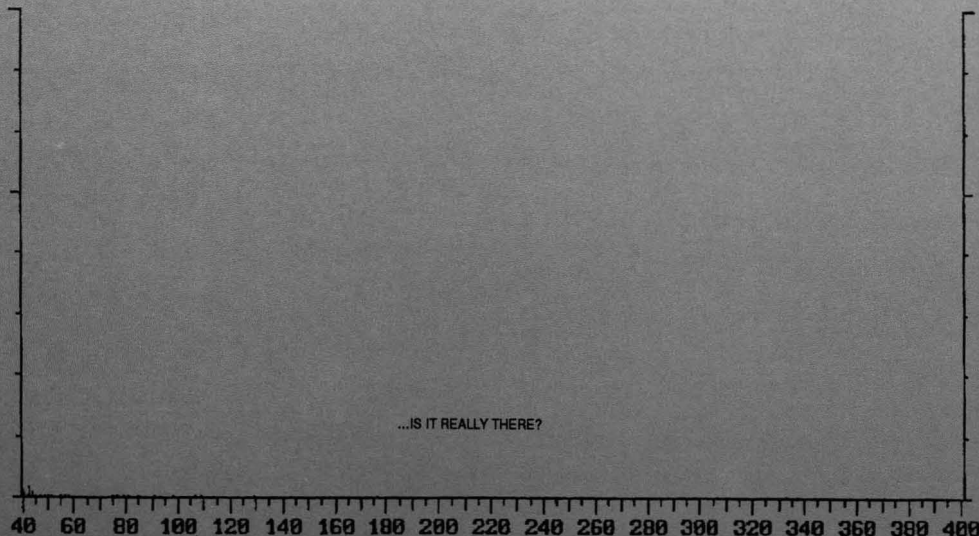


AUGUST 1991
ENVIRONMENTAL SCIENCE & TECHNOLOGY

ES&T

Organohalogenes in nature
Page 1346

IF SATURN™ GC/MS CAN'T SEE IT...



The Ultra Trace Analyzer

Are you confident you're getting the whole picture when confirming compounds? Saturn routinely provides a full scan spectrum at low picogram levels. In fact, through narrow mass range scans, Saturn can determine compounds in sub-picogram levels; therefore outperforming traditional quadrupoles in SIM mode. And, scan rates are fast, without spectral distortion on capillary peaks.

Built by Varian

Now built and supported completely by Varian, the PC-controlled Saturn provides powerful performance. The data system controls all automations, even the in-board diagnostics. New generation ion trap materials and enhanced temperature control of the trap guarantee superb sensitivity even for labile or toxic compounds found in dirty matrices like soil and sludge.

Confirmation Compliance

There is no question Saturn meets absolute confirmation protocols. It starts with the chromatographic excellence of the 3400 Gas Chromatograph. Then, optimum trace analysis is achieved when the 8100 AutoSampler is combined with the SPI temperature programmable inlet system for transfer of sample to the column with complete chromatographic integrity.

Face it. If you don't start with expert chromatographic techniques, how can you trust the final results?



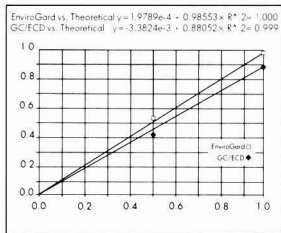
Let us show you how Saturn's superior sensitivity not only gives you complete confidence in your analyses, but how it cuts down analysis time and saves you money. For more information, call **1-800-926-3000**. In Canada, call **416-457-4130**.

GC WITH A FUTURE

varian 

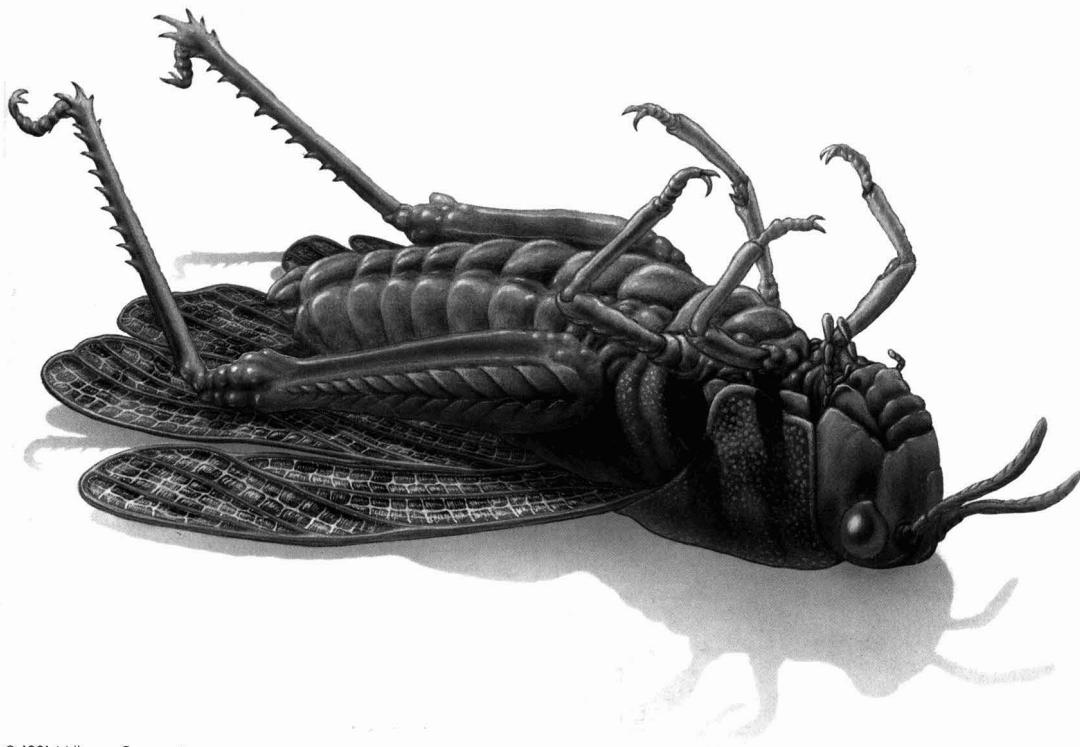
The Same Fate Awaits Anyone Who Can't Detect Pesticides Quickly.

Pesticides can kill more than insects, weeds and fungi. They can kill your bottom line. Particularly if your facility takes days or weeks to conduct pesticide tests. EnviroGard™ immunoassay-based test kits provide results in just 7 minutes (1–2 hours for plate kits). Test



Testing for alachlor shows EnviroGard kits correlate strongly with traditional tests.

for aldicarb, benomyl, triazines and 6 other compounds. Results compare favorably with gas chromatography (chart), mass spectrometry and HPLC. But at \$20 per test, there's no comparison when it comes to price. Order these easy-to-use kits, or get a video and brochure by calling Millipore at 800-225-1380 (in MA: 617-275-9200). **MILLIPORE**

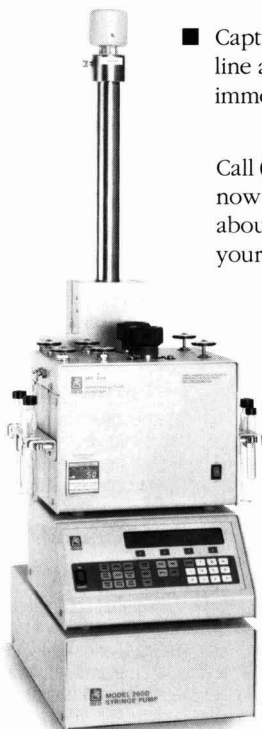


Discover new solutions

Fast, safe priority pollutant sample prep

SFE extracts samples fast for GC and HPLC analysis

- Supercritical fluid extraction uses low-cost, non-toxic CO₂ instead of expensive and hazardous organic solvents.
- Process soils, ash, sediments, and other samples in a fraction of the time required for Soxhlet methods.



- Capture extractants off-line and ready for immediate analysis.

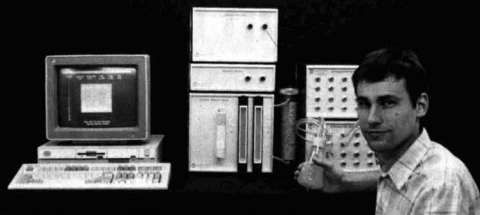
Call **(800)228-4250**
now for details. Ask
about a test extraction of
your sample.

ISCO, Inc.
P.O. Box 5347
Lincoln NE 68505
Tel: (402) 464-0231
Fax: (402) 464-4543



CIRCLE 6 ON READER SERVICE CARD

BIOREMEDIATION O₂/CO₂ Respirometer



The O₂/CO₂ Respirometer optimizes the bioremediation process by monitoring bacterial growth through the measurement of O₂ consumption & CO₂ production. It can monitor up to 20 measuring chambers having volumes ranging from 50 ml to 20 liters. It is capable of 0.2 µL/h sensitivity -- 10 times more sensitive than the Warburg apparatus. It features 24-hour automatic operation under PC computer control. Other applications are in the food & medical fields.



Columbus Instruments

Post Office Box 44049
Columbus, Ohio 43204 USA

PH: (614) 488-6176 Toll Free: 1-800-669-5011

Fax: (614) 276-0529 TLX: 246514

CIRCLE 4 ON READER SERVICE CARD

Oxidations in Organic Chemistry

This volume is the best and most complete source of information on oxidations of organic compounds. It gives a comprehensive, up-to-date, and well-organized review of the subject, with emphasis on preparative aspects and results.

An invaluable aide for the practicing chemist, this volume offers a more experimental rather than theoretical scope with emphasis on the preparative aspects and synthetic usefulness of individual reactions. Reactions described in the text were chosen on the basis of simplicity, clarity of description in the primary literature, availability of oxidants, and yield.

Topics within the volume describe oxidation and dehydrogenation agents and oxidations of various functional groups, with descriptions of the best reagents for a specific reaction. The information is expertly organized and supported by examples, correlation tables, and thorough referencing.

Miloš Hudlický

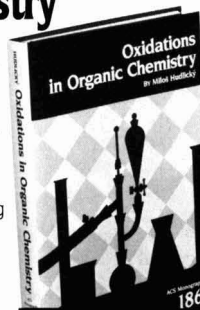
ACS Monograph No. 186

ISBN 0-8412-1780-7 LC 90-34564

433 pages (1990) Clothbound
\$89.95

ISBN 0-8412-1781-5 LC 90-34564

433 pages (1990) Paperbound
\$49.95



Order from: American Chemical Society, Distribution Office, Dept. 74
1155 Sixteenth St., N.W., Washington, DC 20036

or CALL TOLL FREE **800-227-5558**
(in Washington, D.C. 872-4363) and use your credit card!

ES&T CONTENTS

Volume 25, Number 8, August 1991

FEATURES

- 1346 **Organohalogens in nature.** Conclusions drawn from a survey of 135 Swedish lakes. Gunilla Asp-lund and Anders Grimvall, Linköping University, Linköping, Sweden.
- 1352 **Environmental quality criteria.** What type should we be developing? Peter M. Chapman, E.V.S. Consultants, North Vancouver, BC, Canada.

PRÉCIS

- 1360 **Assessing human exposure to airborne pollutants.** Paul J. Lioy summarizes a National Academy of Sciences study on new methods.
- 1363 **Highlights from EPA's Norfolk, VA, conference.** ES&T's Alan Newman describes the recent EPA Conference on Analysis of Pollutants in the Environment.

VIEWS

- 1366 **Assurance levels of standard sample size formulas.** Larry G. Blackwood considers their implications for data quality planning.

REGULATORY FOCUS

- 1369 **Nonpoint source pollution.** Alvin L. Alm explains why success in meeting water quality standards often is elusive.

DEPARTMENTS

- | | |
|-------------------|--------------------------|
| 1341 Editorial | 1373 Products |
| 1342 Currents | 1378 Classified |
| 1345 Earth Summit | 1380 Consulting services |
| 1371 Books | |

UPCOMING

Photocatalyzed destruction of water contaminants

Evaluating uncertainties in risk assessment



Cover: and pp. 1346, 1352, Neal Clodfelter
Credits: p. 1359, Robert Coates Photography

ESTHAG 25(8)1335-1512 (1991)
ISSN 0013 936X

Environmental Science & Technology
©Copyright 1991 by the American
Chemical Society

Editor: William H. Glaze
Associate Editors: Walter Giger,
Ronald A. Hites, Jerald L.
Schnoor, John H. Seinfeld, Joseph
Suflita

ADVISORY BOARD

Roger Atkinson, Joan M. Daisey,
Fritz H. Frimmel, George R. Helz,
Ralph Mitchell, Joseph M.
Norbeck, Walter J. Weber, Jr.,

Alexander J. B. Zehnder, Richard
G. Zepp

WASHINGTON EDITORS

Managing Editor: Stanton S.
Miller
Associate Editors: Julian
Josephson, Alan Newman

MANUSCRIPT REVIEWING

Manager: Yvonne D. Curry
Associate Editor: Marie C. Wiggins
Assistant Editor: Bryan D. Tweedy

MANUSCRIPT EDITING

Journals Editing Manager: Kathleen
E. Duffy

Associate Editor: Lorraine Gibb
Director, Operational Support:
C. Michael Phillippe

GRAPHICS AND PRODUCTION

Head, Production Department:
Leroy L. Corcoran
Composition Systems
Administrator: Vincent L. Parker
Art Director: Alan Kahan
Designer: Neal Clodfelter

Production Editor: Jennie
Reinhardt

PUBLICATIONS DIVISION

Director: Robert H. Marks
Head, Special Publications
Department: Randall E. Wedin
Head, Journals Department:
Charles R. Bertsch

ADVERTISING MANAGEMENT

Centcom, Ltd.
For officers and advertisers, see
page 1380.

RESEARCH

- 1381 **A cometabolic biotransformation model for halogenated aliphatic compounds exhibiting product toxicity.** Lisa Alvarez-Cohen* and Perry L. McCarty

A model that incorporates product toxicity into cometabolic biotransformation kinetics is proposed and evaluated with experimental methanotrophic trichloroethylene transformation data.

- 1387 **Two-stage dispersed-growth treatment of halogenated aliphatic compounds by cometabolism.** Lisa Alvarez-Cohen* and Perry L. McCarty

A two-stage bioreactor that utilizes cometabolic biotransformations for the treatment of halogenated aliphatics is proposed and modeled.

- 1393 **Survey of potable water supplies for *Cryptosporidium* and *Giardia*.** Joan B. Rose,* Charles P. Gerba, and Walter Jakubowski

Cryptosporidium oocysts and *Giardia* cysts are found in 55% and 16% of surface waters used for potable supplies at concentrations averaging 43 oocysts and 3 cysts/100 L.

- 1400 **Influence of the environment on the patina of the Statue of Liberty.** Richard A. Livingston

Acid rain does not affect the Statue of Liberty's copper skin, but sulfur dioxide and sea salt are significant factors.

- 1408 **Long-term processes in a stabilized coal-waste block exposed to seawater.** Daryl E. Hockley* and Hans A. van der Sloot

Chemical and mineralogical profiling of a stabilized waste block reveals processes active during 8-years contact with seawater.

- 1414 **Effect of redox potential and pH on arsenic speciation and solubility in a contaminated soil.** Patrick H. Masscheleyn,* Ronald D. Delaune, and William H. Patrick, Jr.

This study examines the impact of soil redox potential and pH on the speciation and solubility of As in a contaminated soil.

- 1419 **Aqueous-phase oxidation of polychlorinated biphenyls by hydroxyl radicals.** David L. Sedlak and Anders W. Andren*

The degradation of PCBs through oxidation by hydroxyl radicals is studied.

- 1427 **Continuous multiligand distribution model used to predict the stability constant of Cu(II) metal complexation with humic material from fluorescence quenching data.** David M. Grimm, Leo V. Azarraga, Lionel A. Carreira,* and Wisnu Susetyo

By use of a pH-dependent continuous multiligand distribution model, the stability constant between Cu(II) and dissolved humic material is determined.

- 1432 **Extraction efficiencies of organochlorine compounds from Niagara River water.** Mark S. Driscoll, John P. Hassett,* Caryl L. Fish, and Simon Litten

Organochlorine compounds are extracted more efficiently and precisely from water after chromic acid digestion.

- 1439 **Comparison of portable gas chromatographs and passivated canisters for field sampling airborne toxic organic vapors in the United States and the USSR.** Richard E. Berkley,* Jerry L. Varns, and Joachim Pleil

Field results suggest that a combination of canister/TO-14 and portable gas chromatograph methods offers a synergistic approach to source assessment measurements of trace volatile organic compounds in air.

- 1445 **Heuristic model for predicting the intrusion rate of contaminant vapors into buildings.** Paul C. Johnson* and Robert A. Ettinger

This paper presents a heuristic model for screening-level calculations incorporating both convective and diffusive mechanisms, as well as contaminant soil, and building foundation properties.

- 1453 **Biodegradation of polynuclear aromatic hydrocarbons from a bivalve mollusc, *Merccenaria mercenaria* L.** John T. Tanacredi* and Raul C. Cardenas

An experiment utilizing a bivalve mollusc is designed to investigate the ability of naturally occurring bivalves to cleanse themselves after exposure to PAHs found in waste crankcase oil.

- 1461 **Biodegradation of mixed-organic wastes by microbial consortia in continuous-recycle expanded-bed bioreactors.** Tommy J. Phelps,* John J. Niedzielski, Kenneth J. Malachowsky, Richard M. Schram, Stephen E. Herbes, and David C. White*

Please send research manuscripts to Manuscript Reviewing, feature manuscripts to Managing Editor. For editorial policy, author's guide, and peer review policy, see the January 1991 issue, page 45, or write Yvonne D. Curry, Manuscript Reviewing Office, ES&T: A sample copyright transfer form, which may be copied, appears on the inside back cover of the January 1991 issue.

Environmental Science & Technology, ES&T (ISSN 0013-936X), is published monthly by the American Chemical Society at 1155 16th Street, N.W., Washington, D.C. 20036. Second-class postage paid at Washington, D.C., and at additional mailing offices. POSTMASTER: Send address changes to *Environmental Science & Technology*, Membership & Subscription Services, P.O. Box 3337, Columbus, Ohio 43210.

SUBSCRIPTION PRICES 1991: Members, \$39 per year; nonmembers (for personal use), \$73 per year; institutions,

\$329 per year. Foreign postage, \$16 additional for Canada and Mexico, \$36 additional for Europe including air service, and \$45 additional for all other countries including air service. Single issues, \$28 for current year; \$31 for prior years. Back volumes, \$367 each. For foreign rates add \$4 for single issues and \$16 for back volumes. Rates above do not apply to nonmember subscribers in Japan, who must enter subscription orders with Maruzen Company Ltd., 3-10 Nihon bashi 2 chome, Chuoku, Tokyo 103, Japan. Tel: (03) 272-7211.

COPYRIGHT PERMISSION: An individual may make a single reprographic copy of an article in this publication for personal use. Reprographic copying beyond that permitted by Section 107 or 108 of the U.S. Copyright Law is allowed, provided that the appropriate per-copy fee is paid through the Copyright Clearance Center, Inc., 27 Congress St., Salem, Mass. 01970. For reprint permission, write Copyright Administrator,

Publications Division, ACS, 1155 16th St., N.W., Washington, D.C. 20036.

REGISTERED NAMES AND TRADEMARKS, etc., used in this publication, even without specific indication thereof, are not to be considered unprotected by law.

SUBSCRIPTION SERVICE: Orders for new subscriptions, single issues, back volumes, and microform editions should be sent with payment to American Chemical Society, Dept. L-0011, Columbus, OH 43268-0011. Phone orders may be placed, using VISA, MasterCard, or American Express, by calling the ACS Sales Office at (614) 447-3776 or toll free (800) 333-9511 from anywhere in the continental U.S. (For general information, in the Washington, D.C., area call 872-4363 or toll free 800-227-5558.) Changes of address, subscription renewals, claims for missing issues, and inquiries concerning records and accounts should be directed to Manager, Membership and Subscription Services, ACS,

P.O. Box 3337, Columbus, Ohio 43210. Changes of address should allow six weeks and be accompanied by old and new addresses and a recent mailing label. Claims for missing issues will not be allowed if loss was due to insufficient notice of change of address, if claim is dated more than 90 days after the issue date for North American subscribers or more than one year for foreign subscribers, or if the reason given is "missing from files."

The paper used in this publication meets the minimum requirements of American National Standard for Information Sciences—Permanence of Paper for Printed Library Materials, ANSI Z39.48-1984.

The American Chemical Society assumes no responsibility for statements and opinions advanced by contributors to the publication. Views expressed in editorials are those of the author, and do not necessarily represent an official position of the society.

The potential for bioremediation of groundwater contaminated with mixed-organic wastes is demonstrated in laboratory reactors.

- 1466 **Effects of a CO₂ pressure process on the solubilities of major and trace elements in oil shale solid wastes.** Katta J. Reddy,* James I. Drever, and Victor R. Hasfurther

Treatment of moist retorted oil shale with CO₂ reduces alkalinity and the mobility of F and Mo.

- 1470 **Chemical characterization and source apportionment of individual aerosol particles over the North Sea and the English Channel using multivariate techniques.** Chris Xhoffer,* Paul Bernard, René Van Grieken, and Ludo Van der Auwera

The characterization and source of aerosol particles over the North Sea and the English Channel are determined.

- 1479 **Diffusion of 2,3,7,8-tetrachlorodibenzo-*p*-dioxin in soil containing organic solvents.** Michael R. Overcash,* Arnold L. McPeters, Erika J. Dougherty, and Ruben G. Carbonell

The transport of 2,3,7,8-tetrachlorodibenzo-*p*-dioxin in soil containing organic solvents is measured experimentally, and a model that yields effective diffusion coefficients is developed.

- 1485 **Surface reactions of brominated arenes as a model for the formation of chlorinated dibenzodioxins and -furans in incineration: Inhibition by ethanolamine.** T. Lippert, A. Wokaun,* and D. Lenoir

Aryl coupling of bromobenzene over Cu/Al₂O₃ catalysts, a model reaction for dioxin formation, is inhibited by ethanolamine due to competitive adsorption and catalyst deactivation.

- 1489 **Role of plant biomass in the global environmental partitioning of chlorinated hydrocarbons.** Davide Calamari,* Eros Bacci, Silvano Focardi, Carlo Gaggi, Marco Morosini, and Marco Vighi

Concentrations of chlorinated hydrocarbons in plants from sampling areas worldwide are related to air contamination, physicochemical properties, and use patterns of the chemicals.

- 1496 **Mutagenicity of indoor air containing environmental tobacco smoke: Evaluation of a portable PM-10 impactor sampler.** Paris E. Georghiou,* Philip Blagden, David A. Snow, Linda Winsor, and David T. Williams

The sampling characteristics of two PM-10 samplers are compared in coreplicate experiments in indoor air containing ETS, and by mutagenicity testing of the PM-10 extracts.

- 1501 **Influence of sorbate structure on nonequilibrium sorption of organic compounds.** Mark L. Brusseau* and P. Suresh C. Rao

The relationship between sorbate structure and nonequilibrium sorption is investigated by examining the rate-limited sorption of compounds representing eight classes of organic chemicals.

RESEARCH COMMUNICATIONS

- 1507 **Phenol oxidation in supercritical water: Formation of dibenzofuran, dibenzo-*p*-dioxin, and related compounds.** Thomas D. Thornton, Douglas E. LaDue, III, and Philip E. Savage*

Significant concentrations of higher molecular weight products are reported from the oxidation of phenol in supercritical water.

- 1510 **Sonochemical destruction of chlorinated hydrocarbons in dilute aqueous solution.** H. Michael Cheung,* Ashish Bhatnagar, and Greg Jansen

Remediation of contaminated water through ultrasonic irradiation is studied.

*To whom correspondence should be addressed.

This issue contains no papers for which there is supplementary material in microform.

Choosing a graduate school?

Need to know who's doing research critical to yours?

***New edition
just published!***

The ACS Directory of Graduate Research 1989

All the information you need on chemical research and researchers at universities in the U.S. and Canada . . . in a single source.

Includes listings for chemistry, chemical engineering, biochemistry, pharmaceutical/medicinal chemistry, clinical chemistry, and polymer science.

Lists universities with names and biographical information for all faculty members, their areas of specialization, titles of all papers published within the last two years, and individual telephone numbers, FAX numbers, and computer addresses.

Provides a statistical summary of academic chemical research—with information by department on numbers of full- and part-time faculty, postdoctoral appointments, graduate students, and M.S. and Ph.D. degrees granted.

What you'll find inside . . .

Information on . . .

- 683 academic departments
- 11,936 faculty members
- 68,276 publication citations

Listings for . . .

- chemistry
- chemical engineering
- biochemistry
- pharmaceutical/medicinal chemistry
- clinical chemistry
- polymer science

1436 pages (1989) Clothbound

Price:

US & Canada **\$55.00**

Export **\$66.00**

No academic institution or chemically oriented business can afford to be without the ACS Directory of Graduate Research 1989! Order today by calling TOLL FREE (800) 227-5558. In Washington, D.C., call 872-4363. Or use the coupon below.

**Please send me _____ copy(ies) of the ACS Directory of Graduate Research 1989.
Price: US & Canada \$55.00 Export \$66.00.**

☐ Payment enclosed (make checks payable to American Chemical Society).

☐ Purchase order enclosed. P.O.# _____

Charge my: ☐ MasterCard/VISA ☐ American Express ☐ Diners Club/Carte Blanche

Account # _____ Expires _____

Signature _____

Phone _____

Ship books to:

Name _____

Address _____

City, State, ZIP _____

ORDERS FROM INDIVIDUALS MUST BE PREPAID. Please allow 4-6 weeks for delivery. Prices are quoted in U.S. dollars. Mail this order form with your payment or purchase order to:

American Chemical Society, Distribution Office Dept. 705,
P.O. Box 57136, West End Station, Washington, D.C. 20037.

705

Good science and the scientist

It is important for scientists and engineers to take a strong stand on the use of good science in addressing environmental problems. It falls to us, more than any other group, to insist that decision makers understand the nature of the problem and the alternative strategies that may be followed in seeking a solution. We must emphasize the nature and magnitude of the uncertainties involved in each strategy. We must resist irrational, unscientific decisions even if they are to our own benefit. We must counsel politicians, managers, and the general public and hope that they listen.

This is not to say that we have all of the answers. Indeed, one of the strongest messages that we should communicate is that we do not; that there are immense uncertainties in many areas of environmental science and engineering. We should not be afraid to say that more data taking or analysis is needed, even if it appears to be self serving. The fact is, we are now addressing many complex systems that we poorly understand. When a decision could do more harm than good, or when a remediation plan could be extremely expensive and may not lower risk, more research may be the best solution. When the political heat is uncomfortable, no one likes this position, but sometimes it is simply the best science can offer.

We must be humble in expressing opinions, given the nascent resentment against scientists as effete intellectuals, but we must come forward with the best information available and ask that it be taken into account when decisions are made. Too often scientists and engineers have taken a view that public debate is "not my problem"; we are often uncomfortable under adversarial circumstances and we would rather submit the facts, preferably in a written report, and leave. As the debate continues, though, there is often no one to speak for good science, and other arguments prevail. When a solution is proposed, it should be clear to everyone what science has to say about it.

There are innumerable examples that could be cited to reinforce this argument. How many of our readers live in communities where a debate has raged on the locating of a hazardous waste containment or disposal center; and how many times are these debates fraught with unfounded claims of health or ecological effects of trace contaminants? Who speaks up for leaving a contaminant in place when the science says that moving it would be worse? Why do we still fail to recognize uncertainties in analytical measurements and detection limits? Why are we spending hard-to-get public money cleaning up dirt to below natural background levels?

There are two levels at which scientists and engineers can make an impact. Locally, we can offer expertise and counsel to the general public and decision makers. This is particularly valuable because local funds to deal with environmental issues are limited. In addition, we can counsel governmental and, particularly, legislative bodies on environmental issues. Public officials are prone to make decisions on the basis of political considerations, so we must offer the scientific argument, based on the best information and analysis available. That position, if offered articulately again and again with conviction, will have an impact on public health and the environment, and will lead to wiser use of public and private funds for environmental protection.

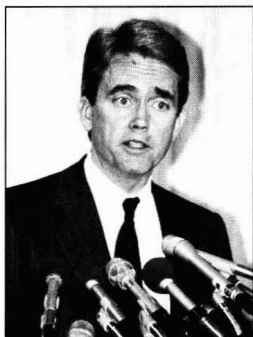


INTERNATIONAL

Eight countries whose territory extends north of the Arctic Circle have signed an agreement to co-operate in monitoring pollution of the Arctic environment and to protect the region's plant and animal life. The United States was one of the signatories of the non-binding agreement, which was initiated by Finland and signed in Rovaniemi, Finland, in mid-June. Provisions include responding to oil spills and monitoring pollution from oil, radiation, heavy metals, organic contaminants, acidification, and noise. Other signatories include Canada, Denmark, Finland, Iceland, Norway, Sweden, and the Soviet Union.

FEDERAL

EPA proposed June 3 to reward companies that voluntarily reduce their toxic air emissions by 90% (95% for particulates) by Jan. 1, 1994. EPA administrator William Reilly offered such companies a "carrot" in the form of a six-year delay for meeting maximum achievable control technology (MACT) provisions of the 1990 Clean Air Act. Any company that wants to participate in this program has until Nov. 15, 1991, to declare its commitment to reduce emissions. The "stick" is that a company that commits to and then fails to meet the Jan. 1, 1994, emissions reduction deadline becomes vulnerable to EPA enforcement actions.



Reilly: Rewarding emission cutters

A company can withdraw its commitment by Dec. 1, 1993, but it then loses the six-year delay and becomes subject to MACT rules. For more information, contact David Beck, Emission Standards Division, EPA, Research Triangle Park, NC 27711; (919) 541-5421.

The National Oceanic and Atmospheric Administration (NOAA) has drafted guidelines for controlling nonpoint source water pollution. Virginia Tippie of NOAA explained to a House subcommittee that the guidelines aim to help state and local governments control nonpoint pollution from agriculture, dams and levees, forestry, marinas, and urban development. In addition, NOAA and EPA are drafting guidelines for state coastal nonpoint pollution control programs. These guidelines may be used in the consideration of Clean Water Act reauthorization.

EPA proposed rules June 11 that would require the use of reformulated gasoline by 1995 in nine metropolitan areas that have the worst tropospheric ozone levels. These areas account for almost 25% of U.S. gasoline consumption. The rules would mandate a fuel composition of at least 2% oxygen, no more than 1% benzene, and no heavy metals. Toxic and volatile compounds in the gasoline must be reduced by 15% initially, and by 25% by 2000, relative to 1990 "base gasoline." Moreover, gasoline makers would be forbidden from putting benzene and other pollutants removed from reformulated gasoline into conventional gasoline sold in the rest of the country. Alternative additives for oxygenating gasoline include methanol, ethanol, and methyl-*tert*-butyl ether.

When will an Environment Department (ED) be added to the President's cabinet? That's still anybody's guess, but in late May the Senate Governmental Affairs

Committee approved creation of an ED. The Committee's version of an enabling act also would create an independent Bureau of Environmental Statistics (BES) within the ED. President Bush wants Congress to make EPA a cabinet department, but he wants no other changes in EPA's operations and opposes the idea of a BES.

STATES

Within 60 days of receipt by EPA, states would learn whether their state implementation plans (SIPs) for controlling air pollution are complete. EPA has proposed. EPA would have to notify states within six months of their filing deadlines (*Fed. Regist.* 1991, 56, 23826); if it does not do so, the SIP would be considered complete as submitted. For more information on streamlining SIP submissions, contact Denise Gerth, Office of Air Quality Planning and Standards, EPA, Research Triangle Park, NC 27711; (919) 541-5550.

Commercial businesses in New York City must start recycling high-grade office paper, corrugated cardboard, metal, and certain types of construction debris. The private trash haulers that pick up this waste also must recycle and offer post-collection separation services. (All commercial trash is taken by private collectors; the city's Department of Sanitation provides only residential trash collection.) The rule went into effect May 29, and enforcement will begin Nov. 29. In May 1992, recycling of newspapers, magazines, and glass containers will be required; by Nov. 1992, plastic containers will be added to the list; and by May 1993, plastic film also will have to be recycled. For more information, call the Department of Sanitation at (212) 334-8590.

A study by the New Jersey Department of Environmental Protection (DEP) suggests that 50 lb (22.75 kg) of chlorofluorocarbons (CFCs) can be recovered for every

100 discarded motor vehicles, DEP Commissioner Scott Weiner announced June 10. He described a pilot project that ran from January to June 1990 and studied the feasibility of recapturing CFCs at commercial scrap yards. Normally when vehicles are scrapped, large amounts of CFCs escape. Several private firms throughout the state allowed scrapped vehicles to be tested for CFCs. An average of 1.2 lb (544 g) of CFCs were recovered from each vehicle. The DEP study also found that workers took 15 min to remove CFCs from each vehicle. A DEP spokesperson said that to make a recovery program feasible, less expensive CFC recapture equipment or a higher market value for recaptured CFCs would be needed.

Revised hazardous waste regulations drafted by the New York Department of Environmental Conservation (DEC) define in more detail than previous regulations required a "significant threat" posed by a site. This means that DEC must document the presence of hazardous waste at a site *and* determine that the waste has caused, or will cause, environmental damage if no remedial action is taken. This draft regulation (6 NYCRR Part 375) follows a 1989 decision by the state Court of Appeals that struck down previous regulations. Under the old rules, the mere presence of hazardous waste could be deemed a significant threat. The court ruled that the old regulations were overly broad. Under New York law, DEC must first determine that a site poses a significant threat before the department can order someone to clean it up.

AWARDS

U.S. environmentalists now have their own Presidential award. As many as 12 Presidential Environment and Conservation Challenge Awards and 30 citations will be presented annually to deserving U.S. residents, organizations, businesses, or governmental agencies. The awards will honor achievements in four arenas: incorporating environmental thinking into sound management practices; fostering cooperative approaches to environmental needs; developing innovative

technologies, programs, or services; and promoting environmental education and communication. Winners receive their awards at a White House ceremony and participate in a national symposium. The first awards will be presented this fall. For more information contact President's Environment and Conservation Challenge Awards, The White House, Council on Environmental Quality, 722 Jackson Place, N.W., Washington, DC 20503; (202) 395-1154.



The Burhennes: Sasakawa laureates

The \$200,000 Sasakawa International Environment Prize was awarded June 5 to Wolfgang Burhenne and Françoise Burhenne-Guilmin of Bonn, Germany. They were honored for having founded and developed the International Union for the Conservation of Nature's Environmental Law Center in Bonn. Wolfgang Burhenne helped establish the World Wide Fund for Nature and the International Council of Environmental Law. Burhenne-Guilmin compiled, analyzed, and indexed the world's most extensive documentation on national and international environmental law. The prize is sponsored by the Japanese Shipbuilding Industry Foundation and administered by the United Nations Environment Programme.

SCIENCE

To identify candidate chemicals for neurotoxicity testing, "EPA should consider the intended use, degree of toxicity, exposure, and other scientific data in deciding whether or not a substance produces an adverse effect on the nervous system," said John O'Donoghue of Eastman Kodak. Addressing EPA June 12 on behalf

of the American Industrial Health Council (Washington, DC), O'Donoghue added that the acceptability of neurotoxicity data "should be determined on the basis of scientific merit and not by comparison to test guidelines." He suggested that EPA's proposed endpoint rule "would vastly overwhelm the national capacity for performing neurotoxicity tests."

The fourth European survey of damage to forests has been completed. All countries participating in the survey used uniform guidelines to determine the level of damage over 114 million hectares (281.5 million acres) of forest in various parts of Europe. The number of countries that report damage to more than 30% of their trees has tripled since 1988, and in seven of those countries, air pollution is viewed as the principal factor. Another reason for the increase in reports of forest decline is that more countries submitted data, according to the International Cooperation Program for Recording and Monitoring the Effects of Air Pollution on Forests. Data are evaluated at the Federal Research Institute for Forestry and Timber Industry (Hamburg, Germany). The principal conclusion is that reduction in levels of air pollution in Europe has become urgent.

Health effects of SO₂ can be evaluated with several uncertainty factors taken out, according to the Electric Power Research Institute (EPRI, Palo Alto, CA). An EPRI project developed a method whereby the distribution of SO₂ concentrations over time and space can be integrated with clinically derived dose-response relationships and with information on the likelihood that asthmatics engaging in exercise will be exposed. Using this method, researchers carried out a risk analysis of asthmatics who lived near two power plants. They concluded that there is a "very low probability of increased pulmonary symptoms due to SO₂ emissions." For more detail, see Wyzga, R. *EPRI Journal* 1991, 16(3), 52-54.

TECHNOLOGY

Hopes for using a deep underground salt chamber for storing lethally radioactive wastes may

be dashed, according to mining experts who testified before a House Government Operations subcommittee in early June. They reported that rock falls have occurred in a deep underground salt chamber near Carlsbad, NM, the site being considered for use beginning this summer under the Waste Isolation Pilot Project. These chambers were carved by rock salt miners almost 20 years ago. Natural closure causes the rock falls and eventually will cause the chamber to collapse. Collapsed salt chambers have been considered ideal "prisons" from which high-level wastes could never escape to the environment. Mining experts fear, however, that the New Mexico chamber will collapse so rapidly that there will not be enough time to evaluate salt chambers as repositories.

A long-standing water supply problem in the British Virgin Islands (BVI) has been solved by a 360,000-gal-per-day reverse osmosis (RO) plant, according to Reliable Water (Billerica, MA). Located on the island of Tortola, BVI, the plant uses RO to convert seawater into drinking water and brine. Operating costs are reduced through energy recovery and reuse and through a design for unattended operation. The plant has an automatic telephone dialer system to alert company staff in case of an emergency. It also features an environmental control and dehumidification system, with a demineralized-water rinsing facility to reduce corrosion. The design allows doubling the plant's

capacity to more than 720,000 gal per day in the future.

North Star Steel Company's Beaumont, TX, plant will be the first industrial user of a new technology for recovering zinc from the hazardous waste dust that forms as a byproduct of electric arc furnace steel production. The recovery plant is expected to be in full operation by late 1992. Zinc concentrations in the dust run as high as 40%. Cadmium and iron also are found in the material. Nationwide, electric arc steel plants produce 550,000 tons of this dust annually. Currently, EPA will allow landfill disposal of dust containing less than 15% zinc. The new technology, the Gas-Fired Flame Reactor process, recovers zinc and other metals on site as metal oxides. It was developed for the Gas Research Institute (Chicago, IL) by Horsehead Resource Development Co., Inc., which will run the Texas reactor. Horsehead plans to sell the crude zinc oxide to the zinc industry and offer the remaining slag to the cement and construction industries. Horsehead has petitioned EPA to delist the slag as a hazardous waste.

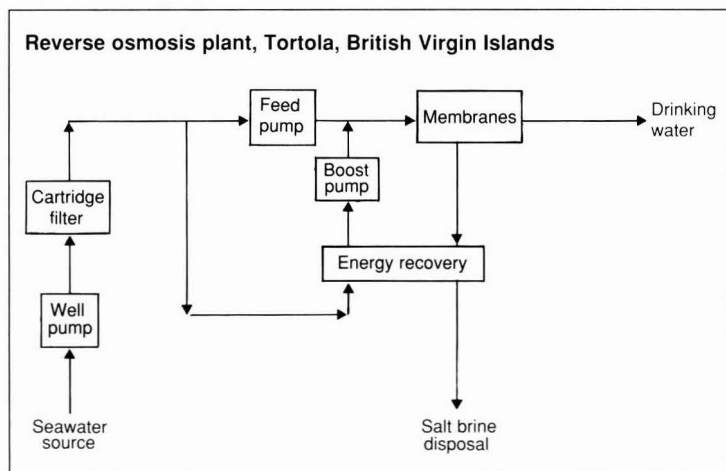
BUSINESS

All nonsmokers should be protected from involuntary exposure to secondhand tobacco smoke in the workplace, in indoor areas open to the public, and in food service establishments, according to the American Industrial Hygiene Association (AIHA, Akron, OH). Employers should provide

smoke-free work areas, forbid smoking in meeting rooms and other common rooms, and set aside areas for smoking with proper venting of air to the outside. AIHA also recommends the establishment of smoking cessation programs with phased-in implementation time, employee participation, training and education, and provisions for enforcement.

Industry, government, and academic groups have formed the Model Evaluation Consortium for Climate Change (MECCA), whose mission will be to evaluate the reliability of current global climate simulation models. These models are used to evaluate possible future climate variations that may arise from human activities and natural events, such as greenhouse gas emissions, deforestation, and volcanic eruptions. "We want to provide policy makers with the scientific information necessary to optimize decisions," says Peter Mueller, MECCA policy chairman, who also is the atmospheric sciences program manager at the Electric Power Research Institute (Palo Alto, CA). MECCA hopes to have initial research results available for the Earth Summit, to be held in Rio de Janeiro in June 1992.

Volvo has launched a road test of five sedans with flexible fuel engines and electrically heated catalytic converters. The cars, to be used in California's Flexible Fueled Vehicle Demonstration Program, run on unleaded gasoline or alcohol-mixed fuels containing as much as 85% methanol. An optical sensor measures methanol concentrations so that fuel injection and ignition computers can adjust flow rates and spark advance. Larger fuel injectors, methanol-resistant fuel lines, and a sensor to adjust air-fuel mixtures have been built into the test cars to handle diverse fuel mixtures. The heated catalytic converter dramatically lowers exhaust pollutants, according to Volvo. To power the converter's heater, a second battery is in the trunk and a larger-than-usual alternator recharges the regular and the converter batteries. Volvo plans a two-year test of the new technology before deciding whether to introduce these advances in production line vehicles.



By Stanton Miller

The United States is active in planning the United Nations Conference on Environment and Development (UNCED) in 1992 and has urged that global climate and forestry agreements be completed, for signing if possible, at that conference (1). But there are some recent observations on this topic from representatives of Brazil, the conference host country. Brazil is leading attempts to improve data on forest losses and conservation. At a meeting in February in Chantilly, VA, deforestation and energy efficiency were discussed by Brazilian spokesmen.

Professor José Goldemberg is the Secretary for Science and Technology of the Presidency of the Republic of Brazil. He is a world-renowned expert on energy strategies who participated in the Second World Climate Conference in Geneva last November (2). At that conference he highlighted the need for better communication of the potential for energy efficiency measures in countries where a lot of fossil-fueled electric generating capacity was being installed, but little was heard about improving end use efficiency.

Luiz Gylvan Meira, Director of Earth Observation at the National Institute for Space Research in São José dos Campos, São Paulo, Brazil, and science adviser of the Brazilian delegation at the Chantilly meeting, spoke about the confused history of attempts to quantify deforestation in Amazonia and the Amazon Basin. [Amazonia is defined by federal law as an area that includes the entire states of Acre, Amazonas, Pará, Rondônia, Amapá, and Roraima, and parts of Mato Grosso, Goiás, and Maranhão. The surface area of the Brazilian Amazon (4,874,000 km²) accounts for 57.6% of Brazil's territory.] Meira said, "Brazilian studies now being conducted with Landsat imaging suggest that the annual rate of deforestation in the legal Amazon is about 20,000 km² a year and has been slowing since the mid- to late 1980s."

Meira mentioned earlier estimates of 40,000 km² by Greenpeace, 50,000 km² by Friends of the Earth, and 60,000–80,000 km² by the World Resources Institute. "The most problematic of these estimates had been the counting of forest fires with satellite imaging; although the fires could be counted and produced visually spectacular images, the assumptions made about the forest that was being lost turned out to create significant overestimates. As a result of taking these annual estimates and then supposing that they held true over a decade, estimated values of as much as 800,000 km² had been produced for the decade of the 80s."

The National Institute for Space Research is now resurveying areas studied in 1975 and 1978 (surveys were conducted for assessing agriculture and therefore had their own areas and assumptions). The Institute is conducting a survey with 1985 images and is analyzing 1980 data. When the survey data are put with 1988 and 1989 surveys in a computer-based Geographical Information System, it will be possible to display the evolution of deforestation through time and space and to better understand its causes. Such data

from 1975 to 1990 from the state of Rondônia are a good example. In Rondônia, there was only cleared and uncleared closed moist forest (i.e., no old clearance or savannah distorted the data on current deforestation).

["Closed" forest refers to vegetation so dense it is very difficult to walk through.] The data indicated a continued slowing in deforestation and the abolition of various tax breaks which had favored deforestation, according to Meira.

Meira says, "Thus, it appears that some 300,000 km² of Amazon forest have been lost to other uses, such as farming, roads, and towns, in recent decades, together with 95,000–97,000 km² of much older clearance. It is now Brazilian policy to reduce the rate of deforestation by 10% each year."

References

- (1) The Council on Environmental Quality; "Environmental Quality, 21st Annual Report"; U.S. Government Printing Office: Washington, DC, 1990, p. 32.
- (2) Phillips, V. *Environ. Sci. Technol.* **1991**, *25*, 574–78.

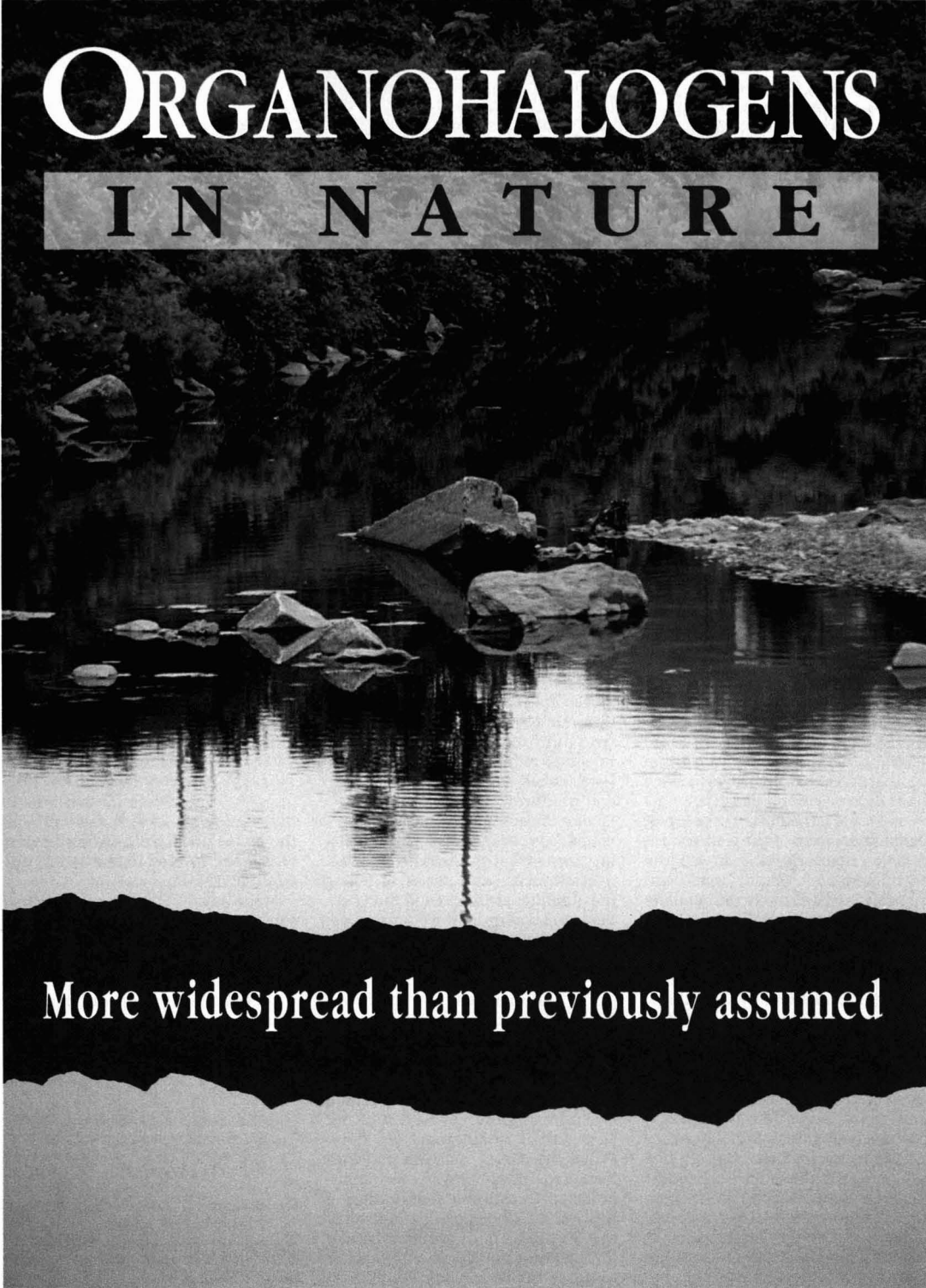
Stanton Miller is the managing editor of ES&T.

Brazil



ES&T FEATURES

ORGANOHALOGENS IN NATURE



More widespread than previously assumed

Although the natural production of organohalogenes has been observed in several studies, it is generally assumed to be much smaller than the industrial production of these compounds (1, 2). Nevertheless, two important natural sources have been known since the 1970s: red algae in marine ecosystems produce large amounts of brominated compounds (3), and methyl halides of natural origin are present in the atmosphere (4, 5). During the past few years it has been shown that organohalogenes are so widespread in ground-water, surface water, and soil (6–10) that all samples in the studies referred to contain measurable amounts of adsorbable organohalogenes (AOX). In addition, the quantities found often exceed the amount that can be explained by human activities in surrounding areas.

We will document the widespread occurrence of organohalogenes in "unpolluted" soil and water and discuss possible sources of these compounds. It has been suggested that these organohalogenes originate from long-range atmospheric transport of industrially produced compounds (11). We will review existing evidence of enzymatically mediated halogenation of organic matter in soil and show that, most probably, natural halogenation in the terrestrial environment is the largest source.

Occurrence in soil and water

To document the natural occurrence of organohalogenes, we conducted a survey of 135 lakes in southern Sweden and found concentrations of AOX ranging from 11 to 185 $\mu\text{g Cl/L}$ (Figure 1). This corresponds well with the results of the studies referred to above, which indicate that all surface waters contain organohalogenes. The highest concentrations in our survey were found in humic-rich, oligotrophic lakes in remote areas where the AOX concentrations were shown to be comparable with those in industrially polluted waters, such as the Rhine River; along a profile from the source of this river to the Dutch border, AOX concentrations varied from 5 to 200 $\mu\text{g Cl/L}$ (12).

To document further the global occurrence of organohalogenes in

terrestrial environments, we analyzed soils from different parts of the world (Table 1). We found that all samples contained organohalogenes and that the ratio of organohalogenes to organic carbon was remarkably stable (0.22–2.8 mg Cl/g C). Moreover, the data presented in Table 1 show that the occurrence of halogenated compounds in soil is not a phenomenon peculiar to Swedish soils; on the contrary, organohalogenes seem to occur worldwide. The variability of the organohalogen-to-organic-carbon ratio for surface water samples (0.84–14.5 mg Cl/g C) was larger, and the median was almost 10 times higher than for soil samples (Figure 2).

In our surveys of AOX in water and soil, we analyzed the water samples according to the German standard procedure (13). For soil samples, however, there is no stan-

many, a survey of rainwater samples resulted in a mean value of 20 $\mu\text{g Cl/L}$ (10).

The total annual deposition of organohalogenes in Sweden (3700 metric tons [tonnes]/year), measured as bulk precipitation, approximately equals the total annual riverine loading (11). However, mass balance calculations for selected river basins strongly indicate that sources other than atmospheric deposition dominate. Large local variations exist between adjacent streams and rivers, and the concentration of AOX in runoff sometimes is 10 times higher than in precipitation (11, 14). Furthermore, as was shown in a mass balance study of a raised bog in Sweden, there must be substantial amounts of naturally produced AOX in soil and water (9); local anthropogenic sources of AOX in the study area were negligible,

“The quantities detected often exceed the amount that can be explained by human activities in the surrounding areas.”

dard method. Nevertheless, a special study of the procedure used in the present investigation gave satisfactory results; the measured AOX concentrations in soil are reproducible, and we found no evidence of artifacts that could jeopardize our conclusion about the widespread occurrence of organically bound halogens in soil.

A nonindustrial source

The prevalence of AOX in remote areas implies that local sources of pollution are not the major explanation for observed concentrations in soil and water. A more substantial contribution could be made by the long-range atmospheric transport of naturally or industrially produced compounds. In Sweden, for example, the average AOX concentration in bulk precipitation has been estimated to be 15 $\mu\text{g Cl/L}$ (11); in Ger-

and the total pool of AOX in the bog (> 1200 tonnes) was found to be more than 300 times larger than the annual atmospheric deposition (< 3.8 tonnes).

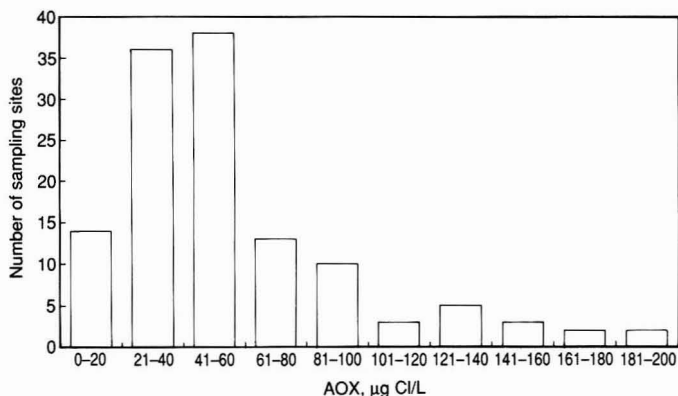
To summarize, these observations indicate that local pollution and atmospheric deposition are responsible for only part of the widespread occurrence of AOX. Natural halogenation processes in terrestrial or limnic (lake and river) environments also must contribute substantially to the AOX in soil and water.

Production in fresh water unlikely

Outflows from lakes seem to have lower concentrations of organohalogenes than do the lakes' tributaries (14). In addition, the highest concentrations in rivers most often are found downstream from peat bogs and in other areas having elevated concentrations of organic matter.

FIGURE 1

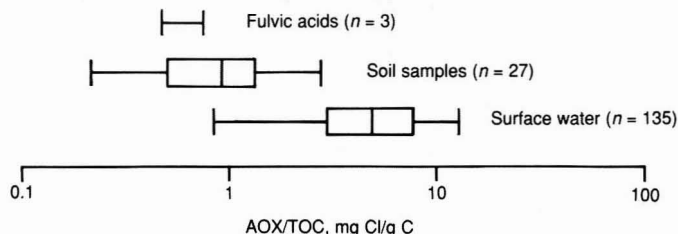
Concentration of adsorbable organohalogens (AOX) in 135 Swedish lakes and rivers^a



^aIn the county of Jönköping.

FIGURE 2

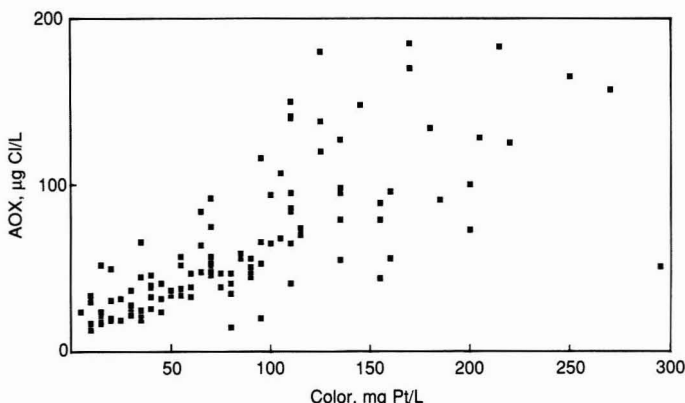
Ratio of adsorbable organohalogens (AOX) to total organic carbon (TOC) in surface water, soil, and fulvic acids^a



^aIsolated from groundwater; box-and-whisker diagrams show medians, quartiles, and minimum and maximum values.

FIGURE 3

Concentration of adsorbable organohalogens (AOX) versus color in 135 Swedish lakes and rivers



This indicates that the halogenated organic compounds are more likely leached from surrounding soils than produced in the water. Furthermore, a large number of terrestrial organisms such as fungi, lichens, bacteria, and higher plants are known to produce halometabolites (2), whereas very few limnic species have been reported to have this capacity.

Thus no evidence is available that strengthens the hypothesis of a net production of organohalogens in fresh water. However, it cannot be totally ruled out that biological production, which is masked by sedimentation, evaporation, or degradation, occurs in lakes.

Terrestrial production

According to Engvold (15), more than 80 plants are known to produce halometabolites. It also has been shown that the concentration of organohalogens in rain falling through spruce trees sometimes is more than 10 times higher than levels in free precipitation (14). These compounds may originate from dry deposition, photochemical oxidation on the needles, or biohalogenation in the tree or on the needles.

Studies recently performed in climate chambers in our laboratory show that organohalogens can be continuously washed from spruce trees. This indicates that such compounds are produced by the tree or possibly by biological or chemical processes on the surface of the needles. Consequently, plants *might* contribute to the organohalogens in the environment, although further investigations are needed to determine the extent of and the mechanisms behind such production.

Several studies have shown that many soil organisms are known to produce halometabolites (2, 16). In addition, as mentioned above, all soils seem to contain organohalogens. Thus, a natural production in soil is another hypothesis that calls for investigation.

Is enzyme action a mechanism?

Haloperoxidases constitute a group of enzymes that catalyze the halogenation of many organic substances in the presence of hydrogen peroxide and halide ion (2). Chloroperoxidases (CPO), which oxidize chloride, bromide, and iodide, have been thoroughly investigated mainly through studies of a specific enzyme (the enzyme EC 1.11.1.10, CPO) from the fungus *Caldariomyces fumago* (17).

TABLE 1

Concentration of adsorbable organohalogens (AOX) in soil samples obtained worldwide

Sampling site	Vegetation	AOX ($\mu\text{g Cl/g d.w.}^a$)	Standard deviation	n	L-o-i ^b	AOX/TOC (mg Cl/g C) ^c
Mochudi, Botswana	Steppe	5	0	2	0.4	2.4
Mochudi, Botswana	Steppe	4	0	2	0.7	1.1
Manaos, Brazil	Campinarana ^d	145	2.6	4	58	0.5
Marondera, Zimbabwe	Savanna	8	2	2	4.6	0.35
N. E. Alberta, Canada	Peat bog, 0–10 cm	254	1.3	2	73	0.7
N. E. Alberta, Canada	Peat bog, 10–40 cm	70	1.9	2	61	0.23
N. E. Alberta, Canada	Peat bog, 40–50 cm	72	4.2	4	65	0.22
Ayer Itam, Malaysia	Deciduous forest	49	3.7	4	12	0.82
Penang Hill, Malaysia	Deciduous forest	54	3.1	2	21	0.51
Penang Hill, Malaysia	Deciduous forest	20	0.2	2	11	0.36
Mount Kintoki, Japan	Bamboo forest	114	2.5	3	17	1.3
Cockle Park Farm, Great Britain	Meadow	62	4.9	4	14	0.89
Cockle Park Farm, Great Britain	Meadow	224	13	5	24	1.9
Klockrike, Sweden	Garden	29	0.9	5	5.8	1.0
Vallmo, Sweden	Pasture	30	1.6	2	4.4	1.4
Axsjön, Sweden	Pine tree forest	360	—	2	86	0.84
Snogerupsån, Sweden	Creek bank	26	—	2	5.4	1.0
Snogerupsån, Sweden	Field	33	—	2	5.9	1.1
Hörby, Sweden	Beech forest, 5–10 cm	348	—	2	29	2.4
Hörby, Sweden	Beech forest, 35–40 cm	196	—	2	14	2.8
Dalir, Iceland	Arctic heath	130	0	2	23	1.1
Dalir, Iceland	Arctic heath	290	13	2	42	1.3
Dalir, Iceland	Arctic heath, brook ravine	180	0	2	17	1.6
Antalya, Turkey	Aleppo pine forest, 0–5 cm	68	5.5	3	72	0.18
Antalya, Turkey	Aleppo pine forest, 5–10 cm	170	3.1	3	37	0.90
Antalya, Turkey	Aleppo pine forest, 10–20 cm	24	1.5	3	7.1	0.68

^a Dry weight.^b Loss on ignition.^c Calculated values of the ratio of AOX to total organic carbon (AOX/0.5 \times L-o-i).^d Central Amazonian term for "forest."

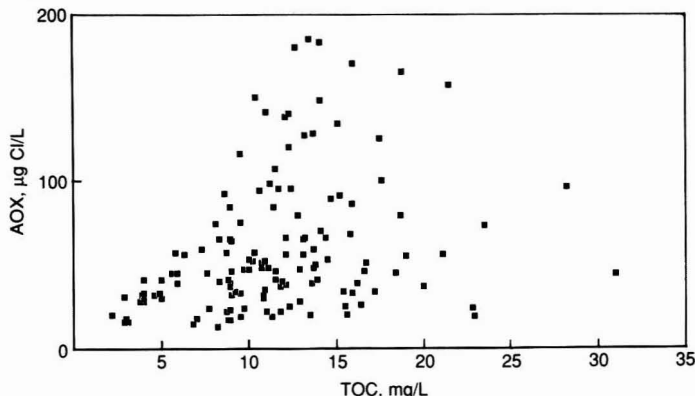
Recently, it has been shown that CPO can catalyze the chlorination of humic substances and that a soil extract obtained by a peroxidase extraction procedure is able to chlorinate monochlorodimedone (18). Further studies of the halogenating capacity of soil extracts have indicated that the catalyst is a chloroperoxidase-like enzyme. Its molecular weight is $> 10,000$ and it is active only in the presence of hydrogen peroxide. The activity is pH-dependent with a pH-optimum close to that of CPO which, under the laboratory conditions of the study, was 3.5–4. In addition, the activity of the soil extract and CPO is inhibited by the addition of specific organic compounds. This implies that enzymatically mediated halogenation of organic matter could be the mechanism that produces organohalogens in soil.

The role of humic substances

Studies of Swedish surface waters previously have shown that the concentration of AOX often is positively correlated to the concentra-

FIGURE 4

Concentration of adsorbable organohalogens (AOX) versus total organic carbon (TOC) in 135 Swedish lakes and rivers



tion of total organic carbon (TOC) (11). In another study, Wigilius et al. (7) showed, by size exclusion chromatography, that halogenated compounds in surface water are present in the same fractions as most of the humic material. Chris-

tiansen (19) showed that iodoperoxidase catalyzes the incorporation of radioactive iodide into humic acids. Furthermore, fulvic acids isolated from groundwater wells have been shown to contain AOX (9).

In our survey of 135 lakes in

southern Sweden, a positive relationship can be seen between the concentration of AOX and water color (Figure 3), but the correlation between the concentration of AOX and that of TOC is less pronounced (Figure 4). The lakes with a high TOC and a low concentration of organohalogens are eutrophic, which implies that only a minor part of the organic matter in these lakes consists of humic material. This suggests that the organohalogens in surface water are related to humic matter, rather than to organic matter in general.

Acknowledgments

We are indebted to Dr. David Hopkins and Dr. Anthony G. O'Donnell, University of Newcastle-upon-Tyne, U.K.; Dr. Larry W. Turchenek, Alberta Research Council; and Prof. Steve Hrukey, University of Alberta, Canada, for providing us with soil samples.

References

- (1) Hoffman, H.-J. et al. *Vom Wasser* **1988**, 71, 125-34.
- (2) Neidleman, S. L.; Geigert, J. *Endeavour, New Series* **1986**, 11, 5-15.
- (3) Fenical, W. In *Elsevier Oceanography Series, 31: Marine Organic Chemistry*; Duursma, E. K.; Dawson, R., Eds.; Elsevier: Amsterdam, 1981; pp. 375-93.

- (4) Lovelock, J. E. *Nature* **1975**, 256, 193-94.
- (5) Harper, D. B. *Nature* **1985**, 315, 55-57.
- (6) Stevens, A. A. et al. *J. Am. Water Works Assoc.* **1985**, 77, 146-54.
- (7) Wigilius, B. et al. *Chemosphere* **1988**, 17(10), 1985-94.
- (8) Grön, C. Dissertation, Institute of Applied Geology, Technical University of Denmark, 1989.
- (9) Asplund, G. *Sci. Total Environ.* **1989**, 81/82, 239-48.
- (10) von Klopp, R.; Kornatzki, K.-H. *Z. Wasser- Abwasser- Forsch.* **1987**, 20, 160-67.
- (11) Enell, M. et al. In *River Basin Management—V*; Laikari, H., Ed.; Pergamon Press PLC: Oxford, 1989; pp. 29-36.
- (12) Keller, M. *Vom Wasser* **1989**, 72, 199-210.
- (13) DIN (Deutsche Industrie Normen); DIN 38409, Teil 14; Beuth-Verlag: Berlin, 1985.
- (14) Grimvall, A. et al. Presented at the 6th European Symposium on Organic Micropollutants in the Aquatic Environment, May 22-24, 1990, Lisbon.
- (15) Engvild, K.C. *Phytochemistry* **1986**, 25, 781-91.
- (16) Siuda, J. F.; de Bernardis, J. F. *Lloydia* **1973**, 36, 107-43.
- (17) Hewson, W. D.; Hager, L. P. In *The Porphyrins, Vol. VII, Biochemistry, Part B*; Dolphin, D., Ed.; Academic Press: New York, 1979; pp. 295-332.
- (18) Asplund, G. et al. In *Lecture Notes in Earth Sciences*; Allard, B.; Borén, H.; Grimvall, A., Eds.; Springer Verlag: Berlin, 1991; pp. 475-83.
- (19) Christiansen, J. Dissertation, Risø-M-

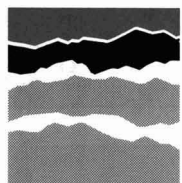
2851, Risø National Laboratory, Denmark, 1990.



Gunilla Asplund is a Ph.D. student in water and environmental studies at Linköping University. She will present a thesis on the natural production of halogenated organic compounds in the terrestrial environment within a year. Asplund holds a B.Sc. degree in biology and terrestrial ecology from Linköping University. Her research interests are in the origin and effects of organohalogens and environmental policy analysis.

Anders Grimvall is a professor of environmental sciences in the department of water and environmental studies at Linköping University. He holds a Ph.D. in probability and statistics from the University of Göteborg, Sweden. His research interests include organic pollutants in water, eutrophication of surface waters, and the statistical analysis of environmental monitoring data.

ENS



ENVIRONMENT NORTHERN SEAS

ENVIRONMENT NORTHERN SEAS CHALLENGES AND BUSINESS OPPORTUNITIES INTERNATIONAL CONFERENCE AND EXHIBITION STAVANGER, NORWAY 26-30 AUGUST 1991

ENS is being launched in August 1991 as a biennial international forum to stimulate innovation and implementation of appropriate technologies and management practices that can efficiently tackle the environmental problems of the northern seas.

The keynote speakers include Gro Harlem Brundtland, prime minister of Norway, and Stephan Schmidheiny, chairman, Business Council for Sustainable Development.

ENS includes six multidisciplinary seminars, with some 150 internationally recognised experts addressing the following major areas:

- emerging technologies in municipal waste water treatment
- measuring and monitoring technology
- aquaculture and agriculture
- clean-up of polluted industrial and mining sites
- offshore activities and shipping
- the ENS challenge for industry

Special workshop sessions will be held on:

- technology transfer and financial aspects
- environmental databases and information systems

The conference, seminars and workshops will be integrated with an exhibition, making ENS a marketplace for present and future environmental technology solutions.

Welcome as an exhibitor or a conference delegate.

International supporters include: • Eureka's Euromar programme • European Association of Metals (EUROMETAUX) • European Water Pollution Control Association (EWPCA) • Helsinki Commission, Baltic Marine Environment Protection Commission • International Chamber of Commerce (ICC) • International Maritime Organisation (IMO) • Nordic Environment Finance Corporation • Nordic Industry Forum • Nordic Investment Bank • The Oslo and Paris Commissions • United Nations Environment Programme (UNEP), industry & environment office • United Nations Industrial Development Organisation (UNIDO).

F I N A N C I A L S U P P O R T E R S

County of Rogaland • City of Stavanger • Den norske Bank • Elf Aquitaine Norge • Mobil Exploration Norway • Norsk Viftfabrikk • SR-Bank • Smedvig • Statoil • Uni Storebrand.

Please send me further details of the

ENVIRONMENT NORTHERN SEAS

Conference programme ☐

Exhibition ☐

(Please use block capitals.)

Name: (Family name, given name.)

Position/Title:

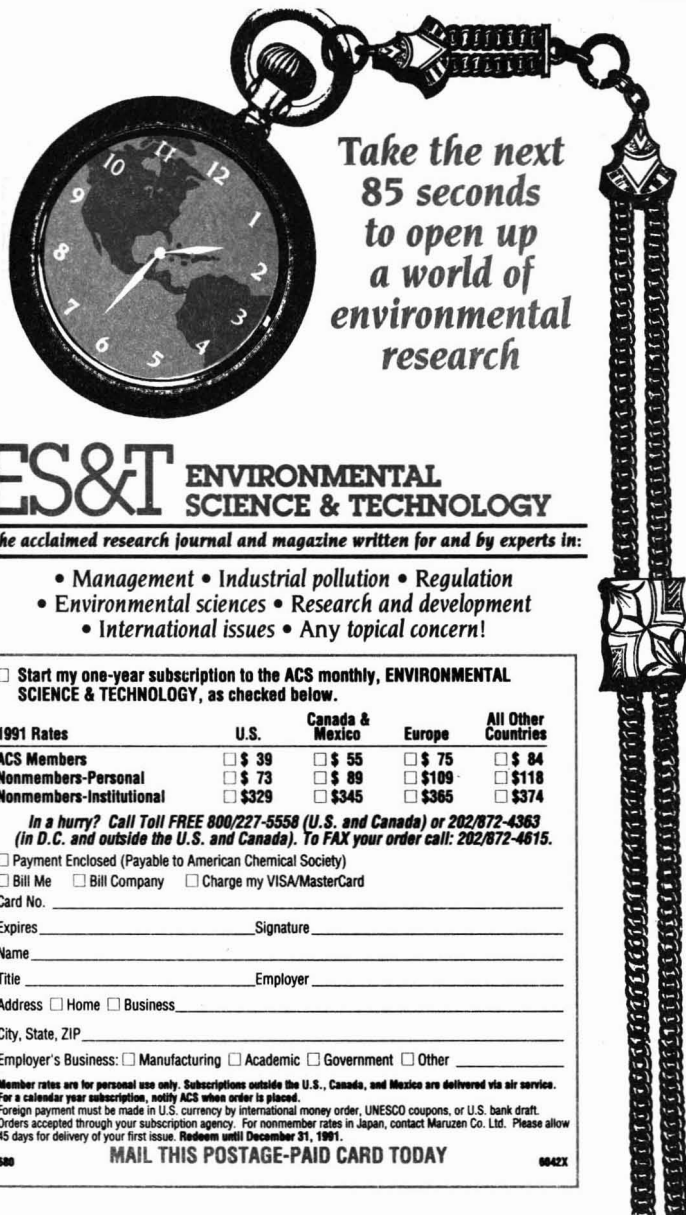
Company/Institution:

Company mailing address:

Tel:

Telefax:

Mail to:
ENS, P.O. Box 410
N-4001 Stavanger, Norway
Tel: +47 4 5581 00
Telex: 33 250 forum n
Telefax: +47 4 5510 15



Take the next
85 seconds
to open up
a world of
environmental
research

ES&T ENVIRONMENTAL SCIENCE & TECHNOLOGY

The acclaimed research journal and magazine written for and by experts in:

- Management • Industrial pollution • Regulation
- Environmental sciences • Research and development
- International issues • Any topical concern!

☐ Start my one-year subscription to the ACS monthly, ENVIRONMENTAL SCIENCE & TECHNOLOGY, as checked below.

1991 Rates	U.S.	Canada & Mexico	Europe	All Other Countries
ACS Members	<input type="checkbox"/> \$ 39	<input type="checkbox"/> \$ 55	<input type="checkbox"/> \$ 75	<input type="checkbox"/> \$ 84
Nonmembers-Personal	<input type="checkbox"/> \$ 73	<input type="checkbox"/> \$ 89	<input type="checkbox"/> \$109	<input type="checkbox"/> \$118
Nonmembers-Institutional	<input type="checkbox"/> \$329	<input type="checkbox"/> \$345	<input type="checkbox"/> \$365	<input type="checkbox"/> \$374

In a hurry? Call Toll FREE 800/227-5558 (U.S. and Canada) or 202/872-4363 (in D.C. and outside the U.S. and Canada). To FAX your order call: 202/872-4615.

☐ Payment Enclosed (Payable to American Chemical Society)

☐ Bill Me ☐ Bill Company ☐ Charge my VISA/MasterCard

Card No. _____

Expires _____ Signature _____

Name _____

Title _____ Employer _____

Address ☐ Home ☐ Business _____

City, State, ZIP _____

Employer's Business: ☐ Manufacturing ☐ Academic ☐ Government ☐ Other _____

Member rates are for personal use only. Subscriptions outside the U.S., Canada, and Mexico are delivered via air service.

For a calendar year subscription, notify ACS when order is placed.

Foreign payment must be made in U.S. currency by international money order, UNESCO coupons, or U.S. bank draft.

Orders accepted through your subscription agency. For nonmember rates in Japan, contact Maruzen Co. Ltd. Please allow 45 days for delivery of your first issue. Redeem until December 31, 1991.

MAIL THIS POSTAGE-PAID CARD TODAY

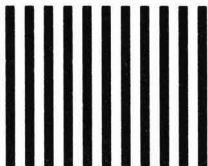
680 0042X



(800)227-5558 (U.S. and Canada)



NO POSTAGE
NECESSARY
IF MAILED
IN THE
UNITED STATES



BUSINESS REPLY MAIL

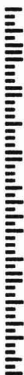
FIRST CLASS

PERMIT NO. 10094

WASHINGTON DC

POSTAGE WILL BE PAID BY THE ADDRESSEE

AMERICAN CHEMICAL SOCIETY
Marketing Communications Department
1155 Sixteenth Street, N.W.
Washington, D. C. 20077-5768





NEW RELEASES FROM THE ACS SYMPOSIUM SERIES

High-Tech Fibrous Materials Composites, Biomedical Materials, Protective Clothing, and Geotextiles

This 25 chapter volume explores the science and technology of high-tech fibrous materials in the areas of composites, biomedical devices, protective clothing, and geotextiles. Contributors from industry, academia, and government survey an array of new products that have unique, high performance features and discuss evolving concepts that could lead to new uses of high-tech fibrous materials.

Tyrone L. Vigo and Albin F. Turbak, Editors

ACS Symposium Series No. 457
408 pages (1991) Clothbound
ISBN 0-8412-1985-0 **\$84.95**

Biotechnology of Amylodextrin Oligosaccharides

International leaders in the field report on the basic biochemical aspects of biotechnology of amylopectin oligosaccharides, including introductions to genetic engineering, enzyme structure, and enzymology; application of specific, new analytical tools essential to characterizing these new types of materials; and specific fields of utility for these polysaccharide biopolymers.

Robert B. Friedman, Editor

ACS Symposium Series No. 458
348 pages (1991) Clothbound
ISBN 0-8412-1993-1 **\$84.95**

Pesticide Transformation Products

Fate and Significance in the Environment

Here is the first available resource on the fate, effects, and significance of pesticide transformation products, highlighting the awareness that pesticides are transformed to other chemicals that are often still biologically active. Covers pesticide degradation mechanisms and products, the fate of transformation products in the physical and biological environment, and the significance of transformation products in crop protection and environmental contamination.

L. Somasundaram and Joel R. Coats, Editors

ACS Symposium Series No. 459
320 pages (1991) Clothbound
ISBN 0-8412-1994-X **\$64.95**

Enzymes in Biomass Conversion

Offering recent worldwide developments, internationally known scientists report on enzymes that are potentially important to large-scale commercial biochemical processes, including fuel and chemical feedstock production, pulp and paper processing, waste degradation and processing, and food processing. Chapters cover basic knowledge of what enzymes are available, what their properties are, and how best to use them.

Gary F. Leatham and Michael E. Himmel, Editors

ACS Symposium Series No. 460
530 pages (1991) Clothbound
ISBN 0-8412-1995-8 **\$99.95**

Coal Science II

Developed in honor of the late Peter H. Given, this new volume presents a comprehensive review of fundamental research on the world's coals. The authors address the chemistry of coal, with specific emphasis on its geochemistry, macromolecular structure, and aspects of the organic reactions of coals. In addition, a variety of modern instrumental techniques are covered, including NMR, mass spectrometry, FTIR, electron microscopy, and gas chromatography.

Harold H. Schobert, Keith D. Bartle, and Leo J. Lynch, Editors

ACS Symposium Series No. 461
352 pages (1991) Clothbound
ISBN 0-8412-2005-0 **\$77.95**

Polymers as Rheology Modifiers

Here is the first publication devoted entirely to the use of polymers as additives to control fluid rheology. Presenting a strong mix of industrial and academic contributions, its 20 chapters cover rheological concepts, gels and latices, associating polymers, polymer-polymer and polymer-solvent interactions, and deformation-related orientations.

Donald N. Schulz and J. Edward Glass, Editors

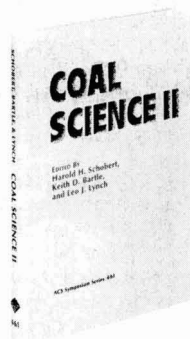
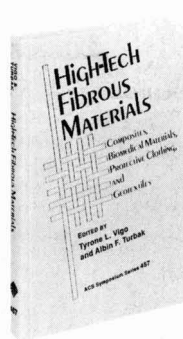
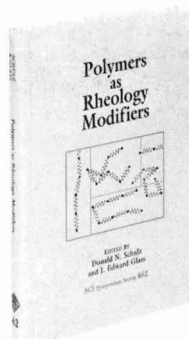
ACS Symposium Series No. 462
357 pages (1991) Clothbound
ISBN 0-8412-2009-3 **\$79.95**

Inositol Phosphates and Derivatives Synthesis, Biochemistry, and Therapeutic Potential

This new volume examines the synthesis, biochemistry, and pharmacological evaluation aspects of inositol phosphate research. Two overview chapters provide comprehensive background information on stereochemistry and nomenclature of inositol phosphates, basic biochemistry, synthetic challenges, and related pharmacology. Subsequent chapters describe novel methods of preparation, including the use of unusual starting materials and mediation by microorganisms, therapeutic potential and bioactivity, and structure-activity relationships.

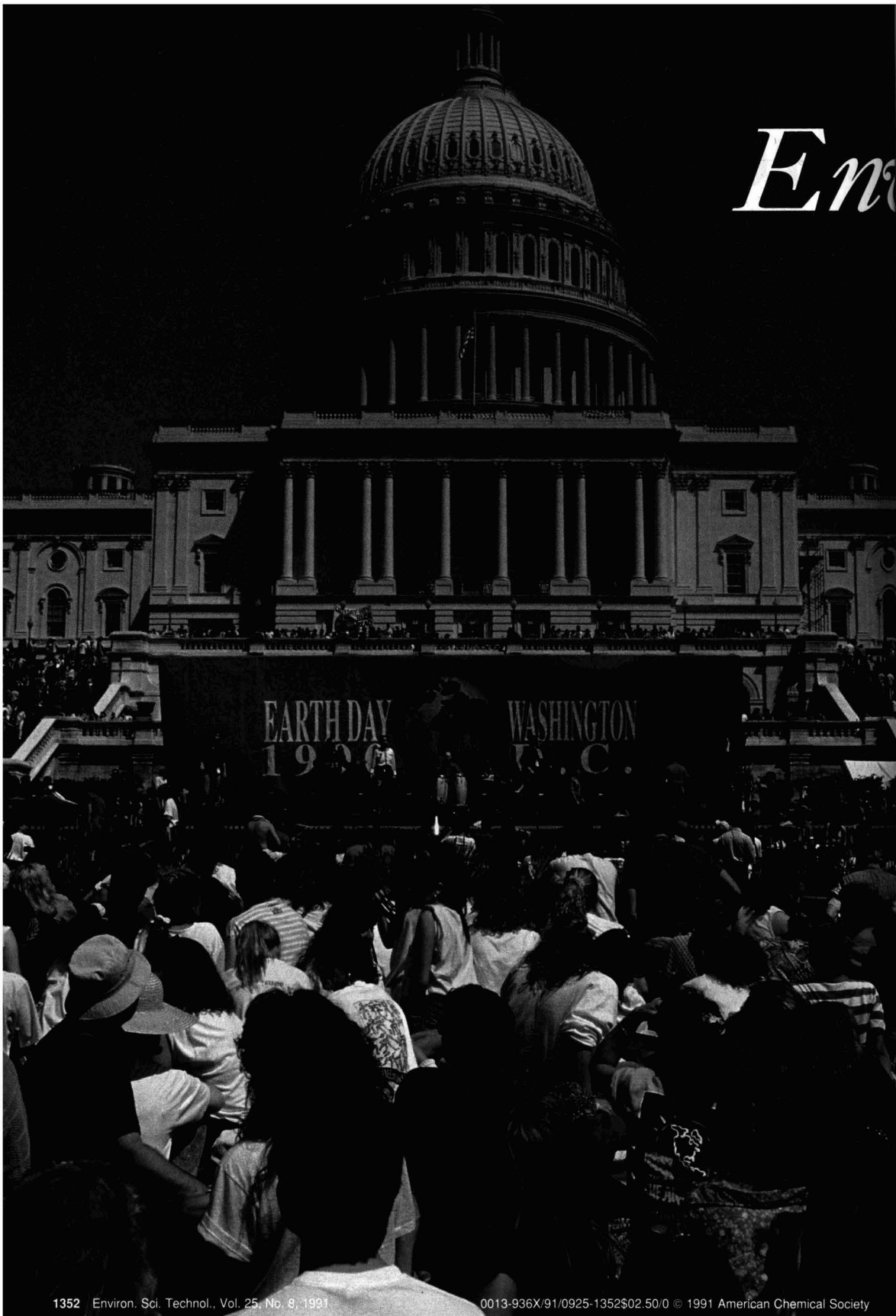
Allen B. Reitz, Editor

ACS Symposium Series No. 463
248 pages (1991) Clothbound
ISBN 0-8412-2086-7 **\$59.95**



Order from: American Chemical Society, Distribution Office, Dept. 10,
1155 Sixteenth St., N.W. Washington, DC 20036 or CALL TOLL FREE
800-227-5558 or in Washington DC (202) 872-4363 and use your
credit card!

En



Environmental Quality

Criteria *What type should we be developing?*

Peter M. Chapman
E.V.S. Consultants
195 Pemberton Avenue
North Vancouver, BC V7P 2R4
Canada

The development of environmental quality criteria is a major global industry; it occupies the time and pays the salaries of professionals in a variety of fields. Scientists provide the data to support or oppose these criteria; lawyers provide the framework for or argue against their promulgation; administrators try to make criteria work or seek loopholes; politicians favor them (or say they do); environmentalists alternately promote and denounce them; and members of the general public hope the criteria will protect the environment but not adversely affect their own jobs or lifestyles.

Is all this activity achieving its objective of improving environmental quality? Are we sure what that objective is? I believe that the answer to both questions is a clear "no." The purpose of this article is to explain this position, to suggest possible remedies, and to urge their immediate implementation.

Criteria vs. guidelines

With respect to environmental quality, the words "criteria" and its singular, "criterion," are inappropriate. A criterion is a narrowly and rigidly defined performance standard. The connotation of this definition in environmental science is that an exceedance of criteria will result in adverse effects such as ecological damage or health impairment. Although this rigidity, which provides a standard on which a de-

cision or judgment may be based, is useful in a court of law, it does not fit the real environment, which is naturally variable and difficult, if not impossible, to define by a series of numbers. For instance, we cannot precisely predict the local daily air temperature in our cities; instead, we use a range of values. This acceptance of reality, which has credence on the television weather forecast, does not seem to carry over into environmental science.

Aquatic toxicologists use laboratory toxicity tests to define ranges of tolerance of organisms to specific chemicals, mixtures of chemicals, or environmental matrices such as effluents, waters, and sediments. Government bodies then accept results of these tests as the basis of environmental quality criteria (in the United States, the EPA Water Quality Criteria; in Canada, the Canadian Council of Environment Ministers [CCEM] Water Quality Criteria). The concept is admirable, but its application is seriously flawed, and not just because such criteria are based on the most sensitive tests and measures with an additional safety factor included. Like weather information, toxicity tests provide only a range of values (1, 2). Thus using them to provide single, inflexible numbers is at best foolish and at worst capricious.

Reporting on the intralaboratory precision of saltwater short-term toxicity tests, Morrison et al. (3) noted: "Coefficients of variation . . . ranged from 1.8 to 46.4%. The precision obtained is comparable to other toxicity tests, but it is uncertain whether the precision of such tests in general is acceptable." The acceptability of such large but real

variation is discussed in greater detail later in this article.

In view of the reality that environmental analyses such as bioassays, chemistry, and community structure provide a range of values rather than a definitive single number, we should not be developing inflexible criteria. Rather, we should be developing *guidelines*. This is not a minor issue in semantics; it is a major issue in attitude and use of data. The term "guidelines," defined as broad performance standards that are applied on the basis of best professional judgment, describes a level of flexibility and a recognition of environmental realities that are not possible with the term "criteria."

The reasons for developing guidelines rather than criteria are best summarized by the following statement attributed to Aristotle: "It is the mark of an instructed mind to rest easy with the degree of precision which the nature of the subject permits and not to seek an exactness where only an approximation of the truth is possible." Clearly, there is a general need for "instructed minds" among professionals and nonprofessionals alike.

Endpoints

To an instructed mind, however, the correct words and attitudes are not sufficient unless we also are measuring the right endpoints. Moreover, we cannot think of endpoints solely in terms of measurements of human inputs and effects. This type of thinking is dangerous; it encourages assumptions that measurements are an end in themselves and that a change in any endpoint has environmental significance. If this change is relative to a

numerical criterion, we tend to give it great weight. Yet all too often such a number is inappropriate and should be replaced by a range of values that might well encompass that endpoint change.

For instance, in North America, discharge permits commonly require that a certain level of success be attained in bioassays (toxicity testing) of fish or other standard organisms. If success (e.g., survival) is less than a specified level, say 49% versus a specified 50%, then remedial action is required. Despite its incorrectness, this clearly arbitrary approach is acceptable even if it is based on a single number, provided that definitive decisions are not made on the basis of one test. Depending on the level of change observed, an appropriate response could include, in increasing level of severity: determining if the next scheduled test follows the same pattern, immediately running additional tests to confirm the results, and conducting further tests to determine the significance of these results. Unless the change approaches the catastrophic (e.g., 100% mortality in a test that previously showed 100% survival) and clearly reflects actual conditions tested, inappropriate responses would include immediately revoking the permit, levying fines, taking legal action, or calling a press conference.

Measurements of endpoints are only a means to the end of assessing, maintaining, and enhancing ecosystem health. As such, endpoints may include measures of that health, of anthropogenic effects, and of "natural" effects. Ecosystem function is the trajectory that gets us to the target of ecosystem health. Endpoints provide measurements that allow us to determine that trajectory; multiple, *never* single, endpoints also may comprise the target.

Clearly, endpoints need to be effects-based because if there is no effect, there is no problem. In this regard, measures of bioaccumulation may be desirable endpoints to protect *human* health, but not necessarily to protect *ecosystem* health. A certain few contaminants, such as mercury, DDT, and PCBs, are of concern because they can biomagnify up the food chain. Hence, measurements of these compounds in tissues of organisms that are eaten by other organisms, including humans, are important. Similarly, the measurement of contaminants such as arsenic in hair and fingernails of humans provides an indication of

direct exposure to a toxicant with known adverse effects. But bioaccumulation per se is a phenomenon, not an effect, for a variety of reasons. For instance, some contaminants such as polycyclic aromatic hydrocarbons must be metabolized to have an effect, and not all organisms can metabolize all compounds. Also, exposure to low levels of contaminants resulting in relatively high tissue levels of contaminants may not have an effect because of gradual acclimation, whereas exposure to high levels of contaminants may have an effect even though contaminants reach only relatively low levels in tissues.

In addition, the definition of endpoints ideally should be based on what we, as human beings, want to protect. There is nothing wrong with using surrogates, including "laboratory white rats," as indicators. For instance, in the field of aquatic toxicity testing, rainbow trout and waterfleas (*Daphnia*, *Ceriodaphnia*) typically fill this role for evaluating the acute endpoints of survival and partial lifecycle testing, respectively. But data on responses of particular species are not necessarily, or always likely to be, applicable to different species, even within the same genus (4). Thus data from these standardized species do not predict the responses of all other species. Moreover, the greater the taxonomic difference, the greater the possible difference in response. If, for example, we are concerned with salmon populations in rivers, we should be conducting tests and assessments with salmon, not with surrogates.

We need to be clear why we are conducting particular tests and using particular organisms in these tests. Surrogates are useful for a variety of purposes, including characterizing relative effects in an area or a discharge plume, deciding on a mode of action, and comparing responses. Surrogates are not useful for absolute determinations of ecosystem health. In fact, they can be misleading if they are used for this purpose. Toxicity tests provide a range of responses. Arguably, this range encompasses a twofold difference under even optimum conditions with standardized, well-established tests on the same species and measurement of short-term lethality. For example, when 10% of fish tested in a bioassay with a particular effluent die in the first test and 20% die in the next test, these results are within the range of varia-

tion of the test itself, irrespective of any effluent toxicity. Moreover, different species will show even more different responses to the same chemical.

Recommended measures or endpoints of ecosystem health

Chapman (5) recommends that measures or endpoints of ecosystem health include the following:

- the presence, absence, or condition of multiple species, but *never* a single, or large number of species;
- persistence of habitat; and
- continuance of normal succession as we know it; change is a normal part of community and ecosystem development.

Ecosystem health

That ecosystem health is the objective of environmental quality guidelines is neither controversial nor arguable. "Ecosystem health," however, is a relative concept established by the user and not subject to an absolute definition (5, 6).

Some definitions of terms, however, are required, if only to determine endpoints. Kelly and Harwell (7) state: "... an ecosystem can be perceived and defined only in an operational context." According to this description, appropriate endpoints would be measures of change in selected indicators relative to a baseline condition, provided that an acceptable and realistic baseline condition can be defined. The International Union for the Conservation of Nature, the United Nations Environment Programme, and the World Wildlife Fund (8) define a healthy ecosystem as one having a high level of biodiversity, productivity, and habitability, which lead naturally to the endpoints of diversity, productivity, and habitat preservation. Although he does not define ecosystem health, Rapport (6) defines *symptoms* of ecosystem breakdown (ecosystem "unhealth") as reduced primary productivity, loss of nutrients, loss of sensitive species, increased instability of component parts and populations, increased disease prevalence, changes in biotic size-spectrum to favor smaller life forms, and increased circulation of contaminants. These symptoms all form possible measurement endpoints for assessing ecosystem health.

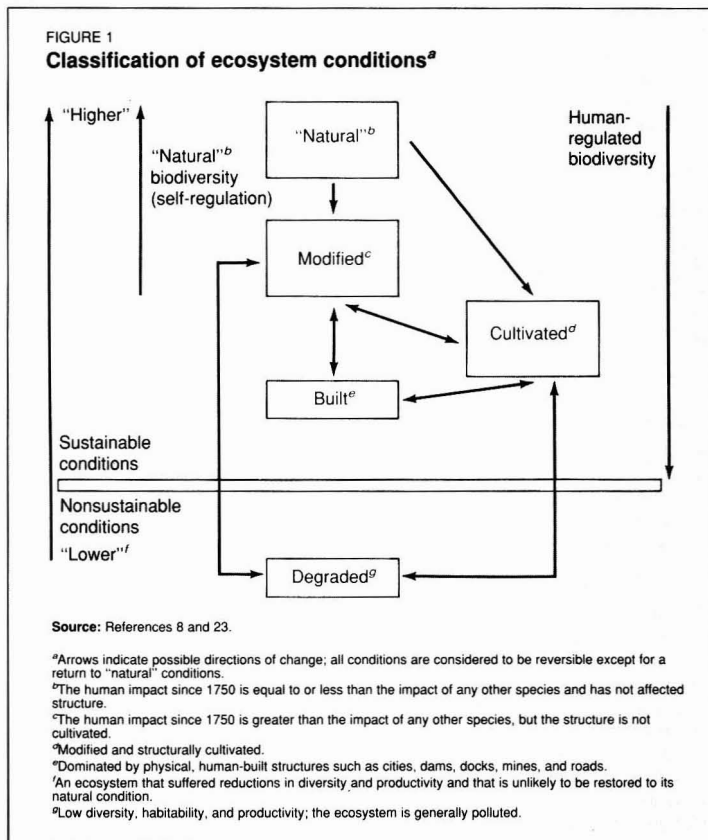
Potential changes to ecosystems and communities are illustrated in

Figure 1. Increasing human regulation of biodiversity is, in itself, neither good nor bad despite a tendency among many members of the public to view "natural" as good and desirable and anthropogenic as bad and undesirable. Natural conditions that are not modified to some extent by human beings and their activity are not common. It is noteworthy but not necessarily alarming that the only nonreversible changes shown in Figure 1 are a return to natural conditions after modification or cultivation; remedial action after a disturbance results in a new state, not a return to predisturbance conditions. This new state comes into existence not only because of the application of science and technology, but also because of social needs and wants, political considerations, available monies, and available scientific and technological expertise.

Particular endpoints used to measure ecosystem health also are subject to scientific and nonscientific modifying factors. These affect the choice of endpoints and the determination of scale for chosen endpoints. For example, the level of acceptable increase in circulation of contaminants is a function of what is measurable (such as laboratory detection limits) and what society finds acceptable. Societal levels of acceptability often are at odds with scientific acceptability. For instance, dioxins are of such general public concern that environmental groups such as Greenpeace have declared: "... the only acceptable standard for dioxin is zero" (9). This goal is unrealistic and unattainable for many reasons, not the least of which is that dioxins also are produced from nonanthropogenic sources such as forest fires. Statements calling for zero levels of chemicals that show a dose-response relationship ignore Paracelsus' (1493-1541) proven statement: "All substances are poisons; there is none which is not a poison. The right dose differentiates a poison and a remedy" (10). Further, nonanthropogenic as well as anthropogenic compounds cause effects such as mutagenicity (11), which many members of the public appear to consider "unnatural."

Reality vs. perception

In describing EPA's list of environmental concerns, Roberts (12) has aptly shown the difference between reality, as determined by the current state of knowledge, and per-



ception, as determined by the current state of anxiety. Roberts does not assign priorities to these concerns, but in terms of degree of ecological risk Roberts' list includes global climate change, ozone depletion, habitat alteration, species extinction, and loss of biodiversity.

EPA's list of concerns related to human health includes outdoor and indoor air pollution (smog, toxic chemicals), radon, drinking water contamination, occupational chemical exposures, pesticide application, and ozone depletion. In contrast, four of the public's seven highest ranked environmental concerns do not appear on EPA's list: active hazardous waste sites (#1), abandoned hazardous waste sites (#2), oil spills (#5), and nuclear power accidents (#7). Maksylewich provides a more detailed comparison (13).

EPA's Science Advisory Board (SAB) (14) recently noted that the U.S. Congress pays the most attention to environmental problems believed by the general public to pose the greatest risks and that EPA follows the will of Congress. Accord-

ing to the SAB, relatively high-risk environmental problems include habitat alteration and destruction, species extinction and loss of diversity, stratospheric ozone depletion, and global climate change. Environmental problems that greatly concern the general public are regarded by the SAB as generally low risk. These include oil spills, groundwater contamination, and radionuclides (14).

Clearly, those with the least knowledge of the subject control the focus of environmental legislation and funding. This situation is illustrated in Figure 2 as an inverse pyramid, in which perception has more importance than reality. Possible solutions are suggested later in this article.

Kimbrough (15) notes: "In spite of our best intentions, public pressure and lack of adequate coordination can lead to attention and resources being devoted to minor problems while important issues are left unattended." An excellent example of this is EPA's National Priorities List (NPL) for hazardous waste sites. Many if not most of the NPL sites

pose relatively little or no risk to human health or the environment, yet they are remediated. It is likely that sites that do pose high risks (e.g., highly contaminated sites in poor rural areas) are not on the list and hence are not being remediated (16).

A line between good and bad?

The question of whether there is a sharp demarcation between good and bad ethical behavior, in the context of human activities, will elicit different answers from different people. Members of a self-righteous minority, who consider themselves to be "totally honest," probably would answer, "yes." Most people, however, probably would answer "no" and, if asked to explain, would say that there is a "gray zone" between good and bad where subjective judgment applies.

A similar situation exists in the field of environmental protection. Although criteria are promulgated on the basis of a line between good (acceptable) and bad (unacceptable) conditions, a sharply definable distinction exists only in legislation. The reality is illustrated in Figure 3. Uncertainty is high unless we choose to be either over- or under-protective. Although it is uncertain whether industrialists would really choose the latter, regulators *will* choose the former. Current regulatory philosophy involves use of the most sensitive measures, "worst case" laboratory tests, and "most sensitive" species. The intent is to ensure that change does not occur and that the question, "How clean is clean?" is answered by "totally clean." Unfortunately, an approach that tries to avoid change does not recognize the following:

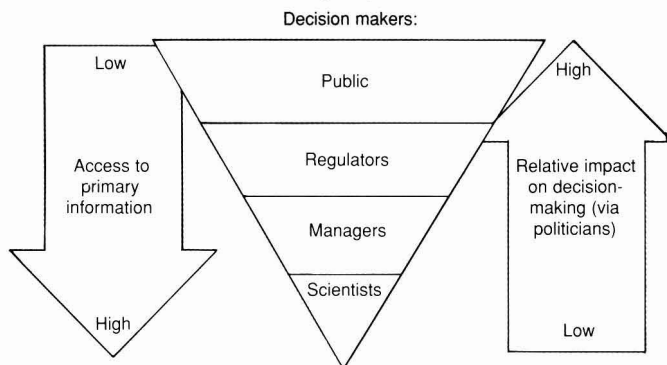
- Contamination (the presence of a chemical or substance) does not necessarily result in pollution (an adverse environmental effect related to contamination).
- Change occurs in nature; biological evolution is a clear example of change. "Natural pollution," such as that caused by volcanic action and forest fires, can also result in change—possibly even evolutionary change. In any case, humans have no control over either of these categories of change.

Prediction vs. reaction

Clearly, it is best to develop methods that allow prediction of environmental problems before they become acute and when they are most reversible. Determinations of effects

FIGURE 2

Current societal decision-making emphasis^a



Source: Reference 5.

^aThis inverse pyramid is highly unstable; an upright pyramid would be highly stable.

based on widespread deaths or diseases in a local population, such as massive fish kills or birth defects in seals, come too late; if we could predict that these events would occur by measuring some enzyme system, for example, perhaps we could act before rather than after the fact.

Although the philosophy of prediction rather than reaction is laudable, it can become dangerous if it is embraced wholly and without question, which is what generally happens when science becomes regulation. Specifically, the more sensitive our early warning systems are, the more likely they will be triggered by non-events such as false positives. An example of such "crying wolf" appears to be the use of animals to test possible carcinogens; a surprisingly large number of false positives may arise from the way the tests are done (11, 17, 18).

Prediction is generally attempted using reductionist or bottom-up approaches, which are based on simplistic laboratory data. Although these can be diagnostic and predictive, they do not describe the real world. At the other extreme are holistic or top-down approaches, based on field data. Holistic approaches describe the real world by evaluating impacts directly, but they are not diagnostic or predictive. As illustrated in Figure 4, reductionist approaches (e.g., the biomarkers concept currently gaining widespread scientific interest) embody the most reversible measures, whereas holistic measures embody the least reversible. However, because ecosystem stability arises from resilience and resistance,

thereby implying that conditions are dynamic rather than static, both measures are needed to assess and maintain ecosystem health adequately. Reductionist and holistic measures are also needed to define environmental problems because we do not have a clear demarcation between "good" and "bad."

What do we want to protect?

We are losing sight of what we want to protect. As human beings we find it easier and much more comfortable to look at a small part of the environment and try to fit it into our artificial schemes (reductionist thinking) than to try to take in the whole picture and adapt our thinking to that reality (holistic thinking).

We have grown used to changing our environment to suit ourselves. This always seemed to work in the past and did not appear to require the consideration of long-term implications. Now that we are more enlightened and want to stop damage, most of it caused by ourselves, we have trouble with long-term implications. More importantly, we have trouble grasping the differences between visually apparent problems that have only short-term, localized implications (e.g., oil spills) and complex problems that have incredibly long-term, global implications (e.g., climate change).

The first step in halting changes that we do not want involves defining the uses to which we as human beings wish to put our environment for our benefit. By defining these, we also define what we want to persist through time. Potential benefits range from the strictly utilitarian to

the aesthetic—from those ecosystem components that provide sustenance to the body to those that are essentially useless for physical needs but that are aesthetically pleasing, such as flowers, or that may be useful in medicine. (It is argued, for instance, that preserving the maximum biodiversity will make possible discoveries in medicine or other fields that will ultimately benefit human beings.) In any case, such benefits, once defined, become endpoints for the evaluation of ecosystem health.

Once these endpoints are defined, we need to structure research, monitoring, regulations, and management accordingly. Further, we want to follow Aristotle's dictum and have "instructed minds." For example, as noted previously, aquatic toxicity tests have a low level of precision because coefficients of variation can approach 50%. Morrison et al. (3) acknowledge this, but then state: "... if variability [for toxicity tests is] in the same range of variability associated with chemical analyses, then, since precision of analytical procedures is generally considered acceptable, precision of toxicological methods must likewise be judged acceptable."

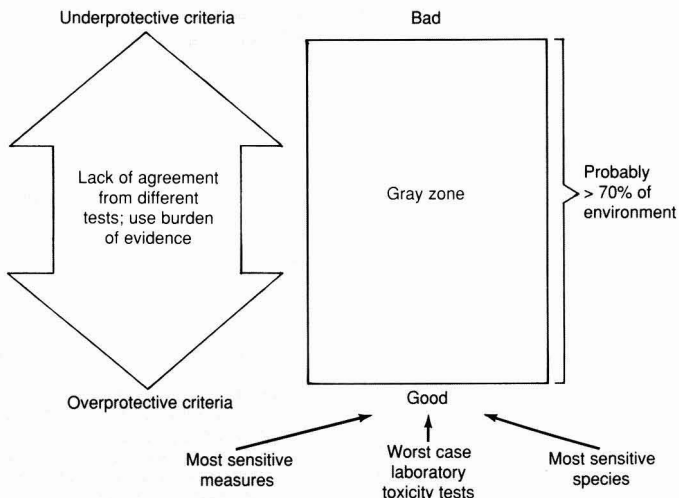
This statement, which, incidentally, is not unique to Morrison et al. (3), is surprising and alarming. In my opinion, it is useful logic only if one agrees with the common position reiterated, but not supported, by Kimbrough (1990): "... that precision and accuracy in chemical analysis are of minor importance because the uncertainties in a risk assessment are usually several orders of magnitude. Thus imprecise and inaccurate chemical analytical data do not have much of an impact" (15).

Kimbrough (15) points out the fallacy of this position: "... because of the action/no action significance attached to numerical standards [such as maximum concentration limits], 'minor' inaccuracies are very important and very costly in practice."

Moreover, numerical criteria tend to be generic. And, although generic criteria may be appealing in theory, all-encompassing numerical limits may be just as ephemeral in practice as the Saprobien concept of indicator species, which European aquatic scientists once looked upon as the ultimate measure of environmental conditions. For instance, Parkerton et al. (19) are correct: "Natural criteria used in formulating enforceable

FIGURE 3

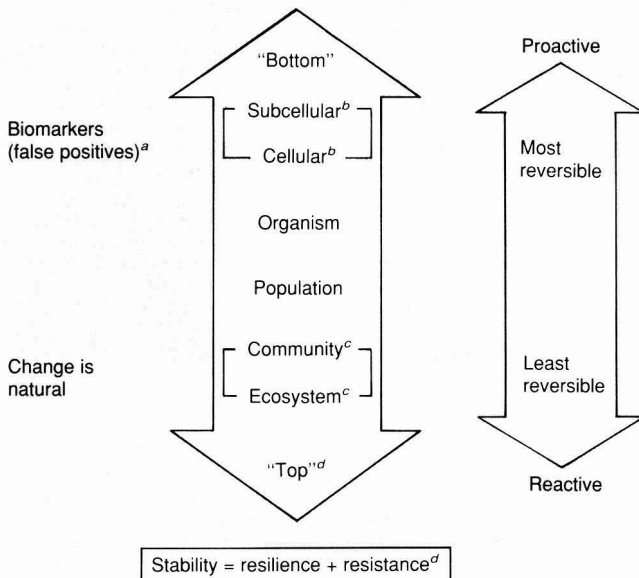
Distinguishing "good" from "bad" environmental conditions^a



^aThe distinction is unclear. Use of "good" conditions to set environmental regulations will be overprotective, whereas use of "bad" conditions will be underprotective. Realistically, one should take into account the inevitability of a certain level of anthropogenic input related to the industrialization necessary for the present level of human civilization. That level normally is determined by human needs and wants.

FIGURE 4

Levels of biological organization



^aFalse positives denotes an effect that is incorrectly detected.

^bBiomarkers at the subcellular and cellular levels would be ideal for environmental protection because they can give an early warning of adverse effects.

^cCommunity and ecosystem are grouped together because these two levels of ecological organization are not readily separable (5).

^dStability at the "top" organization level is defined as resilience and resistance; nevertheless, a wide range of variability is not inconsistent with stability.

water quality standards may be inappropriate when applied generically to all receiving systems due to site-specific interactions that may alter bioavailability."

Numbers do not ensure quality

Developing effective environmental quality guidelines, which allow for both definition of present problems and early warning of potential problems, is not easy. What is easy is developing numerical criteria that do not work and that, even more distressingly, become ends rather than means to improve environmental health. We are deluding ourselves if we think that attaining and maintaining numerical goals will ensure environmental quality. As stated by the EPA's Science Advisory Board (14): "... subjective values always will—and should—influence the ranking of relative environmental risks, no matter how sophisticated the technical and analytical tools become." In this regard, a flexible framework (guidelines) is much more usable than a rigid structure (criteria).

Attaining a clean environment will not be cheap; it has been projected that the cost of complying with environmental regulations will reduce the United States' gross national product by 2.59% over the long term and that by the year 2000, federal, state, and local governments in the United States will be spending \$61 billion annually for environmental protection (22). Accordingly, we clearly need to stop spending "... vast sums of money ... to reduce the levels of chemicals in the environment to levels that cannot be adequately measured and that professional judgment would regard as presenting an acceptable risk" (15).

Guidelines that work must be based on a definition of those uses of the environment that we want to protect, which inevitably leads us to specific, rational endpoints for measurement and assessment. We must structure research, monitoring, regulations, and management so that a "level playing field" exists for human beings and for the environment. Within human society, this "level playing field" must exist for the industrial base that provides the things we require for acceptable human living standards as well as for the environment in which we choose to live.

Ultimately it is a matter of choices. We make choices whether or not we make conscious deci-

Safeguarding environmental quality—Some recommendations

We need to avoid "criteria" and to develop methods and measures that work. Following are several generic and specific recommendations:

Generic

- Avoid using "criterion" and "criteria"; instead, use "guideline" and "guidelines."
- Develop a framework, not a number, to determine environmental quality (health) and avoid the action/no action alternative, which usually is presented as the only choice. This is not to imply that we should never take action, but rather that simplistic yes/no answers and decisions do not commonly fit the complicated reality of the global environment.
- Obtain broad-scale consensus from scientists, managers, lawyers, politicians, and the general public on a strategy or rationale for synthesizing and interpreting information. This would apply to toxicological, bioaccumulation, and other data related to environmental quality.
- Recognize that human existence implies environmental alteration but does not necessarily imply or require destruction; in other words, we change our current *mea culpa* outlook and accept that we are part of the environment, and neither gods nor devils.
- Ensure that we always make "biological sense" by emphasizing high-priority issues such as global climate change and stratospheric ozone reduction and stop wasting precious time, resources, and talent on low-priority issues such as oil spills and "trendy" chemicals.

Specific

- Ensure that the endpoints we are measuring in our tests and monitoring in the environment are as close as possible to what we want to protect and are useful measures of ecosystem health. One of

the major uncertainties in risk assessments arises from extrapolation from measured endpoints to what is to be protected. Measurement endpoints and assessment endpoints should be the same.

- At the level of the individual organism, standardize and, where necessary, develop measures of survival, growth, and reproduction. The latter two measures integrate energetic processes; if an organism can complete all three activities, and a population is at least maintaining its size, the organism is considered healthy. These measures should be applied to key species we want to protect; use of surrogates should be avoided wherever possible.
- Determine community and ecosystem level-specific measures of health; i.e., endpoints for communities and ecosystems we want to protect. These should be based on structure and function and involve generic and specific elements (20). For example, for macrophytes, Painter (21) defines healthy communities as those that have three generic characteristics that could apply to most other communities—diversity, maximized productivity, and complex habitat—and one specific characteristic, a good mix of cover (i.e., coverage of substrate with concomitant exposure to light).
- Determine the appropriateness of current procedures, including different endpoints of different toxicity tests, selected chemical contaminants ("trendy" or "convenient" versus those that pose real threats), selected measures of community structure, and other potential measures of in situ biological alteration.

sions. Informed, rational choices are essential for defining and maintaining the environmental milieu in which we and our descendants will live. We need to return to common sense and basics (i.e., a recognition of complexity rather than further efforts to oversimplify) in order to avoid the increasing use of bad science as a basis for regulation and management. The responsibility is ours; we may not be the best equipped or informed to make the necessary choices and we will undoubtedly make many mistakes, some of them serious, but we must choose what we want and work to

attain this. If we do so, then I am convinced that we will persist and prosper. Can any biological organism ask more than that?

Acknowledgments

This paper was written for my daughter, Jennifer (born May 13, 1990), following a request of Dr. Steve Klaine for a presentation given at the 11th Annual Meeting of the Society for Environmental Toxicology and Chemistry, November 11–15, 1990, Washington, D.C. Although the responsibility for the views expressed is mine alone, useful comments and discussion were provided by Elizabeth Power, Allen Burton, Ilona Kerner, Jennifer Shay, and three anonymous referees.

References

- (1) Munkittrick, K. R.; Chapman, P. M. Presented at the Tenth Annual Meeting of the Society for Environmental Toxicology and Chemistry, Toronto, Canada, November 1989.
- (2) Kovacs, T. G.; Ferguson, S. M. *Environ. Toxicol. Chem.* **1990**, 9, 1081-93.
- (3) Morrison, G. et al. *Res. J. Water Pollut. Control Fed.* **1989**, 61, 1707-10.
- (4) Chapman, P. M.; Farrell, M. A.; Brinkhurst, R. O. *Aquat. Toxicol.* **1982**, 2, 47-67.
- (5) Chapman, P. M. *Journal of Aquatic Ecosystem Health*, in press.
- (6) Rapport, D. J. *Perspect. Biol. Med.* **1989**, 33, 120-32.
- (7) Kelly, J. R.; Harwell, M. A. In *Ecotoxicology: Problems and Approaches*; Levin, A. et al., Eds.; Springer-Verlag: New York, 1988, pp. 9-35.
- (8) IUCN/UNEP/WWF. "Caring for the World: A Strategy for Sustainability"; International Union for the Conservation of Nature; United Nations Environment Programme; World Wildlife Fund: Washington, DC, June 1990, 2nd draft.
- (9) Gladwell, M. In *The Washington Post*, final edition: Washington, DC; May 31, 1990, p. A3.
- (10) In *Toxicology: The Basic Science of Poisons*; Casarett, L. J.; Doull, J., Eds.; MacMillan: New York, 1975, frontispiece.
- (11) Ames, B. N.; Gold, L. S. *Science* **1990**, 249, 970-71.
- (12) Roberts, L. *Science* **1990**, 249, 616-18.
- (13) Maksylewich, W. In *Proceedings of the 17th Annual Aquatic Toxicity Workshop*; Chapman, P. M. et al., Eds.; Canadian Technical Report, Fisheries and Marine Sciences, No. 1774: Ottawa, 1991, pp. 596-609.
- (14) EPA Science Advisory Board. "Reducing Risk: Setting Priorities and Strategies for Environmental Protection"; SAB-EC-90-021; U.S. Environmental Protection Agency, Science Advisory Board: Washington, DC, 1990, pp. 1-26.
- (15) Kimbrough, R. D. *Environ. Sci. Technol.* **1990**, 24, 1442-45.
- (16) Doty, C. B.; Travis, C. C. *Environ. Sci. Technol.* **1990**, 24, 1778-80.
- (17) Ames, B. N.; Magaw, R.; Gold, L. S. *Science* **1987**, 236, 271-80.
- (18) Marx, J. *Science* **1990**, 250, 743-45.
- (19) Parkerton, T. F. et al. *Res. J. Water Pollut. Control Fed.* **1989**, 61, 1636-44.
- (20) Harris, H. J. et al. *Environ. Sci. Technol.* **1990**, 24, 598-603.
- (21) Painter, S. *Journal of Aquatic Ecosystem Health*, in press.

- (22) Nichols, A. B. *Water Environ. Technol.* **1990**, Nov., 47-53.
- (23) Vitousek, P. M. et al. *BioScience* **1986**, 36, 368-73.



Peter M. Chapman is a senior partner of E.V.S. Consultants. He holds a Ph.D. in aquatic ecology from the University of Victoria, Canada. His primary research interests are aquatic ecology and toxicology. He has published more than 80 refereed journal papers, book chapters, technical reports, and proceedings, and he serves on a number of professional committees, councils, and boards, including the Canadian Environmental Advisory Council and EPA's Science Advisory Board.

JOURNAL OF CHEMICAL AND ENGINEERING

DATA

Get a World of Precise, Accurate Data.

Don't miss a single issue.
Subscribe to JCED today!

Multidisciplinary in nature and international in scope, **Journal of Chemical and Engineering Data** features contributions by distinguished scientists from the world over. Their expert reports represent numerical data bases for private technical information systems, particularly in industry, that will broaden your scientific horizons and improve the quality of your work.

This quarterly journal publishes precise, accurate data on physical, thermodynamic, and transport properties of well-defined material. It also keeps you informed about the latest international standards on symbols, terminology, and units of measurement for reporting data properly.

EDITOR: Kenneth N. Marsh, *Texas A&M University*

Volume 36 (1991)	ACS Members		Nonmembers
4 issues per year	1 year	2 years	1 year
U.S.	\$32	\$57	\$234
Canada & Mexico	\$37	\$67	\$239
Europe*	\$41	\$75	\$243
All Other Countries*	\$41	\$75	\$243

*Air service included.

For more information or to subscribe, contact:

American Chemical Society, Marketing Communications Department, 1155 Sixteenth Street N.W., Washington, D.C. 20036

In a hurry?

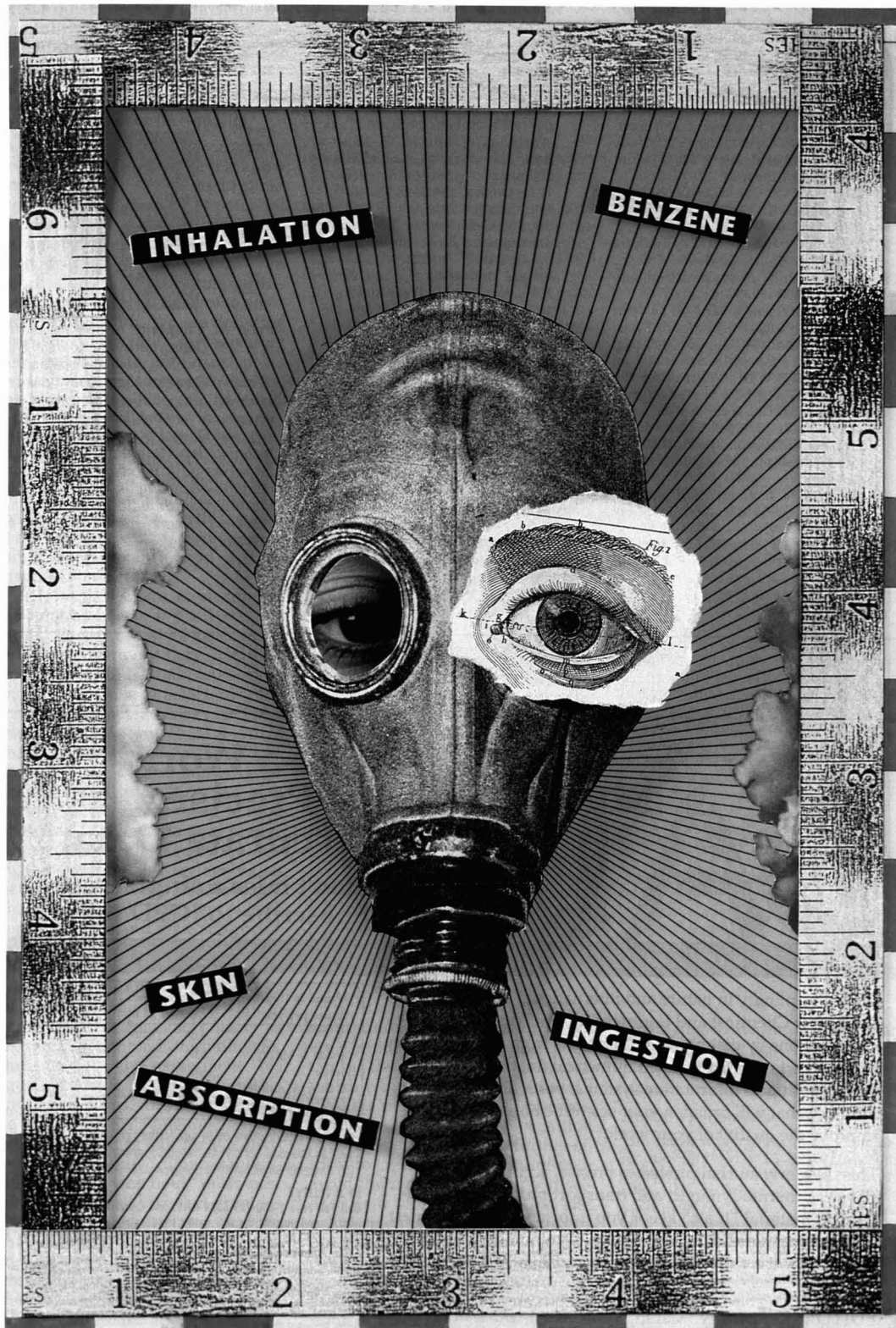
Call Toll Free 1-800-227-5558 (U.S. and Canada)

In D.C. and outside the U.S. and Canada: call (202) 872-4363

Fax: (202) 872-4615; Telex: 440159 ACSPIU or 892582 ACSPIUS

Cable Address: JEICHEM

Member subscription rates are for personal use only. Subscriptions are based on a calendar year. Foreign payment must be made in U.S. currency, by international money order, UNESCO coupons, or U.S. bank draft, or order through your subscription agency. For nonmember rates in Japan, contact Maruzen Co., Ltd. This publication is available on microfilm, microfiche, and the full text is available online through CJO on STN International.



ASSESSING HUMAN EXPOSURE TO AIRBORNE POLLUTANTS

Advances and opportunities

Protecting the general public and sensitive subgroups from the harmful effects of air pollution has proved a difficult task for all levels of government and the regulated community. Passage of the recent Clean Air Act amendments provides new options and responsibilities, but improved scientific techniques need to be employed to better understand and to properly reduce the risks from exposure to unhealthy air. Major outdoor air concerns are photochemical smog, acid aerosols, and air toxics.

A committee I chaired, which was convened by the National Research Council, recently completed an analysis of new methods and technologies for assessing exposure to air pollutants. It included members with expertise in chemistry, mathematical modeling, engineering, physics, air pollution, exposure assessment, medicine, biology, social science, statistics, and environmental policy. The study was sponsored by the Agency for Toxic Substances and Disease Registry of the U.S. Public Health Service.

We realized that the issues associated with human exposure are complex and require a framework for assessing and analyzing total personal exposure of an individual to contaminants. The framework should allow consideration of all the principal ways in which individuals

By Paul J. Liroy

could come into contact with such pollutants. We felt that operating within this framework would help set priorities for reducing risk from actual exposures or provide accurate estimates of exposure to enable management to make decisions about control of potentially harmful pollutants.

Exposure to airborne pollutants is only part of a person's total exposure to a specific pollutant, which includes any inhalation, ingestion, or skin absorption of the pollutant from air, water, food, or soil. Thus, exposure assessments for airborne constituents must take into account the potential contributions from other media, and all routes of exposure must be at least preliminarily assessed for the relative magnitude of their contributions. Such an approach is necessary to define the exposures of concern, to effectively assess risk and make management decisions, to complete environmental epidemiological investigations, and to improve disease diagnosis and intervention.

Even if air is the only route of contact considered, we believe an exposure assessment should account for the locations that might lead to contact with high concentrations of the pollutant studied. It was with this understanding of total human exposure that the committee limited its study to air contaminant exposures.

The carcinogen benzene is an example of how application of a proper exposure assessment might lead to more effective strategies to reduce the health risk from common

airborne chemicals. The Clean Air Act provided the basis for EPA in 1989 to establish regulations for industrial emission of benzene into outdoor air. However, as the Act applies only to outdoor air, no other sources of benzene exposure are included in the subsequent regulation—even though household products, automobile exhaust, and paint may be sources of more than 80% of national benzene exposure. Prioritization of the significance of benzene exposures will help regulators select mitigation measures for outdoor air sources and will truly assist in reducing a population's exposure to benzene. Indoor sources, including tobacco smoke and evaporation from gasoline stored in attached garages, currently require other approaches (e.g., education and product replacement).

The committee identified three major ways of determining human exposure to airborne pollutants. Monitoring the air around an individual with a portable personal air sampler is, of course, the most comprehensive and most accurate. It is also the costliest and most time consuming.

The second method is more indirect and involves techniques such as measuring the amount of a contaminant with a stationary monitor and extrapolating exposure by means of personal activity records or mathematical models. Exposure to carbon monoxide inside a car, for example, might be roughly calculated from the amount of time spent in the car and the quantity of carbon monoxide in the car under typical operating conditions.

The third method involves bio-

Précis articles are reports of meetings of unusual significance, international or national developments of environmental importance, significant public policy developments, and related items.

logical markers as a measure of the integrated dose within the body and of past contact with pollutants. For example, a marker for airborne lead exposure can be elevated lead levels in the blood. However, this must be weighed against contributions from other media. Other biological markers have been developed or are being studied that can detect cellular level changes in the body long before they produce health effects; however, most require validation.

To properly apply these techniques, the committee recommended that researchers use consistent definitions of exposure. The report calls for the scientific and regulatory communities, including journal editors and reviewers of scientific articles, to adhere to standard terms. The committee recommended a set of definitions and defined exposure as contact at a boundary between a human and the environment at a specific environmental contaminant concentration for a specified interval of time. The time interval should, of necessity, be relevant to the biological effect of concern.

Many advances in exposure assessment methods and technology have occurred in recent years. New personal air sampling equipment,

in particular, has been under-used, especially to provide data to support regulatory decision making.

Improved personal air monitors are needed for many potentially harmful contaminants, including certain metals, and various organic chemicals, such as semivolatile compounds and radon and its progeny. Better fixed-site monitors also are needed for many contaminants. Improved instruments—gas chromatographs, mass spectrometers, and electrochemical sensors—should be developed for measuring the concentrations of pollutants in collected air samples. Miniaturization of many instruments is essential if we are concerned with an individual rather than an outdoor site.

Analytical techniques with improved specificity and sensitivity for biological markers are needed, especially ways to test for several markers at the same time and to interrelate measurements of the significant routes of exposure. Researchers who study airborne pollutants should adhere to sound statistical methodology in collecting personal activity data. Basic statistical principles often are ignored in questionnaires and surveys used by exposure analysts.

In order to develop useful models for exposure assessment, researchers also must develop a better understanding of pollutant dynamics. Such fundamental parameters as how, where, when, and at what strength pollutants are dispersed often are lacking. Moreover, many of the methods currently in use for estimating exposure to airborne pollutants have never been verified using independent field measurements. Research should be undertaken to validate these methods.

Using advanced measurement techniques in exposure studies does not in itself ensure better data. Quality assurance programs are critical components of exposure studies; researchers should expect to spend at least 15% of the total study budget on making sure that the data are accurate and precise.

Awareness is increasing of basic principles that place exposure within a continuum, starting with a pollutant emission and continuing through possible cell-level changes and finally being expressed as impaired health. This awareness will make exposure assessment even more important in the future as it leads to the implementation of practical methods for reducing the risk from airborne contaminants and to efforts to mitigate exposure.

A final and major point made in the report is the need to have accurate and realistic assessments to ensure optimal reduction of human exposure. To accomplish this, exposure assessment research should be supported by government programs. Although not stated, such research should also be supported by other sectors, including the regulated community.

The committee's report, *Human Exposure Assessment for Airborne Pollutants: Advances and Opportunities*, is available from the National Academy Press by calling (800) 624-6242 or (202) 334-3313.

The Journal of Organic Chemistry solicits manuscripts that address topics at the interface of organic chemistry and biology.

While such manuscripts should address fundamental problems in organic chemistry (structure, mechanism, synthesis), we encourage submission of manuscripts in which these problems are solved with the use of techniques not traditionally associated with organic chemistry (enzyme kinetics, enzyme isolation and purification, identification of active site residues, etc.). The Journal hopes to foster integrated publications in which the chemical aspects are not separated from the biological aspects.

For manuscript format, see *J. Org. Chem.*, 1990, 55 (1), 7A-10A. Send manuscripts to: C. H. Heathcock, Editor-in-Chief, *The Journal of Organic Chemistry*, Department of Chemistry, University of California, Berkeley, CA 94720

For subscription information

American Chemical Society
Sales and Distribution
1155 Sixteenth Street, N.W.,
Washington, D.C. 20036
(202) 872-4363

Toll Free, 1-800-227-5558



Paul J. Liroy, Ph.D., is a professor in the Department of Environmental and Community Medicine and director of the Exposure Measurement and Assessment Division at the University of Medicine and Dentistry of New Jersey in Piscataway.

ANALYTICAL TECHNIQUES

By Alan Newman

Some new techniques are creeping into EPA's venerable list of analytical methods for organic compounds in the environment. Speakers at the recent EPA Conference on Analysis of Pollutants in the Environment, in Norfolk, VA, described experiments with liquid chromatography/mass spectrometry (LC/MS), supercritical fluid extraction (SFE), and robotic systems. These state-of-the-art techniques offer ways to measure nonvolatile pollutants, improve laboratory efficiency, and reduce costs.

Compared to the number of procedures involving gas chromatography, few EPA methods currently rely on liquid chromatography. However, says William Budde of EPA's Environmental Monitoring Systems Laboratory in Cincinnati, "I predict more growth for LC." Budde lists a host of environmentally important compounds that are too temperature sensitive to survive GC conditions (1-3), for instance, pesticides such as carbamates (e.g., carbaryl and alcarb sulfone), thioureas (e.g., diuron and linuron), and rotenone with five temperature-sensitive ether linkages.

What makes liquid chromatography particularly attractive is that it is now possible to interface high performance liquid chromatography (HPLC) instruments with mass spectrometers. Mass spectrometry offers sensitive and generally unequivocal identification of analytes. A number of different designs are currently available for LC/MS interfaces (4, 5).

At the EPA meeting Budde described experiments with one configuration, labeled a particle beam interface. As the mobile phase elutes off the HPLC column, the solution is sprayed into a heated de-



Highlights from EPA's Norfolk, VA, conference

solvation chamber. Aerosol particles containing the dissolved nonvolatile solute are forced through the chamber and exit via a nozzle or beam collimator. The resulting particle beam travels through two more chambers in which vacuum pumps strip off solvent vapor and reduce the pressure. Particles and solvent vapor that diffuse out of the beam are removed by

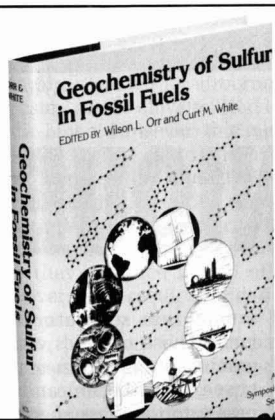
momentum separator skimmers. Those particles with the greatest momentum stay focused in the beam and thus pass into the mass spectrometer. "Momentum carries the particles through the interface to the mass spectrometer," explains Budde.

Using LC/MS, Budde and his colleagues have developed EPA Method 553 for the identification and quantitative analysis of temperature-sensitive benzidines, which are known human carcinogens. Benzidines may be forming in the environment as a result of anaerobic reduction of azo dyes. "There are millions of pounds of azo dyes being produced, and the waste has to go somewhere. It is out there percolating and we don't know if or when it will be a serious problem."

To identify benzidines, samples are run on a reverse-phase liquid chromatography column and eluted with a water-acetonitrile gradient solution containing ammonium acetate to improve separations. Low-bleed HPLC columns are employed in order to minimize the introduction of contaminants that might interfere with the mass spectrum.

The solvent and ammonium acetate that pass through the particle beam interface obscure only the low mass region of the spectrum (63 m/e and lower). The higher mass region reveals patterns similar to standard electron impact spectra for each benzidine congener.

To further evaluate this method, EPA conducted a study with 13 laboratories that used particle beam interfaces. These laboratories employed five different combinations of commercially available mass spectrometers and HPLCs. With benzidine samples that ranged from 5 to 100 ng/ μ L, Budde reported that the mean accu-



Geochemistry of Sulfur in Fossil Fuels

Sulfur in fossil fuels—how it got there and what form it's in—is the subject of this unique, new volume. It is the first to focus entirely on chemical processes occurring in geological environments.

Thirty-two chapters cover the current state of knowledge and address major advances that have established a new era of understanding at the molecular level in sulfur geochemistry. Various fuel systems are examined, as well as the reasons for their differences and similarities. Major advances made during the last decade by improved analytical methods are emphasized.

The volume begins with an introductory section that presents historical background, addresses environmental consequences of the combustion of fossil fuels, describes microbial metabolism of sulfur compounds, and reviews methods for isolating sulfur compounds. Other sections cover:

- studies of depositional environments
- characterization of sulfur in fossil fuel materials
- molecular structure of sulfur compounds and their geochemical significance
- isotopic studies

A 50-page bibliography compiling references from the individual papers is also included.

Wilson L. Orr, Editor, Mobil Research and Development Corporation

Curt M. White, Editor, Pittsburgh Energy Technology Center

Developed from a symposium sponsored by the Division of Geochemistry of the American Chemical Society

ACS Symposium Series No. 429
708 pages (1990) Clothbound
ISBN 0-8412-1804-8 LC 90-839
\$109.95

ORDER FROM

American Chemical Society
Distribution Office, Dept. 76
1155 Sixteenth St., N.W.
Washington, DC 20036

or CALL TOLL FREE

800-227-5558

(in Washington, D.C. 872-4363) and use your credit card!

racy was approximately 97% and, with the 100-ng/ μ L sample, the mean precision was < 10%.

To insure the quality of the LC/MS spectra, Budde's group has evaluated decafluorotriphenylphosphine oxide (DFTPPO) as a performance test compound. This compound features a number of strong peaks in the mass spectrum, ranging from an m/e of 77 to the molecular ion at 458. The spectrum of DFTPPO varies with different spectrometer conditions and thus could indicate system problems that would affect the analysis.

Another new technique offers an easier method for collecting samples for analysis. SFE, explains Merlin Bicking from Twin City Testing Corporation of St. Paul, MN, requires less material and time than traditional solvent extractions. (Supercritical fluids form when materials are raised to temperatures and pressures at which the liquid and gas phases are indistinguishable.) Furthermore, by varying the pressure and temperature, analysts can "fine-tune" the properties of a supercritical solvent for a particular pollutant.

To handle all the variations, Bicking's group employed a statistical approach to determine the best temperature and pressure for extracting a particular pollutant. This approach, labeled a "star-square" or central composite design, determines the percent recovery under nine different extraction conditions. The data lead to a three-dimensional plot of recovery versus temperature and pressure that pinpoints the best extraction conditions.

As an example, Bicking and his colleagues demonstrated the versatility of this approach by adapting it for EPA Method 413.2, which involves the extraction of oil and grease. To simulate this analysis, hexadecane and chlorobenzene were extracted from diatomaceous earth.

The current method calls for the soxhlet extraction of a 20–40-g sample with 300 mL of freon. After 48 h, the solution is concentrated and examined by FT-IR in a 100-mm path length cell. Recovery was determined to be 97%.

The equivalent SFE approach used just 2–5 g of sample and 6 mL of freon—eliminating 98% of the chlorofluorocarbon solvent. After only an hour the extract was diluted to 10 mL and examined by FT-IR using a 10-mm cell. Recovery was about 91%.

Bicking calculated that the cost of

the analysis dropped from \$12.50 for the standard soxhlet extraction to \$1.65 for SFE; "For an analysis that you charge \$30 for, that is a significant cost reduction." He also reported that about six SFE analyses could be performed daily, compared to eight by soxhlet. Automating the supercritical extractions would improve that rate, and thus the efficiency of this new approach.

Bicking has also looked at introducing SFE for the recovery of dioxins and dibenzofurans (EPA Method 8290). The standard SFE fluid, supercritical CO_2 , failed to adequately recover these organics even after long extractions. However, Bicking finds that the extraction improves with methanol mixed in with the CO_2 —another indication of the many variations available with SFE.

As Bicking mentioned, automation is one way to improve the efficiency of a test. W. A. Michalik described the experience of Shell Oil's analytical laboratory in Roxanna, IL, with robotic systems for performing biochemical oxygen demand (BOD) analyses on waste water.

At the heart of the system is a Zymark robotic arm. Arranged in a circle around the arm are various automated stations that transfer the analyte; add the biochemical seed, phosphate buffers, and water; insert and remove the glass stopper; take pH and oxygen measurements; and even wash the bottle for the next analysis. To prepare 30 samples the robot takes 60–90 min, says Michalik. The precision and accuracy of the automated system match the results of human operators.

A technician is needed only to move prepared samples in and out of the incubator and to daily calibrate the peristaltic pumps that transfer solutions. As a result, human involvement in the BOD analyses at Shell has decreased by approximately 75%, yielding another significant savings.

References

- (1) Ho, J. S. et al. *Environ. Sci. Technol.* **1990**, 24, 1748.
- (2) Beller, T. A.; Budde, W. L. *Anal. Chem.* **1988**, 60, 2076.
- (3) Behymer, T. D.; Bellar, T. A.; Budde, W. L. *Anal. Chem.* **1990**, 62, 1686.
- (4) Covey, T. R. et al. *Anal. Chem.* **1986**, 58, 1451A.
- (5) Budde, W. L. et al. *J. Am. Water Works Assoc.* **1990**, 82, 60.

Alan Newman is an associate editor on the Washington editorial staff of ES&T.

INDUSTRIAL & ENGINEERING CHEMISTRY RESEARCH

The one journal recognized as "must" reading throughout the industry

BROAD-BASED, COMPREHENSIVE COVERAGE EVERY MONTH

I&EC RESEARCH reports on important, original work, in the broad field of chemical engineering and industrial chemical research. The contributions include:

Fundamental research on thermodynamics, transport phenomena, chemical reaction kinetics and engineering, catalysis, separations, and materials.

Process design and development techniques for chemical equipment design, system analysis, process control, and scale-up procedures.

New Product innovations involving plastics, elastomers, fibers, fabrics, adhesives, coatings, paper, membranes, catalysts,

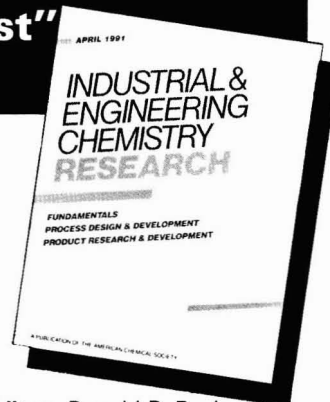
lubricants, fertilizers ceramics, aerosols, and more . . .

Research Notes—Short reports on new ideas or data concerning fundamental concepts, products, and processes that are in the early stages of development.

Correspondence—Comments on corrections to, reinterpretations, and rebuttals of previously published articles.

Reviews—Critical evaluations of the state of the art in timely areas of interest to readers.

The journal also features special sections, or entire issues devoted to timely symposia or to blocks of papers on selected topics.



Editor: Donald R. Paul
*University of Texas,
Austin*

Senior Editor: J. A. Seiner,
PPG Industries

Assoc. Editors: J. L. Anderson,
Carnegie-Mellon Univ.
M. P. Dudukovic
Washington Univ.
J. D. Seader,
Univ. of Utah

Published by the American Chemical Society

**Don't Miss a Single Issue,
Subscribe Today!**

Call Toll Free (U.S. and Canada): 1-800-227-5558
In D.C. and Outside the U.S. and Canada: 202-872-4363
Fax: 202-872-4615
Telex: 440159 ACSPUI or 892582 ACSPUBS
Cable Address: JEICHEM

Or Write:
American Chemical Society
Marketing Communications Department
1155 16th Street, N.W.
Washington, D.C. 20036

Volume 30 (1991) Printed	Canada & Mexico		All Other Countries*	
	U.S.	Europe*	Europe*	Countries*
ACS Members				
One Year	\$ 58	\$ 76	\$ 96	\$104
Two Years	\$104	\$140	\$180	\$196
Nonmembers	\$413	\$431	\$451	\$459

*Air Service Included.

Member subscription rates are for personal use only. Subscriptions are based on a calendar year. Foreign payment must be made in U.S. currency by international money order, UNESCO coupons, or U.S. bank draft, or order through your subscription agency. For nonmember rates in Japan, contact Maruzen Co., Ltd. This publication is available on microfilm, microfiche, and the full text is available online on STN International.

YOU CAN'T AFFORD TO BE WITHOUT USEFUL ARTICLES LIKE THESE:

Optimization of Catalyst Distribution in a Tubular Reactor

by Chengjun Du and Richard Turton

Analysis of the Surface-Enhanced Homogeneous Reaction during Oxidative Dehydrogenation of Propane over a V-Mg-O Catalyst

by Kimmai T. Nguyen and Harold H. Kung

Analysis of Zeolite Catalyst Deactivation during Catalytic Cracking Reactions

by Sebastian C. Reyes and L. E. Scriven

Scale-Up Studies on an Alumina Aerogel Catalyst Support

by Anthony J. Fanelli, Satyajit Verma, Ted Engelmann, and Joan V. Burlew

A Screening and Optimization Approach for the Retrofit of Heat-Exchanger Networks

by Terrence F. Yee and Ignacio E. Grossmann

Adsorptive Drying of Hydrocarbon Liquids by Sudhir Joshi and James R. Fair

Ultrathin Multicomponent Poly(ether sulfone) Membranes for Gas Separation Made by Dry/Wet Phase Inversion
by Ingo Pinnau, Jan Wind, and Klaus-Viktor Peinemann

Fluorescence Spectroscopy Studies of Dilute Supercritical Solutions

by Joan F. Brennecke, David L. Tomasko, Julie Peshkin, and Charles A. Eckert

Partition of Carboxylic Acids in an Emulsion Copolymerization System

by Glenn L. Shoaf and Gary W. Poehlein

Group-Contribution Flory Equation of State for Vapor-Liquid Equilibria in Mixtures with Polymers

by Fei Chen, Aage Fredenslund, and Peter Rasmussen

Experimental Observations of Bubble Breakage in Turbulent Flow

by Robert P. Hesketh, Arthur W. Etchells, and TW Fraser Russell

Pressure Swing Adsorption: Experimental and Theoretical Study on Air Purification and Vapor Recovery

by James A. Ritter and Ralph T. Yang

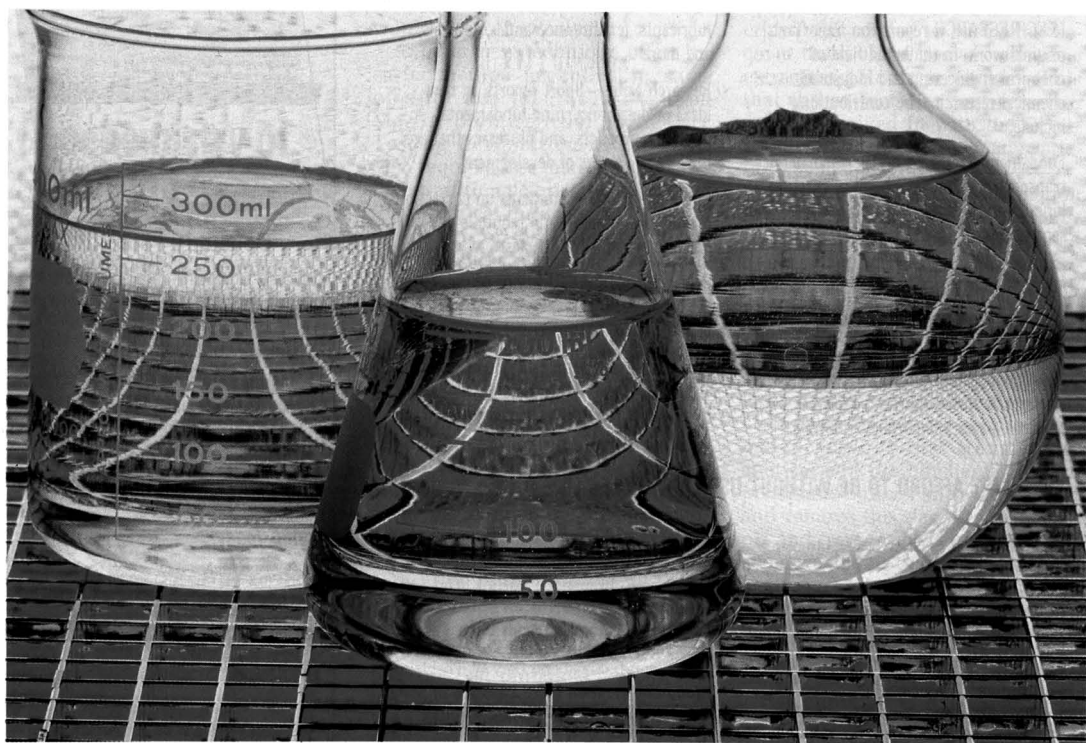
Inadequacy of Steady-State Analysis for Feedback Control: Distillate-Bottom Control of Distillation Columns

by Sigurd Skogestad, Elling W. Jacobsen, and Manfred Morari

Call for Papers! With its policy of expedited manuscript review and industry-wide readership, *Industrial & Engineering Chemistry Research* offers a prestigious home for your research. For information on manuscript submission please contact: Dr. Donald R. Paul, Editor, I&EC Research, Department of Chemical Engineering, University of Texas at Austin, Austin, TX 78712. Phone: (512) 471-5392; Fax: 512-471-0542. Authors do not pay page charges.

ASSURANCE LEVELS OF STANDARD SAMPLE SIZE FORMULAS

Implications for data quality planning



Masterfile

The increased popularity of the data quality objective process in planning for environmental restoration and related programs has resulted in a greater use of sample size formulas as planning tools. (The term "sample size" is used here in the statistical sense, meaning the number of samples obtained rather than sample mass or volume.) Sample size formulas are used as a means of meeting measurement precision requirements with a high level of assurance but with minimal cost.

Views are insightful commentaries on timely environmental topics, represent an author's opinion, and do not necessarily represent a position of the society or editors. Contrasting views are invited.

By Larry G. Blackwood

Sample size formulas based on specifying the required precision of results are readily available. However, these standard formulas generally do not give a reasonable level of assurance that the desired degree of precision will actually be obtained.

The inadequacy of standard sample size formulas is best understood by considering the distinction between confidence levels and assurance levels. A confidence level is the probability that a true value to be estimated will lie within a certain interval (i.e., the confidence interval) about the measurement actually obtained. Planning for the precision of a measurement involves specifying a confidence level and the confidence

interval width we hope to achieve. For example, if we want the estimate of the mean level of a trace constituent in an area of soil to be within 5 ppm of the true value with 95% confidence, the confidence level is 95% and the desired confidence interval width is 10 ppm.

Although we can fix the confidence level prior to a study, the associated confidence interval width is only partially controllable by varying the sample size. The confidence interval width also depends on the sample variance of the data values actually collected, which can only be estimated at the planning stage.

Once the data are collected, the 95% confidence interval width is fixed and we may find that we have

not achieved the desired precision. In the example, the calculated 95% confidence interval may actually be wider than 10 ppm. Therefore the planning process should also involve consideration of the probability that the 95% confidence interval will be of the desired width. This probability is called the assurance level.

Standard sample size formulas allow specification of the desired confidence level and the confidence interval width, but do not allow direct control of the assurance level. This can be illustrated by a simple example. Suppose, as above, we desire to estimate the mean contaminant level in a particular area to within 5 ppm of the actual value with 95% confidence. Also, assume the best estimate of the variance of the data is $\hat{\sigma}^2 = 50$. Then, for $\alpha/2 = \hat{\sigma}^2 (1 - 0.95)/2 = 0.025$, $d = 5$, and assuming independent normally distributed data, two commonly recommended formulas (1, 2) give minimum required sample size values of

$$n = (z_{\alpha/2})^2 \frac{\hat{\sigma}^2}{d^2} = 8$$

or

$$n = (t_{\alpha/2, n-1})^2 \frac{\hat{\sigma}^2}{d^2} = 10,$$

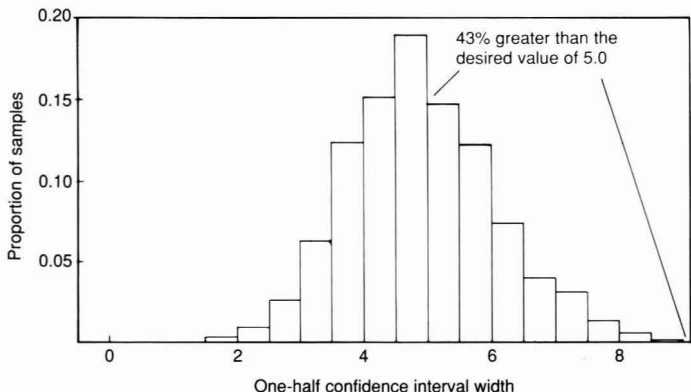
where z and t are critical values from the normal and t distributions, respectively.

A simple simulation exercise shows that the sample size values given by these formulas have little assurance of producing the desired level of precision. From a normal distribution with a mean of 100 (chosen arbitrarily; the results are the same for any mean value) and a variance of 50, generate 1000 samples of the recommended size, $n = 10$. For each simulated data set, calculate the 95% confidence interval for the mean. Any data set with a confidence interval width of 10 or less meets the established precision criteria. The assurance level, or probability that a sample size of 10 will produce the desired precision results, is obtained simply by calculating the proportion of data sets with confidence interval widths that are less than 10 as desired.

The results obtained from one such set of simulations are presented in histogram form in the accompanying figure. The data indicate that 43% of the time the confidence interval width is greater than the desired value. That is, the odds of ob-

FIGURE 1

Results from 1000 simulations with sample size = 10



taining the desired precision with a sample size of 10 are little better than 50–50. This would not be an acceptable assurance level for most data quality planners. If a sample size of eight had been used, less than one-third of the confidence interval results would have met the desired precision criteria.

The poor assurance results are due to the failure of the sample size formulas to take into account the random nature of the sample variances. To control the assurance level of the calculated sample size, it is necessary to account for this variability. Kupper and Hafner (3) give sample size formulas that include a value from a chi-square distribution, which is the distribution of the sample variance. The appropriate chi-square is based on the desired assurance level or what they refer to as the "tolerance probability."

Kupper and Hafner's formulas are more complicated than those used in the example. However, they also give tables in which the correct sample size value can be obtained based simply on knowing the results from the first formula above. Applying their methods to the example, with a desired tolerance probability of 0.95 (i.e., we want a sample size that will give a probability of 0.95 of obtaining a 95% confidence interval width of 10 ppm or less), the required sample size is 17. This is a 70% increase over the largest value specified by the standard formulas.

Employing these new sample size formulas has implications for stating data quality objectives. In particular, the desired assurance level must be stated explicitly. In the above example, although a confi-

dence level of 95% was specified, the desired assurance value was never stated explicitly. We just knew that 57% was not an acceptable result.

By stating the desired assurance level in data quality objective statements and then employing Kupper and Hafner's sample size formula, much better control over the outcome of a data collection effort is obtained. It should therefore become the method of choice in data quality planning.

Acknowledgment

The work described here was performed in part under the auspices of the U.S. Department of Energy, DOE Contract No. DE-AC07-76ID01570.

References

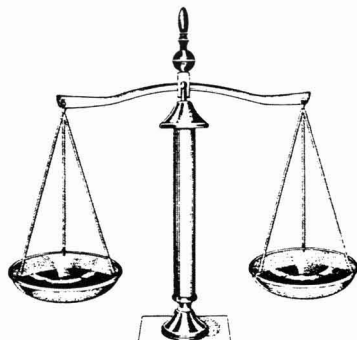
- (1) Snedecor, G. W.; Cochran, W. G. *Statistical Methods* (6th ed.); The Iowa State University Press: Ames, IA, 1967.
- (2) Gilbert, R. O. *Statistical Methods for Environmental Pollution Monitoring*; Van Nostrand Reinhold: New York, 1987.
- (3) Kupper, L. L.; Hafner, K. B. *The American Statistician* **1989**, *43*, 101–05.



Larry G. Blackwood is Senior Scientist in the Measurement Systems Engineering Unit at the Idaho National Engineering Laboratory, Idaho Falls, ID. His research primarily involves statistical methods for data quality planning, data validation, and engineering test analysis.

*Don't let legal jargon put you off...
Learn how to protect your inventions!*

Introduction to Patents



Put aside your fears of the legal system and get an in-depth understanding of the subject of patents. This new audiocassette course, designed for both degree and non-degree persons, is ideal for anyone who wants to learn how to protect intellectual property or who simply wants a basic overview of patents and the patent system.

As complex as it may seem, you'll learn how to read and understand a patent. You'll become more informed about the rights of employed inventors—including a discussion of Shop Rights and Employee Agreements.

You'll also get a better idea how to properly record data and inventive concepts.

**Most importantly, you can use what you learn immediately!
You'll be able to:**

- ☐ read and understand various types of patents
- ☐ appreciate the rights and obligations of inventors
- ☐ distinguish between patents and trade secrets
- ☐ keep proper research records
- ☐ understand the requirements for patentability
- ☐ know the procedures followed to obtain a patent
- ☐ understand differences between the patent systems of various countries
- ☐ and much more!

Presented by expert instructors, this three-hour course will tell you everything you need to know on patents. It is essential for patent departments in corporate and private industry, universities and colleges, small companies that may not have patent departments, secretaries and personnel who handle patent documents, and all researchers who want or need to know how to protect their work. **Order your copy today!**

Brief Outline

General Introduction: Purpose of Course and General Content. Historical Background. Brief Comparison of Patents, Trademarks, Copyrights and Trade Secrets

Trade Secrets

Types of Patents

Requirements of Patentability

Record Keeping

Patent Application and Prosecution: Searching; Patent Gazette; Preparation and Filing and Application; Formal Papers; Examination; Appeals, Interference, Litigation

Organization of a Patent

Patent Marking

Foreign Patents

Employee Rights: Shop Rights, and Employee Agreements

Instructors

Dr. C. Kenneth Bjork is Administration Manager - Patent Operations, Dow Chemical Company. Dr. Bjork is named as patentee on four U.S. and numerous foreign patents.

Richard B. Racine is a partner in the law firm of Finnegan, Henderson, Farabow, Garrett & Dunner, Washington D.C. His practice focuses primarily on inventions in the chemical field.

Unit

Three cassettes (3.0 hours playing time) and 60-page manual: \$350.00, U.S. & Canada; \$420.00, export. Additional manuals: \$18.00 each, U.S. & Canada; \$22.00 each, export. (Catalog No. B7).

Place Your Order Today!

CALL TOLL FREE 1-800-227-5558

ORDER FORM

Send this order form with your payment or purchase order to: American Chemical Society, Distribution Office #30, PO Box 57136, West End Station, NW, Washington, DC 20037

	Qty.	US & Can Price	Export Price	Total Amount
Introduction to Patents Catalog No. B7	_____	\$350.00	\$420.00	\$ _____
Additional Manuals	_____	\$ 18.00	\$ 22.00	\$ _____
		Total Enclosed:		\$ _____

Ship to:

Name _____
Title _____
Organization _____
Address _____
City, State, Zip _____
Phone _____

Bill to:

Name _____
Title _____
Organization _____
Address _____
City, State, Zip _____
Phone _____

Methods of Payment

- ☐ Payment enclosed (make checks payable to ACS)
- ☐ Purchase order enclosed. PO # _____
- ☐ Charge my ☐ Mastercard/Visa ☐ American Express

Account # _____

Expires _____ Interbank # _____ MC/ACCESS

Name of cardholder _____

Signature _____

Phone # _____

**In Washington DC area
call (202) 872-4363.
Fax: (202) 872-6067**

Orders from individuals must be prepaid. Please allow 2-3 weeks for UPS delivery. Foreign payment must be made in US currency by international money order, UNESCO coupons, or US bank draft.

Nonpoint source pollution



Alvin L. Alm

In many respects, the Clean Water Act has been the most successful of environmental statutes. Most industrial firms and municipalities have installed treatment facilities. The Act's technology-based standards and permit programs have been much more workable than the Clean Air Act; the Resource Conservation and Recovery Act; or the Comprehensive Environmental Response, Compensation, and Liability Act. The amount of public funds spent on water treatment facilities dwarfs that spent on treating other media. However, although examples abound of successful cleanups—Lake Erie and the Cuyahoga and Potomac rivers—many water bodies are not meeting quality standards, and national progress is stymied.

There are many reasons success is so elusive. Many water bodies have so little flow that very high levels of waste treatment are required. Toxic air pollutants rain down on some water bodies, notably the Great Lakes.

The most serious problem by far, however, is nonpoint source discharges from agriculture, silviculture, and urban sites. Of the three sources, agricultural runoff is the largest contributor to most water bodies. It deposits massive amounts of sediment into rivers and lakes and carries pesticides and fertilizers into surface water and groundwater. Clearcutting and road building lead to serious sedimentation problems in forests. Runoff from urban construction can result in soil runoff in fast-growing areas.

Historically, Congress has relied on the states to take action to meet the water quality standards. Such

actions have not been particularly effective because states lack explicit regulatory authority. Attempts to require or cajole better management practices have been spotty at best.

As part of the 1987 reauthorization of the Clean Water Act, Congress authorized a \$50 million per year grant program to states to prepare assessments and plans to control nonpoint source runoff. It is too early to determine its success, but the sums are so modest that even if individual grants are meeting objectives, the program cannot be considered an adequate response.

Congress is considering tougher medicine in the process of reauthorizing the Clean Water Act. Because of committee jurisdiction, however, the measures probably will cover only activities that EPA and state environmental agencies can conduct.

Agricultural runoff cannot be controlled without either dramatic changes in the information and incentives that are provided to farmers or new regulatory programs.

Over many decades, the Department of Agriculture and the land grant colleges have transformed U.S. agriculture into the world's most productive system. The tremendous information flow from the land grant colleges to farmers through the Extension Service is probably the best example of technology transfer from the public to the private sector. As a result, soil erosion has been substantially reduced. However, use of pesticides and fertilizers has increased, and runoff has become a more toxic and thereby a more serious water pollution problem.

The Department of Agriculture has not seriously tried to prevent off-farm damage from nonpoint runoff into water bodies until recently. President Bush's Water Quality Initiative, a repackaging of research and outreach activities, is aimed at reducing off-farm damage, but its scope is insufficient.

There are several ways to attack the agricultural nonpoint pollution problem. One is to consider large

farms as point sources and regulate them accordingly. Another option is to create new watershed entities to help manage nonpoint sources, similar to the irrigation districts in the western United States. Such entities could receive federal funds to assist in planning, but an ultimate driver would need to be some form of federal enforcement.

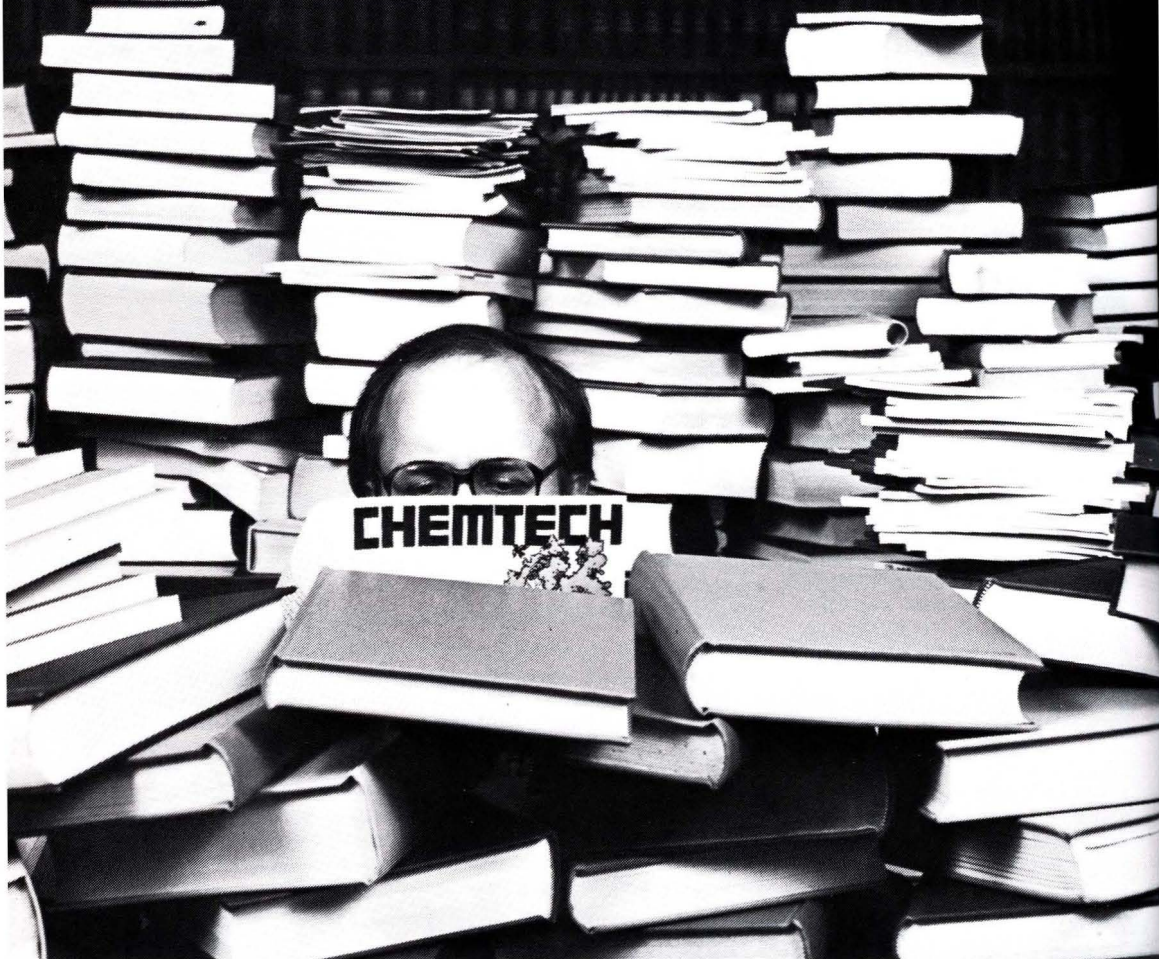
The most realistic option now is a strong congressional mandate to the Department of Agriculture. Although in recent years the Department has been conscientiously promoting control of nonpoint sources, that effort has not resulted in adequate improvement. If Congress fashioned a strong bill that linked subsidies and information programs in an all-out assault on nonpoint sources, the chances for success would be much greater.

Control of urban sediment is more difficult because regulatory control is normally at the county level. Nevertheless, if infrastructure departments (such as HUD and Transportation) had a strong mandate to curb urban runoff, they could provide many incentives. For example, transportation projects contribute heavily to urban runoff and receive major federal funding; thus they are prime candidates for creating incentives to reduce runoff.

The highly touted SAB report, *Reducing Risk*, recommended the integration of environmental concerns with other national policies. In a sense, energy and environmental policies are becoming integrated at the national, and even international, level. But the relationship between water quality, transportation, and urban and agricultural policies is much weaker. Until better integration occurs, nonpoint pollution will remain the largest residual water pollution problem.

Alvin L. Alm is director and senior vice-president for energy and the environment for Science Applications International Corp., a supplier of high-technology products and services related to the environment, energy, health, and national security.

The publication you have time to read



... To keep up the pace with current changes.

Today, trade publications available to industrial chemists concentrate on either chemistry—or chemical engineering—not both. Even though these fields are inter-related. And even though your work depends on your success in knowing what the guy next door is doing. Of course, everyone who wants to keep pace with his own field needs to read the single-discipline journals. But who's got the time to read much more than that?

That's where **CHEMTECH** comes in.

CHEMTECH is published especially for

the busy professional who wants to come up to speed on key developments in the chemical world—up and down the line from where he or she is. **CHEMTECH** helps you solve problems *before* they become red ink at the bottom of the balance sheet.

How does **CHEMTECH** do it?

- By bringing you topics vital to your work. Not just chemical science, but data correlation, economics . . . energy, engineering . . . management, materials, regulations, and more!
- By bringing concepts to you straight from the experts—articles and abstracts written by R&D directors, CEO's, distinguished professors, high-level government officials, and by shirt-sleeves lab and plant people who know

what's happening—because they're at the forefront making it happen!

- And by bringing this timely information to you in a dynamic style that's as entertaining as it is informative. **CHEMTECH**'s scope of coverage will truly stimulate your thinking . . . you'll see.

Keep informed with **CHEMTECH**
CALL TOLL FREE 800/227-5558
Outside U.S. 202/872-4363
Telex: 440159 ACSP UI 89 2582
ACSPUBS

CHEMTECH

American Chemical Society
1155 16th St., N.W., Washington, D.C. 20036

Human Exposure Assessment for Airborne Pollutants: Advances and Opportunities. National Research Council. National Academy Press, 2101 Constitution Ave., N.W., Washington, DC 20418. 1991. xv + 321 pages. \$22.50, cloth.

Human Exposure Assessment explores the need for strategies to address exposure to indoor and outdoor pollutants. It also examines tools available for finding out where and when significant exposures occur and for punishing those responsible. The book presents developments in exposure assessment and examples of how these assessments have been applied to public health issues.

New Developments in Industrial Wastewater Treatment. Ayşen Türkman and Orhan Uslu, Eds. Kluwer Academic Publishers, 101 Philip Dr., Assinippi Park, Norwell, MA 02061. 1991. xi + 226 pages. \$94, cloth.

New Developments in Industrial Wastewater Treatment deals with topics as diverse as biofilm reactors, pretreatment, wastewater analysis, polymers, oil-water separations, and material recovery. The book contains the proceedings of a NATO Advanced Research Seminar held in Izmir, Turkey, Nov. 1989.

Terrestrial and Aquatic Ecosystems: Perturbation and Recovery. Oscar Ravera, Ed. Prentice-Hall, Englewood Cliffs, NJ 07632. 1991. 613 pages. \$159.95, cloth.

Terrestrial and Aquatic Ecosystems discusses human disturbances of ecosystems, biological responses, consequences of altering specific ecological relationships, environmental management and strategies, and restoration of degraded ecosystems.

World Resources Data Diskette. WRI Publications, P.O. Box 4852, Hampden Station, Baltimore, MD 21211. 1991. IBM-compatible software, 5.25-in. and 3.5-in. format. \$89.95; includes user manual and print edition of *World Resources 1990-91*.

Information presented for 146 countries includes basic economic indicators and data on agriculture, forests and rangelands, wildlife habitats, energy, and climate. Data can be downloaded into word processing programs, spreadsheets, and data bases.

The Preservation and Valuation of Biological Resources. Gordon H. Orians et al., Eds. University of Washington Press, P.O. Box 50096, Seattle, WA 98145-5096. 1991. 314 pages. \$40.

The Preservation and Valuation of Biological Resources focuses on methods of preservation in the laboratory and the field, management of biological resources, and economic methods of assessing the value of species. Suggestions for research also are offered.

Acidic Deposition: Regional Case Studies. D. F. Charles, Ed. Springer-Verlag New York, P.O. Box 2485, Secaucus, NJ 07096-2491. 1991. 688 pages. \$98, cloth.

Topics covered include the acid-base chemistry of surface waters, historical trends in sulfur deposition, effects of acid deposition on aquatic ecosystems, and case studies in various regions of the United States and Canada.

Environmental Biotechnology. A. Blažej and V. Privarová, Eds. Elsevier, P.O. Box 882, Madison Square Station, New York, NY 10159. 1991. 436 pages. \$180.

Environmental Biotechnology discusses anaerobic treatment of effluents, denitrification, biofilm cultivation, aerobic thermophilic sludge treatment, and modeling. Sources of bioenergy and positive and negative impacts of biotechnology also are discussed. *Environmental Biotechnology* contains the proceedings of the International Symposium on Biotechnology held in Bratislava, Czechoslovakia, June 1990.

The Clean Air Act Handbook: A Practical Guide to Compliance. Craig A. Moyer and Michael A.

Francis. Clark Boardman Company, 375 Hudson St., New York, NY 10014. 1991. 480 pages. \$85.

This handbook examines the Clean Air Act Amendments of 1990, specifically new regulations for automotive sources, "clean" fuels, the list of hazardous air pollutants, acid deposition controls, stratospheric ozone and climate protection, and enforcement provisions.

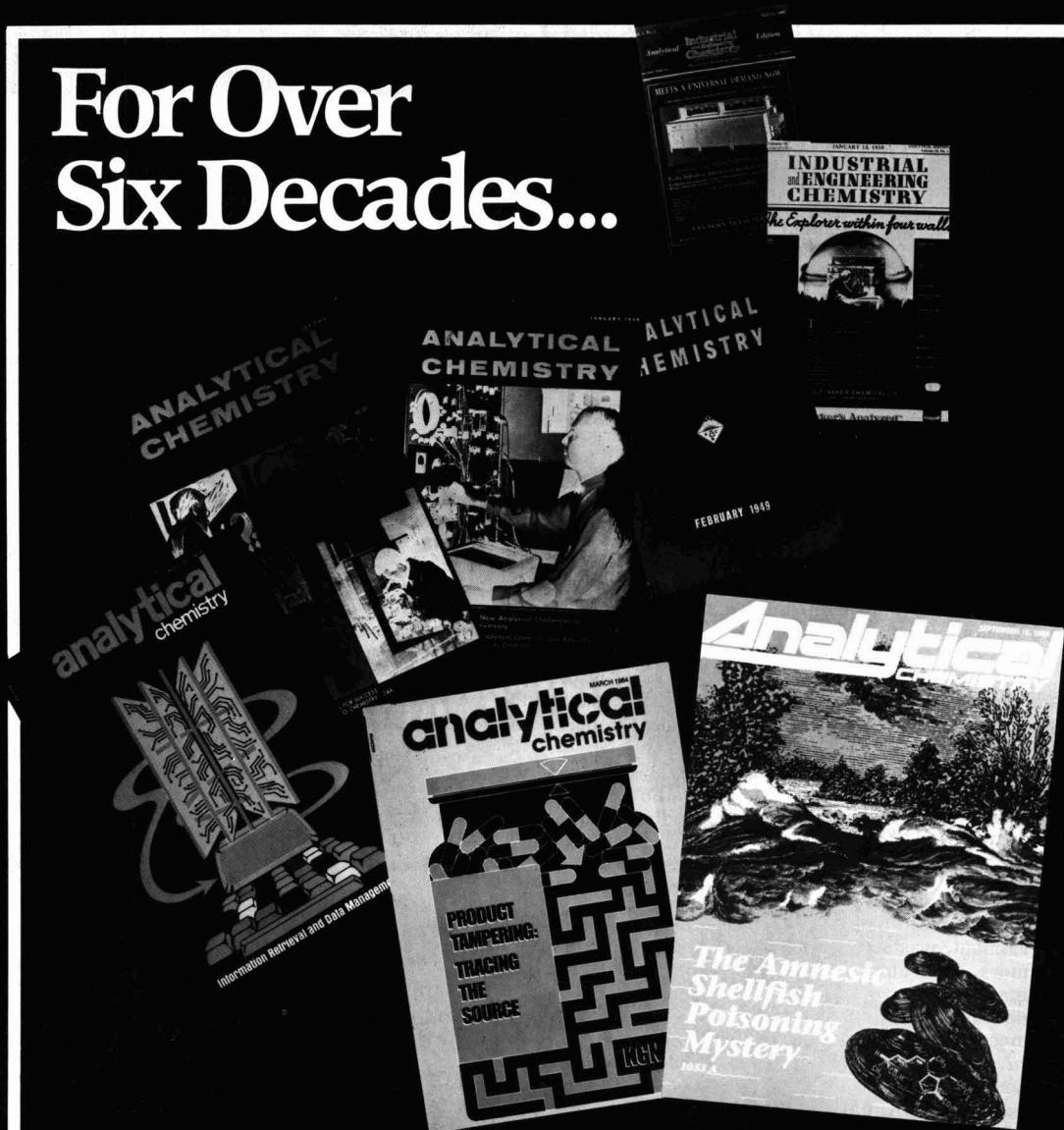
Compilation of EPA's Sampling and Analysis Methods Database. William Mueller and David L. Smith, compilers; Lawrence H. Keith, Ed. Lewis Publishers, 2000 Corporate Blvd., N.W., Boca Raton, FL 33431. 1991. 465 pages. \$124.95 (\$150 outside United States).

This compilation contains all of the 650 method and analyte summaries in *EPA's Sampling and Analysis Methods Database*, also published by Lewis. Each summary includes method name and EPA number, analyte, CAS registry number, instrumentation, method detection limits, sampling and sample container requirements, and more. The *Database* itself is available in a three-volume set of five diskettes, which covers industrial chemicals, pesticides and dioxins, and elements and water quality parameters. The set is available for \$205.

Long-Lived Legacy: Managing High-Level and Transuranic Waste at the DOE Nuclear Weapons Complex. Office of Technology Assessment. Superintendent of Documents, U.S. Government Printing Office, Washington, DC 20402-9325. 1991. 100 pages. \$4.75, paper.

Long-Lived Legacy is a background paper that describes, documents, and analyzes data about high-level and transuranic wastes. The bulk of the Department of Energy's waste management resources will be devoted to handling these high-risk wastes. This paper concludes that the challenge to DOE is to develop safer practices for on-site waste storage and for management of existing and future waste.

For Over Six Decades...



The Leader in the Field.

ANALYTICAL CHEMISTRY, the world's foremost publication in the vital field of measurement science, comes to you semi-monthly packed with *more* research articles, special features and application papers.

Keeping pace with the changes has continued to make *ANALYTICAL CHEMISTRY* the pinnacle of publications in the field . . . for over 6 decades.

For your personal subscription:

CALL TOLL FREE (800) 227-5558 (U.S. only)
Outside U.S. (202) 872-4363

Telex: 440159 UI
89 2582 ACSPUBS



American Chemical Society
1155 16th St., NW
Washington, DC 20036

AIR POLLUTION

Stopping fugitive emissions. "Seal-less" solenoid valves are designed to stop the leakage of fugitive emissions. Principal applications are in corrosive environments. Plast-O-Matic Valves **101**

Air cleaners. Electronic air cleaners handle air exhaust flows of 1200–16,000 ft³/min. Applications include kitchen exhaust systems and asphalt plant emissions. Company reports cleaners have been approved by Los Angeles Testing Laboratory. Universal Air Precipitator **102**

Small particle removal. Tubular electrostatic precipitator removes small particles (<1–3 µm), especially those resulting from municipal sludge incineration. Beltran Associates **103**

Submicron particle removal. Smog-Hog captures particles as small as 0.1 µm by two-stage electrostatic precipitation to meet federal and state opacity and particulate standards. United Air Specialists **104**

Mist elimination. NESTED fiber bed filters eliminate aerosol mist with 99.5% efficiency for submicron particles. Prefilters can be used, if needed, to trap solids that may clog main filters. CECO Filters **105**

HAZARDOUS MATERIALS

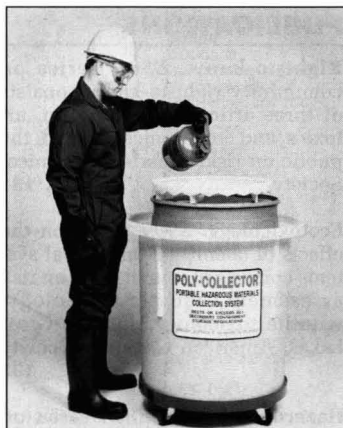
In situ treatment. PermeOx Solid Peroxygen is designed to provide controlled releases of oxygen to dechlorinate, deodorize, and step up biological activity in soils, sludges, and wastewater in situ. FMC **107**

Alternative to UST. EcoVault aboveground vaulted tank stores hazardous materials in an environmentally safe manner, as an alternative to underground storage tanks.

Need more information about any items? If so, just circle the appropriate numbers on one of the reader service cards bound into this issue and mail in the card. No stamp is necessary.

Cylindrical steel tank is encased in six inches of reinforced concrete. EcoVault **109**

Waste incineration. European advanced incineration system is designed to bring about complete waste burnout by means of controlled excess air units that produce higher temperatures. FECO **110**



Liquid collection. POLY-COLLECTOR can be wheeled to hazardous liquid collection sites, in keeping with EPA's container storage regulation. Other applications include draining of used filters and collection of waste oil. ENPAC **106**

INSTRUMENTS

Waste analysis. *Handbook for Waste Analysis* presents a line of simplified equipment and methods for measuring metals, minerals, and wastewater solids in influent, primary effluent, and sludge. Hach **111**

H₂S analyzer. Model 301XM analyzer detects hydrogen sulfide in the parts-per-billion range for process stream or natural gas pipeline applications. Texas Analytical Controls **112**

Companies interested in a listing in this department should send their release directly to Environmental Science and Technology, Attn: Products, 1155 16th St., N.W., Washington, DC 20036.

H₂S analyzer. Model 722R/102 analyzer measures H₂S in fuel gas, coke oven gas, and other gas streams at a range of 0–300 ppm. Houston Atlas **113**

Groundwater sampling. Company offers a line of dedicated sampling systems for measuring groundwater and eliminating losses of volatiles in sampling. American Sigma-Geoguard **114**

Extended TOC analysis. Carbon range extension kit is designed to increase carbon analyzers' upper range capacities to 8% of total organic carbon based on a 10-mg sample. This allows measurement of larger quantities of solid and sludge samples. Rosemount Analytical **115**

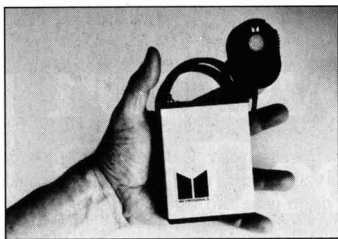
Spectrofluorometer. FluoroMax, a low-cost spectrofluorometer, allows simultaneous acquisition of four wavelength pairs for multiwavelength fluorescence measurements. With proper probes, system can determine Ca²⁺, Mg²⁺, K⁺, Na⁺, Cl⁻, and pH. SPEX **117**

Rapid toxicity test. IQ TOXICITY TEST is designed as a "do-it-yourself" *Daphnia magna* toxicity test or bioassay that can be performed in about 1.25 h. Conventional bioassays require 24–96 h to complete. Aqua Survey **118**

Dust monitor. HAZ-DUST handheld direct reading dust monitor determines total solid particulate and PM₁₀ concentrations for industrial hygiene and hazardous waste site investigations. Device is calibrated according to NIOSH Method 600. Environmental Devices **119**

Water testers. Series 941 single-test water testers are built to test colorimetrically for one analyte. Each model tests for an analyte such as ammonia nitrogen, chlorine, hexavalent chromium, lead, and pH. Orbeco Analytical Systems **121**

Personal CO monitor. The pm-7010 hand-held personal monitor displays the current level of carbon monoxide and sounds an alarm if a user-specified limit is exceeded.



Monitor may be clipped onto a belt or carried inside a shirt pocket. **Metrosonics 120**

Hydrocarbon class analysis. Hydrocarbon Class Analyzer determines the saturated, olefin, and aromatic hydrocarbon content of petroleum fuels with reproducibilities in the 1–3% range. **Suprex 122**

Stack sampling. Emission Parameter Analyzer stack sampling train samples gas stream effluents isokinetically in accordance with EPA standards. It meets or exceeds specifications of Method 5. **Andersen Instruments 123**

Toxic gas analysis. Company offers line of gas chromatography, photo ionization, and flame ionization analyzers for very low levels of toxic gases, intended for use in the workplace. **MSA 124**

Personal alarm. The Compur Monitox personal alarm is a lightweight, rugged, easy-to-wear unit that sounds an alarm when it detects dangerous levels of selected gases or low O₂ concentrations. **Mobay Corporation 125**

Portable GC. The P200D Gas Chromatographic System weighs under 30 pounds yet contains two GCs, each equipped with a heated column, solid state detector, and a sample injection system. The unit includes a rechargeable carrier gas bottle and battery pack. Companion software, the EZChrom 200 data system, operates the unit from an IBM-compatible computer. **MTI Analytical Instruments 126**

Ion laser system. For laser light in red or near-IR regions, the Innova 330 provides 1 W multiline red and 400 mW TEM₀₀ 752.5 nm output from a small frame (1 meter) cavity. Input power is only 208 V ac. **Coherent, Inc. 127**

Liquid chromatography system. SpectraSYSTEM is an integrated LC system of pumps, autosamplers,

and detectors designed to work together in a space-saving design. **Spectra Physics Analytical 128**

Soil toxicity testing. Microtox solid-phase test analyzes samples of soil, sludge, and sediment directly without complex and time-consuming extraction procedures. **Microtox 129**

Airborne fiber monitoring. FM-7400 laser fiber counter determines concentrations per cm³ with a 95% confidence level, in keeping with NIOSH Method 7400. Readings can be provided one minute after startup. **MIE 130**

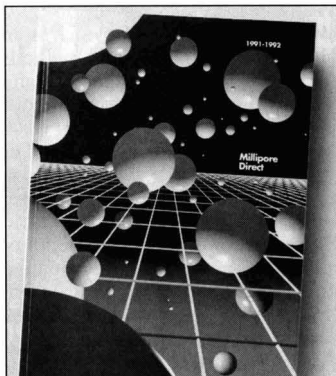
PUBLICATIONS

Right-to-know. *ES&T* series on community right-to-know consists of three articles on pollution, air toxics, and communication with the public on risk. **American Chemical Society 131**

Ecotoxicology. *ES&T* series on the effects of chemicals on natural systems consists of four articles on risk assessment, aquatic toxicology, wildlife toxicology, and the Great Lakes. **American Chemical Society 132**

Hazardous wastes. *ES&T* series on hazardous wastes consists of five articles on remediation technologies. **American Chemical Society 133**

Organic pesticide differentiation. Literature 5091-1011E explains how to differentiate organic pesticides by gas chromatography-mass spectrometry and by GC-Fourier transform infrared spectroscopy. **Hewlett-Packard 134**



Test and analysis equipment. A 475-page catalog lists laboratory water systems, environmental test

kits, sample preparation devices, and chromatography products. **Millipore 136**

SERVICES

PCB transformer reclassification. Company offers services in reclassifying transformers that contain polychlorinated biphenyls (PCBs) into non-PCB transformers with a 10-year warranty on remaining service life. **ENSR 137**

Lead recycling. Company's Total Lead Stewardship (TLS) program recycles old and damaged lead parts and lead-bearing wastes. Customer pays only transport costs. **Vulcan Lead 138**

SOFTWARE

Toxicology data base. Company is publishing a "monumental" toxicology data base, *Toxline Plus*, on CD-ROM. It is based on the four leading sources of toxicological information. **SilverPlatter 139**

Groundwater data management. GROUNDWATER/DMS version 1.20 is designed to enhance groundwater quality data management for monitoring, field work, and laboratory tests. Requirements are IBM AT or 100% compatible, IBM PS/2 Model 50 or above, or a 386-based IBM compatible system. **CSW Data Systems 140**

STANDARDS

Aromatics. BTEX calibration gas is a mixture of 10 ppm each of benzene, ethylbenzene, toluene, and o-xylene. Mixture is stable for up to one year. **Byrne Specialty Gases 141**

WATER TREATMENT

Metals removal. Reverse osmosis water treatment units remove metals, dissolved salts, inorganic molecules, and many organic molecules from water. **Davis Water & Waste 142**

Lead removal. MP500 solid carbon block filters remove dissolved and undissolved lead from drinking water to levels below 1 part per billion. **Multi-Pure 143**

Lead removal. ATS Sorbent, a white granular powder, reduces lead in drinking water "to nondetectable levels." **Engelhard 144**

**CIRCLE
NUMBERS
FOR FREE
INQUIRY
SERVICE**

29-35

ES&T
**Reader
Service
Reply Card**

**It's computer
processed
for fast
response
to your
inquiries
AND, IT'S
FREE**

THE AMERICAN CHEMICAL SOCIETY PRESENTS . . .

25 Unique Sources of Archival-Quality Chemistry Research and News

ACCOUNTS OF CHEMICAL RESEARCH

Editor, Fred W. McLafferty
Cornell University
12 issues a year. ISSN 0001-4842
Member \$25 Nonmember \$143

ANALYTICAL CHEMISTRY

Editor, Royce W. Murray
University of North Carolina, Chapel Hill
24 issues a year. ISSN 0003-2700
Member \$31 Nonmember (Pers.) \$69
Nonmember (Inst.) \$289

BIOCHEMISTRY

Editor, Hans Neurath
University of Washington
51 issues a year. ISSN 0006-2960
Member \$89 Nonmember \$849

BIOCONJUGATE CHEMISTRY

Editor, Claude F. Meares
University of California, Davis
The unifying medium of conjugation chemistry. BIOCONJUGATE CHEMISTRY emphasizes the joining of two different molecular functions by chemical or biological means.
6 issues a year. ISSN 1043-1802
Member \$29 Nonmember \$249

BIOTECHNOLOGY PROGRESS

Editor, Jerome S. Schultz
University of Pittsburgh
Jointly published with the American Institute of Chemical Engineers, this established journal offers *new, bimonthly access* to significant research in process development, product development, and equipment/instrumentation design for the biotechnology industry.
6 issues a year. ISSN 8756-7938
Member \$25 Nonmember \$250

CHEMICAL & ENGINEERING NEWS

Editor, Michael Heylin
51 issues a year. ISSN 0009-2347
Nonmember \$95

CHEMICAL RESEARCH IN TOXICOLOGY

Editor, Laurence J. Marnett
Vanderbilt University
For the latest original findings, in primary research, on the toxicological effects of chemical agents.
6 issues a year. ISSN 0893-228X
Member \$46 Nonmember \$269

CHEMICAL REVIEWS

Editor, Josef Michl
University of Colorado, Boulder
8 issues a year. ISSN 0009-2665
Member \$27 Nonmember \$265

CHEMISTRY OF MATERIALS

Editor, Leonard V. Interrante
Rensselaer Polytechnic Institute
This international journal provides a molecular-level perspective at the interface of chemistry, chemical engineering, and materials science.
6 issues a year. ISSN 0897-4756
Member \$49 Nonmember \$299

CHEMTECH

Editor, Benjamin J. Luberoff
The Concepteam, Inc.
12 issues a year. ISSN 0009-2703
Member \$41 Nonmember (Pers.) \$75
Nonmember (Inst.) \$325

ENERGY & FUELS

Editor, John W. Larsen
Lehigh University
A practitioner's guide to the chemistry of fossil fuels—from formation to methods of utilization.
6 issues a year. ISSN 0887-0624
Member \$48 Nonmember \$294

ENVIRONMENTAL SCIENCE & TECHNOLOGY

Editor, William H. Glaze
University of North Carolina, Chapel Hill
12 issues a year. ISSN 0013-936X
Member \$39 Nonmember (Pers.) \$73
Nonmember (Inst.) \$329

INDUSTRIAL & ENGINEERING CHEMISTRY RESEARCH

Editor, Donald R. Paul
University of Texas, Austin
12 issues a year. ISSN 0888-5885
Member \$58 Nonmember \$413

INORGANIC CHEMISTRY

Editor, M. Frederick Hawthorne
University of California, Los Angeles
26 issues a year. ISSN 0020-1669
Member \$86 Nonmember \$699

JOURNAL OF AGRICULTURAL AND FOOD CHEMISTRY

Editor, Irvin E. Liener
University of Minnesota
12 issues a year. ISSN 0021-8361
Member \$27 Nonmember \$243

JOURNAL OF THE AMERICAN CHEMICAL SOCIETY

Editor, Allen J. Bard
University of Texas, Austin
26 issues a year. ISSN 0002-7863
Member \$79 Nonmember \$750

JOURNAL OF CHEMICAL AND ENGINEERING DATA

Editor, Kenneth N. Marsb
Texas A&M University
4 issues a year. ISSN 0021-9568
Member \$32 Nonmember \$234

JOURNAL OF CHEMICAL INFORMATION AND COMPUTER SCIENCES

Editor, George W.A. Milne, N.I.H.
4 issues a year. ISSN 0095-2338
Member \$19 Nonmember \$129

JOURNAL OF MEDICINAL CHEMISTRY

Editor, Philip S. Portogbesse
University of Minnesota
12 issues a year. ISSN 0022-2623
Member \$44 Nonmember \$399

THE JOURNAL OF ORGANIC CHEMISTRY

Editor, Clayton H. Heathcock
University of California, Berkeley
26 issues a year. ISSN 0022-3263
Member \$59 Nonmember \$518

JOURNAL OF PHYSICAL AND CHEMICAL REFERENCE DATA

Editor, David R. Lide, Jr.
National Institute of Standards & Technology
6 issues a year. ISSN 0047-2689
Member \$75 Nonmember \$350

THE JOURNAL OF PHYSICAL CHEMISTRY

Editor, Mostafa A. El-Sayed
University of California, Los Angeles
26 issues a year. ISSN 0022-3654
Member \$79 Nonmember \$799

LANGMUIR

Editor, William A. Steele
The Pennsylvania State University
12 issues a year. ISSN 0743-7463
Member \$61 Nonmember \$515

MACROMOLECULES

Editor, Field H. Winslow
AT&T Bell Laboratories
26 issues a year. ISSN 0024-9297
Member \$65 Nonmember \$665

ORGANOMETALLICS

Editor, Dietmar Seyferth
Massachusetts Institute of Technology
12 issues a year. ISSN 0276-7333
Member \$62 Nonmember \$620

For subscription information write:

American Chemical Society
Marketing Communications Dept.
1155 Sixteenth Street, N.W.
Washington, D.C. 20036 U.S.A.

Call toll free (U.S. & Canada)

1-800-227-5558.
In Washington, D.C. and outside the U.S.
and Canada call 202-872-4363.
Telex: 440159 ACSP UI or 89 2582
ACSPUBS. FAX: 202-872-4615.

For nonmember rates in Japan contact:

Maruzen Co., Ltd.,
3-10 Nihonbashi 2-chome, Chuo-ku,
Tokyo 103, Japan

Rates are valid through December 31, 1991.

Analytical Chemists—Quality Assurance

San Antonio, TX

We need three professionals to help us develop and monitor quality assurance activities in a major environmental restoration program. Individuals will be responsible for interpretation of environmental data, which characterize potential sources and identify the extent of contamination from hazardous waste sites. In addition, selected individuals will review sampling and analysis plans, work plans and statements of work, and recommend modifications or additions to the documents to meet objectives of project and program requirements. On-site evaluations of environmental laboratories providing analytical services will be conducted by our staff chemists.

Qualifications for these integral positions include an MS or PhD in Chemistry and 8–10 years' hands-on experience in analyzing environmental samples for both organic and inorganic analytes and using SW-846 methods. U.S. citizenship, willingness to travel, and expertise in quality assurance and quality control in chemical measurements are required. Experience in conducting laboratory audits and data validation is highly desirable.

An independent, not-for-profit organization, MITRE works in the public interest, solving complex technical problems by providing system engineering, technical assistance, system integration and acquisition support to government and civil agencies. In addition to competitive salaries, we offer a comprehensive benefits package.

For confidential consideration, please forward your resume to: The Office of Human Resources, Section M08, The MITRE Corporation, 7525 Colshire Drive, McLean, VA 22102. We are an equal opportunity/affirmative action employer.

MITRE

POST-DOCTORAL RESEARCHER

The National Center for Intermedia Transport Research (NCITR) at the University of California, Los Angeles (UCLA) has a postdoctoral position for studies on intermedia and multimedia transport and fate of pollutants, and exposure analysis. The applicant is expected to have experience in numerical computations, software development and working knowledge of IBM and compatible desktop computers. The program includes theoretical and modeling studies of various intermedia transport processes (e.g., rain scavenging, dry deposition and transport in soil). For immediate consideration, please send a curriculum vitae and three letters of reference to Professor Yoram Cohen, Director - NCITR, Dept. of Chemical Engineering, 5531 Boelter Hall, University of California, Los Angeles (UCLA), Los Angeles, California 90024. UCLA is an affirmative action employer.

Nevada Cooperative Extension is seeking candidates for a State Specialist's position in Sustainable Agriculture. Responsibilities include assessing needs, establishing priorities and supporting Area Specialists in conducting educational programs focused on crop production issues and problems. Candidates should be interested in developing crop production systems that are economically profitable and environmentally compatible. A Ph.D. with academic preparation in crop ecology with emphasis in agro-ecosystem management, ecosystem modeling or production economics is required. Salaries are competitive and appointment will be at the assistant, associate, or full professor levels. This is a 12 month, tenure track position located on the University campus in Reno, Nevada. To apply, send a letter of introduction, current resume, summary of research interests and abilities, three letters of reference and official transcripts by August 30, 1991 to Elwood L. Miller (222), Nevada Cooperative Extension, University of Nevada, Reno, NV 89557-0004. AA/EEO. The University employs only U.S. citizens and those lawfully authorized to work in the U.S.

Environmental Engineer

MichCon, one of the nation's leading natural gas companies, has an opportunity available for an engineering professional who thrives on technical challenge. If you'd like to work with a company that gives you the resources, support and freedom you need to succeed, consider the position of Environmental Engineer.

You will conduct toxicological assessments; review legislation/regulations and determine their impact on the organization; coordinate clean-up efforts of contaminated sites; document and ensure disposal of hazardous wastes; and perform other related duties. Qualifications include a Bachelor's degree in Environmental Engineering, Toxicology, Geology, Forestry, or related field. A minimum of 3+ years experience with monitoring and testifying regarding environmental protection regulations and/or experience in toxicological work.

We offer competitive salaries, comprehensive benefits, opportunities for career advancement, and technical challenge. For immediate consideration, please forward your resume in confidence to: Michigan Consolidated Gas Company, 500 Griswold Street, Detroit, MI 48226. Equal Opportunity Employer M/F.

michcon

CLASSIFIED ADVERTISING RATES

Unit	1-T	3-T	6-T	12-T	24-T
1 inch	\$130	\$125	\$120	\$115	\$110

(Check Classified Advertising Department for rates if advertisement is larger than 10".)

SHIPPING INSTRUCTIONS:
Send all material to

Environmental Science & Technology
Classified Advertising Department
500 Post Road East
P.O. Box 231
Westport, CT 06881
(203) 226-7131/Fax (203) 454-9939

LOWEST COST-HIGHEST PERFORMANCE
GAS CHROMATOGRAPHS AND INTEGRATORS
SEVEN DETECTORS FOR ALL EPA-ASTM METHODS
FID TCD ECD FPD
PID ELCD NPD
COMBINE ANY OR ALL
SRI INSTRUMENTS
213-214-5090 fax 5097

FIELD PORTABLE-TEMP. PROG.
DATA SYSTEMS-INTEGRATORS
PURGE AND TRAP
GAS SAMPLING VALVES
THERMAL DESORBERS
AUTOSAMPLERS
GCs STARTING AT \$2495.00
RENTALS AT 0.5% PER DAY
TRAINING CLASSES
TWO YEAR WARRANTY

USE THE CLASSIFIED SECTION

Environmental Engineer

Environmental Engineer to design industrial and municipal water, wastewater and odor control treatment systems to meet local, state and federal standards. Will prepare studies and undertake process design to meet technical and regulatory standards, reduce pollution potential and enhance total resource usage; prepare in-plant studies, develop scope and flowsheets, prepare water and material balances, layouts and specifications, and select equipment for plant and treatment systems to abate or control waste water and hazardous chemicals from pulp and paper effluents and other industrial wastes. MA degree in environmental engineering or environmental science. 1 yr. in job offered or 1 yr. as graduate or postdoctoral research associate/assistant. Required of wastewater and hazardous chemicals from pulp and paper effluents. 9:00am-5:00pm, 40 hrs/wk, \$37,980/yr. Contact or send resume to **Sandra T. Starnes, Alabama State Employment Service, 3440 Third Avenue, South, Birmingham, AL 35222. Refer to J.O. #AL626341.**

LANDAU ASSOCIATES, INC. seeks experienced, solution-oriented professionals for growth-related project management positions in the following specialties:

- Ground Water Engineering
- Geochemistry/Contaminant Mobility
- Sediment Quality/Marine Systems

Candidates should possess an MS or PhD, proven communication skills, problem solving ability, and a relevant technical background. We offer excellent career opportunities in a stable team-oriented atmosphere characterized by technical quality, innovation, challenging projects, and a solid client base.

Send resume and letter of interest to: **Landau Associates, Inc., P.O. Box 1029, Edmonds, WA 98020-9129, Attn: Personnel Manager. AA/EOE. Non-smoking work environment.**

REQUEST FOR PROPOSALS

The Regional Citizens' Advisory Council, a non-profit citizens' group established to monitor the environmental effects of oil industry activities in Prince William Sound and the Gulf of Alaska, is soliciting proposals to conduct the following work:

RFP No. T91-3: Design of a Random Sampling Plan for Incoming Tanker Ballast. Proposals are sought from qualified specialists to design the ideal sampling plan that would most thoroughly describe the chemical composition of ballast water influent entering the ballast water treatment plant at the Alyeska Marine Terminal, a crude oil loading facility in Valdez, Alaska. Ballast water influent consists of seawater and petroleum hydrocarbons, but may include other organic and inorganic substances. Proposals are due by 5 p.m. PST Sept. 6, 1991.

The complete request for proposals and other information will be mailed or faxed upon request. Please contact: **Joe Bridgman or JoAnn Lundfelt, RCAC Terminal Operations & Environmental Monitoring Committee, P.O. Box 3470, Valdez, Alaska 99686, Telephone: (907) 835-5957, FAX (907) 835-5926.**

ENVIRONMENTAL RESEARCH

The Environmental Research Laboratory at SmithKline Beecham, one of the world's largest pharmaceutical research and development companies, is responsible for ensuring that chemicals and processes used in or produced by drug development and manufacture do not endanger the environment. We currently have a position available in this critically important group.

GROUP LEADER

ENVIRONMENTAL ANALYTICAL CHEMISTRY

You will lead the technical efforts to provide state-of-the-art analytical expertise for environmental studies, including methods development and support in HPLC, GC, GC/MS, HPLC/MS and spectroscopy for chemical and microbiological fate and degradation processes, physical chemical property determinations, and environmental process engineering. You will also interact with a multidisciplinary team in generating data to support Environmental Assessment information for IND/NDA submissions to FDA and other regulatory agencies in the U.S. and abroad.

Requirements include a Ph.D. in Chemistry with 4-6 years' experience or an M.S. in Analytical Chemistry with 5-8 years experience in environmental analytical chemistry; proven statistical skills; facility with computers, lab automation systems, and lab data management systems; knowledge of FDA and EPA GLP guidelines; the ability to critically read and interpret scientific literature; demonstrated supervisory skills; excellent interpersonal skills and the ability to work well with all levels of personnel.

SmithKline Beecham offers highly competitive salaries and an excellent benefits package. To apply, please send your resume to: **Central Employment, SmithKline Beecham, 1518 Spring Garden Street, Phila., PA 19101. We are an Equal Opportunity Employer, M/F/H/V.**



SmithKline Beecham
Pharmaceuticals

The Department seeks candidates for Director, Division of Environmental Analysis. Director is responsible for oversight of a statewide regulatory program of laboratory inspection and certification; design of testing programs; advising on matters within disciplines of chemistry, bacteriology, water, and biology. Seek individuals with minimum of ten years in the field of environmental laboratory science with ability to administer a large testing laboratory. Advanced training in chemistry, microbiology, biology, air pollution, engineering or analytical instrumentation. Please send resumes by September 18, to: **Department of Environmental Protection, Affirmative Action Office, One Winter Street, 4th Floor, Boston, MA 02108.**

Environmental Chemists

Law Environmental Inc., a leader in full service Environmental Engineering, is seeking experienced professionals to join our expanding National Laboratories. **Positions available in Atlanta, GA and Pensacola, FLA.**

● **GC/MS ANALYST:** BS or MS in Chemistry and 3+ years of GC/MS Environmental lab experience in volatiles or semi-volatiles.

● **GC ANALYST:** BS or MS Chemistry and 3+ years of GC Environmental lab experience in volatiles or pesticides/PCB analysis.

We offer comprehensive benefits including 401K, ESOP, pension plan. Send resume to: **Law Environmental, Inc., Human Resources, Dept. EST-1, 114 TownPark Drive, Kennesaw, GA 30144. EOE**

MARINE GEOCHEMIST

Southern California Coastal Water Research Project is seeking a Marine Geochemist with experience in trace organic analytical chemistry to study the transport and fate of contaminants in the coastal marine ecosystem off southern California. The successful candidate will have an established publication record and previous extramural funding in marine environmental chemistry. The position involves supervision and management of a small chemistry group, development of research plans and grant proposals, and publication of results in peer-reviewed journals. Experience with GC/MS, GC, HPLC, and related techniques required. Send letter of application and curriculum vitae to: **Personnel, Southern California Coastal Water Research Project, 646 W. Pacific Coast Hwy., Long Beach, CA 90806. SCCWRP is an Equal Opportunity Employer.**

ENGINEERING AND ENVIRONMENTAL POLICY

The National Academy of Engineering is seeking a program officer to handle policy oriented projects related to technology and environment. Responsibilities include development and management of technical and public policy studies, writing or approving background reports, and assisting in administration and budgeting. Requires Ph.D. or equivalent in engineering, economics, public policy or related discipline (or MS/MA with 4 years of experience) and excellent communication skills. Knowledge of energy industries, domestic and global environmental issues related to goods production and consumption, and engineering research and practice in industry desirable. Experience in technology oriented policy analysis or private sector policy and planning work also desirable. Please send resume in confidence to: **NAE, NAS-055-DR, 2101 Constitution Avenue, NW, Washington, D.C. 20418. EOE.**

professional consulting services directory

NATIONWIDE SEARCHES & OPPORTUNITIES

Optimal Resources, Inc.

6750 West Loop South, Suite 455 • Bellaire, Texas 77401-4100
(713) 666-2718 • FAX (713) 666-1402

♦ ♦ ♦

Outstanding Professionals in the following disciplines are encouraged to contact us in complete confidence:

- Environmental / Chemical / Civil Engineering
- Toxicology / Risk Assessment
- Chemodynamics
- Fate & Transport Modeling
- Regulations
- Permitting & Compliance
- Remediation
- Bioremediation
- Hydrogeology
- Environmental Law
- Hazardous Waste Disposal
- Industrial Hygiene
- Environmental / Analytical Chemistry

Environmental Organizations in search of the very best talent for Engineering, Science, R&D, and Regulatory positions pay our fee.

ROUX

GROUND-WATER CONSULTANTS

- SARA RI/FS
- RCRA Compliance
- Property Transfers
- UST Management
- Pesticide Monitoring
- Remediation

ROUX ASSOCIATES INC.

Offices in Atlanta, Chicago, Danbury, Denver, Hartford, Philadelphia, New York, Princeton, San Francisco.

Call 1 - (800) 322-ROUX

THE CONSULTANT'S DIRECTORY

UNIT	Six Issues	Twelve Issues
1" × 1 col.	\$65	\$60
1" × 2 col.	125	115
1" × 3 col.	185	160
2" × 1 col.	125	115
2" × 2 col.	230	210
4" × 1 col.	230	210

ENVIRONMENTAL SCIENCE & TECHNOLOGY

500 Post Road East

P.O. Box 231

Westport, CT 06881

(203) 226-7131

FAX: (203) 454-9939

INDEX TO THE ADVERTISERS IN THIS ISSUE

ADVERTISERS PAGE NO.

Columbus Instruments 1336
Columbus Advertising Agency

Environment Northern Seas 1350
Skandinavisk Media Informasjon

***Isco, Inc.** 1336
Farneaux Associates

Millipore Corporation 1335
Mintz & Hoke, Inc.

Varian IFC
Lanig Associates

Waters/Division of Millipore OBC
Millicomm, Inc.

* See ad in *Environmental Buyers' Guide*.

500 Post Road East
P.O. Box 231
Westport, Connecticut 06880
(Area Code 203) 226-7131
Telex No. 643310
Fax No. (203) 454-9939

Cleveland, OH. . . . Bruce E. Poorman, CENTCOM, LTD., 325 Front St., Berea, OH 44017 (Area Code 216) 234-1333, FAX: (216) 234-3425

Chicago, IL. . . . Michael J. Pak, CENTCOM, LTD., 540 Frontage Rd., Northfield, Ill. 60093 (Area Code 708) 441-6383, FAX: (708) 441-6382

Houston, TX. . . . Michael J. Pak, CENTCOM, LTD., (Area Code 708) 441-6383

San Francisco, CA. . . . Paul M. Butts, CENTCOM, LTD., Suite 1070, 2672 Bayshore Frontage Road, Mountainview, CA 94043 (Area Code 415) 969-4604, FAX: (415) 969-2104

ADVERTISING SALES MANAGER

Bruce E. Poorman

ADVERTISING PRODUCTION MANAGER

Jane F. Gatenby

SALES REPRESENTATIVES

Philadelphia, PA. . . . CENTCOM, LTD. GSB Building, Suite 405, 1 Belmont Ave., Bala Cynwyd, PA. 19004 (Area Code 215) 667-9666, FAX: (215) 667-9353

Los Angeles, CA. . . . Paul M. Butts, CENTCOM, LTD., (Area Code 415) 969-4604

Westport, CT. . . . Edward M. Black, CENTCOM, LTD., 500 Post Road East, P.O. Box 231, Westport, CT 06880 (Area Code 203) 226-7131, FAX: (203) 454-9939

Boston, MA. . . . Edward M. Black, CENTCOM, LTD., (Area Code 203) 226-7131

Atlanta, GA. . . . CENTCOM, LTD., (Area Code 216) 234-1333

New York/New Jersey . . . Dean A. Baldwin, John F. Raftery, CENTCOM, LTD., Schoolhouse Plaza, 720 King Georges Post Road, Fords, NJ 08863 (Area Code 908) 738-8200, FAX (908) 738-6128

Denver, CO. . . . Paul M. Butts, CENTCOM, LTD., (Area Code 415) 969-4604

Advertising Management for the
American Chemical Society Publications

CENTCOM, LTD.

President

James A. Byrne

Executive Vice President

Benjamin W. Jones

Robert L. Voepel, Vice President

Joseph P. Stenza, Production Director

A Cometabolic Biotransformation Model for Halogenated Aliphatic Compounds Exhibiting Product Toxicity

Lisa Alvarez-Cohen^{*†} and Perry L. McCarty[‡]

Environmental Engineering Program, Department of Civil Engineering, University of California, Berkeley, California 94720, and Environmental Engineering and Science, Department of Civil Engineering, Stanford University, Stanford, California 94305-4020

■ A model is proposed to describe the rate and extent of cometabolic transformation of halogenated aliphatic compounds by resting microbial cells. The finite transformation capacity (T_0) of resting cells, which appears to be associated with cometabolic oxidation of many halogenated aliphatic compounds, is used to incorporate the effects of product toxicity and reductant supply into a modified expression of Monod kinetics. Applicability of the model to trichloroethylene transformation by resting cells from a mixed methanotrophic culture is evaluated by comparison with experimental data from batch transformation studies conducted over a range of conditions. A visually good and statistically reasonable fit was obtained between the experimental data and model predictions both with cells alone and with formate added as an exogenous reductant source. A comparison of parameter estimates (k and K_s) derived by use of the cometabolic transformation model and those derived by use of conventional linearized Monod techniques (Lineweaver-Burk and concentration-normalized equations) indicates that, for reactions involving a finite transformation capacity, the linearized Monod equations yield artificially elevated parameters estimates.

Introduction

The widespread occurrence of water contaminated with halogenated aliphatic compounds such as the common solvent trichloroethylene (TCE) has led to development of treatment methods, including air stripping and activated carbon adsorption, for their removal. However, rather than causing complete contaminant destruction, these processes only transfer contaminants from one medium to another. In recent years, a variety of microbial processes have been discovered that can bring about the transformation and frequently the destruction of halogenated aliphatic compounds, stimulating increased interest in the potential of biological treatment. Unlike the biological processes commonly used for water or wastewater treatment, biological processes for the treatment of halogenated aliphatic compounds often depend upon cometabolism. Cometabolism is the transformation of a compound by organisms that do not obtain energy or carbon for cell growth from the transformation and hence require an alternative source of carbon and energy. There have been few engineering

applications of cometabolism, especially for contaminant treatment, and the factors affecting the kinetics of cometabolism have not been studied extensively. Thus, principles upon which to base treatment process design are limited.

The unsuitability of basic Monod kinetics alone for application to methanotrophic TCE transformation reactions (1) hinders process design modeling attempts. However, recent work on cometabolic cofactor dependency, product toxicity, and competitive inhibition makes it possible to more adequately address the issues involved and to propose a model to describe cometabolic transformation rates and extents. This model and its experimental evaluation with data from batch transformation studies are presented in the following study. Throughout this paper the term "resting cells" refers to organisms in the absence of growth substrate (e.g., methanotrophs without methane).

Background

Halogenated aliphatic compounds were first discovered to be biologically transformed under reducing conditions where hydrogenolysis or dihaloelimination to a variety of more reduced products results (2-4), some of which are more hazardous than the parent compound (5). Wilson and Wilson (6) later reported on the possibility of aerobic oxidation of TCE by soil microorganisms that were provided natural gas as a primary source of energy. Here, methanotrophic bacteria were believed to transform TCE through cometabolism, and this has now been adequately confirmed (7-9). The enzyme responsible is methane monooxygenase (MMO), which is used in the initial step of methane oxidation. Since then, other oxygenases have been found to be capable of TCE transformation, including those expressed during oxidation of toluene and other aromatic hydrocarbons (10, 11), propane (12, 13), and ammonia (14). Such oxidations require energy or reducing power, usually in the form of NADH or NADPH (15, 16), and this must be available for TCE cometabolism as well (9).

Hou (17) explored the potential of methanotrophs for cometabolic epoxidation of propene for industrial use and demonstrated that propene oxidation continued for a period in the absence of methane. By supplying a pulse of methanol, an alternative substrate for methanotrophs that does not require MMO, the organisms were able to reestablish propene oxidation for an additional period. Hou

^{*}University of California, Berkeley.

[‡]Stanford University.

attributed the ability of resting cells to carry out limited cometabolism to the presence of endogenous reducing power. Limited TCE oxidation by methanotrophic resting cells has also been demonstrated (1, 8, 9, 18–20). Henry and Grbic-Galic (20) suggested the reducing power of resting methanotrophic cells is related to poly(hydroxybutyrate) (PHB) granule storage within the cells.

Alvarez-Cohen and McCarty (1) defined two terms related to the transformation ability of resting cells: *transformation capacity* (T_c), representing the maximum mass of cometabolized compound (contaminant) that can be transformed per unit mass of resting cells, and *transformation yield* (T_y), the maximum mass of cometabolized compound that can be transformed by resting cells per unit mass of primary substrate used for original cellular growth. For resting cells of a mixed methanotrophic culture grown on methane, they reported a T_c of 0.036 mg of TCE/mg of cells and a T_y of 0.013 mg of TCE/mg of CH_4 .

Recent studies have indicated that T_c for cometabolic TCE transformation is not only a function of the availability of reducing power, but also of the specific cometabolized compound and toxicity of transformation products as well (1, 20, 21). Wackett and Householder clearly demonstrated with a pure culture of toluene-degrading organisms that the intermediate transformation products resulting from epoxidation of TCE were toxic to cells (21). Similar toxicity to methanotrophs has been reported by Alvarez-Cohen and McCarty (1) and Henry and Grbic-Galic (20). In the latter two cases, toxicity was indicated by the greatly reduced methane oxidation rate by the cultures after TCE transformation had occurred.

Studies have been conducted in order to maximize methanotrophic transformation rates of nongrowth substrates by examining the effects of temperature (22–24), cosubstrate addition (1, 9, 20, 23), pH (22, 24), and copper in the growth medium (9, 24).

In the following study, a rate equation for the cometabolic transformation of halogenated aliphatics by resting cells is developed that incorporates the above noted finite transformation capacity. Experimental data are then provided to test the model applicability and to elucidate the important parameters for process design.

Model Development

Monod kinetics have often been used to relate the transformation rate of a compound to its concentration in solution (25):

$$-dS/dt = \frac{kXS}{K_s + S} \quad (1)$$

where S is the solution concentration of cometabolized contaminant (mg/L), k is the maximum rate of contaminant transformation (mg of S (mg of cells) $^{-1}$ day $^{-1}$), K_s is the half-velocity constant (mg/L), and X is the active microbial concentration (mg/L).

For the cometabolic transformation of a contaminant by resting cells, there is no microbial growth over the course of the transformation. Microbial reactions not supporting growth are most commonly modeled by Monod kinetics with a constant active microbial concentration (26, 27), but have also been modeled by Monod kinetics with an active microbial concentration that decays over time (28), or with incorporation of competitive product inhibition (29), as well as by first-order kinetics (9, 19). However, for the cometabolic oxidation of halogenated aliphatic compounds, product toxicity results in a finite transformation capacity of resting cells. Hence, the overall activity of resting cells appears to decrease in proportion to the amount of cometabolized contaminant consumed. On this

basis, the transformation capacity of resting cells might be expressed in the form

$$\frac{1}{T_c} = \frac{dX}{dS} = \frac{\text{mass of cells inactivated}}{\text{mass of contaminant transformed}} \quad (2)$$

which when integrated yields the following expression for the active microbial concentration introduced previously (30):

$$X = X_0 - \frac{1}{T_c}(S_0 - S) \quad (3)$$

where X_0 is the initial active microbial concentration (mg/L), X is the active microbial concentration at time t (mg/L), S_0 is the initial concentration of cometabolized contaminant (mg/L), and S is the concentration of cometabolized contaminant at time t (mg/L).

Combining eqs 1 and 3 and rearranging gives the following:

$$dt = \frac{-(K_s + S)}{k \left(X_0 - \frac{1}{T_c}(S_0 - S) \right) S} dS \quad (4)$$

which can be integrated over time for a batch reactor to yield the following relationship between S and t :

$$t = \frac{1}{k} \left[\left(\frac{K_s}{S_0/T_c - X_0} \right) \ln \left\{ \frac{SX_0}{\left[X_0 - \frac{1}{T_c}(S_0 - S) \right] S_0} \right\} + T_c \ln \left\{ \frac{X_0}{\left[X_0 - \frac{1}{T_c}(S_0 - S) \right]} \right\} \right] \quad (5)$$

Equation 5 relates the cometabolized contaminant concentration remaining at any time t to the initial contaminant and organism concentration for a given transformation capacity. Two notable aspects of eq 5 are the following: (1) $S_0/T_c - X_0$ in the denominator renders the solution discontinuous when $S_0/T_c = X_0$, implying that the complete utilization of transformation capacity will not occur, and (2) real solutions can only be obtained when $X_0 T_c > (S_0 - S)$, indicating that the extent of transformation cannot exceed the transformation capacity. Results of the following experimental study were used to evaluate the suitability of this equation for prediction of TCE transformation by a mixed methanotrophic culture and to evaluate values for the terms k and K_s .

Materials and Methods

Mixed-Culture Development. A 7.5-L stirred tank microbial growth reactor was seeded with effluent from a laboratory column of aquifer material that had been enriched with methane and oxygen as previously described (1). The reactor was operated at a 9-day hydraulic detention time by addition of 833 mL/day of medium and once daily cell wasting. The growth medium consisted of mineral salts dissolved in deionized water after that of Fogel et al. (31). A mixture of 10.3% methane in air was continually injected into the reactor bottom at 280 mL/min and 1.035 atm partial pressure; high-velocity mixing (200 rpm) was maintained to facilitate methane and oxygen transfer to the liquid phase. The measured liquid concentrations of 0.02 mg/L methane and 3.5 mg/L oxygen indicated that cell growth was methane limited. A net growth yield of 0.33–0.37 g of cells/g of CH_4 consumed was

Table I. Parameter Values for the Nonlinear Least-Squares Fit of the Cometabolic Transformation Model to Formate-Free Methanotrophic TCE Disappearance Data (Experiment A)

parameter	value	asymptotic SE	95% confid interv	corr matrix		
k , mg of TCE (mg of cells) ⁻¹ day ⁻¹	0.53	0.017	0.48–0.57	1		
K_s , mg/L	0.37	0.098	0.13–0.61	0.857	1	
S_0 , mg/L	14.7	16.3	14.3–15.1	0.788	0.458	1
$r^2 = 0.9995$						

indicated by the average cell density of 2500 mg/L (ranging from 1800 to 3000 mg/L) and the gas effluent of 8.6% methane.

TCE Solutions and Analyses. Water-saturated TCE solution was prepared at least 24 h before use by adding 10 mL of TCE (99+% pure ACS reagent, Aldrich Chemicals Co., Milwaukee, WI) to a 160-mL glass bottle containing five glass beads and 120 mL of Milli-Q water. The bottle was sealed with a Teflon-lined rubber septum and aluminum crimp-top cap and vigorously shaken. One hour prior to use, the bottle was again shaken and allowed to settle. TCE-saturated water was removed by syringe through the septum, using care to exclude nonaqueous phase TCE.

TCE gaseous concentration was determined from headspace analysis as described previously (1), with a Tracor MT-220 gas chromatograph equipped with a packed column (10% squalene on Chromosorb A/AW) maintained at 70 °C and a linearized electron capture detector, and using an argon/methane mixture as carrier gas. A dimensionless Henry's constant of 0.31 for TCE at 21 °C (32) was used along with known liquid and gas volumes to compute TCE liquid concentrations and total TCE mass present.

TCE Transformation Studies. Transformation experiments were performed in a 21 °C environmental chamber using 62-mL glass bottles sealed with either Mininert Teflon-lined caps or a set of two 50-mil Teflon-lined septa (1). The bottles were inoculated with 20 mL of liquid (mixed-culture medium, cells, or a combination of both). For formate-supplied bottles, 1 mL of mixed-culture medium was replaced with 1 mL of a 400 mM sodium formate solution in Milli-Q water to yield a final concentration of 20 mM formate. Corresponding resting cells received 1 mL of pure Milli-Q water. Saturated TCE solution was added by gas-tight syringe through the Mininert valves, and the bottles were vigorously shaken by hand for 15 s before initial headspace samples for TCE were taken. The bottles were then shaken at 400 rpm (unless otherwise noted) on a circular action shaker table (Lab-Line). Gas samples (200 μ L) were withdrawn periodically with a 500- μ L gas-tight syringe (Pressure-lok) and 22-gauge side-port needle for TCE analysis. TCE transformation rates were determined from changes in total TCE mass, including both that in the liquid and in the gas phases.

Culture Density. Culture density was determined gravimetrically by adding a specific volume of suspended culture to tared 5.1-cm aluminum foil dishes and evaporating the dishes overnight at 105 °C before cooling and reweighing them. Medium controls were used to correct for inorganic dissolved solids in the culture medium. Concentrations reported represent total dry weight of the mixed culture in milligrams per liter.

Results

In experiment A with TCE alone (no formate addition), T_c was estimated by repeated addition of 15 mg of TCE/L to bottles containing 2300 mg/L resting cells (46 mg/

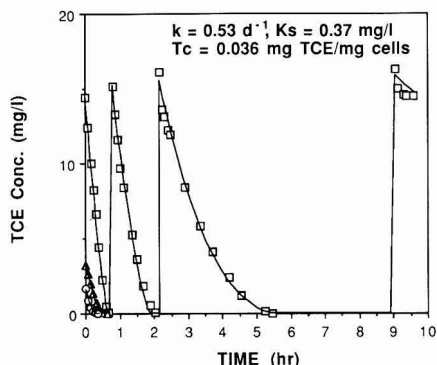


Figure 1. TCE disappearance in batch bottles at three initial TCE concentrations (experiment A). Experimental data (symbols) are plotted along with predictions (lines) by use of the cometabolic transformation model and k and K_s determined from nonlinear regression analysis of initial injection of 14.7 mg/L.

Table II. Residual Sum of Squares (RSS) and Initial TCE Concentrations for Fits of the Cometabolic Transformation Model^a

	S_0 , mg/L	no. of data points	RSS
first TCE addn ^b	14.7	9	0.206
second TCE addn	15.3	10	2.13
third TCE addn	15.6	12	2.75
fourth TCE addn	15.9	5	1.23
dilute cells	3.3	9	0.0624
dilute cells	1.7	6	0.0439

^a Parameters estimated from the first TCE addition to formate-free methanotrophic cells (experiment A). ^b Data used for parameter estimation.

bottle) until TCE transformation no longer occurred. From the results illustrated in Figure 1 (open box data) 1.7 mg of TCE (solution plus headspace mass) was transformed, indicating T_c equaled 0.036 mg of TCE/mg of cells. Next, S_0 , k , and K_s were estimated by a nonlinear regression fit of eq 5 to the disappearance data from only the first TCE addition at the 14.5 mg of TCE/L level. Estimation of S_0 is necessitated by the inherent inaccuracy of a time zero headspace measurement of the volatile TCE due to short-term nonequilibrium between the headspace and liquid phase. Nonlinear regression analysis was performed using Systat 5.0 application software (Systat, Inc.) employing a quasi-Newton estimation method. This analysis resulted in $k = 0.53$ mg of TCE (mg of cells)⁻¹ day⁻¹ and $K_s = 0.37$ mg/L ($r^2 = 0.9995$) with additional statistics summarized in Table I. These values for k , K_s , and T_c were introduced into eq 5, along with appropriate S_0 values, to examine the equation fit for the disappearance of the repeated TCE additions for this case. The results are shown plotted together with the experimental data in Figure 1 and summarized in Table II. In order to test the broader applicability of the model, the same parameters were applied under conditions of more dilute cell con-

Table III. Parameter Values for the Nonlinear Least-Squares Fit of the Cometabolic Transformation Model to Formate-Amended Methanotrophic TCE Disappearance Data (Experiment B)

parameter	value	asymptotic SE	95% confid inter	corr matrix		
k , mg of TCE (mg of cells) ⁻¹ day ⁻¹	7.6	0.438	6.3-8.8	1		
K_s , mg/L	8.2	0.526	6.7-9.6	0.960	1	
S_0 , mg/L	10.1	0.141	9.8-10.5	0.721	0.617	1

$r^2 = 0.9984$

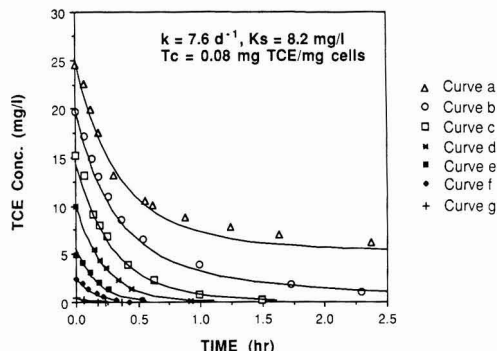


Figure 2. TCE disappearance in formate-amended batch bottles at seven initial TCE concentrations (experiment B). Experimental data (symbols) are plotted along with predictions (lines) by use of the cometabolic transformation model and k and K_s determined from nonlinear regression analysis of curve d.

centration (805 mg/L) and lower initial TCE concentrations (3.2 and 1.6 mg/L), with results also shown in Figure 1 and Table II. The fits between the data and the equation are good, as evidenced by the consistently low residual sum of squares for the repeated TCE additions as well as for the more dilute cell and TCE conditions.

Data from five additional similar experiments, which were fitted with eq 5, yielded the following parameter averages and standard deviations: $T_c = 0.043$ (0.010), $k = 0.84$ (0.29), $K_s = 0.69$ (0.54). The variations here are larger than expected from experimental errors alone, indicating that the model parameters may vary somewhat with change in operational characteristics of the culture. While the transformation capacity of resting cells freshly harvested from the reactor generally showed small variation, caution should be exercised in extending the values to other cultures or operational conditions.

Formate can be used as an external source of reducing power by methanotrophic resting cells (33). In order to determine how the addition of such a nongrowth-inducing and noncompetitive external source of reducing power would affect model parameters, bottles containing 421 mg/L (8.4 mg/bottle) resting cells and 20 mM NaCOOH were supplemented with seven different TCE concentrations in experiment B (Figure 2). The transformation capacity of the cells supplied with formate was determined from the mass of TCE consumed prior to the time that transformation ceased in the bottle initially amended with 25 mg/L TCE (curve a), where TCE utilization was not complete. The value found ($T_c = 0.080$ mg of TCE/mg of cells) was over twice that found with TCE alone, indicating that the addition of reducing power was here highly beneficial for increasing the transformation capacity. The values of S_0 , k , and K_s were obtained from the nonlinear regression fit of the disappearance data from the bottle receiving the middle concentration (10 mg/L) of the range of TCE additions (curve d). The resultant parameter estimates were $k = 7.6$ mg of TCE (mg of cells)⁻¹ day⁻¹ and $K_s = 8.2$ mg/L ($r^2 = 0.9984$), with the additional statistics

Table IV. Residual Sum of Squares (RSS) and Initial TCE Concentrations for Fits of the Cometabolic Transformation Model^a

curve	S_0 , mg/L	no. of data points	RSS
a	25.2	12	7.11
b	19.9	13	2.42
c	14.6	9	2.62
d ^b	10.1	7	0.021
e	5.7	6	0.598
f	2.6	7	0.114
g	0.36	5	0.0135

^aParameters estimated from curve d of formate amended methanotrophic TCE disappearance data (experiment B). ^bData used for parameter estimation.

summarized in Table III. The fit between the TCE disappearance using eq 5 and experimental data from the seven different TCE levels is again good (Figure 2, Table IV), indicating the model is applicable over a wide range of initial TCE concentrations. The estimates of both k and K_s along with their respective 95% confidence intervals are higher with formate added than in the absence of formate, although the ratio k/K_s with formate is somewhat lower (1.4 vs 0.93 L mg⁻¹ day⁻¹). Combining results from three additional similar experiments yielded parameter averages and standard deviations of $T_c = 0.061$ (0.025), $k = 4.8$ (1.9), and $K_s = 7.9$ (0.62). However, the high correlation between k and K_s for experiment B (Table III) indicates that when formate is added to resting cells within the TCE concentration range studied, it may not be possible to obtain unique parameter estimates of k and K_s , suggesting that for those experimental conditions the k/K_s ratio may be a more useful kinetic parameter.

In order to further evaluate the uniqueness of parameter estimates and elucidate the relative importance of parameters over the specific concentration ranges of interest, a sensitivity analysis such as that described by Robinson and Characklis (34, 35) was performed. The sensitivity equations were derived from eq 5 by taking the first derivative of the dependent variable with respect to the parameter of interest (dS/dS_0 , dS/dk , dS/dK_s) by implicit differentiation. The resultant equations were multiplied by their respective parameters to yield consistent units (mg of TCE/L) and are shown plotted against the dependent variable (S) for experiment A in Figure 3 and experiment B in Figure 4. The lack of proportionality between all three curves for both initial concentrations in experiment A (Figure 3) suggests that those experimental conditions should yield unique parameter estimates over most TCE concentrations. However, the relatively low value of the K_s equation at both initial concentrations (note the equation is multiplied by 10 in Figure 3) suggests that, for the conditions of experiment A, the model is relatively insensitive to changes in K_s . For the conditions of experiment B, the sensitivity equations in Figure 4 show a high proportionality of the k and K_s equations for all three initial concentrations, suggesting here that unique estimates of both k and K_s may not have been obtained.

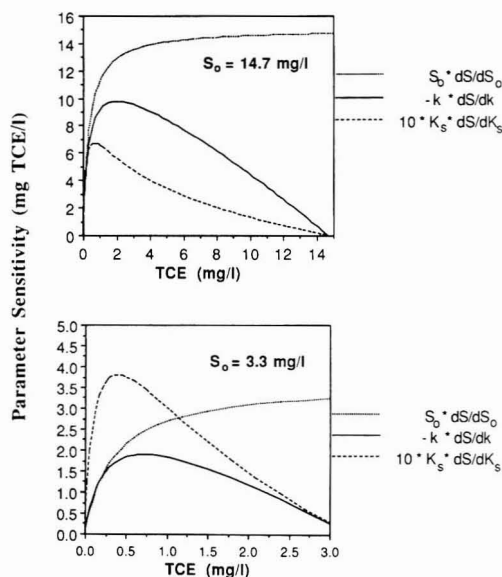


Figure 3. Sensitivity equations for parameters of the cometabolic transformation model applied to methanotrophic TCE transformation under conditions of experiment A for two initial TCE concentrations.

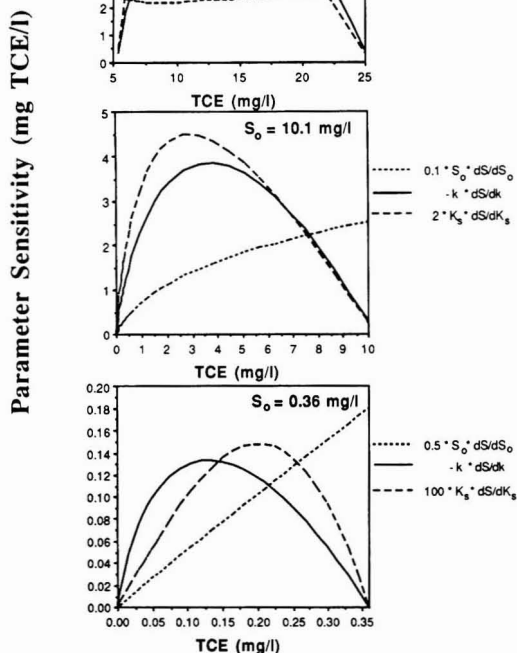


Figure 4. Sensitivity equations of parameters of the cometabolic transformation model applied to methanotrophic TCE transformation under conditions of experiment B for three initial TCE concentrations.

Additionally, Figure 4 shows that at the low initial TCE concentration (0.36 mg/L) the model is extremely insen-

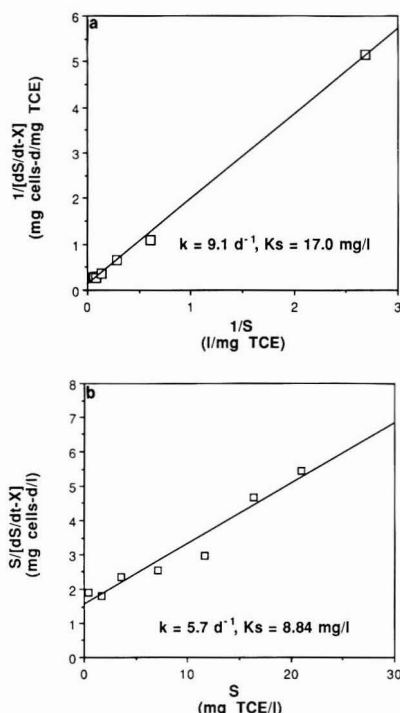


Figure 5. (a) Lineweaver-Burk plot of rate of TCE disappearance within the initial 12 min in formate-fed batch bottles at seven initial TCE concentrations. (b) Concentration-normalized plot of rate of TCE disappearance within the initial 12 min in formate-fed batch bottles at seven initial TCE concentrations.

Table V. Kinetic Parameters for Formate-Amended Methanotrophic TCE Transformation Computed by Three Different Methods

calculation method	k , mg of TCE (mg of cells) $^{-1}$ day $^{-1}$	K_s , mg of TCE/L	k/K_s , L (mg of cells) $^{-1}$ day $^{-1}$	r^2
Lineweaver-Burk	9.1	17.0	0.54	0.998
concentration-normalized	5.7	8.8	0.65	0.943
nonlinear cometabolic transformation model	7.6	8.2	0.93	0.998

sitive to K_s while at the higher initial concentrations much more sensitivity is observed.

In order to compare results obtained with the cometabolic transformation model (eq 5) and more conventional techniques, values for k and K_s were estimated from a Lineweaver-Burk plot (Figure 5a) and a concentration-normalized plot (Figure 5b) of initial disappearance rates computed by linear regression analysis of experiment B data taken within the first 12 min after TCE addition for each TCE concentration, a time period over which cell inactivation might be expected to be small. The parameters derived by these two methods as well as those computed by using nonlinear regression fit of eq 5 to the experimental data are listed in Table V. The parameters computed by use of the Lineweaver-Burk approach are both significantly greater than when eq 5 is used, but are similar when the concentration-normalized method is used. However, both conventional methods produced lower k/K_s

ratios. Based upon the T_c value of 0.080 mg of TCE/mg of cells, it was calculated that the amount of transformation capacity consumed during the first 12 min ranged from 1.8% for the lowest concentration to 35% for the three highest concentrations. This suggests that use of eq 1 alone (basis of both the Lineweaver-Burk and concentration-normalized inverse plots) results in biased parameter estimations, especially at higher contaminant concentrations.

The higher values of K_s obtained by the two traditional methods are artificially elevated as a result of the falloff of the transformation rate associated with toxicity and/or electron donor supply. Consequently, the inflated K_s is accompanied by an artificially elevated k in the Lineweaver-Burk expression since use of the reciprocal plot exaggerates the weighting of the data at the lowest concentrations, where the transformation rate is a function of k/K_s . Conversely, in the normalized-concentration expression the effects of an elevated K_s are less predictable and directly dependent on the range of data since normalization causes the data to be more evenly weighted.

Discussion

The proposed model, which uses TCE transformation capacity to incorporate the effects of toxicity and electron donor supply into a modified expression of Monod kinetics, was capable of predicting the results of methanotrophic TCE transformation reactions over a range of conditions. As yet, the broader applicability of this model to other cometabolic reactions has not been tested. However, evidence of cometabolic finite transformation capacities of resting cells has been noted for many different bacterial systems, including methanogenic reductive dehalogenation reactions (36), TCE oxidation by toluene oxidizers (10) and ammonia oxidizers (14), and methanotrophic propene oxidations (17). A model of the type developed here may be applicable to this broad range of cometabolic reactions; however, further evaluation is needed.

The proposed cometabolic transformation model may also apply to circumstances in which a finite transformation capacity occurs in the absence of overt product toxicity, possibly caused by such phenomena as cofactor dependence, unstable enzymes, and starvation strategies. However, the proposed model by itself would not be applicable for the transformation of compounds that are themselves toxic, since the model presumes that cell activity falls off not as a function of the contaminant itself, but rather as a function of the amount of contaminant consumed. The ability of this model to successfully fit the data for TCE transformation by the methanotrophic culture studied lends further evidence to the hypothesis that, for this culture at least, it is the transformation products, not TCE itself, that are responsible for the observed cell toxicity.

Formate addition to resting methanotrophic cells has been shown to result in an increased maximum TCE transformation rate (1, 9, 24) and capacity (1, 9). The increased maximum rate implies that the reducing power provided by formate may be more readily available than that from the cell's own internal energy reserves. Also, the increased transformation capacity with formate addition suggests that the internal reductant supply may indeed be somewhat limited. Nevertheless, it is still unclear exactly how product toxicity and reductant supply affect transformation capacity since the increased transformation rate caused by formate addition should result in an increased rate of transformation product appearance, and hence increased toxicity. Since the presence of formate enables a given mass of cells to transform a higher mass

of substrate before inactivation, a product toxicity saturation is suggested. That is, the toxic effect is rate limited by some unknown factor such as transport into or within the cell or toxicity reaction kinetics. However, further studies are needed to clarify this issue.

Although it has been previously reported that aeration of methanotrophic resting cells results in decreased transformation rates (1), this effect has not been incorporated into the cometabolic transformation model proposed, since compared to the effect of TCE product toxicity on resting cells at the level studied, the aeration effect was an order of magnitude lower and thus of little importance here. Under other circumstances, inclusion of a term for the decrease due to aeration alone may be appropriate.

The results of this study suggest that individual parameter values may not always be a good indicator of intrinsically higher transformation rates. Therefore, caution should be used when reported parameter values are interpreted, and when possible, experiments designed to directly measure maximum transformation rates at concentrations well above the K_s range.

The proposed cometabolic transformation model, which incorporates the effects of product toxicity and reductant supply into Monod kinetics, was shown to be applicable to methanotrophic TCE transformation by resting cells. A model of this type should be useful for evaluating various reactor designs and configurations for the cometabolic transformation of contaminants by resting microbial cells.

Registry No. TCE, 79-01-6; formate, 71-47-6.

Literature Cited

- Alvarez-Cohen, L.; McCarty, P. L. *Appl. Environ. Microbiol.* 1991, 57, 228-235.
- Bouwer, E. J.; McCarty, P. L. *Appl. Environ. Microbiol.* 1983, 45, 1286-1294.
- Parsons, F.; Woods, P. R.; DeMarco, J. J.—*Am. Water Works Assoc.* 1984, 76, 56-59.
- Vogel, T. M.; Criddle, C. S.; McCarty, P. L. *Environ. Sci. Technol.* 1987, 21, 722-736.
- Vogel, T. M.; McCarty, P. L. *Appl. Environ. Microbiol.* 1985, 49, 1080-1083.
- Wilson, J. T.; Wilson, B. H. *Appl. Environ. Microbiol.* 1985, 49, 242-243.
- Little, C. D.; Palumbo, A. V.; Herbes, S. E.; Lidstrom, M. E.; Tyndall, R. L.; Gilmer, P. J. *Appl. Environ. Microbiol.* 1988, 54, 951-956.
- Tsien, H.-C.; Brusseau, G. A.; Hanson, R. S.; Wackett, L. P. *Appl. Environ. Microbiol.* 1989, 55, 3155-3161.
- Oldenhuis, R.; Vink, R. L.; Janssen, D. B.; Witholt, B. *Appl. Environ. Microbiol.* 1989, 55, 2819-2826.
- Wackett, L. P.; Gibson, D. T. *Appl. Environ. Microbiol.* 1988, 54, 1703-1708.
- Nelson, M. J.; Montgomery, S. O.; Mahaffey, W. R.; Pritchard, P. H. *Appl. Environ. Microbiol.* 1987, 53, 949-954.
- Wackett, L. P.; Brusseau, G. A.; Householder, S. R.; Hanson, R. S. *Appl. Environ. Microbiol.* 1989, 55, 2960-2964.
- Fliermans, C. B.; Phelps, T. J.; Ringleberg, D.; Mikell, A. T.; White, D. C. *Appl. Environ. Microbiol.* 1989, 54, 1709-1714.
- Arciero, D.; Vannelli, T.; Logan, M.; Hooper, A. B. *Biochem. Biophys. Res. Commun.* 1989, 159, 640-643.
- Colby, J.; Stirling, D. I.; Dalton, H. *Biochem. J.* 1977, 165, 395-402.
- Patel, R. N.; Hou, C. T.; Laskin, A. I.; Felix, A.; Derelanko, P. J. *Bacteriol.* 1979, 139, 675-679.
- Hou, C. T. *Appl. Microbiol. Biotechnol.* 1984, 19, 1-4.
- Henson, J. M.; Yates, M. V.; Cochran, J. W.; Shackelford, D. L. *FEMS Microbiol. Ecol.* 1988, 53, 193-201.
- Strand, S. E.; Bjelland, M. D.; Stensel, H. D. *Res. J. Water Pollut. Control Fed.* 1990, 62, 124-129.

- (20) Henry, S. M.; Grbic-Galic, D. *Appl. Environ. Microbiol.* 1991, 57, 236-244.
- (21) Wackett, L. P.; Householder, S. R. *Appl. Environ. Microbiol.* 1989, 55, 2723-2725.
- (22) Hou, C. T.; Patel, R.; Laskin, A. I.; Barnabe, N.; Marczak, I. *Appl. Environ. Microbiol.* 1979, 38, 135-142.
- (23) Patel, R. N.; Hou, C. T.; Laskin, A. I.; Felix, A. *Appl. Environ. Microbiol.* 1982, 44, 1130-1137.
- (24) Brusseau, G. A.; Tsien, H.-C.; Hanson, R. S.; Wackett, L. P. *Biodegradation* 1990, 1, 19-29.
- (25) Lawrence, A. W.; McCarty, P. L. *J. Water Pollut. Control Fed.* 1969, 41, R1-R17.
- (26) Simkins, S.; Alexander, M. *Appl. Environ. Microbiol.* 1984, 47, 1299-1306.
- (27) Schmidt, S. K.; Simkins, S.; Alexander, M. *Appl. Environ. Microbiol.* 1985, 50, 323-331.
- (28) Galli, R.; McCarty, P. L. *Appl. Environ. Microbiol.* 1989, 55, 845-851.
- (29) Barrio-Lage, G.; Parsons, F. Z.; Nassar, R. S. *Environ. Sci. Technol.* 1987, 21, 366-370.
- (30) Alvarez, L. M.; McCarty, P. L.; Roberts, P. V. Presented at the Water Pollution Control Federation Annual Conference, San Francisco, CA, October 1989.
- (31) Fogel, M. M.; Taddeo, A. R.; Fogel, S. *Appl. Environ. Microbiol.* 1986, 51, 720-724.
- (32) Gossett, J. M. *Environ. Sci. Technol.* 1987, 21, 202-208.
- (33) Colby, J.; Dalton, H. *Biochem. J.* 1976, 157, 495-497.
- (34) Robinson, J. A.; Characklis, W. G. *Microb. Ecol.* 1984, 10, 165-178.
- (35) Robinson, J. A. In *Advances in Microbial Ecology*; Marshal, K. C., Ed.; Plenum: New York, 1985; Vol. 8, Chapter 2.
- (36) Freedman, D. L.; Gossett, J. M. *Appl. Environ. Microbiol.* 1989, 55, 2144-2151.

Received for review October 9, 1990. Accepted February 25, 1991. This research was supported in part by fellowships from the National Science Foundation, the Switzer Foundation, and the American Water Works Association (Larson Aquatic Research Support Scholarship), and in part by the Office of Research and Development, U.S. Environmental Protection Agency, through the Western Region Hazardous Substance Research Center, under Agreement R-815738. The contents of this article do not necessarily represent the views of these agencies.

Two-Stage Dispersed-Growth Treatment of Halogenated Aliphatic Compounds by Cometabolism

Lisa Alvarez-Cohen^{*†} and Perry L. McCarty[†]

Environmental Engineering Program, Department of Civil Engineering, University of California, Berkeley, California 94720, and Environmental Engineering and Science, Department of Civil Engineering, Stanford University, Stanford, California 94305-4020

■ A two-stage bioreactor that utilizes cometabolic biotransformations for the treatment of halogenated aliphatics is proposed. Methanotrophic cells are grown in a dispersed-growth reactor prior to transferral to a plug flow transformation reactor in which they are contacted with the waste stream and transformation occurs. A model describing cometabolic biotransformation is used together with basic equations for design of the growth and treatment reactors to predict treatment efficiencies and to evaluate the effects of the finite transformation capacity of resting cells, electron donor supply, and product toxicity on process design. For an example treatment scenario targeting trichloroethylene (TCE), methane transfer and growth reactor size are found to dominate the system design at high contaminant concentrations, while at low concentrations, the treatment reactor size becomes more important. The results of this analysis for a two-stage suspended-growth reactor system suggest that increasing methane and oxygen mass-transfer rates, cell yield, and transformation capacity may have a greater impact on reducing overall reactor size than would an increase in trichloroethylene transformation rate.

Introduction

The growing use of halogenated aliphatic compounds and their subsequent release into the environment indicates the need for the development of a low-cost, highly effective treatment system for their destruction. At present, the most prevalently used treatment processes for halogenated organics include air stripping and activated carbon sorption, which are capable of purifying water and gas streams, but simply transfer the organic contaminants

to a new phase without destroying them.

Many halogenated compounds such as trichloroethylene (TCE) have not been shown to be used by bacteria for energy or growth, but can be transformed through cometabolism by organisms that use a primary substrate, such as methane, for metabolism (1-4). A treatment system based upon the cometabolic transformation of halogenated aliphatics by methanotrophic microorganisms may be a cost-effective and efficient alternative to physical processes due to its potential for high transformation rates, complete compound degradation without formation of undesirable end products, applicability to a broad range of compounds, and a requirement for an inexpensive and widely available primary growth substrate.

Since methanotrophic TCE and methane oxidation both require the same key enzyme, competitive inhibition significantly affects the cometabolic transformation kinetics, as evidenced both in suspended-growth (5) and unsaturated fixed-film bioreactors (6). Competitive inhibition must therefore be factored into process design. Previous studies with methanotrophic bioreactors have used single-stage reactors in which competitive inhibition makes optimization of transformation efficiency difficult (6-9).

However, methanotrophic cells are capable of transforming TCE in the absence of methane (resting cells), and in this way, competitive inhibition can be avoided. A recent finding of significance is that product toxicity and limited electron donor supply result in a finite transformation capacity (T_c) of resting cells (10). Here, T_c is defined as the maximum mass of TCE transformed by a unit mass of resting cells (mg of TCE/mg of cells); a corresponding term, the transformation yield (T_y), represents the maximum mass of TCE transformation per mass of CH_4 used to grow the cells (mg of TCE/mg of CH_4). Formate addition can significantly increase T_c and T_y , presumably due to the increased supply of electron

^{*}University of California, Berkeley.

[†]Stanford University.

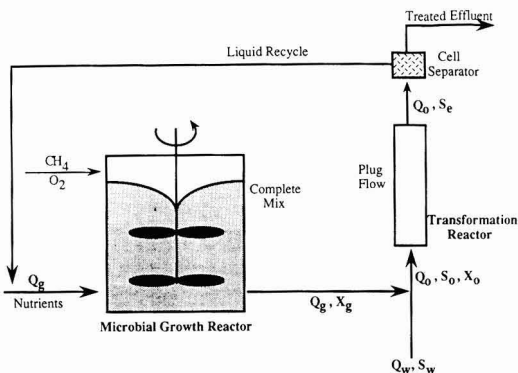


Figure 1. Proposed design for two-stage dispersed-growth methanotrophic treatment system for halogenated aliphatics.

donor produced during formate oxidation (11). Resting cell TCE transformation therefore is affected by the availability of an electron donor supply either from endogenous reserves or from an exogenous source such as formate. Formate addition to methanotrophic resting cells also results in an increased rate of TCE transformation (4, 12, 13) and hence may be useful in optimization of treatment efficiency. TCE transformation product toxicity, evidenced by greatly reduced methane and formate oxidation rates following TCE transformation (10, 14, 15), must also be factored into process design.

The finite transformation capacities of resting cells due to product toxicity or electron donor supply and competitive inhibition are phenomena that appear to be associated with cometabolic oxidation of many halogenated aliphatic compounds. The purpose of this paper is to incorporate these general concepts together with a cometabolic transformation model introduced previously (13, 16) into the design of a dispersed-growth cometabolic treatment system for chlorinated aliphatic compounds. A two-stage reactor is proposed that utilizes methane for cell growth in one reactor while conducting the transformation reaction in a second reactor (thereby excluding competitive inhibition). This work targets TCE for degradation since it is one of the most commonly encountered groundwater contaminants and is representative of a class of common solvents and their degradation products.

Proposed Cometabolic Treatment System

Figure 1 illustrates a two-stage treatment system designed to take advantage of the cometabolic transformation of halogenated aliphatic compounds, while recognizing the limitations imposed. The system consists of a growth reactor in which primary substrate is supplied to produce the organisms of interest under optimal conditions. The cell-rich growth reactor effluent is then mixed with the waste stream containing the compounds to be treated (contaminants), which together enter a treatment reactor without headspace where the contaminants are cometabolically degraded. When separate reactors for growth and contaminant transformation are maintained the reaction rate problems associated with competitive inhibition between the growth substrate and contaminant are also avoided.

The treatment reactor is designed in such a way that the transformation capacity of the cells is expended, or nearly so. Because of product toxicity, the cells are inactivated during treatment (14) and might be removed for disposal rather than being discharged or recycled back to the growth reactor. This is the purpose of the organism sep-

arator. Whatever water may be recycled back to the growth reactor is thus mainly devoid of organisms, but is functional for conveying the microorganisms between reactors. The design of the two reactors can be individually optimized by separating organism growth from treatment.

System Design Model

In the following, basic equations for design of the growth and treatment reactors are developed. The cell separator is not covered here, but there are many possible alternatives for this physical process.

Microbial Growth Reactor. The microbial growth reactor is considered to be a continuously stirred tank reactor (CSTR) without recycle. The reactor influent consists of a liquid stream containing inorganic nutrients and pH buffer for microbial growth. The primary substrate for energy and growth could also enter with the influent. However, with a methanotrophic reactor, the primary substrate is methane, which is preferentially transferred from a gas to the liquid phase. The relationship between hydraulic detention time, rate of methane utilization, and microbial cell concentration is as follows (17):

$$\frac{1}{\theta_g} = \frac{Q_g}{V_g} = \frac{Yr_m}{X_g} - b \quad (1)$$

The rate of primary substrate consumption is expressed as (15)

$$r_m = k_m X_g S_m / (K_m + S_m) \quad (2)$$

In addition, under steady-state operation of a methanotrophic bioreactor where growth is methane limited, the rate of methane consumption is equal to the rate of methane transfer from the gas to the liquid phase. Thus, an alternative expression is

$$r_m = k_L a \left(\frac{P_m}{H_m} - S_m \right) \quad (3)$$

By combination of eqs 1 and 3, the liquid volume of the microbial growth reactor is obtained as a function of the desired active microbial concentration X_g :

$$V_g = \frac{Q_g X_g}{Y k_L a \left(\frac{P_m}{H_m} - S_m \right) - b X_g} \quad (4)$$

Transformation Reactor. The rate of cometabolic transformation of contaminant by resting cells in the transformation reactor can be expressed as (13, 16)

$$r_s = k X S / (K_s + S) \quad (5)$$

The effective concentration of active microbial cells decreases as contaminant is consumed by cometabolism, as described previously (13, 16):

$$dX/dS = 1/T_c \quad (6)$$

Here, T_c is defined as the transformation capacity of the active cells. If the transformation reactor (Figure 1) were operated in a plug flow steady-state mode, then the contaminant concentration, S , would decrease with distance along the reactor. Likewise, eq 6 indicates that the active microbial concentration would decrease as well. The relationship between X and S at any point in the reactor is found by integration of eq 6 to give

$$X = X_0 - (1/T_c)(S_0 - S) \quad (7)$$

Substitution into eq 5 yields the transformation reaction rate as a function of \bar{S} :

$$r_s = \frac{k \left[X_0 - \frac{1}{T_c} (S_0 - S) \right] S}{K_s + S} \quad (8)$$

From a mass balance on S at steady state, the relationship between the hydraulic detention time (θ_t) and contaminant transformation can be expressed as follows (18):

$$\theta_t = V_t/Q_0 = \int_{S_0}^{S_e} -dS/r_s \quad (9)$$

Integration of eq 9 yields the following relationship between detention time and effluent contaminant concentration for an idealized plug flow reactor:

$$\theta_t = \frac{-1}{k} \left[\left(\frac{K_s}{F_r X_0} \right) \ln \left(\frac{S_e/S_0}{F_r + \frac{S_e}{T_c X_0}} \right) + T_c \ln \left(F_r + \frac{S_e}{T_c X_0} \right) \right] \quad (10)$$

Here, a dimensionless term, F_r , defined as the residual capacity factor is introduced:

$$F_r = (X_0 - S_0/T_c)/X_0 \quad (11)$$

F_r represents the fraction of the transformation capacity that would remain if all the contaminant were completely consumed in the transformation reactor. If the cells are exposed to a concentration of contaminant greater than their overall transformation capacity (i.e., $S_0/T_c > X_0$), the resultant F_r will be negative and the contaminant will not be completely consumed. Alternately, when F_r is positive, the full transformation capacity of the cells will not be utilized under the given conditions and transformation of additional contaminant is possible.

For a continuously stirred tank reactor, a similar analysis leads to the following equation for steady-state operation:

$$\theta_t = \frac{1}{k} \left[\frac{(K_s + S_e)(S_0 - S_e)}{X_0 S_e \left(F_r + \frac{S_e}{T_c X_0} \right)} \right] \quad (12)$$

At the entrance to the transformation reactor, the waste flow (Q_w) is mixed with the growth reactor flow (Q_g), yielding the following as the influent microbial cell concentration (X_0) and contaminant concentration (S_0):

$$X_0 = X_g \frac{Q_g}{Q_w + Q_g} = X_g \left(\frac{R}{1 + R} \right) \quad (13)$$

$$S_0 = S_w \frac{Q_w}{Q_w + Q_g} = S_w \left(\frac{1}{1 + R} \right) \quad (14)$$

where R represents the flow ratio (Q_g/Q_w) and S_w the contaminant concentration in the influent waste stream. An implied assumption in the definition of S_0 is that the residual contaminant in the recycle stream (S_e) is destroyed in the growth reactor or otherwise lost. Assuming the transformation reactor is operated devoid of headspace, the transformation reactor volume, V_t , becomes

$$V_t = (1 + R)Q_w \theta_t \quad (15)$$

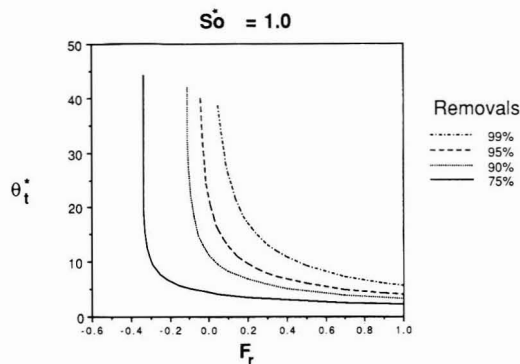


Figure 2. Relationship between dimensionless detention time (θ_t^*) and the residual capacity factor (F_r) for a dimensionless influent TCE concentration (S_0^*) of 1.0 over a range of removal efficiencies within a plug flow transformation reactor. F_r represents the fraction of cell activity remaining following the complete consumption of contaminant (TCE) within the transformation reactor.

System Characteristics

In order to illustrate the relationships between the different variables for reactor design, it is helpful to introduce dimensionless variables:

$$S_e^* = S_e/K_s \quad (16)$$

$$S_0^* = S_0/K_s \quad (17)$$

$$X_0^* = (T_c/S_0)X_0 \quad (18)$$

$$k^* = (t/T_c)k \quad (19)$$

$$\theta_t^* = (k/K_s)X_0 t \quad (20)$$

By introduction of these values into eq 10 for a plug flow reactor and rearrangement, the following equation is obtained:

$$\theta_t^* = \frac{1}{F_r} \left[\left[1 - S_0^* \left(\frac{F_r}{1 - F_r} \right) \right] \ln \left\{ F_r \left(1 - \frac{S_e^*}{S_0^*} \right) + \frac{S_e^*}{S_0^*} \right\} - \ln \left(\frac{S_e^*}{S_0^*} \right) \right] \quad (21)$$

Here θ_t^* represents the dimensionless detention time and is a function of the dimensionless influent concentration, S_0^* , the fraction of contaminant remaining after treatment (S_e^*/S_0^*), and F_r . The residual capacity factor is already dimensionless and can be simplified to

$$F_r = \frac{X_0 - S_0/T_c}{X_0} = \frac{X_0^* - 1}{X_0^*} \quad (22)$$

Equations 21 and 22 indicate θ_t^* is a function of S_e^* , S_0^* , and X_0^* . It is of interest to examine how θ_t^* varies with F_r (and hence X_0^*). Figure 2 illustrates for $S_0^* = 1.0$ the relationship between θ_t^* , F_r , and a range of removal efficiencies expressed as a percentage $[100(S_0 - S_e)/S_0]$. Figure 3 illustrates the same relationship with 95% contaminant removal for a range of S_0^* values. For the case shown in Figure 2, 90% or better removal can be obtained at near-minimal detention times with F_r greater than zero, that is, when the transformation capacity of the cells does not become exhausted. Since θ_t^* tends to increase rapidly as F_r decreases below 0.2, a selected value of 0.2 or higher for F_r seems appropriate as a first estimate for treatment system design. Figure 3 indicates that with S_0^* of 1 or less (i.e., when $S_0 \leq K_s$), the values for θ_t^* and F_r show only slight dependence on S_0^* , but when S_0^* approaches 10 or

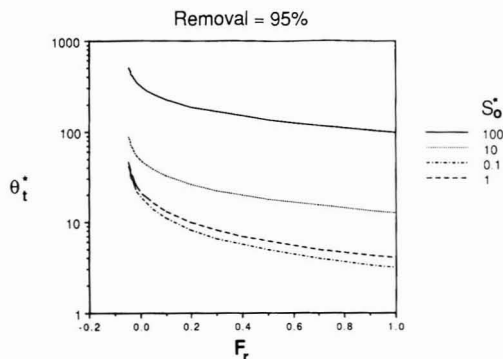


Figure 3. Relationship between dimensionless detention time (θ^*) and residual capacity factor (F_r) over a range of dimensionless influent TCE concentrations (S_0^*) for 95% removal in a plug flow transformation reactor.

Table I. Base-Case Coefficients Used in Growth and Transformation Reactor Design Examples

General Coefficients		
$\theta_g = 9 \text{ day}$	$Q_w = 10^3 \text{ m}^3/\text{day}$	
$K_{La} = 400 \text{ day}^{-1}$	$Y = 0.65 \text{ g of cells/g of CH}_4$	
$H_m = 0.042 \text{ atm}\cdot\text{L/mg}$	$b = 0.1 \text{ day}^{-1}$	
$P_m = 0.09 \text{ atm}$	$F_r = 0.2$	
$S_m = 0.02 \text{ mg/L}$		
TCE-Specific Coefficients		
	TCE alone	TCE + formate
$k, \text{ day}^{-1}$	0.53	7.6
$K_s, \text{ mg/L}$	0.37	8.2
$T_c, \text{ mg of TCE/mg of cells}$	0.036	0.080

higher ($S_0 \gg K_s$), θ^* increases in proportion to increases in S_0^* . This is a consequence of Monod kinetics: the reaction rate is first order with respect to substrate concentration at low concentrations, but zero order at high concentrations.

Design Examples

In order to illustrate the relationship between the respective volumes of the growth and treatment reactors, contaminated water characteristics, and treatment objectives, some examples for a completely mixed growth reactor with a plug flow treatment reactor are provided. Values used for the variables in the base case are listed in Table I. The general values listed in the first column represent operating conditions for the laboratory growth reactor previously described for the corresponding mixed-microbial population grown under nonaseptic conditions (10). Values for Y and b in the second column were determined specifically for the culture used (19), and the value of F_r is the minimum suggested in the preceding to limit treatment reactor size. The TCE-specific coefficients listed represent experimental results with the described mixed-microbial population and reflect the increased transformation rate and capacity of formate-fed cells (13).

Calculations of the system design factors are carried out as follows: X_g is computed from growth reactor coefficients by using eqs 1 and 3; the given F_r is used to compute X_0 (eq 11); R and Q_r are computed by using eq 13 with values of X_0 , X_g , and Q_w ; V_g is computed from eq 4, θ_t from eq 10, and V_t from eq 15. Table II is a summary of resulting system designs for treatment of contaminated streams with two significantly different concentrations of TCE in the waste stream (40 and 0.4 mg/L) in order to help illustrate the interplay between the growth and the treatment re-

Table II. Base-Case Example for Growth and Transformation Reactor Design Parameters Using Two Influent TCE Concentrations and a Removal Efficiency of 95%, $[100(S_w - S_e)/S_w]$, with Resting Cells Alone and in the Presence of Formate

	influent TCE conc (S_w) 40 mg/L		influent TCE conc (S_w) 0.4 mg/L	
	TCE alone	TCE + formate	TCE alone	TCE + formate
Growth Reactor				
cell density (X_g), mg/L	2610	2610	2610	2610
CH ₄ consumptn ^a , kg/day	3970	1790	40	18
volume (V_g , m ³)	4780	2150	48	22
Transformation Reactor				
% TCE removal	95	95	95	95
detention time (θ_t), day	0.096	0.030	0.492	1.37
volume (V_t), m ³	147	37	495	1370
Total System				
flow ratio (R)	0.53	0.24	0.0053	0.0024
net yield, ^b mg of TCE/mg of CH ₄	0.0096	0.021	0.0096	0.021
total volume ($V_g + V_t$), m ³	4930	2190	543	1400

^a Based upon measured cellular net yield of 0.35 mg of CH₄/mg of cells. ^b Represents the estimated mass of TCE consumed per unit mass of CH₄ consumed in reactors.

actors. With the higher influent contaminant concentration, the treatment reactor volume (V_t) is much smaller than for the low influent concentration, while for the growth reactor volume (V_g), the opposite is true. The sum total of reactor volumes is significantly lower for the low TCE concentration. At the high concentration, addition of formate to the treatment reactor to provide an exogenous energy source results in a significant reduction in size for both the treatment and growth reactors, whereas at the lower concentration, the treatment reactor size is surprisingly increased significantly by formate addition. The major reason for the latter is that at the lower concentration the transformation reaction rate is governed more by the ratio k/K_s than by k alone, and this ratio decreased when formate was added. This indicates that the interplay between variables is not always obvious and generalizations about the effect of system changes are sometimes difficult to make.

Table III contains the results of a sensitivity analysis for the base case without formate addition for the same two contaminant concentrations. The results of individually doubling the different important variables are illustrated. At high TCE concentration, the growth reactor size dominates the design. Two major design parameters are particularly significant here, the rate of mass transfer from the gas to the liquid phase (represented by variables k_{La} and P_m) and the transformation capacity (T_c). Increasing these variables can significantly reduce growth reactor size. While changes in other variables can reduce the transformation reactor size, this is not likely to lead to greatly reduced costs for high TCE concentration because of the dominance of the growth reactor size.

At low TCE concentrations, the treatment reactor comes into dominance, and efforts to reduce its size can significantly affect the overall costs. One of the most easily controlled variables here is F_r . When F_r is increased from 0.2 to 0.8, the treatment reactor volume is reduced from 495 to 60 m³. This effect is somewhat offset, however, by an increased methane consumption (from 40 to 159 kg/

Table III. Effect of Doubling Individual System Design Variables on Treatment System Characteristics for a TCE Removal Efficiency of 95%

variable doubled	R , Q_g/Q_w	V_r , m^3	V_g , m^3	consumed CH_4 , kg/day	net yield, ^c mg of TCE/mg of CH_4
$S_w = 40 \text{ mg/L}$					
base case ^a	0.53	147	4780	3970	0.0096
k	0.53	73	4780	3970	0.0096
K_s	0.53	154	4780	3970	0.0096
T_c	0.27	249	2390	1980	0.0192
$K_L a$	0.27	125	2390	3970	0.0096
P_m	0.26	124	2380	3970	0.0096
$1/\theta_g$	0.81	169	3650	3970	0.0096
F_r	0.71	97	6370	5290	0.0072
F_r^b	2.12	42	19100	15900	0.0024
$S_w = 0.4 \text{ mg/L}$					
base case ^a	0.0053	495	48	40	0.0096
k	0.0053	247	48	40	0.0096
K_s	0.0053	892	48	40	0.0096
T_c	0.0027	986	24	20	0.0192
$K_L a$	0.0027	493	24	40	0.0096
P_m	0.0026	493	24	40	0.0096
$1/\theta_g$	0.0081	496	37	40	0.0096
F_r	0.0071	263	64	53	0.0072
F_r^b	0.0212	60	191	159	0.0024

^aBase case makes use of variable values listed in Table I. ^b F_r value doubled again over value in row above to 0.8. ^cRepresents the estimated mass of TCE consumed per unit mass of CH_4 consumed in reactors.

day) and an increase in the growth reactor size (from 48 to 191 m^3). A selection of the best value for F_r requires an economic evaluation, but a value of ~ 0.7 here provides the minimum total volume for growth and treatment reactors (224 m^3).

If eq 12 for a CSTR rather than eq 10 for the plug flow treatment reactor is assumed, then the treatment reactor size increases. For the case with 40 mg/L TCE and no formate addition, the CSTR treatment reactor size is 2–3 times larger than the plug flow case. For this concentration with formate addition, the CSTR is ~ 7 times larger, while at the lower contaminant concentration, with or without formate, it is ~ 10 times larger than the plug flow reactor. Thus, there can be considerable advantage in the design of a treatment reactor that approaches idealized plug flow.

The above examples illustrate that, with relatively high contaminant concentrations, methane transfer and the growth reactor size are likely to dominate the system capital and operating costs, while with low concentrations, the treatment reactor size would most likely dominate costs. The sizes of these reactors are affected by different system variables, and thus it is not clear which particular variables should receive most investigative effort for improvement. In order to successfully apply cometabolic treatment systems for biotransformation of halogenated aliphatic compounds, an understanding of the impact of all the system variables indicated is important.

Summary and Discussion

There have now been several reported studies on reactors for cometabolic transformation of TCE (6–9). The common operational characteristic of the suspended growth (7), unsaturated fixed-film (6, 8) and saturated fixed-film (9) systems reported to date is that growth and transformation have been conducted in the same reactor. When attempts have been made to increase methane transfer to the cells by increasing methane partial pressure in the gas phase, the contaminant transformation rate

often decreases because of competitive inhibition. Thus, with higher contaminant concentrations, where methane transfer has a dominant influence on reactor size, such reactors have significant limitations. In addition, possible toxic effects of contaminant or transformation products on microorganisms have not been well evaluated since the reactors were not operated sufficiently long under the steady-state conditions where toxic effects are likely to become evident.

The use of a two-stage biological treatment system for degradation of contaminants by cometabolism represents an attractive alternative when competitive inhibition between the primary substrate and contaminant is involved, and especially when the products of cometabolism are toxic to the microorganisms. This is the case with TCE transformation by methanotrophic bacteria (10, 14, 15), and also by organisms producing toluene dioxygenase (20, 21). It is probably true for any microbial oxygenase system that may be used for TCE transformation as the epoxide and its transformation products are known to be cytotoxic (22, 23). This is perhaps also true for other halogenated aliphatic compounds, although the degree to which substrate or product toxicity is exhibited in other cases is not yet well-known.

The two-stage reactor concept is related to the well-demonstrated phenomenon that resting methanotrophic cells grown under certain conditions, such as low copper concentration (3, 4), can transform halogenated aliphatic compounds at relatively high rates, comparable to the rates of transformation of the primary substrates themselves. The transformation yields (T_y) of resting cells tend to be of the same order of magnitude as commonly reported for actively growing cells, and thus separation into two stages appears not to result in a loss of efficiency in energy usage. It also provides the marked advantage of permitting cell growth to be optimized for high methane transfer rates and cell activity, using a growth medium that is best suited for this purpose.

This study has illustrated that there are two related characteristic values that affect the design of a two-stage cometabolic treatment system: the transformation capacity, T_c , and the transformation yield, T_y . These terms can be used to relate the energy requirement, in terms of quantity of primary substrate needed, to the amount of contaminant that can be degraded. The lower the value for T_y , the more primary substrate that is required to treat a given amount of contaminant. This generally translates into a larger required growth reactor because of limitations in gas transfer (oxygen in general, but methane also with methanotrophic systems). As illustrated in the examples provided, the growth reactor volume tends to dominate with higher substrate concentrations ($S_0 \gg K_s$), and thus for this case, increasing T_y results in a smaller growth reactor volume.

A high T_y corresponds to a high T_c , which is a limit set by the availability of internally stored reducing power, substrate toxicity, product toxicity, or some combination of all three. As illustrated with a methanotrophic culture (10, 13), T_c can be increased markedly by the addition of formate to the treatment reactor, which serves to increase the methanotrophic reducing power without resulting in competitive inhibition to TCE transformation or organism growth. Formate addition also increases the reaction rate markedly. However, as illustrated, this does not always translate into a smaller treatment reactor volume because K_s tends to increase markedly with formate addition as well. The advantage of added reducing power is effected mainly at high contaminant concentrations. There may

be other ways to increase T_c that need to be explored such as manipulating the cellular growth rate, optimizing the methane/oxygen ratio within the growth reactor, changing the microbial growth medium formulation, or reducing the toxic effects of the contaminant or its transformation products.

An interesting feature found from this reactor analysis is the confounding effects of the several variables on the size of the growth and treatment reactors, effects that tended not to be intuitively obvious. The use of F_r , the residual capacity factor, proved useful in this analysis. F_r indicates the fraction of T_c that will not be consumed during treatment. At higher contaminant concentrations ($S_0 \gg K_s$), designs with F_r as close to zero as practical tended to yield more optimal results because the growth reactor size was dominant. However, with low contaminant concentrations ($S_0 < K_s$), increased values of F_r appeared to provide more optimal reactor volumes as the treatment reactor size dominated here. Under these conditions, it becomes more important to take advantage of the maximum transformation rate by fresh cells, rather than maximizing the use of transformation capacity.

Because of the interplay between so many factors in the design of the two-stage system for cometabolic transformation of halogenated aliphatic compounds, an optimization model that includes capital and operating costs would be useful both for design and to guide future research on ways to reduce treatment costs. In addition, studies on cometabolism of other contaminants and their interactions when present in mixtures is desirable. However, present knowledge is sufficient to indicate that cometabolic treatment is technically feasible; the need is to increase economic feasibility.

Although much work has been done with methanotrophs to maximize the rates of transformation reactions with a range of nongrowth compounds (4, 10–12, 14, 15, 23), the results of the analysis presented here suggest that for a suspended-growth reactor system the development of methods for increasing methane and oxygen mass transfer, or increasing cell yield or transformation capacity, may have a much more significant impact.

Glossary

Growth Reactor

b	microbial decay rate (day^{-1})
H_m	Henry's law coefficient for methane ($\text{atm}\cdot\text{L}/\text{mg}$)
$k_{L,a}$	gas/liquid mass-transfer coefficient (day^{-1})
K_m	primary substrate half-velocity constant (mg/L)
k_m	maximum rate of primary substrate consumption ($\text{mg of } S_m \text{ (mg of cells)}^{-1} \text{ day}^{-1}$)
P_m	partial pressure of methane in growth reactor headspace (atm)
Q_g	growth reactor influent and effluent flow rate (m^3/day)
r_m	rate of primary substrate consumption ($\text{mg}/\text{L}^{-1} \text{ day}^{-1}$)
S_m	steady-state primary substrate solution concentration (mg/L)
V_g	growth reactor volume (m^3)
X_g	steady-state active microbial concentration in growth reactor (mg/L)
Y	microbial growth yield ($\text{mg of cells}/\text{mg of primary substrate}$)
θ_g	growth reactor hydraulic detention time (day)

Transformation Reactor

F_r	residual capacity factor
k	maximum rate of contaminant transformation ($\text{mg of } S \text{ (mg of cells)}^{-1} \text{ day}^{-1}$)
K_s	half-velocity constant for contaminant (mg/L)

Q_0	$Q_w + Q_g$, transformation reactor influent and effluent flow rate (m^3/day)
r_s	rate of contaminant transformation ($\text{mg L}^{-1} \text{ day}^{-1}$)
S	aqueous contaminant concentration at time t (mg/L)
S_e	transformation reactor effluent contaminant concentration (mg/L)
S_0	transformation reactor influent contaminant concentration (mg/L)
T_c	transformation capacity of resting cells ($\text{mg of } S/\text{mg of cells}$)
T_y	transformation yield of resting cells ($\text{mg of } S/\text{mg of primary substrate}$)
V_t	transformation reactor volume (m^3)
X	active microbial concentration at time t (mg/L)
X_0	transformation reactor influent active microbial concentration (mg/L)
θ_t	transformation reactor hydraulic detention time (day)

General Terms

Q_w	waste stream flow rate (m^3/day)
S_w	waste stream contaminant concentration (mg/L)
R	Q_g/Q_w , overall reactor flow ratio

Registry No. TCE, 79-01-6; methane, 74-82-8.

Literature Cited

- Wilson, J. T.; Wilson, B. H. *Appl. Environ. Microbiol.* **1985**, *49*, 242–243.
- Little, C. D.; Palumbo, A. V.; Herbes, S. E.; Lidstrom, M. E.; Tyndall, R. L.; Gilmer, P. J. *Appl. Environ. Microbiol.* **1988**, *54*, 951–956.
- Tsien, H.-C.; Brusseau, G. A.; Hanson, R. S.; Wackett, L. P. *Appl. Environ. Microbiol.* **1989**, *55*, 3155–3161.
- Oldenhuis, R.; Vink, R. L.; Janssen, D. B.; Witholt, B. *Appl. Environ. Microbiol.* **1989**, *55*, 2819–2826.
- Broholm, K.; Jensen, B. K.; Christensen, T. H.; Olsen, L. *Appl. Environ. Microbiol.* **1990**, *56*, 2488–2493.
- Speitel, G.; McLay, D. S. *Proceedings of Environmental Engineering 1990 Specialty Conference*, Arlington, VA; American Society of Civil Engineers: New York, 1990; pp 366–373.
- Strand, S. E.; Bjelland, M. D.; Stensel, H. D. *Res. J. Water Pollut. Control Fed.* **1990**, *62*, 124–129.
- Strandberg, G. W.; Donaldson, T. L.; Farr, L. L. *Environ. Sci. Technol.* **1989**, *23*, 1422–1425.
- Phelps, T. J.; Niedzielski, J. J.; Schram, R. M.; Herbes, S. E.; White, D. C. *Appl. Environ. Microbiol.* **1990**, *56*, 1702–1709.
- Alvarez-Cohen, L.; McCarty, P. L. *Appl. Environ. Microbiol.* **1991**, *57*, 228–235.
- Patel, R. N.; Hou, C. T.; Laskin, A. I.; Felix, A. *Appl. Environ. Microbiol.* **1982**, *44*, 1130–1137.
- Brusseau, G. A.; Tsien, H.-C.; Hanson, R. S.; Wackett, L. P. *Biodegradation* **1990**, *1*, 19–29.
- Alvarez-Cohen, L.; McCarty, P. L. *Environ. Sci. Technol.*, preceding article in this issue.
- Alvarez-Cohen, L.; McCarty, P. L. *Appl. Environ. Microbiol.* **1991**, *57*, 1031–1037.
- Henry, S. M.; Grbic-Galic, D. *Appl. Environ. Microbiol.* **1991**, *57*, 236–244.
- Alvarez, L. M.; McCarty, P. L.; Roberts, P. V. Presented at the Water Pollution Control Federation Annual Conference, San Francisco, CA, October 1989.
- Lawrence, A. W.; McCarty, P. L. *J. Water Pollut. Control Fed.* **1969**, *41*, R1–R17.
- Levenspiel, O. *The Chemical Reactor Omnibook*; OSU Book Stores, Inc.: Corvallis, OR, 1989.
- Smith, L. H., Stanford University, Stanford, CA, personal communication, 1990.
- Wackett, L. P.; Gibson, D. T. *Appl. Environ. Microbiol.* **1988**, *54*, 1703–1708.
- Wackett, L. P.; Householder, S. R. *Appl. Environ. Microbiol.* **1989**, *55*, 2723–2725.
- Henschler, D. In *Bioactivation of Foreign Compounds*;

- Anders, M. W., Ed.; Academic Press: New York, 1985; pp 317-347.
- (23) Miller, R. E.; Guengerich, F. P. *Biochemistry* 1982, 21, 1090-1097.
- (24) Hou, C. T.; Patel, R.; Laskin, A. I.; Barnabe, N.; Marczak, I. *Appl. Environ. Microbiol.* 1979, 38, 135-142.

Received for review October 25, 1990. Accepted February 25,

1991. This research was supported in part by fellowships from the National Science Foundation, the Switzer Foundation, and the American Water Works Association (Larson Aquatic Research Scholarship), and in part by the Office of Research and Development, U.S. Environmental Protection Agency, through the Western Region Hazardous Substance Research Center, under Agreement R-815738. The contents of this article do not necessarily represent the views of these agencies.

Survey of Potable Water Supplies for *Cryptosporidium* and *Giardia*

Joan B. Rose,^{*,†} Charles P. Gerba,[‡] and Walter Jakubowski[§]

Department of Environmental and Occupational Health, College of Public Health, University of South Florida, 13301 Bruce B. Downs Boulevard, Tampa, Florida 33612, Departments of Microbiology and Immunology and Soil and Water Science, University of Arizona, Tucson, Arizona 85721, and U.S. Environmental Protection Agency, Environmental Monitoring Systems Laboratory, Microbiology Research Division, Cincinnati, Ohio 45268

■ The comparative occurrence of *Cryptosporidium* and *Giardia* was evaluated in 257 water samples from 17 states in the United States. *Cryptosporidium* oocysts were detected in 55% of the surface water samples at an average concentration of 43 oocysts/100 L, while *Giardia* cysts were found in 16% of the same samples at an average concentration of 3 cysts/100 L. *Giardia* and *Cryptosporidium* were more frequently detected in samples from waters receiving sewage and agricultural discharges as opposed to pristine waters. There was no correlation between the concentration of water quality indicator bacteria and either protozoa. Both protozoa were more frequently isolated in the fall than other seasons of the year. The concentrations of both organisms were significantly correlated in all waters. *Cryptosporidium* oocysts were detected in 17% of 36 drinking water samples (0.5-1.7 oocysts/100 L) while no *Giardia* cysts were detected. The widespread occurrence of cysts and oocysts in waters used as supplies of potable water suggests that there is a risk of waterborne transmission of *Cryptosporidium* and *Giardia* infections if the water is not adequately treated.

Introduction

Cryptosporidium and *Giardia* are enteric protozoa that cause waterborne disease. Waterborne giardiasis was first recognized in the United States in 1965, and as of 1988, 106 outbreaks have been reported (1). *Cryptosporidium* has only recently been recognized as a cause of waterborne disease. By the 1980s *Cryptosporidium* was well documented as a cause of diarrheal illness in humans and the first waterborne outbreak was reported in 1985 (2).

Giardia is currently the most frequently identified agent of waterborne disease in the United States; however, in the majority of outbreaks the etiological agent has remained undetermined (1). Although *Cryptosporidium* has been documented in only two waterborne outbreaks, it was responsible for one of the largest outbreaks in the United States since 1920, with an estimated 13 000 individuals affected (3). Not only was the size of the outbreak significant, but the water underwent complete treatment including coagulation, sedimentation, rapid sand filtration, and chlorination (4). Water quality standards for coliforms (<1/100 mL) and turbidity (<1 NTU) were met and disinfection (1.5 mg/L chlorine) was not deficient or inter-

rupted. However, improper or poor operational practices were identified, including poor mixing during coagulation and restarting of dirty filters without backwashing.

Many characteristics that enhance the potential for transmission through water are shared by *Cryptosporidium* and *Giardia*. Both are transmitted by the fecal-oral route, with the infected individual excreting *Cryptosporidium* oocysts or *Giardia* cysts. Animals as well as humans may serve as sources of environmental contamination and human infection. The oocyst and cyst are the environmentally stable stages and both are resistant to inactivation by drinking water disinfectants (5, 6). There is no simple or routine test that can be used to evaluate the occurrence of these protozoa in water, and the bacterial indicator system used to assess microbial water quality may be inadequate for the determination of parasitological water quality (7).

The occurrence of the enteric protozoa in drinking water sources indicates a potential risk for waterborne disease, depending on the level of contamination and the effectiveness of the drinking water treatment. In two previous surveys, 10 and 28% of the surface waters sampled were shown to contain *Giardia* cysts at levels between 0.6 and 5/100 L (8, 9). *Cryptosporidium* oocysts were reported in as many as 77% of the waters examined in the western United States at concentrations of 0.1-94 oocysts/100 L (10). In a study limited to a single watershed, *Cryptosporidium* oocyst concentrations in water were correlated to *Giardia* cyst levels (7).

This survey was undertaken to gain additional information on the comparative occurrence of *Cryptosporidium* and *Giardia* in waters used for potable supplies in the United States. In particular we were interested in the occurrence of cyst and oocyst levels in pristine (more protected watersheds) and polluted waters (receiving sewage and agricultural discharges), seasonal occurrence, and association with other water quality variables.

Materials and Methods

Samples were collected from rivers, streams, lakes (or reservoirs), and springs that were used as sources of drinking water. These sites were identified with the assistance of local water authorities and utilities. Samples were categorized as polluted on the basis of the description of the watershed including public access and use, development, farms, and known point discharges from sewage treatment plants, and as pristine if there was no or little human activity, restricted public access, no agricultural activity within the watershed, or sewage treatment plant

^{*} University of South Florida.

[†] University of Arizona.

[§] U.S. Environmental Protection Agency.

discharges impacting the water upstream from the sampling site. Samples were collected over the period of 1985–1988 throughout the year.

Sampling methods and procedures were adapted from those previously described (11). Samples were collected by passing the water through a 10-in.-long polypropylene yarn-wound cartridge filter (Micro Wynd II, AMF/Cuno, Meriden, CT, 1.0- μ m nominal porosity). For surface waters approximately 400-L samples were filtered. Approximately 1000-L samples were also collected from groundwater and treated drinking water by connecting the filter housing directly to a tap. Samples of backwash waters originating from sand filters at the drinking water treatment plants were also collected. Because of the high turbidity of this water only 10–40-L samples could be collected.

After the samples were collected, the filters were removed from the housing, placed in large Zip-loc plastic bags, and shipped on ice to the laboratory for processing. Most filters were processed within 2–4 days; however, in a few cases, the filters were kept at 4 °C for 7–10 days prior to processing.

Oocysts and cysts were recovered from the filter by first backwashing the filter with deionized (DI) water containing 0.1% Tween 80. The filter was cut longitudinally, teased apart, separated in halves, and washed in the eluate in a large container on a shaker at top speed (Gyrotory Shaker, Model G76, New Brunswick Sci. Co., Edison, NJ) for 10 min. The filter material was then rinsed and pressed by hand for 1 min or until clean. The washed filter material was discarded, and the eluate was combined and centrifuged at 1200g for 10 min. Final pellet volumes were recorded, half was resuspended into 10–20 mL of 3.7% formaldehyde for *Giardia* analysis, and the second half of the pellet was resuspended into 10–20 mL of 2.5% potassium dichromate for *Cryptosporidium* analysis. Both storage media have been shown to maintain the cyst and oocyst counts for up to 20 weeks (13), and oocysts have been shown to maintain viability when stored in potassium dichromate.

A volume of resuspended pellet equivalent to 100 L for surface water and 400 L for groundwater or drinking water was processed for each parasite by using procedures described by Rose et al. (12). After being washed, the pellet was resuspended in 10 mL of the Tween 80/sodium dodecyl sulfate solution and homogenized and one drop of antifoam agent A (Sigma, St. Louis, MO) was added. The pellet was resuspended in DI water or Tween 80/SDS solution for *Giardia* or *Cryptosporidium* processing, respectively. The mixture was sonicated for 4 min in a water bath (Branson ultrasonic cleaner 25 KHz, Shelton, CT), and layered onto sucrose [1.24 specific gravity (g/mL), 500 g of sucrose, 320 mL of DI water, and 9.7 mL of liquid phenol, diluted 4/5], for *Cryptosporidium*, and potassium citrate (1.24 g/mL, approximately 56%) was used for *Giardia* (12). Following centrifugation, the top and interface layers and 10 mL of the flotation medium were collected, diluted with DI water in a 1/3 ratio, pelleted, and resuspended in an appropriate volume (1–10 mL) of DI water, depending on the size of the pellet. The final concentrate was filtered through 13-mm-diameter cellulose nitrate membrane filters of 1.2- μ m porosity for *Cryptosporidium* and 5.0- μ m porosity for *Giardia*. Between two and six replicate membranes were needed to filter the entire sample, depending on the turbidity of the suspension.

The samples were stained with monoclonal antibodies directly on the filters while in the housing. Both direct and indirect immunofluorescence procedures were used to

analyze the samples, depending on the antibodies. The development and evaluation of this methodology and antibodies that were used in this study are described in detail by Rose et al. (13). *Cryptosporidium* monoclonal antibodies used in this study were obtained from Dr. Charles R. Sterling, (Dept. of Veterinary Sciences, University of Arizona, Tucson, AZ) and the *Giardia* monoclonal was obtained from Meridian Diagnostics (Cincinnati, OH) (14–16). A second *Giardia* monoclonal antibody was provided courtesy of John L. Riggs (California State Health Department, Berkeley, CA) (17). Goat anti-mouse IgG or IgM(u) antibodies directly conjugated to fluorescein isothiocyanate (FITC) were obtained from Kirkegaard and Perry (Gaithersburg, MD) for an indirect fluorescence procedure.

The filters were removed from the housing and mounted in 50% glycerol phosphate buffered saline (pH 8.0), and cover slips were applied. The entire filter was examined by (200 \times) magnification and epifluorescence microscopy (Olympus BHTU epifluorescence microscope, New Hyde Park, NY). *Cryptosporidium* and *Giardia* were identified at 400 \times magnification from the following criteria: (1) bright apple-green fluorescing objects outlined by specific intense fluorescence on the outside wall of the cyst- or oocyst-like objects; (2) appropriate size and shape. For *Giardia*: oval (8–18 μ m long by 5–15- μ m wide). For *Cryptosporidium*: spherical (4–6 μ m in diameter), characteristic folding in the oocyst wall.

The numbers of cysts and oocysts were calculated per equivalent volume examined.

Methods were evaluated by seeding known levels of oocysts and cysts into tapwater (up to 400 L) or secondary sewage effluent (up to 200 L). After the sample was processed as previously described, percent recoveries were calculated. All data for environmental samples were reported as true oocysts and cyst counts and were not adjusted for recovery efficiencies for each type of water sampled, due to the logistics in running that many seeded samples and potential for contamination of environmental samples.

Grab samples were collected in addition to filtered samples for analysis of turbidity, total coliform bacteria, fecal coliform bacteria, and in a few cases fecal streptococci bacteria and heterotrophic plate count (HPC) bacteria. Standard methods were employed using a turbidimeter, multiple tube fermentation, membrane filtration for coliforms and fecal streptococci, and spread plate techniques on plate count agar for HPC (18).

Each sample was defined by location, date of collection, water type, and treatment (if applicable) and categorized as polluted or pristine. Pristine samples were those coming from watersheds with little human activity, receiving no agricultural discharges or domestic sewage discharges. This information and results of each sample for the protozoa, bacteria, and turbidity were entered on a dBase III Plus program (Ashton-Tate) using an IBM personal computer. Samples were sorted by location, type of water, season, and pristine or polluted categories. Counts for cysts, oocysts, and bacterial colony forming units were transformed for analysis [$\log_{10} (y + 1)$] for all samples. Geometric averages were calculated. Pearson's correlation coefficients were developed for turbidity and each protozoan, total coliforms and the protozoa, fecal coliforms and the protozoa, and *Giardia* and *Cryptosporidium*. The SPSS-X statistical package (SPSS Inc., Chicago, IL) was used on the VAX/VMS computer at the University of Arizona Computer Center. Two-way and two-by-four-way contingency tables were set up for determining association

Table I. Surface Water Samples Collected and Analyzed for *Cryptosporidium* and *Giardia*

state	water type	total sample no. (pristine) ^a	<i>Cryptosporidium</i>		<i>Giardia</i>	
			no. positive (pristine) ^a	av ^b oocysts/ 100 L	no. positive (pristine) ^a	av ^b cysts/100 L
Az	river	32 (20)	14 (6)	4400	3 (2)	3.3
	lake	22 (19)	9 (7)	170	4 (4)	5.0
AR	spring	2 (2)	2 (2)	8	0	<0.25 ^c
CA	river	14 (12)	6 (4)	4	1 (1)	12
	lake	7 (7)	7 (7)	6	0	<1 ^d
CO	river	2 (1)	2	280	0	<1
CN	river	9 (8)	2 (2)	4	1 (0)	2.0
	lake	4 (0)	2	<1	0	<1
FL	river	3 (0)	2	5	0	<1
GA	river	2 (2)	0	<1	0	<1
HI	spring	1 (1)	1	0.25	0	<0.25
MA	lake	1 (1)	1	3	0	<1
MI	river	1 (1)	0	<1	0	<1
MO	river	3 (1)	2 (0)	8	0	<1
NY	river	5 (3)	1 (1)	2	1 (0)	2.0
	lake	6 (3)	2 (1)	1	0	<1
	spring	3 (3)	0	<0.25	0	<0.25
OR	river	7 (4)	4 (2)	3	0	<1
	lake	1 (1)	0	<1	0	<1
	spring	1 (1)	1	13	0	<0.25 ^c
PA	lake	2 (0)	0	<1	0	<1
TX	river	1 (0)	1	20		
	lake	4 (3)	4 (3)	92	1 (0)	3.0
UT	river	29 (5)	23 (4)	1300	8 (1)	140
	lake	23 (0)	16	380	9	30
WA	river	3 (3)	0	<1	0	<1

^a Number of samples in the pristine category. ^b Arithmetic averages for all positive samples. ^c Sample volume was 400 L; detection limit was <1/400 L. ^d Sample volume was 100 L; detection limit was <1/100 L.

Table II. Summary of *Cryptosporidium* and *Giardia* Occurrence in Surface Waters by Pristine versus Polluted Categories

sample category	sample no. in category	sample no. positive for <i>Cryptosporidium</i>	sample no. positive for <i>Giardia</i>	geometric av for oocysts/100 L	geometric av for cysts/100 L
surface waters	181	93	28	43	3
rivers	111 ^a	57 ^a	14	43	4
polluted	38	28	10	66 (29000) ^b	11 (625) ^b
pristine	59	19	4	29 (24000) ^b	0.35 (12) ^b
lakes	70 ^a	39 ^a	14	44	3
polluted	24	14	8	103 (7200) ^b	6.5 (156) ^b
pristine	34	18	4	9.3 (307) ^b	0.5 (7) ^b

^a Values within a category do not add up to the total value since some samples could not be defined as to pollution category. ^b Maximum values in a single sample.

between cyst or oocyst presence and the two water categories and four seasons. Significant associations were tested by using a χ^2 analysis.

Results

Oocyst and cyst method recoveries were evaluated throughout the study by seeded trials using tapwater and activated sludge treated sewage effluent. Sample sizes ranged from 378 (tapwater) to 20 L (sewage effluent). This represented the range of the types of water we were sampling (treated potable waters to those waters highly influenced by sewage discharges). Recovery efficiencies were 29–58% for *Cryptosporidium* and 13–22% for *Giardia* and these are in the ranges previously reported in a variety of wastewaters, surface waters, and tapwaters (9–12).

A total of 188 surface water samples were collected from 17 states (Table I). The majority of surface water samples were taken from the western states, in particular Arizona, California, and Utah (126), while the remaining samples came from the eastern (28), northwestern (14), southern (13), and midwestern (6) states, with one sample from Hawaii. The results in Table I show the arithmetic av-

erages for positive samples only, reflecting peak values without consideration of prevalence (percent positive) in the various water types by state for *Cryptosporidium* oocysts and *Giardia* cysts. Detection limits were 1/100 L for rivers and lakes and 1/400 L for spring waters.

Cryptosporidium oocysts were found in a greater number of samples than *Giardia* cysts and at higher concentrations. In some waters receiving wastewater discharges from sewage treatment plants and agricultural discharges (Arizona, Colorado, Texas, and Utah), high numbers of oocysts were detected. Maximum numbers were 7100, 550, 308, and 29 000/100 L (Arizona, Colorado, Texas, and Utah, respectively) for *Cryptosporidium* oocysts, and a maximum of 625 *Giardia* cysts/100 L was found in Utah waters.

Table II summarizes the occurrence of *Cryptosporidium* and *Giardia* in rivers and lakes as defined by water type and pollution category. Of the 181 river and lake water samples, 93 were categorized as pristine (receiving no sewage, agricultural, or domestic animal discharges). These sites were identified by water authorities and utilities where there was little human habitation and public access

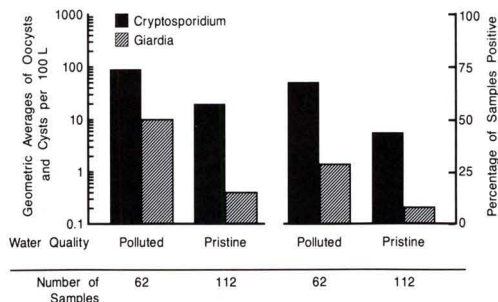


Figure 1. Occurrence of *Cryptosporidium* oocysts and *Giardia* cysts in polluted versus pristine waters.

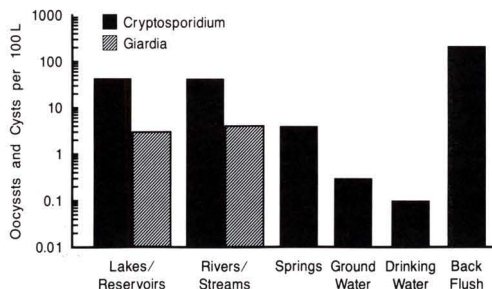


Figure 2. Geometric averages for *Cryptosporidium* oocysts and *Giardia* cysts in various water types.

was controlled. In both river and lake samples, a greater prevalence of *Cryptosporidium* and *Giardia* was observed in the polluted category. Average oocyst and cyst levels were 11 and 13 times greater, respectively, in the polluted as opposed to pristine lake samples. In river samples, average oocysts levels were 2.2 times greater and average cyst levels were 31 times greater in the polluted category.

Seven springs were also included in the pristine category, as well as 12 groundwater samples. Twenty-six samples were undefined by pollution category and were excluded, and six groundwater samples were excluded as fluorescein tracer studies had demonstrated a plume of contamination in the well field. *Cryptosporidium* oocysts and *Giardia* cysts were detected in 39 and 7% of all pristine water samples and averaged 20 oocysts/100 L and 0.4 cysts/100 L, respectively (Figure 1). In contrast, unprotected waters impacted by some type of discharge (sewage or agricultural) had *Cryptosporidium* in 68% of the samples with an average of 91 oocysts/100 L and *Giardia* in 29% of the samples at an average level of 10 cysts/100 L. The association between classification of a water (as polluted or pristine) and frequency of *Giardia* cyst or *Cryptosporidium* oocyst detection was evaluated with a two-way contingency table and χ^2 test of association. The χ^2 was 13.5 and 9.2 with $p < 0.005$ at one degree of freedom for *Giardia* and *Cryptosporidium*, respectively, indicating a statistically significant association between the categories of water defined in our study and the frequency of detection of these organisms.

Geometric means [$\log_{10}(y + 1)$] for all samples were calculated for the protozoa in each category of water type (Figure 2). *Giardia* cysts averaged 3 and 4/100 L in lake/reservoir and river/stream samples, respectively. *Cryptosporidium* oocyst levels were approximately 10 times higher in the surface waters (44/100 L for lake/reservoir samples and 43/100 L for river/stream samples). Spring waters had an average of 4 oocysts/100 L. Six of 36 drinking water samples were positive for oocysts and

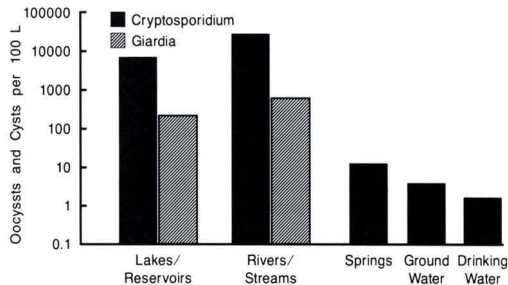


Figure 3. Peak levels of protozoan contamination in a single sample in various water types.

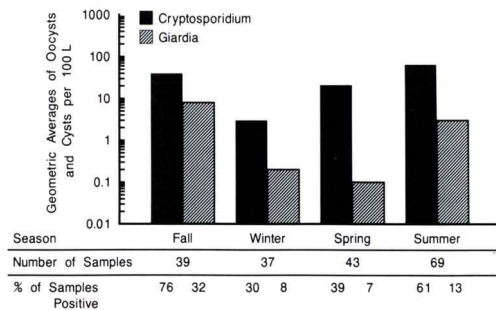


Figure 4. Seasonal occurrence of *Cryptosporidium* oocysts and *Giardia* cysts in surface waters.

the geometric average was 0.1 oocysts/100 L. One of 18 groundwater samples was positive (4/100 L, average of 0.13 oocysts/100 L). Backwash samples from rapid sand filters produced the highest average concentration of oocysts (217/100 L).

The maximum concentrations of *Cryptosporidium* oocysts and *Giardia* cysts found in a single sample were contrasted in the various water types (Figure 3). Table II contains the maximum values in the various water pollution categories. Peak concentrations of oocysts and cysts were approximately 4 and 3 times greater, respectively, in polluted river water as compared to polluted lake water. Peak concentrations of *Cryptosporidium* oocysts were 10–100 times greater than *Giardia* cyst levels. The maximum concentrations of *Cryptosporidium* in pristine and polluted rivers were very similar, while maximum *Giardia* cyst concentrations in the same waters were over 50 times greater in polluted water as compared to pristine water. Maximum *Cryptosporidium* concentrations in springs, groundwater, and drinking water were much lower, ranging from 1.7 to 13 oocysts/100 L.

Surface water samples were sorted by season (June, July, and August as summer; September, October, and November as fall, etc.) and geometric averages were determined for *Cryptosporidium* oocysts and *Giardia* cysts (Figure 4). The average concentrations of oocysts were the highest in the summer and fall (65 and 40/100 L, respectively). A similar pattern was also observed for average cyst concentrations (3 and 8/100 L in the summer and fall, respectively). Both oocyst and cyst concentrations were low in the winter (3 and 0.2/100 L, respectively), and in the spring only oocyst levels increased (21/100 L). The number of samples collected in the summer was 1.7–1.9 times greater than in the fall, winter, or spring. The association of oocyst and cyst occurrence with season was evaluated by using a two by four-way contingency table and the χ^2 test. A significantly greater percentage of samples ($p = 0.01$) were positive for cysts and oocysts in the fall. The

Table III. Geometric Averages for *Cryptosporidium*, *Giardia*, and Bacteria Concentrations by Water Type

water type	<i>Cryptosporidium</i> oocysts/100 L	<i>Giardia</i> cysts/100 L	turbidity, ^a NTU	total coliforms, CFU/100 mL	fecal coliforms, ^b CFU/100 mL	fecal streptococci, ^b CFU/100 mL	HPC, ^c CFU/mL
lakes/reservoirs	44	3	30	21	7.9	7.0	1700
rivers/streams	43	4	25	40	16	3.7	14000
springs	4	<0.25	3.5	7	ND	ND	6000
groundwater	0.3	<0.25	0.18	11	<1	ND	3900
drinking water	0.1	<0.25	0.7	<1	ND	ND	50

^a Arithmetic averages. ^b ND, not determined. ^c Heterotrophic plate count.

Table IV. Correlation Coefficients for Turbidity, Total Coliform Bacteria, Fecal Coliform Bacteria, *Cryptosporidium*, and *Giardia* in Surface Waters

	turbidity ^a	total ^b coliforms	fecal ^c coliforms	<i>Cryptosporidium</i> ^d
<i>Cryptosporidium</i>	0.204	-0.032	0.026	1.0
<i>Giardia</i>	0.208	0.012	0.087	0.544 ^e

^a N = 121. ^b N = 70. ^c N = 73. ^d N = 196. ^e Significant at p < 0.001.

χ^2 was 12.3 and 12.1 for *Giardia* and *Cryptosporidium*, respectively, at three degrees of freedom with p < 0.01.

To determine whether season or pollution category was influencing the results of the statistical associations, the samples were sorted in respect to these variables. The samples were almost equally distributed between polluted and pristine categories for the fall (52 and 48%) winter (55 and 45%), and spring (60 and 40%) collections. In the summer, 81% of the samples fell into the pristine category; however, this apparently did not affect the trend as higher numbers of oocysts and cysts were demonstrated in the summer and fall collections. Samples from the polluted category were fairly evenly distributed among the seasons (34%, fall; 22%, winter; 24%, spring; and 19%, summer). The high percentage of pristine samples (54%) that was collected in the summer as opposed to 20, 11, and 14% that were collected in the fall, winter, and spring, respectively, did not influence the lower prevalence or numbers of oocysts and cysts found in the pristine category.

Geometric averages [log₁₀ (y + 1)] for both positive and negative samples for total coliforms, fecal coliforms, fecal streptococci, and HPC were calculated for samples from various water types and arithmetic averages were calculated for turbidity (Table III). Turbidity averaged 0.7 NTU in drinking water samples, with only one sample greater than 1 NTU (3.0 NTU), and was low in groundwater (0.18 NTU). Turbidity was higher in samples from springs (3.5 NTU), and averaged 25 and 30 NTU in river and lake samples, respectively. Total coliforms ranged from 7 to 40 CFU/100 mL and were not detected in drinking water. Fecal coliforms averaged 16 and 7.9 CFU/100 mL while fecal streptococci averaged 3.7 and 7 CFU/100 mL in rivers and lakes, respectively. The HPC counts averaged 50, 3900, 6000, 14 000, and 17 000 CFU/mL in drinking water, groundwater, springs, rivers, and lakes, respectively.

Correlation coefficients were developed for files with complete data sets in surface water samples, and no associations were observed between either protozoan and turbidity, total coliforms, or fecal coliforms. The concentrations of *Cryptosporidium* oocysts and *Giardia* cysts were significantly correlated, with an r = 0.544 at p < 0.001 (Table IV).

The surface water samples (126) from Arizona (AZ), California (CA), and Utah (UT) were sorted and evaluated separately from a category designated "all other samples" (62, surface water samples). This was done to evaluate the

Table V. Prevalence and Geometric Averages of *Cryptosporidium* Oocysts in Treated Drinking Water

	type of treatment		
	conventional ^a	direct filtration	disinfection only
sample no.	17	11	6
no. of positive samples	2	2	2
geometric av for oocysts/100 L	0.04	0.08	0.20

^a Coagulation, sedimentation, sand filtration, and disinfection.

Table VI. *Cryptosporidium* Oocyst Concentrations, Disinfectant Residuals, and Turbidity in Treated Drinking Water^a

source water ^b	filtration	disinfectant		turbidity, NTU	oocyst/ 100 L
		type	mg/L		
river	conventional	chlorine	0.82	0.24	0.73
	rapid sand				
river	direct ^c	chlorine	0.9	0.5	0.57
river	dual media ^b	chlorine	1.01	0.18	0.5
river	none	chloramine	1.1	0.32	1.7
spring	none	chlorine	0.4	3.0	0.11

^a Total coliforms were <1/100 mL for all five samples. ^b First two rivers in polluted category last two rivers in pristine category; spring influenced by a nearby river flow in polluted category. ^c Coagulant mixer inoperable. ^d No coagulants used.

bias of the large number of samples collected in these states in determining trends. In both groups of samples (AZ, CA, and UT versus all other samples), similar trends were seen between the polluted and pristine categories, as previously described. A greater percentage of samples from the polluted category of waters were positive for *Cryptosporidium* oocysts and *Giardia* cysts as compared to the samples from the pristine category. In addition, the greater percentage of positive samples was found in the fall months.

The occurrences of *Cryptosporidium* oocysts in drinking water were categorized by the type of treatment the water had received. Oocysts were detected in 6 of 36 drinking water samples (400–1000 L) (Table V). In five of the positive samples, data were available on filtration, disinfection, and turbidity (Table VI). Where filtration was not used, one of the positive unfiltered samples had a turbidity (3.0 NTU) exceeding the current standard. The highest oocyst concentration detected (1.7 oocysts/100 L) also came from a water that was unfiltered. Oocysts were detected from a facility using direct filtration; however, the coagulant mixer was inoperable during sample collection. Another oocyst-positive result came from drinking water receiving direct filtration without the use of coagulants. There were no reported problems in the conventional treatment facility using rapid sand filtration in which oocysts were detected.

Table VII. Studies on the Occurrence of *Cryptosporidium* in Water Using Various Antibodies

study/antibodies used	water type	total sample no. collected	% positive	geometric av oocysts/100 L
Ongerth and Stibbs (19)/polyclonal rose (10)/IgG ^b	river ^a	11	100	115
	lake	32	75	91
	river	58	77	94
	pristine waters	6	100	2
	polluted waters	6	83	99
Stetzenbach et al. (27)/IgM ^c	lake	44	29	89
	river	24	29	35
	pristine river	21	65	63
this study/IgG ^b 1985-1986	polluted river	13	83	148
	pristine lake	4	50	34
	polluted lake	14	88	244
	pristine river	38	29	0.9
	polluted river	25	51	24
IgM ^c 1987-1988	pristine lake	30	47	5
	polluted lake	10	38	2

^aPrimarily pristine waters. ^bAntibody courtesy of Dr. Charles R. Sterling. ^cAntibody from Meridian Diagnostics.

Table VIII. Studies on the Occurrence of *Giardia* in Water Using Various Antibodies

study/antibodies used	water type	total sample no. collected	% positive	geometric av cysts/100 L
Ongerth and Stibbs (9)/polyclonal	river ^a	222	43	0.3 ^b
				4
Rose (12)/IgG ^d	pristine river	3	(57) ^c	6
	polluted river	8		0.9 ^b
	polluted lake	10		120
this study/IgG ^d 1985-1986	polluted lake	10		35
	pristine river	21	4	0.08
	polluted river	13	28	13
	pristine lake	4	0	0
	polluted lake	14	47	12
IgG ^c 1987-1988	pristine river	38	9	0.5
	polluted river	25	15	6.1
	pristine lake	30	12	1.2
	polluted lake	10	15	1.3

^aThree separate watersheds, mostly pristine. ^bArithmetic averages. ^cPercentage for all samples. ^dAntibody courtesy of Dr. John Riggs. ^eAntibody from Meridian Diagnostics.

Discussion

Information on the occurrence and concentrations of pathogenic microorganisms in water sources to be used as potable water supplies is critical to ensure proper treatment to protect public health. Surveys such as this one help provide information on what types of supplies may require more treatment than others and help identify seasonal and other environmental factors that influence the occurrence and concentrations of microbial pathogens. This study reports on the most extensive survey to date comparing the relative occurrence of both *Giardia* and *Cryptosporidium* in surface water supplies in the United States. This study attempted to apply the most recent advances in the detection of these protozoan parasites in water (11-13, 19) after a thorough evaluation of the efficiencies of these methods. Hibler reported (8) the most extensive study of waters (more than 4423 samples) for *Giardia* using light microscopy without the aid of antibodies. He found *Giardia* prevalence at 17-41% in lakes, rivers, and creeks. In our study, *Giardia* was detected in 16% of surface waters. Only 3% of the groundwater samples (63 wells) were positive in the Hibler study, and 3.4% of the drinking water samples (357 samples postconventional treatment) were positive for *Giardia*. In our study, no *Giardia* were detected in groundwaters or drinking waters but fewer samples were examined.

This study has demonstrated no association between the protozoa and bacterial indicators. Other surrogates appear to be needed to define water quality to enable determination of the potential risk of enteric protozoan contamination.

In pristine waters indigenous animals may contribute significant numbers of oocysts and cysts to a water system on occasion. Domestic animals, particularly cattle, may also be sources of water contamination (8, 20-23).

Cryptosporidium oocysts were generally detected more often than *Giardia* cysts in every type of water and the concentrations of oocysts averaged 1 log greater than *Giardia* cysts. This may reflect the widespread occurrence of *Cryptosporidium* in a variety of animals. However, the levels of oocysts and cysts in all water samples were found to be significantly correlated. This supports a similar report of concurrent contamination in a single watershed (7).

The seasonal occurrence of *Cryptosporidium* oocysts and *Giardia* cysts in water may be related to the seasonal occurrence of infections. Tzipori (24) in a recent review summarized the frequency of cryptosporidiosis in humans in Asia, the Pacific, America, Europe, and Africa. In 17 of 30 reports, the peak season was found to be in the summer or autumn, while only one study reported peak infections in the winter. Daly et al. (25) found that cases of giardiasis increased in midsummer and peaked in September. In a 7-year period, most of the *Giardia*-positive patients were observed in the late summer, with minimum numbers of patients in the winter (26).

Several previous studies have examined a variety of waters for the occurrence of *Cryptosporidium* and *Giardia* (Tables VII and VIII), (9, 10, 12, 19, 27). Each study employed slightly different recovery methods and different antibodies for detection. The specificity of these antibodies

to human versus animal isolates and their nonspecific binding to other organisms in water samples are variable or unknown. In addition, the method recoveries, water quality, watershed characteristics, and seasonal trends were diverse or unspecified.

Only one investigation to our knowledge has been undertaken to compare various antibodies for cyst and oocyst detection in environmental samples (13). To summarize briefly, the *Cryptosporidium* IgM MAb and the *Giardia* IgG (Riggs) MAb appear to be more specific for the detection of human isolates as they did not demonstrate fluorescence with one bird species (*Cryptosporidium baileyi*) or a mouse isolate (*Giardia muris*), respectively. Both *Giardia* MAb detected fewer cysts when compared to a polyclonal antibody, and the IgG MAb (Riggs) detected less than the other MAb (Meridian). In limited comparisons no differences were observed among antibodies (including those in our study) for sewage samples (13).

In this study and others (10, 19, 27) it appears that the antibodies that were less species specific for *Cryptosporidium*, including the polyclonal and the IgG, resulted in a higher percentage of samples positive and greater concentrations of oocysts than the more specific IgM antibody (Table VII). This was particularly apparent in the pristine water category. Although not as consistent or dramatic for *Giardia*, the more species-specific antibody (the IgG Riggs) did result in data of lower cyst prevalence and cyst concentrations in the pristine water category (9, 12) (Table VIII). The pollution categories remained distinctive regardless of the antibodies except in the case of the lake samples collected in 1987 and 1988.

These data suggest that, particularly in pristine waters, antibodies that are more specific for the species that may infect humans may result in lower counts of *Cryptosporidium* oocysts and *Giardia* cysts and may be more reflective of a human health risk. Further investigations are needed in regard to speciation, cross-infectivity, and antibody specificities for the enteric protozoa.

The occasional finding of *Cryptosporidium* oocysts in drinking water is a concern from a public health viewpoint, considering the low infectious dose of this organism (28) and its resistance to disinfectants (6). The turbidity of the treated water was below the current standard of 1 NTU in most cases, and coliform levels were in compliance. Filtration was being used in three plants, and these data as well as the large outbreaks in Carrollton (3) and Oxford and Swindon (29) demonstrate that currently we have no way of evaluating the operational parameters of a filtration plant for oocyst removal, and the adequacy of disinfection is questionable (6). There is no doubt that filtration can remove oocysts, as in some cases, large numbers of oocysts were detected in the backwash from filters. This could also be significant as backwash waters are often recycled through a plant to conserve water. The recycling of backwash waters was suggested as a possible contributing factor in the outbreak in England (29).

The consumption of nonpotable surface waters has been associated with cryptosporidiosis (30). Bennet et al. (31) have suggested that 60% of all *Giardia* infections in the United States are a result of ingesting contaminated waters (probably from both potable and nonpotable supplies, although this was not defined). The role of potable waters in the acquisition of enteric protozoan infections needs to be further evaluated. In evaluating the health significance of oocyst and cyst contamination of water, we are uncertain of viability, infectivity, and specificity of the pathogen to humans. Currently, we are unable to determine oocyst or cyst viability in environmental samples. Regardless of this

limitation, the occurrence of potential pathogens in source waters may pose a significant health hazard to the exposed population, depending on a number of factors, including the level of the contamination and the degree of treatment to achieve potable water. This survey has demonstrated the widespread occurrence of *Cryptosporidium* and *Giardia* in untreated surface waters. We need to further assess pathogen distributions in water, the potential peaks of contaminants entering a drinking water supply, and the survival, transport, and infectivity of the oocyst and cyst in the environment. These data can then be used with a risk assessment approach to develop appropriate control strategies (32).

Acknowledgments

We thank the numerous individuals in the water industry who assisted us with the sampling of waters. We acknowledge Susan Kutz, Kelley Riley, Hamid Darbin, and Morteza Nakhforoosh for their contribution in processing the samples. We also thank Dr. Judith Sauch and Dr. Frank Schaefer of the U.S. EPA (Cincinnati, OH) for their assistance in preparation of this article.

Literature Cited

- (1) Craun, G. F. *Water Sci. Technol.*, in press.
- (2) D'Antonio, R. G.; Winn, R. E.; Taylor, J. P.; Gustafson, T. L.; Current, W. L.; Rhodes, M. M.; Gary, G. W.; Zajac, R. A. *Ann. Int. Med.* 1985, 103, 886-888.
- (3) Hayes, E. B.; Matte, T. D.; O'Brien, T. R.; McKinley, T. W.; Logsdon, G. S.; Rose, J. B.; Ungar, B. L. P.; Word, D. M.; Pinsky, P. F.; Cummings, M. L.; Wilson, M. A.; Long, E. G.; Hurwitz, E. S.; Juranek, D. D. *N. Eng. J. Med.* 1989, 320, 1392-1376.
- (4) Mason, L. In *Proceedings of the Water Quality Technology Conference*, Nov 15-20, 1987, Baltimore, MD; American Water Works Association: Denver, CO, 1988; pp 889-898.
- (5) Sobsey, M. D. *Water Sci. Technol.* 1989, 21, 179-195.
- (6) Peeters, J. E.; Mañas, E. A.; Masschelein, W. J.; Martinez de Maturana, I. V.; Debacker, E. *Appl. Environ. Microbiol.* 1989, 55, 1519-1522.
- (7) Rose, J. B.; Darbin, H.; Gerba, C. P. *Water Sci. Technol.* 1988, 20, 271-276.
- (8) Hibler, C. P. *Advances in Giardia Research*; Wallis, P., Hammon, B., Eds.; University of Calgary Press: Calgary, AB, Canada, 1988; pp 237-245.
- (9) Ongerth, J. *Am. Water Works Assoc.* 1989, 81, 81-86.
- (10) Rose, J. B. *J. Am. Water Works Assoc.* 1988, 80, 53-58.
- (11) Musial, C. E.; Arrowood, M. J.; Sterling, C. R.; Gerba, C. P. *Appl. Environ. Microbiol.* 1987, 53, 687-692.
- (12) Rose, J. B.; Kaye, D.; Madore, M. S.; Gerba, C. P.; Arrowood, M. J.; Sterling, C. R. In *Advances in Giardia Research*; Wallis, P., Hammon, B., Eds.; University of Calgary Press: Calgary, AB, Canada, 1988; pp 205-209.
- (13) Rose, J. B.; Landeen, L. K.; Riley, K. R.; Gerba, C. P. *Appl. Environ. Microbiol.* 1989, 55, 3189-3196.
- (14) Sterling, C. R.; Arrowood, M. J. *Pediatr. Infect. Dis.* 1986, 5, 5139-5142.
- (15) Garcia, L. S.; Brewer, T. C.; Bouckner, D. A. *J. Clin. Microbiol.* 1987, 25, 119-121.
- (16) Sterling, C. R.; Kutob, R. M.; Gizinski, M. J.; Verastequi, M.; Stetzenbach, L. D. In *Advances in Giardia Research*; Wallis, P., Hammon, B., Eds.; University of Calgary Press: Calgary, AB, Canada, 1988; pp 219-222.
- (17) Stibbs, H. H.; Riley, E. T.; Stockard, J.; Riggs, J. L.; Wallis, P. M.; Isaac-Renton, J. In *Advances in Giardia Research*; Wallis, P., Hammon, B., Eds.; University of Calgary Press: Calgary, AB, Canada, 1988; pp 159-163.
- (18) *Standard Methods for the Examination of Water and Wastewater*, 16th Ed., American Public Health Association (APHA), American Water Works Association, and Water Pollution Control Federation: Washington, DC, 1985.
- (19) Ongerth, J. E.; Stibbs, H. H. *Appl. Environ. Microbiol.* 1987, 53, 672-676.

- (20) Current, W. L. *CRC Crit. Rev. Environ. Control* 1987, 17, 21-51.
- (21) Fayer, R.; Ungar, B. L. P. *Microbiol. Rev.* 1986, 50, 458-483.
- (22) Erlandsen, S. L.; Bemrick, W. J. In *Advances in Giardia Research*; Wallis, P., Hammond, B., Eds.; University of Calgary Press: Calgary, AB, Canada, 1988; pp 227-236.
- (23) Erlandsen, S. L.; Sherlock, L. A.; Januschka, M.; Schupp, D. G.; Schaefer, F. W.; Jakubowski, W.; Bemrick, W. J. *Appl. Environ. Microbiol.* 1988, 54, 2777-2785.
- (24) Tzipori, S. *Adv. Parasitol.* 1988, 27, 63-129.
- (25) Daly, J. J.; Gross, M. A.; McCullough, D.; McChesney, T.; Tank, S. K.; Daly, E. B.; Puskarich, C. L. In *Advances in Giardia Research*; Wallis, P., Hammond, B., Eds.; University of Calgary Press: Calgary, AB, Canada, 1988; pp 71-74.
- (26) Pasley, J. N.; Daly, J. J.; McCullough, D.; Eds.; McChesney, T.; Daly, E. B.; Tank, S. K. *Chronobiol. Int.* 1989, 6, 185-190.
- (27) Stezenbach, L. D.; Arrowood, M. S.; Marshall, M. M.; Sterling, C. R. *Water Sci. Technol.* 1988, 20, 193-198.
- (28) Miller, R. A.; Bronsdon, M. A.; Morton, W. R. *J. Infect. Dis.* 1990, 161, 312-315.
- (29) Smith, H. V.; Rose, J. B. *Parasitol. Today* 1990, 6, 8-12.
- (30) Gallaher, M. M.; Herndon, J. L.; Nims, L. J.; Sterling, C. R.; Grabowski, D. J.; Hull, H. F. *Am. J. Public Health* 1989, 79, 39-42.
- (31) Bennett, J. V.; Holmberg, S. D.; Rogers, M. F.; Solomon, S. L. *Am. J. Prev. Med.* 1987, 3, 102-114.
- (32) Rose, J. B.; Haas, C. N.; Regli, S. *Am. J. Public Health*, in press.

Received for review December 5, 1989. Revised manuscript received July 10, 1990. Accepted February 25, 1991. This document has been reviewed in accordance with U.S. Environmental Protection Agency policy through CR-813536 to the University of Arizona and approved for publication. Approval does not signify that the contents necessarily reflect the view or policies of the Agency, nor does mention of trade names or commercial products constitute endorsement or recommendation for use.

Influence of the Environment on the Patina of the Statue of Liberty

Richard A. Livingston*

Geology Department, University of Maryland, College Park, Maryland 20742

■ The copper corrosion layer, or patina, of the Statue of Liberty now shows a variation in color from one point to another that is associated with local variations in the mineralogy of the patina. It has been proposed that the color patterns are the result of attack by acid rain. To investigate this problem, a set of copper mineral phase diagrams has been prepared, which display the stability domains and solubilities as a function of the major anions (SO_4^{2-} , Cl^- , H^+ , and HCO_3^-) found in rainwater. These diagrams provide the basis for a geochemical model of the patina's mineralogy. The model predicts that acid rain, at the pH levels observed in rainfall in New York City, cannot affect the mineralogy or solubility of the patina. The color patterns appear to be related to the direction of the prevailing wind, which determines where the rainwater contacts the Statue. The rainwater in turn stabilizes the sulfate copper minerals over the chloride ones. These patterns may be more prominent now than in the past because of reductions in ambient SO_2 levels in the intervening years.

I. Introduction

The restoration work on the Statue of Liberty, which was completed in 1986, was designed to eliminate the galvanic corrosion between the copper skin and the wrought iron framework. However, during the course of the work another aspect of the corrosion of the copper came to light. Baboian and Cliver (1) observed that there were systematic differences in the composition of the minerals of the corrosion layer, or patina, at different points around the Statue of Liberty. This caused concern for two reasons. First, since antiquity the patina of a copper or bronze object has been regarded as an important esthetic factor (2). Second, the mineralogy of the patina affects its ability to protect the metal substrate.

Regarding this second point, Nielsen (3) compared samples of the present-day patina with a sample taken

from the Statue of Liberty in 1905 and subsequently kept in storage. He noted that while the basic copper sulfate mineral brochantite ($\text{Cu}_4(\text{OH})_6\text{SO}_4$) was found in samples from both periods, antlerite ($\text{Cu}_3(\text{OH})_4\text{SO}_4$), a mineral with a higher sulfate content, was found only in the modern sample. Acid rain, a phenomenon that has appeared only in the last two or three decades, consists largely of sulfuric acid (4). Nielsen theorized that the acid rain was attacking the brochantite and converting it to antlerite (2). Since the latter is more soluble than the former, Nielsen also conjectured that acid rain may thus be increasing the rate of copper loss from the Statue. Baboian and Cliver extended this conjecture to explain the spatial pattern of color on the Statue. Analysis of old photographs indicated that the patina was uniformly green in the 1960s so that the present distribution of patina color seems to have developed over the same time period during which rain has become more acid in the Northeast United States.

However, acid rain is not the only environmental factor capable of affecting the mineralogy of the patina. Sulfur dioxide gas can react directly with the copper to produce sulfate minerals. Sea salt is another possibility, since Nielsen also found atacamite ($\text{Cu}_4(\text{OH})_6\text{Cl}_2$) in the patina of the Statue. This basic copper chloride is often found in copper patinas in coastal areas exposed to sea-salt particles (5), and therefore, it is not surprising to find it on the Statue, which looks out upon the Atlantic Ocean. Thus, to understand the mineralogy of the patina it is necessary to consider the effects of the aqueous species H^+ , SO_4^{2-} , and Cl^- as well as OH^- , HCO_3^- , and NO_3^- , which are also present.

A basic tool for studying the effect of environmental chemistry on corrosion layer mineralogy is the equilibrium-phase diagram, which is derived from chemical thermodynamics. These phase diagrams were originally developed by Pourbaix (6) to model metallic corrosion as a function of pH and redox potential, pE , but have subsequently been extended to a wide range of environmental variables. Since thermodynamic equilibrium is the basic requirement for constructing these diagrams, they are usually unsuitable for studying short-term kinetics.

* Present address: R. A. Livingston Associates, 2737 Devonshire Place N.W., Washington, D.C. 20008.

However, they can provide constraints on the assemblage of minerals that will be stable over long-term exposure to a given set of environmental conditions.

A number of researchers have previously explored the copper mineral-phase relationships involving these components. Pourbaix himself (7) drew a phase diagram for the five-dimensional system $\text{Cu}-\text{Cl}-\text{CO}_2-\text{SO}_3-\text{H}_2\text{O}$. This system also would be suitable for the situation of the Statue of Liberty. However, Pourbaix's phase diagram used only single values of SO_3 , CO_2 , and Cl based on the chemical composition of drinking water in Brussels. Subsequently, Leckie and Davis (8) prepared a conventional Pourbaix diagram at a fixed level of sulfur (0.1 M). Silman (9) drew up a three-dimensional diagram using Cu^{2+} , pH, and SO_4^{2-} as the axes. Kucera and Mattson (10) constructed a two-dimensional diagram with axes of pH and SO_4^{2-} at a fixed level of Cu^{2+} , as did Graedel (11). To investigate the stable minerals under a wider range of conditions including carbonate, sulfate, and chloride ions, Woods and Garrels (12) prepared two-dimensional diagrams involving the composite components $(\text{H}^+)^2(\text{Cl})^2$ and $(\text{H}^+)^2\text{SO}_4^{2-}$ rather than pH, Cl^- , and SO_4^{2-} separately. Mann and Deutscher (13) also studied copper mineral stability involving these ions. Their approach consisted of selecting discrete levels of these ions and, for each set of values, finding the least soluble mineral. Boundary lines connecting these known points were then drawn by interpolation.

However, all these previous studies have in common the drawback that Pourbaix-type diagrams are inconvenient for investigating the region of greatest interest concerning the effect of acid rain on the Statue of Liberty, i.e., the interface between the solution and the solid phases of the corrosion layer. At this interface, the presence of the cation Cu^{2+} in the solution introduces an additional variable, leading to a three- or four-dimensional figure. As noted above, previous investigators have usually dealt with this problem by selecting one or more discrete values of Cu^{2+} . This then makes it possible to construct two-dimensional phase diagrams in which the solution/surface interface appears as a set of contours. However, during reactions with acid rain Cu^{2+} concentration varies continuously. These processes are difficult to portray graphically on such a set of contours.

The approach used here eliminates the problem by treating Cu^{2+} as a dependent variable that is a function of the environmental variables SO_4^{2-} , OH^- , and Cl^- . The resulting phase diagram has a unique curve representing the solution/surface interface, which makes it much easier to visualize the processes of environmental degradation of the Statue's patina.

II. Patina Mineral Stability Diagrams

Since the primary concern with acid rain is the potential effect of H^+ (or OH^-) and SO_4^{2-} on the Statue's patina, Figure 1 has been prepared to display the copper mineral stabilities as a function of these two variables. The chemical equations and equilibrium constants used to generate this diagram are summarized in Table I. This diagram was constructed in the usual way established by Pourbaix (5), except for the boundary lines between the solution and the solid phases. Therefore, away from this region of the diagram, the boundaries between solid phases have the same slopes as in a conventional Pourbaix diagram.

The major difference is that the set of lines at the solution/surface interface has been drawn by imposing the constraint of a specified electroneutrality condition on the solubility product of the saturated mineral. This procedure

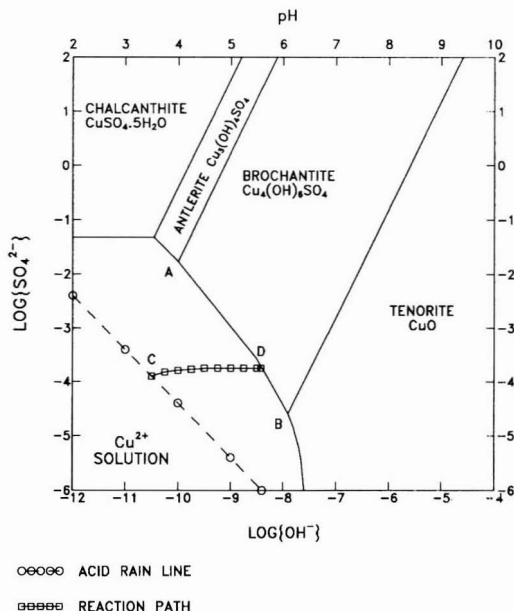
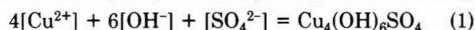


Figure 1. Equilibrium phase diagram for copper minerals as a function of SO_4^{2-} and OH^- activities at 25 °C, $P_{\text{CO}_2} = 10^{-3.5}$ bar and $[\text{Cl}^-] = 0$. Note that the mineral saturation lines are solution bound. All thermodynamic data are taken from Woods and Garrels (16).

Table I. Reactions and Equilibrium Constants

Brochantite Solubility	
$\text{Cu}_4(\text{OH})_6\text{SO}_4 = 4\text{Cu}^{2+} + 6\text{OH}^- + \text{SO}_4^{2-}$	$\log K_{\text{br}} = -68.9$
Antlerite Solubility	
$\text{Cu}_3(\text{OH})_4\text{SO}_4 = 3\text{Cu}^{2+} + 4\text{OH}^- + \text{SO}_4^{2-}$	$\log K_{\text{ant}} = -47.1$
Chalcantite Solubility	
$\text{CuSO}_4 \cdot 5\text{H}_2\text{O} = \text{Cu}^{2+} + \text{SO}_4^{2-} + 5\text{H}_2\text{O}$	$\log K_{\text{ch}} = -2.65$
Tenorite Solubility	
$\text{CuO} + \text{H}_2\text{O} = \text{Cu}^{2+} + 2\text{OH}^-$	$\log K_{\text{tn}} = -20.25$
Atacamite Solubility	
$\text{Cu}_4(\text{OH})_6\text{Cl}_2 = 4\text{Cu}^{2+} + 6\text{OH}^- + 2\text{Cl}^-$	$\log K_{\text{at}} = -69.8$
Antlerite/Chalcantite Stability	
$\text{Cu}_3(\text{OH})_4\text{SO}_4 + 2\text{SO}_4^{2-} + 5\text{H}_2\text{O} = 3\text{CuSO}_4 \cdot 5\text{H}_2\text{O} + 4\text{OH}^-$	$\log K_{\text{antch}} = -39.2$
Brochantite/Antlerite Stability	
$3\text{Cu}_4(\text{OH})_6\text{SO}_4 + \text{SO}_4^{2-} = 4\text{Cu}_3(\text{OH})_4\text{SO}_4 + 2\text{OH}^-$	$\log K_{\text{brant}} = -18.0$
Tenorite/Brochantite Stability	
$4\text{CuO} + 4\text{H}_2\text{O} + \text{SO}_4^{2-} = \text{Cu}_4(\text{OH})_6\text{SO}_4 + 2\text{OH}^-$	$\log K_{\text{tnbr}} = -16.8$
Brochantite/Atacamite Stability	
$\text{Cu}_4(\text{OH})_6\text{SO}_4 + 2\text{Cl}^- = \text{Cu}_4(\text{OH})_6\text{Cl}_2 + \text{SO}_4^{2-}$	$\log K_{\text{brat}} = -0.929$

can be illustrated by the example of the saturation of brochantite. Its precipitation is given by the relationship



The solubility product for this reaction is then

$$K_{\text{br}} = \{\text{Cu}^{2+}\}^4 \{\text{OH}^-\}^6 \{\text{SO}_4^{2-}\} \quad (2)$$

where the braces represent activities and the brackets are concentrations, e.g.:

$$\{\text{SO}_4^{2-}\} = \gamma_{\text{SO}_4^{2-}} [\text{SO}_4^{2-}] \quad (3)$$

Note that eq 2 describes a three-dimensional surface in the

space with axes $\{Cu^{2+}\}$, $\{OH^{-}\}$, and $\{SO_4^{2-}\}$.

However, since rainwater is a very dilute solution, it is reasonable to assume that during contact with the Statue's surface, its chemistry will become dominated by the ions supplied by dissolution of the corrosion products. Therefore, the electroneutrality condition would be approximated by

$$[Cu^{2+}] = [SO_4^{2-}] + \frac{1}{2}[Cl^{-}] + \frac{1}{2}[Alk] \quad (4)$$

where $[Alk]$ is the carbonate alkalinity defined as

$$[Alk] = [HCO_3^{-}] + 2[CO_3^{2-}] + [OH^{-}] - [H^{+}] \quad (5)$$

and the activities of the carbonate species HCO_3^{-} and CO_3^{2-} are fixed by the pH of the solution and the partial pressure of carbon dioxide (14).

Since the water film is open to the atmosphere, the partial pressure of carbon dioxide remains constant at $10^{-3.5}$ bar. Hence the alkalinity is solely a function of pH, and eq 3 can be restated in terms of the single variable, OH^{-} , by using appropriate equilibrium constants:

$$[Alk] = 10^{2.68}[OH^{-}] + 10^{6.65}[OH^{-}]^2 + [OH^{-}] - 10^{-14}/[OH^{-}] \quad (6)$$

With this expression for Alk , eq 4 can be used to substitute for $\{Cu^{2+}\}$ in eq 2, giving

$$K_{br} = \gamma^4_{Cu^{2+}}(10^{2.68}[OH^{-}] + 10^{6.65}[OH^{-}]^2 + [OH^{-}] - 10^{-14}/[OH^{-}] + [SO_4^{2-}] + [Cl^{-}])^4[OH^{-}]^6[SO_4^{2-}] \quad (7)$$

This equation thus presents the saturation of brochantite as a function of the three major environmental anions: SO_4^{2-} , OH^{-} , and Cl^{-} .

In the two-dimensional phase diagram with the axes $\{SO_4^{2-}\}$ and $\{OH^{-}\}$, $[Cl^{-}]$ is an adjustable parameter, which can be initially set to zero for simplicity. It is then possible to solve eq 7 by iteration. This is done by selecting a value for $[OH^{-}]$ and then testing various values of $[SO_4^{2-}]$ until the closure error is less than a specified amount, in this case, 0.01%. The result of the iterative computations is the line segment in Figure 1 connecting points A and B.

The iterative solution of eq 7 shows that in the range of values where the solution is saturated with respect to brochantite, $10^{-2} < [SO_4^{2-}] < 10^{-5}$ mol/L and $[OH^{-}] < 10^{-7}$. Thus, in this region of the phase diagram, $[SO_4^{2-}] \gg [Alk]$, according to eq 6. With this result, it is possible to solve eq 7 analytically. It becomes first

$$K_{br} = \gamma^4_{Cu^{2+}}[SO_4^{2-}]^4[OH^{-}]^6[SO_4^{2-}] \quad (8)$$

This is a mixed type of solubility product because it includes both concentrations and activities of SO_4^{2-} as well as the activity coefficient of Cu^{2+} . However, in this particular case, such complications can be avoided because over the range of ionic strengths involved

$$\gamma_{Cu^{2+}} \approx \gamma_{SO_4^{2-}} \quad (9)$$

and therefore eq 8 can be rewritten solely in terms of activities by using this relationship together with eq 3:

$$K_{br} = \gamma^4_{SO_4^{2-}}[SO_4^{2-}]^4[OH^{-}]^6[SO_4^{2-}] = [OH^{-}]^6[SO_4^{2-}]^5 \quad (10)$$

Finally, taking logarithms of eq 10 and rearranging gives

$$\log [SO_4^{2-}] = 0.2 \log K_{br} - 1.2 \log [OH^{-}] \quad (11)$$

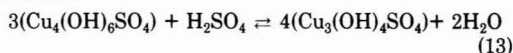
This is a simple linear relationship between the logarithms of $[SO_4^{2-}]$ and $[OH^{-}]$ as indicated by the line segment between A and B in Figure 1. The slope of this line is -1.2 in contrast to a slope of -6 that would appear in a conventional Pourbaix diagram (8, 9). Note that the linearity is fortuitous. In general, where Alk is not negligible, or the activity coefficients cannot be equated as in eq 9, the

saturation line will be curved.

The same procedure is used to determine the saturation line for antlerite. In this case also, the ultimate result is a simple linear relationship in the logarithms of the activities:

$$\log [SO_4^{2-}] = 0.25 \log K_{ant} - \log [OH^{-}] \quad (12)$$

The intersection of these two saturation lines occurs at point A, which has the coordinates $\log [SO_4^{2-}] = -1.77$, $\log [OH^{-}] = -10.04$ (or pH = 3.96). It also marks the intersection of the brochantite/antlerite boundary line with the solution field. Hence, it is the only point on the diagram where both antlerite and brochantite can be stable in contact with each other and the solution. For solution compositions above this point, i.e., at lower pH and higher $[SO_4^{2-}]$, only antlerite is stable and brochantite must dissolve, and vice versa for values below this point. Moreover, this point also constitutes a buffer for sulfuric acid, as can be seen from the reaction for conversion of brochantite to antlerite:



In other words, adding sulfuric acid to a stable assemblage of a water film + antlerite + brochantite will not affect the solution chemistry. It will only change the proportion of brochantite to antlerite in the patina. This reaction is also significant because it implies that as antlerite dissolves, it can react with water yielding solid brochantite and sulfuric acid.

The solution field in Figure 1 is completed by the saturation lines of two other copper minerals. At higher values of $[SO_4^{2-}]$ it is saturated with respect to chalcantite ($CuSO_4 \cdot 5H_2O$). Since this is not a basic copper salt, its dissolution does not involve changes in $[OH^{-}]$. Hence, its saturation line is horizontal. Chalcantite has not been observed in the patina of the Statue, which suggests that the level of $[SO_4^{2-}]$ in the environment does not exceed $10^{-2.5}$ mol/L. Tenorite (CuO) is the phase shown as bounding the lower end of the solution field. This mineral has been observed in the Statue's patina. However, because of the presence of Cl^{-} , as discussed below, the actual saturated phase could also be atacamite.

The phase diagram in Figure 1 is "surface bound", in the sense that it includes a specific electroneutrality condition which is determined by equilibrium with the mineral assemblage of the surface. This is typical of water in thin surface films or in porous materials. However, in the case of large water-to-surface volumes, such as an object immersed in the sea, or water flowing through a pipe, the bulk solution electroneutrality condition may differ from that at the immediate interface. It would still be possible to use surface-bound phase diagrams under these conditions, although steady state instead of true equilibrium would be implied.

It should also be noted that the surface-bound constraint only requires that the variability in the electroneutrality condition be completely determined by the ions found in the surface minerals. It is possible to use an electroneutrality condition that includes additional ions, provided that these do not react with the surface. The result would be a phase diagram with the same general features. However, the positions of the saturation lines and intersection points may be shifted because of the common ion effect, ion pairing, and the influence of these additional ions on the ionic strength and, hence, activity coefficients. These complications can be modeled, but a discussion of this is beyond the scope of this article. In this particular case, because rainwater is a very dilute solution, any ad-

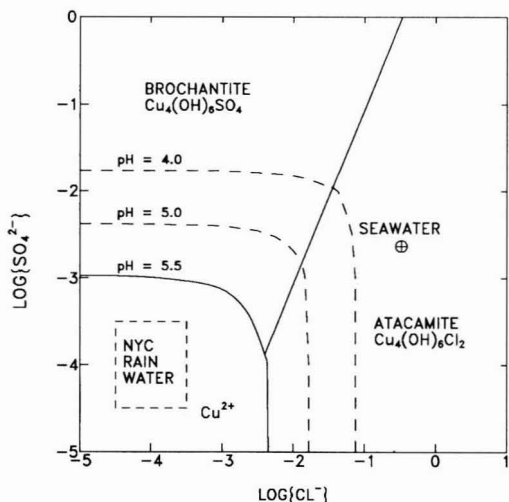


Figure 2. Equilibrium phase diagram for copper minerals as a function of SO_4^{2-} and Cl^- activities at 25 °C and $P_{\text{CO}_2} = 10^{-3.5}$ bar. Note that the mineral saturation lines are solution bound. All thermodynamic data are taken from Woods and Garrels (16).

ditional ions can be ignored.

To evaluate the effect of chlorides on the patina, it is necessary to assign nonzero values to $[\text{Cl}^-]$, which again creates a three-dimensional surface. This could be handled by introducing a set of contours for various levels of $[\text{Cl}^-]$ in the phase diagram of Figure 1. However, to visualize the relationship between atacamite and brochantite more conveniently, a second phase diagram has been constructed with axes of $\log [\text{SO}_4^{2-}]$ and $\log [\text{Cl}^-]$, which is presented in Figure 2. In this diagram the third component becomes $\log [\text{OH}^-]$, which cannot be set to zero. Consequently, instead of a unique curve representing the solution/surface interface, there is a set of contours at specified levels of pH. For each contour, there is a single point where brochantite and atacamite can coexist in contact with the solution. However, unlike the invariant point A in Figure 1, this point does not represent a true acidity buffer.

With these two phase diagrams, it is then possible to visualize the influence of the environment on the Statue of Liberty's patina. First the effect of acid rain is evaluated, and then the effects of sulfur dioxide and sea-salt deposition are considered.

III. Effect of Acidic Deposition on the Patina Stability

Acid rain falling in the Northeast United States is produced by the long-range transport and transformation of sulfur dioxide emitted from certain large fossil-fueled power plants, located primarily in the Midwest (3). In New York City, rainfall pH typically ranges from 3.8 to 4.2 (15). The anthropogenic acidity is a mixture of sulfuric and nitric acids. Since these dominate over any natural acids present, the acidity can be given as

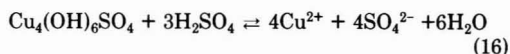
$$[\text{H}^+]_{\text{rain}} = 2[\text{SO}_4^{2-}]_{\text{rain}} + [\text{NO}_3^-]_{\text{rain}} \quad (14)$$

The ratio of sulfate to nitrate anions is roughly 2:1. Assuming this ratio remains relatively constant, it is possible to approximate eq 14 by

$$[\text{H}^+]_{\text{rain}} \approx 2.5[\text{SO}_4^{2-}]_{\text{rain}} \quad (15)$$

This relationship has also been plotted in Figure 1. A point on this line represents the composition of a given acid rain event. This line does not coincide with the boundary

for the solution field, which indicates that the rain is not in equilibrium with the patina. Therefore, upon contact with the surface, the acid will tend to be neutralized by reaction with brochantite:



The path of this reaction is shown graphically in Figure 1 as the line CD moving in the direction of increasing $[\text{OH}^-]$ from the starting point C on the acid rain line. It continues until it intersects with the brochantite saturation line at point D. This indicates that equilibrium between the solution and the solid phase has been reached, and the reaction stops.

The equation describing these neutralization reaction paths can be derived from stoichiometry and mass balances. From eq 16, the amount of SO_4^{2-} added to the solution at any point along the path by the reaction with brochantite is

$$\Delta[\text{SO}_4^{2-}] = -0.165\Delta[\text{H}^+] \quad (17)$$

Combining eqs 15 and 17 ultimately gives a relationship describing the SO_4^{2-} concentration as a function of the solution $[\text{H}^+]$ and the initial $[\text{H}^+]$ in the rain:

$$[\text{SO}_4^{2-}] = -0.165[\text{H}^+] + 0.56[\text{H}^+]_{\text{rain}} \quad (18)$$

The particular neutralization path that intersects the saturation line at the invariant point A is important because it defines a geochemical divide. Any solution with a starting composition that falls below this divide will eventually reach equilibrium with brochantite, while any composition above the divide will end in equilibrium with antlerite. This means that only those rainwater compositions above the geochemical divide can convert brochantite to antlerite. Substituting the coordinates of point A ($\log [\text{H}^+] = -3.96$, $\log [\text{SO}_4^{2-}] = -1.77$) into eq 18 and solving gives a pH value in the rain of 1.36. Therefore, only rain with pH less than this value will be able to transform brochantite to antlerite, but this pH level is much lower than the minimum ever observed in acid rain. Consequently, the acid rain falling on the Statue of Liberty cannot convert the brochantite in the patina to antlerite.

While it has no effect on the stability of brochantite vs antlerite in the patina, the acidity of the rain could still conceivably increase the solubility of brochantite itself. The solubility of brochantite can be expressed as a function of $[\text{SO}_4^{2-}]$, because of the assumption that the solution is surface bound. Consequently, the $[\text{SO}_4^{2-}]$ in the solution is due solely to dissolution of brochantite. Then from stoichiometry, the amount of brochantite in solution in grams per liter is equivalent to $454[\text{SO}_4^{2-}]$. This computation is simplified by the fact that for the relevant range of solution compositions there is negligible complexing of copper.

It is then necessary to define a reference solubility that would be observed in the absence of manmade acidity. Conceptually, this would be the solubility measured in a layer of water on the surface created by condensation. There are two cases for surface conditions. The first is that both antlerite and brochantite are present, and the second is that only brochantite is found.

In the first case, because of the antlerite/brochantite buffer given by eq 13, the acid rain has no effect on $[\text{SO}_4^{2-}]$, which is fixed at $10^{-1.76}$ or 17.4 mmol/L. At this solution chemistry, the activity coefficient for SO_4^{2-} is 0.48. Hence $[\text{SO}_4^{2-}]$ is 36 mmol/L, and the brochantite solubility is simply 16.5 gm/L regardless of the acidity of the rain.

However, in the second case, in the absence of antlerite there is no unique value for the solubility of brochantite

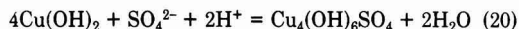
since it can be in equilibrium with the solution at any point along line AB. To establish a reference solubility, it is then necessary to specify either $\{SO_4^{2-}\}$ or pH. In a simple brochantite/water system, the pH would be fixed at 5.6 by equilibrium with atmospheric CO_2 . This value of pH at line AB gives a value of 0.20 mmol/L for $\{SO_4^{2-}\}$, and hence a reference brochantite solubility of 0.1 gm/L. For comparison, the lowest value of pH measured in acid rain in the New York area is 3.5. The neutralization path for this rain acidity is shown as line CD in Figure 1. This intersects the brochantite saturation line at $\{SO_4^{2-}\} = 0.18$ mmol/L, which is slightly lower than that for the reference brochantite solubility. In other words, even the worst case acid rain slightly reduces the solubility of brochantite rather than increases it under these conditions.

In reality, the system is more complicated, and the pH of the solution is probably not determined by CO_2 equilibria. While the surface is wet, corrosion of the copper metal of the Statue's skin can proceed. The overall reaction can be summarized as



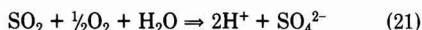
This process injects base into the solution and thus tends to drive the equilibrium toward higher pH and therefore lower brochantite solubility.

Moreover, eq 19 also suggests the possibility of the formation of solid $Cu(OH)_2$ as a separate phase. In fact, most investigators have observed that in the precipitation of brochantite, $Cu(OH)_2$ initially appears as a colloid, which subsequently converts to brochantite (16). The equation for this reaction



suggests that brochantite can dissolve incongruently by hydrolysis to form $Cu(OH)_2$ and sulfuric acid. The coexistence of these two phases would create another buffer. However, it is not possible to locate this on the phase diagram because of the uncertainty of the Gibbs energy of $Cu(OH)_2$, which is dependent on the particle size of the colloid. As a result, $Cu(OH)_2$ is generally regarded as being only metastable with respect to CuO (17). This explains why tenorite rather than $Cu(OH)_2$ is shown as the stable phase at point B in Figure 1.

While the copper is corroding, sulfur dioxide gas is also simultaneously depositing from the atmosphere, giving rise ultimately to sulfuric acid according to the overall reaction



which would tend to drive the equilibrium in the other direction toward lower pH and higher brochantite solubility.

Consequently, the pH, and hence the brochantite solubility, is determined by the balance at any given moment between the two competing processes of copper corrosion and SO_2 deposition. Unfortunately, the details of these processes, which are controlled by kinetics and not thermodynamic equilibria, are not known. The problem of estimating the SO_2 deposition rate is discussed more fully below.

The most that can be said at the present state of knowledge is that the solubility of brochantite shifts up and down along line AB in response to fluctuating environmental conditions. Nevertheless, it has been shown above that, even in the case of the extreme acid rain event (pH = 3.5), the solubility of brochantite is not affected if the reference pH is less than 5.6. For more typical rain acidities (pH > 4), the reference pH would have to be greater than 6 for the brochantite solubility to show sen-

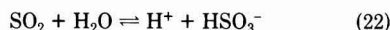
sitivity. However, this reference pH lies along line AB very close to point B, and in this region of the phase diagram, there is a great deal of uncertainty about whether the stable phase is brochantite, antlerite, or copper hydroxide, as discussed above. Moreover, when the effect of Cl^- is taken into account, it is likely that an additional stable mineral, atacamite, coexists with brochantite in this region. The effect of this mineral assemblage on solution chemistry is discussed in the next section. It would effectively keep the reference pH below 5.0.

Therefore, practically speaking, acid rain does not affect the solubility of brochantite or the conversion between brochantite and antlerite at the Statue of Liberty. This conclusion is supported by laboratory investigations that have found no effect of pH on copper corrosion product mineralogy (16, 18). Thus, Nielsen's conjecture that acid rain is altering either the composition or the solubility of the Statue's patina does not appear viable.

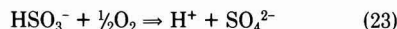
This conclusion contradicts the conventional wisdom about the effect of acid rain on copper or bronze sculpture. Another way of stating the issue is that the patina of the Statue itself produces sulfuric acid in contact with water. This is a consequence of the incongruent dissolution of the basic copper sulfate minerals antlerite and brochantite, as shown in eqs 13 and 20. The resulting pH levels are comparable to those found in acid rain. Moreover, the amount of acidity that can be delivered by acid rain is limited by the processes of atmospheric chemistry that operate during long-range transport and further by the fact that it rains only about 1–2% of the time over the period of a year. In contrast, sulfur dioxide produced by sources in the New York City region can react with copper skin to produce sulfates a much greater percentage of the time.

IV. Influence of Sulfur Dioxide and Sea-Salt Deposition on the Patina

Given that acid rain has negligible effect on the patina of the Statue, the sulfate that forms the dominant corrosion minerals must come from other sources, primarily deposition of sulfur dioxide gas. The overall equation for the formation of sulfuric acid from sulfur dioxide is given by eq 21. However, this is actually a two-step process. The first is the hydration of sulfur dioxide, which yields sulfurous acid:

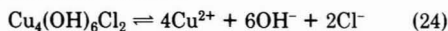


This is followed by oxidation to form the sulfate:



The process given by eq 22 can be characterized by a thermodynamic equilibrium, in which the pH of the solution plays an important role in determining the HSO_3^- concentration in the solution. However, the subsequent oxidation step HSO_3^- to SO_4^{2-} is effectively irreversible, and the relationship between the two chemical species is determined by kinetics rather than equilibrium considerations. There are many possible SO_2 oxidation reactions involving copper compounds as catalysts (19), but unfortunately, it is not yet known which would be the rate-limiting step. Nevertheless, it is possible to state qualitatively that the concentration of SO_4^{2-} will increase monotonically with the partial pressure of SO_2 , but it is also regulated to some degree by the solution pH, which in turn depends on the rate of corrosion of copper and the rate of brochantite precipitation. Therefore, it is unlikely that the SO_2 deposition rate achieves a steady state except at the brochantite/antlerite buffer, point A, where the pH is fixed.

The effect of chlorides deposited by rainwater or by seawater, either as spray droplets or sea-salt suspended particulate matter can be evaluated by using Figure 2. The chemistry range of New York rainwater (13) and of seawater has also been plotted in this figure. It can be seen that seawater plots in the stability field of atacamite. Hence, if it came into contact with a brochantite layer, it would convert the brochantite into atacamite. In contact with atacamite, it would simply precipitate more atacamite to remove Cu^{2+} and Cl^- from the solution until equilibrium with the surface is reached.



On the other hand, rainwater plots in the solution field. If it came into contact with atacamite, the solution chemistry would move toward saturation by dissolving the atacamite to increase the Cl^- activity of the solution according to the reaction. However, this reaction also releases OH^- , thereby increasing the pH. Since this reaction has no effect on the $\{\text{SO}_4^{2-}\}$, its path would be a horizontal line moving toward the right. This path would appear to reach equilibrium with atacamite. However, because the pH is also increasing, the saturation line of brochantite is also moving lower, as shown by the contours in Figure 2. Even for the lowest values of $\{\text{SO}_4^{2-}\}$ found in rainwater, the end result of the reaction is equilibrium with brochantite rather than atacamite. Consequently, on surfaces regularly washed by rainwater, atacamite would be unstable, but on sheltered surfaces, the accumulation of sea salt would tend to favor a mixture of brochantite and atacamite. The instability of atacamite in the presence of rainwater has also been pointed out by Opila (20) and Graedel (11), but neither of these authors considered the possibility of sea-salt deposition.

The coexistence of brochantite and atacamite does not necessarily create a pH buffer, unless either $\{\text{SO}_4^{2-}\}$ or $\{\text{Cl}^-\}$ is also held constant, as can be seen from Figure 2. As discussed above, the deposition of SO_2 to form SO_4^{2-} requires the presence of a film of water and varies with solution chemistry. On the other hand, the deposition of sea-salt particles is a mechanical process that can take place on either a wet or a dry surface. This means that the sea-salt deposition rate would be much less variable and, hence, more likely to be the controlling factor in establishing a quasi-buffer with the atacamite/brochantite mineral assemblage. Dry deposition rates of chlorides have been measured in lower Manhattan at 0.5–3.0 mmol/ m^2month (15). However, to translate this deposition rate into a Cl^- concentration requires detailed knowledge about the adsorption and/or condensation of moisture on the surface, and the rate of removal by runoff. In the absence of this detailed information, the composition of water lying on the surface can be bracketed by seawater and by rainwater. From Figure 2, seawater has a $\{\text{Cl}^-\}$ of 0.38 mol/L, which yields a pH of 3.9 at the atacamite/brochantite boundary. This lies very close to the brochantite/antlerite buffer at point A of Figure 1. At the other extreme, a typical value of $\{\text{Cl}^-\}$ in rainwater of 4 mmol/L gives a pH of 5 at equilibrium.

Therefore, there appears to be two points in the $\text{SO}_4^{2-}\text{--OH}^-\text{--Cl}^-$ system where the solution chemistry would be most stable: the antlerite/brochantite buffer and the brochantite/atacamite quasi-buffer. Away from these two points the pH would float, and hence the solution chemistry would fluctuate in response to environmental factors. Higher partial pressures of SO_2 would tend to drive the solution toward the antlerite/brochantite buffer, while lower partial pressures would tend to drive the solution toward the brochantite/atacamite point. Hence, it is likely

that the solution chemistry spends most of the time at one buffer or the other, and not at values in between.

V. Spatial Pattern of the Patina Color and Its Historical Development

It is thus the relative magnitudes of the deposition rates of sulfates vs chlorides at a given point on the Statue's surface that determine the local proportions of antlerite, brochantite, and atacamite in the patina. In turn, the controlling factor in the spatial variability of the deposition rates seems to be the relative frequency of occurrence of a stagnant moisture film, due to adsorption and condensation of humidity vs the occurrence of flowing water from rain. The latter destroys atacamite and washes away the sea salt while promoting the deposition of sulfate and the formation of brochantite. Thus, where the water flows the color of the patina will be the light bluish-green of brochantite, and where it does not, the color will be darker because of the presence of translucent olive-green atacamite.

On the left side of the Statue's face, this distribution creates the effect of a photographic negative (Figure 3). This part of the head is oriented due east and so is protected from the prevailing winds, which blow from the west (21). This part of the Statue is thus sheltered from direct contact with rainwater because of this lee-side effect, combined with the overhang of the crown above that protects against rain falling vertically. However, some water flows off the crown down along recessed areas such as the grooves in the hair and the folds of the eyelids. These concave areas, which would normally be in shadow and thus dark, are lightened because of the formation of significant amounts of brochantite. In contrast, the areas of high relief such as the cheek, which one would expect to be highlighted, are darker because of the presence of atacamite.

This model of the formation of the Statue's patina has been derived from geochemical thermodynamics theory. A test of this model would ideally consist of systematic sampling of the Statue's surface for correlation with local environmental conditions. Some analyses of samples of the Statue of Liberty's patina have been made in the past using a variety of techniques including X-ray diffraction (1, 2, 22, 23), Auger electron spectroscopy (18), and ion chromatography (24). These studies generally found the patina to consist mainly of brochantite, antlerite, and atacamite. An inner layer of cuprite (Cu_2O) and, in some places, nantokite (CuCl) also exists. These cuprous compounds reflect the reduced supply of oxygen below the patina surface (7). Also, as Opila points out, neither brochantite nor atacamite is stable in direct contact with copper metal (20).

Unfortunately, the specimens of patina that were taken during the restoration of the Statue are very few in number. Moreover, the samples were often restricted to areas that would be hidden from public view, which may make them unrepresentative. In some cases, the analyses are contradictory. For example, on the specimen of copper that was removed in 1905, Nielsen (3) found atacamite, while Baboian and Cliver (1), analyzing the same piece, did not. These differences may be due in part to the difficulty of analyzing the mineralogy of poorly crystallized thin layers. Consequently, it is impossible to make any statistically significant test of this model with the available data. It is suggestive, though, that Nassau et al. (23) found the highest proportions of atacamite in the two specimens from the left cheek of the Statue. In the absence of any further sampling of the Statue's patina, another test would be to put out samples of copper patinated with either



Figure 3. Left elevation of the head of the Statue of Liberty. This is a positive print, as can be seen from the figure of the man in the lower left corner. Photograph by J. T. Lowe, courtesy of the Library of Congress.

atacamite or brochantite around the Statue and observe which minerals remain stable over time.

Concerning the historical development of the patina, Nielsen's (3) examination of a piece of the patina that had been indoors since 1905 found that it consisted primarily of atacamite and brochantite, but no antlerite. This presumably reflects a lower SO_4^{2-} in 1905 than in recent decades. The data on air pollution in the past are ex-

tremely limited, but based on fuel consumption data, it is likely that sulfur dioxide levels in 1905 were not as high as they are now. In succeeding decades, the levels increased greatly and may have reached their peak in the 1940s and 1950s. The levels of SO_2 in New York City in the late 1950s went as high as $400 \mu\text{g}/\text{m}^3$ (25). Following the introduction of air pollution controls in the 1960s, the sulfur dioxide dropped to roughly $20 \mu\text{g}/\text{m}^3$ (26).

The photographic evidence presented by Baboian and Cliver (1) seems to show that, in the 1960s, the patina was uniformly light green. This suggests that at that time the SO_2 level was high enough that sulfate deposition dominated other processes over the entire surface of the Statue. Hence the patina was uniformly brochantite/antlerite. However, after the SO_2 level dropped by more than 1 order of magnitude, the associated sulfate deposition might not have been sufficient to overcome the deposition rate of sea-salt particles, which presumably has stayed constant over time. Thus atacamite could become stable at certain places, and the patina would vary in composition spatially.

While this geochemical model provides an explanation of the differences in the patina between the windward and leeward sides of the Statue as a whole, it fails to explain the particular pattern observed on the right arm and torch surfaces. Here the patina is very thin and more brownish in color, which indicates a higher percentage of tenorite (CuO). Traces of brochantite are found only in areas sheltered from the rain. Moreover, the boundary between the different types of patina is aligned with the edges of particular panels of copper. These features suggest that the patina pattern depends upon metallurgical rather than environmental factors. Franey and Davis (27) found that the only major differences among the copper panels were grain size and hardness. The panels without patina had the greater hardness and significantly smaller grain size. The brochantite patina was found on the softer panels of copper, which also had the larger grain sizes, which suggests that these panels had been annealed.

For a possible explanation of this phenomenon, it is necessary to consider mass balances. A certain amount of the patina minerals dissolves in rainwater and is carried off in the runoff. To maintain a stable patina, this loss must be made up by the corrosion of more copper coupled with SO_2 deposition. Apparently, at present SO_2 levels, the corrosion rate of the annealed copper is still high enough to preserve the brochantite patina, but the corrosion rate of the unannealed copper on the torch arm is insufficient. The corrosion rate is described by the copper's polarization curve. However, the necessary electrochemical measurements to determine if the polarization curves are significantly different between the two types of copper have not yet been made.

It is interesting that Pourbaix (7) investigated a somewhat similar problem in connection with the corrosion of copper drinking water pipes in Brussels. In this case, annealed copper pipes corroded much more rapidly than unannealed ones. Pourbaix found that the annealed copper had a much more positive electrode potential, about +350 to 420 mV (SHE) vs the unannealed metal. This potential exceeds the critical level for active corrosion (+270 mV (SHE) in this case). The difference in potential is associated with a carbon film found on the surface of the annealed copper. This film apparently formed during annealing when the copper was heated under reducing conditions. The copper had a residual layer of oil on the surface from the lubricant used as part of the sheet-rolling process. The high temperatures and low oxygen conditions during annealing caused the oil to break down, leaving the carbon film behind.

VI. Conclusions

It is possible to explain many of the phenomena observed on the patina of the Statue of Liberty by means of a geochemical model involving the deposition rates of sulfates and chlorides. The reactions between rainwater and the copper minerals comprising the patina can be readily visualized by use of surface-bound equilibrium-

phase diagrams. The model indicates that acid rain, at the levels measured in New York City, has no effect on either the mineralogy of the patina or its solubility. The color patterns on some parts of the Statue, particularly the left side of the face, seem to result from the combination of sea-salt deposition and sheltering from rainwater, which promote the formation of atacamite. On other parts of the Statue, rainwater driven by the prevailing westerly winds favors the formation of brochantite. In the past, higher levels of SO_2 may have produced a uniform brochantite layer over the entire Statue. The particular patina pattern on the right arm and torch of the Statue may be a result of metallurgical considerations associated with the rolling and annealing of the copper sheets.

However, a complete understanding of the problem requires more information about several aspects of copper corrosion under these environmental conditions. These include the phase relationships among copper hydroxide, tenorite, and brochantite as a function of SO_4^{2-} and OH^- activities, and particularly whether incongruent dissolution is involved. Another critical area of research concerns the kinetics of the coupled processes of copper corrosion and SO_2 deposition and the role of solution pH in regulating the process. A third area for future research would be the rate of chloride deposition to the Statue's surface, and the actual Cl^- concentrations to be found in surface water films. Another important research topic would be the effect of rolling, working, and annealing on the polarization curves of the copper. Finally, as a way of testing this geochemical model, it would be desirable to conduct long-term exposure experiments using artificial patina samples at different locations around the Statue.

Acknowledgments

I thank P. Candela for several very helpful discussions on the development of the phase diagrams, and T. Woods for explaining her research concerning basic copper minerals. E. deLony provided a valuable insight on the prevailing winds effect. The support and assistance of E. Cliver is also much appreciated.

Literature Cited

- (1) Baboian, R.; Cliver, E. B. *Mater. Perform.* **1986**, 25(5), 80.
- (2) Weil, P. D. In *Corrosion and Metal Artifacts*; Brown, B. F., et al., Eds.; National Bureau of Standards: Gaithersburg, MD, 1977; pp 77-92.
- (3) Nielsen, N. A. *Mater. Perform.* **1984**, 23(4), 78.
- (4) Schwartz, S. E. *Science* **1989**, 243, 753.
- (5) Graedel, T. E.; Nassau, K.; Franey, P. J. *Corros. Sci.* **1987**, 27, 639.
- (6) de Zoubov, N.; Vanleugenhaghe, C.; Pourbaix, M. In *Atlas of Electrochemical Equilibria in Aqueous Solutions*; Pourbaix, M., Ed.; Pergamon: Oxford, U.K., 1966; pp 384-392.
- (7) Pourbaix, M. J. *J. Electrochem. Soc.* **1976**, 123(2), 25C.
- (8) Leckie, J. O.; Davis, J. A., III. In *Copper in the Environment*; Nriagu, J. N., Ed.; Wiley: New York, 1979; pp 90-121.
- (9) Silman, J. F. B. Ph.D. Dissertation, Harvard University, 1958.
- (10) Kucera, V.; Mattson, E. In *Corrosion Mechanisms*; Mansfeld, F., Ed.; M. Dekker, Inc.: New York, 1987; pp 211-284.
- (11) Graedel, T. E. *Corros. Sci.* **1987**, 27, 741.
- (12) Woods, T. L.; Garrels, R. M. *Appl. Geochem.* **1986**, 1, 181.
- (13) Mann, A. W.; Deutscher, R. L. *Chem. Geol.* **1977**, 19, 253.
- (14) Stumm, W.; Morgan, J. J. *Aquatic Chemistry*; Wiley: New York, 1981; pp 180-182.
- (15) Toonkel, L. E. *Environmental Measurements Laboratory Environmental Report: Appendix, EML-395*; NTIS: Springfield, VA, 1981; pp B11-B31.
- (16) Woods, T. L.; Garrels, R. M. *Econ. Geol.* **1986**, 81, 1989.

- (17) Stumm, W.; Morgan, J. J. *Aquatic Chemistry*; Wiley: New York, 1981; pp 297-299.
- (18) Nassau, K.; Miller, A. E.; Graedel, T. E. *Corros. Sci.* 1987, 27, 703.
- (19) Hoffmann, M. R.; Jacob, D. J. *SO₂, NO and NO₂ Oxidation Mechanisms: Atmospheric Considerations*; Calvert, J., Ed.; Butterworth Publishers: Boston, MA, 1984; pp 101-173.
- (20) Opila, R. L. *Corros. Sci.* 1987, 27, 685.
- (21) NOAA, *Local Climatological Data—Central Park, New York, NY*; National Climatic Center: Asheville, NC, 1981.
- (22) Osborn, D. H. *Mater. Des. Eng.* 1963, June, 80.
- (23) Nassau, K.; Gallagher, K. P.; Miller, A. E.; Graedel, T. E. *Corros. Sci.* 1987, 27, 639.
- (24) Muller, A. J.; McCrory-Joy, C. *Corros. Sci.* 1987, 27, 695.
- (25) Blade, E.; Ferrand, E. F. J. *Air Pollut. Control Assoc.* 1969, 19, 973.
- (26) Department of Environmental Conservation. *New York State Air Quality Report, Continuous and Manual Air Monitoring Systems*; New York State DEC: Albany, NY, 1981; p 25.
- (27) Franey, J. P.; Davis, M. E. *Corros. Sci.* 1987, 27, 659.

Received for review June 19, 1990. Revised manuscript received April 8, 1991. Accepted April 15, 1991. This work was funded by the North Atlantic Historic Preservation Center of the National Park Service through a grant from the Andy Warhol Foundation.

Long-Term Processes in a Stabilized Coal-Waste Block Exposed to Seawater

Daryl E. Hockley* and Hans A. van der Sloot

Netherlands Energy Research Foundation, (ECN), P.O. Box 1, 1755 ZG Petten, The Netherlands

■ A stabilized waste block, formed by cementation of coal combustion wastes with portland cement and lime, was retrieved after 8-years exposure to a marine environment. The block was analyzed to obtain concentration profiles for major and minor elements. Combination of the major element profiles with semiquantitative X-ray diffraction results allowed identification of diffusion-limited precipitation and dissolution processes. The precipitation and dissolution processes moved as a sharp boundary from the surface toward the center of the block, penetrating about 10–20 mm in the 8 years. Leaching of minor elements was limited to the region between the surface and the boundary. Concentration profiles for sea salts suggest that precipitation in the matrix pores of the boundary region restricted diffusion further into the block. This process, known as “pore refinement” in concrete durability literature, may also restrict degradation of the waste block matrix and the leaching of contaminants.

Introduction

Background. According to recently compiled statistics, approximately 280 million tonnes of fly ash is produced each year by the combustion of coal. Less than 10% of this volume is utilized, primarily as a cement replacement (1). Disposal of the remainder is complicated by the fact that many fly ashes contain appreciable amounts of contaminants, especially metals and oxy anions. In the United States, coal combustion wastes have historically been disposed in landfills near the combustion facility. Disposal in the ocean has been a more common practice in the United Kingdom (2). A more recent alternative is to combine coal wastes with other cementing agents to produce hardened blocks of “stabilized waste”. In principle, these stabilized forms are better able to retain contaminants than the bulk wastes and are therefore more acceptable for utilization or disposal.

The Coal Waste Artificial Reef Program (CWARP) studied the environmental consequences of utilizing stabilized coal combustion wastes as construction material for artificial fishing reefs. On September 12, 1980, some 16000 blocks of stabilized waste were released from a hopper barge to form a 500-tonne artificial reef in the New York Bight. The blocks consisted of coal fly ash and flue gas desulfurization residues stabilized with lime and portland cement additives. Results of the CWARP re-

search, which ended in 1984, were generally encouraging. The coal-waste blocks showed little deterioration and no decrease in compressive strength. Elements of environmental concern remained inside the blocks or were leached at very slow rates. Biological communities developed on the coal-waste reef and showed no evidence of contaminant uptake (3–8).

Divers from the State University of New York returned to the coal-waste reef in the summer of 1988. The biological communities growing on the coal-waste blocks were surveyed and found to be identical with those observed on nearby blocks of uncontaminated concrete, suggesting that the contaminants in the waste blocks continued to have little or no adverse impact on their immediate surroundings. Subsequent strength testing of blocks retrieved during the 1988 dives showed no decrease in compressive strength, indicating that the blocks had not been adversely affected by further exposure to the marine environment. One of the retrieved blocks was forwarded to the Netherlands Energy Research Foundation (ECN) for detailed chemical and mineralogical profiling. The results of these analyses are reported herein and the chemical and mineralogical processes responsible for the apparently favorable behavior of the coal-waste reef are identified.

Experimental Section

Retrieved Block. Details of the mixing, forming, and curing of the coal-waste blocks were reported previously in the CWARP publications (3, 6). The reef was constructed on sandy sediments at a water depth of 40 m. The block forwarded to ECN was retrieved in July 1988, after 409 weeks in the sea. It was one of the type referred to as “Conesville” blocks in the earlier reports. It measured approximately 20 × 20 × 40 cm and weighed approximately 25 kg. The block was found lying on the seabed and was overgrown by an encrusting biological community on all exposed surfaces. The underside was partially buried and remained clean of biological growth. The pattern and extent of the biological growth suggests that the block had remained in the same orientation on the seabed for several years.

Chemical Analyses. Samples measuring 4 × 4 × 10 cm were cut from selected locations in the block with a wet-cutting diamond blade stone saw. The samples were subsequently sliced in a dry-cutting device fitted with a high-volume dust sampler. Starting from the surface of

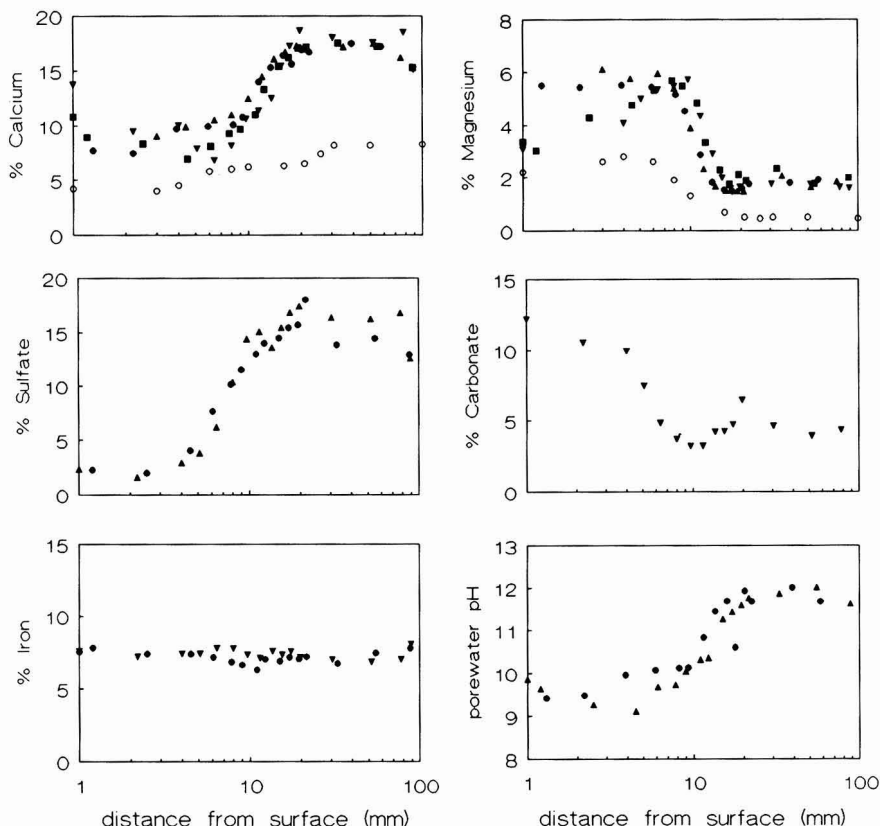


Figure 1. Concentration profiles for major elements in the coal-waste reef block. Filled shapes indicate profiles from the block retrieved in 1988 after 8-years exposure. Open circles show profiles measured in a block retrieved after 80-weeks exposure (7).

the block, thin slices were removed by the diamond blade saw and the dust was collected on a microsorban filter mounted in the dust sampler. A new filter was inserted for each slice.

The dust was removed from the filters and analyzed for major, minor, and trace elements. Ca, Mg, and Mo were measured by inductively coupled plasma emission spectrometry after dissolution of the dust in a pressure bomb containing a $\text{HCl-HClO}_4\text{-HNO}_3$ mixture. Na was measured by atomic absorption spectrometry. Fe, Mn, Br, As, Sb, Se, W, La, and Sc were measured by neutron activation analysis. Cl, SO_4 , and F were measured by ion chromatography after dissolution of the sample in NaOH melt. This procedure measures both SO_3 and SO_4 as sulfate. Carbonate was measured by acidification, volatilization as CO_2 , trapping in a solution of barium perchlorate, *tert*-butyl alcohol, and glycerine, and titration by NaOH. All concentrations were reported as weight percentages and subsequently normalized by Sc to account for porosity changes. The reference NBS coal fly ash 1633a was analyzed along with the other samples as a check on the accuracy of the analytical results.

To obtain pH profiles indicative of porewater conditions in the block, portions of the dust from the microsorban filters were rewetted with demineralized water at a liquid/solid ratio of 2 mL/g. Measurements were taken with a pH electrode after a 5-min contact time.

Morphological Examination. The retrieved block was inspected visually and photographed. The profile samples were also inspected and a dark layer was noted about 10–20 mm from the surface. A scanning electron microscope

(SEM) was used to examine the dark layer and to search for crystalline precipitates. Energy dispersive X-ray (EDX) mapping was used to identify regions of increased Ca and Mg concentrations.

Mineralogical Analysis. Samples were taken from depths of 1, 4.0, 6.4, 9.7, 13.6, 17.4, 30.5, and 78 mm in a single profile and analyzed by powder X-ray diffraction. The diffractograms were examined and mineralogically distinct regions were identified. Diffractograms from samples representative of each region were then used for semiquantitative analysis.

Results and Discussion

Concentration Profiles. As mentioned above, all concentrations were normalized by Sc so that the resulting Sc profile is, of course, flat. Before the normalization, the Sc profiles showed a slight (<10%) increase near the surface. Since Sc is relatively insoluble in seawater, the normalization procedure interprets the increase in the weight percentage of Sc as indicating an increase in porosity. To ensure that the normalization by Sc did not bias any of the other profiles, all normalized profiles were compared with the original data. Only the profile features that appeared significant in both data sets are discussed herein.

Concentration profiles for Ca, Mg, SO_4 (and SO_3), CO_3 , pH, and Fe are shown in Figure 1. The filled shapes represent profiles from different locations in the block. For comparison, profiles from a block retrieved in 1982 (7) are included and shown as open circles. The most notable features in the Ca, Mg, SO_4 , CO_3 , and pH profiles are the

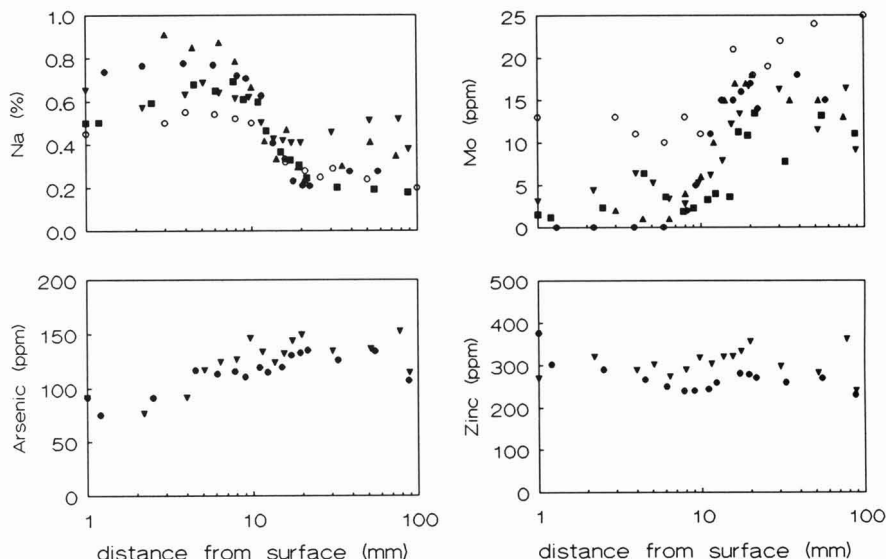


Figure 2. Concentration profiles for selected minor and trace elements in the coal-waste reef block. Open circles again show profiles measured in the block retrieved earlier (7).

sharp discontinuities at distances of about 10–20 mm from the surface. In contrast, the Fe profiles show no significant concentration changes. Reaction and transport processes have clearly had a more significant effect on the Ca, Mg, SO_4 , and CO_3 than on the Fe. The discontinuity in the pH profiles confirms the presence of two chemically different regions and implies that the concentration changes in the discontinuous profiles were caused by reaction. In the discussion below, Ca, Mg, SO_4 , and CO_3 will be referred to as the “reactive” components.

Another noteworthy feature in Figure 1 is the overall consistency of the profiles. Concentration measurements from the region of the discontinuity are very reproducible. The samples taken from the surface itself produce less consistent results. These inconsistencies are removed if profiles from the biologically encrusted surfaces of the block are separated from those from the cleaner underside.

Figure 2 shows concentration profiles for Na, Mo, As, and Zn. The Na and Mo profiles again show discontinuities at about 10–20 mm from the surface. These profiles are discussed further below. Profiles for Cl and Br are less consistent than those presented here but show behavior very similar to the Na. The As profiles in Figure 2 show discontinuities located slightly nearer the surface. Profiles for B and Sb showed similar behavior. These profiles are also discussed further below. The Zn profiles show a reasonably constant concentration except near the surface. Cu, La, and W profiles showed similar behavior. Since surface enrichment of these elements is only seen in profiles from the underside of the block, it is believed that they were scavenged from the sediment porewater. Scavenging effects have also been noted by earlier workers (4). Profiles for Mn, F, and Se showed too much scatter to assign them to any of the above groups. However, they all show some evidence of a discontinuity within 10–20 mm of the surface.

Morphology. Figure 3 shows a photograph of a cross section cut from the retrieved block. The change in tone about 10–20 mm from the surface corresponds with the concentration profile discontinuities. A similar darker region was observed at the same distance from the surface of all sections cut from the block. In areas where the

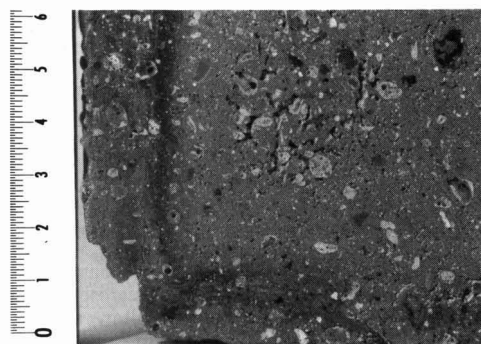


Figure 3. Cross-section cut from the coal-waste reef block showing darkened region near the surface. Scale is in centimeters.

surface of the block was irregular or fractured, the darker region paralleled the surface. Surface darkening has been noted in earlier examinations of coal-waste reef blocks. Labotka et al. (8) noted a uniform darkening in the surface region of reef blocks retrieved after 80-weeks submersion and took this as evidence of recrystallization. In the 1988 block, the darkening process appears to have created two distinct layers, a lighter one near the surface and a darker one in the 10–20-mm region. These results are more consistent with those of Conjeaud (10), who examined cement pastes exposed to seawater and noted a light-colored calcite-rich layer at the surface underlain by a darker brucite-rich layer.

SEM and EDX examinations of numerous samples from near the block's surface showed that dark regions are indeed enriched with Mg. However, no distinct crystals of Mg minerals were apparent in any of the SEM–EDX examinations, even at magnifications of 2000 \times . It appears that the Mg enrichment results either from the precipitation of an amorphous Mg phase or from substitution of Mg into other phases such as calcite.

XRD Results. Examination of the X-ray diffractograms revealed that the samples taken at 17.4, 30.5, and 78 mm from the surface had an identical mineralogy.

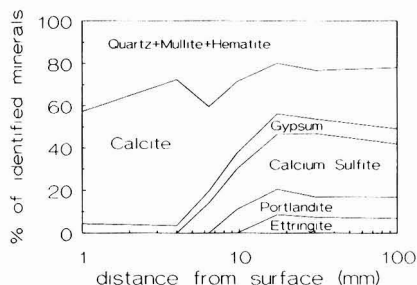


Figure 4. Summary of semiquantitative XRD results.

Quartz, calcite, portlandite, ettringite, gypsum, calcium sulfite, mullite, and hematite peaks were identified in diffractograms from these locations. The samples taken at 1 and 4.0 mm from the surface showed a very different mineralogy. Portlandite, ettringite, and calcium sulfite were not detected in these samples and calcite peaks were much more prominent than in the samples from the inner block. Samples taken at 6.4, 9.7 and 13.6 mm showed a transition between the surface and internal mineralogies.

All major peaks in the diffractograms were identified. The diffractograms were checked for any evidence of an Mg precipitate, such as that noted by Fuhrmann and Colombo (9), but none was found. The inability to identify an Mg phase by XRD concurs with the SEM-EDX findings and suggests that the Mg near the block's surface is present as an amorphous phase.

Results of the semiquantitative analysis of the X-ray diffractograms are shown in Figure 4. The difficulties involved in quantitative XRD analysis of samples containing so many phases should not be underestimated. Cullity (11) presented a thorough discussion of this subject. To limit potential errors in the quantitative analysis of the reef block samples, only mineral phases with peaks corresponding to three or more significant peaks in the diffractogram were included in the quantitative analysis. Despite these precautions, the results should be interpreted as being indicative of trends rather than as accurate quantities. The dominant trends apparent in Figure 4 are the increase in calcite and the disappearance of portlandite, ettringite, and calcium sulfite across a region 10–20 mm from the surface. This region corresponds to the locations of the morphological and chemical discontinuities discussed above.

Reactive Mineralogy. A more complete picture of the present mineralogy of the waste block can be obtained by combining information from both the XRD and concentration profiles. The summary concentration profiles shown in Figure 5 were obtained by averaging the individual profiles, converting to molar units, and summing the reactive cations and reactive anions. Similarities between these profiles and Figure 4 are immediately apparent. For example, the decrease in sulfate concentrations moving toward the block's surface corresponds to the disappearance of the sulfur-containing minerals, ettringite and calcium sulfite, in the XRD profiles. The residual sulfate evident in the near-surface region corresponds to the gypsum phase in the XRD profile.

Similar correspondence is evident between the carbonate and calcite profiles. The XRD evidence shows that the dominant calcium phases at the block's surface are calcite and gypsum. Comparison of the anion profiles with the calcium profile supports this conclusion. In the inner region of the block, the calcium profile exceeds the sum of anion profiles by about 1 mol/kg. The excess calcium is accounted for by the hydroxide phase, portlandite. The

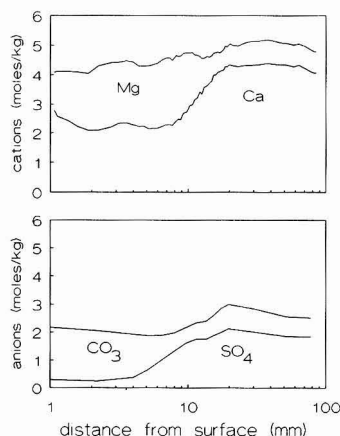


Figure 5. Summary profiles for reactive cations (upper) and anions (lower).

pH profiles in Figure 1 show that porewater in the inner regions of the block had a pH of about 12, consistent with the presence of a calcium hydroxide phase.

The identity of the magnesium phase remains questionable. However, if the above interpretation of the calcium mineralogy is correct, all of the carbonate or sulfate present in the near-surface region is accounted for. Substitution of Mg into calcite minerals is therefore unlikely to account for more than a small amount of the observed Mg enrichment. The remaining possibilities are that the magnesium is present as hydroxide, oxide, or silicate phases. Neither magnesium oxides nor silicates are likely to have precipitated in the near-surface region. At most, these phases could account for the background Mg present throughout the profile. We therefore tentatively conclude that the magnesium enrichment in the near-surface region is due to precipitation of a hydroxide phase. This conclusion is also supported by the pH profiles in Figure 1, which show that the porewater pH in the near-surface region was between 9 and 10, as would be expected in the presence of magnesium hydroxide in equilibrium with seawater.

Long-Term Processes. Comparison of the concentration and mineralogical profiles from this study with information from earlier studies (7, 8) shows that the inner region of the block has been relatively unaffected by contact with the seawater. In contrast, the region of the block within 10–20 mm of the surface has undergone significant alterations. Some of the alteration processes have been hypothesized in earlier reef block research, (e.g., ref 8) and in concrete durability research (e.g., ref 12 and references therein). Results of the present study provide support to these hypotheses and allow a more complete picture to be formed.

Exchange of magnesium for calcium as the principal reactive cation is the most notable feature in the present reef block profiles. The fact that the most soluble calcium phases, portlandite and calcium sulfite, have disappeared from the near-surface region suggests that dissolution and precipitation processes, rather than a simple ion exchange, are responsible. Since seawater is undersaturated with respect to portlandite and calcium sulfite, dissolution of calcium phases is to be expected. The net loss of Ca, as shown by the profiles in Figure 2, indicates that a portion of the Ca released by dissolution diffuses out of the block. The remainder is consumed by precipitation with carbonate ions, which tend to diffuse inward from the seawater.

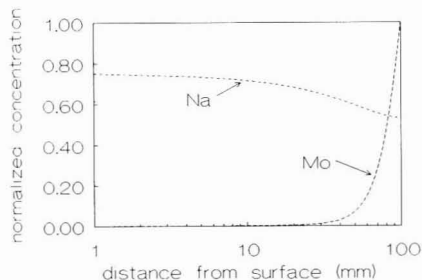


Figure 6. Na and Mo profiles predicted by a simple diffusion model. Diffusion coefficients were calculated according to leaching test methods (14). Results have been normalized by the scales of Figure 2 to allow easy comparison.

The OH^- ion released by the portlandite dissolution produces the high pH's measured in the inner block and creates a hydroxyl concentration gradient toward the block's surface. In the near-surface region, where no portlandite remains, the outward-diffusing hydroxyl ion is consumed by precipitation with the inward-diffusing Mg ion. As is evident from Figure 5, the net result of these processes is an approximately 1:1 exchange of Ca for Mg.

The Ca-Mg exchange creates surprisingly sharp discontinuities in the concentration profiles. Discontinuities such as these are not usually associated with either diffusion or dissolution. They are a result of the combination of the two processes and are known in mathematical literature as moving boundaries (13). The dissolution process is focused at a "boundary" between the region where the solid phase has been completely dissolved and the region where the solid phase is still present. Dissolution behind the boundary is limited because ion products remain higher than or equal to the solubility product. In front of the boundary, diffusion carries the dissolution products away and toward the surface. The continuing dissolution and diffusion result in a slow movement of the boundary toward the block's center.

We know of no previous work wherein the leaching of compounds from a solidified waste has been treated as a moving boundary problem. The "leach testing" procedures currently used in laboratory studies measure only the element leaving the waste block and the results are then interpreted by use of simple diffusion models (e.g., refs 14 and 15). Although these models produce empirically correct descriptions of the leaching test data, the profiles shown herein indicate that they do not accurately reflect the complexity of the underlying phenomena.

Researchers in the field of concrete durability have shown that precipitation in the pores of concrete exposed to seawater reduces hydraulic permeability (10, 12, 16). This process is referred to as "pore refinement" because new, smaller pores are created between the fine crystals of precipitate. We believe that discontinuities observed in the Na profiles indicate that this mechanism has been active in the reef block. In contrast to the Ca and Mg profiles, the Na profile is not likely to have been affected by dissolution or precipitation. However, as Figure 6 shows, the profile is certainly not what would be expected from diffusion alone. The magnitude of the increase in Na concentrations in the near-surface region is consistent with complete replacement of the surface porewater by seawater (assuming a bulk density to porosity ratio of 3 g/mL). The sudden drop at the 10–20-mm boundary suggests a local reduction in the diffusion coefficient. As mentioned above, similar profiles were obtained for two other conservative sea salts, Cl and Br. In each of these

cases, the increase in concentration is consistent with complete mixing of seawater in the near-surface region and a restriction of diffusion across the boundary region. We suggest that pore refinement, resulting from precipitation of calcium carbonate and magnesium hydroxide, causes the localized change in diffusion.

Further evidence for pore refinement is obtained by a comparison of results from this block with one retrieved after 80-weeks submersion. Discontinuities in the chemical profiles and in the block's color were evident in the earlier studies (7, 8). Since diffusion-controlled processes (including these moving boundary processes) vary with the square root of time, these discontinuities would be expected to have moved about twice as far into the block over the 8-year period. As is shown in Figures 1 and 2, the discontinuities were at approximately the same location in both blocks, indicating that the diffusion-controlled processes had been stopped or at least slowed by the time of the earlier studies.

The indirect evidence indicates the extent of pore refinement and the time scale over which it occurs. Unfortunately, since effective pore refinement requires only localized precipitation in the necks of connected pores, direct measurement of porosity changes may be impossible. Certainly the inhomogeneity of the reef blocks precludes any meaningful measurement of porosity changes over such short distances. Further experiments under better controlled conditions may provide more direct evidence of pore refinement and its effects.

Implications for Coal-Waste Block Integrity. Both for structural performance and for the containment of contaminants, it is essential that the stabilized waste blocks not be overly weakened through reactions with their surroundings. Although the mechanisms of strength loss upon exposure of concrete to seawater are still in question, a number of reactions have been identified that may also affect stabilized coal wastes. The formation of expansive ettringites, "magnesium ion attack" of calcium silicate hydrates, and mass loss due to "carbonic acid attack" were mentioned by Mehta (12). The first of these possibilities is unlikely to occur in the reef block because of the initially high concentration of sulfates. Ettringite formation occurred during the pouring and setting of the blocks and the present profiles indicate a subsequent dissolution rather than an uptake of sulfate. The latter two possibilities are also unlikely, at least in the near to medium future. The coal-waste block contains sufficient reactive Ca minerals to ensure that the cementing materials, the calcium silicate hydrates, are not attacked. Only when the supply of portlandite, calcium sulfite, and gypsum are consumed will the less soluble matrix materials be attacked. Although this process may be occurring in the near-surface region, the center of the block is still well protected after 8 years in seawater.

Pore refinement acts to slow down all reactions between seawater and the interior of the block and may therefore contribute significantly to the long-term integrity of the waste block in marine environments. Evidence for this effect is provided by a comparison of the CWARD results with those from an experiment wherein coal-waste blocks were submerged in Lake Ontario (17). The freshwater environment provided no source of magnesium ion and hence no pore refinement was possible. In contrast to blocks retrieved from the marine environment, blocks of the same original composition exhibited marked surface softening after a 1-year exposure to freshwater.

It is interesting to note that the primary source of ions for the pore-refining precipitation was unreacted calcium

hydroxide. In conventional concrete practice, complete reaction of calcium hydroxide is considered desirable since it leads to minimum porosity and to a matrix less likely to react with its environment (12). Further research is needed to determine whether, in the case of waste stabilization for use in marine environments, the design criteria should include additional calcium hydroxide for pore refinement.

Implications for Contaminant Leaching. The central question in most utilizations of stabilized waste is the rate at which contaminants are leached to the surroundings. As mentioned above, the current understanding of leaching processes is based on information gained from laboratory leach testing, which measures only the element leaving the stabilized block. Leach tests undoubtedly serve many useful regulatory and investigative purposes; they are rapid and repeatable and can be easily interpreted. However, the present results show that contaminant profiles in leached blocks can be much different from those predicted by simple leaching models. This observation suggests the importance of using chemical and mineralogical profiling, in conjunction with leach testing, to develop a better fundamental understanding of the processes controlling contaminant leaching in the field.

The discontinuities in the As profiles in Figure 2 show that major elements are not the only ones affected by moving boundary processes. The profiles indicate that As leaching is restricted by reactions in the boundary region, perhaps by sorption or coprecipitation with the magnesium hydroxide phase. Total leaching of this element, as determined by integrating the concentration profiles and comparing them with As profiles in the original blocks, is less than 5%. The leaching of other elements associated by sorption or coprecipitation with a dissolving mineral phase will also be controlled by the dissolution of that phase. Although the mathematical proof is beyond the scope of this paper, it can be shown that the resulting moving boundary processes cannot be distinguished from simple diffusion by leach test methods; concentration profiles are required.

A number of elements showed concentration profiles similar to that of Zn in Figure 2. These elements have apparently not been affected by the moving boundary processes. In fact, the smooth concentration profiles suggest that no leaching of these elements has occurred. This point is confirmed by comparison of total concentrations in the present block with those from blocks retrieved earlier. Apparently, these elements are present either as insoluble minerals or in association with non-reactive phases, such as the glassy fly ash particles present in the original waste and the calcium silicate hydrate matrix.

Pore refinement also appears to have significant effects on contaminant leaching. The Mo profile in Figure 2 is a mirror image of the Na profile, suggesting that Mo leaching is limited by the same physical restriction. For comparison, Figure 6 shows the very different Mo profile that would be expected from a simple diffusion process. Concentration profiles for other contaminants also show leaching limited to the near-surface region. The negligible impact of waste block contaminants on the local biota (3, 5) can be partially explained by the fact that leaching has been limited to, at most, the outer 10–20 mm of the block.

Conclusions

The combination of concentration and XRD profiles provides a more complete picture of the present mineralogy of the coal-waste block than can be obtained by either

method alone. The combined results allow identification of the dissolution and precipitation processes active in the block during the 8 years of exposure to seawater. Dissolution of calcium hydroxide, calcium sulfite, and ettringite began at the block surface and proceeded as a moving boundary toward the interior. Some of the calcium released by dissolution was reprecipitated as a carbonate phase. The remainder was lost to the surrounding seawater. Magnesium ions infiltrating from the seawater were precipitated, apparently as a hydroxide phase. Concentration profiles of As, Sb, and B showed that minor elements also exhibit moving boundary effects, perhaps through association with the mineral phases. The alteration and leaching processes were confined to within 10–20 mm of the block's surface. Many concentration profiles showed sharp discontinuities in this region, a feature that cannot be explained by the simple diffusion-based models presently used to interpret leaching data.

Sharp discontinuities in the concentration profiles of nonreactive sea salts led to the hypothesis that the precipitation of small crystals in pores near the block's surface restricted diffusion. This process is fundamentally similar to the pore refinement identified by earlier workers. It causes a slowing of all diffusion-controlled processes, including the degradation of the block matrix and the leaching of contaminants. These effects are favorable for proposed utilizations of stabilized energy waste in the marine environment. Further research is required to determine the potential for optimizing the pore refinement process and to establish its limitations.

Acknowledgments

The waste reef block was made available to ECN by P. M. J. Woodhead of the Marine Sciences Research Center, State University of New York. Slicing, sampling, and analysis of the block were performed at ECN by J. Wijkstra and D. Hoede. The X-ray diffractograms were produced by V. Govers of the Institute of Earth Sciences, University of Utrecht. Mr. Govers also made available computer facilities for quantitative analysis of the XRD results. R. N. J. Comans of ECN proofread the manuscript and made valuable suggestions. The skill and cooperation of each of these individuals were appreciated by the authors.

Registry No. Ca, 7440-70-2; Mg, 7439-95-4; Fe, 7439-89-6; As, 7440-38-2; Zn, 7440-66-6; Mo, 7439-98-7; Na, 7440-23-5.

Literature Cited

- (1) Manz, O. E.; Faber, J. H.; Takagi, H. In *Third CANMET/ACI International Conference on Fly Ash, Silica Fume, Slag and Natural Pozzolans In Concrete, Supplementary Papers*; compiled by M. Alasali; Conference Organizing Committee (CANMET): Ottawa, ON, Canada, 1989; pp 1–15.
- (2) Duedall, I. W.; Kester, D. R.; Park, P. K.; Ketchum, B. H. In *Wastes in the Ocean*; Duedall, I. W., Kester, D. R., Park, P. K., Ketchum, B. H., Eds.; John Wiley and Sons: New York, 1985; Vol. 4, pp 3–42.
- (3) Parker, J. H.; Woodhead, P. M. J.; Duedall, I. W.; Colussi, J.; Hilton, R. G.; Pfeifferberger, L. E. In ref 2, pp 537–555.
- (4) Roethel, F. J.; Oakley, S. A. In ref 2, pp 691–717.
- (5) Woodhead, P. M. J.; Jacobson, M. E. In ref 2, pp 597–612.
- (6) Woodhead, P. M. J.; Parker, J. H.; Carleton, H. R.; Duedall, I. W. *Coal-Waste Artificial Reef Program, Phase 4b*; EPRI CS3726; Electric Power Research Institute, Palo Alto, CA, 1984.
- (7) van der Sloot, H. A.; Wijkstra, J.; van Stigt, C. A.; Hoede, D. In ref 2, pp 467–497.
- (8) Labotka, A. L.; Duedall, I. W.; Harder, P. J.; Schlotter, N. J. In ref 2, pp 717–739.

- (9) Fuhrmann, M.; Colombo, P. *Radioact. Waste Manage. Nucl. Fuel Cycle* 1989, 33, 365-380.
- (10) Conjeaud, M. L. In *Performance of Concrete in the Marine Environment*; ACI Publication SP65; American Concrete Institute: Detroit, MI, 1980; pp 39-61.
- (11) Cullity, B. D. *Elements of X-Ray Diffraction*; Addison-Wesley Publishing Co.: Reading, MA, 1978.
- (12) Mehta, P. K. *Concrete: Structure, Properties, and Materials*; Prentice-Hall Inc.: Englewood Cliffs, NJ, 1986.
- (13) Crank, J. *Free and Moving Boundary Problems*; Clarendon Press: Oxford, U.K., 1984.
- (14) American Nuclear Society Standards Committee Working Group ANS16.1. *American National Standard Measure-*

- ment of the Leachability of Solidified Low-Level Radioactive Wastes by a Short-Term Test Procedure*; American Nuclear Society: La Grange Park, IL, 1986.
- (15) Edwards, T.; Duedall, I. W. In ref 2, pp 741-755.
- (16) Regoud, M. In ref 10, pp 63-82.
- (17) Flynn, G. B.; Scudato, R. J.; Gannon, J. E. In ref 2, pp 651-665.

Received for review August 28, 1990. Revised manuscript received March 5, 1991. Accepted March 14, 1991. Funding for the project was obtained from NOVEM, the Netherlands Agency for Energy and the Environment.

Effect of Redox Potential and pH on Arsenic Speciation and Solubility in a Contaminated Soil

Patrick H. Masscheleyn,* Ronald D. Delaune, and William H. Patrick, Jr.

Laboratory for Wetland Soils and Sediments, Center for Wetland Resources, Louisiana State University, Baton Rouge, Louisiana 70803-7511

■ The influence of redox potential and pH on arsenic speciation and solubility was studied in a contaminated soil. Alterations in the oxidation state of arsenic, as influenced by redox potential and pH, greatly affected its solubility in soil. At higher soil redox levels (500-200 mV), arsenic solubility was low and the major part (65-98%) of the arsenic in solution was present as As(V). An alkaline pH, or the reduction of As(V) to As(III), released substantial proportions of arsenic into solution. Under moderately reduced soil conditions (0-100 mV), arsenic solubility was controlled by the dissolution of iron oxyhydroxides. Arsenic was coprecipitated [as As(V)] with iron oxyhydroxides and released upon their solubilization. Upon reduction to -200 mV, the soluble arsenic content increased 13-fold as compared to 500 mV. The observed slow kinetics of the As(V)-As(III) transformation and the high concentrations of Mn present indicate that, under reduced soil conditions, arsenic solubility could be controlled by a $Mn_3(AsO_4)_2$ phase.

Introduction

Because the solubility, mobility, bioavailability, and toxicity of arsenic depends on its oxidation state (1-5), studies of As speciation and transformations among species are essential to understanding the As behavior in the environment. Arsenate [As(V)] and arsenite [As(III)] are the primary As forms in soils. Both As(V) and As(III) are subjected to chemically and/or microbiologically mediated oxidation-reduction and methylation reactions in soils and natural waters (3, 6-8). Numerous studies have dealt with As sorption on specific minerals and soils. Amorphous iron and aluminum hydroxides (9, 10), clay content (11), and pH (9-12) are the soil properties reported to be most related to As sorption. Methylated arsenic oxyacids can be produced by a variety of microorganisms, and their presence has been reported in a wide range of natural waters (8, 13) and soils and sediments (7, 14).

Although of great environmental importance, little detailed information is available about the influence of redox potential on the behavior of As in contaminated soils. Deuel and Swoboda (2) reported an increase of total soluble As under reduced conditions and attributed this increase to the reduction of ferric arsenate compounds. Using an equilibrium thermodynamics approach, Sadiq et

al. (15) developed solubility isotherms for several metal arsenates. Under oxidized conditions, they predicted that As solubility would be determined by a $Ca_3(AsO_4)_2$, $Mn_3(AsO_4)_2$ or a $Pb_3(AsO_4)_2$ phase. Similar conclusions were reported by Hess and Blanchard (16). Under reducing conditions, arsenite minerals are too soluble to persist in soils, but arsenic sulfides were predicted to be stable (15). Livesey and Huang (17) concluded that soluble arsenate was controlled by adsorption reactions in soils, rather than through the precipitation of arsenate compounds.

The purpose of this paper is to report the effect of soil redox potential and pH on the speciation and solubility of As in a contaminated soil. Results generated identified soil redox-pH conditions that can limit or enhance As translocation and movement in the environment. Interpretations are based on results of laboratory experiments and simple equilibrium thermodynamic calculations.

Experimental Section

Soil. A soil known to be contaminated with As was collected near Kolin, LA. The soil, located in the vicinity of an As dipping vat, had been exposed to As contamination for a period of greater than 20 years. A detailed description of the sampling site was given by Kotuby-Amacher and Gambrell (18). Surface (0-20 cm) samples were taken from the soil, belonging to the Acadia-Kolin Association (Aeric Ochraqualf). This association consists of loamy upland soils that have a clayey subsoil. Upon arrival in the laboratory, the soil was air-dried, ground to pass a 1-mm sieve, homogenized by thorough mixing, and stored at room temperature in 4-L polyethylene flasks until use.

The organic matter content and pH of the surface soil were determined to be 1.8% and 5.6, respectively. The surface soil had a total (aqua regia digestion) As content of $555 \pm 18 \text{ mg kg}^{-1}$ ($n = 5$) dry soil. Quartz constituted more than 90% of the X-ray (Cu K α radiation) detected mineral fraction of bulk powder samples. Minor concentrations of both potassium feldspars and plagioclase minerals were also detected. The clay fraction contained mostly kaolinite and mixed layered illite-montmorillonite (>85%). Using selective extraction techniques, Kotuby-Amacher and Gambrell (18) determined the manganese oxide, and amorphous iron oxide content of the surface soil

to be in the order of 0.03 and 0.15%, respectively. Correlation analysis revealed that the major part of the As present was associated with the amorphous iron oxide phase (18). No crystalline As minerals were detected by the X-ray diffraction technique.

Experiments. In a first experiment, 60-g portions of dry soil were placed in a set of plastic canisters (19) and gently compacted with intermittent additions of distilled deionized water followed by incubation under flooded conditions for a desired period of time. The saturated soil created a 6-cm-deep layer in the core. Then, water was introduced from the bottom with the help of a syringe and needle until an overlying floodwater depth of ~2 cm was created. Adding water from the bottom helped to release entrapped air. To ensure reducing conditions the canisters were sealed with the supplied caps. Duplicate canisters were opened after 1, 3, 15, 35, 65, and 105 days of submergence. An Eh–pH depth profile was taken by using a system similar to that described by Patrick and Delaune (20). Rather than measuring continuous profiles, we decided to gradually lower the microelectrodes to preselected depths (0.25, 0.5, 1.5, 2.5, 3.5, and 4.5 cm). Preliminary experiments had shown that an equilibration period of 4 h was necessary to obtain constant redox readings. After an Eh–pH depth profile was taken, the overlying water was removed from the cores with a plastic syringe followed by horizontal sectioning at 0.5-, 1.0-, 2.0-, 3.0-, 4.0-, and 5.0-cm core depths. The volume (0.5–0.8 mL) of saturation extracts, recovered from soil sections by centrifugation and filtration, was not sufficient for the determination of all elements of interest. Therefore, each section was immediately transferred to a 40-mL polycarbonate centrifuge tube to which a known volume of oxygen-free deionized distilled water was added. The lids of the centrifuge tubes were equipped with rubber septa, which facilitated the displacement of air with argon. The soil suspensions were shaken for 1 h on a mechanical shaker, centrifuged (20 min at 7000 rpm, Sorvall GSA-400 rotor, Du Pont Co., Wilmington, DE) and filtered through a 0.45- μ m micropore filter under an inert argon atmosphere by use of a pressure–vacuum system (21). Each supernatant was divided into two aliquots. One was used for the determination of soluble As species and sulfides. Concentrated HNO_3 (200 μL /10 mL of extract) was added to the second aliquot in which selected soluble metals (Ca, Mg, K, Na, Al, Fe, Mn, Cu, Pb, Cd, Ni, and Zn) and total P were determined. After the extraction, the dry weight of the soil in each tube was determined. This allowed the calculation of the soil to water ratio, which varied from 2.70 to 3.40.

In the next series of experiments, soil suspensions were equilibrated under controlled redox and pH conditions. The soil was equilibrated (at $28 \pm 2^\circ\text{C}$) in laboratory microcosms at various redox–pH conditions by using a modification (22) of the pH–redox control system developed by Patrick et al. (23). Suspensions were prepared by mixing an amount of soil equivalent to 200 g of dry weight with deionized distilled water so that the final soil/water ratio was 1 to 6. The following redox–pH conditions were used: redox –200, 0, 200, and 500 mV; pH 5, 8, and uncontrolled. In the uncontrolled pH experiments, the microcosms were sampled at 3-day intervals over a 24-day period. The other microcosms were sampled at the end of the 24-day equilibration period. Natural (uncontrolled) pH values at the end of the incubation period were 5.2 for 500 mV, 6.7 for 200 mV, 7.0 for 0 mV, and 7.2 for –200 mV. All experiments were run in duplicate. Sampling proceeded as follows. Two soil suspension aliquots were withdrawn from each microcosm,

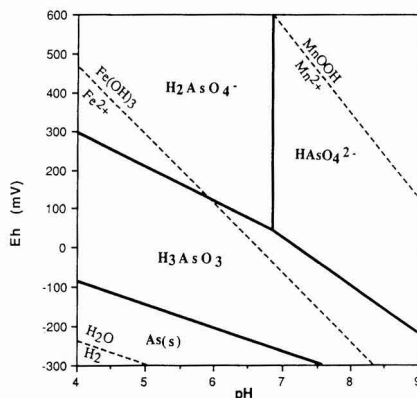


Figure 1. Eh–pH diagram for the system As–H₂O system. Activities of As, Mn, and Fe were all taken to be 10^{-4} .

centrifuged, and filtered through a 0.45- μ m micropore filter under an inert argon atmosphere for reduced treatments. One filtered supernatant was used for the determination of As and sulfides, the other was treated as described above and used for cation and metal analysis.

Analysis. The water extracts were analyzed for As species with a pH-selective hydride generation/separation technique followed by atomic absorption spectrophotometry detection (24). The arsines from inorganic As(III) were selectively generated and purged for analysis from a solution buffered at pH 6.5 with Tris [tris(hydroxymethyl)aminomethane] buffer. The solution was then further acidified with concentrated HCl (to a final concentration of 3 M HCl) and analyzed for As(V). Although our analytical technique was optimized for the determination of methylarsonic acid and dimethylarsenic acid in the presence of large concentrations of inorganic As species, we were not able to detect any organic arsenicals present. The performance of the analyzing step involving hydride generation, cryogenic condensation, and volatilization was assessed by analysis of EPA reference standards for total inorganic As [As(III) + As(V)] and yielded values of 25 and 241 $\mu\text{g L}^{-1}$ compared with the true values of 26.7 and 235 $\mu\text{g L}^{-1}$. Absorbance was found linear over the range 2–120 ng of As and had a sensitivity of 0.0083 absorbance units/ng of As. Six measurements of absorbance at the 50-ng level gave a relative standard deviation of 2.3%. All As species in the extracts were analyzed within 5 h after sampling.

Metals, major cations, and total P in solution were analyzed with a Jarrel Ash ICP. The performance of the ICP was checked with EPA reference samples. Sulfide was measured by an ion-specific Ag/S electrode in an anoxic buffer solution (sulfide electrode operating instructions; Lazar Research Laboratories, Los Angeles, CA), and titration alkalinity determinations (25) were used to estimate the concentrations of soluble carbonate species.

Possible mineral saturation was evaluated through the use of the equilibrium computer model (PC version 1.23) GEOCHEM (26). Statistical analysis were performed with PC-SAS (27).

Results and Discussion

Arsenic Speciation, Transformations, and Solubility as Affected by Soil Redox Potential. The predicted effect of redox potential (Eh) and pH on the oxidation state of As is summarized in Figure 1, which was constructed by use of critically evaluated thermodynamic data (28, 29). It can be seen that H_3AsO_3 , H_2AsO_4^- ,

HAsO_4^{2-} , or As(s) will be the thermodynamically dominant As species present in a soil, depending on its Eh and pH. It is important to remember that this Eh–pH diagram is really a “predominance-area” diagram because the outlined fields are those areas where the designated species make up more than 50% of the total concentration. To make the diagram more useful, the redox couples $\text{Fe}(\text{OH})_3/\text{Fe}(\text{II})$ and $\text{MnOOH}/\text{Mn}(\text{II})$ were also included. Since both manganese and iron oxides and hydroxides exist in various degrees of crystallinity (amorphous, meta-stable poorly crystalline, and crystalline), the actual stability fields for these compounds may differ from computed boundaries from soil to soil. In using the term Eh, it is also important to distinguish between the quantity that is calculated from the activities of a specific redox pair (as in Figure 1) and the quantity measured with a platinum electrode. In the reported experiments Eh was used in the latter sense and it is to be understood that the measured “equilibrium” Eh represents a mixed redox potential, i.e., the composite of different ongoing redox processes. In order to make the measured Eh values amenable to quantitative interpretation, we also measured the $\text{As}(\text{III})/\text{As}(\text{V})$, soluble Mn [$\text{Mn}(\text{II})$], soluble Fe [$\text{Fe}(\text{II})$], and the S (–II) redox species. As will be illustrated, the measured Eh corresponded to buffering with respect to particular redox pairs.

In the first experiment, a time series evaluation between Eh, pH, soluble redox elements, and As species in soil cores was made. Changes in vertical distribution of Eh, $\text{As}(\text{III})$, $\text{As}(\text{III}+\text{V})$, Mn, and Fe upon flooding are presented in Figure 2. During the equilibration under submerged conditions, the pH increased from 5.6 to 7.1 (Figure 2A–D). Little variation in pH (± 0.2) was found throughout a particular profile. Flooding periods longer than 35 days did not significantly alter the vertical distribution of Eh and redox elements studied. Flooding (reducing conditions) of the soil did not have an influence on soluble Al, Ca, Mg, Na, and K concentrations. However, as early as 3 days after flooding, there was a considerable increase in soluble Mn throughout the soil core (Figure 2, parts A vs B). As more reducing conditions ($\text{Eh} < 150$ mV) developed, dissolved Mn increased to a near constant value of approximately 35 mg kg^{-1} soil. No Fe was solubilized after 3 days of flooding (Figure 2B). When, between the 15th and 35th day of submergence, redox levels dropped below 100 mV, soluble Fe concentrations reached a maximum (Figure 2, parts C vs D) and stayed unchanged for the rest of the equilibration period.

Some arsenic was reduced and released into solution before the solubilization of the ferric hydroxide layer. Differences in depth profiles presented in Figure 2A and B clearly illustrate this. While soluble Fe concentrations remained unchanged, dissolved As concentrations increased by a factor of 2, and $\text{As}(\text{III})$ became the major species present. Solubilization of As was occurring simultaneously with the reduction of $\text{As}(\text{V})$ to $\text{As}(\text{III})$ (Figure 2B).

The constructed phase diagram (Figure 1) adequately depicts the sequence of redox reactions encountered in our soil. Quantitative inferences could not always be made with respect to critical redox levels at which particular redox pairs are unstable. Manganese became mobilized when the measured Eh dropped from 300 to ~ 150 mV, while according to the equilibrium thermodynamic considerations, the reduction of MnOOH to Mn^{2+} should occur at approximately 600 mV (pH 7.0). On the other hand, at redox levels below 100 mV (pH 6.4) $\text{As}(\text{III})$ became the predominant As species in solution, this in agreement with the computed phase diagram for the $\text{As}-\text{H}_2\text{O}$ system.

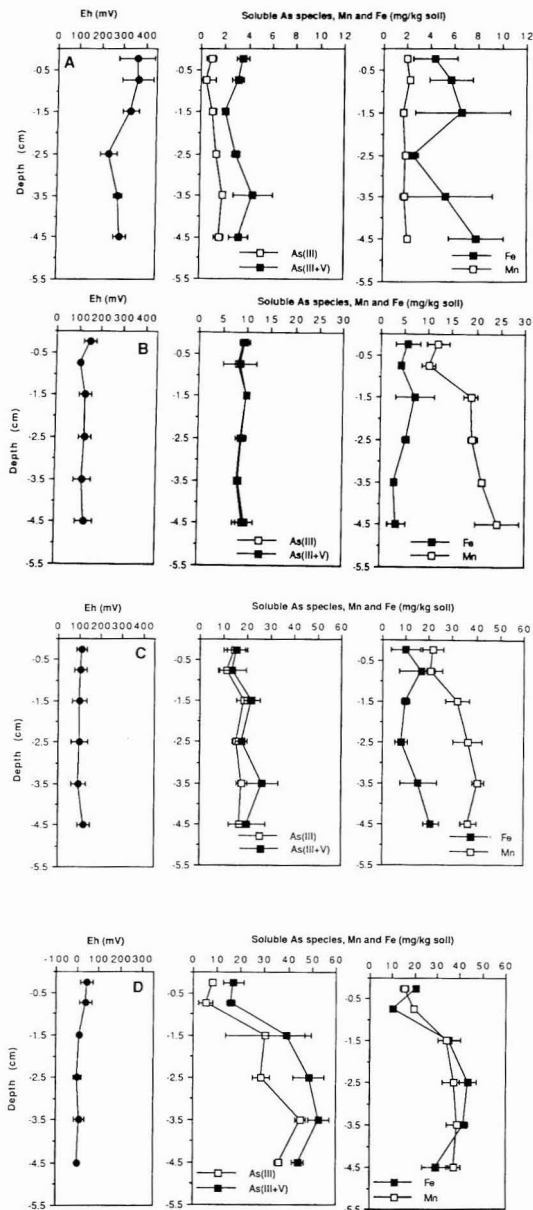


Figure 2. Vertical distribution of Eh, soluble As species, Mn, and Fe. (A) after 1 day of flooding (pH = 5.7 ± 0.1). (B) after 3 days of flooding (pH = 6.4 ± 0.2). (C) after 15 days of flooding (pH = 7 ± 0.2). (D) after 35 days of flooding (pH = 7 ± 0.3). Note changes in scale.

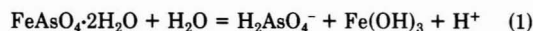
Furthermore, the observed mobilization of Fe at an Eh of ~ 50 mV (pH 7.0) is in reasonable agreement with the calculated $\text{Fe}(\text{OH})_3/\text{Fe}^{2+}$ stability boundary.

Data for equilibrations at 35 days show a sharp and correlative increase ($P < 0.01$) of total soluble As and Fe. When expressed on a molar basis, the dissolution of As occurred at Fe to As ratios varying from 0.8 to 1.7. Although it is very difficult to distinguish between adsorption and coprecipitation reactions without direct examination of the solid surfaces involved (30, 31), consideration of the molar Fe/As ratios released upon reduction suggests that As was coprecipitated with the iron oxyhydroxides. It

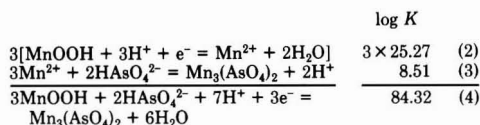
appears that As(V) was released upon solubilization of the hydroxides and slowly reduced to As(III).

Generally, observed increase in soluble As upon reduction have been attributed to the solubilization of ferric arsenate and other forms of iron combined with arsenic (2, 32–34). From our experiment, however, it can be seen that the reduction and release of As may occur before the dissolution of iron oxyhydroxides. Apparently, the dissolution of the ferric hydroxide layer led to a further increase in As concentrations. Up to 10% of the total As present in the soil became soluble. Although thermodynamically unfavorable, a considerable amount of As(V) was observed under reduced conditions after solubilization of the ferric hydroxide layer (Figure 2C,D). Our study indicates that As(V) served as an effective electron acceptor in microbial mineralization of organic matter and thereby became reduced to the more mobile and toxic As(III) species. A possible explanation for the slow and incomplete As(V) reduction is the competition of Fe(III) as a terminal electron acceptor in microbial respiration. It has been shown that manganese(IV) oxides are effective oxidants with respect to As(III) (35, 36); however, the abiotic oxidation of As(III) was not of major importance in our soil. Although there were enough manganese(IV) oxides in the soil to oxidize all of the As(III) to As(V), As(III) remained the predominant soluble As species (Figure 2B–D).

Possible arsenic mineral saturation was evaluated by comparing ion activity products of $(\text{Al}^{3+})(\text{AsO}_4^{3-})$, $(\text{Ca}^{2+})^3(\text{AsO}_4^{3-})^2$, $(\text{Mg}^{2+})^3(\text{AsO}_4^{3-})^2$, $(\text{Mn}^{2+})^3(\text{AsO}_4^{3-})^2$, and $(\text{Fe}^{3+})(\text{AsO}_4^{3-})$ with their most recent tabulated solubility products (16, 29). Other metal arsenates (Cu, Ni, Pb) were ignored because the soluble concentrations of the corresponding metals were very low ($<0.2 \text{ mg kg}^{-1}$ soil). Under oxidized conditions, soil extracts were undersaturated with respect to aluminum, calcium, magnesium, manganese, and iron arsenate minerals. Although the experimental data clearly indicated that As solubility was mainly controlled by an iron phase, the Fe(III) activity in solution was not sufficient for precipitation of FeAsO_4 . Furthermore it has been predicted (16, 29) that an FeAsO_4 mineral formed in soil incongruently will dissolve to iron hydroxide and soluble arsenate, according to the following equation:



The release of high concentrations of Mn upon reduction and the slow kinetics of arsenate–arsenite transformations made the precipitation of a $\text{Mn}_3(\text{AsO}_4)_2$ phase under reduced conditions a likely event, as was indicated by GEO-CHEM (26). The following reactions, based on thermodynamic data (15, 28), illustrate this:



After rearranging eq 4, assuming activities of solid phases and H_2O equal to 1, and substituting values of 7 and 0.5, respectively, for pH and pe ($E_h = 30 \text{ mV}$), we obtain $\log a_{(\text{HAsO}_4^{2-})} = -16.91$. From this expression it can be seen that, upon reduction, MnOOH becomes unstable and very small amounts of soluble As(V) are sufficient to obtain supersaturation with respect to a manganese arsenate phase. The formation of $\text{Mn}_3(\text{AsO}_4)_2$ could set an upper limit for dissolved arsenate concentrations under reducing conditions.

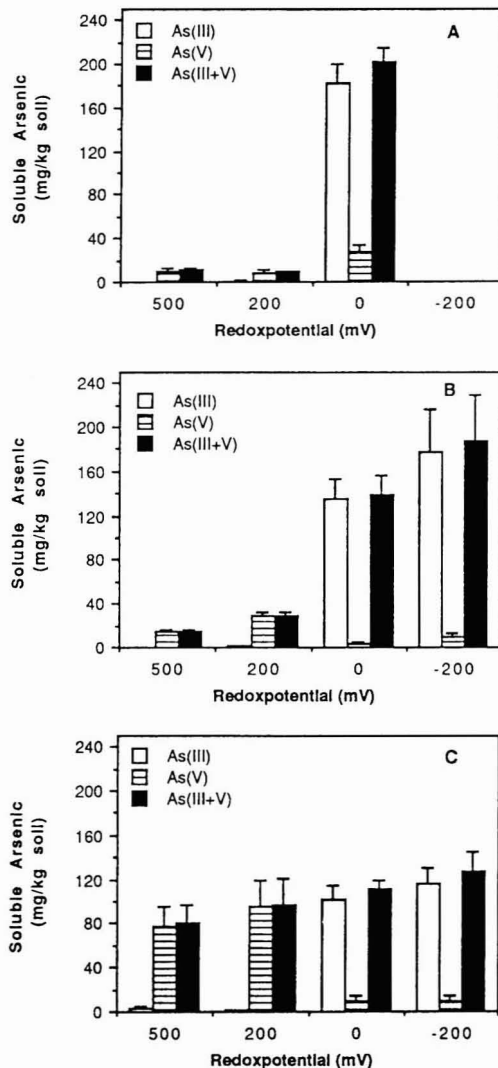


Figure 3. Distribution of soluble arsenic species after a 24-day equilibration period under controlled redox and pH conditions. (A) at pH 5.0. (B) at natural pH (5.2 for 500 mV, 6.7 for 200 mV, 7.0 for 0 mV, and 7.2 for -200 mV). (C) at pH 8.0.

Sulfide concentration stayed well below the detection limit (0.05 ppm) of our analytical technique and its influence on As solubility in the soil can therefore be neglected.

Redox–pH Chemistry of Arsenic. The redox–pH chemistry of As was studied by equilibrating soil suspensions under controlled E_h –pH conditions. Parts A–C of Figure 3 show the species distribution of As at three suspension pH levels (5.0, natural, and 8.0) in combination with four different redox levels (–200, 0, 200, and 500 mV). After ~10 days of equilibration, the preselected redox and pH were reached and maintained during a 2-week period. Upon acidification of the soil to pH 5, strongly reduced conditions (–200 mV) could not be achieved, and results are therefore not available.

Both redox status and pH affected the speciation and solubility of As. At redox potentials of 200 and 500 mV, As(V) was the major dissolved As species, constituting

Table I. Concentration of Soluble As Species, Mn, and Fe as a Function of Soil Redox-pH Conditions

day	pH	Eh, mV	concn, mg kg ⁻¹ soil			
			As(III)	As(V)	Mn	Fe
0	5.6	340	1.4	5.6	1.9	17.5
3	6.7	100	46.8	3.1	20.8	15.3
6	6.8	20	76.5	6.6	21.2	72.0
0	5.8	440	0.9	7.9	2.4	27.3
3	6.6	80	34.3	1.2	17.4	29.5
6	7.0	-100	69.4	3.4	16.2	75.8

>95% of the total soluble As. Upon reduction (0 and -200 mV), As(III) became the major dissolved As species, although concentrations of As(V) up to 14 mg kg⁻¹ dry soil remained, and As solubility generally increased. Up to 40% of the total As present in the soil became soluble. While the first experiment gave an idea of As transformations under natural conditions, the stirred suspension experiment indicated maximum transformations rates.

Similar mechanisms controlling As solubility were observed in both experiments. Table I contains data obtained during two of the controlled Eh experiments. The increase in As solubility before the solubilization of the iron oxyhydroxides was characterized by a reversal in As speciation. Although Mn was reduced after 3 days of incubation, As(III) remained the dominant soluble As species, suggesting that the abiotic oxidation of As(III) to As(V) by Mn(IV) compounds was not important in our soil. A sharp increase of soluble As concentrations coincided with the solubilization of iron oxyhydroxides and the released As(V) was slowly reduced.

Interesting information was obtained from the alkaline (pH 8) equilibrations (Figure 3C). Under oxidized conditions, soluble As concentrations were as much as 3 times higher than in the equilibrations at lower pH. Almost all As was present as As(V). This can be explained by the pH-dependent adsorption characteristics of As(V) onto the oxide surfaces (9, 30). The decreasing positive surface charge of the oxides with increasing pH facilitated the desorption of arsenate. Under reducing conditions, As(III) became the major dissolved species with total soluble As being less than in the more acidic equilibrations. The reason for this is somewhat unclear. An incomplete or slower solubilization of iron oxyhydroxides under alkaline conditions could be responsible for the lower As concentrations observed. At pH 8, dissolved Fe concentrations did not significantly increase upon reduction. Furthermore, the presence of soluble organics under alkaline conditions (pH 8.0) and the formation of iron oxyhydroxides-organic matter complexes could have retarded Fe reduction (37) and the release of As into solution.

In summary, redox potential and pH were shown to control the speciation and solubility of As in a contaminated soil. Both parameters are, therefore, important in assessing the fate of As-containing compounds in soil. Qualitatively, As speciation changed according to thermodynamic predictions. At higher redox levels, As(V) was the predominant As species and As solubility was low. Alkaline conditions and/or reduction of As(V) to As(III) led to a mobilization of As. Under moderately reduced conditions (0-100 mV), As solubility was controlled by the dissolution of iron oxyhydroxides. Data indicate that As was coprecipitated [as As(V)] with the oxyhydroxides and released upon their solubilization. Due to the slow kinetics of the As(V)-As(III) transformation, a considerable amount of the thermodynamically unstable As(V) species was observed under reducing conditions. This slow

transformation rate and the release of high concentrations of Mn upon reduction make the precipitation of a Mn₃(AsO₄)₂ phase possible. When disposal of As-containing wastes is planned, consideration should be given to maintaining high redox and nonalkaline conditions necessary for minimum As solubility and mobilization.

Registry No. As, 7440-38-2; Mn, 7439-96-5; Fe, 7439-89-6.

Literature Cited

- (1) Penrose, W. R. *CRC Crit. Rev. Environ. Cont.* **1974**, *4*, 465-482.
- (2) Duel, L. E.; Swoboda, A. R. *Soil Sci. Soc. Am. J.* **1972**, *36*, 276-278.
- (3) Brannon, J. R.; Patrick, W. H., Jr. *Environ. Sci. Technol.* **1987**, *21*, 450-459.
- (4) U.S. Environmental Protection Agency. *Quality criteria for Water*; U.S. Government Printing Office: Washington, DC, 1976.
- (5) National Research Council. In *Committee on Medical and Biologic Effects of Environmental Pollutants*; National Academy of Sciences: Washington, DC, 1977.
- (6) Ferguson, J. F.; Gavis, J. *Water Res.* **1972**, *6*, 1259-1274.
- (7) Johnston, S. W. M.S. Thesis, Louisiana State University, Baton Rouge, LA, 1978.
- (8) Braman, R. S.; Foreback, C. C. *Science* **1973**, *182*, 1247.
- (9) Pierce, M. I.; Moore, C. B. *Water Res.* **1982**, *16*, 1247-1253.
- (10) Sakata, M. *Environ. Sci. Technol.* **1987**, *21*, 1126-1130.
- (11) Elkhatib, E. A.; Bennet, O. L.; Wright, R. J. *Soil Sci. Soc. Am. Proc.* **1984**, *48*, 1025-1029.
- (12) Pierce, M. L.; Moore, C. B. *Environ. Sci. Technol.* **1980**, *14*, 214-216.
- (13) Andreae, M. O.; Klumpp, D. K. *Environ. Sci. Technol.* **1979**, *13*, 738-740.
- (14) Woolson, E. A. *Weed Sci.* **1977**, *25*, 412-416.
- (15) Sadiq, M.; Zaid, T. H.; Mian, A. A. *Water, Air, Soil Pollut.* **1983**, 369-377.
- (16) Hess, R. E.; Blanchar, R. W. *Soil Sci. Soc. Am. J.* **1976**, *40*, 847-852.
- (17) Livesey, N. T.; Huang, P. M. *Soil Sci.* **1981**, *131*, 88-94.
- (18) Kotuby-Amacher J.; Gambrell, R. P. PB 88-224829; U.S. Environmental Protection Agency, ADA, OK, 1988.
- (19) Jugsujinda, A.; Khind, C. S.; Patrick, W. H., Jr.; Lindau, C. W. *Soil Sci. Am. J.* **1987**, *51*, 837-838.
- (20) Patrick, W. H., Jr.; Delaune, R. D. *Soil Sci. Soc. Am. J.* **1972**, *36*, 573-576.
- (21) Patrick, W. H., Jr.; Henderson, R. E. *Soil Sci. Soc. Am. J.* **1981**, *45*, 855-859.
- (22) Masscheleyn, P. H.; Delaune, R. D.; Patrick, W. H., Jr. *Environ. Sci. Technol.* **1990**, *24*, 91-96.
- (23) Patrick, W. H., Jr.; Williams, B. G.; Moraghan, J. T. *Soil Sci. Soc. Am. J.* **1973**, *37*, 331-332.
- (24) Masscheleyn, P. H.; Delaune R. D.; Patrick, W. H., Jr. *J. Environ. Qual.* **1991**, *20*, 96-100.
- (25) *Standard Methods for the Examination of Water and Wastewater*, 15th ed.; American Public Health Association: Washington, DC, 1988; p 278.
- (26) Sposito, G.; Mattigod, S. V. *GEOCHEM: A computer program for the calculation of chemical equilibria in soil solution and other natural waters*. University of California, Riverside, CA, 1979.
- (27) *SAS User's Guide*; SAS Institute, Inc.: Cary, NC, 1985.
- (28) Lindsay, W. L. *Chemical Equilibria in Soils*, 1st ed.; Wiley: New York, 1979.
- (29) Dove, P. M.; Rimstidt, J. D. *Am. Mineral.* **1985**, *70*, 838-844.
- (30) Evans, L. J. *Environ. Sci. Technol.* **1989**, *23*, 1046-1056.
- (31) Sposito G. In *Geochemical Processes at Mineral Surfaces*; Davis, J. A., Hayes, K. F., Eds.; ACS Symposium Series 323; American Chemical Society: Washington, DC, 1986, pp 217-228.
- (32) Aggett, J.; O'Brien, G. A. *Environ. Sci. Technol.* **1985**, *19*, 231-238.

- (33) Aggett, J.; Roberts, L. S. *Environ. Sci. Technol.* 1986, 20, 183-186.
- (34) Seyler, P.; Martin, J. M. *Environ. Sci. Technol.* 1989, 23, 1258-1263.
- (35) Oscarson, D. W.; Huang, P. M.; Defosse, C.; Herbillon, A. *Nature* 1981, 291, 50-51.
- (36) Oscarson, D. W.; Huang, P. M.; Liaw, W. K. *J. Environ. Qual.* 1980, 9, 700-703.

- (37) Theis, L. T.; Singer, P. C. *Environ. Sci. Technol.* 1974, 6, 569-573.

Received for review February 4, 1991. Accepted March 22, 1991. The proposed research was partially funded by Cooperative Agreement CR816805-01 from the U.S. Environmental Protection Agency, Environmental Research Laboratory, Duluth, MN.

Aqueous-Phase Oxidation of Polychlorinated Biphenyls by Hydroxyl Radicals

David L. Sedlak and Anders W. Andren*

Water Chemistry Program, University of Wisconsin—Madison, Madison, Wisconsin 53706

■ Hydroxyl radicals (OH[•]s), generated with Fenton's reagent, rapidly oxidized polychlorinated biphenyls (PCBs) in aqueous solutions. The observed product distributions indicated that the reaction proceeds via addition of a hydroxyl group to one of the nonhalogenated sites. The unreactive nature of the halogenated sites accounts for the lower reaction rates observed for the more highly chlorinated congeners. Within homologue groups, chlorine substitution in the meta or para positions results in lower reaction rates due to steric hindrance occurring when hydroxyl radical attacks at the site ortho to the aromatic ring. Estimates of environmental half-lives, based upon kinetic measurements, reported steady-state OH[•] concentrations, or estimates of radical production rates, suggest that aqueous-phase oxidation by OH[•]s may be an important PCB loss mechanism in cloudwater and surface waters under certain conditions.

Introduction

Polychlorinated biphenyls (PCBs) are a group of chlorinated aromatic compounds that have been used in dielectric fluids, plasticizers, and cutting oils (1). Concerns about the potential deleterious effects of these compounds on aquatic and terrestrial ecosystems prompted the United States to ban their production subsequent to 1979 (2). Despite a reduction in total emissions, PCBs persist in the environment. To assess the efficacy of the ban and to predict future PCB levels it is necessary to quantify both the amount of PCBs entering the environment and the rate at which they are removed through various pathways. Residence times for individual PCB congeners in the atmosphere and in lakes have recently been investigated in some detail. Calculations indicate residence times of 2-4 months in the atmosphere (3). Residence times in lakes vary as a function of such factors as depth, size, hydraulic residence times, productivity, and sedimentation rates. Recent estimates for Lakes Michigan and Superior seem to indicate residence times on the order of 2-10 years (4, 5). Although physical removal mechanisms appear to be of primary importance, both in the atmosphere and in lakes, the extent of chemical and microbial degradation remains to be determined.

Biodegradation studies have shown that reductive dehalogenation and metabolic oxidation occur under both aerobic (1, 6) and anaerobic conditions (7-9). Although biodegradation is possible, significant concentrations may be required to induce enzymatic activity. Furthermore, organisms capable of metabolizing PCBs have only been observed in a few specific environments, such as anaerobic river sediments (7-9). Biodegradation is probably not an

important loss mechanism for PCBs, except in certain highly contaminated environments.

Direct photodegradation of PCBs by ultraviolet light also occurs to some extent, and recent evidence suggests that atmospheric half-lives for PCBs due to this pathway may be on the order of weeks (10). One of the important direct photolysis reactions results in production of less chlorinated PCB congeners through reductive dehalogenation, and total PCB concentrations may only decrease slowly through this process. Without detailed information on the importance of the various photolysis pathways it is difficult to determine the effect of these reactions on the atmospheric lifetimes of PCBs. Reactions of PCBs with common environmental oxidants such as hydroperoxy radicals (HO₂[•]) and ozone (O₃) have not been reported and are probably not very important because only very strong oxidant species can react with PCBs.

One potentially important degradation mechanism for PCBs is oxidation by hydroxyl radicals (OH[•]s). Hydroxyl radicals are among the strongest environmental oxidants known (11) and their reaction with biphenyl and monochlorobiphenyl has been observed in both the gas (12) and liquid (13) phases. Hydroxyl radicals are ubiquitous in the environment and are present in low concentrations under normal conditions in surface water (14, 15) and in the atmosphere (16, 17). It is believed that OH[•]s are responsible for the degradation of many environmental contaminants such as NO₂ (16) and PAHs (16, 17) and for the formation of natural organic polymers (18). Provided that OH[•] fluxes in the environmental media are sufficient, they could provide an important removal pathway for PCBs.

Atkinson (19) and Leifer (20) estimated atmospheric decay rates for gas-phase PCBs using average steady-state values for atmospheric OH[•] concentrations, an extension of the Hammett coefficient linear free energy relationship, and measured rate constants for biphenyl and chlorobiphenyl. Atmospheric half-life estimates for all of the different congeners derived by Atkinson ranged from 3 to 120 days, which is approximately equal to the atmospheric residence times estimated for PCBs (3). This reaction is especially important from a global standpoint because a significant portion of the world's PCB burden is transported through the atmosphere in the gaseous phase. It should be noted that results from these calculations are somewhat uncertain because actual rate constant measurements are only available for biphenyl and monochlorobiphenyl and the Hammett coefficient relationship may not be very accurate for the more highly chlorinated congeners.

Understanding the reactions of PCBs with OH[•]s is crucial to predicting the future persistence of PCBs and

the hazards associated with their presence. It is especially important to determine reaction rates for all of the important PCB congeners because the toxicity, concentrations, and fate and transport properties vary greatly within this group of chemicals (1). To develop a model of PCB oxidation rates in the environment we have studied in detail the reactions of OH[•]s with PCBs. The initial products of the reaction were followed in the oxidation of 2-chlorobiphenyl with OH[•]. Relative reaction rates for PCB congeners with as many as five chlorines were then determined by examining the oxidation of Aroclor 1242 by OH[•]. Results from these experiments were then used to develop a simple model to predict environmental oxidation rates for PCBs. These results provide information important for the prediction of decay rates for PCBs in aqueous systems and may also be extended to estimate removal rates for gas-phase reactions or the prediction of removal rates for other substituted aromatic compounds.

Materials and Methods

Stock solutions of chlorobiphenyl isomers and PCB mixtures were prepared with Millipore Milli-Q water. The appropriate quantity of PCB, dissolved in acetone, was added to a 4-L vessel. PCB concentrations were below solubility for all isomers present in the solutions. After evaporation of the solvent, water was added to the vessel and the solution was stirred for at least 1 week with a Teflon-coated stir bar. All reaction solutions were maintained at 25 °C with a recirculating water bath.

The oxidation of 2-chlorobiphenyl (2-ClBp) was achieved by adding 1 mL of 20 mM H₂O₂ to a rapidly stirring 100-mL solution of 0.01 mM 2-ClBp with 0.8 mM Fe²⁺. The initial pH was adjusted to the appropriate value with either HCl (pH < 3.0), acetic acid buffer (pH = 4.2), or phosphoric acid buffer (pH = 7.2). Available data for OH[•] rate constants (21) indicated that the buffers would not significantly scavenge OH[•]s at the buffer strengths used. Samples (25 mL) were solvent extracted between 15 and 20 min after initiation of the reaction. Under these conditions H₂O₂ will be the limiting reactant, and kinetic calculations using the published second-order rate constant for the initiation step of the Fenton's reagent reaction (11) and the initial reactant concentrations were performed. Assuming that the initial reaction of H₂O₂ and Fe²⁺ is the rate-limiting step and that the reaction follows second-order kinetics, our calculations indicate that more than 95% of the H₂O₂ was consumed in the first minute after the H₂O₂ was added. By the time the samples were extracted, all of the OH[•] was consumed and the product-forming reactions were complete. The extracts were acidified with HCl (to pH values between 1 and 2), extracted three times with 30 mL of petroleum ether, and analyzed by GC/MS as described previously (22). Quantification of the amount of oxidation that occurred was achieved by comparing concentrations in the extracts with a control sample to which water was added instead of H₂O₂.

Oxidation products were identified by concentrating the petroleum ether extracts to 1 mL and analyzing by GC/MS. The concentrated extracts were also analyzed after derivatization with diazomethane. The chromatograms and mass spectra were compared with a standard of 5-hydroxy-2-chlorobiphenyl (2-chloro-5-biphenylol) obtained from Ultra Scientific (Providence, RI).

Prior to performing competition experiments using an Aroclor 1242 mixture, the extent of reactant adsorption onto the glass walls of the reaction flask was assessed. These experiments were conducted in triplicate with 100 mL of 0.1 mg/L Aroclor 1242 stock solution added to a 100-mL volumetric flask. After a specified time interval,

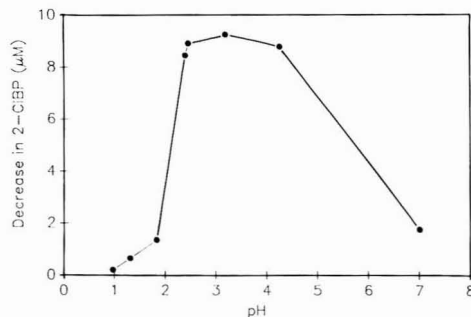


Figure 1. pH dependence for oxidation of 2-chlorobiphenyl with Fenton's reagent. Initial conditions: [Fe²⁺] = 0.8 mM; [H₂O₂] = 0.2 mM; [2-chlorobiphenyl] = 0.01 mM.

50 mL was removed and extracted three times with 50 mL of petroleum ether. PCB concentrations in these samples were compared with those obtained by extracting the remaining 50 mL of solution and the inside of the flask three times with 50 mL of petroleum ether. All samples were analyzed by GC/ECD using a Hewlett-Packard 5890 gas chromatograph with an electron capture detector as described previously (3).

Competition experiments were conducted by adding 70 mL of the Aroclor 1242 stock solution with 0.080 mM H₂O₂ to 30 mL of a rapidly stirring 0.25 mM Fe²⁺ solution with 1.5 mM acetic acid buffer. GC peak areas from samples collected after 4 min were compared with control samples (without H₂O₂) after correction for variability between runs by using the internal standards. Decreases in concentrations for each isomer were converted to relative rate constants by setting the rate constant for 2,3'-dichlorobiphenyl at unity and averaging the results of duplicate experiments. Only the 28 most predominant peaks, which account for approximately 90% of the total amount of PCBs present, are reported because variability in peak areas of the less prevalent congeners observed in duplicate analyses made interpretation of the results difficult. Results for the 28 congeners that were quantified varied by less than approximately ±5% between duplicate analyses.

The relative reaction rates were compared with absolute reaction rates in a separate competition experiment between 2,3'-dichlorobiphenyl and biphenyl. The absolute rate constant for biphenyl used in our analysis is discussed below. The experiment was performed as described above and extracts were analyzed by GC/MS.

Results and Discussion

Oxidation of 2-Chlorobiphenyl. Aqueous solutions of 2-chlorobiphenyl were readily degraded with Fenton's reagent. In a series of experiments conducted at different pHs, as much as approximately 95% of a 0.01 mM 2-ClBp solution was oxidized with 0.8 mM Fe²⁺ and 0.2 mM H₂O₂ after 15 min (Figure 1). Degradation of 2-ClBp was observed over the entire range tested, and approximately 90% of the 2-ClBp was oxidized by H₂O₂ in the pH range of 2.3–4.3. A similar pH dependence was also observed in the oxidation of chlorobenzene with Fenton's reagent (22). The pH dependence of the Fenton's reagent reaction may be directly related to the concentration of Fe(OH)⁺, which is reportedly much more reactive than Fe²⁺ in the Fenton's reagent reaction (23). The inability of the Fenton's reagent reaction to degrade most of the 2-ClBp outside of the pH range of 2.3–4.3 does not imply that OH[•] reactions are only important within this narrow pH range because a variety of other reactions (see below) result in the formation of OH[•]s in the environment. The pH effect could diminish

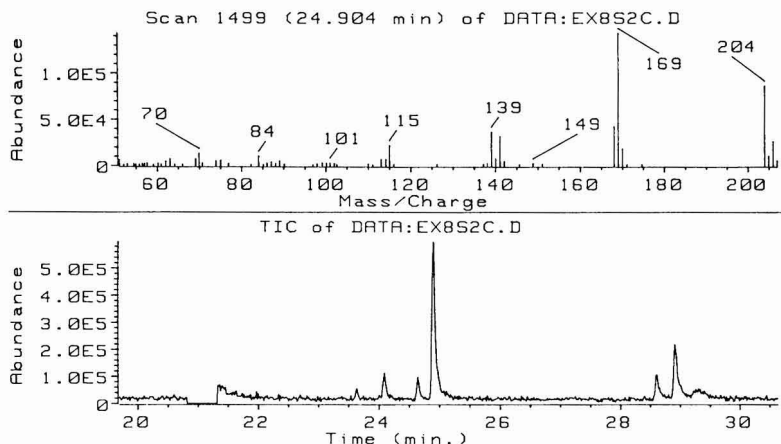


Figure 2. GC/MS chromatogram and typical mass spectrum for underivatized products of 2-chlorobiphenyl oxidation.

Table I. Mass Spectral Data for Diazomethane-Derivatized Reaction Products from Oxidation of 2-Chlorobiphenyl with Fenton's Reagent

peak ^a	RT ^b	<i>m/e</i> fragment ^f					ID ^c
		[M - CH ₃ Cl] ⁺	[M - CH ₃ Cl] ⁺	[M - Cl] ⁺	[M - CH ₃] ⁺	[M] ⁺	
1	25.07	1.00 ^d	—	0.50	—	0.78	ortho
2	25.74	0.71	—	—	0.38	1.00	ortho
3 ^e	26.96	—	0.33	—	—	1.00	meta
4	27.19	—	0.43	—	—	1.00	meta
5	27.33	—	0.38	—	0.50	1.00	para
6	27.59	—	0.36	—	0.27	1.00	para
7	27.75	—	0.37	—	—	1.00	meta

^a Order of elution of peaks. ^b Retention time. ^c Tentative identification of hydroxylation position based on mass spectral data. ^d Relative intensity of mass spectral peak. ^e Retention time and mass spectra correspond to methylated 5-hydroxy-2-chlorobiphenyl standard. ^f —, indicates not present.

the importance of the reactions in environments where the Fenton's reagent reaction is an important source of OH[•]s. Other common OH[•] sources may not exhibit the same pH effect.

Several intermediate compounds isolated from the oxidized solutions were identified as hydroxychlorobiphenyls (HCIBps). The GC/MS chromatograms indicated the presence of several compounds with almost identical mass spectra (Figure 2), which closely matched the mass spectra of the 5-hydroxy-2-chlorobiphenyl standard and the NBS mass spectral library entry for hydroxymonochlorobiphenyls. Derivatization of these extracts with diazomethane resulted in seven distinct peaks with several different mass spectral patterns (Figures 3 and 4, Table I). The mass spectrum for one of the methylated intermediates (peak 3) was similar to that of the 5-hydroxy-2-chlorobiphenyl standard and the other mass spectra were similar to those described for hydroxychlorobiphenyls by Tulp et al. (24). The location of OH substitution on the derivatized HCIBp isomers was determined by evaluation of the different mass fragments of the compounds in a manner similar to that described by Tulp et al. (24). The compound identified as the product of meta hydroxylation (peak 3) had the same retention time as the 5-hydroxy-2-chlorobiphenyl standard. In addition, relative retention times for the identified isomers corresponded to the order observed by Tulp et al. (24) (i.e., ortho, meta, para).

The seven hydroxychlorobiphenyls result from hydroxylation at each of the nonhalogenated sites. Concentrations of the different isomers were approximately the same order of magnitude and were not quantified

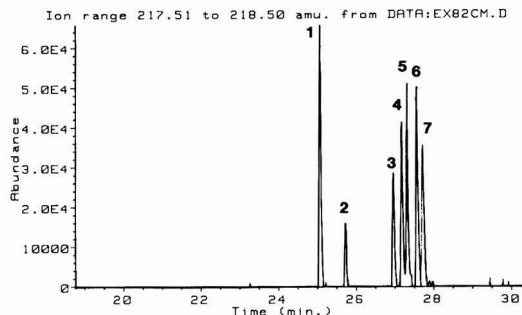


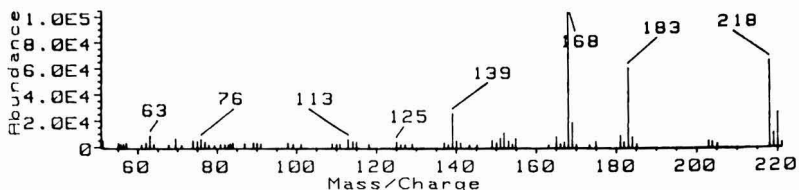
Figure 3. GC/MS chromatogram for derivatized reaction products from oxidation of 2-chlorobiphenyl with Fenton's reagent. Peak numbers correspond to spectra in Figure 4.

because analytical standards for all seven compounds were unavailable and it was not possible to determine the amount of each isomer that underwent further reactions with OH[•]s. Additional qualitative analysis of the chromatogram suggested the possible presence of dihydroxylated chlorobiphenyls. Other oxidation products were not observed in the chromatograms. However, the existence of more polar intermediate products resulting from ring cleavage or additional ring hydroxylation was not disproven since these compounds might not be amenable to the solvent extraction and/or gas chromatography procedures used in this analysis.

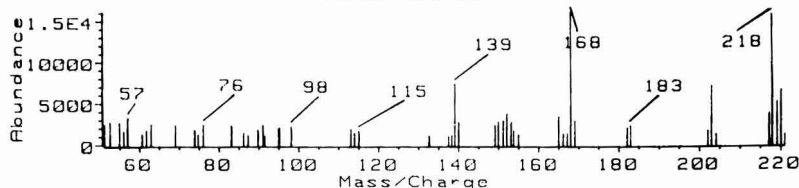
Oxidation of PCB Isomers in Aroclor 1242. To test the effect of chlorine substitution on PCB reactivity, a

PEAK #

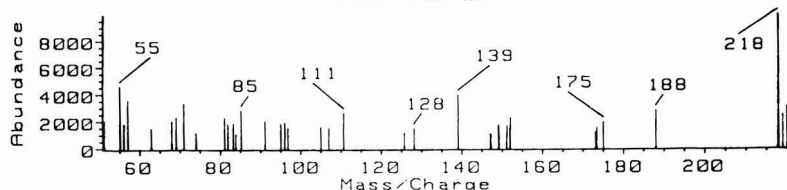
1



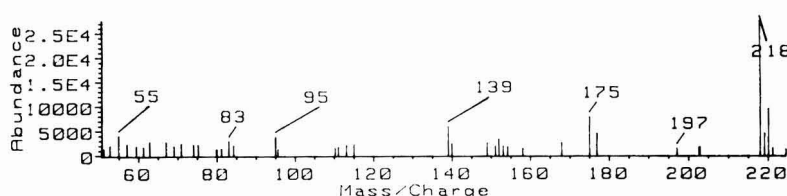
2



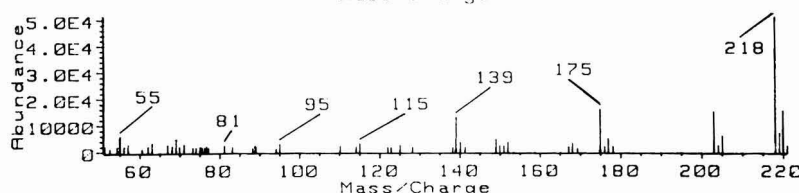
3



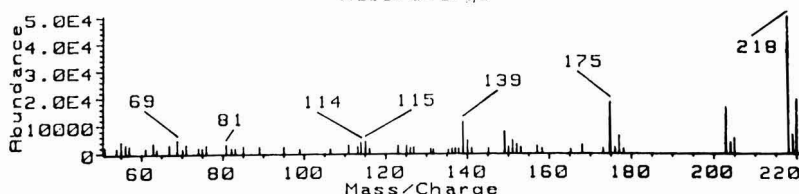
4



5



6



7

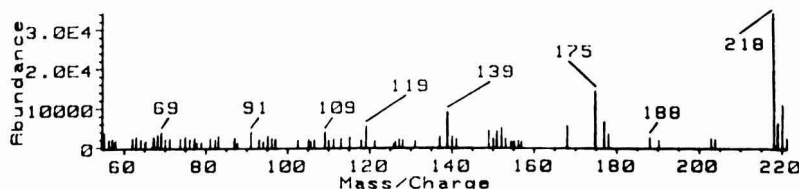


Figure 4. Mass spectra for derivatized reaction products for oxidation of 2-chlorobiphenyl with Fenton's reagent. Peak 3 was found to have the same retention time and mass spectrum as the derivatized 5-hydroxy-2-chlorobiphenyl standard.

series of experiments were conducted in which an aqueous PCB mixture, prepared from a sample of Aroclor 1242, was oxidized with Fenton's reagent. Relative rate constants for a group of PCB congeners were measured by monitoring congener concentrations in the Aroclor solutions before and after reaction with OH^\cdot . Thus, it was possible to test the effect of chlorine substitution through one ex-

periment rather than through a series of individual measurements for different congeners.

In evaluating reactions involving hydrophobic organic compounds (such as highly chlorinated PCBs), it is important to consider adsorption to container walls, which may result in heterogeneous reactions occurring via different mechanisms at rates different from homogeneous

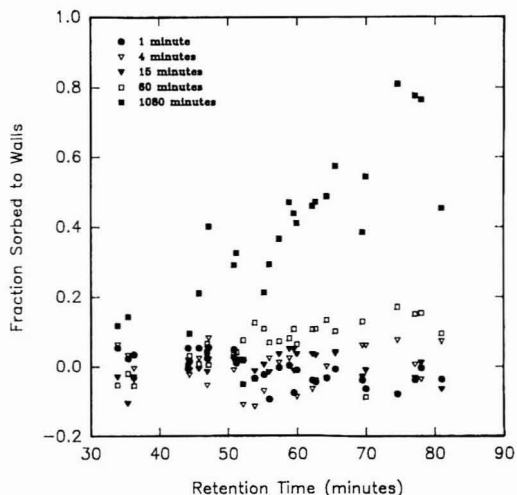


Figure 5. Time dependence of adsorption of Aroclor 1242 onto a glass reaction vessel.

reactions. To avoid confounding effects of heterogeneous reactions it was important to generate OH's only in the presence of dissolved PCBs. Previously, reaction kinetics for hydrophobic compounds were conducted in nonaqueous solvents such as 1,1,2-trichlorotrifluoroethane to avoid such heterogeneous reactions (25). Although it is possible to produce OH's via Fenton's reagent in nonaqueous solutions, we chose to conduct our experiments in aqueous solutions, because results from experiments in organic solvents are often difficult to apply to environmental settings. Analysis of the adsorption kinetics of PCB congeners with as many as five chlorines (Figure 5) demonstrated that insignificant quantities of all congeners were adsorbed within the first 15 min after addition to the vessel. Thus, the rapid kinetics of the OH[•] reactions relative to adsorption assured that the reaction was complete before any PCBs were adsorbed to the container wall.

The absence of nonhalogenated products in the experiments with 2-chlorobiphenyl and previous experiments with chlorobenzene demonstrated that dechlorination reactions are insignificant relative to hydroxylation reactions in the initial attack of OH's on chlorinated aromatic compounds. Furthermore, product analysis showed that hydroxylation occurred to some extent at all nonhalogenated sites despite steric hindrance and/or resonance effects. If dechlorination reactions (chlorine abstractions) are insignificant relative to OH addition at nonhalogenated sites, PCBs with fewer chlorines should be oxidized more readily than the more highly substituted congeners. Thus, the unreactive nature of the halogenated site should be an adequate predictor of relative oxidation rates between homologue groups.

Relative rate constants were calculated from peak areas for the congeners measured before and after the reactions with the following equation:

$$k_{rel} = k_2/k_1 = [\ln(c_2/c_{2,init})]/[\ln(c_1/c_{1,init})] \quad (1)$$

where k_{rel} is the relative rate constant for congener 2; k_1 and k_2 are the absolute rate constants for reactions 1 and 2, respectively; c_1 and c_2 are the final peak areas for congeners 1 and 2, respectively; and $c_{1,init}$ and $c_{2,init}$ are the initial peak areas for congeners 1 and 2, respectively.

The rate constants for all of the congeners were calculated relative to 2,3'-dichlorobiphenyl (2,3'-DCB). The observed trend for the measured relative rate constants

Table II. Results from Competition Experiments with Aroclor 1242 Mixture

peak ^a	name ^b	no. of Cl	rel rate ^c	abs rate, ^d $\times 10^9 \text{ dm}^3 \text{ mol}^{-1} \text{ s}^{-1}$
7	2,4-DCB	2	0.88	7.1
6	2,3'-DCB	2	1.00	8.0
5/8	2,3-DCB	2	0.98	7.9
18	2,2',5'-TCB	3	0.86	6.9
17	2,2',4'-TCB	3	0.93	7.5
24/27	2,3',6'-TCB	3	0.94	7.6
16	2,2',3'-TCB	3	0.89	7.2
32	2,4',6'-TCB	3	0.99	8.0
26	2,3',5'-TCB	3	0.78	6.3
25	2,3',4'-TCB	3	0.89	7.2
28/31	2,4,4'-TCB	3	0.90	7.2
33	2',3,4'-TCB	3	0.89	7.2
22	2,3,4'-TeCB	3	0.92	7.4
45	2,2',3,6'-TeCB	4	0.83	6.7
52	2,2',5,6'-TeCB	4	0.71	5.7
49	2,2',4,5'-TeCB	4	0.77	6.2
48/47	2,2',4,5'-TeCB	4	0.79	6.4
44	2,2',3,5'-TeCB	4	0.69	5.5
37/42	2,2',3,4'-TeCB	4	0.79	6.4
41/71	2,2',3,4'-TeCB	4	0.71	5.7
40	2,2',3,3'-TeCB	4	0.76	6.1
74	2,4,4',5'-TeCB	4	0.67	5.4
70/76	2,3',4',5'-TeCB	4	0.69	5.5
66	2,3',4,4'-TeCB	4	0.63	5.1
56/60	2,3,3',4'-TeCB	4	0.67	5.4
92/84	2,2',3,5,5'-PeCB	5	0.59	4.7
101	2,2',4,5,5'-PeCB	5	0.57	4.6
110	2,3,3',4',6'-PeCB	5	0.53	4.3

^aCoeluting peaks are listed together. The predominant peak [according to Manchester-Neesvig and Andren (3)] was used in model formulation. ^bAbbreviations: DCB, dichlorobiphenyl; TCB, trichlorobiphenyl; TeCB, tetrachlorobiphenyl; PeCB, pentachlorobiphenyl. ^cRate normalized relative to rate for congener 6, value is average of duplicate experiments. ^dEstimated rate based upon competition experiments with congener 6 and biphenyl. Rate used for biphenyl oxidation is described in text.

(Table II) demonstrates a decrease in oxidation rates for the more highly chlorinated PCBs. As the number of chlorines increased from two to five the rate constant decreased by approximately a factor of 2. The relative rate constant also varied considerably within each homologue group. This decrease in reaction rates with increasing degree of chlorination is considerably smaller than that predicted by gas-phase structure-activity relationship (SAR) models that are based upon measurements of reaction rate constants for biphenyl and monochlorobiphenyl (19, 20).

The relative rate constants were converted to absolute values by comparing the relative reaction rates for biphenyl and 2,3'-DCB to measurements of the absolute rate constant for biphenyl. Results from the competition experiment using 2,3'-DCB and biphenyl yielded a relative reaction rate of 1.12 ($k_{biphenyl}/k_{2,3'-DCB}$). The reported absolute rate constant for the reaction of biphenyl and OH[•] is $9.0 \times 10^9 \text{ dm}^3 \text{ mol}^{-1} \text{ s}^{-1}$ (13), which was measured from the formation of radical cations in the reaction of biphenyl and OH[•]. This measured absolute rate constant approaches the diffusion-controlled limit for the reaction calculated from application of kinetic theory (26).

Structure-Activity Relationships. If the number of available nonhalogenated sites is the only factor responsible for controlling the reaction rates of OH's with PCB congeners, then a linear relationship should exist between the relative rate constants and the number of nonhalogenated sites. A correlation ($R^2 = 0.95$, using a least-squares simple linear regression model) was observed between the number of nonchlorinated sites and the ob-

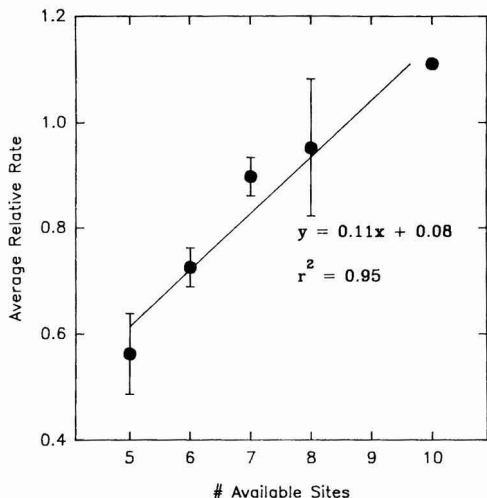


Figure 6. Relationship between number of nonchlorinated sites and average relative reaction rates. Error bars represent 95% confidence interval for each homologue group.

served average relative rate constant for each homologue group (Figure 6). The observed slope of the regression line (0.11) is consistent with the expected results if each additional chlorinated site prevents 10% of the effective collisions from resulting in a reaction and the more highly chlorinated congeners have slightly smaller diffusivities.

Although the relationship between the number of available sites and the average rate constant for the homologue groups is consistent with our hypothesized reaction mechanism, it does not adequately explain the high degree of variability observed within homologue groups. The most obvious explanations for this variability are resonance and steric effects. Structure-activity relationships such as the Hammett coefficient relationship used for predicting rate constants for gas-phase reactions (19, 20) discriminate between congeners within homologue groups on the basis of resonance effects. However, such a model should not be applied to analysis of these data because it assumes that OH substitutions will occur only at the most energetically favored site(s), which is clearly not supported by product analysis.

Measurements of reductive potentials for dehalogenation half-reactions of PCB congeners (27) have shown that PCBs containing ortho chlorinated sites are better reductants than other congeners in the same homologue group. A valid explanation of this effect is that congeners with chlorine groups adjacent to the ring are subject to more steric strain than other congeners and a greater change in free energy occurs upon dehalogenation. Using this observation to explain reaction rates of PCBs with OH \cdot , we have assumed that hydroxylation in positions located ortho to the aromatic ring will be less favorable than hydroxylation at other sites because ortho hydroxylated compounds will experience more steric strain than meta or para hydroxylated compounds. This effect was tested by fitting a multiple regression model in which available ortho sites were treated separately from meta and para sites. (In cases where coeluting peaks were quantified, the congener present in higher concentrations was used in the model.) The model provided a highly significant prediction of the rate constants when all of the data were used ($R^2 = 0.85$; coefficient for substituent location: ortho = 0.112; meta/para = 0.168; intercept = -0.160) (Figure 7). The coefficients for the predictor variables indicate

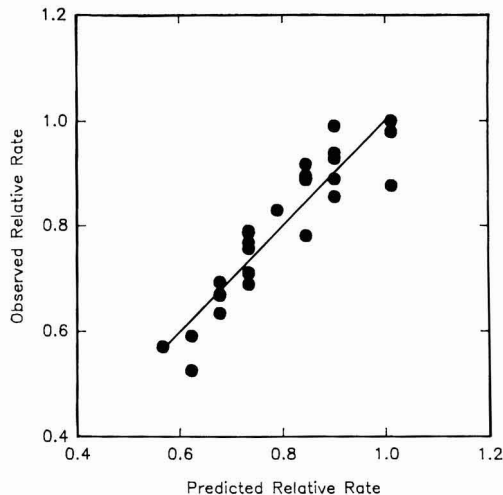


Figure 7. Relationship of measured relative rates and rates predicted by separate consideration of ortho and meta/para hydroxylation sites for oxidation of PCBs by OH \cdot . Line indicates exact agreement.

that meta and para sites were more reactive than ortho sites.

Prediction of Environmental Decay Rates. To determine the significance of hydroxyl radical oxidation as a PCB loss mechanism it is necessary to evaluate both the reaction rate constants and reactant (PCB, OH \cdot) concentrations. If the oxidant (OH \cdot) is present at relatively constant, low concentrations, it may be reasonable to make a steady-state approximation and model the process as a pseudo-first-order decay, with a rate constant expressed as the product of the absolute rate constant (k_a) and the steady-state OH \cdot ([OH \cdot] $_{ss}$) concentration:

$$-d[\text{PCB}]/dt = k_a[\text{OH}\cdot]_{ss}[\text{PCB}] = k[\text{PCB}] \quad (2)$$

Data on steady-state OH \cdot concentrations are available for the atmosphere (19) and some surface waters (14, 15) and may be used to predict PCB decay rates in this manner.

In surface waters, OH \cdot s are produced by processes including photochemical excitation of organic chromophores and photolysis of nitrate ions (15). These OH \cdot s quickly react nonselectively with many organic and inorganic chemicals present in the water and very low steady-state OH \cdot concentrations are typically observed. As a result of these low oxidant concentrations, reactions of organic contaminants with OH \cdot s are often relatively unimportant in surface waters. Persistent contaminants, which are not amenable to degradation by other processes, may eventually degrade through OH \cdot reactions. For example, by use of published rate constant values (21), the half-lives for aromatic compounds were calculated to range from approximately 8 to 800 days at the steady-state OH \cdot concentrations (14, 15) observed in several freshwater samples.

Steady-state OH \cdot concentrations have not been determined in cloudwater or rain because processes contributing to OH \cdot formation and degradation vary considerably over time and space and calculation of steady-state OH \cdot concentrations is very difficult. Consideration of estimated OH \cdot production rates or fluxes in cloudwater suggests that aqueous OH \cdot s are among the most important cloudwater oxidants and may be responsible for the oxidation of hydrophilic compounds in clouds. Aqueous OH \cdot s may be produced in cloudwater via the mechanisms described above for surface waters as well as via diffusion of OH \cdot s from the gas phase (28), reaction of Fe $^{2+}$ with H $_2$ O $_2$ (29)

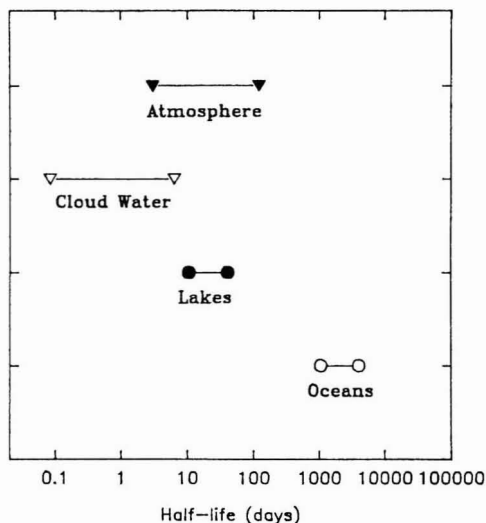


Figure 8. Estimated half-lives for PCBs in various environmental media. Atmospheric vapor phase half-lives from Atkinson (19).

(Fenton's reagent reaction), and photoreduction of ferric complexes (29, 30). Recent evidence suggests that the latter two trace-metal-mediated processes may be more important to liquid-phase OH^\bullet generation than previously believed: A considerable portion of the iron present in cloudwater (up to 0.2 mM) was found to be in the reduced form (31), possibly as the result of photochemical reduction of Fe^{3+} or reactions of Fe^{3+} with HO_2^\bullet (32). Reduced iron in cloudwater readily reacts with H_2O_2 , which is present as the result of diffusion into cloudwater from the gas phase, as evidenced by measurements from cloudwater (33, 34) and rain (35).

An evaluation of PCB and OH^\bullet reaction rates in fog, rain, and cloudwaters must also consider the physicochemical state of the reactants as well as the presence of other OH^\bullet scavengers. Homogeneous liquid-phase reactions of biphenyl are known to occur. The extent to which heterogeneous reactions take place is presently unknown. PCB concentrations in fog, rain, and cloudwaters are controlled by gas-phase partitioning into water droplets and by the presence of particle-associated PCBs. Observed concentrations in rainwater are usually less than 10–15 ng/L but are higher than those predicted by Henry's law coefficients (36). Such deviations are thought to result from the influence of dissolved organic matter, colloids, and particulate matter. An average of 50% of the total PCB mass in 10 precipitation events was found in "dissolved" (filterable) form. It has also been reported that fogwater, which is thought to be similar in chemical composition to cloudwater, shows even higher enrichments. Reported total PCB concentrations are in the range of 7–22 $\mu\text{g/L}$ (37). In our analysis we have not attempted to account for the effect of sorption on decay rates for PCBs in cloudwater, fog, or rain. If heterogeneous reactions do not occur, or occur at much slower rates than homogeneous reactions, the OH^\bullet oxidation reactions will still be important because a substantial fraction of the PCB mass is dissolved.

The estimated rate constants and reported or predicted steady-state OH^\bullet concentrations were used to calculate environmental half-lives in surface water for PCBs with as many as eight chlorines (Figure 8). The estimates were not extended to PCBs with more than eight chlorines

Table III. Constituents Present in Cloudwater and Associated Contribution to OH^\bullet Removal

component	concn, ^a M	rate const, ^{b,c}	sum
H^+	10^{-4}	NR	
SO_4^{2-}	10^{-4}	NR	
NO_3^-	10^{-4}	NR	
NH_4^+	10^{-4}	1×10^8	1.0×10^4
Na^+	10^{-4}	NR	
Cl^-	10^{-4}	NR	
Fe^{3+}	10^{-6}	7.9×10^7	7.9×10^1
Mn^{4+}	10^{-6}	7.9×10^7	7.9×10^1
formate	2×10^{-4}	3.4×10^9	6.8×10^5
acetate	8×10^{-4}	2.3×10^7	1.8×10^5
phenols	2×10^{-6}	1.0×10^{10}	2.0×10^4
alkanes	4×10^{-6}	1.0×10^9	4.0×10^3
total			8.9×10^5

^a Concentrations for first eight constituents are upper range from ref 32; values for constituents 9–12 from ref 37. Assumed molecular weights: phenols, 78; alkanes, 207. ^b Rate constant for OH^\bullet reaction from Buxton et al. (21). ^c NR, no reaction.

because few PCBs with more than eight chlorines are present in the environment and the model could not be extrapolated beyond this range. OH^\bullet concentrations in marine surface waters (10^{-18} M) are approximately 2 orders of magnitude lower than freshwater because bromide ion present in seawater at a concentration of approximately 0.8 mM (38) has a reaction rate constant of approximately $10^9 \text{ dm}^3/\text{mol-s}$ (21) and effectively scavenges OH^\bullet s. In the ocean, low steady-state OH^\bullet concentrations and low dissolved PCB concentrations probably render this oxidation pathway insignificant. In freshwater systems, half-lives range from approximately 4 to 11 days and OH^\bullet oxidation could remove a substantial amount of the PCBs in the water column, provided that residence times are sufficient and particle-bound PCBs react with OH^\bullet s. From a global perspective, OH^\bullet oxidations may not be very important because PCBs in the water column represent only a small fraction of the total mass in the environment.

A different method was employed for the calculation of half-lives of PCBs in cloudwater because estimates of steady-state OH^\bullet concentrations were unavailable. This calculation is intended to provide a preliminary estimate of PCB oxidation half-lives and may not account for some of the factors important to atmospheric modeling efforts. In the calculation it was assumed that the sole source of OH^\bullet s in cloudwater is gas-phase transfer, which Chameides and Davis (28) estimated to occur at a rate of approximately 0.5–10 nM/s. Constituents present in the cloudwater (Table III) compete for available OH^\bullet s. The pseudo-first-order rate constant for oxidation of any PCB congener by OH^\bullet s is equivalent to the product of the absolute rate constant and the steady-state OH^\bullet concentration (which is expressed as the rate of OH^\bullet production divided by the rate constant for OH^\bullet loss):

$$k' = k_a(\text{rate of } \text{OH}^\bullet \text{ diffusion}) / \sum [k_i(i)] \quad (3)$$

where the sum of the rates and concentrations of all reactive constituents in the rainwater (i) are given by the data in Table III.

The constituents listed in Table III do not include those unidentified compounds such as lignins, carbohydrates, and tannins. These unidentified materials may be very important in terms of their contribution to dissolved organic carbon (DOC). However, without any experimental data it is difficult to assess their reactivity with OH^\bullet s. For the purposes of this analysis it was assumed that these constituents were unimportant relative to the chemicals listed in Table II. The half-lives for PCBs may be readily

calculated by solving for the pseudo-first-order rate constant:

$$t_{1/2} = \ln(2)/k' \quad (4)$$

And, if the sum of the non-PCB constituents in the solution scavenge OH's much more effectively than the PCBs (i.e., $\sum[k_i(i)] \gg k_{\text{PCB}}[\text{PCB}]$), then the half-life can be expressed as a function of only those parameters listed in eq 3.

The cloudwater half-lives depicted in Figure 8 serve only as a preliminary estimate of the contribution of OH[•] reactions to the oxidation of PCBs occurring in the environment. Factors such as competition for OH's by unidentified organic compounds may increase half-lives, while OH[•] sources not considered, including the Fenton's reagent reaction, photolysis of Fe³⁺, and other sources of OH's, will decrease half-lives. These calculations suggest that cloudwater half-lives may be as much as 1 order of magnitude lower than half-lives in other environmental media.

Conclusions

Although the half-lives presented in Figure 8 have not been substantiated with field measurements or a detailed evaluation of OH[•] concentrations, they do provide estimates of the importance of these various PCB loss mechanisms. From a global standpoint, oxidation by OH's in surface waters probably does not remove a significant quantity of PCBs. In oceans, very low steady-state OH[•] concentrations and low aqueous PCB solubility preclude the removal of large amounts of PCBs. Despite modest removal rates for dissolved PCBs in lakes and streams, OH[•] oxidation reactions in freshwater environments are not important because PCBs in the water column account for a small fraction of the global PCB burden. In the atmosphere, gas-phase oxidation may be an important mechanism for PCB loss; however, additional measurements or more appropriate SARs are necessary to more accurately assess half-lives. PCB oxidation by OH's in cloudwater could be an important mechanism for PCB degradation, and further work may provide a sufficient substantive basis for evaluating the global significance of this pathway. Absolute oxidation rates may be at least as high, if not 1 order of magnitude greater than gas-phase rates, but the hydrophobic nature of PCBs may prevent large quantities of PCBs from partitioning into cloudwater and DOC may effectively compete for OH's. Further research to more accurately determine cloudwater PCB concentrations and OH[•] production and loss rates and to monitor for the presence of PCB oxidation products in the environment may provide information necessary for evaluating the relative importance of these degradation pathways.

Acknowledgments

We thank David Degenhardt of the Wisconsin State Laboratory of Hygiene for his advice on the derivatization of reaction products.

Registry No. 2,4-DCB, 33284-50-3; 2,3'-DCB, 25569-80-6; 2,3-DCB, 16605-91-7; 2,2',5-TCB, 37680-65-2; 2,2',4-TCB, 37680-66-3; 2,3',6-TCB, 38444-76-7; 2,2',3-TCB, 38444-78-9; 2,4',6-TCB, 38444-77-8; 2,3',5-TCB, 38444-81-4; 2,3',4-TCB, 55712-37-3; 2,4,4'-TCB, 7012-37-5; 2',3,4-TCB, 38444-86-9; 2,3,4'-TCB, 38444-85-8; 2,2',3,6-TeCB, 70362-45-7; 2,2',5,6'-TeCB, 41464-41-9; 2,2',4,5'-TeCB, 41464-40-8; 2,2',4,5-TeCB, 70362-47-9; 2,2',3,5'-TeCB, 41464-39-5; 2,2',3,4'-TeCB, 36559-22-5; 2,2',3,4-TeCB, 52663-59-9; 2,2',3,3'-TeCB, 38444-93-8; 2,4',5-TeCB, 32690-93-0; 2,3',4',5-TeCB, 32598-11-1; 2,3',4,4'-TeCB, 32598-10-0;

2,3,3',4'-TeCB, 41464-43-1; 2,2',3,5,5'-PeCB, 52663-61-3; 2,2',4,5,5'-PeCB, 37680-73-2; 2,3,3',4',6-PeCB, 38380-03-9; Aroclor 1242, 53469-21-9; hydroxyl, 3352-57-6.

Literature Cited

- (1) Hutzinger, O.; Safe, S.; Zitko, V. *The Chemistry of PCBs*; CRC Press: Cleveland, OH, 1974.
- (2) U.S. EPA Fed. Regist. 1979, 44, 31514-31568.
- (3) Manchester-Neesvig, J. B.; Andren, A. W. *Environ. Sci. Technol.* 1989, 23, 1138-1148.
- (4) Swackhamer, D. L.; Armstrong, D. E. *Environ. Sci. Technol.* 1986, 20, 879-883.
- (5) Eisenreich, S. J. In *Sources and Fates of Aquatic Pollutants*; Hites, R. A., Eisenreich, S. J., Eds.; Advances in Chemistry 216; American Chemical Society: Washington, DC, 1987; Chapter 13.
- (6) Baxter, R. M.; Sutherland, D. A. *Environ. Sci. Technol.* 1984, 18, 608-610.
- (7) Brown, J. F.; Wagner, R. E.; Feng, H.; Bedard, D. L.; Brennan, M. J.; Carnahan, J. C.; May, R. J. *Environ. Toxicol. Chem.* 1987, 6, 579-593.
- (8) Quensen, J. F.; Tiedje, J. M.; Boyd, S. A. *Science* 1988, 242, 752-754.
- (9) Rhee, G. Y.; Bush, B.; Kane, M.; Shane, L. *Water Res.* 1989, 8, 957-964.
- (10) Bunce, N. J.; Landers, J. P.; Langshaw, J.; Nakai, J. S. *Environ. Sci. Technol.* 1989, 23, 213-218.
- (11) Walling, C.; Johnson, R. A. *J. Am. Chem. Soc.* 1975, 97, 363-367.
- (12) Atkinson, R.; Arey, J.; Zielinska, B.; Aschmann, S. M. *Environ. Sci. Technol.* 1987, 21, 1014-1022.
- (13) Sehested, K.; Hart, E. J. *J. Phys. Chem.* 1975, 79, 1639-1642.
- (14) Mill, T.; Hendry, D. G.; Richardson, H. *Science* 1980, 207, 886-887.
- (15) Haag, W. R.; Hoigne, J. *Chemosphere* 1985, 14, 1659-1671.
- (16) Seinfeld, J. H. *Science* 1989, 243, 745-752.
- (17) Atkinson, R. *Chem. Rev.* 1985, 85, 69-201.
- (18) Larson, R. A.; Hufnagel, J. M. *Limnol. Oceanogr.* 1980, 25, 505-512.
- (19) Atkinson, R. *Environ. Sci. Technol.* 1987, 21, 305-307.
- (20) Leifer, A. Atmospheric Oxidation of Chlorinated Biphenyls. In *Environmental Transport and Transformations of Polychlorinated Biphenyls*; EPA-560/5-83-025, NTIS No. PB84-142579, 1983.
- (21) Buxton, G. V.; Greenstock, C. L.; Helman, W. P.; Ross, A. B. *J. Phys. Chem. Ref. Data* 1988, 17, 513-586.
- (22) Sedlak, D. L.; Andren, A. W. *Environ. Sci. Technol.* 1991, 25, 777-782.
- (23) Zepp, R. G. Environmental Research Laboratory, U.S. EPA, Athens, GA, personal communication, 1990.
- (24) Tulp, M. T. M.; Olie, K.; Hutzinger, O. *Biomed. Mass Spectrom.* 1977, 4, 310-316.
- (25) Dilling, W. L.; Gonsior, S. J.; Boggs, G. U.; Mendoza, C. G. *Environ. Sci. Technol.* 1988, 22, 1447-1453.
- (26) Dorfman, L. M.; Matheson, M. S. In *Progress in Reaction Kinetics*; Porter, G., Ed.; Pergamon Press: Oxford, 1965; p 237.
- (27) Rusling, J. F.; Miaow, C. L. *Environ. Sci. Technol.* 1989, 23, 476-479.
- (28) Chameides, W. L.; Davis, D. D. *J. Geophys. Res.* 1982, 87, 4863-4877.
- (29) Graedel, T. E.; Mandich, M. L.; Weschler, C. J. *J. Geophys. Res.* 1986, 91, 5205-5221.
- (30) Faust, B. C.; Hoigne, J. *Atmos. Environ.* 1990, 24A, 79-89.
- (31) Behra, P.; Sigg, L. *Nature* 1990, 344, 419-421.
- (32) Schwartz, S. E.; Weinstein-Lloyd, J. *Natl. Meet.-Am. Chem. Soc., Div. Environ. Chem.* 1990, 30, 173-177.
- (33) Penkett, S. A.; Jones, B. M. P.; Brice, K. A.; Eggleston, A. E. *J. Atmos. Environ.* 1979, 13, 123-127.
- (34) Daum, P. H.; Kelly, T. J.; Schwartz, S. E.; Newman, L. *Atmos. Environ.* 1984, 18, 2671-2684.
- (35) Cooper, W. J.; Lean, D. R. S. *Environ. Sci. Technol.* 1989, 23, 1425-1428.
- (36) Murray, M.; Andren, A. W., submitted to *Atmos. Environ.*
- (37) Capel, P. D.; Gunde, R.; Zurcher, F.; Giger, W. *Environ. Sci. Technol.* 1990, 24, 722-727.

(38) Stumm, W.; Morgan, J. J. *Aquatic Chemistry*; Wiley: New York, 1981.

Received for review September 28, 1990. Accepted March 4, 1991. This work was funded by the U.S. Air Force Office of Scientific

Research, Grant AFOSR-88-0301. Funding was also obtained from the University of Wisconsin Sea Grant College Program under grants from the Office of Sea Grant, NOAA, U.S. Department of Commerce, and the State of Wisconsin (Federal Grant NA84AA-D-00065).

Continuous Multiligand Distribution Model Used To Predict the Stability Constant of Cu(II) Metal Complexation with Humic Material from Fluorescence Quenching Data

David M. Grimm,[†] Leo V. Azarraga,[‡] Lionel A. Carreira,^{*,§} and Wisnu Susetyo[§]

Technology Application, Inc., U.S. Environmental Protection Agency, Athens, Georgia 30613, Environmental Research Laboratory, U.S. Environmental Protection Agency, Athens, Georgia 30613, and Department of Chemistry, University of Georgia, Athens, Georgia 30602

■ We report the use of a pH-dependent continuous multiligand distribution model to determine the stability constant between Cu(II) and dissolved humic material. Fluorescence quenching of the humic material by Cu(II) is used to produce spectral titration curves. The values from the titration curves are then fit, by use of a least-squares fitting routine, to the calculated values produced by the model. Three titrations at pH 2.5, 3.5, and 4.5 were conducted using this method, and the observed and calculated values are compared. A single stability constant for Cu(II) with the humic material is reported. The results of these titrations are compared with the results of experiments carried out using a new technique that relies on the spectral properties of the Eu(III) ion to probe metal binding sites in humic material.

Introduction

Naturally occurring organic materials, in both terrestrial and aquatic systems, have been studied by researchers for many years. The conclusions that can be drawn from these studies are that the structure and physical properties of these organic materials, more commonly referred to as humic and fulvic substances, vary from region to region and are important in many environmental processes. Recently, particular interest in humics and fulvics has increased because of their ability to bind and transport potentially toxic metals in the environment (1-5).

In an effort to understand and quantify metal humic complexation, researchers have used an assortment of techniques. The most common methods used to study the metal binding characteristics of naturally occurring dissolved organic matter (DOM) have been ultrafiltration, ion-exchange, equilibrium dialysis, and potentiometric methods (5-11). All of these techniques employ an indirect method of determining the amount of metal complexed to the humic material under study. Namely, the free metal ion concentration is measured and subtracted from the total metal added to determine the amount of metal bound.

A more direct method of studying the metal binding characteristics of DOM would be to examine a property exhibited by either the humic material itself or a property of the metal to which it is complexed. In recent years, such a method was proposed by Ryan and Weber (12). Their

method utilizes the well-documented (12-14) ability of the Cu(II) ion to quench the naturally occurring fluorescence of humic material. Ryan and Weber's work included the development of a model that uses this quenching property of Cu(II) to determine copper's stability constants with humic material (12). The major assumption made in employing this fluorescence quenching technique is that the quenching varies linearly with bound copper.

The models developed, from both indirect and direct binding studies, and the binding parameters determined from the fluorescence as well as the other previously mentioned techniques all have one thing in common: they yield conditional constants that are functions of ligand or proton concentrations. These methods normally produce conditional binding constants that often vary greatly with ionic strength and particularly with pH. An example is a paper by Ryan and Weber (12) that reports the binding constant of Cu(II) to vary by a factor of 6 as the pH changed from 5 to 7. These models are of limited utility for predicting the metal binding properties of DOM over a wide range of environmental conditions.

In the last few years, however, a new technique that yields thermodynamic values for metal-humic interaction has proven useful as a predictive tool in determining metal-organic speciation. This method, developed by Dobbs et al. (15), uses the fluorescence properties of the Eu(III) ion to probe metal binding sites in DOM. The technique utilizes the fluorescence spectrum of the Eu(III) ion, which is sensitive to ligation with humic material, to produce spectral titration curves. This method is unique in its ability to simultaneously measure both the free and bound europium concentrations. The spectral data from this technique are fitted by using a continuous multiligand distribution model (16) to determine the number of metal binding sites in the system and to examine the effect of competition between protons and other metals of interest with that of the probe metal for the available DOM sites (17). This model is unique in its ability to determine binding constants for metal ions with humic material that are not conditional constants that depend on ligand concentration or changing pH conditions. This method has been used to measure the binding constants of several metals as a function of pH and ionic strength (17). While using this technique to study the competition for binding sites between Eu(III) and Cu(II), we observed very strong fluorescence quenching of both the Eu(III) and DOM. The quenching was strong enough to interfere with the signal being monitored from the bound Eu ion at concentrations below 10^{-5} M Eu(III). Although a reasonable fit to the

[†]Technology Application, Inc., U.S. EPA.

[‡]Environmental Research Laboratory, U.S. EPA.

[§]University of Georgia.

titration curve above 10^{-5} M Eu(III) could be made, we felt it necessary to confirm our results with another method.

In this paper, we report the use of the continuous multiligand distribution model to evaluate the fluorescence quenching effect on DOM by the Cu(II) ion. These titrations were conducted at three different pH values and the data from the titrations were then fit by use of a modified version of the continuous multiligand distribution model, which takes into account ionic strength effects as well as proton competition for binding sites. This paper will also try to address the assumptions used in modeling the fluorescence quenching experiments recently criticized and defended in the literature (18, 19).

Experimental Section

Instrumentation. The experimental setup for the fluorescence quenching experiment is virtually the same as that used in the lanthanide ion probe technique described by Dobbs et al. (20). Some modifications were made to the system, however; so a brief outline of the system configuration will be presented here. A Lambda Physik EMG 101 MSC excimer laser with a power output of 1.3 J at 308 nm was used to pump a FL3002 tunable dye laser. The laser dye (QUI) provided the excitation wavelength of 394 nm. The beam was focused with a 200-mm lens and directed vertically through a 1-cm disposable UV cuvette. The fluorescence emission was collected 90° off axis to minimize stray radiation. Two lenses were used to collect, collimate, and focus the fluorescence onto the monochromator slits. A GCA/Mcpherson 0.5-m double monochromator was used to disperse the fluorescence emission and a gated RCA C31034A02 photomultiplier tube (PMT) was used for fluorescence detection. A Stanford Research Systems Model SR535 digital delay/pulse generator was used to control the timing of the experiment.

The timing sequence and data collection method for this experiment are virtually the same as for the experiment outlined by Dobbs et al. (20). The only modifications were to change the delay time to zero in this experiment and to add a circuit that utilized the toggle mode on the boxcars (Model 510 Stanford Research Systems) to eliminate any background drift. The circuit allowed the pulse generator to operate at twice the pulse rate of the laser, to take a sample between pulses, and to subtract this dark count from the actual sample signal. This technique helped reduce electronic noise as well as any base-line drift from the PMT. The beam from the dye laser was monitored by splitting a small fraction of the beam onto a photodiode, and this signal was used as a reference to reduce the effect of fluctuations in the laser power output. The measurements were taken as a ratio of fluorescence signal over reference signal.

Reagents and Sample Preparations. The DOM used in this experiment was obtained from the Suwannee River in southern Georgia by Serkiz and Perdue (21) in May 1987. Reverse osmosis was used to extract and concentrate the DOM from the river water; the DOM was then further processed with XAD resins (21). A concentrated solution of the DOM was prepared by dissolving 0.55 g of the dry organic material in 50 mL of deionized water to give an 11 g/L solution with a pH < 2.6. This solution was kept in an amber reagent bottle and stored at 4 °C. A stock solution of the DOM was prepared by diluting 200 μ L of the concentrated solution to 37 mL with deionized water to give a 60-ppm DOM solution.

A stock Cu(II) solution was made by dissolving 0.672 g of CuCl₂ in 100 mL of deionized water. Eleven serial dilutions, from 2×10^{-2} to 5×10^{-6} M, gave a 4 order of

magnitude range of Cu(II) solution concentrations. The pH of each solution was adjusted with dilute HCl or NaOH.

The samples were prepared by mixing 1:1:1 volumes of deionized water, DOM, and dilute Cu(II) solutions in order to give 3 mL of 20-ppm DOM solution with various Cu(II) concentrations. The samples were continuously stirred during the monitoring period with a Teflon-coated micro stir bar (Hellma Model 333 Cuv-o-stir). The fluorescence from the sample was monitored at 500 nm. Thirty data points were taken over a 5-min period, and the average fluorescence signal was recorded. Duplicate samples for each concentration at the three different pHs were monitored to ensure that the signal did not change significantly during each run.

Theory

Ryan and Weber have described in detail the fluorescence quenching of a ligand by complexation with the Cu(II) ion (12). The total fluorescence intensity (I) is equal to the fluorescence of both the free ligand (I_L) and the bound ligand (I_{ML}) in the sample. The equation for this relationship is

$$I = \chi_L I_L + \chi_{ML} I_{ML} \quad (1)$$

where χ_L is the mole fraction of the free ligand and χ_{ML} is the mole fraction of the metal-ligand complex. The quantities I_L and I_{ML} are, respectively, the maximum and minimum fluorescence signal that can be monitored in the sample and are limiting factors in a titration. The quantity I , therefore, is directly proportional to the number of binding sites available for metal complexation and can be expressed in the following form:

$$I = I_L - \frac{\sum [ML_i]}{C_L} (I_L - I_{ML}) \quad (2)$$

where ML_i is the concentration of metal bound to the i th site, C_L is the total concentration of the ligand, and the χ_{ML} is now expressed as the $\sum [ML_i]$ over C_L . A plot of the fluorescence intensity, I , vs the log of the metal concentration yields a plot that is sigmoidal in form. From eqs 1 and 2, the total concentration of the bound metal can be derived as is shown in eq 3. The concentration of

$$\sum [ML_i] = \left(1 - \frac{I}{I_L}\right) \left(\frac{C_L I_L}{I_L - I_{ML}}\right) \quad (3)$$

free metal $[M]$ can be calculated from the mass balance equation for the total metal concentration, C_M . The total free metal then can be expressed in the form

$$[M] = C_M - \sum [ML_i] \quad (4)$$

This analysis of the experimental data provides the means to determine quantitatively the concentrations of the bound and free metal species at any point in the titration process.

As stated previously, the model used in this study is a continuous multiligand distribution model that works under the assumption that DOM is comprised of a large number of various monoprotic acids whose protonated binding sites are normally distributed with respect to their log K values. Perdue et al. (22) and Simms (23) have discussed the validity of this approach thoroughly. The individual ligand concentrations, C_i , the total ligand concentration, C_L , the mean log K_i value, μ , and the width of the distribution, σ , for the log K_i distribution of the ligand sites are estimated by nonlinear regression analysis of the titration data (15). These parameters are used to functionally describe the metal-humic complexation behavior

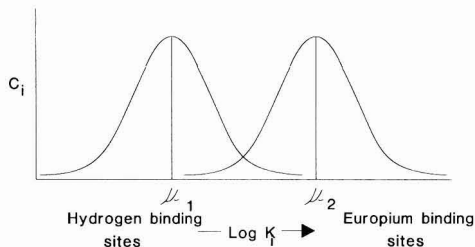


Figure 1. Hydrogen model assumption. Distribution of metal and proton binding sites.

and may vary from humic material to humic material. The higher the μ value the stronger the metal is bound. The larger the σ , the wider the distribution of the $\log K_i$ constants that reflect the amount of structural variation of the humic material.

When the metal-proton competition model is used, an assumption needs to be made. The distribution of the ligand sites available for binding are assumed to be the same for the two species. Since the same set of binding sites is available for both species, the widths of the two distributions are equal. (A pictorial representation of this is given in Figure 1.) This implies that the difference in free energy associated with binding at site i remains constant for the two species as a function of i . Therefore, the ratio K_{M_i}/K_{H_i} , where K_{M_i} is the binding constant for the metal at the i th binding site and K_{H_i} is the humic acid ionization constant at site i , remains constant (17).

Once this assumption is made, an expression for $[ML_i]$ can be developed in terms of all known variables (17):

$$[ML_i] = \frac{K_{M_i}[M]C_i}{1 + K_{M_i}[M] + K_{H_i}[H]} \quad (5)$$

The Gaussian distribution model yields the following expression for the ligand distribution:

$$C_i = \frac{C_L}{\sigma\sqrt{2\pi}} e^{-[(\mu_M - \log K_{M_i})^2]/2\sigma^2} \quad (6)$$

where C_i is the concentration of the ligand of type i , C_L is the total concentration of ligand in the humic substance, μ_M is the mean of the metal binding constant, and σ is one standard deviation of the mean.

This expression for C_i then is substituted into eq 5. The solution to this equation yields the total concentration of the metal at the i th binding site. To equate the value predicted by the model to the experimentally observed values given by the fluorescence titration, eq 5 must be summed or integrated over all i 's to obtain the total bound metal concentration $\Sigma[ML_i]$. The summation is expressed as the following:

$$\Sigma[ML_i] = \frac{C_L}{\sigma\sqrt{2\pi}} \int_{-\infty}^{+\infty} \frac{K_{M_i}[M]}{1 + K_{M_i}[M] + K_{H_i}[H]} e^{-[(\mu_M - \log K_{M_i})^2]/2\sigma^2} \times d \log K_M \quad (7)$$

Evaluation of this integral provides an expression for the total bound metal.

Ionic strength is also a factor that must be taken into account when the system is modeled. The relation between concentration quotients K_{M_i} and K_{H_i} and their respective thermodynamic constants $K_{M_i}^T$ and $K_{H_i}^T$ are given as

$$K_{M_i}^T = \frac{\{ML_i\}}{\{M\}\{L_i\}} = \frac{[ML_i]}{[M][L_i]} \frac{g_{M_i}}{g_M g_{L_i}} = K_{M_i} \Gamma_{M_i} \quad (8)$$

$$K_{H_i}^T = \frac{\{HL_i\}}{\{H\}\{L_i\}} = \frac{[HL_i]}{[H][L_i]} \frac{g_{H_i}}{g_H g_{L_i}} = K_{H_i} \Gamma_{H_i} \quad (9)$$

where braces $\{\}$ and brackets $[\]$ denote activities and concentrations, respectively; g then denotes activity coefficients. Debye-Hückel theory indicates that the activity coefficient ratio Γ equals 1 at zero ionic strength. K values, therefore, equal K^T values at zero ionic strength and decrease with increasing ionic strength. The ionic strength effect can be incorporated into the model by substituting K_{M_i} and K_{H_i} with their respective thermodynamic constants and activity coefficient ratios in eqs 8 and 9 to give the following equation for $[ML_i]$:

$$[ML_i] = \frac{(K_{M_i}^T/\Gamma_{M_i})[M]C_i}{[1 + (K_{M_i}^T/\Gamma_{M_i})[M] + (K_{H_i}^T/\Gamma_{H_i})[H]]} \quad (10)$$

This expression then can be substituted into eq 7. The effect of ionic strength on the system is discussed in detail by Susetyo et al. (17).

To fit the data, initial guesses are made for the modeling parameters μ_M , μ_H , C_L , and σ . The values for the total metal concentration and hydrogen ion concentration are known. The integral limits are set at $\pm 4\sigma$, and the resulting expression is evaluated. The modeling parameters are allowed to vary by using a least-squares fitting routine until the best possible fit can be obtained between the actual experimentally observed values and the calculated values. For fitting these titrations, however, all of the parameters with the exception of K_{Cu} were held to the values previously determined (17) for the DOM.

Results and Discussion

The pH-dependent multiligand distribution model was first used to calculate parameters in conjunction with the lanthanide ion probe spectrofluorometry technique (15). This technique utilizes the fluorescence properties of Eu(III) to probe the metal binding sites in humic materials at environmental concentrations. The model was expanded to predict not only proton competition but competition from other metal ions and the effect of ionic strength on humic material. This technique and model are described in detail by Susetyo et al. (17). This method is unique in its ability to simultaneously measure both free and bound europium metal concentrations, unlike ion selective electrode methods that measure only the free metal concentration or fluorescence quenching methods that measure only the bound metal concentration. As stated in the introduction, we have used the Eu(III) fluorescence technique to measure the competition of Cu(II) and Eu(III) for DOM binding sites. Because the fluorescences of the Eu(III) and the DOM were quenched by Cu(II), our studies could only be carried out at Eu(III) concentrations greater than 10^{-5} M, which resulted in a larger than normal uncertainty in the measured binding constant ($\mu_{Cu} = 4.9 \pm 0.4$). In order to substantiate our calculated value of the Cu(II) binding constant, we have undertaken a fluorescence quenching titration that uses the same model for metal binding.

Three titrations at different pH conditions were conducted using Cu(II) as the probe metal. Before the titrations were conducted, speciation studies of Cu(II) in an aqueous environment were simulated by using a new metal speciation model (MINTQA2) to determine the pH range at which all the Cu(II) would remain in solution (24). The MINTQA2 simulation runs concluded that at a pH of 6 and a Cu(II) concentration of 5×10^{-5} M 96% of the Cu ion in solution was free Cu(II). If the pH of the solution was increased to 7, the percentage of the free Cu(II) ion in

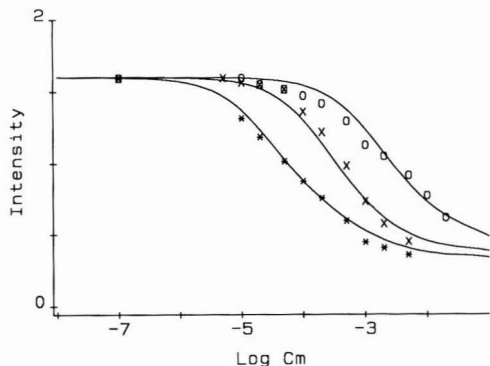


Figure 2. Plot of Cu(II) quenching titrations. Calculated curves are represented by lines. Observed data at pH 2.5 (O), pH 3.5 (X), and pH 4.5 (*).

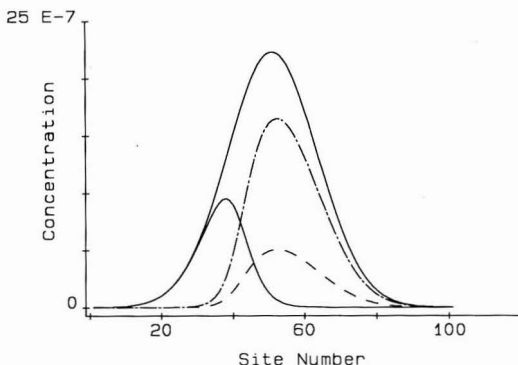


Figure 3. Species in solution at a Cu(II) concentration of 7×10^{-4} M at a pH of 2.5. Continuous lines represent both free (lower curve) and total ligand concentration. The area under the --- line represents bound metal; area under the -.- line represents bound hydrogen.

solution dropped to 31% with 62% of the Cu forming $\text{Cu}(\text{OH})_2$. To ensure that all of the Cu in solution exists as free Cu(II), the three fluorescence quenching titrations were conducted below a pH of 5.

The data from these three titrations then were fitted to the calculated data by means of a modified version of our pH-dependent multiligand distribution model. A plot of the observed and calculated values is given in Figure 2. The single set of humic-dependent parameters used to fit the data were taken from experiments done previously using the lanthanide ion probe technique. These parameters (C_L , σ , μ_H) were held constant and only the μ_M for Cu(II) was allowed to vary in order to get the best fit between calculated and observed data. The observed values are almost identical with the calculated curves for the three titrations at pH 2.5, 3.5, and 4.5. The large displacement between the three curves reflects the different pH conditions under which the titrations were conducted. This is illustrated graphically in Figures 3–5, where the concentration of copper is held constant at 7×10^{-4} M. The area under the upper curve in the graph represents the total ligand concentration, whereas the other curves represent the amount of bound copper, bound hydrogen, and free ligand. The area under these three curves sums to equal the area under the upper curve. At the low pH of 2.5 most of the binding sites are occupied by a proton due to the large proton concentration in solution, but at the higher pH of 4.5 and lower proton concentration, most of the binding sites are occupied by the metal ion.

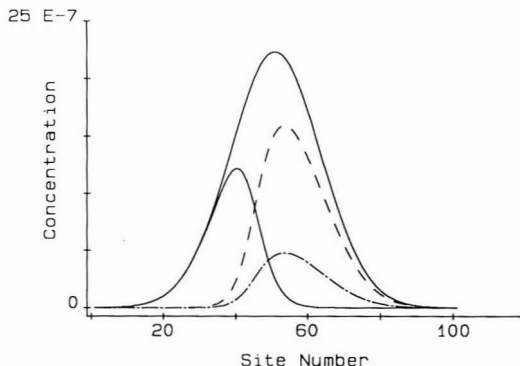


Figure 4. Species in solution at a Cu(II) concentration of 7×10^{-4} M at a pH of 3.5. Continuous lines represent both free (lower curve) and total ligand concentration. The area under the --- line represents bound metal; area under the -.- line represents bound hydrogen.

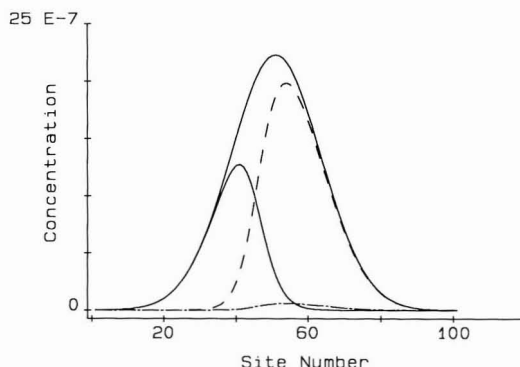


Figure 5. Species in solution at a Cu(II) concentration of 7×10^{-4} M at a pH of 4.5. Continuous lines represent both free (lower curve) and total ligand concentration. The area under the --- line represents bound metal; area under the -.- line represents bound hydrogen.

Table I. Fitting Parameters for Cu(II) Fluorescence Quenching Technique

I_L	1.60	σ	1.72	μ_H	3.87
I_{ML}	0	C_L	9.6×10^{-6}	μ_M	4.2

The final calculated μ_M for Cu(II) that best fits all three sets of data in Figure 2 was 4.2 ± 0.2 . It should be reemphasized that the values C_L , μ_H , and σ are the same values that were used to fit the binding of Eu(III) as a function of pH and the competitive binding of Al(III) (17). It should also be emphasized that the value of μ_M determined for Cu(II) is the same for all three pH conditions. The difference in the appearance of the three curves is solely a result of competitive binding with a proton. The parameters used to fit the data are given in Table I. It should also be noted that the value of I_{ML} is constant and not a function of pH. In the analysis of Ryan and Weber (12) both the values of I_{ML} and K_{Cu} changed significantly with pH. In addition, we find the value of I_{ML} to be zero. This does not imply that all binding sites are fluorophoric, but that all (or nearly all) fluorophoric sites have a site capable of binding Cu(II). The leveling off observed in the calculated and observed plots of Figure 2 is a direct result of the competitive Langmuir/Gaussian distribution model employed in the analysis and the competition for binding sites by protons. There is no need to invoke any assumptions as to "the useful measurement range" of the fluorescence quenching technique as described in some

recently published correspondence (19).

The value calculated for the μ_M of the Cu(II) ion in the fluorescence titrations was slightly lower than the 4.9 ± 0.4 calculated for Cu(II) by use of the partial titration curve obtained with the lanthanide ion probe technique. The difference in the results can be explained if one considers what is actually being observed in the fluorescence quenching titrations. When the ability of Cu(II) to quench the natural fluorescence of the DOM is used, it is assumed that all the ligands available for Cu(II) complexation are ligands that are fluorophoric in nature, and that they lose their fluorescence upon binding with Cu(II). This is undoubtedly not the case. The DOM, in fact, may contain organic moieties that bind Cu(II) but do not fluoresce, in which case the calculated μ_M for Cu(II) would be underestimated by the fluorescence quenching method. The values obtained by the two different techniques are, however, quite close.

Conclusions

The natural fluorescence property of humic material can be used to study the metal binding characteristics of these materials. The fluorescence quenching technique when coupled with the pH-dependent multiligand distribution model can be used to predict Cu(II) complexation with different humic materials at different pH and ionic strength conditions. Additional benefits are that this technique can be used with samples containing humic material at environmental concentrations and that measurements can be made quickly and easily.

The results from the fluorescence quenching technique agree quite well with those from the lanthanide ion probe technique. The fact that two very different spectroscopic methods were used to collect the data and that, by holding all the parameters constant, with the exception of K_{Cu} , the model was able to fit both sets of data demonstrates the utility of the pH-dependent multiligand distribution model. The fact that the two techniques gave a slightly different Cu(II) binding constant is explained by the dependence of the fluorescence quenching technique on the complexed ligand being fluorophoric or near a fluorophoric site. The lanthanide ion probe technique may be a more precise way of measuring humic metal complexation, because the fluorescence signal being monitored is from the bound and free metal and does not rely on the probe metal being bound to a fluorophoric ligand.

Registry No. Cu(II), 7440-50-8.

Literature Cited

- (1) Sposito, G. *CRC Crit. Rev. Environ. Control* **1986**, *16*, 193-229.

- (2) Tan, K. H.; Binger, A. *Soil Sci.* **1986**, *141*, 20-25.
- (3) Florence, T. M.; Batley, G. E. *CRC Crit. Anal. Chem.* **1980**, *9*, 219-296.
- (4) Saar, R. A.; Weber, J. H. *Anal. Chem.* **1980**, *52*, 2095-2100.
- (5) Hering, J. G.; Morel, F. M. M. *Environ. Sci. Technol.* **1988**, *22*, 1234-1237.
- (6) Shuman, M. S.; Woodward, G. P. *Anal. Chem.* **1973**, *45*, 2032-2035.
- (7) Shuman, M. S.; Woodward, G. P. *Environ. Sci. Technol.* **1977**, *11*, 809-813.
- (8) McKnight, D. M.; Wershaw, R. L. *Open-File Rep.—U.S. Geol. Surv.* **1989**, No. 87-557, 59-79.
- (9) Truit, R. E.; Weber, J. H. *Anal. Chem.* **1981**, *53*, 337-342.
- (10) Mantoura, R. F. C.; Dickson, A.; Riley, J. P. *Estuarine Coastal Mar. Sci.* **1978**, *6*, 387-408.
- (11) Matsunaga, K.; Negishi, M.; Fukase, S. *Geochim. Cosmochim. Acta* **1980**, *44*, 1615-1619.
- (12) Ryan, D. K.; Weber, J. H. *Anal. Chem.* **1982**, *54*, 986-990.
- (13) Ryan, D. K.; Weber, J. H. *Environ. Sci. Technol.* **1982**, *16*, 868-872.
- (14) Schnitzer, M.; Ghosh, K. *Soil Sci. Soc. Am. J.* **1981**, *45*, 25-29.
- (15) Dobbs, J. C.; Susetyo, W.; Carreira, L. A.; Azarraga, L. V. *Anal. Chem.* **1989**, *61*, 1519-1524.
- (16) Perdue, E. M.; Charles, R. L. *Environ. Sci. Technol.* **1983**, *17*, 654-660.
- (17) Susetyo, W.; Dobbs, J. C.; Carreira, L. A.; Azarraga, L. V.; Grimm, D. M. *Anal. Chem.* **1990**, *62*, 1215-1221.
- (18) Ryan, D. K.; Ventry, L. S. *Anal. Chem.* **1990**, *62*, 1523-1526.
- (19) Cabaniss, S. E.; Shuman, M. S. *Anal. Chem.* **1990**, *62*, 1528-1531.
- (20) Dobbs, J. C.; Susetyo, W.; Knight, F. E.; Castles, M. A.; Carreira, L. A.; Azarraga, L. V. *Anal. Chem.* **1989**, *61*, 483-488.
- (21) Serkiz, S. M.; Perdue, M. E. Isolation of Dissolved Organic Matter From The Suwannee River Using Reverse Osmosis. Submitted to *Water Res.*
- (22) Perdue, E. M.; Reuter, J. H.; Parrish, R. S. *Geochim. Cosmochim. Acta* **1984**, *48*, 1257-1263.
- (23) Simms, H. S. *J. Am. Chem. Soc.* **1926**, *48*, 1239-1250.
- (24) Allison, J. D.; Brown, D. S.; Novo-Gradac, K. J. *MINTEQA2/PRODEFA2, A Geochemical Assessment Model for Environmental Systems: Version 3.0 User's Manual*; U.S. Environmental Protection Agency: Athens, GA, 1990.

Received for review December 4, 1990. Revised manuscript received February 20, 1991. Accepted March 25, 1991. L.A.C. gratefully acknowledges support provided by the National Research Council, which provided him a senior research associateship at the Athens Environmental Research Laboratory. L.A.C. and W.S. acknowledge the U.S. Environmental Protection Agency's Cooperative Agreement CR813461-01-3. Note: Mention of trade names or commercial products does not constitute endorsement or recommendation for use by the U.S. Environmental Protection Agency.

Extraction Efficiencies of Organochlorine Compounds from Niagara River Water

Mark S. Driscoll, John P. Hassett,* and Caryl L. Fish

Department of Chemistry, State University of New York, College of Environmental Science and Forestry, Syracuse, New York 13210

Simon Litten

New York State Department of Environmental Conservation, 50 Wolf Road, Albany, New York 12233

■ A chromic acid digestion extraction technique was compared to conventional solvent extraction for recovery of a series of organochlorine compounds (chlorinated benzenes, polychlorinated biphenyls, DDT, DDE, mirex, and photomirex) from centrifuged Niagara River water. The digestion technique was more efficient than conventional solvent extraction. Relative recovery (undigested/digested) decreased exponentially with increasing log K_{ow} . This implies that digestion-extraction recovers both the fraction dissolved and the fraction bound to dissolved organic matter (DOM), while conventional solvent extraction only recovers the dissolved fraction. As the time compounds equilibrated with the DOM increased, the extraction efficiencies by conventional extraction decreased while the efficiencies by digestion extraction remained 100%. Results obtained with the digestion technique were also more reproducible than those with conventional solvent extraction.

Introduction

The interactions between humic substances [humic acids, fulvic acids, humins, and dissolved organic matter (DOM)] and hydrophobic organic compounds have been studied by several groups. Cholesterol (1), polychlorinated biphenyls (PCB) (2-9), phthalate esters (10-14), alkanes (11-13, 15), fatty acids (11, 13), polynuclear aromatic hydrocarbons (PAH) (5, 12, 14-19), mirex (20-22), chloranil (23, 24), DDT (3, 8, 9, 14, 25-28), and other pesticides (9, 14, 29-31) bind to humic substances. Binding interactions affect bioavailability (5, 16, 18, 32-34), gas exchange (2, 6, 7, 20, 21, 35-37), solubility (8, 10, 14, 15, 24, 25, 38), particle adsorption (35, 39-41), photolysis (21, 42, 43), and hydrolysis (30, 44) reactions. Only a few investigators have looked at how these interactions affect the extraction efficiencies of hydrophobic compounds from water. Hassett and Anderson (1) found that the solvent extraction efficiency of cholesterol from water was reduced in the presence of DOM. Landrum et al. (45) showed that C_{18} bonded-phase adsorbents did not remove DOM-bound compounds from natural water under some conditions. Carlberg and Martinsen (12) showed that the extraction efficiencies of alkanes, PAHs, chlorinated hydrocarbons, and phthalate esters were less than 100% by either solvent or XAD-2 extraction in the presence of humic acids. The extraction efficiencies of these compounds decreased as the time after spiking was increased from 4 to 60 days. These results indicate the time between spiking and extraction is very important. Preliminary work (46) showed that the hexane extraction efficiencies of many chlorinated hydrocarbons from Niagara River water were less than 100%. Some studies (11, 13) have shown that methylation of humic substances increased the recovery of hydrophobic compounds from water. Fish et al. (46) found that adding chromic acid to water increased the extraction efficiencies of many organochlorine compounds. Maguire and Tkacz

(47) found that raising the pH of water to 12 increased the amount of PCB congeners extracted as compared to yields at the water's natural pH, while lowering the pH to 1 decreased the extraction efficiencies. There may be two explanations for this; binding of PCBs to humic acids decreases with increasing pH (7); also, at low pH humic acids will precipitate, possibly trapping the PCBs in the matrix.

In this study, the extraction efficiencies of 22 organochlorine compounds from Niagara River water were determined. Conventional liquid-liquid extraction with hexane was compared to chromic acid digestion, to break down dissolved organic matter, combined with hexane extraction.

Experimental Section

Reagents. All extractions were done with pesticide-grade hexane or dichloromethane (Baker Chemical) and digestion extractions used chromic acid cleaning solution of 90-96% sulfuric acid and 1% CrO_3 (Mallinckrodt). Acetone and petroleum ether (30-60 °C boiling range) used for cleaning were glass distilled. Stock solutions were made with pesticide-grade benzene (Fisher Scientific). Humic acid was obtained from Aldrich Chemical.

Standard Compounds. Table I lists the 22 compounds used with amounts spiked into 1-L water samples (column A) and the log of the octanol-water partition coefficients (K_{ow}) (column B) (48-51). Amounts spiked were at least 50 times below the solubility limits of the compounds in water. Unspiked samples were analyzed at the start of this project, and the native concentrations were at least 2 orders of magnitude less than the spiked concentrations. The chlorinated benzenes were obtained from Aldrich; unlabeled mirex was donated by the United States Environmental Protection Agency; [^{14}C]mirex (6.13 mCi/mmol) was purchased from Pathfinder Lab., Inc.; photomirex was donated by Environment Canada. All other compounds were obtained from Ultra Scientific Inc.

Accurate amounts of each standard compound were prepared by weighing on a microbalance, with the exception of 1,2,4-trichlorobenzene, which was measured volumetrically. Each standard was dissolved in benzene and diluted to 10 mL. Mixed standards were prepared by diluting appropriate volumes of the stock solutions with hexane. One mixed standard contained mirex and photomirex; the other contained the remaining 20 compounds.

Sampling. Samples were collected approximately bi-weekly from January 22, 1986, to January 7, 1987, at sampling stations established by Environment Canada on the Niagara River at Fort Erie and Niagara-on-the-Lake, ON. The sites have been described in more detail elsewhere (52). Samples were centrifuged on site with Westfalia continuous-flow centrifuges with a flow rate of 6 L/min. Quadruplicate samples for direct solvent (undigested) extraction were collected in 1-L glass Wheaton bottles with aluminum foil lined screw caps from each site.

Table I. Results of the Spiked Study

no. diff at 95%	compound	amt spiked, ng/L	log K_{ow} (ref)	method					recovery					rel rec (R)			no. diff at 95%
				S UN, ng (N)	S DIG, ng (N)	V UN	V DIG	UN	S (n)	H	I	J	S (n)	av	L	M	
1	1,2,4-trichlorobenzene	145.4	3.98 (48)	15.1 (25)	11.6 (26) ^a	10.1	7.96	1.021	0.112 (52)	0.991	0.039 (53)	1.033	0.119 (24)	1.033	0.119 (24)	14:10	1
2	1,2,3-trichlorobenzene	76.6	4.04 (48)	12.2 (25)	9.42 (26) ^a	15.6	12.3	1.003	0.098 (52)	0.998	0.059 (53)	1.022	0.114 (24)	1.022	0.114 (24)	14:10	0
3	1,2,3,4-trichlorobenzene	26.6	4.55 (48)	3.31 (25)	1.73 (26) ^a	13.0	6.52	0.933	0.101 (52)	1.005	0.032 (53)	0.956	0.106 (24)	0.956	0.106 (24)	9:15	3
4	2-PCB	984.0	4.46 (49)	87.5 (25)	65.9 (26) ^a	11.2	6.70	0.782	0.197 (52)	0.991	0.033 (53)	0.794	0.200 (24)	0.794	0.200 (24)	10:14	4
5	penta-chlorobenzene	39.3	5.03 (48)	2.22 (25)	2.49 (26) ^a	5.72	6.34	0.966	0.075 (52)	1.007	0.031 (53)	0.988	0.081 (25)	0.988	0.081 (25)	12:13	2
6	4-PCB	2720.0	4.69 (49)	310 (25)	239 (26) ^a	15.3	8.79	0.738	0.267 (52)	0.993	0.043 (53)	0.746	0.270 (25)	0.746	0.270 (25)	7:18 ^b	7
7	2,4-PCB	249.0	5.07 (49)	19.0 (26)	19.5 (27)	7.72	7.84	0.962	0.063 (53)	1.010	0.038 (55)	0.991	0.074 (26)	0.991	0.074 (26)	9:17	2
8	hexachlorobenzene	41.2	5.47 (48)	2.91 (29)	2.33 (30)	7.15	5.66	0.975	0.069 (59)	0.998	0.028 (61)	0.989	0.074 (28)	0.989	0.074 (28)	12:16	2
9	4,4'-PCB	675.0	5.30 (49)	105 (35)	59.9 (36) ^a	16.5	8.88	0.923	0.109 (75)	1.002	0.043 (76)	0.943	0.117 (33)	0.943	0.117 (33)	13:21	4
10	2,4,4'-PCB	103.9	5.67 (49)	7.19 (35)	4.06 (36) ^a	7.37	3.91	0.917	0.124 (75)	1.009	0.021 (76)	0.393	0.126 (33)	0.393	0.126 (33)	10:23 ^b	6
11	2,2',3,4-PCB	49.1	5.69 (49)	4.08 (36)	3.12 (36) ^a	8.94	6.37	0.911	0.081 (75)	0.999	0.031 (76)	0.930	0.087 (37)	0.930	0.087 (37)	9:28 ^b	9
12	<i>o,p'</i> -DDE	30.5	6.27 (49)	2.08 (36)	2.65 (36)	7.46	8.69	0.896	0.063 (75)	1.002	0.042 (76)	0.913	0.076 (37)	0.913	0.076 (37)	3:34 ^b	9
13	2,2',4,5,5'-PCB	99.1	6.38 (49)	6.87 (36)	4.15 (36) ^a	7.57	4.19	0.895	0.071 (75)	1.005	0.022 (76)	0.916	0.074 (37)	0.916	0.074 (37)	5:32 ^b	12
14	<i>p,p'</i> -DDE	34.7	6.40 (49)	4.69 (36)	3.82 (36) ^a	15.7	11.0	0.843	0.083 (75)	0.999	0.053 (76)	0.860	0.098 (37)	0.860	0.098 (37)	2:35 ^b	12
15	3,3',4,4'-PCB	243.0	6.36 (49)	64.0 (36)	37.9 (36) ^a	31.5	15.6	0.826	0.151 (75)	0.994	0.069 (76)	0.836	0.166 (37)	0.836	0.166 (37)	6:31 ^b	7
16	2,3',4,4',5-PCB	95.6	6.65 (49)	12.3 (36)	10.2 (36)	14.9	10.7	0.847	0.099 (75)	1.003	0.052 (76)	0.864	0.112 (37)	0.864	0.112 (37)	4:33 ^b	12
17	<i>o,p'</i> -DDT	12.9	6.59 (49)	2.19 (36)	1.17 (36) ^a	19.3	9.08	0.862	0.107 (75)	1.000	0.044 (76)	0.881	0.116 (37)	0.881	0.116 (37)	10:27 ^b	4
18	2,2',4,4',5,5'-PCB	117.0	6.92 (49)	12.7 (36)	10.2 (36)	12.8	8.73	0.825	0.093 (75)	1.008	0.042 (76)	0.848	0.102 (36)	0.848	0.102 (36)	1:35 ^b	16
19	<i>p,p'</i> -DDT	139.0	6.36 (50)	16.9 (36)	10.0 (36) ^a	14.0	7.22	0.847	0.112 (75)	1.006	0.035 (76)	0.866	0.117 (36)	0.866	0.117 (36)	6:30 ^b	15
20	photomirex	57.8	7.20 (51)	7.66 (36)	4.00 (36) ^a	16.6	6.91	0.773	0.119 (75)	1.009	0.034 (76)	0.798	0.124 (37)	0.798	0.124 (37)	1:36 ^b	21
21	2,2',3,4,4',5,5'-PCB	96.6	7.36 (49)	13.1 (36)	13.2 (36)	17.8	13.7	0.746	0.127 (75)	0.999	0.056 (76)	0.760	0.139 (37)	0.760	0.139 (37)	2:35 ^b	18
22	mirex	63.4	7.50 (51)	10.1 (36)	4.82 (36) ^a	22.5	7.61	0.692	0.144 (75)	0.994	0.036 (76)	0.707	0.148 (37)	0.707	0.148 (37)	1:36 ^b	24

^a Statistically smaller at the 95% confidence level. ^b The proportion n_{av}/n_d is statistically different at a confidence level of 95%.

Bottles were weighed before and after sampling to determine the amount of water collected. Quadruplicate samples for digestion extraction were collected in 2-L round-bottom flasks with glass stoppers. The flasks were filled to an approximate 1000-mL mark, and the exact amount was determined by weighing.

Spiking. Two samples of each set of four collected in both Wheaton bottles and round-bottom flasks from both sites were spiked with 5 μ L of the mirex-photomirex stock solution and 10 μ L of the other combined standard solution. The samples were then shaken for 24 h at 25 °C.

Undigested Sample Extraction. Samples collected in Wheaton bottles were extracted by pouring the contents of the sample bottle into a 2-L separatory funnel, rinsing the bottle with 70 mL of hexane, pouring the hexane into the separatory funnel, shaking the funnel vigorously for 2 min, allowing the phases to separate, and removing the hexane layer. This process was repeated twice more, including rinsing the sample bottle. The combined hexane layers were passed through a column of 8 g of anhydrous sodium sulfate to remove traces of water and evaporated to 5–10 mL in a Kuderna–Danish concentration apparatus. Spiked samples were analyzed without further concentration. Unspiked samples were concentrated further to ~100 μ L by evaporating the hexane with slow bubbling by use of a glass capillary tube and purified nitrogen. All the compounds used in this study were concentrated quantitatively with this bubbling procedure.

Digested Sample Extraction. Samples collected in round-bottom flasks were treated by adding 5 mL of chromic acid and 200 mL of hexane, fitting the flask with a reflux condenser, placing the flask in a heating mantle, and refluxing at the hexane boiling point for 2 h. The sample refluxed smoothly without boiling chips or stirring. After being cooled, the sample was transferred to a 2-L separatory funnel and shaken vigorously. After the phases separated, the hexane layer was removed, passed through a column containing 8 g of anhydrous sodium sulfate, and evaporated to 5–10 mL in a Kuderna–Danish concentration apparatus. Spiked samples were analyzed without further concentration. Unspiked samples were concentrated to ~100 μ L as above.

Gas Chromatography. Extracts were analyzed by using a Varian 3400 gas chromatograph with a splitless capillary column injector, auto injector, a 60-m \times 0.25-mm (i.d.) SPB-1 (0.25- μ m film thickness) fused-silica capillary column (Supelco Inc.) and a ^{63}Ni electron capture detector. Data were collected by a Keithley DAS Series 500 data acquisition system connected to a Leading Edge Model D microcomputer and stored on floppy disks. Data acquisition was controlled with Labtech Notebook software. The output from the gas chromatograph was also sent to a strip-chart recorder. Prior to injection, 2,2',3,3',5,5',6,6'-octachlorobiphenyl was added to the extracts as an internal standard. The spiked samples received 100 μ L (93 ng) and the unspiked 10 μ L (9.3 ng). The column temperature was held at 60 °C for 5 min, raised to 270 °C at a rate of 10 °C/min, and held at 270 °C for 30 min. Compounds in the unspiked samples were quantified by comparing peak heights to a standard curve and making volume corrections based on the internal standard response. Although internal standard was added to all extracts in the spiked studies, the peaks were compared to 2,2',5,5'-tetrachlorobiphenyl due to an unknown compound that interfered with the internal standard in some samples. 2,2',5,5'-Tetrachlorobiphenyl was chosen because it was quantitatively recovered by both methods in the uncontaminated samples.

Time of Equilibration. A humic acid solution was prepared by dissolving humic acid (sodium salt) in distilled water adjusted to pH 10 with 2 N NaOH and was then filtered through a 0.2- μ m cartridge filter. The solution was diluted to obtain a dissolved organic carbon (DOC) concentration of 5.0 mg/L. Water from Labrador Pond, Tully, NY, was collected in 20-L glass carboys and centrifuged before use. The water had 6.1 mg/L DOC. Ten 4-L bottles each of humic acid water and pond water were spiked with ^{14}C -labeled mirex at a concentration of 28.5 ng/L. Bottles were stored at 20 °C. At intervals of 5 min to 5 days after spiking, the contents of a bottle of each water sample were divided into four 1-L aliquots for duplicate solvent and digestion extraction. The extracts were concentrated to ~1 mL and combined with 15 mL of scintillation cocktail, and ^{14}C activity was determined with a Packard Series 4000 liquid scintillation counter.

Results and Discussion

This study compared the ease of use, precision, and accuracy of conventional hexane extraction of Niagara River water to hexane extraction coupled with chromic acid digestion. The compounds used in this study were chlorobenzenes, PCB congeners, DDT, DDE, mirex, and photomirex (Table I). Water samples were collected approximately biweekly from January 22, 1986, to January 7, 1987. Recovery studies evaluated average recoveries, seasonal variations, spiked vs unspiked samples, and time of equilibration after spiking.

Centrifugation was used instead of filtration since it allowed water to be processed quickly and was less likely to adsorb the compounds of interest. Using the same model centrifuge, Allan (53) showed up to 70% of the particles recovered were less than 0.2 μ m, and 90–95% of the total particles were removed. Kuntz (54) showed that centrifugation removed 83% of the particulate carbon and nitrogen from samples collected from the Niagara River.

Often with conventional liquid–liquid extraction, emulsions form due to the presence of surface-active organic matter. In this study, emulsions in undigested samples frequently interfered with separation of the hexane and water phases. The emulsion and phase-separation problems were never encountered in the digested samples, suggesting that the surface-active organic matter was destroyed. This lack of emulsions makes the digestion method easier to use.

One problem with using a digestion extraction technique is the possibility of degrading the compound of interest. All the compounds used in this study were stable even at chromic acid concentrations 10 times greater than normally used for the digestions.

Spiked Samples. Precision of the two methods was compared by evaluating the standard deviation. Standard deviations (*S*) for recovery of each spiked compound were estimated from duplicate results (55) as

$$S = (\sum D^2 / 2N)^{0.5} \quad (1)$$

where *D* is the absolute difference between a pair of duplicates, and *N* is the number of duplicates. The data from both sampling sites were pooled when the standard deviations were calculated. Table I lists the standard deviations in nanograms, the number of duplicate samples, and the coefficients of variance for amounts of each compound recovered by each method (columns C–F). Standard deviations of the two methods were compared with an *F* test (Table I). Of the 22 compounds studied, 14 showed a significant difference at the 95% confidence level. In every case where there was a real difference, the standard deviation was lower among the digested samples (Table

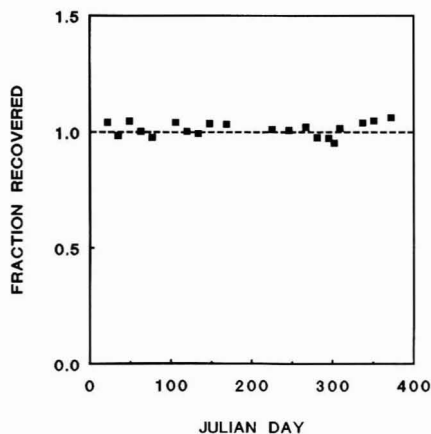


Figure 1. Fraction of spiked mirex recovered by the digestion method vs sampling period.

I columns C and D). These differences ranged from 30% for 1,2,3-trichlorobenzene to 109% for mirex. When a Wilcoxon signed rank test is applied, the digestion method is more precise, overall, than the solvent extraction method (95% confidence level). The average coefficients of variance of 8.4% for digested and 13.6% for undigested also show that the digestion method is overall more precise. The superior precision obtained with sample digestion may be due to the lack of emulsions, allowing better phase separation and thus more reproducible recoveries.

The average absolute recoveries and their standard deviations are listed in Table I (columns G–J) for both methods. All the compounds were quantitatively recovered by the digestion method but not all were by conventional solvent extraction. The quantitative recoveries by digestion are reproducible over time, as can be seen from the small standard deviations (Table I, column J). For example, Figure 1 is a plot of fraction recovered for mirex by digestion over the sampling period.

The two methods were also compared by evaluating relative recoveries. Relative recoveries (R) were calculated for each sample set by using

$$R = f_u/f_d \quad (2)$$

where f_u and f_d are the concentration (average of duplicates) of a compound recovered from undigested and digested samples, respectively. Relative recoveries were used to nullify any possible variation in spiking and concentration of the stock solution from week to week. Over the entire study period, 20 of the 22 test compounds were recovered, on average, less efficiently from undigested Niagara River water than from digested water ($R < 1$). The average relative recoveries ranged from 1.033 for 1,2,4-trichlorobenzene to 0.707 for mirex (Table I, column K). The number of sample sets for which undigested extraction was more efficient (n_u) was compared to the number for which digestion was more efficient (n_d) for each compound in Table I. If the results were random, the average expected outcome would be $n_u \approx n_d$. The proportions $n_u:n_d$ range from 14:10 (nearly random) for the two trichlorobenzenes to 1:36 for mirex and photomirex. These results show that 13 of the compounds were extracted better by the digestion method (sign test) while none were extracted better by undigested extraction (confidence level of 95%) (Table I, column M).

By use of the standard deviations and the average of duplicate samples, the methods were compared for individual sample dates with a t test (95% confidence level).

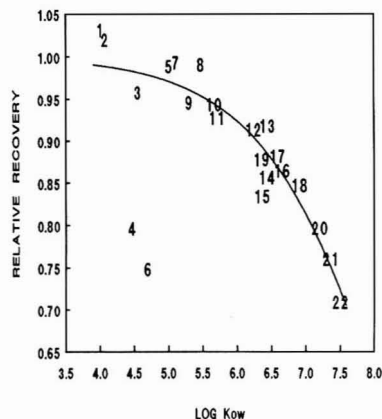


Figure 2. Relative recovery of spiked compounds vs $\log K_{ow}$. The numbers correspond to the compound numbers in Table I. The line is the nonlinear least-squares fit to the data using eq 7.

The number of times that the digestion method was better ranges from 0 for 1,2,3-trichlorobenzene to 24 for mirex (Table I, column N). Hexane extraction was not significantly better than digestion extraction for any sample set.

Most of the compounds that are recovered less efficiently with hexane extraction have high octanol–water partition coefficients (K_{ow}) (Table I, column B), and the relative recoveries tend to decrease with increasing $\log K_{ow}$ (Figure 2). This result may appear counterintuitive, since compounds with high K_{ow} should partition more readily from water to an organic solvent. It can be explained if some fraction of a compound bound by dissolved organic matter was recovered more efficiently from digested samples than from undigested samples (dissolved organic carbon is 2.1–7.0 mg/L). This could occur due to partial or complete destruction of the DOM by reaction with chromic acid, which would release DOM-bound compounds and make them more available for extraction. Compounds with higher K_{ow} values tend to be bound to a greater extent by DOM (14). These results can be explained quantitatively from

$$C_T = C_b + C_f \quad (3)$$

where C_T is the total concentration of the organochlorine compound in water, C_b is the bound concentration, and C_f is the free concentration. The binding constant K_{DOC} is defined as

$$K_{DOC} = C_{DOC}/C_f = C_b/[C_f(DOC)] \quad (4)$$

where C_{DOC} is the concentration of the bound compound in the dissolved organic carbon and (DOC) is the concentration of the dissolved organic carbon.

K_{DOC} is related to K_{ow} (56) by an equation that takes the form

$$\log K_{DOC} = a \log K_{ow} + b \quad (5)$$

Combining eqs 3–5

$$C_T/C_f = (DOC)10^{(a \log K_{ow} + b)} + 1 \quad (6)$$

Assuming that the digestion–extraction method extracts both bound and free compounds (C_T), and that solvent extraction of undigested samples recovers only the free compounds (C_f), then relative recovery (R) equals C_f/C_T , and

$$R = 1/[(DOC) 10^{(a \log K_{ow} + b)} + 1] \quad (7)$$

Equation 7 predicts that relative recovery will decrease with increasing K_{ow} . The line in Figure 2 is the nonlinear

Table II. Results of the Unspiked Study

compound	concn digested, ng/L	unspiked		spiked	
		rel rec	SD	rel rec	SD
2,2',3,4-PCB	0.195	0.696	0.230	0.930	0.087
2,2',4,5,5'-PCB	0.475	0.782	0.261	0.916	0.074
<i>p,p'</i> -DDE	0.132	0.844	0.132	0.860	0.098
2,3',4,4',5-PCB	0.501	0.675	0.211	0.864	0.112
2,2',4,4',5,5'-PCB	0.589	0.688	0.181	0.848	0.102

least-squares fit of eq 7 to the experimental points. Compounds 4 (2-chlorobiphenyl) and 6 (4-chlorobiphenyl) are not included in the regression because of anomalous behavior discussed below. By use of an average DOC concentration of 4.4 mg/L for Niagara River water, the regression yields *a* and *b* values of 0.443 and 1.614, respectively. These values are similar to previously published results for correlation of K_{DOC} with K_{ow} . Kenaga and Goring (57) reported *a* and *b* values of 0.54 and 1.38 and Henry and Suffet (9) reported values of 0.59 and 1.37. These results support the hypothesis that the DOM-bound compounds are not efficiently recovered from undigested samples.

Some compounds showed little difference between the two extraction methods ($R \approx 1$) throughout the study period. These compounds are 1,2,4-trichlorobenzene, 1,2,3-trichlorobenzene, 1,2,3,4-tetrachlorobenzene, pentachlorobenzene, 2,4-PCB, and hexachlorobenzene. Other compounds such as 2,2',4,5,5'-PCB show that the digestion method is significantly better than undigested extraction ($R < 1$), but the differences between the two methods are small. Compounds with larger K_{ow} s such as mirex show that digestion is much better. Figure 3a is a graph of relative recovery (averages of both sampling sites) vs day of sampling for mirex. The relative recoveries vary over time from ~1 to as low as 0.3. The graph of 4-PCB (Figure 3b) shows very interesting results. There was little difference between the methods for most samples, but for three consecutive sampling dates (77, 106, and 120) the differences were large, with relative recoveries less than 0.55. In one sample pair from the Fort Erie site, 4-PCB was not recovered at all in the two solvent extraction samples ($R = 0$) yet it was extracted quantitatively from the digested samples. The fact that the other 20 compounds were recovered rules out improper spiking. The other monochlorobiphenyl, 2-PCB, showed similar results. The most plausible explanation for this decrease in relative recovery is a strong specific association between the two monochlorobiphenyls and a transient component of the dissolved organic matter in the river.

Unspiked Samples. Table II lists five compounds studied in the unspiked samples, the average native concentrations by digestion extraction, and the average relative recoveries and standard deviations, both spiked and unspiked. These compounds were chosen because they were always detected in the unspiked samples from both sites. The unspiked relative recoveries range from 0.844 for *p,p'*-DDE to 0.675 for 2,3',4,4',5-PCB. Figure 4 is a graph of unspiked relative recovery (averages of both sampling sites) vs date of sampling for 2,3',4,4',5-PCB. For all of the sampling days, undigested extraction was less efficient than digested extraction ($R < 1$).

Relative recoveries from spiked and unspiked samples were compared to evaluate the use of spiked compounds as surrogates for native compounds in extraction studies. The relative recoveries are less from the unspiked samples than from the spiked samples for all the compounds (Table II). The differences range from 2% for *p,p'*-DDE to 34% for 2,2',3,4-PCB. Assuming that digestion extraction is

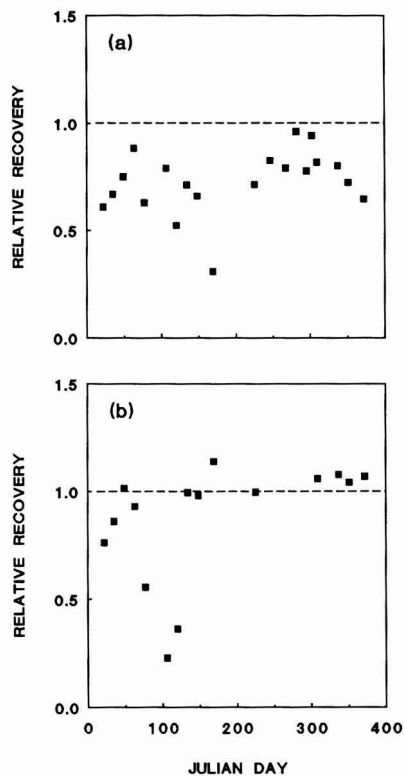


Figure 3. (a) Relative recovery of spiked mirex vs sampling date. (b) Relative recovery of spiked 4-chlorobiphenyl vs sampling date.

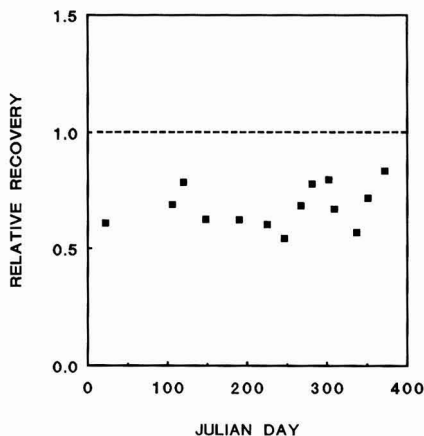


Figure 4. Relative recovery of unspiked 2,3',4,4',5-pentachlorobiphenyl vs sampling date.

quantitative for unspiked samples, hexane extraction efficiencies in unspiked and spiked samples can be compared

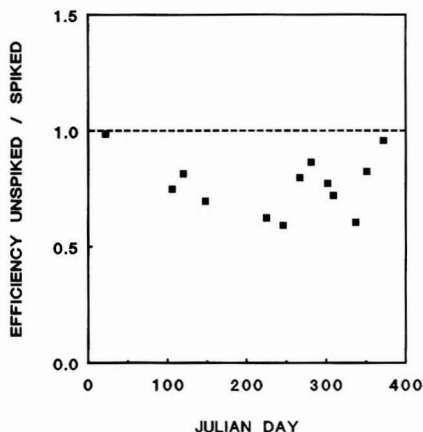


Figure 5. Unspiked/spiked solvent extraction efficiency vs sampling date for 2,3',4,4',5-pentachlorobiphenyl.

by dividing the unspiked relative recoveries by those of the spiked samples. If the ratio is less than 1, the hexane extraction efficiency is lower in the unspiked sample. Figure 5 is a plot of this ratio vs date of sampling for 2,3',4,4',5-PCB. Hexane extraction efficiency of each unspiked sample is always less than the corresponding spiked sample. The other PCBs gave similar results, but there is no difference in the recovery of *p,p'*-DDE from spiked and unspiked samples. The explanation for the different behavior of PCBs and *p,p'*-DDE could be either differences in rates of interaction with DOM or different exposure time to DOM in the environment. As these results show, the use of spiked surrogate compounds is not a valid method for determining extraction efficiencies from natural water samples.

The lower recoveries from the unspiked samples may be due to lower water concentrations of the pollutants. This hypothesis seems unlikely since the binding constants of hydrophobic compounds to particles (K_{POC}) (22) and DOM (K_{DOC}) (7) do not appear to be concentration dependent. A more plausible explanation for the lower recoveries in the unspiked samples is differences in time of equilibration. The spiked samples were allowed to equilibrate for only 24 h while the unspiked samples may have equilibrated in the environment much longer. This time of equilibration will be important if the association kinetics between the compounds of interest and the DOM is on the order of days and not minutes or hours. This hypothesis is supported by laboratory studies with mirex. Figure 6 is a plot of the fraction recovered by both methods for mirex in humic acid and pond water vs time after spiking. The humic acid water and the pond water had organic carbon concentrations of 5.0 and 6.1 mg/L, respectively. Immediately after spiking, mirex is recovered efficiently by solvent extraction, but recovery declines over a 5-day period. Mirex is quantitatively recovered by digestion throughout the study period. Therefore, time of equilibration after spiking is very important when extraction efficiencies are studied. These data suggest that at least 5 days is needed for equilibration. The report of Carlberg and Martinsen (12) also supported this hypothesis, showing that extraction efficiencies of many organic compounds from natural water decreased as the time after spiking increased from 4 to 60 days.

Some researchers prefer to use other solvents for extraction. The U.S. EPA priority pollutant method specifies dichloromethane (58). Extraction with hexane and with

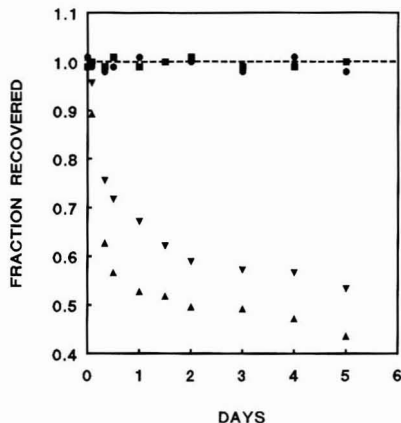


Figure 6. Fraction of mirex recovered by both methods vs time in days after spiking for pond and Aldrich humic acid water. Key: undigested pond Δ , humic acid ∇ , digested pond \circ , humic acid \blacksquare .

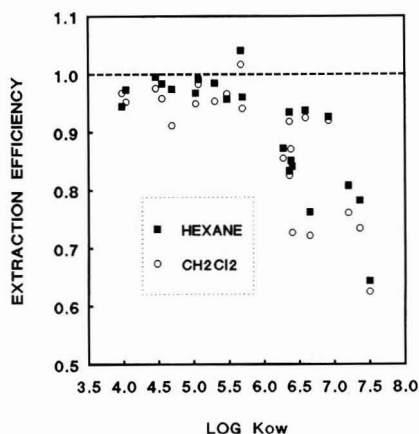


Figure 7. Extraction efficiency vs log K_{ow} for hexane and dichloromethane extraction.

dichloromethane was compared on duplicate Niagara River water samples. Figure 7 is a plot of extraction efficiency vs log K_{ow} for both solvents. Extraction with dichloromethane was not superior to hexane extraction. Extraction of mirex from these water samples gave efficiencies of 62.5% and 64.4% for dichloromethane and hexane, respectively.

Conclusion

Emulsions and phase separation were a problem in the undigested samples. These problems were not encountered in the digested samples, thus making the digestion technique easier to use.

The digestion extraction technique is more efficient than conventional solvent extraction for recovering organochlorine compounds from natural water. The extraction efficiency for the digestion technique is essentially 100%, while at times solvent extraction is much less. As the K_{ow} s of the compounds increase, the efficiency of solvent extraction decreases. This decrease is presumably due to binding of the more hydrophobic compounds to DOM. The digestion technique degrades this DOM, thus allowing efficient extraction of these compounds.

The digestion technique is also more precise than conventional solvent extraction. Average coefficients of var-

iance are 8.40 and 13.6, respectively.

Using spiked compounds as surrogates for estimating extraction efficiencies is not always valid. Solvent extraction recovery of spiked compounds varies with sampling date, hydrophobicity of the compound, and time after spiking and does not correspond well to recovery of native compounds.

Caution

The digestion used in this study does not react violently. Some strong oxidizing agents present fire and explosion hazards when mixed with some organic compounds and other oxidizable substances (59). Therefore, investigators who want to try other oxidant-solvent combinations are advised to proceed with extreme caution.

Acknowledgments

We thank Environment Canada, especially Serge Metikosh, Kenneth Kuntz, and Hans Biberhofer, for their assistance in sampling.

Registry No. 1, 120-82-1; 2, 87-61-6; 3, 634-66-2; 4, 2051-60-7; 5, 608-93-5; 6, 2051-62-9; 7, 33284-50-3; 8, 118-74-1; 9, 2050-68-2; 10, 7012-37-5; 11, 52663-59-9; 12, 3424-82-6; 13, 37680-73-2; 14, 72-55-9; 15, 32598-13-3; 16, 31508-00-6; 17, 789-02-6; 18, 35065-27-1; 19, 50-29-3; 20, 39801-14-4; 21, 35065-30-6; 22, 2385-85-5; water, 7732-18-5; chromic acid, 7738-94-5.

Literature Cited

- (1) Hassett, J. P.; Anderson, M. A. *Environ. Sci. Technol.* **1979**, *13*, 1526.
- (2) Griffin, R. A.; Chian, E. S. K. EPA-600/2-80-027; U.S. Government Printing Office: Washington, DC, 1980.
- (3) Chiou, C.; Malcolm, R. L.; Brinton, T. I.; Kile, D. E. *Environ. Sci. Technol.* **1988**, *22*, 502.
- (4) Gschwend, P.; Wu, S. *Environ. Sci. Technol.* **1985**, *19*, 90.
- (5) Landrum, P. F.; Nihart, S. R.; Eadir, B. J.; Herche, L. R. *Environ. Toxicol. Chem.* **1987**, *6*, 11.
- (6) Hassett, J. P.; Milicic, E. *Environ. Sci. Technol.* **1985**, *19*, 638.
- (7) Jota, M. A. T.; Hassett, J. P. *Environ. Toxicol. Chem.* **1991**, *10*, 483.
- (8) Kile, D. E.; Chiou, G. T. In *Aquatic Humic Substances: Influence on Fate and Treatment of Pollutants*; Suffet, I. H., MacCarthy, P., Eds.; Advances in Chemistry 219; American Chemical Society: Washington, DC, 1988; pp 131-157.
- (9) Henry, L. L.; Suffet, I. H. In *Aquatic Humic Substances: Influences on Fate and Treatment of Pollutants*; Suffet, I. H., MacCarthy, P., Eds.; Advances in Chemistry 219; American Chemical Society: Washington, DC, 1989; pp 159-171.
- (10) Matsuda, K.; Schnitzer, M. *Bull. Environ. Contam. Toxicol.* **1973**, *6*, 200.
- (11) Khan, S. U.; Schnitzer, M. *Geochim. Cosmochim. Acta* **1972**, *36*, 745.
- (12) Carlberg, G. E.; Martinsen, K. *Sci. Total Environ.* **1982**, *25*, 245.
- (13) Ogner, G.; Schnitzer, M. *Geochim. Cosmochim. Acta* **1970**, *34*, 921.
- (14) Carter, C. W. Ph.D. Thesis, Drexel University, 1984.
- (15) Boehm, P. D.; Quinn, J. G. *Estuarine Coastal Mar. Sci.* **1976**, *4*, 93.
- (16) McCarthy, J. F. *Environ. Contam. Toxicol.* **1983**, *12*, 559.
- (17) Landrum, P. F.; Giesy, J. P. In *Advances in the Identification and Analysis of Organic Pollutants in Water*; Keith, L. H., Ed.; Ann Arbor Science: Ann Arbor, MI, 1981; pp 345-355.
- (18) McCarthy, J. F.; Jimenez, B. D. *Environ. Sci. Technol.* **1985**, *19*, 1072.
- (19) Gauthier, T.; Seltz, W. R.; Grant, C. *Environ. Sci. Technol.* **1987**, *21*, 243.

- (20) Yin, C.; Hassett, J. P. *Environ. Sci. Technol.* **1986**, *20*, 1213.
- (21) Mudambi, A. R.; Hassett, J. P. *Chemosphere* **1988**, *17*, 1133.
- (22) Yin, C.; Hassett, J. P. *Chemosphere* **1989**, *19*, 1289.
- (23) Melcer, M. E.; Zalewski, M. S.; Brisk, M. A.; Hassett, J. P. *Chemosphere* **1987**, *16*, 1115.
- (24) Melcer, M. E.; Zalewski, M. S.; Hassett, J. P.; Brisk, M. A. In *Aquatic Humic Substances: Influence on Fate and Treatment of Pollutants*; Suffet, I. H., McCarthy, P., Eds.; Advances in Chemistry 219; American Chemical Society: Washington, DC, 1989; pp 173-183.
- (25) Wershaw, R. L.; Burcar, P. J.; Goldberg, M. C. *Environ. Sci. Technol.* **1969**, *3*, 271.
- (26) Porrier, M. A.; Bordelon, B. R.; Laseter, J. L. *Environ. Sci. Technol.* **1972**, *6*, 1033.
- (27) Ballard, T. M. *Soil Sci. Soc. Am. Proc.* **1971**, *35*, 145.
- (28) Carter, C. W.; Suffet, I. H. *Environ. Sci. Technol.* **1982**, *16*, 735.
- (29) Mather, S. P.; Morley, H. V. *Bull. Environ. Contam. Toxicol.* **1978**, *20*, 268.
- (30) Perdue, E. M.; Wolfe, N. L. *Environ. Sci. Technol.* **1982**, *16*, 847.
- (31) Means, J. C.; Wijayaratne, R. *Science* **1982**, *215*, 968.
- (32) Leverssee, G. J.; Landrum, P. F.; Giesy, J. P.; Fannin, T. *Can. J. Fish. Aquat. Sci.* **1983**, *40*, 63.
- (33) Muir, D. C. G.; Yarechewski, A. L.; Knoll, A.; Webster, G. R. B. *Environ. Toxicol. Chem.* **1986**, *5*, 261.
- (34) Landrum, P. F.; Reinhold, M. D.; Nihart, S. R.; Eadie, B. J. *Environ. Toxicol. Chem.* **1985**, *4*, 459.
- (35) Hassett, J. P.; Anderson, M. A. *Water Res.* **1982**, *16*, 681.
- (36) Brownawell, B. J.; Farrington, J. W. In *Marine and Estuarine Geochemistry*; Sigleo, A. C., Hattori, A., Eds.; Lewis: Chelsea, MI, 1985; pp 97-120.
- (37) Caron, G.; Suffet, I. H.; Belton, T. *Chemosphere* **1985**, *14*, 993.
- (38) Chiou, G. T.; Kile, D. E.; Brinton, T. I.; Malcolm, R. L.; Leenheer, J. A.; MacCarthy, P. *Environ. Sci. Technol.* **1987**, *21*, 1231.
- (39) Gschwend, P. M.; Wu, S. C. *Environ. Sci. Technol.* **1985**, *19*, 90.
- (40) Baker, J. E.; Eisenreich, S. J.; Johnson, T. C.; Halfman, B. M. *Environ. Sci. Technol.* **1985**, *19*, 854.
- (41) Baker, J. E.; Capel, P. D.; Eisenreich, S. J. *Environ. Sci. Technol.* **1986**, *20*, 1336.
- (42) Zepp, R. G.; Wolf, N. L.; Gordon, J. A.; Fincher, R. C. *J. Agric. Food Chem.* **1976**, *24*, 727.
- (43) Zepp, R. G.; Braun, A. M.; Hoigne, J.; Leenheer, J. A. *Environ. Sci. Technol.* **1987**, *21*, 485.
- (44) Macalady, D. L.; Tratnyek, P. G.; Wolfe, N. L. In *Aquatic Humic Substances: Influence on Fate and Treatment of Pollutants*; Suffet, I. H., MacCarthy, P., Eds.; Advances in Chemistry 219; American Chemical Society: Washington, DC, 1989; pp 323-332.
- (45) Landrum, P. F.; Nihart, S. R.; Eadie, B. J.; Gardner, W. S. *Environ. Sci. Technol.* **1984**, *18*, 187.
- (46) Fish, C. L.; Driscoll, M. S.; Hassett, J. P.; Litten, S. In *Aquatic Humic Substances: Influence on Fate and Treatment of Pollutants*; Suffet, I. H., MacCarthy, P., Eds.; Advances in Chemistry 219; American Chemical Society: Washington, DC, 1989; pp 223-229.
- (47) Maguire, R. J.; Tkacz, R. J. *Chemosphere* **1989**, *19*, 1277.
- (48) Sarna, L. P.; Hodge, P. E.; Webster, G. R. B. *Chemosphere* **1984**, *13*, 975.
- (49) Hawker, D. W.; Connell, D. W. *Environ. Sci. Technol.* **1988**, *22*, 382.
- (50) Lyman, W. J.; Reehl, W. F.; Rosenblatt, D. H. *Handbook of Chemical Property Estimation Methods*; McGraw-Hill: New York, 1982; Chapter 1.
- (51) Hansch, C.; Leo, A. *Substituent Constants for Correlations Analysis in Chemistry and Biology*; Wiley-Interscience: New York, 1979.
- (52) Data Interpretation Group Joint Evaluation of Upstream/Downstream Niagara River Monitoring Data, for the Period April 1987 to March 1988; A joint publication of NYSDEC, EC, U.S. EPA, and MOE, 1989; pp 13-15.
- (53) Allan, R. J. *Sediment-Related Fluvial Transmission of Contaminants*, Scientific Series No. 107; IWD, Western and

- Northern Region: Regina, SK, Canada, 1979.
- (54) Kuntz, K. Canada Centre for Inland Waters, personal communication, 1991.
- (55) Anderson, R. L. *Practical Statistics for Analytical Chemists*; Van Nostrand Reinhold: New York, 1987; pp 35-40.
- (56) Karickhoff, S. W.; Brown, D. S.; Scott, T. A. *Water Res.* 1979, 13, 241.
- (57) Kenaga, E. E.; Goring, C. A. I. In *Aquatic Toxicology*, ASTM STP 707; Eaton, J. G., Parrish, P. R., Hendricks, A. C., Eds.; American Society for Testing Materials: Philadelphia, PA, 1980; pp 78-115.

- (58) Guidelines establishing test procedures for the analysis of pollutants. *Fed. Regist.* 1979, 44, No. 233.
- (59) *Prudent Practices for Handling Hazardous Chemicals in Laboratories*; National Research Council; National Academy Press: Washington, DC, 1981; p 36.

Received for review September 24, 1990. Revised manuscript received March 4, 1991. Accepted March 20, 1991. We thank the New York State Department of Environmental Conservation for funding this study.

Comparison of Portable Gas Chromatographs and Passivated Canisters for Field Sampling Airborne Toxic Organic Vapors in the United States and the USSR

Richard E. Berkley,* Jerry L. Varns, and Joachim Pleil

Atmospheric Research and Exposure Assessment Laboratory, U.S. Environmental Protection Agency, Research Triangle Park, North Carolina 27711

■ Collection of samples in passivated canisters is widely used in analysis of trace volatile organic compounds in air because preconcentration is usually required to detect analytes. Sample integrity can be compromised by deterioration or artifact formation during storage and preconcentration. A laboratory-tested portable gas chromatograph (PGC) equipped with a highly sensitive photoionization detector (PID) offers the advantage of near real-time data without preconcentration, but its limitations as a field-portable instrument must be recognized. This paper presents data produced simultaneously by the canister/TO-14 method and by PGCs. Data were obtained in U.S. and overseas field studies at industrial, hazardous waste, and roadway sites. Field results suggest that a combination of canister and PGC methods offers a synergistic approach to source assessment measurements.

Introduction

The low part per billion (ppb) concentrations of toxic organic compounds found in ambient air have generally eluded direct detection, and samples must undergo preconcentration prior to analysis. Sample collection may actually be a preconcentration process in which analytes are stripped from the air matrix by a cryogenic trap or a sorbent bed, or whole air samples may be collected in passivated canisters and kept for later analysis (1). Use of a portable gas chromatograph (PGC) equipped with a photoionization detector (PID) of sufficient sensitivity to detect organic compounds without preconcentration at sub-ppb levels offers a significant alternative approach to this difficult analytical problem.

Reviews by Verner and Driscoll (2, 3) in 1984-1985 describe more than a decade of PID applications in gas chromatography. Several reports describe analyses of organic vapors in air with PID-equipped chromatographs that were not portable and required preconcentration (4-8). Leveson developed a 10.6-eV photoionization detector with significantly enhanced sensitivity, which was incorporated into a portable gas chromatograph (9). The photon source was an electrodeless discharge tube excited by a radio-frequency oscillator. It was claimed to detect benzene without preconcentration at 0.1 ppb (10-13). With this instrument, Berkley estimated a benzene detection limit equivalent to 0.03 ppb. The smallest sample actually analyzed, 1 μ L containing 1.6 pg of benzene,

produced a 2.3-V-s peak at maximum gain. Linear response over a wide range of concentration (0.5-130 ppb benzene) could be maintained, and air injections as large as 1 mL could be made without unacceptable loss of chromatographic resolution. Comparable sensitivities to other aromatic compounds and chloroalkenes were also found (14). A portable instrument of such sensitivity would obviously be suitable for air monitoring, but relatively few reports of such use have appeared (15-17).

Potential sampling errors with canisters include breakthrough of analytes from the preconcentration trap, chemical reactions between collected compounds, and sample degradation during storage. Sample integrity during storage in passivated canisters has been demonstrated in the absence of highly reactive compounds (18), but HCl, for example, was shown to cause artifact formation (19). Parallel use of a PGC method that does not store or preconcentrate samples could call attention to the occurrence of such problems. PGCs are more easily transported than a large number of canisters and can more readily obtain a large volume of data in the field. On the other hand, they are presently limited to low-resolution chromatography, they identify the limited number of compounds that they can detect at ambient levels by retention time only, and they require a skilled operator. The analytical trade-offs in field sampling between the widely used canister method and the near-real-time PGC are listed in Table I.

We have operated PGCs in both laboratory and field tests, (20, 21), but those evaluations included minimal comparison with data obtained by other methods. The objective of this report was to compare PGC data with method TO-14 canister data for volatile organic compounds. Herein are data obtained in two field studies, conducted in Delaware and Lithuania.

Experimental Section

Canister Analysis. Spherical 6-L electropolished canisters (SIS, Inc.) were used to collect air samples and to store PGC calibration standards. Canisters were cleaned by heating to 90 °C while they were evacuated through a liquid nitrogen trap to a final pressure below 10- μ m (mercury equivalent) for 2 h.

For direct comparison between canister and PGC results, a canister was held with its inlet less than 10 cm from the end of the PGC probe and the valve was opened to fill it

Table I. Relative Advantages of Canister and PGC Methods for Ambient Air Sampling

comparative criteria	canister	portable GC
no. of compds analyzed	typically 41 ^a	typically <15
quantitation limit	typically 0.2 ppbv	typically <0.1 ppbv ^a
specificity	identification by retention time, multiple detectors, GC/MS ^a	identification by retention time and 10.6-eV PID minutes ^a
data delay	weeks	direct analysis, no sample preparation ^a
sample integrity	samples stored, pressurized, preconcentrated	multiple samples per GC ^a
multiple sampling	one sample per canister	analyzes a few compounds at many sites quickly
field screening	analyzes many compounds at one site very slowly	trained analyst required at field site
critical personnel	trained analyst remains in laboratory ^a	

^a Indicates which instrument (if any) is best for each criterion.

during the time the PGC sample pump was running. It should be emphasized that this procedure did not result in perfectly equivalent sampling. Of approximately 50 mL of air that entered the PGC sample probe, only 1 mL was analyzed, whereas the canister analysis was representative of the entire sample collected (up to 6 L). Nevertheless, both methods would be expected to produce similar results from sampling the same air at the same time.

Less direct comparison was made by performing consecutive PGC analyses while time-integrated canister samples were being collected nearby. For time-integrated measurements, evacuated canisters were fitted with pre-calibrated mechanical flow controllers, and air was sampled at 25 mL/min for 2 h.

Air samples collected in canisters were transported to a laboratory, cryogenically preconcentrated, and analyzed by using a modified Hewlett-Packard Model 5880A gas chromatograph equipped with flame ionization and electron capture detectors. A Hewlett-Packard Model 5970A mass selective detector was used for some samples. GC/MS calibration was based upon 41 organic compounds cited in the TO-14 method (1). They were analyzed following 1:1000 dilution of commercially prepared cylinder standards (Scott Specialty Gases; 10 ppm each in nitrogen). The dilution was accomplished by metering the calibration gases and humid zero-grade diluent air into a manifold with mass flow controllers. After an 8-h system equilibration, 5% of the stream was diverted into a clean evacuated canister to a positive pressure of 200 kPa (3 atm absolute) by a steel diaphragm pump. Canister samples collected in Delaware were analyzed by Battelle Memorial Institute (Columbus, OH), and canister samples taken in Lithuania were analyzed at the Environmental Protection Agency Laboratory in Research Triangle Park, NC.

Portable GC Analysis. The microprocessor-controlled PGC (Photovac Model 10S70) was equipped with a constant-temperature column enclosure, which contained a 0.53 mm i.d. \times 10 m wall-coated open-tubular column, 1.0 m of which was a back-flushable precolumn. A chemically bonded stationary liquid phase was used, either CPSil5CB or CPSil19CB (Chrompak). Ultrazero air (<0.1 ppm carbon) was used as carrier gas. An IBM-compatible laptop computer used vendor-provided software via an RS-232 interface to automate chromatograph operation and data storage.

Chromatographic peaks were identified and quantitated by use of retention times and response factors, which were stored in the nonvolatile memory of the PGC microprocessor. The calibration library was created by analyzing mixtures of analytes (10 ppb) produced by flow dilution of commercially prepared standards, as described above. Compounds that had ionization potentials greater than 10.6 eV were not detected by the PGCs below 100 ppb. During sampling, PGCs were automatically recalibrated every four or five runs with a standard containing a single compound, chlorobenzene or tetrachloroethylene. These

standards were prepared by flow dilution as described above, certified by GC/FID analysis, and shipped to the site in canisters along with other equipment. After each field study, the remaining field calibrant was recertified by GC/FID. No statistically significant change in concentration was observed. After each recalibration run, the microprocessor corrected the retention time and response factor for the calibrant and then proportionally corrected retention times and response factors of all compounds in the library. Retention times and responses of calibrant peaks were not reported by the PGC during autosampling runs. Peak recognition windows were set to $\pm 5\%$ of retention time, and minimum peak area was set to 5 mV-s. At this setting, the smallest detectable concentration for each calibrated compound was below 0.1 ppb.

PGC samples were collected at intervals of 15 min. Air was drawn into the sample probe (3 m \times 2 mm i.d. stainless steel tubing) for 45 s, then the sample loop was switched into the carrier stream for 15 s, and finally the sample loop was removed from carrier flow to minimize peak tailing. The precolumn was back-flushed by the carrier stream except when calibrated compounds were actually passing through it. Calibration runs differed from sample runs only in that the loop received calibration mixture instead of an air sample. The 10-s flow of calibrant (120 mL/min) ended 2 s before injection. A typical chromatogram with quantitation list and setup table is shown in Figure 1.

PGCs were sheltered from drafts and direct sunlight inside an automobile or a mobile laboratory during field operation, and the stainless steel sample probe was extended through a window or a sampling port. Before automatic sampling was started, a stable base line was observed and the library was recalibrated with single-compound standard. Chlorobenzene or tetrachloroethylene was used as calibrant. A different calibrant was used for each PGC when two of them were operated together. External rechargeable 12-V batteries (Johnson Controls GC12800 or PP12120 gel cell and Sears Die-Hard Marine) were used to supply power. In Lithuania, 240-V 50-Hz electric current was stepped down with a transformer (Triad N-9M) and adjusted to 115 V with a powerstat (Staco Energy Products) for charging batteries.

Field Sites. Samples were taken during April 1989 at several hazardous waste sites near Wilmington and New Castle, DE. This was done in cooperation with the Delaware Department of Natural Resources and Environmental Control as part of a preliminary investigation of airborne emissions from Superfund hazardous waste sites in the area. Three of the rural sites were inactive landfills under Superfund remediation. Others included an abandoned industrial waste lagoon, a waste treatment and incineration plant, and a chemical plant that manufactured chlorinated aromatic compounds.

In June 1989 a field study was conducted near Vilnius, Lithuanian SSR under project 02.01-12 of the U.S.-USSR Environmental Agreement, in which Soviet and American

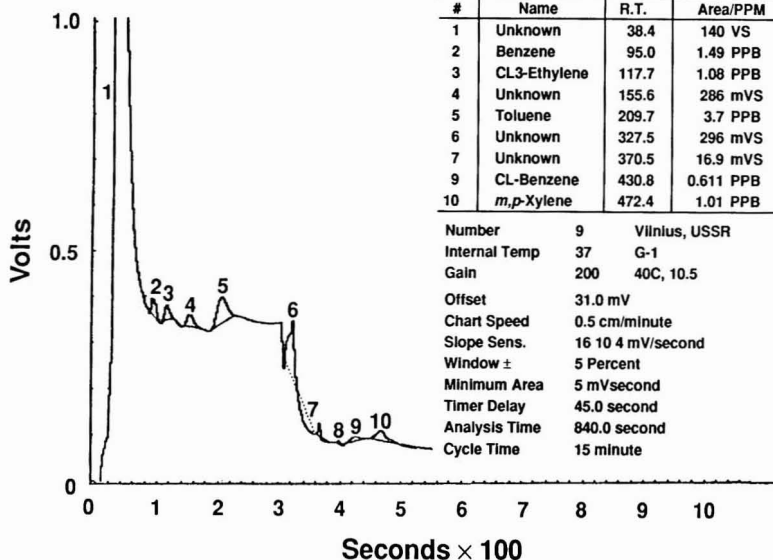


Figure 1. Typical PGC chromatogram showing setup and quantitation list.

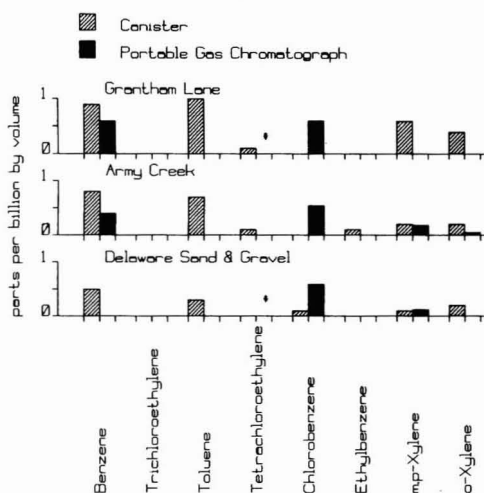


Figure 2. Comparison of PGC and canister responses at three Superfund sites near New Castle, DE. (*) Tetrachloroethylene was not detected by the PGC due to a persistent base-line disturbance caused by programmed valve operation.

methods of analyzing air pollution from automobile exhaust were compared. Benzene, toluene, and higher homologues were of special interest in this study. Two identically equipped PGCs were used. Their performance was compared in side-by-side operation, and then they were operated as an upwind/downwind pair. Five weeks in transit, prolonged storage, and use of converted electric power provided a stringent test of PGC performance at a remote location.

During the Lithuanian study, samples were taken at a site on the Vilnius-Kaunas Highway (A-227) ~12 km from the center of Vilnius. This four-lane divided highway ran from southeast to northwest through rolling countryside. A mobile laboratory provided by the Lithuanian Institute of Physics was placed ~20 m northeast of the highway on ground that was ~2 m below the level of the roadway. Open uneven fields extended more than 150 m from the

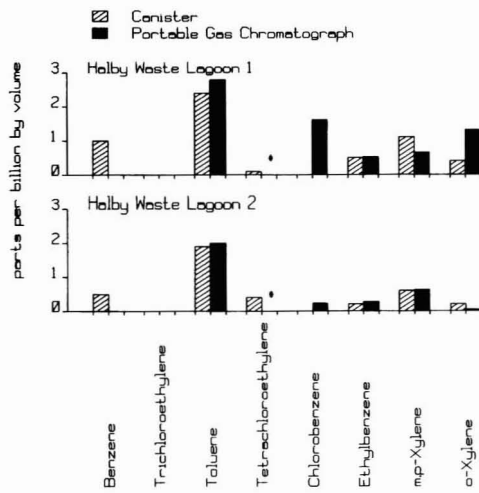


Figure 3. PGC and canister comparison at an abandoned waste lagoon in Wilmington, DE. (*) Tetrachloroethylene was not detected by the PGC due to a persistent base-line disturbance caused by programmed valve operation.

road on either side. The speed limit was 100 km/h, and daytime traffic volume was moderate to heavy without stop-and-go congestion. No industrial activity was visible in the immediate vicinity.

Results and Discussion

Delaware Field Study. Figures 2-4 contrast PGC and canister data from colocated simultaneous sampling in Delaware. Figure 2 shows samples taken at three Superfund sites. Concentrations were low, typical of sub-ppb ambient background levels in areas remote from vehicular traffic or other sources, suggesting that these compounds were not emitted in significant quantities from waste buried at the sites. Samples taken downwind of a waste lagoon are shown in Figure 3. Concentrations were low at this urban/industrial site but slightly higher than at the rural Superfund sites.

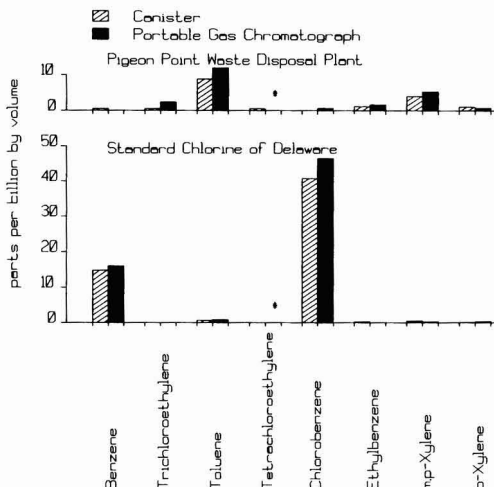


Figure 4. PGC and canister responses at the Pigeon Point waste disposal plant in Wilmington, DE (above) and at Standard Chlorine of Delaware chemical plant (below). (*) Tetrachloroethylene was not detected by the PGC due to a persistent base-line disturbance caused by programmed valve operation.

The low analyte concentrations in Figures 2 and 3 call attention to some limitations of PGCs. Sub-ppb to 1 ppb benzene levels were not always detected by the PGC when reported by the canister method. The PGC peak recognition algorithm sometimes did not respond to a very small peak emerging where the base line was tailing from a large peak or where it had been disturbed by programmed valving. PGC data for tetrachloroethylene in the Delaware study were obliterated by such a base-line disturbance. Also, chlorobenzene, the field recalibrant, persistently contaminated sample runs at approximately 0.5 ppb due to a valve leak. PGC and canister comparisons at concentrations substantially above 10 ppb were in close agreement.

Samples taken by both methods near the waste incineration plant at Pigeon Point show toluene and higher homologues at significant levels (Figure 4). This active waste disposal operation produced an intense stench caused by compounds that were detectable by neither method. Also shown in Figure 4 are high levels of benzene and chlorobenzene measured downwind of an industrial complex that produced chlorinated aromatic compounds.

The large relative discrepancies between PGC and canister results at the lowest concentrations tend to obscure how well they agree overall. In Figure 5 PGC data are plotted versus canister data for each occasion when a compound was detected by either method during the Delaware study. The plot shows that the two methods do produce equivalent data and enhances perspective on relative differences at the lowest concentrations. Agreement was reasonably close over the entire concentration range. It would have been better if more points had been measured at higher concentrations, but the number of canisters available was limited, and sites with high-level emissions were found only after most canisters had already been filled.

Lithuanian Field Study. Of the 36 canisters taken to Vilnius, all were dedicated to 2-h time-integrated sampling. PGC data were compared to canister data by autosampling during the canister sampling period. Two PGCs were operated side by side in the mobile laboratory with colocated sample probes extended to a point 1 m above and 18 m northeast of the roadway. Figure 6 compares analyses

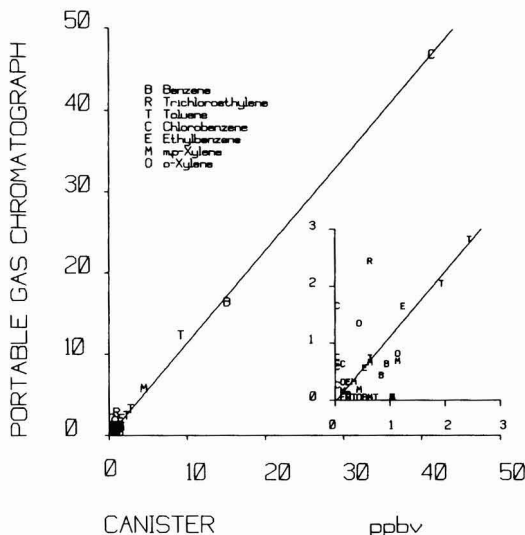


Figure 5. PGC versus canister responses from the Delaware field study. Inset shows the region near the origin. Slope, 1.141; intercept, -0.027; correlation coefficient, 0.996; 41 points.

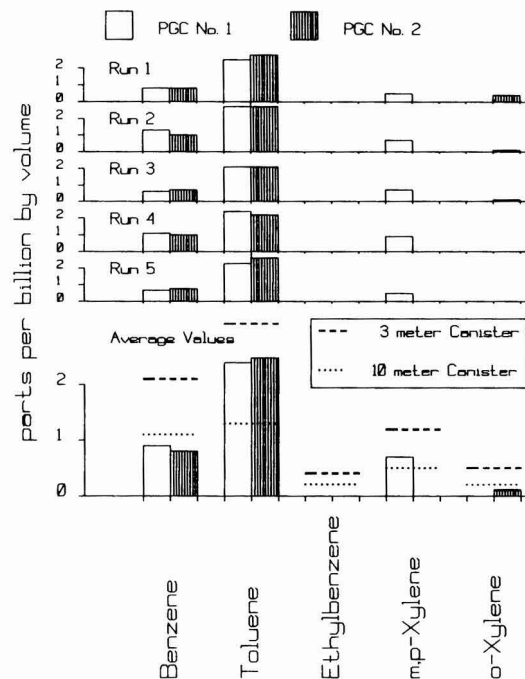


Figure 6. Side-by-side downwind PGC responses observed at 15-min intervals during a 2-h time-integrated canister sampling period at highway site in USSR.

made by the colocated PGCs which coincided with time-integrated sampling by canisters placed 3 and 10 m from the edge of the highway. This comparison was completed during nonturbulent movement of air across the site and while traffic density was fairly constant. Average levels of benzene, toluene, ethylbenzene, *m*-,*p*-xylene, and *o*-xylene found by the PGCs were in reasonable agreement with data from the 3- and 10-m canisters; however, the PGC levels sometimes exceeded the 10-m average canister concentrations, even though the PGCs were further re-

Table II. Retention Time Stability during Vilnius Field Study^a

unit	benzene		toluene		<i>m,p</i> -xylene		<i>o</i> -xylene	
	peak no.	RSD, %	peak no.	RSD, %	peak no.	RSD, %	peak no.	RSD, %
PGC-1	5	0.8	5	0.2	5	0.1	0	
PGC-2	26	1.3	26	2.4	15	1.1	0	
June 1, 1989								
PGC-1	16	0.8	16	1.5	14	0.8	0	
PGC-2	14	0.2	16	0.4	0		5	0.5
June 2, 1989								
PGC-1	13	0.7	13	0.5	2		3	0.1
PGC-2	45	0.5	45	0.7	14	0.3	37	0.6
June 4, 1989								
PGC-1	44	1.5	49	1.8	1		4	3.1
PGC-2	32	0.2	48	0.2	8	0.5	23	0.6
June 6, 1989								
PGC-2	31	0.4	21	0.7	7	0.4	8	0.9
June 7, 1989								

^aRSD, relative standard deviation.

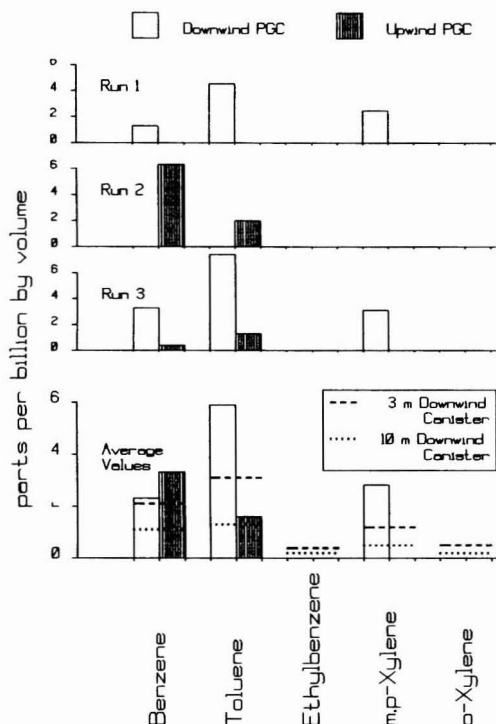


Figure 7. Upwind/downwind PGC responses observed at 15-min intervals terminating at the end of a 2-h time-integrated canister sampling period at highway site in USSR.

moved (18 m) from the highway. This discrepancy in source dilution suggested that sampling variation and/or site influences were being revealed by the near-real-time measurements of the PGCs. Additionally, the toluene/benzene (T/B) ratios for the 3- and 10-m canisters were 1.2 and 1.5, respectively, whereas the T/B ratio for the paired PGCs averaged 2.9. The agreement between the paired PGCs for toluene and benzene measurements shown in Figure 6 also suggested that the differences in the T/B ratio may have arisen from short-term variations in concentrations.

For upwind/downwind operation, the PGCs were deployed across the highway from each other with PGC-1

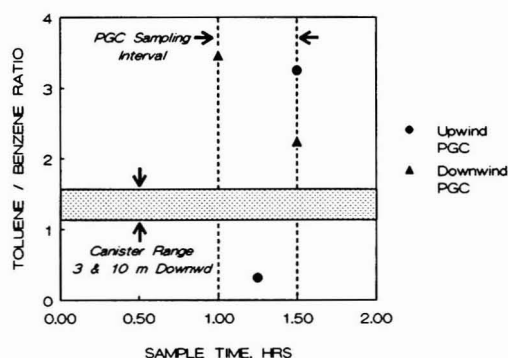


Figure 8. Toluene/benzene ratios from upwind/downwind PGC data and time-integrated canister data at highway site in USSR.

inside a van parked 12 m downwind (southwest) of the highway while PGC-2 remained inside the mobile laboratory. Canisters were again placed 3 and 10 m downwind of the highway. Data obtained in three PGC runs toward the end of the canister sampling period are shown in Figure 7. During run 1 the upwind PGC was recalibrating and reported no data. During run 2 the downwind PGC was recalibrating. Scheduling constraints allowed only 0.5 h of PGC sampling to be compared to the canisters, but this was sufficient to demonstrate (Figure 8) that the range of T/B ratios detected by the PGCs can be averaged out and "lost" by a time-integrated technique. PGC quantitative results were substantially in agreement with the canister results. Unlike the canister T/B ratios, the averaged T/B ratio for both PGCs was higher (2.3) and included a much wider range of values (0.32–3.4).

The T/B ratio discrepancy highlights an advantage of PGC sampling. Time-integrated canister samples average data over the duration of the sample period, while PGCs take a "snapshot" of what is in the air during an interval of 1 min or less and are influenced by emissions from vehicles that happen to be passing while the sample is being taken. In the United States, the T/B ratio in ambient air is usually greater than 1, although the ratio of toluene to benzene produced in combustion/pyrolysis processes is generally less than 1. This happens in the United States because hydrocarbon constituents of engine exhaust are mostly unburned fuel that has eluded emission control devices. Benzene in U.S. gasoline is limited to 4%,

and averages $\sim 1.3\%$. Toluene is permitted in higher concentrations since it is less toxic, and it strongly enhances octane rating. Toluene and benzene are not present in diesel fuel because they are outside its distillation range (typically C_{10} - C_{25}). Diesel combustion produces more benzene than toluene, but since gasoline-powered engines predominate on U.S. highways, the ambient T/B ratio in the United States is usually greater than 1. Different circumstances prevail in the USSR. Benzene in fuel is not regulated, and emission control devices are absent. Diesel-powered trucks, buses, tractors, and self-propelled machinery in enormous variety use Soviet highways, often outnumbering automobiles. Thus T/B ratios in the USSR could be more variable than in the United States.

A great advantage of using a 10.6-eV PID is that the compounds it is best able to detect are volatile aromatics that are among the most prolific of the volatile toxic compounds in engine exhaust. Paraffins, which are of somewhat less concern, are also present and can produce interferences when universal detectors are used, but they are not detectable by 10.6-eV PIDs at concentrations below 100 ppb. Apparently there were few if any interferences at the Vilnius site. Evidence for this is shown in Table II, where relative standard deviations of retention times for each compound are displayed for each sampling period. The PGCs were operated in autosampling mode, uninterrupted most of the time, and produced many more data than were shown in Figures 6 and 7. The number of times each compound was detected during each sampling period is displayed with the relative standard deviation of its retention time during that period. In most cases relative standard deviations were below 2%. If several compounds with similar (but not identical) retention times had been detected, the scatter in retention times would have been larger. It is unfortunate that these data cannot be compared with retention times from calibration runs, which were not reported by the PGCs when operating in auto-sampling mode. Because no data from authentic standards are included in Table II it can provide evidence that positive interferences were absent, but it cannot prove it.

Conclusions

On the basis of comparisons with canister data from domestic and foreign field studies, portable gas chromatographs can rapidly produce valid estimates of ambient background concentrations of many volatile nonpolar and semipolar organic air pollutants that ionize below 10.6 eV. Because of the specificity of the PID detector to compounds that ionize below 10.6 eV, little difficulty is encountered with interferences due to coeluting peaks, in spite of limited chromatographic resolution. Because the PGC can process data immediately, it is of great value for rapid screening of hazardous waste sites, chemical spills, and other sources of airborne organic vapors. Our comparison of T/B ratios from the respective methods is one example of how combined data can yield information on specific emission sources that might otherwise be missed by time-integrated sampling.

Results of these studies show acceptable agreement between PGC data and data from the canister/TO-14 method. They suggest that the canister/TO-14 method is generally valid for sampling atmospheres not contaminated with highly reactive compounds, even when analyses must be delayed. Combined canister/PGC analyses would be useful at uncharacterized sites or where highly reactive compounds are suspected. Positive interferences do occasionally affect canister data and could affect PGC data as well, but negative interferences would be less likely to

influence PGCs since they do not store or preconcentrate samples. Furthermore, when analyses using different sampling methodologies produce similar results, a preponderance of evidence is created that the data are substantially correct.

PGC analysis can be applied to nonpolar organic compounds that ionize below 10.6 eV and that are sufficiently volatile to elute from the column at 50 °C or below. Comparison of canister and PGC sampling should be expanded to include additional classes of compounds, especially polar solvents.

Literature Cited

- (1) *Compendium of Methods for the Determination of Toxic Organic Compounds in Ambient Air*; EPA-600/4-84-017; Environmental Protection Agency, Atmospheric Research and Exposure Assessment Laboratory, Research Triangle Park, NC, 1988.
- (2) Verner, P. J. *Chromatogr.* **1984**, *300*, 249-264.
- (3) Driscoll, J. N. *J. Chromatogr. Sci.* **1985**, *23*, 488-492.
- (4) Driscoll, J. N.; Atwood, E. S.; Hewitt, G. F. *Ind. Res. Dev.* **1982**, *24*, 188-191.
- (5) Cox, R. D.; Earp, R. F. *Anal. Chem.* **1982**, *54*, 2265-2270.
- (6) Rudolph, J.; Jensen, C. *Int. J. Environ. Anal. Chem.* **1983**, *13*, 129-139.
- (7) Nutmagul, W.; Cronn, D. R.; Hill, H. H., Jr. *Anal. Chem.* **1983**, *55*, 2160-2164.
- (8) Langhorst, M. L. *J. Chromatogr. Sci.* **1981**, *19*, 98-103.
- (9) Leveson, R. Ger. Offen. DE 3031358, Mar 19, 1983. Leveson, R. C. U.S. Patent 4398152, Aug 9, 1983. Leveson, R. C.; Barker, N. J. Canadian Patent 1158891 A1, Dec 20, 1983.
- (10) Barker, N. J.; Leveson, R. C. *Am. Lab.* **1980**, *12*, 76.
- (11) Leveson, Richard C.; Barker, N. J. *Proceedings of the Annual ISA Analytical Instruments Symposium*, 27th; St. Louis, MO, Mar 23-26 1981; pp 7-12.
- (12) Collins, M.; Barker, N. J. *Am. Lab.* **1983**, *15*, 72.
- (13) Clark, A. I.; McIntyre, A. E.; Lester, J. N.; Perry, R. *Int. J. Environ. Anal. Chem.* **1984**, *17*, 315-326.
- (14) Berkley, R. E. *Evaluation of Photovac 10S50 Portable Photoionization Gas Chromatograph for Analysis of Toxic Organic Pollutants in Ambient Air*; EPA/600/4-86/041; Environmental Protection Agency, Research Triangle Park, NC, 1986.
- (15) Lipsky, D. *Proceedings of the APCA Mid-Atlantic States Section Conference*; Wilmington, DE Apr 18-19, 1983; Paper D.
- (16) Hawthorne, A. R.; Matthews, T. G.; Gammage, R. B. *Proceedings, 78th Annual Meeting—APCA*, Detroit, MI, June 16-21, 1985; Paper 85-30B.
- (17) Jerpe, J.; Davis, A. J. *Chromatogr. Sci.* **1987**, *25*, 154-157.
- (18) Oliver, K. D.; Pleil, J. D.; McClenny, W. A. *Atmos. Environ.* **1986**, *20*, 1403-1411.
- (19) Gholson, A. R.; Storm, J. F.; Jayanty, R. K. M.; Fuerst, R. G.; Logan, T. J.; Midgett, M. R. *JAPCA* **1989**, *39*, 1210-1217.
- (20) Berkley, R. E. *Field Evaluation of Photovac 10S50 Portable Photoionization Gas Chromatograph for Analysis of Toxic Organic Pollutants in Ambient Air*; EPA/600/D-88/088; Environmental Protection Agency, Research Triangle Park, NC, 1988.
- (21) Berkley, R. E.; Varns, J. L.; McClenny, W. A.; Fulcher, J. *Proceedings of the 1989 EPA/AWMA Symposium on Measurement of Toxic and Related Air Pollutants*; AWMA: Pittsburgh, PA, 1989; pp 19-26.

Received for review October 3, 1990. Revised manuscript received April 2, 1991. Accepted April 12, 1991. This work was funded in part by the EPA Superfund Innovative Technology Evaluation (SITE) Program. The information in this document has been funded wholly or in part by the United States Environmental Protection Agency. It has been subjected to Agency review and approved for publication. Mention of trade names or commercial products does not constitute endorsement or recommendation for use.

Heuristic Model for Predicting the Intrusion Rate of Contaminant Vapors into Buildings

Paul C. Johnson* and Robert A. Ettinger

Shell Development, Westhollow Research Center, Houston, Texas 77251

■ The intrusion into and subsequent accumulation of contaminant vapors in buildings and family dwellings is of concern for health and safety reasons. When preparing environmental and health risk assessments, one must be able to quantify this exposure pathway in order to decide if site-specific conditions correspond to unacceptable indoor contaminant vapor concentrations. For cases in which contaminated-site soil cleanup levels can be negotiated based on site-specific conditions, a related problem is the determination of residual contaminant levels below which associated adverse health effect risks are deemed negligible. Unfortunately, there are currently no accepted models for predicting vapor intrusion rates, and there is considerable debate over which transport mechanisms govern the process. This paper presents a heuristic model for screening-level calculations. It incorporates both convective and diffusive mechanisms, as well as contaminant soil, and building foundation properties. Sample calculations are presented for a range of parameter values to illustrate use of the model and the relative contributions of individual transport mechanisms.

Introduction

The intrusion and subsequent accumulation of radon vapors in commercial buildings and family dwellings has received considerable attention in the last decade. Of growing interest is the related problem of vapor transport from contaminated soils into buildings and dwellings. When preparing health and environmental risk assessments, regulators may require one to determine a residual contaminant level below which the associated adverse health effect risk is deemed negligible. To accomplish this, however, predictive transport models are required. Despite the attention focused on radon intrusion, no such validated models are available.

The current level of understanding is that both diffusion and convection contribute to vapor intrusion, and specific site characteristics will determine the significance of each. Nazaroff et al. (1) attempted to correlate radon concentrations in basements with building ambient pressure differences, wind speed, temperature differences, soil radon activity, and indoor air-exchange rates. In summary, for the three dwellings studied, typical building underpressurizations (ambient basement pressure drop) ranged between 1 and 50 Pa, and radon intrusion rates increased with increasing building underpressurization. Through the use of a tracer gas and controlled building underpressurization, Nazaroff et al. (2) studied the coupling between building underpressurization, induced soil depressurization, and flow of soil gas to a building. In another field study, Hodgson et al. (3) studied the transport of vapors from a landfill to a residential basement; they concluded that convective transport was negligible for the conditions at that site. By building a scale model of a building, Arnold (4) attempted to correlate building underpressurization, wind speed, soil type, soil gas intrusion rates, and pressure distributions in surrounding soils.

Attempts to model radon intrusion have produced both semianalytical solutions and detailed numerical codes. Landman (5), who considered only vapor-phase diffusion,

modeled radon transport through cracks in slabs and predicted that a slab with 1% open cracks by area will reduce the radon flux by 75% relative to the case of a bare dirt floor. Landman and Cohen (6) later tried to simplify this analysis and incorporate convective transport. Other authors, such as Zapalac (7), have attempted to model and measure radon fluxes through intact (i.e., no macroscopic cracks) concrete barriers.

Recently, numerical models have been employed by Garbesi and Sextro (8) and Loureiro et al. (9). The former model soil gas entry through "permeable" walls, rather than through cracks and openings, and predict reasonable soil gas entry rates for the cases studied. The latter couple soil gas flow field solutions with a contaminant transport model to predict radon intrusion rates through cracks and openings in basement floors and walls. It should be noted that one must be careful when extending results and conclusions from radon intrusion studies to the problem addressed in this study. In the case of radon intrusion, vapors are typically generated within the soil matrix adjacent to the foundation, while contaminant vapors of the type discussed in this report must migrate from a source located a distance from the building.

The goal of this work is similar to those of Nazaroff (10) and Nazaroff and Sextro (11); we want to develop a less computationally complex screening-level model for estimating contaminant vapor intrusion rates. Nazaroff (10) outlined a semianalytical approach for predicting indoor radon concentrations in the limit of convective-dominated transport, while Nazaroff and Sextro (11) described a more empirical technique based on a site-specific *in situ* measurement. Here we utilize the results and observations of these authors to formulate a heuristic model for predicting the intrusion rate of contaminant vapors into buildings through foundations in a more general scenario: contaminant vapors originating an arbitrary distance away from a building. This model can be used as a risk assessment screening-level tool; it can be used to identify sites, or contaminant levels, for which contaminant exposures through a vapor inhalation pathway may cause adverse health effects. It can also be used as a tool to help identify sites where more detailed numerical simulations or field sampling are appropriate. Below, the basis for the model is discussed, model equations are derived, and sample calculations are presented that illustrate the use of the model.

Heuristic Model Basis

While the formal development of the heuristic model is presented below, it is necessary to identify relevant phenomena that govern contaminant vapor transport into dwellings. In the following section, a dimensional analysis is conducted to assess the relative importance of each phenomenon. The transport of contaminants through soil matrices is often modeled by solving the following transport equation:

$$\frac{\partial \sum \epsilon_i C_i}{\partial t} + \sum_i \mathbf{u}_i \cdot \nabla C_i = \sum_i \nabla \cdot \mathbf{D}_i^{\text{eff}} \nabla C_i + \sum_i R_i \quad (1)$$

where i is a subscript that specifies the phase (i.e., v = vapor, s = sorbed, f = free phase or precipitate, and m = soil moisture), t is time (s), ϵ_i is the volume fraction of phase i (volume of phase i /volume of soil, dimensionless), C_i is the concentration of contaminant in phase i (mass/volume of phase i , g/cm³), u_i is the Darcy velocity vector associated with phase i (cm/s), ∇ is the del operator (1/cm), D_i^{eff} is the effective porous medium diffusion coefficient of contaminant in phase i (cm²/s), and R_i is the formation rate of contaminant in phase i (g/cm³-s).

For the special case where residual contaminant levels are low enough that no contaminant free-liquid/precipitate phase is present in the soil pores, under equilibrium conditions contaminant levels in the vapor, sorbed, and soil moisture phases are often assumed to be proportional to each other and the total contaminant level [Johnson et al. (12)]. Equation 1 can then be written in terms of a single phase concentration. One can assume, without any loss of generality, that contaminant levels in the soil moisture and vapor phases are related by a Henry's law constant, H (cm³ of H₂O/cm³ of vapor):

$$C_v = HC_m \quad (2)$$

A similar equation can be written for the relationship between sorbed and soil moisture phases, except that H is replaced by a sorption coefficient. If one assumes that diffusive transport is significant only in the vapor and soil moisture phases, then it follows from eq 2 that

$$\sum_i \nabla \cdot D_i^{\text{eff}} \nabla C_i = \nabla \cdot (D_v^{\text{eff}} + D_m^{\text{eff}}/H) \nabla C_v = \nabla \cdot D^{\text{eff}} \nabla C_v \quad (3)$$

where D^{eff} , defined by eq 3, is the "effective porous medium diffusion coefficient based on vapor-phase concentrations". The effective porous medium diffusion coefficients (D_m^{eff} and D_v^{eff}) are related to the pure component molecular diffusivities in water and air, $D^{\text{H}_2\text{O}}$ and D^{air} , total soil porosity, $\epsilon_T = (\epsilon_v + \epsilon_m)$, vapor-filled porosity, ϵ_v , and moisture-filled porosity, ϵ_m , by the Millington-Quirk [Bruell and Hoag (13)] expression:

$$D_m^{\text{eff}} = D^{\text{H}_2\text{O}} \epsilon_m^{3.33} / \epsilon_T^2 \quad (4)$$

and

$$D_v^{\text{eff}} = D^{\text{air}} \epsilon_v^{3.33} / \epsilon_T^2 \quad (5)$$

where ϵ_m and ϵ_v are related to ϵ_T , the moisture content θ_m (cm³ of H₂O/g of soil), and the bulk soil density ρ_b (g/cm³):

$$\epsilon_m = \theta_m \rho_b \quad (6)$$

and

$$\epsilon_v = \epsilon_T - \theta_m \rho_b \quad (7)$$

For most compounds (except those with very small Henry's law constants), the contribution due to diffusion through the soil moisture will be insignificant in comparison with vapor-phase diffusion.

For the purpose of this analysis, we also assume that significant convective transport occurs only in the vapor phase, and vapor flow is described by Darcy's law:

$$u_v = -\frac{k_v}{\mu} \nabla P \quad (8)$$

where k_v is the soil permeability to vapor flow (cm²), μ is the vapor viscosity (g/cm-s), P is the pressure in the vapor phase (g/cm-s²), and u_v is the vapor-phase mass-average velocity (cm/s).

Table I. Dependence of Pe on Soil Type^a

soil type	permeability, k_v (darcy or 10 ⁻⁸ cm ²)	Pe
silt	0.01-0.1	0.08-0.08
silty sand	0.1-1	0.08-0.8
fine sand	1-10	0.8-8
medium sand	10-100	8-80

^a $Pe = (k_v \Delta P_r L_D / D^{\text{eff}} \mu L_P)$, where $\Delta P_r = 10$ Pa = 100 g/cm-s² = 10⁻⁴ atm, $D^{\text{air}} = 0.087$ cm²/s (benzene at 20 °C); $D^{\text{H}_2\text{O}} = 1.0 \times 10^{-5}$ cm²/s; $H = 0.18$ cm³ of H₂O/cm³ of vapor (benzene at 20 °C); $\epsilon_T = 0.38$; $\theta_m = 0.07$ g of H₂O/g of soil (sandy soil at field capacity moisture content); $\rho_b = 1.7$ g of soil/cm³ of soil; $\mu = 1.8 \times 10^{-4}$ g/cm-s; $L_D = L_P$; $D^{\text{eff}} \approx D_v^{\text{eff}} = 0.087$ cm²/s $\times (0.26^{3.33}/0.38^2) = 6.8 \times 10^{-3}$ cm²/s.

Inserting eqs 3 and 8 into eq 1 and nondimensionalizing the resulting equation yields

$$\frac{\partial \sum_i \epsilon_i C_i^*}{\partial t^*} - \left(\frac{L_P}{L_D} \right) (\nabla^* P^*) \cdot (\nabla^* C_v^*) = \nabla^* \cdot \left[\frac{D^{\text{eff}} \mu L_P}{k_v \Delta P_r L_D} \right] \nabla^* C_v^* + \sum_i R_i^* \quad (9)$$

where ΔP_r is the reference or characteristic indoor-outdoor pressure difference and * denotes nondimensional variables:

$$C_i^* = C_i / C_r \quad \nabla^* = L_D \nabla \quad P^* = P / \Delta P_r \\ t^* = t (k_v \Delta P_r / L_P L_D \mu) \quad R_i^* = R_i L_P L_D \mu / C_r k_v \Delta P_r$$

where C_r , L_D , and L_P are characteristic concentration, diffusion pathway length, and convection pathway length values, respectively, chosen to give the dependent concentration variable and derivatives of C_i^* and P^* magnitudes of order unity. Then the dimensionless group

$$[k_v \Delta P_r L_D / D^{\text{eff}} \mu L_P] = Pe \quad (10)$$

determines the relative significance of convective and diffusive transport mechanisms. Here Pe is the Peclet number, expressed in terms of the driving pressure ΔP_r . If $Pe \gg 1$, convective transport dominates; if $Pe \ll 1$, diffusive transport dominates. Note that the Peclet number defined by eq 10 contains two length scales L_D and L_P . This is appropriate for the problem of contaminant vapor intrusion into buildings, where the characteristic length scales for diffusion and convection may be quite different. Logical choices for L_D and L_P are the contaminant source-basement separation and the distance between ground surface and the basement floor, respectively.

It is useful to examine the magnitude of Pe before formulating any simpler vapor intrusion models. Based on the Nazaroff et al. (1, 2) studies, typical values of ΔP_r are 1-10 Pa (10-100 g/cm-s²), so we will choose the following representative parameter values: $\Delta P_r = 10$ Pa = 100 g/cm-s² = 10⁻⁴ atm; $D^{\text{air}} = 0.087$ cm²/s (benzene at 20 °C); $D^{\text{H}_2\text{O}} = 1.0 \times 10^{-5}$ cm²/s; $H = 0.18$ cm³ of H₂O/cm³ of vapor (benzene at 20 °C); $\epsilon_T = 0.38$; $\theta_m = 0.07$ g of H₂O/g of soil (sandy soil at field capacity moisture content); $\rho_b = 1.7$ g of soil/cm³ of soil; $\mu = 1.8 \times 10^{-4}$ g/cm-s; $L_D = L_P$. Table I presents values for Pe for different soil types. While θ_m , ϵ_T , ρ_b , and hence D^{eff} will vary with soil type, it has been assumed that all soils listed in Table I have similar total porosities, soil moisture contents, and bulk densities (an assumption that would not be valid for comparing sandy and clayey soils). The diffusion coefficients in water and air are also compound-specific; however, compounds whose molecular weights range from 70 to 300 have diffusion coefficients that differ by only a factor of ~ 2 [Lyman et al. (14)]. Of the parameters appearing in eq 10, the soil

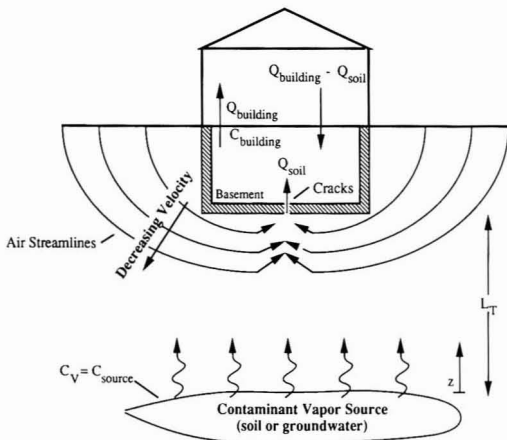


Figure 1. Vapor intrusion scenario.

permeability, k_v , is the most variable at any given site; it is not unusual for k_v to vary by 3 orders of magnitude across a site the size of a typical residential lot. As can be seen in Table I, Pe ranges between 0.01 and 100 for the soil types listed there. The significance of this observation is that any vapor intrusion model based only on either convective or diffusive transport mechanisms cannot reasonably describe the relevant phenomena over the typical range of soil types. Any proposed model, therefore, must include both transport mechanisms.

Formulation of the Heuristic Model

This discussion will be limited to problems in which chemical or biological transformations are not significant (i.e., $R_i = 0$). Recall that the goal of this development is to produce a predictive model suitable for screening-level calculations. Given that biological transformations in the unsaturated zone are presently not very well understood, it is not appropriate to attempt to incorporate them into this level of modeling. The reader should understand, however, that degradation due to microorganisms does occur; any model that includes them will predict lower intrusion rates than the model presented here (unless the contaminant of concern is produced by the biological transformation).

At this point we will restrict the analysis to steady-state (nondiminishing source) problems, although it will be shown later how one might adapt the results to diminishing source problems. Figure 1 presents a simplified sketch of the problem under consideration, in which a contaminant vapor source of concentration C_{source} is located some distance L_T below the floor of a basement or building slab. We want to predict the intrusion rate of vapors into the building. To accomplish this, the following assumptions are made:

- (i) Contaminant vapors enter structures primarily through cracks and openings in the walls and foundation (electrical outlets, wall-floor seams, sump drains, etc.).
- (ii) Convective transport is likely to be most significant in the region very close to a basement, or foundation, and vapor velocities decrease rapidly with increasing distance from a structure.
- (iii) Vapor-phase diffusion is the dominant mechanism for transporting contaminant vapors from contaminant sources located away from the foundation to the soil region near the foundation.
- (iv) All contaminant vapors originating from directly below the basement will enter the basement, unless the

floor and walls are perfect vapor barriers.

Assumption i reflects the current thinking that vapor intrusion is mainly due to cracks, seams, and openings in basement floors and walls, while ii and iii are based on the analysis presented above, the Peclet numbers appearing in Table I, and analogy to known solutions of fluid mechanics problems. In this simplistic model, contaminants volatilize from the source and diffuse toward the foundation. When convection is significant, they are "swept" into the building through cracks; otherwise, the contaminant vapors diffuse through the cracks and openings. Assumption iv restricts contaminant vapors from leaking around a building to ground surface and, therefore, adds a level of conservation to the model. Vapor leakage to the surface will be significant whenever the resistance to transport into a building is much greater than the resistance to transport to ground surface, such as buildings built on relatively intact slab foundations. It should be noted that the final results will not be limited by the validity of assumption i; if one follows the analysis below for the case where vapors are transported through intact porous walls, the final equations are identical in form with the results presented below (this will be shown later).

In addition to assumptions i-iv listed above, there are also assumptions inherent in the simplistic mathematical models described below. One-dimensional transport models form the basis for the heuristic model; therefore, it is assumed that the soil is homogeneous within any horizontal plane with respect to effective diffusion coefficients (heterogeneity in the vertical direction is accounted for). Also, it is assumed that convective vapor flow in the region near the foundation is uniform. This assumption, however, does not preclude application of the model to scenarios where there is a uniform layer of gravel adjacent to the foundation; in fact, the idealization described in assumption ii accurately represents this scenario, and one only needs to be sure to predict the soil gas entry rate based on properties of this region (and not the permeability of surrounding soils).

In the following, the heuristic vapor intrusion model is formulated by combining approximate mathematical descriptions of the relevant transport phenomena:

(a) **Diffusive Transport from the Source to a Region near the Structure.** As described above, it is assumed that contaminant vapors are transported from the contaminant source to a region near the structure, primarily by a molecular diffusion through pore vapor and soil moisture phases. The rate can be approximated by the expression

$$E_1 = A_B (C_{\text{source}} - C_{\text{soil}}) D_T^{\text{eff}} / L_T \quad (11)$$

where E_1 is the mass-transport rate toward the structure (g/s), A_B is the cross-sectional area through which vapors pass (cm^2), C_{source} is the vapor concentration at the contaminant source (g/cm^3), C_{soil} is the vapor concentration in the region near the structure (g/cm^3), L_T is the distance from contaminant source to foundation (cm), and D_T^{eff} is the "overall" effective porous media diffusion coefficient based on vapor-phase concentrations for the region between the source and foundation (cm^2/s).

The cross-sectional area, A_B , can be approximated by the total basement area (floor and walls). Assuming that convection, when significant, is only dominant in a region very near the foundation allows us to approximate the total diffusion length, L_T , as the distance between the source and foundation. The soil permeability to vapor flow, building underpressurization, and physical setting will determine the actual thickness of the convection-dominated region, which will increase with increasing permea-

bility to vapor flow and increased building underpressurization. In general, the unsaturated soil zone may be composed of several soil types with varying moisture contents and porosities, and the effective overall diffusion coefficient for a region between $z = 0$ and $z = L_T$ is

$$D_T^{\text{eff}}/L_T = \left[\int_0^{L_T} dz/D^{\text{eff}}(z) \right]^{-1} \quad (12)$$

where $D^{\text{eff}}(z)$ is the effective porous media diffusion coefficient at z , which is a function of the contaminant type and soil characteristics as defined by eqs 3–7.

For systems composed of n distinct soil layers defined by thicknesses L_i and uniform effective overall porous media diffusion coefficients D_i^{eff} , eq 12 reduces to

$$D_T^{\text{eff}}/L_T = \left[\sum_{i=0}^n L_i/D_i^{\text{eff}} \right]^{-1} \quad (13)$$

(b) Transport from Soil Gas into Building. The transport of contaminants from soil gas adjacent to a foundation is assumed to occur by a combination of convective and diffusive transport mechanisms. As a first approximation, the steady-state, one-dimensional solution to eq 9 for vapor transport through a crack (or porous medium) with a constant uniform convective velocity ($Q_{\text{soil}}/A_{\text{crack}}$) is used to predict the total rate of contaminant intrusion into a building:

$$E = Q_{\text{soil}}C_{\text{soil}} - \frac{Q_{\text{soil}}(C_{\text{soil}} - C_{\text{building}})}{[1 - \exp(Q_{\text{soil}}L_{\text{crack}}/D_{\text{crack}}A_{\text{crack}})]} \quad (14)$$

where E is the entry rate of contaminant into the building (g/s), Q_{soil} is the volumetric flow rate of soil gas into the building (cm^3/s), D_{crack} is the effective vapor-pressure diffusion coefficient through the crack (cm^2/s), L_{crack} is the thickness of the foundation (cm), C_{building} is the contaminant vapor concentration in the building (g/cm^3), and A_{crack} is the area of cracks/openings through which contaminant vapors enter the building (cm^2).

The only "unknown" in eqs 11 and 14 is the soil gas contaminant concentration, C_{soil} , which can be obtained by requiring that the rates E_1 and E be equal at steady state. The result

$$C_{\text{soil}} = \left[C_{\text{source}} \left[\frac{D_T^{\text{eff}}A_B}{Q_{\text{soil}}L_T} \right] \left[\exp\left(\frac{Q_{\text{soil}}L_{\text{crack}}}{D_{\text{crack}}A_{\text{crack}}} \right) - 1 \right] + C_{\text{building}} \right] / \left[\left[\frac{D_T^{\text{eff}}A_B}{Q_{\text{soil}}L_T} \right] \left[\exp\left(\frac{Q_{\text{soil}}L_{\text{crack}}}{D_{\text{crack}}A_{\text{crack}}} \right) - 1 \right] + \exp\left(\frac{Q_{\text{soil}}L_{\text{crack}}}{D_{\text{crack}}A_{\text{crack}}} \right) \right] \quad (15)$$

can be substituted into eq 14 to obtain E , the rate of contaminant entry into a building through the foundation:

$$E = \left[\frac{D_T^{\text{eff}}A_B C_{\text{source}}}{L_T} \right] \left[\exp\left(\frac{Q_{\text{soil}}L_{\text{crack}}}{D_{\text{crack}}A_{\text{crack}}} \right) - \left[\frac{C_{\text{building}}}{C_{\text{source}}} \right] \right] / \left[\left[\frac{D_T^{\text{eff}}A_B}{Q_{\text{soil}}L_T} \right] \left[\exp\left(\frac{Q_{\text{soil}}L_{\text{crack}}}{D_{\text{crack}}A_{\text{crack}}} \right) - 1 \right] + \exp\left(\frac{Q_{\text{soil}}L_{\text{crack}}}{D_{\text{crack}}A_{\text{crack}}} \right) \right] \quad (16)$$

When eq 16 is written this way, E is the product of the steady-state diffusive rate of contaminant transport from a source to a bare dirt floor foundation (first term on

right-hand side) and a factor containing a number of dimensionless groups whose significance will be discussed below.

Indoor Air Quality. Equation 16 can be incorporated into a steady-state mass balance for a basement (or building) to produce an explicit expression for the indoor contaminant vapor. Assuming no other contaminant sources or sinks (i.e., sorption to walls or furniture) and a well-mixed building, this expression can be written

$$Q_{\text{building}}C_{\text{building}} = E \quad (17)$$

where Q_{building} denotes the basement (or building) ventilation rate, expressed as a volumetric flow rate. Often, this term is expressed as the product of an "air-exchange rate" and a basement (or building) volume; however, here these terms are combined into Q_{building} . Substituting eq 16 into eq 17 and rearranging yields

$$C_{\text{building}} = \left[C_{\text{building}}^* \times \exp\left(\frac{Q_{\text{soil}}L_{\text{crack}}}{D_{\text{crack}}A_{\text{crack}}} \right) \right] / \left[\exp\left(\frac{Q_{\text{soil}}L_{\text{crack}}}{D_{\text{crack}}A_{\text{crack}}} \right) + \left[\frac{D_T^{\text{eff}}A_B}{Q_{\text{building}}L_T} \right] + \left[\frac{D_T^{\text{eff}}A_B}{Q_{\text{soil}}L_T} \right] \left[\exp\left(\frac{Q_{\text{soil}}L_{\text{crack}}}{D_{\text{crack}}A_{\text{crack}}} \right) - 1 \right] \right] \quad (18)$$

where

$$C_{\text{building}}^* = \left[\frac{D_T^{\text{eff}}A_B C_{\text{source}}}{Q_{\text{building}}L_T} \right] \quad (19)$$

In eqs 18 and 19, C_{building}^* represents the indoor vapor concentration corresponding to the case where vapors diffuse from the source to a bare soil foundation. As will be derived later, this is the limiting case in which Q_{soil} becomes very small and the diffusional resistance through the basement floors/walls is significantly less than the diffusional resistance through the soil zone between the contaminant vapor source and building. Equation 18 can also be arranged to produce the "attenuation coefficient" α :

$$\alpha = C_{\text{building}}/C_{\text{source}} \quad (20)$$

or equivalently

$$\alpha = \left[\left[\frac{D_T^{\text{eff}}A_B}{Q_{\text{building}}L_T} \right] \times \exp\left(\frac{Q_{\text{soil}}L_{\text{crack}}}{D_{\text{crack}}A_{\text{crack}}} \right) \right] / \left[\exp\left(\frac{Q_{\text{soil}}L_{\text{crack}}}{D_{\text{crack}}A_{\text{crack}}} \right) + \left[\frac{D_T^{\text{eff}}A_B}{Q_{\text{building}}L_T} \right] + \left[\frac{D_T^{\text{eff}}A_B}{Q_{\text{soil}}L_T} \right] \left[\exp\left(\frac{Q_{\text{soil}}L_{\text{crack}}}{D_{\text{crack}}A_{\text{crack}}} \right) - 1 \right] \right] \quad (21)$$

Both eqs 18 and 21 depend on three dimensionless groups:

$$\frac{Q_{\text{soil}}L_{\text{crack}}}{D_{\text{crack}}A_{\text{crack}}} \quad \frac{D_T^{\text{eff}}A_B}{Q_{\text{building}}L_T} \quad \frac{Q_{\text{soil}}}{Q_{\text{building}}}$$

The first represents the equivalent Peclet number for transport through the foundation, the second is the attenuation coefficient (as defined in eq 20) for diffusion-dominated transport from a constant source to a bare dirt floor, and the third is the attenuation coefficient for con-

vective transport from a source located adjacent to the building.

At this point it is useful to examine the behavior predicted by eq 21 in certain limiting situations, in order to verify that the mathematics represents the phenomena incorporated into their derivation and that the results fall within appropriate bounds:

(a) $(Q_{\text{soil}}L_{\text{crack}}/D_{\text{crack}}A_{\text{crack}}) \rightarrow \infty$. In this limit convection is the dominant transport mechanism through the basement (building) floor and walls. Equation 21 becomes

$$\lim_{D_{\text{crack}}A_{\text{crack}}} \frac{Q_{\text{soil}}L_{\text{crack}}}{D_{\text{crack}}A_{\text{crack}}} \rightarrow \infty \quad \alpha \rightarrow \frac{\left[\frac{D_T^{\text{eff}}A_B}{Q_{\text{building}}L_T} \right]}{\left[\frac{D_T^{\text{eff}}A_B}{Q_{\text{soil}}L_T} \right] + 1} \quad (22)$$

If the source lies directly beneath the foundation ($L_T \rightarrow 0$), then $\alpha \rightarrow Q_{\text{soil}}/Q_{\text{building}}$, which is the proper result for convection-dominated transport of a vapor stream with concentration C_{source} . If the source is "far" from the basement (i.e., $D_T^{\text{eff}}A_B/Q_{\text{soil}}L_T \rightarrow 0$), then transport is limited by diffusion from the source to foundation, and $\alpha \rightarrow D_T^{\text{eff}}A_B/Q_{\text{building}}L_T$. Note that in the limit $Q_{\text{soil}}L_{\text{crack}}/D_{\text{crack}}A_{\text{crack}} \rightarrow \infty$ the results are independent of the cracked area of the floor and walls. This is because contaminant vapors are swept into the building as fast as they are transported to the soil adjacent to the floor and walls.

(b) $(Q_{\text{soil}}L_{\text{crack}}/D_{\text{crack}}A_{\text{crack}}) \rightarrow 0$. In this limit diffusion is the dominant transport mechanism through the basement floor and walls, and eq 21 reduces to

$$\lim_{D_{\text{crack}}A_{\text{crack}}} \frac{Q_{\text{soil}}L_{\text{crack}}}{D_{\text{crack}}A_{\text{crack}}} \rightarrow 0 \quad \alpha \rightarrow \frac{\left[\frac{D_T^{\text{eff}}A_B}{Q_{\text{building}}L_T} \right]}{1 + \left[\frac{D_T^{\text{eff}}A_B}{Q_{\text{building}}L_T} \right] + \left[\frac{D_T^{\text{eff}}A_B L_{\text{crack}}}{D_{\text{crack}}A_{\text{crack}} L_T} \right]} \quad (23)$$

Equation 23 contains two dimensionless groups. As discussed above, $D_T^{\text{eff}}A_B/Q_{\text{building}}L_T$ represents the attenuation coefficient for diffusive transport to a bare dirt floor. The second dimensionless group, $D_T^{\text{eff}}A_B L_{\text{crack}}/D_{\text{crack}}A_{\text{crack}} L_T$, is a measure of the diffusion rates through the soil relative to those through the floor and walls. If $D_T^{\text{eff}}A_B L_{\text{crack}}/D_{\text{crack}}A_{\text{crack}} L_T \ll 1$, then $\alpha \rightarrow D_T^{\text{eff}}A_B/Q_{\text{building}}L_T$ because $D_T^{\text{eff}}A_B/Q_{\text{building}}L_T$ will typically be much less than unity unless $Q_{\text{building}} \rightarrow 0$. If $D_T^{\text{eff}}A_B L_{\text{crack}}/D_{\text{crack}}A_{\text{crack}} L_T \gg 1$, then $\alpha \rightarrow D_{\text{crack}}A_{\text{crack}}/Q_{\text{building}}L_{\text{crack}}$, which is the appropriate attenuation coefficient for transport from a source located adjacent to the floor and walls. When $D_T^{\text{eff}}A_B L_{\text{crack}}/D_{\text{crack}}A_{\text{crack}} L_T \gg 1$, then diffusion through the floor and walls is the rate limiting mechanism, and there is a vapor concentration "buildup" below the building or basement.

(c) $Q_{\text{building}} \rightarrow 0$. This limit corresponds to a perfectly sealed basement, Q_{soil} must also approach zero, and the model predicts that $\alpha \rightarrow 1$; that is, the indoor contaminant vapor concentration approaches the contaminant vapor concentration in the soil gas.

Sample Calculations

On the basis of the analysis above, it appears that model predictions fall correctly within the appropriate bounds for all limiting cases examined. These results, however,

Table II. Parameter Values Used To Generate Figures 2-5

$A_B = 7 \text{ m} \times 10 \text{ m} + 2(2 \text{ m} \times 7 \text{ m}) + 2(2 \text{ m} \times 10 \text{ m}) = 138 \text{ m}^2 = 138 \times 10^4 \text{ cm}^2$
$L_{\text{crack}} = 6 \text{ in.} = 15 \text{ cm}$
$Q_{\text{building}} = 7 \text{ m} \times 10 \text{ m} \times 3 \text{ m} \times 0.5 \text{ volume exchanges/h} = 105 \text{ m}^3/\text{h} = 2.9 \times 10^4 \text{ cm}^3/\text{s}$
$D^{\text{air}} = 0.087 \text{ cm}^2/\text{s}$ (benzene)
$D^{\text{H}_2\text{O}} = 1.0 \times 10^{-5} \text{ cm}^2/\text{s}$
$H = 0.18 \text{ cm}^3$ of $\text{H}_2\text{O}/\text{cm}^3$ of air (benzene)
$\theta_m = 0.07 \text{ g}$ of $\text{H}_2\text{O}/\text{g}$ of soil
$\epsilon_T = 0.38 \text{ cm}^3/\text{cm}^3$ of soil
$\rho_b = 1.7 \text{ g}/\text{cm}^3$
$\Delta P = 1.0 \text{ Pa} = 10 \text{ g}/\text{cm} \cdot \text{s}^2$

give no indication of what "typical" values of these dimensionless groups might be. It is useful at this point, therefore, to examine model predictions for a sample case. Consider a $10 \text{ m} \times 7 \text{ m} \times 3 \text{ m}$ (length \times width \times height) basement whose floor lies 2 m below grade. It is assumed that the floor/wall cracks and openings are filled with dust and dirt characterized by a density, porosity, and moisture content similar to that of the underlying soil. Model parameters A_B , L_{crack} , Q_{building} , D^{air} , $D^{\text{H}_2\text{O}}$, H , θ_m , ϵ_T , and ρ_b are given in Table II. The remaining unspecified parameters are the convective flow rate from the soil into the basement, Q_{soil} , the area of cracks, A_{crack} , and the distance between the contaminant source and the foundation, L_T . The soil gas flow rate, Q_{soil} , is likely to be dependent on the basement crack area, A_{crack} , soil type and stratigraphy, building underpressurization, and basement geometry. For simplicity, however, we will estimate Q_{soil} as suggested by Nazaroff (10):

$$Q_{\text{soil}} = \frac{2\pi\Delta P k_v X_{\text{crack}}}{\mu \ln [2Z_{\text{crack}}/r_{\text{crack}}]} \frac{r_{\text{crack}}}{Z_{\text{crack}}} \ll 1 \quad (24)$$

Equation 24 is an analytical solution for flow to a cylinder of length X_{crack} and radius r_{crack} located a depth Z_{crack} below ground surface; this is an idealized model for soil gas flow to cracks located at floor/wall seams. Here ΔP , k_v , and μ are as defined above. For this sample problem, $Z_{\text{crack}} = 2 \text{ m}$ (as stated above), X_{crack} is taken to be the total floor/wall seam perimeter distance (34 m), and for consistency r_{crack} is given by

$$r_{\text{crack}} = \eta A_B / X_{\text{crack}} \quad (25)$$

where the ratio $\eta = A_{\text{crack}}/A_B$, so that $0 \leq \eta \leq 1$. For reference, $\eta = 0.01$ corresponds to $r_{\text{crack}} = 4.1 \text{ cm}$ for the values of A_B and X_{crack} given above; $r_{\text{crack}} = 1 \text{ cm}$ corresponds to $\eta = 0.0025$.

In the Nazaroff et al. studies (1, 2), estimates for Q_{soil} are in the $280\text{--}2800 \text{ cm}^3/\text{s}$ ($1\text{--}10 \text{ m}^3/\text{h}$) range, for induced building underpressurizations of $5\text{--}30 \text{ Pa}$ and very permeable soils ($k_v > 10^{-8} \text{ cm}^2$). Note that $1 \text{ m}^3/\text{h}$ corresponds to $\sim 1\%$ of the assumed total basement air exchange rate ($0.5/\text{h}$). For the purpose of this sample calculation we choose $\Delta P = 1 \text{ Pa}$ ($10 \text{ g}/\text{cm} \cdot \text{s}^2$), which is probably a reasonable long-term average value for screening calculations.

Figure 2 presents soil gas flow rates predicted by eq 24 for $\eta = 0.01$ and $\eta = 0.001$. This figure illustrates the strong dependence of Q_{soil} on soil type, and a weaker dependence on crack size (as reflected in the value of η). For very permeable soils ($k_v \geq 10^{-6} \text{ cm}^2$), the predicted Q_{soil} values are of the same order of magnitude as the values observed by Nazaroff (1, 2). For example, $Q_{\text{soil}} = 260 \text{ cm}^3/\text{s}$ for $\eta = 0.01$ and $k_v = 1 \times 10^{-6} \text{ cm}^2$. For reference, medium sandy soils correspond to $10^{-7} < k_v < 10^{-6} \text{ cm}^2$.

Figures 3-5 present predicted attenuation coefficients α , for $\eta = 0.01$, and $\eta = 0.001$, as a function of k_v , for L_T

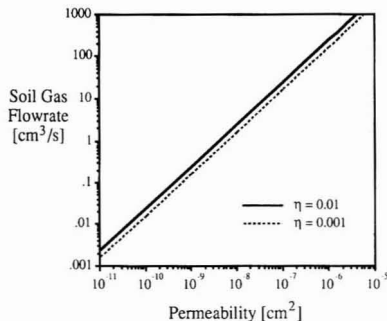


Figure 2. Dependence of soil gas entry flow rates, Q_{soil} , on soil permeability, k_v , as predicted by eq 24 for the parameters listed in Table II.

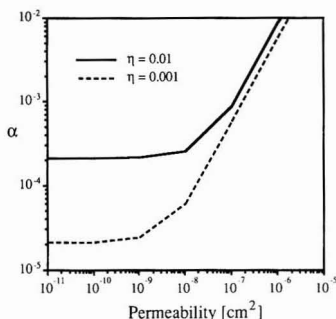


Figure 3. Dependence of attenuation coefficient, α , on soil permeability, k_v , as predicted by eq 21 for the parameters listed in Table II and $L_T = 0$.

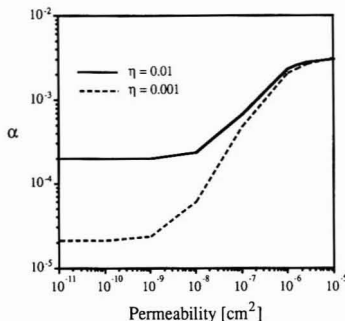


Figure 4. Dependence of attenuation coefficient, α , on soil permeability, k_v , as predicted by eq 21 for the parameters listed in Table II and $L_T = 100$ cm.

$= 0, 100$, and 1000 cm. Recall that $\alpha = C_{\text{building}}/C_{\text{source}}$, and it is a measure of both the indoor contaminant vapor concentration and contaminant vapor intrusion rate. The results are plotted in this way to facilitate comparison with numerical modeling results presented by Loureiro et al. (9). Figure 3 corresponds to the case where the contaminant vapor source lies adjacent to the building foundation ($L_T = 0$) and is roughly equivalent to the radon intrusion scenario modeled by these authors. The screening model predicts results that are in good qualitative and quantitative agreement with the detailed numerical modeling results [i.e., see Loureiro et al. (9), Figure 11]; both predict that α (and hence the intrusion rate) is independent of k_v for "small" values of k_v and becomes proportional to k_v at "large" values of k_v . The transition between these two regimes occurs near $k_v = 10^{-8}$ cm². For $k_v < 10^{-8}$ cm², the

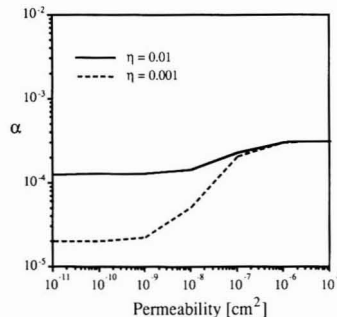


Figure 5. Dependence of attenuation coefficient, α , on soil permeability, k_v , as predicted by eq 21 for the parameters listed in Table II and $L_T = 1000$ cm.

soil gas flow rate through the cracks becomes so low that diffusion is the dominant transport mechanism and α is therefore independent of k_v . For $k_v > 10^{-8}$ cm², on the other hand, containment vapors are swept into the building primarily by convection. In this limit, $\alpha \rightarrow Q_{\text{soil}}/Q_{\text{building}}$ and becomes proportional to the resistance to flow (as measured by k_v). In this case the proposed screening model predicts $0.001 < \alpha < 0.01$ for $10^{-7} < k_v < 10^{-6}$ cm², which happens to fall in the range of values typically reported for radon intrusion studies. Figure 3 also indicates that the screening model predicts a dependence of intrusion rate and attenuation on the size of the crack, with the effect being more pronounced at lower permeabilities. As the crack size decreases, resistance to both diffusive transport and soil gas flow increases; thus, α is always predicted to be less for $\eta = 0.001$ than for $\eta = 0.01$. The decrease in flow rate predicted by eq 24 is apparently not as significant, however, as the increased resistance to diffusion through foundation cracks. Thus, for practical purposes, it can be concluded that the effect of crack size on contaminant vapor intrusion rates will be relatively insignificant in the limit of convective-dominated transport.

Figures 4 and 5 present model predictions for cases where the contaminant vapor source is located some distance L_T away from the foundation. In each figure the dependence of α on k_v is a sigmoidal-shaped curve, where α becomes independent of k_v in the limits of "large" and "small" soil permeabilities. In the limit of less permeable soils, soil gas flow rates are so low that vapor intrusion is governed entirely by the relative rates of diffusion through the soil and foundation. As the soil becomes more permeable, the "sweeping" of contaminant vapors into the building by soil gas flow increases the intrusion rate. At some point, however, diffusion from the containment vapor source to the region of soil gas flow limits the rate of contaminant vapor transport. For highly permeable soils, therefore, α becomes independent of k_v and only weakly dependent on foundation properties. The transition between Figures 4 and 5 also illustrates that α and the intrusion rate become less dependent on foundation properties as L_T increases. This is evidenced by the convergence of the "low" and "high" k_v asymptotes, and the $\eta = 0.001$ and $\eta = 0.01$ predictions as L_T increases; in the limit $L_T \rightarrow \infty$, diffusion through soil becomes the limiting transport mechanism.

Figures 3–5 illustrate the necessity of developing models that incorporate both convective and diffusive transport mechanisms. Single transport process based models cannot predict the wide range of behavior exhibited in these figures, nor can they explain the difference in the obser-

variations of Nazaroff (1, 2) for radon intrusion, and those of Hodgson et al. (3) for vapor transport of contaminant vapors from a landfill. The sample calculations also illustrate that the soil type can have a significant impact on the indoor vapor concentration, since Q_{soil} will be dependent on the soil permeability, and the effective porous media diffusion coefficient is sensitive to changes in soil porosity and moisture content. Being an analytical solution, eq 21 is easily used to study the sensitivity of model predictions over a range of reasonable soil and building characteristics. The major limitation to practical applications of the model is the lack of site-specific η values. It is not likely that such values can be easily measured; however, one can use the model to examine predictions for a realistic range of such values in order to determine the effect of this parameter at any given site. Clearly, predictions are insensitive to η in the limit of "permeable" soils and large source-foundation separations. A realistic range for η can be proposed by considering physical realizations corresponding to specific values of η . For example, $\eta = 0.01$ corresponds to a 1-cm-wide crack running the length of basement floor/walls every 100 cm.

It should be noted that Figures 2-5 contain model predictions for specific soil characteristics and building dimensions and are presented for illustrative purposes. The results should not be extrapolated to other sites not corresponding to the chosen parameters.

Extension of Theory to Relatively Permeable Foundation Walls

In the work of Garbesi and Sextro (8) it is assumed that vapor intrusion occurs through permeable below-grade walls, rather than through foundation cracks and openings. On the basis of this assumption, one can follow the approach used to derive eq 21 to obtain the following equivalent expression:

$$\alpha = \left[\left[\frac{D_T^{\text{eff}} A_B}{Q_{\text{building}} L_T} \right] \exp \left(\frac{Q_{\text{soil}} L_F}{D^F A_B} \right) \right] / \left[\exp \left(\frac{Q_{\text{soil}} L_F}{D^F A_B} \right) + \left[\frac{D_T^{\text{eff}} A_B}{Q_{\text{building}} L_T} \right] + \left[\frac{D_T^{\text{eff}} A_B}{Q_{\text{soil}} L_T} \right] \left[\exp \left(\frac{Q_{\text{soil}} L_F}{D^F A_B} \right) - 1 \right] \right] \quad (26)$$

which is similar to eq 21, except A_{crack} is replaced by A_B , D^{crack} is replaced by D^F , the effective diffusion coefficient through the porous foundation floor and walls, and L_{crack} is replaced by the foundation/wall thickness L_F . Equations 4-7 and 12 should be used to calculate D^F . While eqs 26 and 21 appear similar, they can predict quite different results. Equation 26 is independent of the area of cracks/openings because intrusion is assumed to occur uniformly over the floor/wall area. For a given Q_{soil} , therefore, the soil gas velocity through the floor/walls is lower for the permeable floor/wall case. The impact of this is that eq 26 may predict that transport through the foundation is diffusion dominated, while eq 21 predicts that it is convection dominated, for a given Q_{soil} and $D^{\text{crack}} = D^F$.

Extension of the Theory to Transient Problems

Equation 21 provides a screening estimate of indoor vapor concentrations, but does not account for depletion of the contaminant vapor source. This assumption is reasonable when short-term exposures are being estimated and does provide a conservative (upper bound) estimate for long-term exposures. There are situations, however, when more realistic long-term exposure estimates are de-

sired and it is unlikely that the source will remain constant for a long period of time (usually ~ 70 years for most exposure estimates). Many processes can contribute to an unsteady source, including the depletion due to transport away from the source, biodegradation, and chemical reaction. Of the three processes, the depletion due to transport is most often modeled, due to the current uncertain quantification of the other two. A first-order estimate of whether or not significant changes will occur over a given time period τ is obtained by calculating the mass of contaminant emitted from the source over that time period (τE) and comparing it with the initial residual contaminant mass in the soil directly below the building ($\rho_b C_R \Delta H_c A_B$):

$$\tau E \stackrel{?}{=} \rho_b C_R \Delta H_c A_B \quad (27)$$

where C_R and ΔH_c denote the average residual contaminant level in the soil (g/g of soil) and the thickness of the vertical interval (cm) over which the contaminant is distributed, respectively, and E is given by eq 16. If the left-hand side of eq 27 is greater than the initial mass of contaminant right-hand side, then it is possible that the contaminant lying beneath (or adjacent to) the building will eventually volatilize and enter the building. The validity of this assumption will depend on site characteristics.

The simplest extension of the model is derived by invoking the quasi-steady-state assumption used by Thibodeaux and Hwang (15) for single-component contaminants or mixtures of compounds having similar vapor pressures and molecular weights. In this approach it is recognized that the source-building separation increases with time due to depletion; however, it is assumed that the rate at which a steady-state vapor concentration profile is established is much greater than the rate at which depletion occurs. At any time, therefore, the emission rate is given by eq 16 with L_T replaced by the source-building separation at that time. Implicit in this approach is the assumption that depletion occurs first from the layers of contaminant closest to the building floor and walls, and a hypothetical "depletion zone" grows with time. In a sense, the mass of contaminant incorporated in the soil "dries up", beginning at the edge closest to the building. This is a reasonable assumption for diffusion-dominated transport to the building-soil interface, but not valid for convection-dominated transport from contaminated soil adjacent to a building floor. With this limitation in mind, eq 16 combined with a mass balance provides a mathematical expression of the quasi-steady-state assumption:

$$\rho_b C_R A_B \frac{d\delta}{dt} = \left[\frac{D_T^{\text{eff}} A_B C_{\text{source}}}{(L_T^0 + \delta)} \right] \left[\exp \left(\frac{Q_{\text{soil}} L_{\text{crack}}}{D^{\text{crack}} A_{\text{crack}}} \right) - \left[\frac{C_{\text{building}}}{C_{\text{source}}} \right] \right] / \left[\left[\frac{D_T^{\text{eff}} A_B}{Q_{\text{soil}} (L_T^0 + \delta)} \right] \times \left[\exp \left(\frac{Q_{\text{soil}} L_{\text{crack}}}{D^{\text{crack}} A_{\text{crack}}} \right) - 1 \right] + \exp \left(\frac{Q_{\text{soil}} L_{\text{crack}}}{D^{\text{crack}} C_{\text{crack}}} \right) \right] \quad (28)$$

where δ , t , and L_T^0 denote the "depletion zone" thickness ($\delta = 0$ at $t = 0$) (cm), time (s), and initial contaminant-building floor separation (cm), respectively. Equation 28 can be rearranged and rewritten in the form

$$d\delta^*/dt = \psi/(\beta + \delta^*) \quad (29)$$

where

$$\delta^* = \delta/L_T^0 \quad (30)$$

$$\psi = D_T^{\text{eff}} C_{\text{source}} / (L_T^0)^2 \rho_b C_R \quad (31)$$

$$\beta = \left(\frac{D_T^{\text{eff}} A_B}{L_T^0 Q_{\text{soil}}} \right) \left[1 - \exp \left(- \frac{Q_{\text{soil}} L_{\text{crack}}}{D_{\text{crack}} A_{\text{crack}}} \right) \right] + 1 \quad (32)$$

In this analysis it is assumed that the residual contaminant level in soil C_R is uniform, D^{eff} is constant as δ increases, and the ratio $C_{\text{building}}/C_{\text{source}} \ll 1$. Equation 29 can be solved to obtain

$$\delta^* = -\beta + \sqrt{\beta^2 + 2\psi t} \quad (33)$$

The time τ_D required to deplete a contaminated zone of thickness ΔH_c can be obtained from eq 33, by setting $\delta^* = \Delta H_c / L_T^0$

$$\tau_D = \frac{[\Delta H_c / L_T^0 + \beta]^2 - \beta^2}{2\psi} \quad (34)$$

Equation 34 predicts that τ_D increases with increasing L_T^0 and C_R ; increasing L_T^0 decreases the initial diffusive driving force, while increasing C_R increases the contaminant capacity of the contaminated soil zone. If $\tau \geq \tau_D$, the average emission rate into the basement (E) over the time period τ_D is obtained by a simple mass balance:

$$\langle E \rangle = \rho_b C_R \Delta H_c A_B / \tau \quad (35)$$

For time periods $\leq \tau_D$, the average emission rate is given by

$$\langle E \rangle = \frac{\rho_b C_R \Delta H_c A_B}{\tau} \left(\frac{L_T^0}{\Delta H_c} \right) [(\beta^2 + 2\psi\tau)^{1/2} - \beta] \quad (36)$$

which can be derived by substituting eq 33 for δ^* (δ/L_T^0) into the right-hand side of eq 28 and then averaging the resulting expression over the time period τ . As expected, eq 36 predicts a decrease in $\langle E \rangle$ with increasing τ . The corresponding long-term average attenuation coefficient (α) is then

$$\langle \alpha \rangle = \frac{\rho_b C_R \Delta H_c A_B}{Q_{\text{building}} C_{\text{source}} \tau} \left(\frac{L_T^0}{\Delta H_c} \right) [(\beta^2 + 2\psi\tau)^{1/2} - \beta] \quad (37)$$

While eqs 28–37 form a more sophisticated model than eq 21, one must be aware that increasing the level of sophistication usually increases the amount of site-specific information required. More sophisticated screening models are usually also based on additional assumptions, and one must be careful to ensure that these assumptions are valid for specific site characteristics.

Vapor Equilibrium Models

The models presented above require an estimate of the source vapor concentration, C_{source} . Two main approaches are used in vapor transport modeling; in the first C_{source} is assumed to be proportional to the residual level in the soil, and in the second C_{source} is independent of the residual level, but is a function of composition. The former is applicable in the limit of "low" residual levels where compounds are sorbed to the soil, dissolved in the soil moisture, and present in the vapor space; the latter is applicable for "high" residual levels where free-phase liquid or precipitate is trapped in the soil interstices. A more detailed description of this topic can be found in Johnson et al. (12), and it is not appropriate to repeat the discussion here. It is important to note, however, that if one chooses an incorrect model for predicting C_{source} , then it is possible to

over- or underpredict the actual C_{source} value by orders of magnitude.

Conclusions

We have derived and illustrated the use of a heuristic model of the intrusion rate of subsurface contaminant vapors into buildings through basement, or foundation, floors and walls. The model provides an exposure assessment screening-level tool; it can be used to identify sites, or contaminant levels, where contaminant exposures through a vapor inhalation pathway may cause adverse health effects. It can also be used to help identify sites where more detailed numerical simulation, or field sampling, is appropriate. The model was used to make predictions of basement vapor concentrations over a range of realistic parameters. It is clear from the wide range of results that field data will only be correlated by models such as this that incorporate both convective and diffusive transport mechanisms.

Currently, there are few reported experimental studies that are sufficiently detailed to compare with model predictions. However, the range of behavior, dependence on relevant parameters, and limiting bounds of the model are in qualitative agreement with published case histories. At this point, more detailed field studies and numerical simulations are needed to help validate this screening-level model.

Acknowledgments

We thank James D. Colthart for his thoughtful review and contributions to the presentation and technical content of this article.

Registry No. Radon, 10043-92-2.

Literature Cited

- (1) Nazaroff, W. W.; Feustel, H.; Nero, A. V.; Revzan, K. L.; Grimsrud, D. T.; Essling, M. A.; Toohey, R. E. *Atmos. Environ.* **1985**, *19*, 31–46.
- (2) Nazaroff, W. W.; Lewis, S. R.; Doyle, S. M.; Moed, B. A.; Nero, A. V. *Environ. Sci. Technol.* **1987**, *21*, 459–466.
- (3) Hodgson, A. T.; Garbesi, K.; Sextro, R. G.; Daisy, J. M. Presented at 81st Annual Meeting of APCA, June 19–24, 1988, Dallas, TX, 88-95B.1.
- (4) Arnold, L. J. Ph.D. Dissertation, Rutgers, The State University of New Jersey, 1988.
- (5) Landman, K. A. *Health Phys.* **1982**, *43*, 65–71.
- (6) Landman, K. A.; Cohen, D. S. *Health Phys.* **1987**, *44*, 249–257.
- (7) Zapalac, G. H. *Health Phys.* **1982**, *43*, 65–71.
- (8) Garbesi, K.; Sextro, R. G. *Environ. Sci. Technol.* **1989**, *23*, 1481–1487.
- (9) Loureiro, C. O.; Abriola, L. M.; Martin, J. E.; Sextro, R. G. *Environ. Sci. Technol.* **1990**, *24*, 1338–1348.
- (10) Nazaroff, W. W. *Radiat. Prot. Dosim.* **1988**, *24*, 199–202.
- (11) Nazaroff, W. W.; Sextro, R. G. *Environ. Sci. Technol.* **1989**, *23*, 451–457.
- (12) Johnson, P. C.; Hertz, M. B.; Byers, D. L. In *Petroleum Contaminated Soils*; Kosteki, P. T., Calabrese, E. J., Eds.; Lewis Publishers: Chelsea, MI, 1990; Vol. III, pp 295–326.
- (13) Bruell, C. J.; Hoag, G. E. In Proceedings of the NWWA/API Conference on Petroleum Hydrocarbons and Organic Chemicals in Groundwater: Prevention, Detection, and Restoration, November 12–14, 1986, Houston, TX.
- (14) Lyman, W. J.; Reehl, W. F.; Rosenblatt, D. H. *Handbook of Chemical Property Estimation Methods*; McGraw-Hill: New York, 1982.
- (15) Thibodeaux, L. J.; Hwang, S. T. *Environ. Prog.* **1982**, *1*, 42–46.

Received for review August 14, 1990. Revised manuscript received February 21, 1991. Accepted April 1, 1991.

Biodepuration of Polynuclear Aromatic Hydrocarbons from a Bivalve Mollusc, *Mercenaria mercenaria* L.

John T. Tanacredi^{*†} and Raul R. Cardenas^{‡§}

National Park Service, Gateway NRA, Division Natural Resources, Brooklyn, New York 11234, and Environmental Health Science Program, Department of Civil and Environmental Engineering, Polytechnic University, Brooklyn, New York 11201

■ *Mercenaria mercenaria*, exposed in vitro for 48 h to nine parent polynuclear aromatic hydrocarbons (PAHs) found in waste crankcase oil (WCCO) and analyzed by multi-parametric analysis over a 45-day depuration period in an activated carbon filtration aquaria system, did not depurate PAHs, but rather maintained them at detectable levels. Uptake of PAHs was shown to be directly related to clam weight. A cluster analysis of empirical results reaffirmed a biostabilization in PAH groupings in clam tissue over a 45-day depuration period and exhibited no evidence of a decreasing trend in total PAHs when subjected to ANOVA. Due to the commercial importance of hard-shell clams, the practices of clam depuration and clam relaying are reviewed in light of potential long-term public health exposures to low-level xenobiotics and the implications for human consumers.

Introduction

Oil pollution of our coastlines and estuaries continues to be a chronic global environmental problem. A considerable quantity of the petroleum hydrocarbons, estimated at 0.86 million metric tons annually (1) entering the marine environment from the land via storm and sanitary sewers and urban and river runoff, can be attributed to waste crankcase oil (WCCO) (2, 3). Polynuclear aromatic hydrocarbons (PAHs) are found in WCCO (4, 5). Impacts from waste petroleum hydrocarbons may be considerable when one takes account of the fact that the estuaries and coastal seas receiving these wastes, despite comprising only 10% of the total global marine environment, support approximately 99% of the total world fish population and shellfish production (6). WCCO contains heavy metals and volatile organics, as well as a variety of PAHs formed by the high-temperature combustion in automobile engines (7). PAHs are a class of compounds that are toxic, carcinogenic, and mutagenic. Table I shows the distribution of 10 common PAHs found in WCCO as well as other media. The presence of PAHs in the natural environment is a global phenomenon (8) with absolute concentrations being highest for samples taken in the vicinity of human activity and lowest for samples taken from more primitive environments. Mueller et al. (9) noted that urban runoff, which contains a considerable quantity of WCCO, is responsible for a substantial portion of the petroleum-related hydrocarbons entering the marine environment of New York.

The availability of petroleum-related pollution from PAHs to commercially important marine organisms is of major concern to many coastal ecologists (10). Chronic petroleum pollution of commercial shellfish species has been suggested to be so widespread that carcinogen contamination of seafoods may occur not only in obviously polluted waters, but also in waters deemed suitable for commercial seafood production (11).

The shellfish industry in New York has been adversely affected in recent years by a host of anthropogenic pollutants as well as the overharvesting of available shellfish stocks. Because of the possibility of contamination by a variety of pollutant sources, the clamming industry has developed several practices to aid in the rejuvenation of shellfish harvesting. One practice, called "relaying", involves the removal of clams from "contaminated" natural waters and placement of these organisms in "certified" natural waters to allow depuration, or self-cleansing of bacteria, and then commercial harvesting of the transplanted clams for human consumption. Bacteriological standards for the human consumption of shellfish are assumed to have been met by clams depurated in certified waters (waters that meet coliform test standards and water temperatures of 50 °F or better) for 21 days. However, PAHs, such as those in WCCO, react similarly to other lipophilic compounds and accumulate in biological tissue. Moreover, PAHs may not be subject to the normal metabolic processes exhibited by filter-feeding bivalves. Thus, the potential persistence of compounds such as PAHs beyond a 21-day bacteriological depuration period is highly probable (12).

It is also possible that shellfish and other organisms taken from areas with a history of oil contamination have levels of compounds that, in turn, "bioactivate" other complex compounds found in WCCO into mutagens and carcinogens (13). Neither the mechanism nor the quantitation of partitioning of PAHs between aqueous media and various types of lipid tissue has been fully explored, and the long-term public health risks of ingestion of seafood containing subtoxic levels of chronically contributed xenobiotic contaminants such as PAHs is lacking (14). Since seafood is a major source of global food, the impact of bioavailable, bioconcentratable, petroleum-related compounds such as PAHs to human health was a major concern of this investigation. In an effort to investigate the ability of naturally occurring bivalves to cleanse themselves after exposure to a variety of PAHs (all found in WCCO), a laboratory experiment utilizing the bivalve mollusc *Mercenaria mercenaria* was designed.

Experimental Section

Nine parent PAHs frequently exhibited in WCCO, yet only a small part of the host of PAHs found in any petroleum product (4, 32) was of interest in this study: naphthalene, biphenyl, fluorene, phenanthrene, fluoranthene, pyrene, chrysene, benzo[a]pyrene, and benz[a]anthracene. In order to establish the aqueous stability of the nine PAHs, a UV-fluorescence spectroscopy synchronous excitation technique (15, 16) was used to pre-screen total PAHs added to a control synthetic seawater aquarium tank (no clams) over 45 days.

Laboratory exposure of bivalve molluscs (*Mercenaria mercenaria* L.) to the nine reference PAHs was carried out in three additional 20-gall (75.7-L) glass aquarium tanks each with 20 clams. A 1.147 ppm PAH standard acetone solution (Supelco Co., Inc.) in seawater (Instant Ocean Aquarium Systems, Inc., Eastlake, OH) was added to each

[†] National Park Service.

[‡] Polytechnic University.

[§] Present address: Carpenter Environmental Associates, Inc., 70 Hilltop Road, Ramsey, NJ 07446.

Table I. Mean Percentage Distribution of Waste Crankcase Oil PAH Characterizations^a

PAH	Peake and Parker (4) WCCO	Hoffman et al. (32)				Tanacredi ^b WCCO
		urban runoff	atmos fallout	STP ^c	sediment	
naphthalene	ND	1.3	0.7	32.0	0.5	45.2
biphenyl	ND	0.8	0.5	1.7	0.4	4.4
fluorene	6.0	2.7	2.9	2.4	1.2	4.4
phenanthrene	32.1	10.0	15.7	4.7	7.1	13.8
fluoranthene	17.9	25.2	33.5	3.0	17.9	4.5
pyrene	27.5	12.6	10.3	2.9	18.3	ND
benz[a]anthracene	3.6	11.6	8.7	0.2	7.4	4.7
chrysene	10.2	15.8	3.4	0.7	13.2	21.4
benzo[a]pyrene	1.4	4.8	3.0	0.2	17.3	1.5
anthracene	1.3	NT	NT	NT	NT	NT

^aND, none detected. NT, not tested. ^bWCCO from oil change in 1978 Ford with 107 200 miles and a previous oil change after 4023 miles. 10W/40 SAE oil analyzed by HPLC for this investigation. ^cSTP, sewage treatment plant.

Table II. Summary of HPLC Findings. PAHs Extracted and Distributed in *M. mercenaria* from Exposure Tanks

	Tank 2 (Postexposure Sample Taken)						total
	2 h	10 h	2 day	14 day	30 day	45 day	
Naph	101.0	22.0	55.0	29.0	21.0	0.0	228.0
Bi	51.3	34.8	79.2	54.1	64.0	73.3	356.7
Fl	61.2	20.7	32.7	47.3	48.1	65.2	275.2
Phen	1040.0	94.7	169.0	390.0	633.0	392.0	2718.7
Flor	1320.0	241.0	199.0	376.0	663.0	335.0	3134.0
Pyr	470.0	131.0	61.9	205.0	201.0	203.0	1271.9
BaA	25.9	18.8	25.5	27.3	33.5	13.4	144.4
Chr	166.0	78.3	26.5	61.3	48.4	100.0	480.5
BaP	260.0	72.2	46.6	97.8	99.4	67.8	643.8
PAH totals	3495.4	713.5	695.4	1287.8	1811.4	1249.7	9253.2

	Tank 3 (Postexposure Sample Taken)						total
	2 h	2 day	7 day	14 day	30 day	45 day	
Naph	0.0	ND	57.0	117.0	52.0	48.0	274.0
Bi	84.1	87.2	114.0	72.0	45.5	68.5	471.3
Fl	39.3	68.1	62.2	42.4	34.3	45.2	291.5
Phen	161.0	548.0	766.0	316.0	221.0	415.0	2427.0
Flor	265.0	521.0	757.0	239.0	511.0	730.0	3023.0
Pyr	201.0	300.0	ND ^b	128.0	126.0	243.0	998.0
BaA	20.9	25.5	4.7	16.8	19.8	19.0	106.7
Chr	31.6	255.0	13.9	81.7	222.0	15.7	619.9
BaP	52.3	147.0	52.8	127.0	43.5	211.0	633.6
PAH totals	855.2	1951.8	1827.6	1139.9	1275.1	1795.4	8845.0

	Tank 4 (Postexposure Sample Taken)						total
	2 h	10 h	2 day	7 day	14 day	30 day	
Naph	114.0	95.3	ND	438.0	0.0	119.0	766.3
Bi	63.0	48.7	76.9	285.0	65.6	48.0	587.2
Fl	58.0	39.8	32.3	89.8	75.1	51.0	346.0
Phen	368.0	892.0	193.0	442.0	612.0	300.0	2807.0
Flor	195.0	1010.0	364.0	423.0	779.0	1450.0	4221.0
Pyr	113.0	223.0	104.0	28.2	359.0	97.2	924.4
BaA	33.0	43.0	20.5	15.8	33.3	9.7	155.3
Chr	877.0	163.0	93.8	9.9	204.0	90.5	1438.2
BaP	131.0	368.0	313.0	48.6	250.0	67.5	1178.1
PAH totals	1952.0	2882.8	1197.5	1780.3	2378.0	2232.9	12423.5

^aAll values in nanograms per gram of wet tissue weight. ^bND, not detected.

tank. Filter systems were operated initially without any carbon for 48 h in order to afford maximum uptake and exposure of PAHs to clams. "Mother-stock" clams were maintained in separate tanks from which the experimental exposure clams were randomly selected. Because the stage in the life cycle of organisms at the time of analysis may influence hydrocarbon distribution, all clams were 7–8 years old, or in the commercial "cherry-stone" age group, though this age differentiation can be variable from estuary to estuary. The mean wet weight (MWW) for exposure clams was 32.9 ± 5.14 g. All tanks were maintained in the

dark and kept at constant temperature (21.5 ± 1 °C), pH (8.2), and salinity (‰) (27 ppt). All parameters were monitored every other day.

Two clams, selected randomly from each tank, were established as "background organism" samples, shucked, and extracted. The remaining clams were left in the exposure tanks for the 48-h PAH exposure time. Carbon filters were added to the filter pumps only after the 48-h exposure period. Two clams were sequentially, yet randomly, removed for HPLC analysis (Table II). Each two-clam sample from each of the three exposure tanks

represented the pooled clam sample for that particular sample "depuration" time. Water samples of exposure tanks were periodically analyzed for quality assurance/quality control (QA/QC) purposes by GC-MS after carbon filtration and during the clam depuration period.

All exposure aquaria had Instant Ocean seawater previously recirculated continuously for 60 days through activated charcoal, 250 L/h pump rate, Eheim filtration pump systems (Eheim Filter Co., Inc.) prior to clam exposure experiments. All water samples were extracted with methylene chloride in separatory funnels. All organism samples were Soxhlet extracted for 8 h in research grade hexane. (Fisher Scientific, Inc.)

The sample extracts were rotary evaporated to 35 mL. In order to reduce a variety of interferences, sample extracts were applied to a chromatographic column (1% water-deactivated silica/alumina gel) and the benzene-methanol elutriate was collected for analysis. All extracts were concentrated to 1–2 mL and subjected to either HPLC (clams) or GC-FID/GC-MS (water, activated-carbon extracts) analysis. Clam specimens were rinsed several times in distilled water, blotted dry, and weighed for total wet tissue weight (TWTW). Original clam tissue was stored in a freezer at -10°C . Extraction for analysis started within 48–52 h of removal from exposure tanks. Three times the TWTW of anhydrous sodium sulfate was added to each two-clam sample. The sample was blended and ground for 2 min at high speed. Tissue homogenates were placed in hexane-prewashed Soxhlet thimbles and Soxhlet extracted for 8 h at approximately 20 cycles/h.

Water and periodic control clam samples were analyzed by gas chromatography on a Perkin-Elmer Sigma 3 and a Hewlett-Packard 5880A gas chromatograph, both equipped with capillary glass columns and flame ionization detectors (FID). The columns were 0.25 mm \times 30 m DB-1 glass capillaries attached to a spitless injector. Temperature programming was initiated at 80°C (held for 2 min), and programmed temperature increases of $4^{\circ}\text{C}/\text{min}$ were maintained to a final temperature of 310°C and held for 12 min isothermal. Injector port temperature was 260°C and detector temperature was 310°C . All peak resolution and identification were accomplished by comparison of retention times for eluted compounds to retention times of eluted internal standard PAHs.

The GC-MS analysis conducted on water and on invertebrate food extracts was done by using a computerized Perkin-Elmer GC-MS equipped with a 6 ft \times 0.1 in. i.d. glass capillary column packed with 1% SP-1000 on Carbowax B (60/80 mesh). The GC-MS was capable of scanning from 20 to 260 amu every 7 s, utilizing 70-V electron energy in the electron impact ionization mode.

HPLC analyzes of exposure clam extracts were conducted on a Hewlett-Packard 1084B HPLC (U.S. EPA ID 167831), with a 25 cm \times 4.6 mm i.d. Vydac 201TP column. A calibration range for the HPLC-UV detector system was prepared and analyzed by using Supelco PAH mixture 610M. The solvent and oven temperatures were 30°C . The gradient used was 50% acetonitrile and 50% water for the first 2 min, then increased to 100% acetonitrile by 15 min, and held there for 5 min. The UV-fluorescence detector was set at 254 nm, the instrument flow rate was 1.50 mL/min, and a 25- μL injection size was used on each sample run. When chromatograms posed matrix interferences, direct quantification of the analyses was made impossible by either area estimation or by peak height measurements. Under these circumstances the sample was diluted by one-fourth and analyzed by a method of standard additions. The linearity of the range was eval-

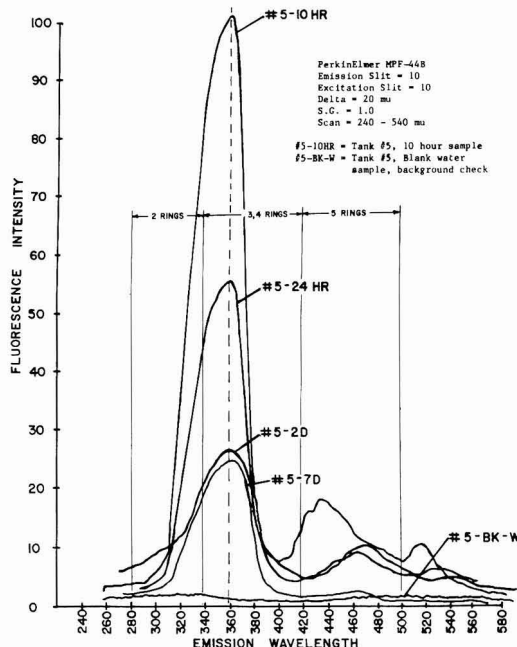


Figure 1. Synchronous fluorescence excitation emission spectra for control tank 5 water samples.

uated for each compound by comparing the center standard to the upper and lower standards and calculating the percent relative error. The relative percent error for each parameter was consistently less than 15% for all compounds and was considered acceptable.

A synchronous excitation (SE) fluorescence spectroscopic method was used, which was previously described by Frank (17) and Frank and Gruenfeld (18). All UV-fluorescence analyses were conducted on a Perkin-Elmer MPF-3 UV-fluorescence spectrophotometer with two independent monochromators, a 150-W xenon arc light source, and 10-mm path length. Synchronous excitation of the individual water sample was accomplished by exciting it at 20-nm wavelength intervals between 240 and 480 nm. The excitation wavelength was maintained 20 nm less than the emission wavelength during the synchronous scan.

Results

The control tank (T5) contained PAH-contaminated water, no clams, and no carbon filtration system. Results of UV-fluorescence analysis (Figure 1) were corroborated by GC/GC-MS quantification of the nine PAH standard concentration of 1.147 ppm added initially to the control tank T5 water. This was done to establish total PAH concentration stability over a 45-day clam depuration period as a control reference for bioavailability to clams in exposure tanks (T2, T3, T4). The total PAH concentrations retained in nanograms per gram of wet tissue weight and detected by HPLC in organisms over the 45-day depuration period are shown in Figure 2. For each interval there were three replicates, each composed of two clams, providing for six clams per depuration time sample. Measured concentrations from each two-clam sample were then averaged for further analysis, yielding 18 sample data points for each PAH (Table II and Figure 2).

The means and standard deviations (probable error) for the averaged PAH values ($N = 18$) exhibited a diverse

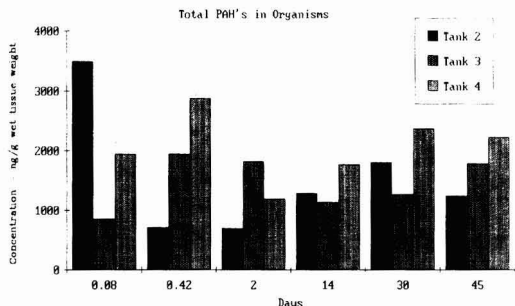


Figure 2. Days of depuration in activated-carbon-filtered aquaria.

pattern of standard deviation values, prompting some concern regarding the stability of statistical results for individual PAHs. Furthermore, it was strongly suspected that the results from some PAHs were significantly correlated, possibly due to the similarity in chemical structure. Specifically, the mean values of each compound in Figure 3 exhibited a general clustering of compounds across depuration times samples, and Figure 4 shows this clustering is consistently observable within each exposure tank. Nevertheless, it was also clear that both inter- and intratank variability exists in measured concentrations. Though tanks 2–4 were exposure tank replicates, intratank clam extracts exhibited a variance between amounts of each PAH individually retained (Figure 4). Further work on the specific mechanism driving the depuration kinetics of PAHs in clam tissue is clearly required.

To address the above concerns, a hierarchical cluster analysis was performed on the known PAHs. Basically, this type of analysis classifies PAHs with similar patterns and levels of nanogram per gram concentrations across the eight sequential time samples (2 h to 45 days). Technically, the objective measure of similarity used is the cosine of the angle between two octuple vectors representing the nanogram per gram levels per time sample for two compounds. PAH pairs with smaller angles (i.e., cosines near 1.0) are considered to be more similar. Note that this is an empirical, rather than analytical, grouping process and may not replicate for other types of organisms. The cluster analysis method is then used on a 9×9 similarity matrix to construct groups with high internal similarities of PAHs and low external similarities to PAHs in other groups.

When this similarity matrix, given in Table III, was analyzed with the unweighted pair group average (UPGMA) method (19, 20), three groups emerged between a rescaled distance 10 and 15 of the dendrograms in Table III (Phen + Flor + Pyr + BaP + BaA), (Naph + Bi + Fl), and (Chr). This grouping is somewhat parallel to a logical grouping based on molecular weight, solubility, and ring structure. In particular, group I compounds (Naph + Bi + Fl) have the highest solubilities, lowest molecular weights, and two-ring structures; group II compounds (Phen + Flor + Pyr) have intermediate values for solubility and molecular weight, and three- or four-ring structures; finally, group III compounds (BaA + Chr + BaP) have the lowest solubilities, the highest weights and four- or five-ring structures. Given this parallel to the empirical results, and the small sample size, the logical grouping probably makes more sense. Therefore, results were pooled within these groups for the following analyses.

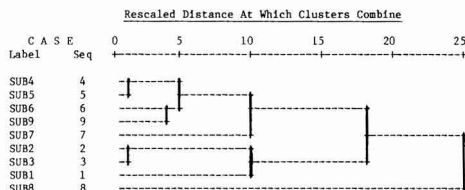
In Figure 5, a graphic representation is given of depuration rates in the three PAH logical clusters. The locally weighted regression technique is used to smooth the actual data points to enhance interpretability of the trend. An

Table III. Hierarchical Cluster Analysis Summary of All Results

A. Cosine Similarity Coefficient Matrix

Variable	SUB1	SUB2	SUB3	SUB4	SUB5	SUB6	SUB7	SUB8
SUB2	.8496							
SUB3	.6775	.8974						
SUB4	.5467	.7250	.8976					
SUB5	.5258	.6471	.8398	.9044				
SUB6	.3371	.5811	.8305	.8709	.82			
SUB7	.5004	.5905	.7748	.7172	.88	.7091		
SUB8	.4102	.4558	.6274	.5430	.45	.5355	.5513	
SUB9	.3947	.5873	.7634	.8490	.80	.8515	.6990	.5466

B. Dendrogram



C. Cluster Membership of Cases Using Average Linkage (UPGMA)

Label	Case	Number of Clusters						
		8	7	6	5	4	3	2
SUB1	1	1	1	1	1	1	1	1
SUB2	2	2	2	2	2	1	1	1
SUB3	3	3	2	2	2	1	1	1
SUB4	4	4	3	3	3	2	2	1
SUB5	5	4	3	3	3	2	2	1
SUB6	6	5	4	4	3	2	2	1
SUB7	7	6	5	5	4	3	2	1
SUB8	8	7	6	6	5	4	3	2
SUB9	9	8	7	4	3	2	2	1

examination of the smoothed data trends reveals no evidence of a decrease in total PAHs from clam tissue. Group II shows the highest overall readings although there is a slight dip in the trend at intervals 2 and 4. Group III shows some downward trend, but levels off at interval 4. Group I readings are uniformly low throughout the time sample sequence. It is important to note that the total sample is dominated by Group II (Phen + Flor + Pyr) since this group accounts for the majority of the detected PAHs (Figure 3).

A statistical analysis was also performed to test the null hypothesis that the nanogram per gram concentration maintained a uniform value across time intervals (i.e., $H^0: \mu_1 = \mu_2 = \dots = \mu_8$). The null hypothesis was rejected only for biphenyl at $\alpha = .05$. This result was probably due to an unusually high reading for the 7-day sampling, which was 100% higher than the next largest reading. Thus, the ANOVA results show no evidence of a downward trend across the eight time intervals, which corresponds to the graphical results in Figure 5. However, average PAH concentrations for every PAH did test as significantly different from 0. These findings strongly suggest that PAHs (1) do accumulate in clam tissues and (2) do not depurate significantly within a period of 45 days. Thus, the nine PAHs at the detectable bioavailability values were sequestered and appear to have been stabilized in clam tissue over the entire 45-day depuration period. Detectable levels of all nine reference PAHs were recovered in clam tissues after the full 45-day period. Clams in all exposure tanks were observed with extended siphons so that normal pumping or filtering activity by the clam species continued after exposure.

Discussion

The majority of previous investigations have shown that marine organisms are able to release petroleum hydrocarbons from their tissues rapidly when they were returned to petroleum-free environments, (21, 22). Boehm and

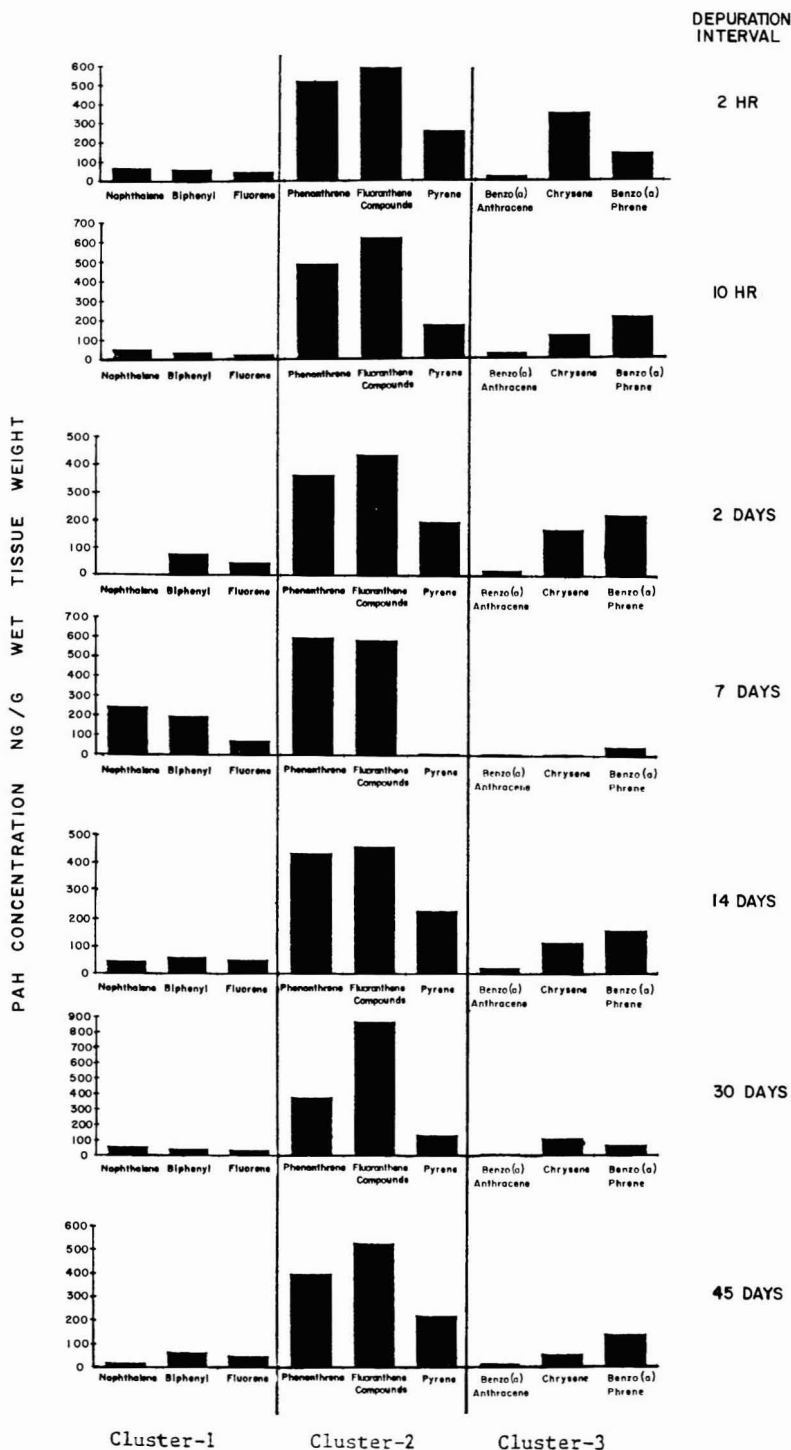


Figure 3. Mean PAH values per compound per time. Clusters I-III are, respectively, groups I-III.

Quinn (23), however, have reported that *M. mercenaria* *L.* chronically exposed to petroleum hydrocarbons accumulated them to high levels in their tissues and failed to release them when returned to clean seawater over a 120-day depuration period. They suggested that hydro-

carbons released from molluscs exposed to xenobiotics for long periods of time would be extremely slow due to (1) an accumulation of hydrocarbons in a more stable tissue compartment (e.g., lipids) and (2) the organisms being in a positive nutritional balance. In this investigation, clams

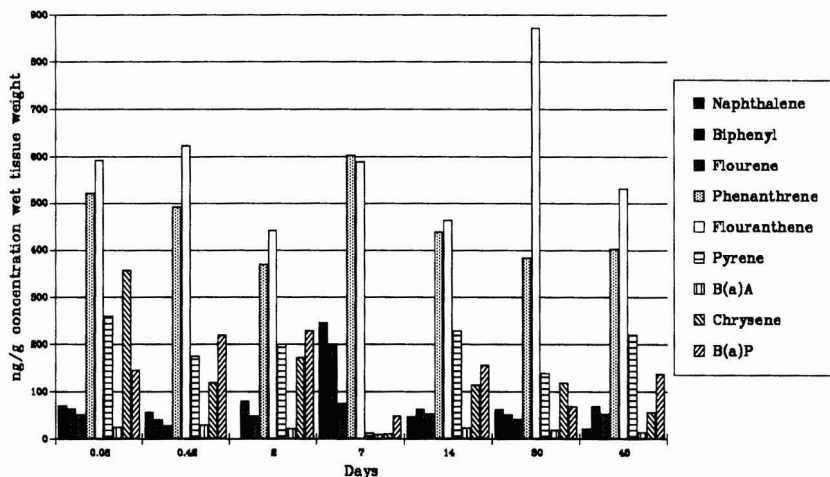


Figure 4. Mean values of organism exposure in tanks 2-4.

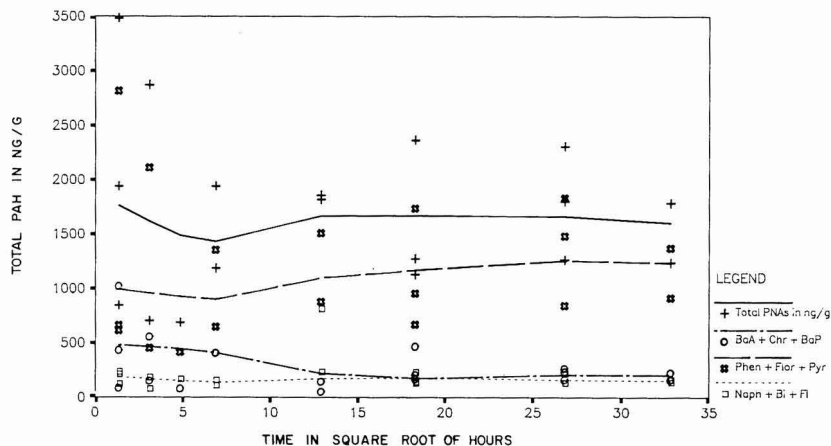


Figure 5. PAHs in clam tissue over time by use of locally weighted regression for smoothing.

exposed to the nine PAHs, mostly found in WCCO and associated with urban-influenced estuarine ecosystems, were not supplementally fed over the depuration period and yet the accumulated PAHs were still not depurated. The nine PAHs were immediately sequestered (i.e., within 48 h) and remained at relatively constant concentrations. Elimination of PAHs over the 45-day depuration period was not achieved. The results lend evidence to PAH maintenance being initiated in hard-shell clams over relatively short term periods. Unlike other marine taxa, this "sequestering" in molluscs may support the apparent inability of molluscs to metabolize PAHs to more water soluble and thus easily secreted polar metabolites. This increased "stabilization" and accumulation of parent PAHs is in agreement with Brown and Pancirov (24) and may, as they have suggested, show a long-term selective uptake of these specific aromatics. With PAH adsorptive ability and low water solubility, investigations have suggested that estuarine colloids contribute considerably to materials available for ingestion by filter-feeding bivalves (25).

These findings are also in agreement with those of Stein, Hom, and Varanasi (26), who showed that one PAH, BaP, reached steady-state concentrations in tissue by the first day of exposure in a fish (*Parophrys retulus*, English sole), known to be able to metabolize BaP. Food-web transfer

is a major concern in the commercial fishing industry, one that may be warranted in light of the results of this investigation.

The generalization noted by Fowler (27) that there is an initial rapid discharge of PAHs, followed by a much slower loss of those PAHs associated with a more stable compartment within the organism, appears to be borne out to some degree in this work, but not according to statistical analysis of data in Figure 5, for example. Clams in this research had been maintained in carbon-filtered clean waters for over 1 year prior to initial exposure to the nine PAHs for 48 h, so the clams cannot be considered to be "chronically exposed" to PAHs. In addition, chromatographic profile background control checks of nonexposed background clams did not reveal any of the nine parent PAHs. There was no evidence that clams contaminated with PAHs for 48 h were able to rapidly eliminate these compounds in 1-5 days as observed by Lee et al. (22).

There is little knowledge of the effects on humans from ingestion of petroleum hydrocarbons, especially PAHs at subtoxic levels. Though previous research has emphasized the effects of single PAHs, it is possible that parent PAH byproducts and substituted PAHs may play a more important role in the environment, with some organisms acting as reserves for these compounds (28). Dunn and

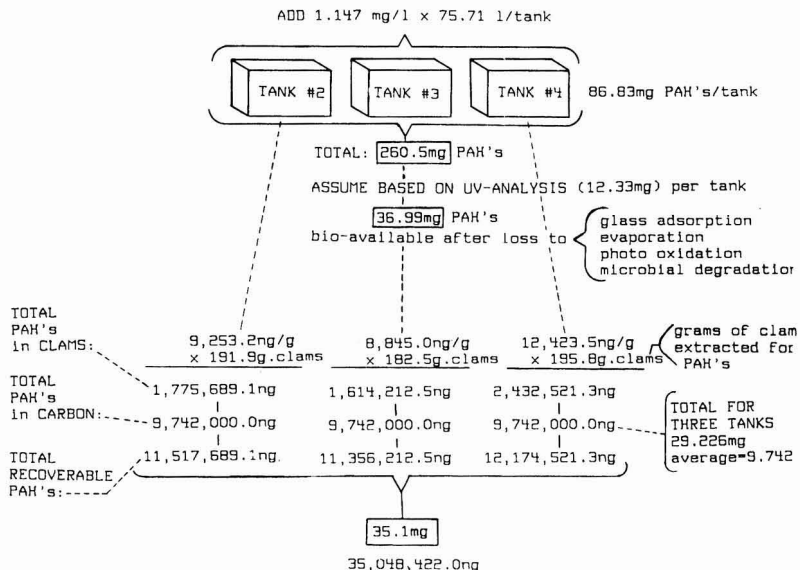


Figure 6. PAH bioavailability to clams in aquaria.

Fee (11) noted that commercial seafood contained low-level PAH contamination, and Pruel et al. (29) noted that there was a consistent level of PAH content in commercially sold *M. mercenaria* ranging from 1.5 to 17.0 ng/g based upon 100-g wet tissue weight for analysis. *Mercenaria* may very well be considered an "estuarine quality" indicator based upon its PAH levels. Values of PAHs after exposure, acute or chronic, are important if we are to attempt to establish a public health exposure threshold for PAHs in bivalves.

Depuration has been described by several investigators as being different for different hydrocarbons and different organisms. Neff and Anderson (28) demonstrated depuration of hydrocarbons from exposure to no. 2 fuel oil for 8 h although small quantities of substituted naphthalenes remained in oyster tissues 672 h (28 days) after exposure. Naphthalene and phenanthrene percent distribution values in WCCO were higher than any of the other seven PAHs (Table I). In the literature, however, they consistently provide low (naphthalene) and high (phenanthrene) values in clam tissue (29, 30). Lee et al. (22) noted that *Mytilus edulis* took up 20 µg of [¹⁴C]naphthalene and [³H]-3,4-benzo[a]pyrene from a seawater solution but after 24 h in fresh seawater had discharged 80% of these compounds. This investigation exhibited that 94% of the subsequently recoverable PAH initial concentrations were retained in the closed aquarium system; most previous work utilized a seawater flow-through system or a considerably less sophisticated exposure system (Figure 6). The PAHs in this investigation were either sequestered by siphoning organisms or adsorbed to glass or activated carbon filters (Figure 7).

Similar to work of Dunn and Stitch (31), BaP in this investigation was sequestered by *M. mercenaria* at a low concentration and biostabilized by not depurating over the 45-day depuration period. Phenanthrene and fluoranthene consistently exhibited higher values in clam extracts throughout the sampling period, and though this result has been expressed in sediment values of previous investigations (32, 33), its significance for bivalves is unclear. As noted by Hoffman et al. (32), urban street runoff PAHs (WCCO) are similar in composition to atmospheric fallout PAHs, but different from municipal effluent PAHs. Urban

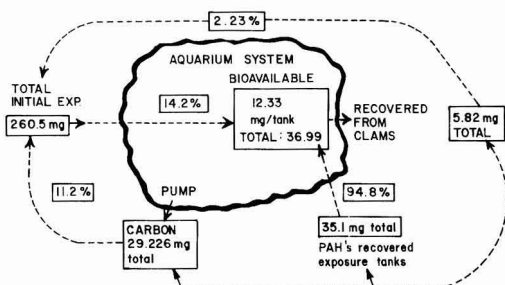


Figure 7. Summary of percentage distribution of PAHs in aquaria.

street runoff is a major source of high molecular weight PAHs to the estuary with a contribution of over 70% of the high molecular weight PAHs.

Jackim and Wilson (34) exposed *Mya arenaria* to ¹⁴C-labeled no. 2 fuel oil, and testing concentrations of six PAHs after 5 1/2 weeks concluded that depuration rates were appreciably slower after chronic exposure than after an acute exposure. These observations are not in agreement with the present work since once a stable residual equilibrates, depuration of the range of PAHs, even after an acute 48-h exposure time, did not occur. Previous depuration experiments involved removal of clams from either "polluted" waters and transferring the clams to "clean" waters in continuous flow-through filtered seawater systems for depuration of contaminants. The use of carbon filtration systems in this experiment eliminated the need to move organisms at any time during their depuration periods, thus avoiding any metabolic stress to the clam or their pumping rates. In addition, a "closed-system aquarium" provides an ideal observation environment for in situ exposure and mass balance tracking.

An ancillary finding from this study was that heavier clams tended to collect higher concentrations of PAHs. The initial accumulation by bivalves of PAHs influenced by clam weight with possible correlations of PAH associations based upon lipid content is in general agreement with Fong (35) and supports the uses of bivalves as sentinel organisms for monitoring xenobiotics in coastal waters (36).

Pearson correlation coefficients were computed between combined weight of the two-clam sample and the PAH concentration; eight out of nine were positive. Fluorene and benz[a]anthracene had the highest correlations, 0.57 and 0.47, respectively; both were significant at the 0.05 level with a two-tailed test.

Phenanthrene, fluoranthene, and pyrene were detected in clam tissues at higher concentrations per sample time in relation to the other six PAHs. In most cases, these three PAHs exhibited the highest values for the sample under study at any particular depuration time. The most recoverable PAH from clam tissue extracts was fluoranthene, and BaA was the quantitatively least recovered PAH. Neff and Anderson (28) found phenanthrene was accumulated most rapidly by *Rangia cuneata* and released most slowly. For this compound, this investigation appears to be in agreement. Most previous investigations have concentrated on the water-soluble fraction (WSF) of petroleum products, specifically naphthalene and phenanthrene. Farrington et al. (37) found that phenanthrene, fluoranthene, and pyrene in bivalves were indicative of waste petroleum input. A propensity to bioaccumulate a particular PAH may reflect PAH bioavailability, previous exposure extent and duration, and PAH variable volatility and solubility.

Conclusions

The most important implication of the present study is that consumers of bivalve molluscs chronically exposed to persistent levels of PAHs at or above ambient PAH concentrations in urban estuaries may be at higher than normal health risk. Programs in highly urbanized estuarine ecosystems advocating the relaying or transferring of bivalves from "marginal waters" for ultimate commercial harvesting to "approved waters", while well intentioned, may be unduly exposing the shellfish-consuming public to higher than normal levels of PAHs. Even though individual clams may have "low or acceptable" PAH levels (levels difficult to establish and for which there are no present U.S. FDA or WHO threshold standards), cumulative effects of consumption could provide the necessary threshold concentrations of these carcinogenic/mutagenic PAHs in human lipid tissue potentially resulting in long-term health concerns. The usual 21-day depuration or relay period for bacteriological quality improvement in bivalve molluscs appears to be inappropriate and insufficient for chemical depuration. Due to the relative stability of PAHs in clam tissue under ideal depuration conditions, in situ depuration environments may never afford acceptable exposure concentrations of PAHs for consumers of shellfish from urban systems.

The following are recommended:

- (1) Clam relay programs in urbanized estuarine systems should be reevaluated in light of potentially increased long-term public health risk from xenobiotics.
- (2) Research should be undertaken to investigate the complexity of a myriad of compounds bioaccumulated by bivalve molluscs and their level of biomaintenance in lipid tissue compartments.
- (3) Future investigations should concentrate on trophic transfer of low-level, chronic concentrations of a complex group of petroleum-derived compounds attributable to WCCO PAHs because WCCO has been established as the major contributor of PAHs in urban estuarine ecosystems.

Acknowledgments

We gratefully acknowledge the HPLC and GC-MS analyses on clam tissue conducted by the U.S. Environ-

mental Protection Agency, R & D Labs, Edison, NJ under National Park Service/Environmental Protection Agency IAG 1770-84-0001. We acknowledge G. Camilli, Rutgers University, Graduate School of Education, for conducting the specialized computer statistic analyses of results; P. A. Buckley, National Park Service; and J. G. Quinn, University of Rhode Island, Graduate School of Oceanography, for their helpful reviews of the manuscript. A special thank you to C. Fredo for the final manuscript preparation and A. Scaglione for meticulous maintenance and operation of the aquarium systems.

Registry No. Naphthalene, 91-20-3; biphenyl, 92-52-4; fluorene, 86-73-7; phenanthrene, 85-01-8; fluoranthene, 206-44-0; pyrene, 129-00-0; benz[a]anthracene, 56-55-3; chrysene, 218-01-9; benzo[a]pyrene, 50-32-8.

Literature Cited

- (1) *World Resources: A Guide to the Global Environment: 1990-1991*; World Resources Institute: Oxford University Press: New York, 1990; p 186.
- (2) *Oil in the Sea; Inputs, Fates and Effects*; National Academy of Science, National Research Council, National Academy Press: Washington, DC, 1985.
- (3) Kneip, T. J.; Custshall, N. H.; Field, R.; Hart, F. C.; Lioy, P. J.; Mancini, J.; Mueller, J. A.; Sobotowski, C.; Szelligowski, J. In *Ecological Stress and the New York Bight*; Mayer, G., Ed.; Estuarine Research Federation: Columbia, SC, 1982; pp 145-161.
- (4) Peake, E.; Parker, K. In *Polynuclear Aromatic Hydrocarbons: Chemistry and Biological Effects*, Fourth International Symposium; Battelle Press: Columbus, OH, 1980; p 1025.
- (5) Tancredi, J. T. J.—*Water Pollut. Control Fed.* **1977**, *49*, 216.
- (6) *Oil and Hazardous Spills in U. S. Waters: 1971-1982*. Council on Environmental Quality Report. Table A048 *Water Quality*; 1983; p 311.
- (7) Pruell, R. J.; Quinn, J. G. *Environ. Pollut.* **1988**, *49*, 89-97.
- (8) LaFlamme, R. E.; Hites, R. *Geochim. Cosmochim. Acta* **1977**, *42*, 289-303.
- (9) Mueller, J. A.; Garrish, T. A.; Casey, M. C. Contaminant Inputs to the Hudson-Raritan Estuary. NOAA Technical Memorandum OMPA-121, 1982.
- (10) Smith, C. M.; Hackney, C. T. *Estuaries* **1989**, *12*, 42-48.
- (11) Dunn, B. P.; Fee, J. J. *Fish. Res. Board Can.* **1979**, *36*, 1469-1476.
- (12) Boehm, P. D.; Quinn, J. G. *Mar. Biol.* **1977**, *44*, 227-233.
- (13) Dobrowski, C. J., Jr.; Epifano, C. E. *Can. J. Fish. Aquat. Sci.* **1980**, *37*, 2318-2322.
- (14) Segar, D. A.; Davis, P. G. Contamination of Populated Estuaries and Adjacent Coastal Ocean—A Global Review. NOAA Technical Memo. NOS, OMA11, 1984.
- (15) Frank, U. *Toxicol. Environ. Chem. Rev.* **1978**, *73*.
- (16) Frank, U.; Stainken, D.; Gruenfeld, M. In Proceedings of USCG/USEPA/API National Conference on Control of Hazardous Material Spills, Los Angeles, CA; 1979; p 323.
- (17) Frank, U. In *Proceedings, Joint Conference on Prevention and Control of Oil Pollution*; American Petroleum Institute: San Francisco, CA, 1975; pp 87-91.
- (18) Frank, U.; Gruenfeld, M. Determination of Petroleum Oils in Sediments by Fluorescence Spectroscopy Spectroscopy and NMR. Abstracts of the Pittsburgh Conference on Analytical Chemistry and Applied Spectroscopy; U.S. EPA/API; 1971; Paper 400.
- (19) Anderberg, M. R. *Cluster Analysis for Application*; Academic Press: New York, 1973.
- (20) Everitt, B. S. *Cluster Analysis*, 2nd ed.; Heineman Books: London, 1980.
- (21) Stegeman, J. J.; Teal, J. M. *Mar. Biol.* **1973**, *22*, 37-44.
- (22) Lee, R. F.; Gardner, W. S.; Anderson, J. W.; Blaylock, J. W.; Barwell-Clarke, J. *Environ. Sci. Technol.* **1978**, *12*, 832-838.
- (23) Boehm, P. D.; Quinn, J. B. *Estuarine Coastal Mar. Sci.* **1976**, *93*-105.

- (24) Brown, R. A.; Pancirov, R. J. *Environ. Sci. Technol.* 1979, 13, 878-879.
- (25) Wijayaratne, R. D.; Means, J. C. *Mar. Environ. Res.* 1984, 11, 77-89.
- (26) Stein, J. E.; Hom, T.; Varanasi, V. *Mar. Environ. Res.* 1984, 13, 97-119.
- (27) Fowler, S. W. In *Pollutant Transfer and Transport in the Sea*; Kullenberg, G., Ed.; CRC Press: Boca Raton, FL, 1982; Vol. 2, pp 1-66.
- (28) Neff, J. M.; Anderson, J. W. *Response of Marine Animals to Petroleum and Specific Petroleum Hydrocarbons*; John Wiley and Sons, Inc.: New York, 1981; pp 177.
- (29) Pruell, R. J.; Hoffman, E. J.; Quinn, J. G. *Mar. Environ. Res.* 1984, 11, 163-181.
- (30) Teal, J. M.; Howarth, R. W. *J. Environ. Manage.* 1984, 8, 27-44.
- (31) Dunn, B. P.; Stith, H. F. *Bull. Environ. Contam. Toxicol.* 1976, 15, 398-401.
- (32) Hoffman, E. J.; Mills, G. L.; Latimer, J. S.; Quinn, J. G. *Environ. Sci. Technol.* 1984, 18, 580-587.
- (33) Bates, T. S.; Murphy, P. P.; Curl, Jr., H. C.; Feely, R. A. *Environ. Sci. Technol.* 1987, 21, 193-198.
- (34) Jackim, E.; Wilson, L. In *Proceedings, 10th Annual National Shellfish Sanitation Meeting*; 1977; p 27.
- (35) Fong, W. C. *J. Fish. Res. Board Canada* 1976, 33, 2774-2780.
- (36) Burns, K. A.; Smith, J. L. *Estuarine Coastal, Shelf Sci.* 1981, 13, 433-443.
- (37) Farrington, J. W.; Goldberg, E. D.; Risebrough, R. W.; Martin, J. H.; Bowen, V. T. *Environ. Sci. Technol.* 1983, 17, 490-496.

Received for review October 26, 1990. Revised manuscript received March 13, 1991. Accepted March 14, 1991. This research was supported in part through funding provided by the United States Department of the Interior, National Park Service under Cooperative Agreement 1771-4-21(04) with the Polytechnic University, and Interagency Agreement 1770-84-0001 with the U.S. Environmental Protection Agency, MERL-Ci; Edison, NJ.

Biodegradation of Mixed-Organic Wastes by Microbial Consortia in Continuous-Recycle Expanded-Bed Bioreactors

Tommy J. Phelps,*[†] John J. Niedzielski,[†] Kenneth J. Malachowsky,[†] Richard M. Schram,[†] Stephen E. Herbes,[†] and David C. White*^{†,‡,§}

Institute for Applied Microbiology, University of Tennessee, 10515 Research Dr. Suite 300, Knoxville, Tennessee 37932-2567, Environmental Sciences Division, Oak Ridge National Laboratory, Oak Ridge, Tennessee 37831, and the Department of Microbiology, University of Tennessee, Knoxville, Tennessee 37996-0845

■ Microbial consortia enriched from subsurface sediments contaminated with chlorinated hydrocarbons proved capable of degrading mixed-organic wastes. Methane and/or propane as foodstock enabled aerobic mineralization of greater than 20 mg L⁻¹ trichloroethylene (TCE) plus 1 mg L⁻¹ vinyl chloride, benzene, and toluene in cell suspension or bioreactor experiments. The microbial consortia degraded 80-95% of TCE at 20 mg L⁻¹ within 5 days in continuous-recycle expanded-bed bioreactors requiring 50-100 mol of foodstock/mol of TCE degraded. When the bioreactors were challenged with groundwaters contaminated with mixed-organic wastes, the microbial consortia degraded greater than 99% of the benzene, toluene, xylene, vinyl chloride, and nine chlorinated hydrocarbons, 85% of the TCE, and 60% of the tetrachloroethylene within 21 days, while requiring 80 μmol of methane plus propane per micromole of mixed-organic waste degraded. The potential for bioremediation of groundwater contaminated with mixed-organic wastes was demonstrated in laboratory reactors.

Introduction

Chlorinated and aromatic hydrocarbons are major components of mixed-organic wastes contaminating soils, sediments, and groundwaters (1-6). As a consequence of high usage and improper disposal technologies, many soils and subsurface aquifers are contaminated; some containing greater than 1000 mg L⁻¹ chlorinated hydrocarbons, often in combination with other organic wastes (2, 6, 7). Remediation of subsurface contamination may require long treatment times and considerable expense (3, 4, 8). Some

treatments often result in the mere transfer of wastes from poorly controlled environments to storage sites (2). Waste storage facilities or atmospheric venting may alleviate an immediate concern without detoxifying the waste. Remediation technologies that destroy or mineralize toxicants on-site would be more desirable than transfer of wastes from one environment to another.

Bacteria capable of utilizing aromatic hydrocarbons as sources for energy are well documented (1, 5, 9) and successful examples of bacterial remediation of contamination plumes have been demonstrated (1, 3, 8). Chlorinated alkenes such as trichloroethylene (TCE) are degraded fortuitously or cometabolically by methanotrophic (10, 11) and heterotrophic microorganisms (6, 12, 13). Methane and propane have been shown to stimulate biodegradation of trichloroethylene in soil columns (10, 14) and bioreactors (15-17). Several microorganisms have the capability to degrade specific chlorinated or aromatic compounds, but in this study we investigated the ability of microbial consortia to degrade a mixture of organic toxicants. Mixed-organic waste degradation in continuous-recycle expanded-bed bioreactors was successful. Biological degradation of organic waste from groundwater, which contained TCE, benzene, toluene, xylene, and several other chlorinated aliphatic hydrocarbons, is reported.

Materials and Methods

Bioreactor Design and Operation. Each bioreactor consisted of two borosilicate glass chromatography columns (Pharmacia, Piscataway, NJ) linked in series (Figure 1). The expanded bed consisted of 70 g of 60-80-mesh crushed glass and a liquid displacement of 45 mL. Bed expansion was 20 mL at a flow rate of 20 mL min⁻¹. Liquids flowed upward through the expanded bed, into the gas recharge column, and through the peristaltic pump. A detailed description of the bioreactor construction, maintenance,

[†] Institute for Applied Microbiology, University of Tennessee.

[‡] Oak Ridge National Laboratory.

[§] Department of Microbiology, University of Tennessee.

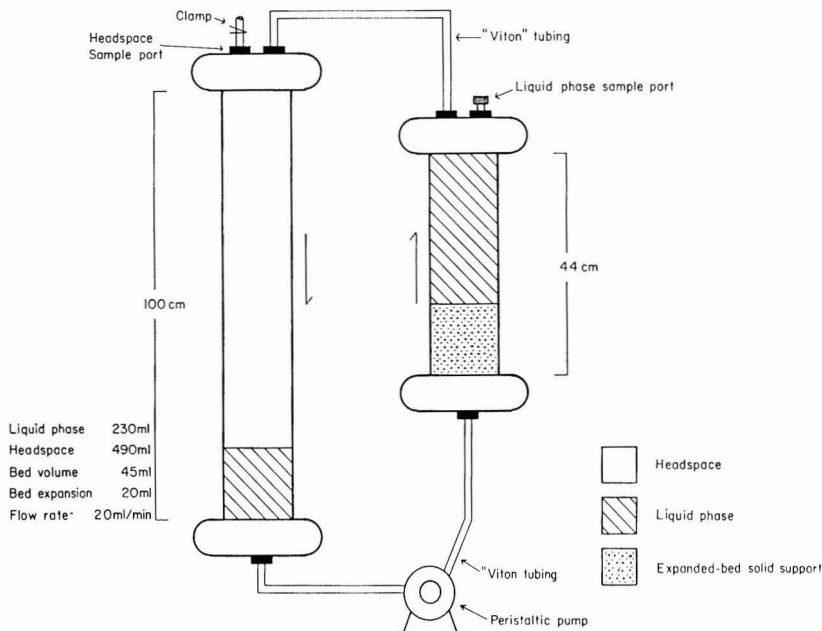


Figure 1. Diagram of expanded-bed bioreactor and gaseous recharge column. Recirculation was accomplished by peristaltic pumping through Viton tubing.

and operation has been given (15). Each bioreactor contained 230 mL of medium to which mineral salts and 2.0 mM phosphate/bicarbonate buffer were added, and the pH of the medium was 7.2. Temperature was maintained at 22 °C. Resazurin, 2 mg L⁻¹, was added as a redox indicator. Bioreactors were fed methane (5% v/v) and/or propane (3% v/v) as foodstock while oxygen served as the terminal electron acceptor (15). Methane and propane were added daily by syringe to maintain their respective concentrations unless stated otherwise. Each day samples were obtained from the headspace sampling port. Losses of TCE, methane, and propane from the inhibited control reactor averaged less than 5% of the initial concentrations after 20 days. The control reactor was inhibited with 0.2% sodium azide plus 0.5% formalin. Contaminated groundwater was obtained from a shallow monitoring well in a waste disposal site near Oak Ridge, TN. Field measurements indicated the groundwater had a pH = 6.5, temperature of 18 °C, oxidation-reduction potential of 26 mV, and dissolved oxygen concentrations of 1.2 mg L⁻¹.

Bacterial Cultures. Three consortia with TCE-degrading capabilities were used as inocula. Culture SRP was isolated from the Savannah River Site and was capable of degrading TCE at concentrations exceeding 100 mg L⁻¹ (6). The PM-M culture contained mixtures of propane- and methane-oxidizing cultures obtained from soils near the vicinity of Ada, OK, in addition to the TCE-degrading consortium from SRP. The additional methane- and propane-oxidizing cultures added to the PM-M consortium appeared incapable of degrading 20 mg L⁻¹ TCE. A methanotroph capable of degrading TCE at concentrations less than 1 mg L⁻¹ (11) was also added to the PM-M consortium. Consortium SM-1 consisted of the SRP consortium plus the TCE-degrading methanotroph (11). Consortium SM-1 and PM-M had been maintained in the continuous-recycle bioreactors for >3 months (15). Culture maintenance and cell suspension studies utilized crimp-top serum vials with Teflon septa as previously described (6). Cultures for cell suspension studies were centrifuged and

resuspended in 10 mL of 2 mM phosphate plus 10 mM bicarbonate-buffered medium at an approximate density of 1.0 g dry weight L⁻¹. Duplicate vials of controls and cell suspensions were sacrificed at each time point.

Analytical Procedures. TCE was analyzed by headspace analyses using a Hewlett-Packard 5890 gas chromatograph (GC) equipped with a 50 m × 0.2 mm Hewlett-Packard ultraperformance cross-linked methyl-silicone column and an electron capture detector (6). Benzene, xylene, and toluene were analyzed from liquid-phase samples by use of a similar GC and column equipped with a flame ionization detector. Propane and methane in headspace gases were analyzed with a Shimadzu GC-9A equipped with a packed column and flame ionization detector. Standard calibration curves used the same headspace/liquid-phase ratio as the columns. Analyses of multiple chlorinated hydrocarbons were performed from water samples collected in 40-mL Teflon sealed vials in accordance with U.S. EPA procedure 624. Analyses were conducted by Oak Ridge National Laboratory (ORNL).

Results and Discussion

Cell Suspension Studies. Our laboratory previously demonstrated degradation of greater than 99% of 50 mg L⁻¹ TCE to carbon dioxide by mixed populations of heterotrophic microorganisms (6). Nelson et al. (12) reported that heterotrophic TCE-degrading microorganisms could be induced by toluene, suggesting that microorganisms may possess the ability to simultaneously degrade mixed-organic wastes. Results in Table I show that cell suspensions of microbial consortia were capable of degrading mixed-organic wastes. Cell suspensions inhibited with 0.1% sodium azide and 0.5% formalin did not degrade the mixed-organic wastes in the 10-day experiment when compared to uninoculated controls. Increased benzene and toluene in the inhibited suspensions after 10 days was attributed to variability of the uninoculated and inhibited controls when compared to standard curves. Suspensions of the SRP consortium degraded >80% of the mixed-or-

Table I. Removal of Organic Contaminants by Cell Suspensions^a

suspension	mixed-waste component ^b (initial concn)			
	TCE (20 mg L ⁻¹)	vinyl chloride (1 mg L ⁻¹)	benzene (1 mg L ⁻¹)	toluene (1 mg L ⁻¹)
inhibited cells	26	11	+7	+27
SRP consortium	85	82	87	90
reactor consortium	87	96	93	99
SRP consortium maximum from separate expts	>99.99	99.9	>99	>99

^a Experimental procedure: Stationary-phase cultures were centrifuged and resuspended into duplicate 10-mL volumes of 2 mM phosphate plus 10 mM bicarbonate-buffered basal medium to which one or more toxicants were added. Oxygen (10 mL) was added to each suspension and the 28-mL vials were sealed with Teflon septa. Results were analyzed after 10 days and the average value was reported. The SRP maximum values represent results obtained in similar experiments performed in different months. ^b Data reported as percent loss of initial concentration relative to controls containing no cells.

Table II. Utilization of TCE and Propane during Degradation of Mixed-Organic Wastes^a

day	reactor	TCE, μg L ⁻¹	TCE loss, μmol	propane loss, μmol
0	control	2200	0	0
	PM-M	2200	0	0
	SM-1	2200	0	0
3	PM-M	2000	0.5	700
	SM-1	1900	0.5	600
6	PM-M	1300	1.7	1300
	SM-1	1300	1.6	1300
15	PM-M	560	3.0	2000
	SM-1	420	3.1	2000
21	control	2400	0	70
	PM-M	440	3.3	2700
	SM-1	400	3.3	2600

^a Experimental conditions: Each reactor (Figure 1) contained 230 mL of groundwater from a contaminated site. Control reactor was inhibited with 0.1% sodium azide plus 0.5% formalin. Culture PM-M contained the SRP consortium plus several methane- and propane-oxidizing cultures. Culture SM-1 consisted of the SRP consortium and a TCE-degrading methanotroph. Propane was maintained at 5% (v/v) and bioreactors were recirculated for 21 days.

ganic wastes in these experiments. In other experiments performed in different months, the SRP consortium maximally degraded >99.9% of the toxicants (Table I). The reactor consortium included the PM-M consortium plus uncharacterized microorganisms that colonized the reactor after it was challenged with groundwater containing a diverse microbial community in addition to mixed-organic wastes. The reactor consortium, which was inoculated with more methane- and propane-oxidizing cultures

than the SRP consortium, appeared to degrade toxicants to a greater extent than the SRP consortium alone (Table I). In previous bioreactor experiments fed methane plus propane (17), TCE degradation by the PM-M consortium was significantly greater than the less complex SM-1 consortium (95% level by Student's *t* test) (17). Furthermore, the difference between the consortia was significantly greater than zero at the 99% confidence level with a *Z* score (standard error of the mean) of 3.4 (data not shown) (17). These results suggest that complex microbial consortia may have a greater ability to simultaneously degrade mixtures of organic wastes (11–13, 17) than pure cultures. However, the addition of pure cultures to a consortium may further enhance its ability to degrade mixtures of organic wastes.

Bioreactor Experiments. Previous reports described the ability of these consortia to degrade 20 mg L⁻¹ TCE in expanded-bed bioreactors (17). Table II illustrates the utilization of TCE and propane after bioreactors were challenged with groundwaters contaminated with mixed-organic wastes. Laboratory analyses determined the bioreactors contained 2.2 mg L⁻¹ TCE at the time of inoculation. TCE loss within the reactors averaged 115 μg L⁻¹ day⁻¹ for the first 15 days versus 12 μg L⁻¹ day⁻¹ for days 15–21. The TCE degradation rate thus decreased by 1 order of magnitude while propane consumption decreased 50%, possibly due to limiting availability of inorganic nutrients. However, in other experiments when the concentrations of phosphate, nitrate, and minerals were doubled, the propane consumption rate was linear for >8 days (data not shown) but the rate of TCE degradation decreased to <60% of the initial rate and 50% more propane was required per micromole of TCE degraded

Table III. Degradation of Mixed-Organic Wastes by a Propane-Fed Bioreactor

organic wastes	toxicant concn in reactors, ^a μg/L				
	control day 0	control day 0	control day 21	PM-M day 21	SM-1 day 21
vinyl chloride	4000	4400	1200	10	10
chloroethane	27	30	13	10	10
methylene chloride	10	11	9	1	1
1,1-dichloroethylene	690	780	5	<5	<5
1,1-dichloroethane	1100	1200	820	<5	<5
1,2-dichloroethylene	3000	3100	3600	29	13
1,2-dichloroethane	21	23	18	<5	<5
1,1,1-trichloroethane	1200	1300	940	15	6
trichloroethylene	1700	1900	2600	435	235
1,1,2-trichloroethane	52	54	46	<5	<5
tetrachloroethylene	2100	2300	2100	805	860
benzene	86	90	49	<5	<5
toluene	49	51	26	<5	<5
xylene	26	28	10	<5	<5

^a Analyses performed by ORNL in accordance with EPA procedure 624. Values below detectable concentrations are noted by "<".

Table IV. Comparison of TCE and Mixed-Organic Waste Degradation in Recycled Bioreactors^a

experiment	initial TCE concn, $\mu\text{g/L}$	total wastes degraded, μmol	foodstock consumed, μmol	foodstock/TCE loss, $\mu\text{mol}/\mu\text{mol}$
TCE control	20000	2	na ^b	na ^b
TCE with propane plus methane ^c	20000	31	3700	123 \pm 16
TCE with propane and methane at day = 0 only ^c	20000	31	1730	55 \pm 1
TCE with propane ^c	20000	29	2650	91 \pm 12
TCE with propane plus methane	4000	4.1	860	215 \pm 40
mixed organics	1700	32	2700	84
with propane	1900	34	2600	76

^aExperimental design: Each reactor contained 230 mL of medium, which in the mixed-waste experiments was replaced with well water. Propane and methane were maintained at 3–5% (v/v) in the headspace. Experiments receiving propane and methane at day = 0 only did not receive additional methane or propane after initiation of the experiment. Standard deviations were calculated for those experiments repeated four times. ^bna, not applicable. ^cData summarized from Phelps et al. (17).

(17). These results agreed with other studies (16, 17) which suggested that microbial degradation of TCE in bioreactors becomes slower and less efficient as TCE concentrations decrease to approximately 500 $\mu\text{g L}^{-1}$.

Degradation of mixed-organic wastes in the expanded-bed total-recycle bioreactors is shown in Table III. The analyses performed by EPA procedure 624 showed TCE to be 1700–1900 $\mu\text{g L}^{-1}$ in the reactors versus 2200 $\mu\text{g L}^{-1}$ by headspace analysis. Variability between replicate samples analyzed by EPA procedure 624 rarely varied by more than 10%, as shown by the day = 0 controls. Results after 21 days are expressed as averages of duplicate analyses. Seven of the 14 toxicants present in the groundwaters were degraded to the detection limits of the methods employed. Vinyl chloride and 1,1-dichloroethylene were the only toxicants whose concentrations decreased more than 60% in the control reactor. In the experimental reactors vinyl chloride was reduced >99% to concentrations less than the detection limits. The EPA procedure 624 analyses, which were in agreement with Table II, showed that >80% of the TCE was degraded in both bioreactors. Dichloroethylenes and ethanes were decreased >99.5% to nondetectable concentrations.

Tetrachloroethylene decreased 60% in both test reactors, but less than 5% in the control reactor. In preliminary experiments in which cell suspensions of these consortia have been exposed to <0.6 mg L^{-1} tetrachloroethylene, loss of tetrachloroethylene has been observed under aerobic conditions. However, due to the low specific activity of [¹⁴C]tetrachloroethylene, verification of degradation products has not been achieved (data not shown). It was also possible that tetrachloroethylene degradation in these bioreactors occurred via reductive dechlorination in anaerobic microniches as observed previously (18). Although the bulk-phase liquid remained oxidized, as monitored by the blue color of resazurin, it is likely that anaerobic microniches existed within biofilms.

Benzene, toluene, and xylene were also degraded in the bioreactors. Nelson et al. (12) reported that a heterotrophic toluene degrader could degrade TCE when induced with toluene. Inducers were not required for TCE degradation by these consortia (6), nor did the presence of methane and propane eliminate the degradation of aromatics and chlorinated hydrocarbons. In all, greater than 91% of the total mixed-organic contaminants were degraded. Chlorinated intermediates of TCE decomposition such as dichloroethylenes and vinyl chloride did not accumulate within the bioreactors. These results substantiated previous studies, which accounted for >60% of [¹⁴C]TCE being converted to carbon dioxide by the SRP consortium (6).

Foodstock Utilization. Previous studies (6, 17) showed that these consortia could use methane or propane as

foodstock for bioremediation of chlorinated hydrocarbons, but efficiency per mole of foodstock and degradative rates were less with methane alone. Table IV compares the efficiency of TCE degradation and mixed-organic waste degradation in expanded-bed total-recycle bioreactors. When 20 mg L^{-1} TCE was the only contaminant present and propane plus methane were continuously available as foodstocks, each mole of TCE degraded required an average of 123 mol of foodstock. When no methane or propane was added, 10% of the TCE was lost during starvation of the consortia. During pulsed feeding of the consortia, when methane and propane were provided only at day = 0 and the reactors depleted their foodstocks, stable and reproducible TCE degradation proceeded for 5 days. Pulsed feeding reduced methane and/or propane consumption by half with no adverse effect on degradation of TCE with an efficiency of 55 mol of foodstock consumed/mol of TCE degraded (Table IV). When propane was the foodstock, 91 mol of propane were required per mole of TCE degraded. As the TCE concentration decreased, the TCE degradation rate and degradative efficiency decreased. At 4 mg L^{-1} TCE, 215 mol of propane plus methane were required per mole of TCE degraded versus 123 mol at higher TCE concentrations (Table IV). Degradation efficiencies for TCE from Table II correspond to an approximate foodstock/TCE ratio of 500 for the first 15 days versus a ratio of 5000 for the final 6 days; however, mixed-organic wastes were also degraded.

A total of 33 μmol of mixed-organic wastes (2.6 μmol of TCE plus 30.4 μmol of other contaminants) were degraded in the mixed-organic waste experiments requiring 2650 μmol of propane or 80 μmol of foodstock per micromole of contaminant degraded. If TCE had been the only organic waste, the expected foodstock/TCE ratio for TCE at 2 mg L^{-1} would have been >200 (Table IV). The observed ratio of 80 suggests that mixed-waste degradation may require fewer moles of foodstock than TCE degradation. Possible explanations for the apparent efficiency of mixed-waste degradation include the following: (1) less chlorinated hydrocarbons may be more readily degraded than TCE (16) or PCE, (2) degradative products may be available as energy or carbon sources, (3) toxicants such as benzene, xylene, or toluene could serve as energy sources. Bioremediation of gasoline and jet fuel plumes supports the notion that light aromatics can serve as substrates for bioremediation (1, 5, 8), and toluene is known to induce TCE degradation by *Pseudomonas* sp. (12). The groundwater used in these studies contained 161 $\mu\text{g L}^{-1}$ light aromatics, an amount that would be insignificant as an energy source for the reactor biomass. The apparent efficiency of mixed-waste degradation by these consortia likely resulted from the less chlorinated aliphatics being more susceptible to oxidation (4); consequently they

may have readily undergone transformations by fortuitous or cometabolic processes (16).

Each bioreactor contained approximately 20 mg dry weight of biomass as estimated by phospholipid fatty acids (17). When TCE was degraded at a concentration of 20 mg L⁻¹, each milligram of biomass degraded an average of 40 µg of TCE each day with a maximum of 80 µg of TCE/mg of biomass each day (calculations not shown). During mixed-waste degradation at 2 mg L⁻¹ TCE and 230 mL of groundwater per reactor, the daily TCE consumption was 1.3 µg of mixed-organic wastes (mg of biomass)⁻¹ day⁻¹. When considering all contaminants, the average degradation rate was 7 µg of mixed-organic wastes (mg of biomass)⁻¹ day⁻¹. Although the quantity of foodstock required per micromole of contaminant degraded was similar between the mixed-organic waste and TCE experiments, the biomass required more time to degrade the lower concentration of mixed-organic wastes. As shown in Tables II and III, several weeks were required to decrease the TCE concentration 80%, with little degradation occurring over the final 6 days. These results suggest that as the concentration of TCE decreases, degradation rates decrease dramatically. Results also suggest that highly chlorinated constituents, such as PCE and TCE, may decrease the degradation rate and the metabolic efficiency of mixed-waste bioremediation, while lesser chlorinated aliphatics or light aromatics may be degraded more rapidly and efficiently. Fortunately, degradation of many components of mixed-organic waste may not require additional nutrients or degradative time and may even contribute to foodstock pools and energy flow.

Conclusions

Bioremediation of mixed-organic wastes from contaminated groundwaters was demonstrated in laboratory bioreactors. The feasibility of remediating organic waste mixtures including PCE, TCE, less chlorinated aliphatics, benzene, toluene, and xylene from groundwaters by microbial consortia fed gaseous hydrocarbons was established. Degradation required less than 100 mol of methane or propane/mol of contaminant degraded. The closed-system reactors appeared well suited for perturbation and metabolic studies. Future plans include use of these systems to assess the resiliency and efficiency of bioremediation processes.

Acknowledgments

We thank Tony Palumbo, Gerry Strandberg, and Terry Donaldson of Oak Ridge National Laboratory and Carl Fliermans and Terry Hazen from Westinghouse Savannah River Site for assistance, guidance, and fruitful discussions.

Registry No. H₂C=CHCl, 75-01-4; ClCH₂CH₃, 75-00-3; CH₂Cl₂, 75-09-2; Cl₂C=CH₂, 75-35-4; Cl₂CHCH₃, 75-34-3; ClC-

H=CHCl, 540-59-0; ClCH₂CH₂Cl, 107-06-2; Cl₃CCH₃, 71-55-6; Cl₂C=CHCl, 79-01-6; Cl₂CHCH₂Cl, 79-00-5; Cl₂C=CCl₂, 127-18-4; benzene, 71-43-2; toluene, 108-88-3; xylene, 1330-20-7; methane, 74-82-8; propane, 74-98-6.

Literature Cited

- (1) Bartha, R. *Microbiol. Ecol.* **1986**, *12*, 155-172.
- (2) U.S. Department of Energy. *Evaluation of Mid-to-Long Term Basic Research for Environmental Restoration*; DOE/ER-0419; U.S. Government Printing Office: Washington, DC, September 1989.
- (3) Roberts, P. V.; et al. *In-Situ Aquifer Restoration of Chlorinated Aliphatics by Methanotrophic Bacteria*; EPA/600/2-89/033; U.S. Environmental Protection Agency: Ada, OK, July 1989.
- (4) Vogel, M. T.; et al. *Environ. Sci. Technol.* **1987**, *21*, 722-36.
- (5) Atlas, R. M.; Bartha, R. *Microbial Ecology*, 2nd ed.; The Benjamin/Cummings Publishing Co., Inc.: New York, 1987; pp 403-438.
- (6) Fliermans, C. B.; et al. *Appl. Environ. Microbiol.* **1988**, *54*, 1709-1714.
- (7) Phelps, T. J.; et al. *Geomicrobiol. J.* **1988**, *6*, 157-170.
- (8) Wilson, J. T.; et al. *In Situ Bioremediation of Spills from Underground Storage Tanks: New Approaches for Site Characterization Project Design, and Evaluation of Performance*; EPA/600/S2-89/042; U.S. Environmental Protection Agency: Ada, OK, September 1989.
- (9) Rochkind, M. L.; et al. *Microbial Decomposition of Chlorinated Aromatic Compounds*; EPA/600/2-89/090; U.S. Environmental Protection Agency: Cincinnati, OH, 1989.
- (10) Wilson, J. T.; Wilson, B. H. *Appl. Environ. Microbiol.* **1985**, *49*, 242-243.
- (11) Little, C. D.; et al. *Appl. Environ. Microbiol.* **1988**, *54*, 951-956.
- (12) Nelson, M. J. K.; et al. *Appl. Environ. Microbiol.* **1987**, *53*, 949-954.
- (13) Wackett, L. P.; Gibson, D. T. *Appl. Environ. Microbiol.* **1988**, *54*, 1703-1708.
- (14) Henson, J. M.; et al. *FEMS Microbiol. Ecol.* **1988**, *53*, 193-201.
- (15) Niedzielski, J. J.; et al. *J. Microbiol. Methods* **1989**, *10*, 215-223.
- (16) Strandberg, G. W. *Environ. Sci. Technol.* **1989**, *23*, 1422-1425.
- (17) Phelps, T. J.; et al. *Appl. Environ. Microbiol.* **1990**, *56*, 1702-1709.
- (18) Vogel, T. M.; McCarty, P. L. *Appl. Environ. Microbiol.* **1985**, *49*, 1080-1083.

Received for review May 1, 1990. Revised manuscript received January 28, 1991. Accepted April 3, 1991. This research was supported by the Oak Ridge National Laboratory Y-12 Plant Remedial Action Project, U.S. Department of Energy, under Contract DE-AC05-84OR21400 with Martin Marietta Energy Systems Inc.; Savannah River Laboratory, under contract AX681901 with E. I. du Pont de Nemours and Co. Portions of this research were supported by Grant ERKP219 from DOE-OHER to the Environmental Sciences Division of Oak Ridge National Laboratory.

Effects of a CO₂ Pressure Process on the Solubilities of Major and Trace Elements in Oil Shale Solid Wastes

Katta J. Reddy,^{*,†} James I. Drever,[‡] and Victor R. Hasfurther[†]

Wyoming Water Research Center, P. O. Box 3067, University Station, Laramie, Wyoming 82071, and Department of Geology and Geophysics, University of Wyoming, Laramie, Wyoming 82071

■ Processing of oil shale at high temperatures produces a highly alkaline solid waste. The waste can be stabilized by a recarbonation process. In order to test a method for accelerating the recarbonation process, we exposed three moist oil shale solid waste (OSSW) samples to 5 psi CO₂ pressure for 1 h. The treated and untreated samples were equilibrated with water for 7 days and the chemical composition of the aqueous extracts determined. Before CO₂ treatment, the Ca²⁺ and Mg²⁺ concentrations appeared to be controlled by silicate phases present in the waste such as wollastonite (CaSiO₃), forsterite (Mg₂SiO₄), and talc (Mg₃Si₄O₁₀(OH)₂), which buffered the pH at ~12.0. The CO₂ treatment lowered the pH from 12.0 to ~9.0 through the formation of calcite. The Ca²⁺ concentrations from CO₂-treated samples suggested a close approach to saturation with respect to calcite (CaCO₃) whereas the Mg²⁺ concentrations appeared to be controlled by either magnesite (MgCO₃) or possibly a silicate. The CO₂ treatment generally decreased F and Mo concentrations in aqueous extracts. The F⁻ concentration before and after CO₂ treatment appeared to be controlled by fluorite (CaF₂). Our results demonstrate that the CO₂ pressure process is an effective means of reducing the pH and the concentrations of F and Mo in aqueous extracts from alkaline solid wastes.

Introduction

Oil shale contains mainly kerogen and carbonate minerals. Oil is recovered from the oil shale by thermally degrading the kerogen at elevated temperatures, which results in production of large amounts of oil shale solid wastes (OSSW). These solid wastes are often alkaline (typical slurry pH may range from 10.0 to 13.0) and often contain elevated levels of toxic elements.

Reclamation of OSSW is often affected by the high pH and high solubilities of toxic elements. In addition, soluble toxic elements may leach from the disposal environment and migrate to groundwater (1-8).

During the processing of oil shale, high temperatures drive off CO₂ from carbonate minerals resulting in the formation of oxide and silicate phases. These phases react rapidly with water, and as a result, the pH of aqueous extracts of OSSW approach 12.0, and this affects the solubility relationships of many elements. The high pH increases the solubility and mobility of anionic trace elements, e.g., As, B, F, Mo, and Se (1-6). Among these trace elements, F and, to some extent, Mo have shown considerable mobility in OSSW disposal environments (4).

The high pH of OSSW decreases slowly as the CO₂-deficient materials absorb CO₂ from the atmosphere (recarbonation). However, natural recarbonation of OSSW occurs slowly, and this may hinder reclamation efforts intended to minimize potential pollution of natural resources (land/water) associated with the disposal of these materials.

The objectives of the research were as follows: (1) to investigate a process for accelerating the recarbonation process by reacting moist oil shale wastes under CO₂ pressure; (2) to examine the effects of CO₂ pressure treatment on the pH and solubilities of major (e.g., Ca and Mg) and trace (e.g., F and Mo) elements in aqueous extracts.

Materials and Methods

The samples used in this study were Western Reference Green River Formation oil shale from the Piceance Creek Basin in Colorado, which had been processed at 770, 1000, and 1295 K to produce PP3, Lurgi, and PP6 oil shale solid wastes, respectively. More details regarding the processing conditions are reported in Merriam et al. (9) and Nowacki (10).

Samples were ground to pass a 0.25-mm sieve to enhance the recarbonation process. However, under oil shale processing conditions samples may vary in particle size. For CO₂ pressure treatment experiments, a pressure vessel was designed (Figure 1) to react oil shale solid waste samples. The reaction vessel consisted of 30 cm by 30 cm polyvinyl chloride (PVC) cylinder with an o-ring seal lid and a pressure release valve to control the internal pressure. A stainless steel screen covered with filter paper was placed in the middle of the reaction vessel to hold samples. The gas inlet of the reaction vessel was connected to a CO₂ tank through a distilled H₂O flask to saturate the CO₂ with H₂O.

Fifty grams of each sample containing 15-20% moisture was spread over the filter paper. Before the gas outlet was connected to the pressure gauge, CO₂ from a gas tank was bubbled through distilled H₂O, using a sparger, to purge the initial air from the reaction vessel. Approximately 5 psi pressure was maintained inside the reaction vessel. After a reaction period of 1 h, the sample was removed and sufficient distilled H₂O was added to the sample to prepare a saturated paste. The saturated paste was immediately measured for pH. After few days, samples were air-dried and subjected to solubility measurements. For solubility measurements, duplicate 20-g samples of treated and untreated samples were placed into 250-mL Nalgene bottles with 100 mL of distilled-deionized H₂O. Three drops of toluene was added to each bottle to suppress microbial activity. Each sample bottle was tightly capped, placed on a mechanical shaker, and reacted in an incubator at a constant temperature of 25 °C (298 K). After 3- and 7-day reaction periods, sample suspensions were filtered through 0.45-μm Millipore filters under an atmosphere of argon gas to prevent uptake of atmospheric CO₂.

Each filtered solution was divided into two subsamples. One subsample was acidified to pH 5-6 with HNO₃. The other subsample was left unacidified. The unacidified samples were analyzed immediately for pH and concentration of carbonate species. The acidified samples were analyzed for Ca, Mg, Na, K, F, Mo, Cl, SO₄, and Si.

The pH was measured with an Orion combination pH electrode. Ca, Si, Mg, and Mo were measured with inductively coupled plasma optical emission spectroscopy

^{*} Wyoming Water Research Center.

[†] University of Wyoming.

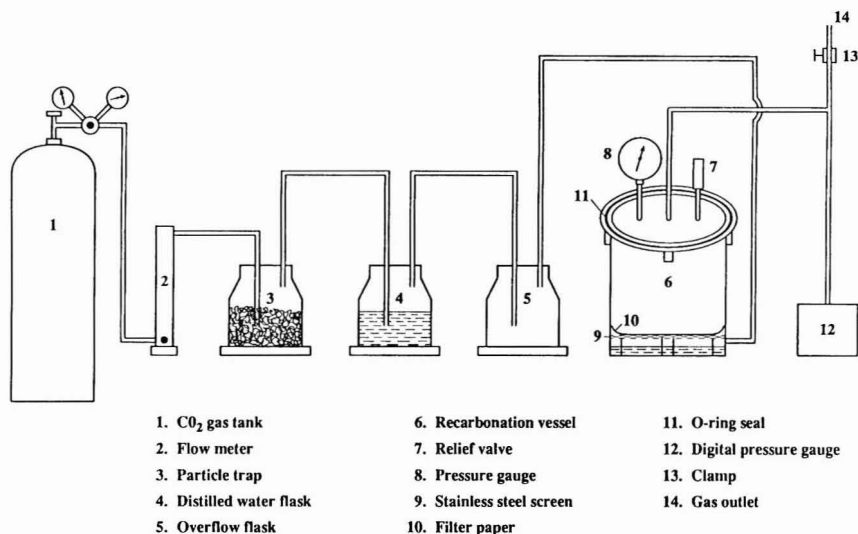


Figure 1. Experimental design of CO₂ pressure process to hasten recarbonation process of oil shale solid wastes

Table I. Effect of CO₂ Treatment on pH and Concentrations of Different Elements in Aqueous Extracts of Oil Shales^a

raw oil shale		PP3		Lurgi		PP6	
		BR ^b	AR ^c	BR ^b	AR ^c	BR ^b	AR ^c
3 Days							
pH	7.93	10.28	9.00	11.62	9.05	11.65	9.07
Ca	108.0	0.22	11.04	156.0	18.32	205.0	252.0
Mg	44.0	0.24	12.18	BD ^d	313.0	BD ^d	266.0
Si	10.0	1.0	0.45	8.5	1.7	10.0	1.1
C ^e	176.0	351.0	157.0	1.4	68.0	4.2	5.3
F	3.5	15.1	9.5	8.5	1.9	2.13	6.74
Mo	0.43	1.6	1.45	1.1	0.83	4.80	1.10
7 Days							
pH	8.21	10.68	8.83	12.07	9.10	12.10	9.13
Ca	139.0	7.63	6.96	179.0	14.0	50.50	201.0
Mg	53.1	0.24	10.13	0.22	286.0	0.21	232.0
Si	9.7	0.77	0.40	3.87	1.77	17.32	7.05
C ^e	113.6	367.0	202.0	2.02	76.8	3.51	21.10
F	8.10	25.63	10.68	5.12	1.9	3.79	6.74
Mo	0.60	1.70	1.35	0.90	0.95	2.58	0.76

^a Mean of duplicate analyses, units are milligrams per liter except for pH. ^b Before CO₂ treatment. ^c After CO₂ treatment. ^d BD, below detection limit of 0.001 mg/L. ^e Total carbonate and bicarbonate species measured as CO₂.

(ICP-OES); Na and K were measured with atomic absorption (AA) spectrometry. F and Cl were measured with specific ion electrodes, and SO₄ was measured by BaCl₂ precipitation. Carbonate and bicarbonate species in the aqueous extracts were analyzed by the CO₂ gas release method (11) to avoid possible interference from inorganic and organic anions. In this method, solutions were acidified to pH 4.5 and evolved CO₂(g) was trapped in a basic solution under an atmosphere of argon. Aqueous extracts of OSSW were also analyzed for B, As, and Se, but the concentrations of these elements were found to be less than 0.01 mg L⁻¹. The Ca²⁺ activity in aqueous extracts was analyzed with a specific ion electrode to test for possible effects of organic complexation on Ca²⁺ activity (11).

The total elemental concentrations and pH of aqueous extracts were used as input to the GEOCHEM (12) speciation model to calculate ion activities. Solution species (e.g., HSiO₄³⁻, SiO₄⁴⁻, CaH₃SiO₄⁺, NaMoO₄⁰, CaMoO₄⁰) that may be significant in alkaline solid waste solutions were added to the GEOCHEM database (13). From ion activities, ion activity products (IAPs) were calculated and compared

with solubility products (K_{sp} s) to evaluate the solid phases controlling the solubilities of Ca, Mg, F, and Mo before and after CO₂ treatment. We assumed that IAPs within ± 0.50 log unit of K_{sp} s of solid phases represented equilibrium, and that the solid phase was a probable control on the concentrations of the ions involved.

Results and Discussion

The effect of CO₂ treatment on the pH and the solubilities of major and trace elements in aqueous extracts of oil shales is presented in Table I. The complete results of the chemical analyses are reported in Reddy et al. (14), and only data from the 7-day reaction period will be discussed here. The chemical analyses of aqueous extracts of raw oil shale are also included in Table I for comparison.

The processing of raw shale at different temperatures caused significant differences in the chemical composition of the aqueous extracts both before and after CO₂ treatment. The CO₂ treatment had least effect on the PP3 sample, presumably because it was processed at a temperature low enough for carbonates to be preserved.

Table II. Saturation Indexes Indicating Potential Controls on the Solubilities of Ca, Mg, F, and Mo in Aqueous Extracts of Oil Shales^a

solid phase	log K_{sp} ^c	saturation index ^b					
		PP3		Lurgi		PP6	
		BR ^d	AR ^e	BR ^d	AR ^e	BR ^d	AR ^e
CaSiO ₃ (wollastonite)	13.27			0.03	-3.34	-0.33	-2.52
CaCO ₃ (calcite)	-8.48	-0.32	0.33		0.28		0.08
Mg ₂ SiO ₄ (forsterite)	28.87					-0.17	-1.92
MgSiO ₃ (clinoenstatite)	11.42				0.01		-0.25
Mg ₃ Si ₄ O ₁₀ (OH) ₂ (talc)	22.26	0.44	0.17	0.14			
MgCO ₃ (magnesite)	-7.46		-0.29		0.85		-0.44
CaF ₂ (fluorite)	10.42	-0.09	-0.42	0.41	-1.84	-0.39	0.23
CaMoO ₄ (powellite)	-8.05	-2.13	-1.60	-0.32	-2.30	-0.85	-1.17

^a Mean of duplicate analyses. ^b log (IAP/ K_{sp}). ^c Values were taken from Reddy et al. (13) and Reddy and Drever (20). Values for calcite and powellite were taken from Plummer and Busenburg (21) and Essington (5), respectively. ^d Before CO₂ treatment. ^e After CO₂ treatment.

Potential solubility controls on Ca, Mg, F, and Mo in aqueous extracts from treated and untreated samples are presented in Table II. A complete list of saturation indexes for different solid phases are reported in Reddy et al. (14), and only the few solid phases relevant to the comparison of before and after CO₂ treatment are discussed here. Before CO₂ treatment, IAPs for the PP3 sample extracts show a close approach to saturation with respect to calcite and talc. These results suggest that concentrations of Ca²⁺ and Mg²⁺ in PP3 aqueous extracts are probably controlled by calcite and a magnesium silicate phase such as talc. The IAPs for Lurgi and PP6 samples show a close approach to saturation with respect to wollastonite. The IAPs also show a close approach to saturation with respect to forsterite (for PP6) and talc (for Lurgi). These results suggest that silicate phases formed during high-temperature processing are controlling the concentrations of Ca²⁺ and Mg²⁺ in aqueous extracts from untreated Lurgi and PP6 samples.

Park et al. (15), Reddy and Lindsay (22), and Reddy et al. (13) have reported that processing raw shale at elevated temperatures causes production of oxides (e.g., CaO, MgO) and several silicate phases including wollastonite and forsterite. The oxide phases are more soluble than silicate phases and often dissolve upon contact with moisture. The IAPs of oxide phases for untreated Lurgi and PP6 samples also indicated a high degree of undersaturation. Thus, silicate phases produced during the process of heating usually buffer the pH and control Ca²⁺ and Mg²⁺ concentrations. However, for the PP3 sample, which was produced by processing raw shale at moderate temperatures (to minimize decomposition of carbonates), calcite is probably buffering the pH and controlling the concentration of Ca²⁺ in aqueous extracts.

The CO₂ treatment effectively lowered the pH of OSSW aqueous extracts from 12.0 to ~9.0 (Table I). The IAPs for the PP3 samples show a close approach to saturation with respect to calcite. The IAPs for Lurgi and PP6 samples show a high degree of undersaturation with respect to wollastonite and a close approach to saturation with respect to calcite. These results suggest that CO₂ treatment caused dissolution of wollastonite (and probably other silicate phases), precipitation of calcite, and reduction of pH.

Several other studies have also reported a decrease in pH of OSSW aqueous extracts due to recarbonation. Bell and Berg (16) reported that exposing OSSW to the atmosphere over a period of 20–160 days lowered the pH of extracts from 11.4 to 9.0 by recarbonation. Harbert et al. (17) attributed the decrease in pH of OSSW aqueous extracts to the precipitation of calcite. Reddy et al. (3) reported that bubbling CO₂ through aqueous extracts of

OSSW for 6 months caused dissolution of silicate phases, precipitation of calcite, and reduction of pH from 12.0 to ~8.0. In our experiments, reacting moist OSSW under slightly elevated CO₂ pressures for 1 h accelerated the recarbonation process and lowered the pH through the precipitation of calcite.

The Mg²⁺ concentrations in aqueous extracts of OSSW after CO₂ treatment appeared to be controlled by either the silicate or carbonate phase, the IAPs show a close approach to saturation with respect to talc, clinoenstatite, and magnesite.

The CO₂ treatment caused a decrease in the concentration of F for PP3 and Lurgi extracts, but not for PP6. The CO₂ treatment also caused a decrease in the concentrations of Mo for PP3 and PP6 samples. Reddy et al. (3) reported that lowering the pH of OSSW causes reduction in the concentrations of F and, in some cases, Mo in extracts. Garland et al. (7) and Essington and Spackman (23) have reported similar results. Thus, the decrease in the concentrations of F and Mo in CO₂-treated samples is probably due to the reduction in the pH of extracts. The IAPs both before and after CO₂ treatment show a close approach to saturation with respect to fluorite (except Lurgi after treatment) and a high degree of undersaturation with respect to powellite (except Lurgi before treatment). These results suggest that fluorite may be controlling the solubility of F, and that powellite does not control the solubility of Mo in aqueous extracts from either treated or untreated samples.

Stollenwerk and Runnells (2), Reddy and Hasfurther (6), Essington et al. (18), and Essington and Spackman (19) have reported that fluorite and powellite probably control the solubilities of F and Mo in aqueous extracts of OSSW, respectively. However, our study and that of Essington (5) suggest powellite does not always control the solubility of Mo in OSSW extracts.

Conclusions

The processing of oil shale at high temperatures results in production of large quantities of oil shale solid wastes. These waste materials are often alkaline and often contain elevated levels of toxic elements. Before CO₂ treatment, the solubility measurements suggested that silicate phases including wollastonite and forsterite (produced during the heating process) buffer the pH and control Ca²⁺ and Mg²⁺ concentrations in aqueous extracts of OSSW. Reacting moist OSSW at 5 psi CO₂ pressure for 1 h lowered the pH from 12.0 to 9.0 through the precipitation of calcite and also decreased the concentrations of F and Mo in aqueous extracts. The Ca²⁺ concentrations in CO₂-treated samples were controlled by the solubility of calcite. The Mg²⁺ concentration appeared to be controlled by silicate and

carbonate phases. The F^- concentrations from treated and untreated samples suggested a close approach to saturation with respect to fluorite. The MoO_4^{2-} concentrations appeared to be highly undersaturated with respect to powellite.

The CO_2 pressure process described in this study involves treatment of waste materials in a solid phase containing moisture, not a slurry or an aqueous solution phase, and requires only short reaction times (e.g., 1 h) to effectively lower the pH and the solubilities of F and Mo. Since this process uses CO_2 , which can be obtained either from the combustion process itself or from other sources, another potential benefit is that it may help to minimize emission of CO_2 into the atmosphere. Further detailed research to examine the efficiency of the CO_2 pressure process for chemical stabilization of alkaline solid wastes (e.g., coal combustion solid waste) is needed.

Acknowledgments

We thank Steven P. Gloss for his suggestions on the original manuscript. We also thank Philip C. Singer, Associate Editor, and anonymous reviewers for their comments on the manuscript.

Registry No. Ca, 7440-70-2; Mg, 7439-95-4; Si, 7440-21-3; Mo, 7439-98-7; $CaSiO_3$, 13983-17-0; $CaCO_3$, 13397-26-7; Mg_2SiO_4 , 15118-03-3; $MgSiO_3$, 14654-06-9; $Mg_3Si_4O_{10}(OH)_2$, 14807-96-6; $MgCO_3$, 13717-00-5; CaF_2 , 14542-23-5; $CaMoO_4$, 14020-51-0; CO_2 , 124-38-9.

Literature Cited

- (1) Parker, H. W.; Betha, R. W.; Gruven, N.; Grazdor, M. N.; Watta, J. C. Interactions between groundwater and in-situ retorted oil shale. *2nd Pacific Engineering Congress Proceedings*; 1977; Vol. 1, pp 450-454.
- (2) Stollenwerk, K. G.; Runnells, D. D. *Environ. Sci. Technol.* **1981**, *15*, 1340-1346.
- (3) Reddy, K. J.; Lindsay, W. L.; Boyel, F. W.; Redente, E. F. *J. Environ. Qual.* **1986**, *15*, 129-133.
- (4) Stark, J. K.; Redente, E. F. *J. Environ. Qual.* **1986**, *15*, 282-288.
- (5) Essington, M. E. *Environ. Sci. Technol.* **1990**, *24*, 214-220.
- (6) Reddy, K. J.; Hasfurther, V. R. *Water Res.* **1989**, *23*, 833-836.

- (7) Garland, T. R.; Wildung, R. E.; Harbert, H. P. Influence of irrigation weathering reactions on the composition of percolates from retorted oil shale field lysimeters. *12th Oil Shale Symposium Proceedings*; Colorado School of Mines, Golden, CO, 1979; pp 52-93.
- (8) Fransway, D. F.; Wagenet, R. J. *J. Environ. Qual.* **1981**, *10*, 107-113.
- (9) Merriam, N. W.; Cha, C. Y.; Sullivan, S. U.S. Department of Energy Report DOE/FE/60177-2439, 1987.
- (10) Nowacki, P. *Oil Shale Technical Data Handbook*; Noyes Data Corp.: Park Ridge, NJ, 1981.
- (11) Reddy, K. J.; Lindsay, W. L.; Workman, S. M.; Drever, J. I. *Soil Sci. Soc. Am. J.* **1990**, *54*, 67-71.
- (12) Sposito, G.; Mattigod, S. V. *GEOCHEM: A computer program for the calculation of chemical equilibria in soil solutions and other natural water systems*; The Kearney Foundation of Soil Science; University of California: Riverside, CA, 1980.
- (13) Reddy, K. J.; Drever, J. I.; Hasfurther, V. R. U.S. Department of Energy, DE-FC21-86MC11076, 1988.
- (14) Reddy, K. J.; Drever, J. I.; Hasfurther, V. R. U.S. Department of Energy, DE-FC21-86M11076, 1990.
- (15) Park, W. C.; Lindemorris, A. E.; Tabb, G. A. *In Situ* **1979**, *3*, 353-381.
- (16) Bell, R. W.; Berg, W. A. *Agron. Abstr.* **1977**, 168.
- (17) Harbert, H. P., III.; Berg, W. A.; McWhorter, D. B. U.S. Environmental Protection Agency, EPA 600/7-79-188, 1979; p 26.
- (18) Essington, M. E.; Spackman, L. K.; Harbour, J. D.; Hartman, K. D.; U.S. Department of Energy, DE-FC21-86ME1111076, 1987.
- (19) Essington, M. E.; Spackman, L. K. U.S. Department of Energy, DOE/FE/60/77-2433, 1986.
- (20) Reddy, K. J.; Drever, J. I. U.S. Department of Energy, DOE/MC/11076-2443, 1987.
- (21) Plummer, L. N.; Busenburg, E. *Geochim. Cosmochim. Acta* **1982**, *46*, 1011-1040.
- (22) Reddy, K. J.; Lindsay, W. L. *J. Environ. Qual.* **1986**, *15*, 1-4.
- (23) Essington, M. E.; Spackman, L. K. U.S. Department of Energy, DE-FC21-86MC11076, 1988.

Received for review April 23, 1990. Revised manuscript received February 11, 1991. Accepted March 28, 1991. We express thanks to the United States Department of Energy for funding of this work through Western Research Institute Cooperative Agreement DE-FC21-86M11076.

Chemical Characterization and Source Apportionment of Individual Aerosol Particles over the North Sea and the English Channel Using Multivariate Techniques

Chris Xhoffer,* Paul Bernard, and René Van Grieken

Department of Chemistry, University of Antwerp (UIA), B-2610 Antwerp-Wilrijk, Belgium

Ludo Van der Auwera

Royal Meteorological Institute, Ringlaan 3, B-1180 Brussels, Belgium

■ More than 25 000 individual aerosol particles in 51 particulate matter samples, all taken from a research vessel over the North Sea and the English Channel, in a time range of 4 years, were analyzed by automated electron probe X-ray microanalysis (EPXMA). Multivariate methods were used to reduce the total data set. Single-particle analysis combined with hierarchical cluster analysis yields nine major particle types. The North Sea aerosol is predominantly composed of sea salt, sulfur-rich particles, silicates, and calcium sulfate particles. Their abundance is dependent on meteorological conditions and sample location. Differences between all samples were studied on the basis of the abundance variations by using principal component analysis. Three factors explain 91% of the total covariance between the samples. The first component represents the marine-derived aerosol fraction and is more important as wind speed increases or at more remote sampling locations. The second component differentiates anthropogenically derived CaSO_4 -rich samples. Their relative abundance is much more pronounced as the sampled air masses spend longer residence times over the south of England. The samples of the third cluster are related to high silicate and sulfur abundances. Source apportionment of this group was obtained by a second principal component analysis. Two different clusters separate mixed marine/continental samples from pure continental-derived silicate and sulfur-rich particulate samples.

Introduction

Since the North Sea is surrounded by the western and northern parts of the European continent and by Great Britain, it undergoes strong influences from industrial, agricultural, and domestic activities. On a long term, accumulation into the North Sea could change the chemical environment. Therefore, attempts are made to estimate the impact of the surrounding anthropogenic activities on the North Sea. The man-made pollutants can reach the North Sea by several pathways including river transport, direct discharges by pipelines, dumping activities, and atmospheric transport. The North Sea aerosol is a mixture of many components, some derived from the sea itself and some having descended from aloft.

Because of internal heterogeneity of the aerosol samples (i.e., the chemical diversity of the particles as a consequence of their different production mechanisms), individual particle analysis can advantageously be applied for the source identification of various atmospheric pollution processes. The relative percentage abundance of the specific particle types can be a measure for the source strength. Besides source apportionment, microanalysis can also be useful for the investigation of the behavior of particles during transport (e.g., gas-to-particle conversion, coagulation processes, etc.). A reduced sampling time and the small amount of material needed for individual mi-

croanalysis can be advantages in the study of different dynamic processes.

Experimental Procedure

Samples and Sample Preparation. A total of 51 aerosol samples were collected over the North Sea and English Channel during various cruises in a time range of 4 years (1984-1987) aboard the R/V *Belgica*. Atmospheric aerosols were sampled on 47-mm-diameter Nuclepore filters with a pore size of 0.4 μm . The filtration units are provided with a hat-type inlet to avoid the collection of large droplets and rain. The whole is mounted in the mast on the foredeck of the ship, 6 m above deck, 11 m above the sea surface, and facing 0.5 m upwind from the mast itself. When the relative wind direction to the ship is unfavorable, or not within $+45$ to -45° , the power supply of the pump is cut off in order to avoid contamination by the vessel. Figure 1 shows different tracks for the various cruises. Comparison of the particle sizes for samples simultaneously collected with and without the hat-type inlet showed no differences in size range below 15 μm (1).

Depending on weather conditions and sampling area, the sampling time was ~ 8 h in order to collect 5-10 m^3 of air. For sampling sites near coastal regions, smaller sampling volumes are needed compared to "off-shore" locations. In contrast, higher sampling volumes are necessary during or after rain events because of reduced particle number concentration in the air by "rain-out" effects. To reduce chemical changes as well as compositional and morphological transformations of the atmospheric aerosol, each filter was immediately put between Petri dishes and stored in a refrigerator. A part of the Nuclepore filter was mounted on a plastic ring that fit into the electron microprobe sample holder. All samples were coated with a thin carbon layer of approximately 40 nm to improve electrical conductivity.

Instrumentation. Single-particle analysis was performed by electron probe X-ray microanalysis (EPXMA) using a JXA-733 superprobe of JEOL (Tokyo, Japan). This superprobe is equipped with energy- and wavelength-dispersive X-ray spectrometers, a secondary and transmission electron detector, and two simultaneously operating backscattered electron detectors (for topographic and compositional imaging). The probe is automated with a Tracor Northern TN 2000 system and an LSI 11/23 microcomputer controlling all EPXMA parameters. The obtained data can be stored either on magnetic tape or on double-density floppy discs. All information can, at any time, be transferred to a VAX 11/780 computer for additional off-line data processing.

Automation Methodology. During the execution of the automated particle recognition and characterization (PRC) program, the electron beam scans over a preset area of interest. When the backscattered electron intensity of

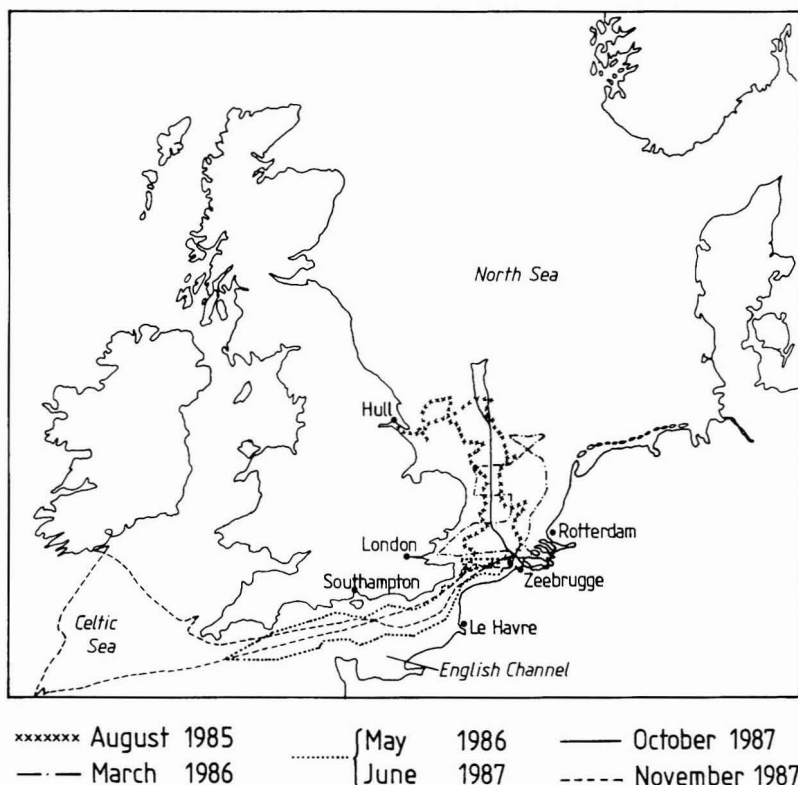


Figure 1. Different sampling routes on the North Sea, English Channel, and Celtic Sea.

the particle contour exceeds a predefined threshold value, the object is considered detected. Size parameters such as the perimeter, average diameter, and shape factor $[(\text{perimeter})^2/4\pi \text{ area}]$ are calculated. The diameter measured by EPXMA is based on the projected area of the particle and might differ from the aerodynamic diameter. An X-ray spectrum can be accumulated at the center of the particle or by performing cross scans over the particle. Subsequently an X-ray spectrum is calculated and deconvoluted. Thus, the whole PRC program is set up in three sequential steps: localizing, sizing, and chemical characterization, after which the beam scans for the next particle.

For each aerosol sample, ~500 particles in a size range from 0.2 to 15 μm were automatically analyzed. X-ray spectra were accumulated for 15 s with a beam current of 1 nA and an acceleration voltage of 20 kV. This whole operation takes less than 3 h per sample and yields a huge data set. To reduce the data, two hierarchical and one nonhierarchical cluster analysis were applied for each sampling campaign (2). First a hierarchical cluster analysis performed on the elemental composition data of 500 particles resulted in an average composition data set. For this, every particle i is presented in a N -dimensional space as an object vector with coordinates according to its N -elemental composition. Here N is the number of variables and equals the number of different elements detected in one sample. The method starts from m objects ($m = 500$ particles) that are to be classified, and at each step the two most similar objects (particles) or already formed clusters are merged into a single cluster. The similarity between two objects was derived from the Euclidian distance coefficient between the objects. The Ward method (error

sum of squares method) was used for the calculation of the distances between newly formed clusters and the remaining objects and/or clusters. So, the more close two objects or clusters are, the more similar they are. A second hierarchical clustering was performed on the average composition data of the samples and resulted in a set of training vectors (centroids) that are representative for that sampling campaign. Finally, a nearest centroid sorting (non-hierarchical cluster analysis) is used to classify all particles from one campaign according to their distance from the centroids of the clusters. The method of Forgy (3) minimizes the sum of squares of the distances to the centroids for a fixed number of clusters. This procedure results in an average composition data set for each North Sea sample according to the centroids of the corresponding campaign.

The whole particle classification procedure involves thus a series of cluster analyses and is followed by a principal component analysis (PCA). The purpose of the PCA method is to represent the variations present in the data in such a way that, without losing significant information, the dimensionality is reduced. To achieve this, new variables (components) are constructed, according to a linear combination of the original variables, in such a way that the newly formed principal components are uncorrelated and that they are constructed with decreasing degree of importance. The principal components obtained in this way represent the linear independent variance present in the data of original variables. The most important sources for the variance in the data are examined by studying the first principal components. General information about the PCA technique can be found elsewhere (4). Several papers discuss expert systems to sort out individual particle data (2, 5–8).

Table I. Range for the Particle Identification Bases on the Mean Percent Abundance for Each Cluster Group

particle type	criteria: based on relative X-ray intensities		
sea salt	Cl > 75%	7% < Na < 10%	
aged sea salt	24% < S < 44%	38% < Cl < 60%	
sulfur-rich	S > 71%		
calcium sulfate	23% < Ca < 45%	46% < S < 60%	
calcium-rich	12% < Ca < 90%	5% < P < 58%	S < 16%
aluminosilicates	17% < Al < 30%	50% < Si < 62%	4% < Fe < 8%
quartz	88% < Si < 91%		
titanium-rich	72% < Ti < 82%		
iron-rich	72% < Fe < 91%		

The accuracy for the X-ray measurements is close to 1% for abundant elements. The reliability (2σ values) of the relative abundances of the particle types can be calculated from binomial statistics and is between 2 and 5% absolute when 500 particles are measured. It has been shown (9) that the variability on the composition of the clusters is almost entirely due to the variation in the particles' composition and is therefore a reliable measure for the heterogeneity of the clusters. The accuracy of particle sizing depends mainly on two different factors: (a) threshold setting of the backscattered image signal and (b) the magnification used. Accuracies within 20% are obtained (10). The reproducibility for particle sizing using the backscattered electron image is within 6% for the mean diameter.

Results and Discussion

Conventional X-ray microanalysis makes it possible to detect elements from $Z \geq 11$. The measured X-ray output data consist of relative peak intensities obtained by a fast filter algorithm (FFA), namely, a symmetrical convolution function by the Hardeman transformation (11). The relative percent X-ray intensity expresses the ratio of the net X-ray intensity of that element to the total net X-ray intensities collected from that particle. This information is important for chemical intercomparison of particles and can thus be used for the assignment of particles to various particle types. The hierarchical clustering procedure applied to the elemental composition of more than 25 000 particles collected from different parts over the North Sea, the English Channel, and the Celtic Sea resulted in the identification of nine major relevant particle types. Some low-abundance particle types were encountered; although their abundance cannot be determined with high accuracy, their occurrence in the aerosol can be important with regard to the deposition and source apportionment of some specific trace elements. The characteristics of these minor particle types will be discussed separately. Table I gives an overview of the nine major particle types with the range of the average composition of the groups for each sampling campaign. These data give an idea of the criteria by which a particle was assigned to a specific particle type by hierarchical cluster analysis. Note that the relative X-ray intensity of Na in NaCl is much lower than that of Cl. Indeed, Na has much lower sensitivity due to physical effects and because the absorption effects of the X-ray signal by the detector window are more important for Na than for Cl. Typical relative percent X-ray ratios of $1/12 \leq \text{Na/Cl} \leq 1/8$ are observed.

Relative abundances or particle number concentrations (expressed in percent) of each particle type for every individual sample are given in Table II. The standard deviations of the relative abundances are given by binomial

statistics. For the individual EPXMA measurements, where a total of 500 particles were analyzed, the standard deviations are between 1 and 5% on a 95% confidence interval.

The number concentration of particles present in 1 m^3 marine air can be derived from the number of particles analyzed, multiplying these with the ratio of the filter area to the analyzed area. Table III tabulates the range of number concentrations of particles between 0.2 and $15 \mu\text{m}$ above the North Sea calculated for the 51 samples analyzed. Accuracies were estimated to be $\sim 10\%$ as based on uncertainties in analyzed filter area and sampled air volume. The findings of these data are in good agreement with aircraft measurements performed over the North Sea at sea level (12). There is clearly a tendency of increasing particle number concentration as the sampled air masses originate from over the continent. Knowing the total number concentrations of aerosol particles above the North Sea, the percent abundance of each particle type, the assumed density for each particle class, and the mean equivalent spherical diameter of each particle belonging to that particle class, one can calculate the mass concentrations for each particle type. However, the accuracy for mass concentrations is worse than 60% and is highly dependent on the accuracy for the diameter determination.

The nature, source and relative abundance variations for each particle type will subsequently be discussed in more detail.

Different Particle Types. (1) Sea-Salt Particles.

A particle type is defined as sea salt when the average content of Cl exceeds 75% in relative X-ray intensity. No other element, except Na, is of any significance. It is postulated that the total contribution of freshly generated NaCl present in the marine atmosphere is attributed to a marine source. The main process for the generation of fresh sea salt into the atmosphere is the breaking of waves. This process is more effective as the wind speed increases (13).

Very large variations in number concentrations for sea-salt aerosols are found ranging from 0 to 94% of the total number fraction. High sea-salt abundances were found in the August campaign of 1985 when samples were taken under stormy southwest winds: whitecap formation and sea spray induced by wind action are predominantly responsible for the ejection of sea salt into the atmosphere. The anthropogenic particle fraction is not necessarily low but is totally suppressed by the domination of sea salt. Contrarily, for the cruise of May 1986, the air mass trajectory went through the Channel, via the south coast of England, until the influence of the Atlantic Ocean was clearly observed. Nearing more westerly regions is reflected by an increase in sea-salt concentrations. Back-trajectories of the sampled air evolved from far over the Atlantic Ocean without continental interferences. No anthropogenically derived particulate matter was detected.

(2) Transformed or Aged Sea-Salt Particles.

This particle type is rich in S and Cl. Also mixtures of NaNO_3 , Na_2SO_4 , and NaCl are possible (14). These S- and Cl-rich particles are identified as aged sea salt. They are formed by the conversion of NaCl into Na_2SO_4 by SO_2 , implying the release of HCl in the marine atmosphere. These results are consistent with the findings of other authors (15-18).

The contribution of S enrichment in sea-salt aerosols is more pronounced in the samples for which an important anthropogenic influence on the marine atmosphere is expected. The mixing of air masses is always observed on passing from continental conditions toward more marine ones or vice versa. This was clearly observed for the

Table II. Relative Percent Abundances of Nine Particle Types for 51 North Sea Samples

date	sea salt	aged sea salt	S-rich	CaSO ₄	Ca-rich	alumino- silicates	Si-rich	Ti-rich	Fe-rich
Dec 84	0	2	19	0	20	47	4	0	8
	63	10	4	0	9	3	0	0	10
	33	7	7	0	7	36	4	0	5
	0	0	35	0	15	12	2	0	36
Aug 85	77	0	2	11	0	6	4	0	1
	26	0	3	9	1	50	5	1	6
	8	0	2	8	0	71	8	0	3
	0	0	5	5	0	74	7	1	7
	0	0	33	21	0	6	9	1	30
	0	0	11	48	2	14	8	0	18
	0	0	61	0	0	18	10	0	12
Mar 86	0	0	32	4	0	42	11	0	11
	0	0	67	3	0	14	5	0	11
	0	0	61	3	0	21	8	0	7
	1	0	24	12	0	27	8	0	29
May 86	18	0	53	5	10	5	5	1	5
	20	20	35	3	10	6	3	0	3
	60	27	0	3	2	7	0	0	0
	52	40	0	2	5	1	1	0	0
	68	17	3	2	9	0	0	0	0
	84	8	4	1	3	0	0	0	0
	91	6	2	0	1	0	0	0	0
	77	4	4	5	7	2	2	0	1
	94	5	0	0	1	0	0	0	0
	91	9	0	0	1	0	0	0	0
	83	14	0	0	2	1	1	0	0
	90	4	0	2	2	2	1	0	0
	77	12	1	2	5	3	0	0	0
	56	26	7	4	8	0	0	0	1
	11	11	32	18	7	18	2	0	1
	2	0	38	9	1	32	5	5	8
	0	0	13	82	0	4	1	0	0
	0	0	69	17	0	6	2	2	4
	0	0	12	5	0	59	21	1	3
June 87	0	0	19	72	0	4	4	0	0
	0	0	2	94	0	2	0	0	1
	1	0	33	50	0	9	7	0	1
	0	0	21	68	0	3	7	0	1
	0	0	4	84	0	10	2	0	0
	0	0	85	6	0	3	6	0	0
	0	0	32	13	0	36	17	0	2
	3	2	21	37	0	30	0	0	7
	2	36	8	8	0	46	0	0	1
	1	42	6	3	0	47	0	0	1
	1	4	41	14	0	39	0	0	0
	0	1	43	17	0	24	0	4	10
Nov 87	0	1	38	9	0	11	0	37	4
	1	0	60	19	0	8	0	9	3
	0	0	50	13	0	24	0	8	5
	0	0	56	8	0	6	0	27	2
	0	0	35	20	0	22	0	19	4
	(diam), μm	0.8	0.7	0.8	0.8	1.3	1.3	1.0	0.8

Table III. Particle Number Concentrations (m^{-3}) Observed for Three Types of Sampled Air Masses above the North Sea

air mass type	range	mean
marine	$(7.9 \pm 0.2) \times 10^3$ – $(6.9 \pm 0.7) \times 10^4$	$(3.9 \pm 0.4) \times 10^4$
mixed	$(2.9 \pm 0.3) \times 10^4$ – $(4.7 \pm 0.7) \times 10^5$	$(2.5 \pm 0.5) \times 10^5$
continental	$(8.7 \pm 0.9) \times 10^5$ – $(2.9 \pm 0.6) \times 10^6$	$(1.9 \pm 0.7) \times 10^6$

campaign of May 1986. The corresponding back-trajectory (Figure 2) shows originally marine air traveling over the southern part of England.

(3) Sulfur-Rich Particles. In general, the S concentration is greater than 70% for this particle type, and no associations with Ca are present. Studies on particulate S present in urban sites showed that numerous secondary reactions can take place (19, 20). Industrial SO₂ gas emissions are oxidized in homogeneous or heterogeneous

reactions and form SO₄²⁻. Anthropogenic emissions like combustion of fossil fuel constitute the main source for the SO₄²⁻ release into the atmosphere. Often NH₄⁺ is present in continental aerosols in concentrations high enough for partial or complete neutralization of H₂SO₄ with the formation of various ammonium salts as (NH₄)₂SO₄, (NH₄)-HSO₄, and (NH₄)₃H(SO₄)₂ (21). Similar particles were found in the Phoenix urban aerosol (22), where the only detectable element was S. Here, several of these Phoenix S-bearing particles were detected, indicating that the cores are soot. It was also observed (23) that biological particles (composed of light elements, such as H, C, O, and N) with their complex morphology and wet surfaces provide an attractive nucleating surface for SO₂ absorption and conversion to sulfate. In analogy to the North Sea aerosol, probably S-rich compounds have condensed onto or reacted with existing carbonaceous particles that have acted as condensation nuclei. The shape of the spectrum with its very high background is typical for organic and bio-



Figure 2. Air mass back-trajectory for aerosols collected during the May 1986 campaign. The shaded area corresponds to ca. 36-h air mass back-trajectories calculated for a height of 10 m above the North Sea. The air masses have traveled from point A toward B.

logical material, although carbon X-rays cannot readily be detected with conventional EDX analysis (23). However, X-ray spectra can distinguish between carbonaceous particles and, e.g., crustal particles, whereas morphology studies often differentiate botanical particles from soot (24). Signals from organic particulate matter can exceed the backscattered electron image threshold above the Nuclepore filter necessary for the localization of particles. The image signals from the filter backing material are normally completely suppressed by this threshold setting. So, if a localized and detected particle is composed almost entirely of elements lighter than Na, the organic nature can be ascertained from the relatively noisy background in its collected X-ray spectrum (25, 23). However, one must keep in mind that the total X-ray counts are still much lower than what is observed for, e.g., mineral particles.

Carbonaceous particles enriched in $(\text{NH}_4)\text{HSO}_4$ and $(\text{NH}_4)_2\text{SO}_4$ or mixtures at their surface are present over the North Sea as was also inferred from laser microprobe mass analysis (LAMMA) results (14). Most of these S-rich particles have a diameter in the submicrometer range. This might be an indication that they are formed by gas-to-particle conversion processes. Combustion processes are almost exclusively responsible for the high pollution gaseous sulfur compounds, although a smaller fraction can have a marine origin, as is the case for dimethyl sulfoxide (DMSO) and derived compounds. For the most westerly located sampling place of the May 1986 campaign, where only pure marine conditions were encountered, low concentrations of marine S-bearing compounds were detected.

The S-rich particulate matter was the most important particle type encountered in the sampling campaigns of March 1986 and November 1987. In March 1986, the atmosphere above the North Sea had been influenced by a long period of easterly wind and at the time of sampling the sea surface was smooth and the visibility strongly reduced due to a persistent fog. The particle concentration was very high, because of the presence of an inversion layer. The 36-h air mass back-trajectories (Figure 3) showed a steady supply of continental air traveling over West Germany, The Netherlands, and Belgium. For the November 1987 cruise, no fog and inversion conditions

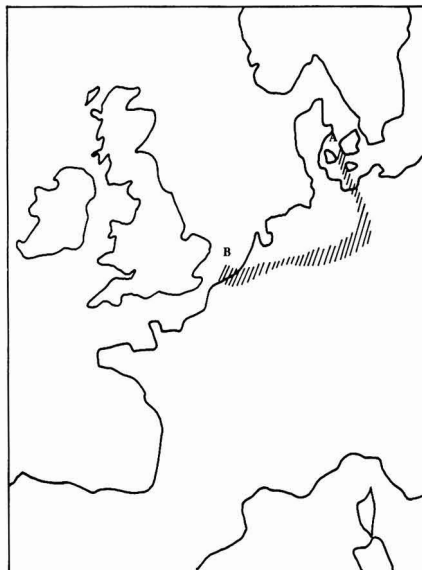


Figure 3. Air mass back-trajectory for aerosols collected during the March 1986 campaign.

were observed. All filters have collected air masses originating from above Eastern European countries. Comparable S concentrations were found in the June 1987 campaign, although the air masses had long residence times above the south of England. Consequently, high S emissions must be related to industrial and automotive sources from all over Europe.

(4) Calcium Sulfate Particles. Both Ca and S are present in the same particles, with their elemental composition ranges given in Table I. These particles are very often found in both marine and continental aerosols. They are identified as CaSO_4 . Some possible marine formation mechanisms are postulated (27), e.g.: (1) CaSO_4 can be produced by fractional crystallization of marine aerosols, a process that is especially efficient with high relative humidity. Possibly breakup of the CaSO_4 crystal from the sea-salt aerosol particle takes place either by impaction on the filter or during its atmospheric residence. (2) CaSO_4 could result from the aerosol interaction between marine or airborne CaCO_3 with atmospheric SO_2 or H_2SO_4 , e.g., within clouds.

The abundance of CaSO_4 particles under purely marine conditions (May 1986) does not vary proportionally with sea salt. Furthermore, in the samples with highest CaSO_4 contributions, NaCl is virtually absent. Actually much higher abundances are present in the samples influenced by the continent (June 1987). The March 1986 and June 1987 campaigns were both characterized by high S-rich and Ca-rich particle number concentrations. For the reaction of particles with SO_2 and/or SO_4^{2-} , particles need to have the appropriate surface chemistry (in this aspect, calcite scores better than clay minerals and much better than silicates) and long suspension times in the air (23). Such sampling conditions, high humidity, persistent fog, and an inversion layer, were observed for the March 1986 sampling campaign, favoring such transformation reactions. It is, however, not evident that in the June 1987 campaign acid transformation reactions between CaCO_3 (may partly be derived from the cliffs of Dover) and SO_2 or SO_4^{2-} components are dominant for the formation of CaSO_4 particles. If such reactions would have taken place, it implies that

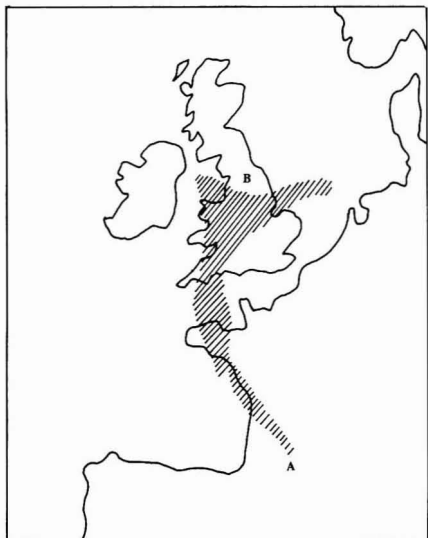


Figure 4. Air mass back-trajectory for aerosols collected during the October 1987 campaign.

all CaCO_3 particles had been fully transformed. Indeed, in the June samples with exceptionally high number concentrations of CaSO_4 , the Ca-rich (CaCO_3) particle type, which is the obvious precursor for CaSO_4 , was not observed at all. This means that CaSO_4 is predominantly emitted by anthropogenic sources such as combustion processes and by eolian transport from the continent to the North Sea. CaSO_4 has also been found in the fly ash particles collected from coal power plants (28). It is remarkable that all CaSO_4 -rich filters were influenced by continental air masses traveling over the south of England (June 1987 and October 1987) (Figure 4). In some particular samples, the relative intensity of S is much higher than what is normally measured for CaSO_4 . Hence, this particle type can partly be identified as CaSO_4 enriched with S, in the form of, e.g., $(\text{NH}_4)_2\text{SO}_4$. The formation of $\text{CaSO}_4(\text{NH}_4)_2\text{SO}_4$ aerosols can be explained by the coagulation of CaSO_4 particles with submicrometer sulfate aerosols (19). These results were confirmed by LAMMA measurements (14).

(5) Calcium-Rich Particles. For the Ca-rich particle type, we can only postulate that they are mainly characterized as CaCO_3 although C and O cannot be detected by our method.

All Ca-rich aerosols that contain less than 16% S are classified in this group. They can originate both from the marine environment and from continental sources.

As seawater evaporates, various dissolved salts begin to crystallize out sequentially. First calcite (CaCO_3) and dolomite [$\text{CaMg}(\text{CO}_3)_2$] precipitate, then gypsum [$\text{CaSO}_4(\text{aq})$], followed by halite (NaCl), and finally the Mg salts (29). If this crystallization effect takes place in an aerosol droplet, CaSO_4 as well as other salts (e.g., the remaining residues) would be detected on the filter. Only Ca-rich particles, CaSO_4 , and NaCl were identified. Mg was detected in low abundances, never as the major cation in individual particles. Mg is mostly associated with Ca-rich or Ca-S-rich particles. Probably also the mixed salt [$\text{CaMg}(\text{CO}_3)_2$] can undergo further reaction with gaseous S-rich components. A small fraction of Ca-rich particles show up to 15% S in the relative X-ray spectrum but are not classified in the CaSO_4 group according to the criteria of Table I. This can be an indication of the initiation of Ca-S-rich particle formation from CaCO_3 and/or derived

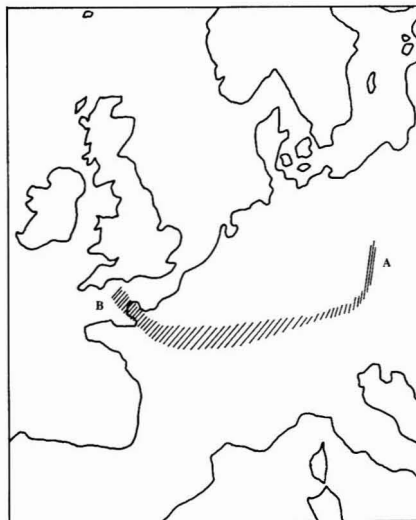


Figure 5. Air mass back-trajectory for aerosols collected during the November 1987 campaign.

components with atmospheric SO_2 or H_2SO_4 . According to the obtained data set, Ca-rich particles above the North Sea cannot unambiguously be apportioned to one source type.

(6) Aluminosilicate-Rich Particles. These particles are characterized by the presence of Al, Si, S, K, Ca, and Fe as major elements and Ti, Cr, Mn, Ni, and Zn as minor ones. This mineral type of particle finds its origin on the continent. X-ray spectra cannot distinguish whether these particles are soil dust or fly ash derived. Only morphology can sometimes differentiate their source. The soil dust particles have variable shapes and diameters ranging from submicrometer to $\sim 5 \mu\text{m}$. However, sometimes 40% or more of all aluminosilicates have a smooth and nearly perfect spherical shape. This is especially true for the November 1987 cruise, when the sampled air masses were influenced by Eastern European emissions (Figure 5). Hence, these particles must be fly ash derived. They are formed during high-temperature combustion processes of fossil fuel and obtain their typical shape after solidification of the molten material. Smaller fly ash contributions are also observed during air mass trajectories over England and western Europe. In $\sim 5\%$ of all aluminosilicates, a rather high S concentration was present in the aerosol during the March 1986 campaign. Because meteorological conditions favored high continental influences over marine ones, anthropogenic S from SO_2 emissions is very likely to be responsible for secondary reactions. H_2SO_4 derived from SO_2 emissions can have long residence times during calm weather conditions at high relative humidities. During long fog periods, high humidity, and inversion layer conditions, mineral particles that were initially hydrophobic can most probably be wetted with acidified water droplets and are left behind as possible cloud condensation nuclei (CCN) for further reactions (27). These CCN can in an initial state be composed of an aluminosilicate nucleus covered by a S-rich surface coating. But further transformation of element-specific extraction processes are also possible. Such reactions are responsible for the further breakdown of silicate mineral particles, forming silicon-rich clusters.

(7) Silicon-Rich Particles. In the Si-rich group, the Si-K X-rays constitute more than 88% of the character-

istic X-ray spectrum. These mineral quartz particles are irregularly shaped. They can be derived from soil dust and therefore are often found in the presence of aluminosilicates. Another fraction of the quartz particles are emitted during the combustion of coal in power plants (30, 31). Most of the Si-rich particles are present in the size range below 1 μm . The fact that these particles, just as the Fe-rich particles, are found in the smallest size range could strengthen the hypothesis that they are formed during combustion processes.

(8) Titanium-Rich Particles. For some North Sea samples (November 1987), rather high abundances of Ti-rich particles were observed. The mean relative X-ray intensity for Ti ranges between 65 and 85%.

The mean diameter of the Ti-rich particles is 1.0 μm and the shape factor of 3 deviates far from 1 for spherical particles. The main source for Ti release into the atmosphere is pigment spray, but minor pollution processes and sources such as soil dispersion, asphalt production, and coal-fired boilers and power plants are also known (6). Sometimes chromium is detected in this particle group beside some contributions of Si, Zn, Pb, and Ba.

(9) Iron-Rich Particles. The samples taken near the continents show high contributions of Fe-rich particles. Within this cluster, three different Fe-rich particle types are recognized. The first subgroup consists of pure iron oxide. Most of these particles are spherical, but irregularly shaped particles are found as well. They are mainly produced by ferrous metallurgy processes. The second subgroup consists of Fe-Zn-Mn-rich particles. Within this group, the abundances for Zn and Mn are much more pronounced. They are derived from ferrous manganese furnace processes. Very often S is associated with Fe-rich particles: the Fe-S-rich particles constitute the third subgroup. These particles, probably pyrite and iron sulfate, can be formed by reaction between iron oxide and sulfuric acid, during their release in ferrous metallurgy related combustion processes.

(10) Minor Particle Type. Rare particles are also interesting because they can sometimes be apportioned unambiguously to one specific source.

Characteristic X-ray spectra showed that some S-bearing aerosols have P and Cl as detectable elements. Also, a very high X-ray background is often observed originating from an organic matrix. Organic phosphorus is primarily formed through biological activities. Bubble bursting can cause enrichments of P in the sea-salt aerosol particles by fractionation out of the sea surface microlayer (32). When these P-rich particles mix with anthropogenic air masses, the S components can also react with these sea-salt particles forming aged sea salt enriched in P. The major sources for particulate P in marine aerosols of New Zealand (33) are soil particles containing both naturally occurring and fertilizer-derived P, as well as sea-salt particles and industrial emissions. Na, Al, and V were associated with P as indicators or markers for, respectively, a marine source, a crustal weathering source, and an anthropogenic pollution source (e.g., burning of biological material). For the North Sea samples, no association between P and Al or V was detected and hence these particles probably have a marine origin.

Alternatively, the presence of P is often associated with Ca. These particles are classified into the Ca-rich group, although their percent abundance of relative X-ray intensities from Ca and P are, respectively, 13 and 55%. This particulate matter can be fertilizer derived or is a residual from biological material (e.g., pollen) and can be transported over the North Sea by wind action. Ca- and

Table IV. Cumulative Eigenvalues and the Loadings for the First Three Principal Components Derived from the Covariance Matrix for Two PCA Performed on the North Sea Data

	principal components					
	for all samples (51)			for the third cluster (29)		
	1	2	3	1	2	3
cum %	54	75	91	61	80	88
variables	loadings					
sea salt	0.99	0.01	-0.09			
aged sea salt	0.42	-0.10	0.22			
marine fraction				-0.50	0.86	-0.10
sulfur	-0.66	-0.40	-0.62	0.97	-0.04	-0.21
calcium sulfate	-0.41	0.91	-0.01	0.25	-0.13	0.06
calcium-rich	0.24	-0.19	0.00	-0.08	0.29	0.39
aluminosilicates	-0.41	-0.39	0.80	-0.90	-0.37	-0.22
quartz	-0.39	-0.18	0.26	-0.21	-0.46	0.01
titanium-rich	-0.23	-0.14	-0.23	0.29	-0.06	0.02
iron-rich	-0.33	-0.21	0.00	0.11	-0.22	0.90

P-rich particles were also found in aerosol samples taken above the equatorial Pacific Ocean where only marine influences were expected (31). The relative X-ray intensities of 60% for Ca and 30% for P, compared to what we found here, suggest indeed an other, still unidentified source.

For some samples, higher abundances of heavier elements like Pb and Br together with Cl were detected. These Pb-rich particles originate from automobile exhaust emissions. Pb is added to the gasoline together with ethylene dihalide compounds (Br, Cl). Pb/Cl/Br compounds can be identified as $2\text{PbBrCl}\cdot\text{NH}_4\text{Cl}$ (34). The emitted lead halides can readily be converted to lead sulfates by reaction with SO_2 , H_2SO_4 , or $(\text{NH}_4)_2\text{SO}_4$ with the loss of HBr (35). However, none of the transformed lead halide particles were observed in spite of the very high S concentrations present in the sampled air masses.

Principal Component Analysis

To study variations in the abundance data set, principal component analysis (PCA) was applied using a software package, the so-called Data Processing Program (DPP) (36). We used the relative percent abundances of nine particle types (nine variables) for 51 North Sea samples from Table II as input data for the PCA. The covariance matrix was used for the calculation of the principal components. The first three principal components explain 91% of the total variance present in the original data set. The loadings of the first three principal components, listed in Table IV, are plotted in Figure 6a, while the scores are represented in Figure 6b. Three main clusters are recognized. The first group with a high score on the first principal component contains 14 samples with high abundances of sea salt and aged sea salt. A second cluster of eight samples is separated by the second principal component. The samples in this cluster are characterized by high CaSO_4 abundances. Because of the low negative score on the first principal component, the emission of CaSO_4 particles has to be related to continental anthropogenic sources. The third cluster of 29 samples is elongated in the direction of the first and third principal components. The third component is related to high sulfur and aluminosilicate abundance variations. To validate the robustness of these identified clusters, a hierarchical cluster analysis (Ward's method, unstandardized variables) was performed on the data. When the result was studied at a three-cluster level, exactly the same clusters were found.

Table V. Mean Relative Percent Abundances of Each Particle Type Calculated for the Four Clusters That Were Formed by Principal Component Analysis

type	no.	sea salt	aged sea salt	S-rich	CaSO ₄	Ca-rich	alumino-silicate	Si-rich	Ti	Fe	MF ^a
marine	14	76	13	2	2	4	2	1		1	100
CaSO ₄	8	1		16	67		9	4		4	1
mixed	7	16	17	21	7	5	30	3		3	37
S/silic	22	1		41	9	2	27	6	5	9	1
mean	51	23	6	23	16	3	18	4	2	5	33

^aMF, marine fraction.

The third group, however, cannot be attributed unambiguously to a specific source. Therefore, further separation within this group is necessary to differentiate marine influences from continental ones.

A second PCA was applied to these 29 samples. To enhance the difference between marine and continental aerosols, a new variable, the marine fraction (%) was introduced, replacing the sea-salt and aged sea-salt variables. The marine fraction was defined as

$$\text{marine fraction (\%)} = \frac{\langle \text{ss} + \text{aged ss} \rangle}{\langle \text{ss} + \text{aged ss} \rangle_{\text{marine cluster}}} \times 100$$

ss and aged ss represent the abundance of, respectively, the sea-salt and aged sea-salt particle type for each sample, and $\langle \text{ss} + \text{aged ss} \rangle_{\text{marine cluster}}$ is the mean of the sum of the sea-salt and aged sea-salt particle-type abundances for the marine cluster. The calculated value for the latter was 89%.

The loadings of the resulting first three principal components, listed in the three columns at the right side of Table IV, are plotted in Figure 7a and the scores are represented in Figure 7b. This figure shows two distinct clusters. One of them, with high score on the second principal component, consists of seven samples, and all have a high marine fraction (mean marine fraction of 37%). This means that these analyzed particles originate from mixed marine/continental air masses. The other identified cluster contains nearly 100% continent-derived particles (22 samples), e.g., mean marine fraction of 1%. Variations in this group are mainly due to a different silicate/sulfur ratio. Principal component 1 describes this and even a negative linear relationship between the silicate and sulfur is present ($r = -0.82$). The determination of the silicate/sulfur ratio reflects the contribution ratio of their respective emission sources. The mixing ratio combined with bulk trace metal analysis can probably be used to determine the trace metal content of the distinct emission sources. Besides the relative importance of the silicate and sulfur particulate sources, iron particulate source contributions are superimposed (principal component 3). In the mixed marine/continental group, the same dependency on the silicate/sulfur ratio is found.

Table V summarizes the relative particle abundances for each of the four cluster groups as well as the mean abundance for all particles analyzed. Also the marine fraction is calculated and listed. Note that the marine fraction obtained for the mixed continental/marine sample group has a value of 37%, whereas the mean marine fraction for all samples is 33%. This suggests that the mean of all samples taken during the six campaigns is also representative for mixed sampling conditions.

Conclusions

The aerosol concentrations near sea level vary greatly depending on proximity to natural and man-made sources. From the data set resulting from 25 000 individual particle

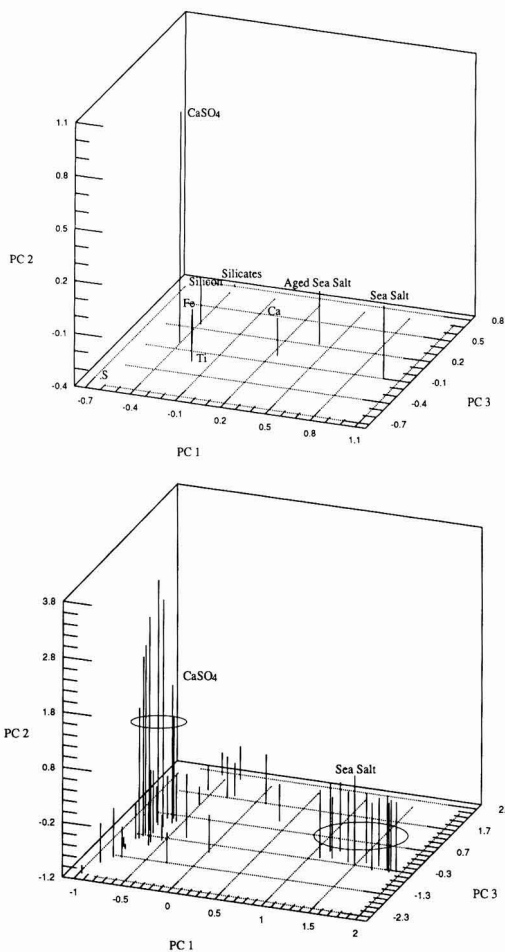


Figure 6. (a, top) Loadings of the first three principal components (51 samples), obtained by PCA of EPXMA of North Sea aerosol results. (b, bottom) Component scores of the first three principal components (51 samples), obtained by PCA of EPXMA of North Sea aerosol results.

analyses of 51 North Sea aerosol samples, four different aerosol groups could be differentiated on the basis of their composition. These groups were apportioned according to distinct particle emission sources.

More than 21% of all particles detected above the North Sea and surrounding waters represent sea-salt particles. Within this group, the marine contributions for S-rich, CaSO₄, and Ca-rich particles were estimated to be 0.5, 0.6, and 1.1%, respectively. Anthropogenic-derived S-rich particles and aluminosilicates represent 21 and 16%, respectively, of the aerosol composition, whereas industrial-derived CaSO₄ contributes almost 15% of all particles

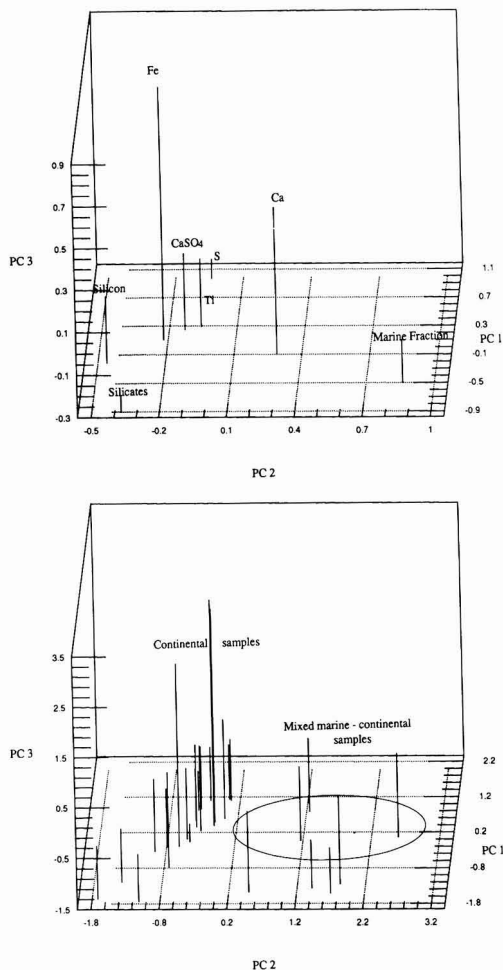


Figure 7. (a, top) Loadings of the first three principal components, obtained by a second PCA on the third cluster (29 samples) resulting from the first PCA. (b, bottom) Component scores of the first three principal components, obtained by second PCA on the third cluster (29 samples) resulting from the first PCA.

analyzed. About 13% of all North Sea particles is a mixture of particles from both marine/natural and continental/anthropogenic emission sources. For all other particle types detected, their contribution is less than 5% of the total North Sea aerosol and they are derived from various emission sources.

Registry No. S, 7704-34-9; CaSO_4 , 7778-18-9; Ca, 7440-70-2; Si, 7440-21-3; Ti, 7440-32-6; Fe, 7439-89-6; quartz, 14808-60-7.

Literature Cited

- Otten, Ph., private communications, 1986.
- Bernard, P.; Van Grieken, R.; Eisma, D. *Environ. Sci. Technol.* **1986**, *20*, 467-473.
- Forgy, E. W. *Biometrics* **1965**, *21*, 768.
- Massart, D. L.; Kaufman, L. *The Interpretation of Analytical Data by the Use of Cluster Analysis*; Wiley: New York, 1983.
- Shattuck, T. W.; Germani, M. S.; Buseck, P. R. *Environmental Applications of Chemometrics*; Breen, J. J., Robinson, P. E., Eds.; ACS Symposium Series 292; American Chemical Society: Washington, DC, 1985; pp 118-129.
- Hopke, P. K. *Receptor Modelling in Environmental Chemistry*; John Wiley and Sons: New York, 1985.
- Saucy, D. A.; Anderson, J. R.; Buseck, P. R. *Atmos. Environ.* **1987**, *21*, 1649-1657.
- Kim, D. S.; Hopke, P. K.; Massart, D. L. *Sci. Total Environ.* **1987**, *59*, 141-155.
- Van Borm, W.; Adams, F. *Atmos. Environ.* **1988**, *22*, 2297-2307.
- Raeymaekers, B. Ph.D. Thesis, University of Antwerp, 1987.
- Op de Beek, J. P.; Hoste, J. *At. Energy Rev.* **1975**, *13*, 151-189.
- Rojas, C. M.; Otten, P.; Van Grieken, R. *J. Aerosol Sci.* **1989**, *20*, 1257.
- Blanchard, D. C. *Air-Sea Exchange of Gases and Particles*; Liss, P. S., Slinn, W. G. N., Eds.; Riedel Publishing Co.: Dordrecht, The Netherlands, 1983; p 407.
- Bruynseels, F.; Storms, H.; Van Grieken, R.; Van der Auwera, L. *Atmos. Environ.* **1988**, *22*, 2593-2602.
- Martens, C. S.; Wesolowsky, J. J.; Harris, R. C.; Kaifer, R. *J. Geophys. Res.* **1973**, *78*, 8778.
- Erikson, E. *Tellus* **1960**, *12*, 63.
- Hitchcock, D. R.; Spiller, L. L.; Willson, W. E. *Atmos. Environ.* **1980**, *14*, 165-182.
- Clegg, S. L.; Brimblecombe, P. *Atmos. Environ.* **1985**, *19*, 465-470.
- Harrison, R. H.; Sturges, W. T. *Atmos. Environ.* **1984**, *18*, 1829-1833.
- Van Borm, W.; Adams, F.; Maenhaut, W. *Atmos. Environ.* **1989**, *23*, 1139-1151.
- Charlson, R. J.; Covert, D. S.; Larson, T. V.; Waggoner, A. P. *Atmos. Environ.* **1978**, *12*, 39-53.
- Post, J. E.; Buseck, P. R. *Environ. Sci. Technol.* **1984**, *18*, 35-42.
- Mamane, Y.; Noll, K. E. *Atmos. Environ.* **1985**, *19*, 611-622.
- Dzubay, T. G.; Mamane, Y. *Atmos. Environ.* **1989**, *23*, 467-476.
- Mamane, Y.; Miller, J. L.; Dzubay, T. G. *Atmos. Environ.* **1986**, *20*, 2125-2135.
- Reference deleted in proof.
- Andreae, M. O.; Charlson, R. J.; Bruynseels, F.; Storms, H.; Van Grieken, R.; Maenhaut, W. *Science* **1986**, *232*, 1620-1623.
- Parungo, F.; Ackerman, E.; Proulx, H.; Pueschel, R. *Electron Microscopy and X-Ray Applications to Environment and Occupational Health Analysis*; Russel, P. A., Hutchings, A. E., Eds.; Ann Arbor Science: Ann Arbor, MI, 1979.
- Borchert, B. In *Chemical Oceanography*; Skirrow, G., Riley, J. P., Eds.; Academic Press: London, 1965; Vol. 2.
- Husain, L. *Toxic Metals in the Atmosphere*; Nriagu, J. O., Davidson, C. L., Eds.; Advances in Environmental Science and Technology 17; John Wiley and Sons: New York, 1987.
- Xhoffer, C. M.Sc. Thesis, University of Antwerp (UIA), 1987.
- Graham, W.; Piotrowicz, S. R.; Duce, R. A. *Mar. Chem.* **1979**, *7*, 325-342.
- Chen, L.; Arimoto, R.; Duce, R. A. *Atmos. Environ.* **1985**, *19*, 779-787.
- Post, J. E.; Buseck, P. R. *Environ. Sci. Technol.* **1985**, *19*, 682-685.
- Sturges, W. T.; Harrison, R. M. *Atmos. Environ.* **1986**, *20*, 1485-1496.
- Van Espen, P. *Anal. Chim. Acta* **1984**, *165*, 31-49.

Received for review October 15, 1990. Accepted March 21, 1991. This work was partially supported by the Belgian Ministry for Science Policy under Contract 84-89/69 and by a NATO research grant. C. X. acknowledges a research fellowship from the Belgian Instituut ter Aanmoediging van Wetenschappelijk Onderzoek in Nijverheid en Landbouw. H. Storms carried out some of the EPXMA measurements.

Diffusion of 2,3,7,8-Tetrachlorodibenzo-*p*-dioxin in Soil Containing Organic Solvents

Michael R. Overcash,* Arnold L. McPeters, Erlka J. Dougherty, and Ruben G. Carbonell

Department of Chemical Engineering, North Carolina State University, Raleigh, North Carolina 27695-7905

■ The transport of 2,3,7,8-tetrachlorodibenzo-*p*-dioxin (TCDD) in soils containing various organic liquids has been measured experimentally. A model has been developed that considers diffusive transport in the liquid phase and takes into account the rate of adsorption and desorption of TCDD from the soil particles. Effective diffusion coefficients for TCDD were fit to the data, and the results compared well with estimates using the Wilke-Chang correlation.

Introduction

Removal of 2,3,7,8-tetrachlorodibenzo-*p*-dioxin (TCDD) from contaminated soil is of recent interest in many areas of the country and the world. The chemical has extremely low water solubility and volatility and thus can be very persistent once introduced into the soil environment (1, 2). Other chemicals such as PCBs and chlorinated furans exhibit similar behavior. In spite of the recalcitrant nature of the contaminant, public concern mandates that effective cleanup methods be found.

A number of remediation technologies have been proposed and, in some cases, have reached the development stage (3-5). There is an active EPA program for emerging concepts in remediation of soils (6) and another program to verify the more developed methodologies (7).

In a significant number of these technology concepts the migration of trace concentrations of the contaminant occurs in a larger, bulk liquid phase (e.g., waste oil, tank leakage of trichloroethylene, spills of solvents). This migration is potentially by diffusion and convection of the organic fluid in the soil. TCDD can also be solubilized by surfactants. After a site or area has had the direct source removed (e.g., a leaking tank), migration of trace substances can be primarily by diffusional processes in the organic fluid, particularly when the contaminant has low water solubility. Contaminants with higher water solubility can be transported primarily by convection during rainfall or after reaching the water table.

For TCDD in water-saturated soils, diffusion would appear to be the primary mode of transport in the absence of physical movement of the soil particles since the water solubility of the compound is extremely low (<20 ppt (8)). If an organic phase is present in the soil, it is important to understand the diffusional transport of TCDD in the porous material. Possible situations where this might be applicable include the application of TCDD-contaminated oil to land, the residual migration in solvent plumes when a leaking tank source is removed, or in other circumstances when solvents in soils may cause leaching or removal of TCDD. For example, one possible cleanup technique for TCDD-contaminated soil involves the application of organic solvents to the contaminated soil and the subsequent solubilization, movement, and photodegradation of the TCDD (9, 10).

In previous analyses of solvent-based systems to clean up soil, the adsorption/desorption behavior and microscale diffusion of trace contaminants have not been measured. The lack of data is particularly acute with difficult to analyze compounds such as TCDD. Since understanding

Table I. Composition of Norfolk Loamy Sand

particle size	composition, %	diameter (13) (d_p), μ	external surface area (A_p), $\text{cm}^2 \text{g}^{-1}$
sand	84.8	50-840	41 ^a
silt	10.7	2.0-50	9.1×10^4 ^a
clay (primarily kaolinite)	4.5	≤ 2.0	1.5×10^5 (13)

^a External area calculated as surface area of spheres with the given diameter.

of the underlying phenomena at the microscale in soil is so broadly necessary and applicable, studies were undertaken to provide both experimental and theoretical information for TCDD diffusive transport in the presence of organics.

The main purpose of these diffusion studies was to quantify TCDD movement through a soil column in which a solvent or solvents were present. The ability of the solvent to remove the chemical from Norfolk loamy sand and the diffusive flux through the soil were both considered in this analysis. Quantitative measurements and models of the adsorption and desorption kinetics of TCDD in this soil have already been carried out (11). A model of the unsteady-state desorption/diffusion process is presented and the model is used to calculate effective diffusivities for TCDD in the solvent-laden soil.

Experimental Procedures

To determine a group of effective solvents for TCDD solubilization, desorption tests had previously been conducted (11). From this information, several solvents were chosen for these diffusion studies: ethyl oleate, tetradecane, dimethyl sulfoxide, 1-butanol, and 2-propanol.

The soil used was a Norfolk loamy sand (Table I) spiked with ¹⁴C-labeled TCDD from ethanol in a manner previously described (11), to yield a concentration of 50-60 ng of TCDD g^{-1} . When the soil is spiked by this procedure, it is postulated that ~60% of the TCDD chemically or physically adsorbs to the soil particles (11). The remainder of the chemical is assumed to be contained in the soil as a film on the soil particles, without actually being adsorbed. This situation is comparable to the state of TCDD contamination in the field, as a spill of contaminated solvent would evaporate and leave the TCDD in much the same manner.

For tests involving TCDD-spiked solvent, stock TCDD solutions containing 600-2000 ng mL^{-1} TCDD in ethanol or isooctane were diluted with the relatively nonvolatile solvents to be used in the diffusion studies. The new solution was then left open under a hood until weight loss indicated that all the volatile solvent had evaporated, leaving the TCDD in the less volatile organic. To prepare solutions of TCDD in volatile alcohols, drops of the stock TCDD solution were added to large volumes of the desired solvent. The concentrations were adjusted to produce an applied level of ~60 ng of TCDD g^{-1} of soil.

The experiments involved two soil/solvent cells. One cell was spiked with ¹⁴C-labeled TCDD and one cell contained no TCDD. The TCDD spike was added to either

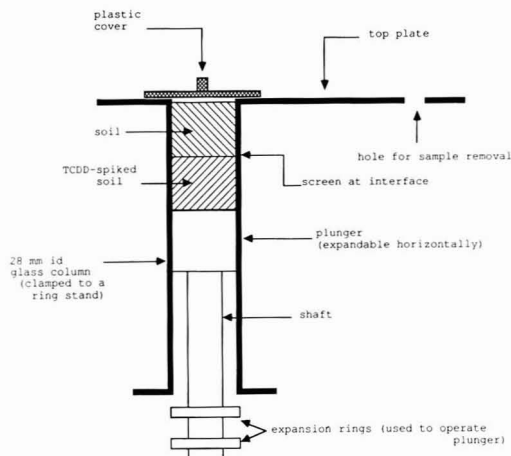


Figure 1. Diffusion apparatus.

the soil or the solvent in the spiked cell as described above. For both cells the soil samples were treated with a set amount of the organic solvent, depending on the test being conducted, so that no net solvent movement would occur between cells. Known weights of the desired solvent were added to the soil samples contained in plastic cups, and the mixtures were stirred thoroughly with a spatula. The soil samples were then loaded into the diffusion apparatus (Figure 1). The apparatus was prepared by alteration of a 50-mL gas/liquid syringe with addition of a glass plate perpendicular to and flush with the barrel top. It consisted of a glass cylinder 28 mm in diameter with an adjustable Teflon plunger to hold the soil column during the experiment and a shaft to move the soil column up for sampling after exposure. The plunger used a spring assembly to enable expansion in the horizontal direction, with the expansion controlled by rings at the bottom of the shaft. This allowed the plunger to be tightened into any desired position and discouraged solvent seepage. The cylinder could accommodate samples as deep as 50 mm. The syringe barrel had etched calibration lines 1.6 mm apart, which were used to determine plunger movement and thereby control sample size.

To load the samples, the Teflon plunger was tightened at the desired depth and the cylinder clamped in a vertical position. The soil/solvent mix, prepared immediately before the start of the experiment, was then added by spatula portions to fill the cylinder, with intermittent tamping to eliminate air pockets. Based on the amount of solvent needed to bring the system to apparent full saturation, the average porosity of the packed soil column was 0.38. The bottom cell, usually the TCDD-spiked sample, was loaded through a funnel to prevent contamination of the upper cylinder surface. After the loading of the bottom cell to a depth of approximately 15 mm with an even surface, a circular piece of PVC screen with square 0.16-cm holes was added to delineate the interface between the two cells. The screen weight before the test was 0.06 g, and the weight before and after the tests did not differ appreciably, showing little, if any, solvent absorption. The second (usually unspiked) soil/solvent sample was then loaded to the same depth as the first, and any excess soil was removed with a razor blade to make the top surface flush with the glass plate. These experiments utilized a vertical column rather than a horizontal one because the soil/solvent samples were semiliquid and solvent would seep away from the soil if not well-contained. On some

tests, minor seepage was observed around the plunger at the bottom. For this reason, almost all tests were run so that TCDD diffusion would be in the direction opposite of gravity. The apparatus was covered with a Saran cover during studies involving more volatile solvents to restrict solvent evaporation and then left undisturbed for 96 h. The laboratory temperature was relatively constant during any 96-h period, generally in the 25–28 °C range.

During the experiment, some of the TCDD from the spiked cell diffused to the unspiked cell. At the end of the test, the soil column was divided into successive equal segments of 3–6 mm in depth, depending on the particular test being done. The diffusion apparatus was held vertically on a ringstand and a plastic sample cup positioned beneath a small hole in the glass plate at the top of the cylinder. The Teflon plunger was then pushed up the desired distance, which caused the soil column to protrude above the glass plate. The sample layer was separated from the soil below by sliding a single-edge razor blade along the top plate surface. The sample was then moved over the hole in the plate where it dropped into the tared cup. Soil layers from lower depths in the column were removed in successive samples. In all tests a cut was made just above the screen to divide the two original soil cells at the interface. This procedure provided a reproducible and convenient method of sampling soil columns over a range of depths. Sample cuts of a given depth did show some variability in weight; therefore actual soil weights were used as the basis for all TCDD concentration calculations.

The soil from each cut was extracted with ethanol, and the extracts were analyzed by scintillation counting for ^{14}C . To extract the TCDD, 60–90 mL (depending on the size of the soil sample) of denatured ethanol was added to the 1–4 g sample in a 125-mL capped plastic bottle. After 16 h of shaking on a wrist-action shaker and 24 h of settling time, an aliquot from the extract solutions was added to ~15 mL of Scintiverse II liquid (Fisher Scientific, Fair Lawn, NJ) in a glass scintillation vial. Scintillation counting was then done using a Packard TriCarb scintillation spectrometer, Model 2405. Blanks containing ethanol in Scintiverse II were run with each sample to determine the background radiation, which varied from 24 to 40 dpm. Corrections were made for counting efficiency, and final determinations of sample activities varied from 50–1000 dpm. Since TCDD is virtually inert to biological activity, there was no appreciable TCDD degradation during the course of the experiment. Thus, the amount of ^{14}C was directly related to the amount of TCDD, and this procedure produced a profile of the TCDD concentration in the diffusion cells. Results were expressed as dpm g^{-1} of sample.

Twenty diffusion studies of TCDD in soil with single solvents were completed. The conditions of the experiments are shown in Table II. The amount of solvent needed to bring the system to full saturation with all pore space filled with solvent was determined by inspection. The amount of solvent needed to fill lower percentages of the total soil pore space was then determined by calculation. Three different degrees of saturation (full saturation, ~70% saturation, and ~30% saturation) were used as shown in the table. The degree of saturation is defined as the fraction of the total pore volume that is filled with solvent. It can vary from zero for completely dry soil to 1 for full saturation.

Results and Discussion

Table II shows the results for percentage of TCDD that crossed the interface separating the two cells after 96 h.

Table II. Conditions and Results for Diffusion Studies

test	degree of saturation	spike location	T, °C	% across interface in 96 h
Ethyl Oleate				
698	1.00	solvent	16	13.2
700	1.00	soil	16	6.70
743	1.00	solvent	27	18.5
744	1.00	solvent	27	20.3
745	1.00	soil	27	12.0
727	1.00	solvent	28	21.8
776	0.70	solvent	28	16.3
831	0.70	soil	30	14.0
Tetradecane				
910	1.00	soil	24	25.5
725	1.00	solvent	28	30.1
726	1.00	soil	28	25.0
778	0.69	solvent	28	18.0
Dimethyl Sulfoxide				
767	1.00	solvent	29	33.7
768	1.00	soil	29	33.5
777	0.70	solvent	28	30.7
756	0.70	soil	28	22.9
790	0.35	soil	26	16.5
2-Propanol				
812	0.70	soil	28	32.8
813	0.70	soil	28	28.1
1-Butanol				
920	0.67	soil	25	20.2

The theoretical maximum value is 50%, since when the concentration is the same in both cells the driving force for diffusion is no longer present. The values of percentage transferred range from 6.7 in test 700 with ethyl oleate to 33.7 in test 767 in dimethyl sulfoxide, showing that none of the tests had reached equilibrium after 96 h.

To model the diffusion studies, several assumptions were utilized. First, it was assumed that TCDD transport occurs only in the liquid phase. This is reasonable since the vapor pressure of TCDD is only 3.46×10^{-9} mmHg at 30 °C (12). The concentration of TCDD in the air spaces in the soil that were present in the unsaturated tests would be less than 4.6×10^{-10} volume percent.

Second, it was assumed that the soil behaved identically with each solvent; that is, the physical properties of the soil remained constant. Any changes that did occur that would affect TCDD adsorption were implicitly accounted for in the modeling equations by the use of previously measured rate and equilibrium constants for adsorption and desorption. However, these rate constants and partition coefficients were measured at 25 °C. In the present model it was assumed that the change in temperature to that of the diffusion studies had little effect on the kinetic behavior, so the rate and equilibrium constants were used without modification.

Finally, it was postulated that convective solvent movement was negligible so diffusion was the main TCDD transport pathway. To test this assumption one of the studies in ethyl oleate was conducted with the spiked soil half on the top of the diffusion column, the reverse of the usual procedure. The study that was reversed, 743, did show a lower transport rate than the other similar studies, 727 and 744; however, the difference was within the range of experimental variation. The percentage that crossed the plastic screen delineating the cell boundary in test 743 was 18.5%, as opposed to an average of 21.1% for 727 and 744. Although less TCDD movement occurred in the reversed study, this difference was quite small (2.6% of the total TCDD), comparable to the difference between 727 and 744. Ethyl oleate has a low vapor pressure, and solvent

Table III. Equilibrium Coefficients and Rate Constants for TCDD Adsorption/Desorption in Various Solvents

solvent	K, cm ³ g ⁻¹	10 ³ k _a , h ⁻¹	10 ³ k _d , cm ³ g ⁻¹ h ⁻¹
dimethyl sulfoxide	0.096	16	1.5
1-butanol	0.19	24	4.6
tetradecane	0.26	2.4	0.62
ethyl oleate	0.56	1.9	1.1

loss by evaporation was negligible. These observations led to the conclusion that convective solvent transport was not a significant factor in the TCDD movement between cells.

Under these assumptions, the experimental setup can be described with the following two mass balances. First, the rate of change of the concentration of TCDD in the organic is directly related to the rate of diffusion of the chemical by

$$\epsilon_1 \frac{\partial C}{\partial t} + \epsilon_p \rho_p a \frac{d\Gamma}{dt} = D_{\text{eff}} \frac{\partial^2 C}{\partial x^2} \quad (1)$$

where C is the bulk concentration of TCDD in solution (g cm⁻³), Γ is the surface concentration of adsorbed TCDD (g cm⁻²), x is the distance down the length of the diffusion cell, and t is time (s). Other variables include a , the ratio of surface area of the soil particles to particle mass (cm² g⁻¹); ρ_p , the particle density (g cm⁻³); ϵ_1 , the fluid-filled porosity, also known as volume wetness (cm³ fluid cm⁻³ total); ϵ_p , the fraction of total volume occupied by particles (cm³ particles cm⁻³ total); and D_{eff} , the effective diffusivity of TCDD through the soil matrix (cm² s⁻¹). Note that the sum of ϵ_p and ϵ_1 is 1.0 for a saturated column.

The time rate of change of the adsorbed TCDD concentration is given by

$$a(d\Gamma/dt) = k_a \theta C - k_d a \Gamma \quad (2)$$

where k_a is the rate constant for TCDD adsorption from solvent to soil (cm³ g⁻¹ s⁻¹) and k_d is the rate constant for desorption from the soil to the solvent (s⁻¹). The fraction of the soil surface open and available for adsorption, θ , is taken to be 1.0 since the TCDD concentration is so low. This equation has been shown to describe the desorption of TCDD from soil in the presence of organic solvents with reasonable accuracy and has been used to evaluate rate constants for TCDD adsorption/desorption behavior (11). Values of k_a , k_d , and $K = k_a/k_d$, the equilibrium constant for TCDD partitioning between the soil and the solvent, are shown in Table III.

The adsorption/desorption process of eq 2 has the effect of slowing the transport of TCDD. If the original spike is on the soil, time for desorption is required as well as time for diffusion. As shown by short-time desorption studies (11), approximately 40% of the TCDD is quickly solubilized. However, the remainder takes days or weeks to desorb from the soil. When the equations are written in this way, the retardation effect can be separated from the diffusion.

To make the governing equations dimensionless, one can define

$$\bar{t} = t D_{\text{eff}} / l^2 \quad (3)$$

$$\bar{x} = x / l \quad (4)$$

$$\alpha = \epsilon_1 C / (\epsilon_1 C_0 + \rho_p \epsilon_p a \Gamma_0) \quad (5)$$

$$\beta = \rho_p \epsilon_p a \Gamma / (\epsilon_1 C_0 + \rho_p \epsilon_p a \Gamma_0) \quad (6)$$

where Γ_0 is the initial TCDD concentration on the soil (g cm⁻²), C_0 is the original TCDD concentration in the solvent (g cm⁻³), and l is the total length of the diffusion cells (cm).

Table IV. Effective Diffusion Coefficients at Full Saturation					
test	<i>T</i> , °C	10 ⁶ <i>D</i> , cm ² s ⁻¹	10 ⁶ <i>D</i> _{eff} , cm ² s ⁻¹	<i>R</i> ²	<i>m</i>
Ethyl Oleate					
698	16	1.64	0.18	0.99	2.3
700	16	1.64	0.43	0.97	1.4
743	27	2.15	0.32	0.99	2.0
744	27	2.15	0.40	0.99	1.7
745	27	2.15	0.73	0.99	1.1
727	28	2.21	0.56	0.98	1.4
Tetradecane					
910	24	5.74	0.67	0.96	2.2
725	28	5.82	0.97	0.96	1.9
Dimethyl Sulfoxide					
767	29	5.07	1.0	0.96	1.7
768	29	5.07	1.5	0.98	1.3

The dimensionless variables defined include \bar{t} , dimensionless time, and \bar{x} , dimensionless distance. Also given are α and β , the dimensionless concentrations of TCDD in the solvent and adsorbed to the particles, respectively. These are defined as the ratio of TCDD concentration to initial TCDD concentration. The dimensionless variables are then substituted into eqs 1 and 2 to obtain

$$\frac{\partial \alpha}{\partial \bar{t}} + \frac{\partial \beta}{\partial \bar{t}} = \left(\frac{1}{\epsilon_1} \right) \frac{\partial^2 \alpha}{\partial \bar{x}^2} \tag{7}$$

and

$$d\beta/d\bar{t} = A\alpha - B\beta \tag{8}$$

where *A* and *B* are dimensionless groups defined by

$$A = k_a l^2 / D_{\text{eff}} (\rho_p \epsilon_p / \epsilon_1) \tag{9}$$

$$B = k_d l^2 / D_{\text{eff}} \tag{10}$$

A and *B* represent the ratio of the adsorption and desorption rates to the diffusion rate.

The initial conditions at $\bar{t} = 0$ are

$$h/l \leq \bar{x} \leq 1 \quad \alpha = 0, \beta = 0 \tag{11}$$

where *h* is the length of the cell containing the original TCDD spike (cm). For the case of the initial TCDD added in the solvent (just prior to the beginning of the diffusion time)

$$0 \leq \bar{x} \leq h/l \quad \alpha = 1, \beta = 0 \tag{12}$$

or, for the case of the initial TCDD already on the soil

$$0 \leq \bar{x} \leq h/l \quad \alpha = 1 - P, \beta = P \tag{13}$$

where *P* is the fraction of TCDD that is actually adsorbed to the soil particles and desorbs relatively slowly according to eq 2. The remainder of the TCDD is assumed to dissolve very quickly in the solvent. For this type of soil and spiking procedure, *P* is approximately 0.6 (11). There are no-flux boundary conditions at the end of the cells ($\bar{x} = 0$ and $\bar{x} = 1$), given by

$$\partial \alpha / \partial \bar{x} = 0 \tag{14}$$

The particle density, ρ_p , was 2.65 g cm⁻³, a common value for soils of this type (13), and the fraction of the total volume occupied by particles, ϵ_p , was 0.62. For the saturated tests, ϵ_1 was equivalent to $1 - \epsilon_p$. Under unsaturated conditions ϵ_1 was set to a value corresponding to the fraction of solvent saturation multiplied by $1 - \epsilon_p$. The dimensionless equations were solved numerically by using an IMSL packaged equation solver, MOLCH (14). This package solves a system of partial differential equations

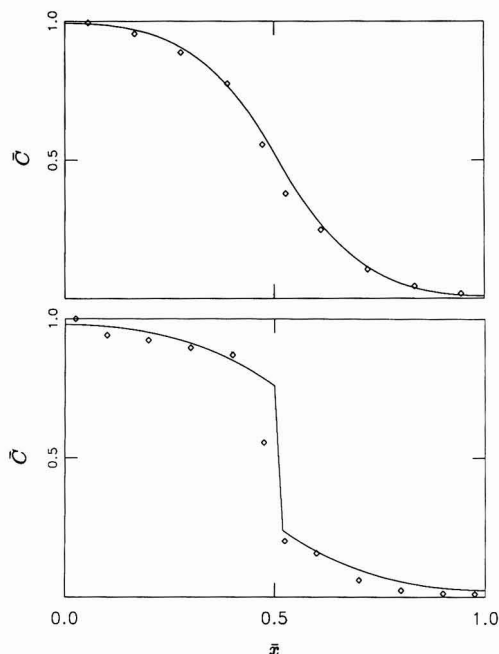


Figure 2. Dimensionless concentration (\bar{C}) versus position (\bar{x}) for TCDD in ethyl oleate, degree of saturation 1.0, at 16 °C. Tests 698 (top) and 700 (bottom).

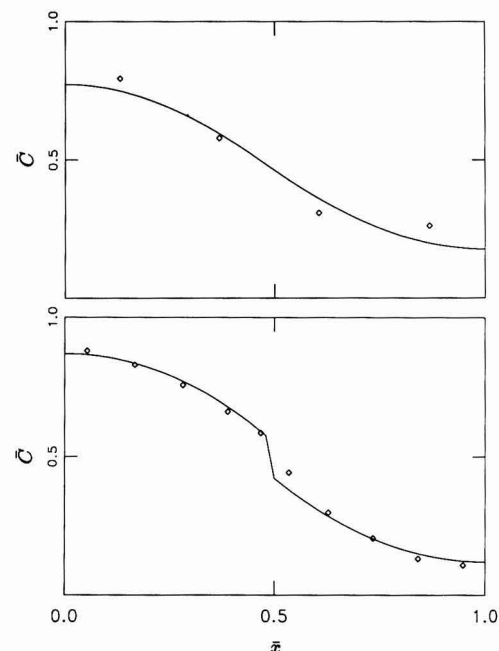


Figure 3. Dimensionless concentration (\bar{C}) versus position (\bar{x}) for TCDD in dimethyl sulfoxide, degree of saturation 0.69, at 28 °C. Tests 777 (top) and 756 (bottom).

by the method of lines with cubic Hermite polynomials. The D_{eff} was adjusted until the least-squares sum was minimized for each case.

Tables IV and V give the values of D_{eff} calculated from the model. Figures 2 and 3 show examples of results for dimensionless concentration, \bar{C} , versus dimensionless

Table V. Effective Diffusion Coefficients at Less Than Full Saturation

test	<i>T</i> , °C	$10^6 D$, cm ² s ⁻¹	ϵ_1	$10^6 D_{\text{eff}}$, cm ² s ⁻¹	<i>R</i> ²	<i>m</i>
Ethyl Oleate						
776	28	2.21	0.26	0.20	0.99	1.8
831	30	2.35	0.26	0.54	0.98	1.1
Tetradecane						
778	28	5.82	0.26	0.21	0.98	2.5
Dimethyl Sulfoxide						
756	28	5.05	0.26	0.67	0.99	1.5
777	28	5.05	0.26	0.74	0.95	1.4
790	26	5.02	0.13	0.28	0.99	1.4
2-Propanol						
812	28	5.14	0.26	1.1	0.95	1.1
813	28	5.14	0.26	1.2	0.94	1.1
1-Butanol						
920	25	2.29	0.25	0.84	0.99	1.1

position, \bar{x} . Dimensionless concentration is defined as total concentration divided by original total concentration. The total concentration is equal to the bulk liquid concentration plus the adsorbed concentration, and the original total concentration is total concentration at the beginning of the test. The position x is made dimensionless by scaling it with the total length of the sample cells, l . Points are plotted at the position corresponding to the center of the depth of the sample taken. Correlation coefficients (R^2) were calculated for each test, using

$$R^2 = (\text{TS} - \text{RS})/\text{TS} \quad (15)$$

where TS is the total sum of the squares of the differences between the predicted and actual data points and RS is the residual sum of squares, the sum of the differences between the data points and the average value of the concentration. The model appears to fit the data quite well. Correlation coefficients were above 0.94 for all tests except test 726. The data from this sample were so widely scattered that useful results could not be found with the model. The causes of the scatter in the data from this test are unknown.

It is interesting to note the difference in the model results depending on the location of the original TCDD spike. For instance, when test 698 and test 700 are compared (Figure 2), a discontinuity is observed in the model (and the data) of the latter test, in which the TCDD was originally on the soil. This effect is due to the nature of the desorption process. Approximately 40% of the TCDD dissolves very quickly. The remainder is adsorbed on the soil particles and must come to equilibrium according to the rate equation (eq 2). This process does not come to steady state over the course of the experiment, and the result is the observed discontinuity. The discontinuity is less pronounced when organic liquids with higher desorption rate constants, such as dimethyl sulfoxide, are used in the diffusion test (Figure 3).

In order to further verify the model, the diffusivity of TCDD in each solvent was compared against the effective diffusivity calculated by using the model. The pure solution diffusivity was either directly measured (11, 15) or, in the case of ethyl oleate, estimated by the method of Wilke and Chang (16). The Wilke-Chang estimation technique utilizes a correlation with the molar volume of the solute at the boiling point (in cm³ gmol⁻¹; \bar{V}_A), the viscosity of the solvent (in cP; μ), and the molecular weight of the solvent (M_B)

$$D_{\text{WC}} = 7.4 \times 10^{-8} [(\Psi_B M_B)^{1/2} T] / \mu \bar{V}_A^{0.6} \quad (16)$$

where T is temperature (K) and Ψ_B is an association parameter having to do with the polarity of the solvent. The molar volume of the solute, TCDD, was calculated from an estimated value of the density of liquid TCDD at its normal boiling point (12). The density is given as 1.02 g cm⁻³; so the molar volume was found to be 315 cm³ mol⁻¹. The viscosity of ethyl oleate is 6.1 cP at 25 °C (17), and the association parameter was assumed to be 1.0 as information concerning the actual value was not available in the literature. This could affect the accuracy of the prediction, which has been shown to be within 10% on the average (16). The diffusivity of TCDD in ethyl oleate at 25 °C was calculated to be 2.04×10^{-6} cm² s⁻¹, a very low value due to the high viscosity of the solvent.

Diffusivities were available for TCDD in the remainder of the organic liquids at 25 °C. Because the experiments were conducted at temperatures ranging from 16 to 29 °C, pure solution diffusivities had to be estimated at these temperatures. The Wilke-Chang diffusivity can be seen in eq 16 to vary linearly with temperature, inversely with solvent viscosity, and with the square root of solvent molecular weight. The Wilke-Chang temperature dependence relationship was used to find values for diffusivity at the temperatures in question.

The effective diffusivities found by using the model for diffusion studies at full saturation are compared with the pure solution diffusivity (D) at the experiment temperature in Table IV. To further study the results of the model, a measure of the predicted tortuosity was used. The tortuosity (τ) of a soil specimen can be defined as the ratio of the average length of the pore passages in the soil matrix to the length of the specimen, and is given by

$$\tau = D\epsilon/D_{\text{eff}} \quad (17)$$

where D is the diffusivity of the component in free solution (cm² s⁻¹) and ϵ (cm³ of voids cm⁻³ of total) is porosity of the soil matrix. One form for describing tortuosity was first proposed by Bruggeman (18), and is given by

$$D_{\text{eff}} = D(\epsilon^m) \quad (18)$$

Tortuosity is always greater than 1 and Bruggeman showed theoretically that for spherical particles $m = 3/2$. Table IV gives calculated values for the exponent m , where D_{WC} was used as an estimate of D in the case of ethyl oleate. Since transport was assumed to occur only in the solvent phase, the porosity (ϵ) used in the calculation of m in eq 18 was considered to be equivalent to volume wetness (ϵ_1), the fraction of the total volume that is fluid-filled (cm³ of fluid cm⁻³ of total). For the saturated tests ϵ_1 is equal to ϵ since all pore space is filled with solvent.

Calculation of m provides a check on the effective diffusivities found with the model. This factor shows the relationship between TCDD diffusivity in pure solution and effective diffusivity in the soil medium. The higher the value of m , the greater the tortuosity, and the greater the obstructions encountered by TCDD molecules along the diffusion path. Under ideal experimental conditions, with completely homogeneous soil samples and the same pore space distribution within each soil column, the m values would be the same for each test if the model was calculating the effective diffusivities correctly.

The average value of m in the diffusion studies was found to be 1.6, with a standard deviation of 27%. The scatter in these values is to be expected, since the soil and packing structure cannot be expected to be uniform from sample to sample.

Some of the values for the tortuosity exponent found in the saturated studies are less than $3/2$, the m Bruggeman calculated for a matrix of spheres. Since the m values are

somewhat lower than those found by other researchers under similar conditions (19, 20), the lowered values raise questions about the mode of transport of TCDD in these studies. Nonuniform structures in the soil through which diffusion could more effectively occur could account for some increased movement. The possibility of TCDD transport in the vapor phase playing a part in increased transport is remote, since the vapor pressure of TCDD is so low. In addition, in the saturated studies solvent filled the pores, leaving no space for vapor transport. Capillary movement of the solvent driven by evaporation is also an improbable explanation, since the solvents in question have relatively low vapor pressures, the diffusion cells were covered with a plastic cover, and the soil mixtures did not lose an appreciable amount of weight during the course of the experiment (generally less than 1%). One last possibility is that the estimate of porosity (0.38) could be too low. The estimation procedure for ϵ was based on observation of apparent saturation with organic fluids. If all pores were not filled with solvent, this could lead to underprediction of ϵ , which could be enough to account for the low observed tortuosity.

Tests 743, 744, and 745 were all conducted with ethyl oleate at full saturation at the same temperature (27 °C). Test 727 also had these same conditions with a temperature reading 1 °C higher. Tests 727 and 744 were identical, with the TCDD spike originally in the solvent. Test 743 was done with the spiked cell in the top of the diffusion apparatus, the opposite of the usual procedure, and test 745 contained the original TCDD spike on the soil rather than the solvent. The difference in the calculated D_{eff} values for tests 727 and 744 is 29%, with only 1% accounted for by the differing temperature conditions. However, the corresponding difference in the percentages of the TCDD that passed the screen that delineated the boundary of the two cells was 1.5% of the total TCDD, which is equivalent to a 6.9% change. This small difference in amount of transferred TCDD could be caused by many different factors, soil variability and the lack of strict temperature control among them. Thus the model can be seen to be quite sensitive to small changes in the amount of TCDD transport. A similar effect is observed in comparing test 743 with 727 and 744.

The effective diffusivities found from the diffusion experiments do follow the general trend that would be expected from the Wilke–Chang diffusivity calculations. For instance, the D_{eff} calculated for ethyl oleate, the most viscous of the solvents studied, is lower than that for tetradecane or dimethyl sulfoxide.

In the unsaturated diffusion tests (Table V), the correlation coefficients again showed close agreement between model and data. The rate of diffusion would be expected to decrease with fluid-filled porosity according to eq 18. This effect was observed in the diffusion experiments. Some of the calculated m values are less than $3/2$ in the unsaturated tests as well. When the unsaturated tests are compared with those at full saturation, this measurement of tortuosity shows no consistent pattern of change. This observation leads to the conclusion that the cause of the variation is probably not due to some systematic under- or overprediction by the model, but rather to unavoidable variation in the soil columns.

Two solvents that were not represented in the saturated tests were included in the unsaturated tests, 1-butanol and 2-propanol. The calculated TCDD diffusivity in 1-butanol follows the trend already described, showing a relatively high value since it is a low molecular weight solvent of relatively low viscosity. 2-Propanol also shows high D_{eff}

values for the same reasons.

One of the objectives of the diffusion experiments was to choose a solvent that would be appropriate for application to soil to effect TCDD removal and transport. The desirable attributes of a solvent used for this purpose include high equilibrium coefficient for removal, high TCDD diffusion rates, and low volatility so that the solvent would not need frequent reapplication. To maximize TCDD diffusivity in the solvent, it is apparent that low molecular weight and low viscosity are important. As price and environmental stability are also determining factors, tetradecane and 1-butanol appear to be the most promising of the solvents studied. The transport of TCDD in soil containing low levels of these solvents could be estimated by extrapolation from the results of the present study.

Conclusions

The model results show that movement of TCDD through soil with organic solvents can be adequately predicted by using adsorption and desorption rate constants, measured or estimated diffusivities, and tortuosity appropriate to the soil under consideration. The effective diffusivities calculated by the model can be used in the diffusive flux in other situations involving TCDD and organic solvents on soil, such as the case of the addition of solvents to contaminated soil in the presence of UV light.

The results of these experiments clearly show the need for including adsorption/desorption kinetics in a model for TCDD transport. The difference in transport between samples with a soil TCDD spike and those with TCDD in the solvent was marked. The model does a good job of describing this difference mathematically, as shown by the generally high R^2 values.

The tortuosity of the soil bed as determined by the Bruggeman m factor was calculated to be low in these studies. The most likely causes of this effect appear to be nonuniform soil structures or inability to accurately estimate soil porosity.

Of the solvents studied, tetradecane appears to have the best combination of properties for TCDD removal from soil. This chemical is relatively harmless to the environment, has a low vapor pressure to limit solvent loss, and shows relatively high rates of TCDD solubilization and diffusion.

Glossary

a	ratio of particle surface area to particle mass ($\text{cm}^2 \text{g}^{-1}$)
C	TCDD concentration in solution phase (g cm^{-3})
\bar{C}	dimensionless total concentration
C_0	original TCDD concentration in bulk solution phase (g cm^{-3})
D	TCDD diffusivity in solution ($\text{cm}^2 \text{s}^{-1}$)
D_{eff}	effective diffusivity of TCDD ($\text{cm}^2 \text{s}^{-1}$)
D_{WC}	Wilke–Chang estimated diffusivity ($\text{cm}^2 \text{s}^{-1}$)
h	length of cell containing original TCDD spike (cm)
K	equilibrium constant ($\text{cm}^3 \text{g}^{-1}$)
k_a	rate constant for adsorption ($\text{cm}^3 \text{g}^{-1} \text{s}^{-1}$)
k_d	rate constant for desorption (s^{-1})
l	total length of the diffusion cells (cm)
m	Bruggeman tortuosity factor
M_B	molecular weight of solvent (g mol^{-1})
P	fraction of TCDD spike actually adsorbed to soil particles
R^2	correlation coefficient
RS	residual sum of squares
t	time (s)
T	temperature (K)
\bar{t}	dimensionless time
TS	total sum of squares

\bar{V}_A	molar volume of solute ($\text{cm}^3 \text{mol}^{-1}$)
x	distance (cm)
\bar{x}	dimensionless distance
α	dimensionless solution concentration
β	dimensionless adsorbed concentration
Γ	TCDD concentration adsorbed to particle surfaces (g cm^{-2})
Γ_0	initial TCDD concentration adsorbed to particle surfaces (g cm^{-2})
ϵ	porosity ($\text{cm}^3 \text{cm}^{-3}$)
ϵ_1	fluid-filled porosity (volume wetness) ($\text{cm}^3 \text{cm}^{-3}$)
ϵ_p	fraction of total volume occupied by particles ($\text{cm}^3 \text{cm}^{-3}$)
θ	fraction of surface area left open for adsorption
μ	viscosity (cP)
ρ_p	particle density (g cm^3)
τ	tortuosity
Ψ_B	association parameter for use in Wilke-Chang estimation

Literature Cited

- (1) Kearney, P. C.; Isensee, A. R.; Helling, C. S.; Woolson, E. A.; Plimmer, J. R. *Adv. Chem. Ser.* 1973, No. 120, 105-111.
- (2) Young, A. L.; Cairney, W. J.; Thalken, C. E. *Chemosphere* 1983, 12, 713-726.
- (3) Kostecki, P. T.; Calabrese, E. J. *Petroleum Contaminated Soils*; Lewis Publishers: Chelsea, MI, 1989.
- (4) Lucero, G.; Moertl, K.; Holmes, R.; Arnstein, C. *Superfund Handbook*; EIVSR Corp.: Acton, MA, 1989.
- (5) Sims, R.; Sorensen, D.; Sims, J.; McLean, J.; Mahmood, R.; Dupont, R.; Jurinak, J. *Contaminated Surface Soils: In-Place Treatment Techniques*; Noyes Publications: Park Ridge, NJ, 1986.

- (6) U.S. E.P.A. *The Superfund Innovative Technology Evaluation Program: Technology Profiles 1989*; EPA/540-5-89-013; ORWER: Washington, DC, 1989.
- (7) U.S. E.P.A. *Technological Approaches to the Cleanup of Radiologically Contaminated Superfund Sites*; EPA 540/2-88/002; ORD: Washington, DC, 1989.
- (8) Marple, L.; Brunck, R.; Throop, L. *Environ. Sci. Technol.* 1986, 20, 180-182.
- (9) Exner, J. H. *Hazard Waste* 1984, 1, 217-224.
- (10) Liberti, A.; Brocco, D.; Allegrini, I.; Cecinato, A.; Possanzini, M. *Sci. Total Environ.* 1978, 10, 97-104.
- (11) Dougherty, E. J. Ph.D. Dissertation, North Carolina State University, 1990.
- (12) Schroy, J. M.; Hileman, F. D.; Cheng, S. C. *Chemosphere* 1985, 14, 877-880.
- (13) Hillel, D. *Fundamentals of Soil Physics*; Academic Press: New York, 1980.
- (14) *IMSL Math/Library—FORTRAN Subroutines for Mathematical Applications*; IMSL: 2500 ParkWest Tower One, 2500 CityWest Blvd., Houston, TX, 77042-3020, 1987.
- (15) Dougherty, E. J.; Overcash, M. R.; Carbonell, R. G. *Hazard. Waste Hazard. Mater.* 1991, 8, 43-53.
- (16) Wilke, C. R.; Chang, P. *AIChE J.* 1955, 1, 264-270.
- (17) Hamazaki, T.; Kobayashi, S.; Urakaze, M.; Yano, S.; Fujita, T. *Biorheology* 1985, 22, 221-226.
- (18) Bruggeman, D. A. G. *Ann. Phys.* 1935, 24, 636-664.
- (19) Currie, J. A. *Br. J. Appl. Phys.* 1960, 11, 318-324.
- (20) Hoogschagen, J. *Ind. Eng. Chem.* 1955, 47, 906-913.

Received for review June 21, 1990. Revised manuscript received September 10, 1990. Accepted September 11, 1990. This research was supported in part by Southern California Edison Co., but the contents of this paper do not necessarily reflect the views and policies of the company.

Surface Reactions of Brominated Arenes as a Model for the Formation of Chlorinated Dibenzodioxins and -furans in Incineration: Inhibition by Ethanolamine

T. Lippert,[†] A. Wokaun,^{*,†} and D. Lenoir^{‡,§}

Physical Chemistry II and Ecological Chemistry and Geochemistry, University of Bayreuth, D-8580 Bayreuth, Germany

■ The aryl coupling reaction of bromobenzene on alumina-supported copper catalysts has been studied as model for dioxin formation. The reaction was monitored in situ by transmittance FTIR spectroscopy. Time-dependent changes in the spectra were recorded during addition of bromobenzene to the carrier gas stream. Both coupling of phenyl intermediates to yield biphenyls and formation of phenol and phenolate were observed. Novel approaches to inhibit the coupling reaction of aryl halides by addition of ethanolamine to the catalyst surface were studied. The resulting inhibition was attributed to site blocking and irreversible deactivation of the copper surface due to imine and nitride formation.

Introduction

The mechanisms leading to the formation of chlorinated dibenzodioxins and -furans (PCDD/F) generated during

incineration processes, e.g., in municipal waste incineration (MWI), are a subject of current research interest and controversial discussion (1, 2). Evidence is emerging that catalytic reactions occurring between 300 and 400 °C on the surface of fly-ash particles in the postcombustion zone play an important role in the formation of these micropollutants (3-6). Fly ash has been identified as a catalytically active reagent for electrophilic chlorination of aromatic structures (7). Halogenation and dehalogenation reactions of aryl bromides catalyzed by fly ash from MWI at 300 °C (8) have recently been observed.

As a consequence of these findings an inhibition method has been developed (9), which is based on deactivation of the catalytic surfaces of fly-ash particles through the addition of suitable compounds (9) to the postcombustion zone. The results of appropriate laboratory experiments (10) have been extended to a technical pilot plant burning refuse-derived fuel (RDF); an overall reduction of PCDD/F concentration by 96% has been observed (11). The results of preliminary experiments in a technical plant have also been reported (12).

In order to obtain a more detailed understanding of the heterogeneous chemical reactions occurring on the fly-ash surfaces we have tested an appropriate catalytic model

[†]Physical Chemistry II.

[‡]Ecological Chemistry and Geochemistry.

[§]Present address: GSF-Forschungszentrum für Umwelt und Gesundheit, Institut für Ökologische Chemie, Ingolstädter Landstr. 1, W-8042 Neuherberg, München, Germany.

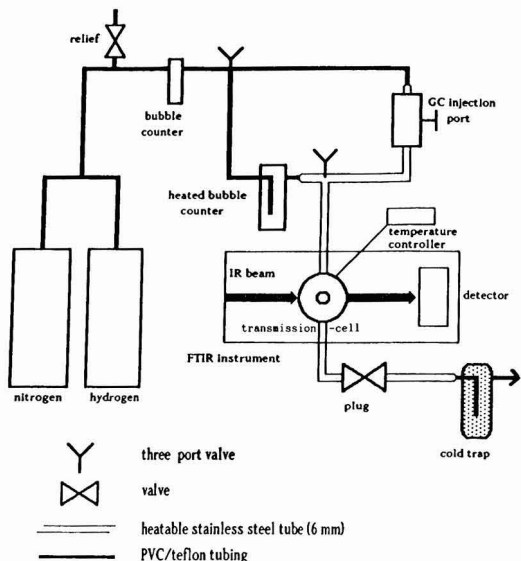
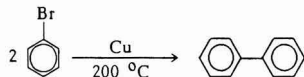


Figure 1. Block diagram of the apparatus used for the in situ transmittance FTIR experiments.

reaction, i.e., the conversion of bromobenzene to biphenyl on a copper surface (Ullmann I reaction).



Copper-catalyzed coupling reactions of halogenated arenes (Ullmann type I reaction) have been the subject of extensive investigations (13); a strong dependence on the method of preparation of the copper particles has been found (13).

This reaction is widely used for syntheses of various bisaryl compounds in organic chemistry (14), and several mechanistic pathways have been proposed (13, 14). As the effluents of MWI plants contain chlorobenzenes and chlorophenols, this reaction and the corresponding Ullmann type II reaction (15) (formation of bisaryl ether compounds from halobenzenes and phenols) can be used as a model for the formation of halogenated biphenyls, dibenzodioxins, and dibenzofurans. Copper has been detected in MWI fly ash (16) and is considered to act as a catalyst in the formation of PCDD/F. The conversion of chlorophenols to chlorinated dibenzodioxins at ca. 300 °C on the surface of catalytically active fly-ash particles has been demonstrated (9) experimentally.

An analysis system has been developed to study this reaction by surface-sensitive transmittance FTIR spectroscopy (17). The effect and fate of two established inhibitors, triethylamine and ethanolamine, were studied in detail by use of this method. Reference information used for the spectral interpretation includes the work of Kagel (18), who studied the adsorption of 1-(*o*-chlorophenyl)-ethanol, as well as recent spectroscopic investigation on copper catalysts (19–21). A more extensive survey on spectroscopic references is given in ref 17.

Experimental Section

Apparatus. An in situ transmission cell similar to the one used by Hecker and Bell (22) was used for the FTIR investigations. A block diagram of the apparatus is presented in Figure 1. The temperature in the reactor

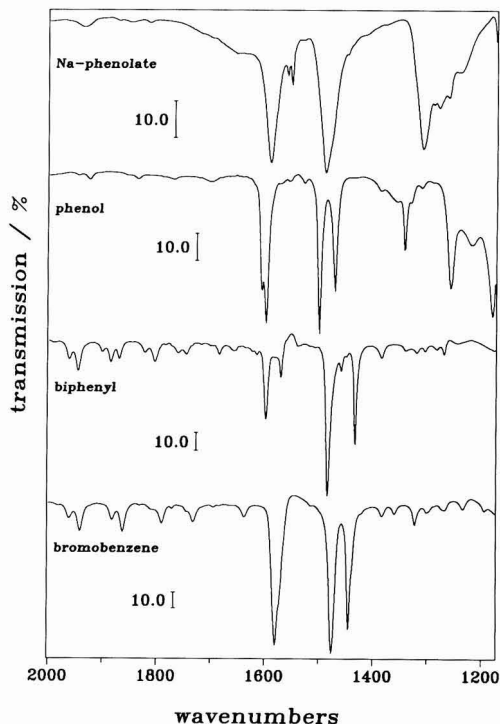


Figure 2. FTIR spectra of reference compounds recorded at room temperature in transmission.

was controlled to within ± 3 K. Stepwise addition of the reactant was achieved by redirecting the carrier gas stream through a heated bubble column containing the reactant; the concentration was adjusted by varying the temperature of the bubble column. Alternatively, reactants were added in a pulsed fashion through a modified gas chromatography injection port. The system is a slightly modified version of a design described in ref 19. Spectra were recorded with an FTIR instrument (Mattson, Model Polaris) equipped with a transmission cell; 25 scans at a resolution of 4 cm^{-1} were coadded for each spectrum at a given temperature.

Subsequent to the spectroscopic experiments, the contents of the cold trap as well as compounds adsorbed on the catalyst material were analyzed by GC/MS (Hewlett-Packard, gas chromatograph, Model 5890 A, and mass selective detector, Model 5970).

Reagents. Traces of water were removed from bromobenzene (Aldrich, purity >98%) by storing the liquid over a molecular sieve. Ethanolamine (Aldrich, >98%) and triethylamine (Fluka, p.a.) were used without purification.

Catalysts: Preparation and Pretreatment. The catalyst, which contained 10 wt % of copper on alumina, was prepared according to the procedure described elsewhere (23). The alumina modification of the support was identified as $\gamma\text{-Al}_2\text{O}_3$ by X-ray diffraction. For the IR studies, 40 mg of the catalyst was pressed into thin wafers of 20-mm diameter, using a pressure of 12 tons cm^{-2} . The catalyst wafers were pretreated in a flow (35 $\text{cm}^3 \text{min}^{-1}$) of pure nitrogen (Linde, 99.999%) at 473 K for 2 h.

Results and Discussion

1. Reactions of Bromobenzene on Copper Catalyst Surfaces. Reference spectra of sodium phenolate, phenol, biphenyl, and bromobenzene recorded at room tempera-

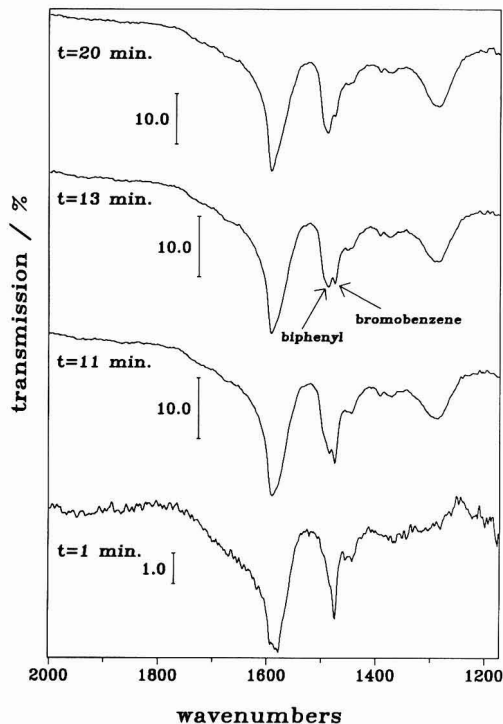


Figure 3. Time-dependent transmittance FTIR spectra recorded over a Cu/ γ -Al₂O₃ catalyst surface at 200 °C, subsequent to stepwise addition of bromobenzene to the nitrogen carrier gas stream. Experimental conditions are described in the text.

ture in the setup described above are presented in Figure 2. The reactions of bromobenzene on the surface of our copper/ γ -Al₂O₃ catalyst at 200 °C were followed over a period of 20 min (Figure 3).

The reaction of bromobenzene, to yield biphenyl, is clearly seen from the appearance of the corresponding biphenyl absorptions in the FTIR spectra. In particular, one observes the time-dependent growth of the characteristic 1483-cm⁻¹ vibration of biphenyl on the high-frequency side of the 1474-cm⁻¹ band of bromobenzene (cf. spectrum recorded at $t = 13$ min in Figure 3). In ref 17, various types of catalyst surfaces have been compared with respect to the observed rate of biphenyl formation. Copper/ γ -Al₂O₃ catalysts are generally more active than Cu/gibbsite systems. The activity of Cu/ γ -Al₂O₃ is increased by in situ reduction of the copper, followed by dehydration. Tables summarizing the relative dehalogenation activities, as well as details of the spectroscopic assignments for reactant and product bands, are given in ref 17.

Note that the 1445-cm⁻¹ vibration of biphenyl, and the corresponding 1432-cm⁻¹ feature of bromobenzene, are comparatively weak on the catalyst surface. These vibrations are characterized by a dynamic dipole moment that is parallel to the surface and is therefore screened by the presence of metallic copper. A mechanism for biphenyl formation that involves copper organic species on the surface of the catalyst is proposed in the reaction scheme of Figure 4. In addition, formation of phenolate is observed. This side reaction is generally not observed when the reaction is performed in solution (13, 14). The reaction conditions on the solid phase may favor a substitution reaction of the aryl bromide with nucleophilic O²⁻ anions

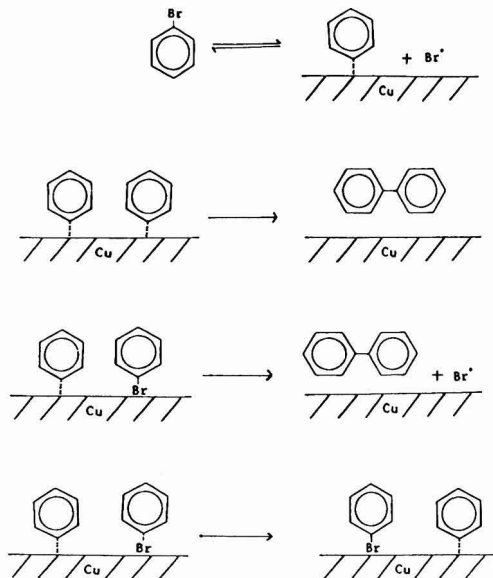
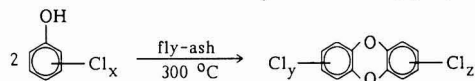


Figure 4. Proposed mechanism for reactions of bromobenzene over a copper catalyst surface. Subsequent to adsorption and formation of a surface phenyl species (top), biphenyl is formed by a recombination reaction (second trace) or reaction of a surface phenyl species with the bromobenzene reactant (third trace). In addition, halide-exchange reactions are known to occur on the copper surface (bottom trace).

of the support material (γ -Al₂O₃).

The presence of the biphenyl product was verified by GC/MS analysis of the contents of the cold trap subsequent to the spectroscopic runs. Furthermore, biphenyl was identified upon extraction of the spent catalyst with CCl₄, followed by GC/MS analysis.

2. Effects of Inhibitors. The reaction of chlorophenols to chlorinated dibenzodioxins occurring on the surface of various fly-ash samples from standard MWI reactions has been used as model for PCDD/F formation (9, 10).



A set of 11 compounds was tested for their ability to block the reaction (9, 10). Alkanolamines, such as triethanolamine and ethanolamine, were found to be most efficient as inhibitors. The dose-response relationship has been studied for the triethanolamine inhibitor (9).

Encouraged by this success, the laboratory experiments have been transferred to a pilot plant incinerator burning a special kind of refuse-derived fuel. By an appropriate technique, a mixture of triethanolamine and triethylamine was added to the stack gas in the 400 °C postcombustion zone. The addition (1:1) resulted in a significant overall reduction of the PCDD/F concentration, by a factor of 12–15 (9). It is worthwhile mentioning that the incinerator must be operated with inhibitor injection for an induction period of about 12 h before the full reduction in PCDD/F levels is achieved (8, 9). Some preliminary results of inhibition studies on a larger technical municipal waste incinerator have also been reported (12, 24).

To understand the mechanism of inhibition, ethanolamine was added together with bromobenzene to the copper catalyst described above, and the surface reactions were studied at 200 °C. Ethanolamine was added pulse-wise into a continuous stream of bromobenzene passing

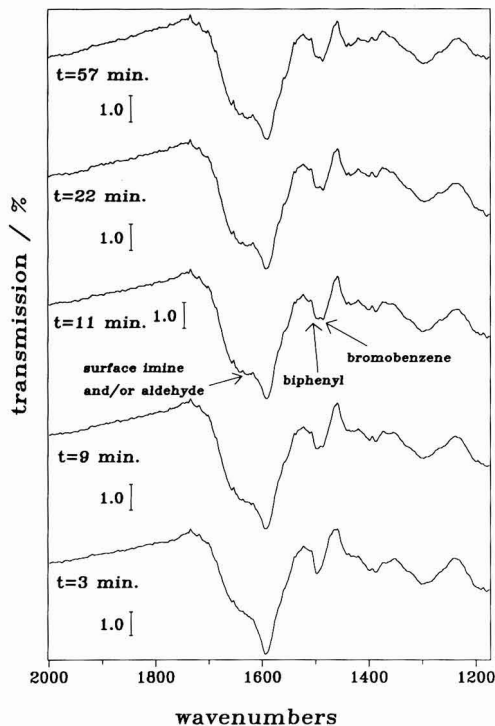


Figure 5. Time dependence of transmittance FTIR spectra recorded over a Cu/ γ -Al₂O₃ catalyst at 200 °C, subsequent to ethanolamine addition to a continuous bromobenzene/nitrogen carrier gas stream. Note that the biphenyl product, which initially prevails on the surface, is progressively displaced by the bromobenzene reactant as the catalyst is being deactivated by ethanolamine. Additional surface species observed are discussed in the text.

over the surface, while the reaction was monitored by FTIR; see Figure 5.

The addition of ethanolamine to the reaction system by this technique was observed to block the formation of biphenyl from bromobenzene. In the presence of ethanolamine, bromobenzene resides on the catalyst surface without further reaction to products. In a complementary experiment, it was impossible to detect a 5- μ L pulse of bromobenzene on a catalyst surface loaded with ethanolamine before addition of bromobenzene. The control experiment, performed in the absence of ethanolamine, proved that 5 μ L of bromobenzene is easily detected on the catalyst surface over a period of 90 min. The reaction and fate of the inhibitor, ethanolamine, can be deduced from new bands observed between 2100 and 2300 cm⁻¹, and a broad band extending from 1610 to 1680 cm⁻¹ which is assigned to a surface-bound aldehyde (19) or a surface imine species (21, 25). The bands in the 2100–2300-cm⁻¹ range are attributed to either azide or cyanide groups formed on the surface of the catalyst (cf. Figure 6). The width and intensity of these bands correspond to those observed in the spectra reported in refs 20 and 21. Azides and imines have been found as intermediates during reaction of primary alkylamines on transition-metal surfaces, in which nitrides are formed as the final state of deactivation (21, 26, 27). It is known that these surface species deactivate the copper catalyst surfaces in various catalytic reactions, such as the dehydroamination reaction (26).

The model of catalyst deactivation by nitride formation is supported by the fact that nitrogen, as well as bromine, is detected in an energy-dispersive X-ray analysis of the

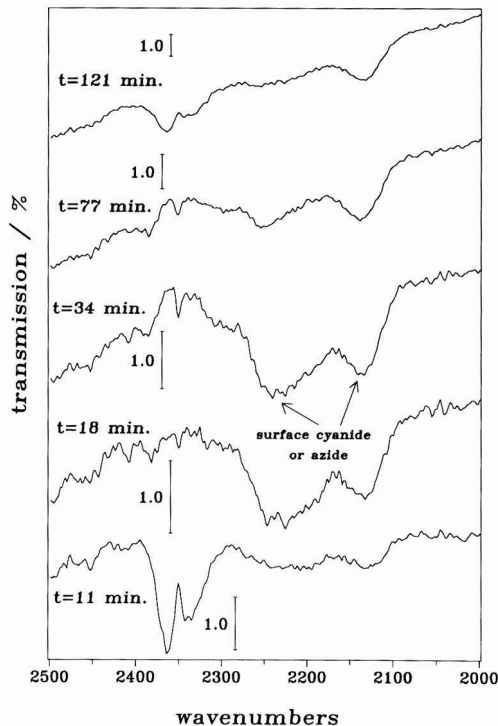


Figure 6. Surface species produced by addition of the ethanolamine inhibitor to the copper catalyst surface. The series of time-dependent spectra shown in Figure 5 is extended to longer reaction times. Attention is focused on the 2100–2300-cm⁻¹ region, where vibrations of surface azides and cyanides are being observed (see text).

catalyst surface subsequent to the inhibition run.

In an experiment using triethylamine, no evidence for a corresponding inhibitory action was found. We only observed a band at 1653 cm⁻¹, which is due to a surface imine (25). This is consistent with the laboratory inhibition tests (11).

In summary, it appears that amines are well suited to inhibit the catalytic action of copper. Primary amines are converted to copper nitride, and the catalyst is deactivated by the formation of the nitride layers. Tertiary amines, such as triethylamine, for which nitride formation has not been observed, are less active as inhibitors.

The second mechanism of inhibition identified in this study is the displacement of the aryl dehalogenation by competitive reactions that are favored on the catalyst surface by preferential adsorption. The dehydroamination reaction, which is known to inhibit other catalytic processes on copper surfaces (26), has been identified as a likely candidate for the competitive inhibition mechanism. The inhibitor studied, ethanolamine, contains both the amine and the alcohol functionalities required for this reaction. The γ -alumina support provides strong adsorption sites for the hydroxyl group of the inhibitor. During dehydroamination, an aldehyde intermediate is formed; the observation of this species provides evidence for the involvement of this reaction in the inhibitory action of ethanolamine.

Conclusion

The conversion of bromobenzene to biphenyl on a defined copper catalyst surface has been monitored by FTIR spectroscopy. By use of this reaction as a model for

PCDD/F formation on fly ashes, the effect of inhibitors was studied by this technique. While no inhibitory action was observed for triethylamine, ethanolamine was shown to act as a very efficient inhibitor, by blocking the active sites of copper surfaces. At this point it is important to draw attention to the differences between the carefully prepared surfaces investigated in this study, and the highly heterogeneous fly ash in the complex environment of an incinerator. Details of the phenomena observed in the laboratory cannot be transferred to the technical plant, and we cannot exclude the possibility that other modes of inhibitory action are important in the incinerator environment. However, the relevant results on the inhibition of dioxin formation obtained in the pilot plant are consistent with the mechanisms proposed in this study.

Acknowledgments

We thank O. Hutzinger for his support, and M. McLachlan for reading the manuscript.

Registry No. Cu, 7440-50-8; PhOH, 108-95-2; Ph₂, 92-52-4; BrPh, 108-86-1; sodium phenolate, 139-02-6; ethanolamine, 141-43-5.

Literature Cited

- (1) Altwicker, E. R.; Schonberg, J. S.; Konduri, R. K. N. V.; Milligan, M. S. *Chemosphere* **1990**, *20*, 1935.
- (2) Shaub, W. M.; Tsang, W. *Environ. Sci. Technol.* **1983**, *17*, 721.
- (3) Karasek, F. W.; Dickson, L. C. *Science* **1987**, *237*, 754.
- (4) Vogg, H.; Stieglitz, L. *Chemosphere* **1986**, *15*, 1373.
- (5) Hagenmaier, H. P.; Kraft, M.; Brunner, H.; Haag, R. *Environ. Sci. Technol.* **1987**, *21*, 1080.
- (6) Gullett, B. K.; Bruce, K. R.; Beach, L. O. *Chemosphere* **1990**, *21*, 1945.

- (7) Hoffmann, R. V.; Eicemann, G. A.; Long, Y.-T.; Collins, M. C.; Lu, M.-Q. *Environ. Sci. Technol.* **1990**, *24*, 1635.
- (8) Zier, B.; Lenoir, D.; Lahaniatis, E.; Ketrup, A. *Chemosphere*, in press.
- (9) Dickson, L. C.; Lenoir, D.; Hutzinger, O.; Naikwadi, K. P.; Karasek, F. W. *Chemosphere* **1989**, *19*, 1435.
- (10) Lenoir, L.; Dickson, L. C.; Hutzinger, O. *Chemosphere*, in press.
- (11) Lenoir, D.; Hutzinger, O.; Mützenich, E.; Horch, K. Z. *UWSF Umweltchem. Okotox.* **1990**, *1*, 3.
- (12) Karasek, F.; Naikwadi, K. P. *Proceedings of "Dioxin 90"*; Ecoinforma: Bayreuth, Germany, 1990; Vol. 3, p 127.
- (13) Fanta, P. E. *Synthesis* **1974**, *1*, 9.
- (14) Koshelev, V. J. *Ser. Khim. Nauk.* **1983**, No. 4, 86.
- (15) Moroz, A. A.; Shvartsberg, M. S. *Russ. Chem. Rev. (Engl. Transl.)* **1974**, *43*, 1443.
- (16) Dickson, L. C. Thesis, Waterloo, 1987; p 112.
- (17) Lippert, T.; Lenoir, D.; Wokaun, A. *Ber. Bunsenges. Phys. Chem.* **1990**, *94*, 1465.
- (18) Kagel, R. O. *J. Catal.* **1970**, *16*, 316.
- (19) Jobson, J.; Baiker, A.; Wokaun, A. *Ber. Bunsenges. Phys. Chem.* **1989**, *93*, 64.
- (20) Jobson, E.; Baiker, A.; Wokaun, A. *J. Chem. Soc., Faraday Trans.* **1990**, *86*, 1131.
- (21) Krittenberger, J.; Jobson, J.; Wokaun, A.; Baiker, A. *Catal. Lett.* **1990**, *5*, 73.
- (22) Hecker, W. C.; Bell, A. T. *J. Catal.* **1981**, *71*, 216.
- (23) Baiker, A.; Richarz, W. *Synth. Commun.* **1987**, *8*, 27.
- (24) Morello, T.; Eng, P. *Proceedings, Meeting on Dioxin Inhibition in MWI Plants*, Augsburg, April 2, 1990.
- (25) Sokoll, R.; Hobert, H.; Schmuck, J. *J. Catal.* **1990**, *121*, 153.
- (26) Baiker, A.; Kijenski, J. *Catal. Rev. Sci. Eng.* **1985**, *27*, 653.
- (27) Baiker, A.; Monti, D.; Son Fan, Y. *J. Catal.* **1984**, *88*, 81.

Received for review December 1, 1990. Revised manuscript received April 29, 1991. Accepted May 3, 1991. This work has been supported by grants of the Deutsche Forschungsgemeinschaft (SFB 213).

Role of Plant Biomass in the Global Environmental Partitioning of Chlorinated Hydrocarbons

Davide Calamari,* Eros Bacchi, Silvano Focardi, Carlo Gaggi, Marco Morosini, and Marco Vighi

Institute of Agricultural Entomology, University of Milan, via Celoria 2, 20133 Milan, Italy, and Department of Environmental Biology, University of Siena, via delle Cerchia 3, 53100 Siena, Italy

■ Plant biomass plays a significant role in the global environmental partitioning phenomena and plants are good indicators of tropospheric contamination levels by chlorinated hydrocarbons. In the present research 300 samples of plants were collected in 26 areas distributed worldwide and analyzed for HCB, α -HCH, γ -HCH, p,p' -DDT, o,p' -DDT, and p,p' -DDE. Global HCB distribution is strongly dependent on the temperature, the HCB being present mainly in samples from cold areas. The sum of DDTs show higher concentrations in samples from tropical areas, while the sum of HCHs is higher in the plants from the Northern Hemisphere. These results are discussed, taking into account the role of physicochemical properties in determining the global distribution as well as the air concentrations, the use patterns of the chemicals, and the age of the contamination.

Introduction

In recent years there has been increasing interest in global contamination from persistent organic chemical

substances, such as chlorinated hydrocarbons. Concentrations in air have been measured and attempts have been made to evaluate the role of the atmosphere in world transport and contamination of remote areas (1-3).

Some groups have attempted to reconstruct the cycling mechanisms of these molecules (4), others to quantify the atmospheric inputs to the world's oceans (5) and to compile a global mass balance (6).

Remote and especially cold areas have been the subject of particular attention and analyses of atmospheric chlorinated pesticides have been performed in Antarctica, Sweden, and Arctic Canada (2, 7, 8).

In terrestrial ecosystems, plant biomass is believed to play a significant role in the circulation and bioaccumulation phenomena of these chemicals, and the air to leaf transfer of gaseous organics can be considered a key process, particularly for less soluble compounds (9-14).

To contribute to a better understanding of both issues, this research group has measured chlorinated hydrocarbons in foliage as an indication of tropospheric contamination levels (15), their contents in lichen and moss samples from the Antarctic Peninsula as base-line levels of world contamination (16), and organochlorine residues in mango foliage from West Africa (17). This paper is an

* University of Milan.
University of Siena.

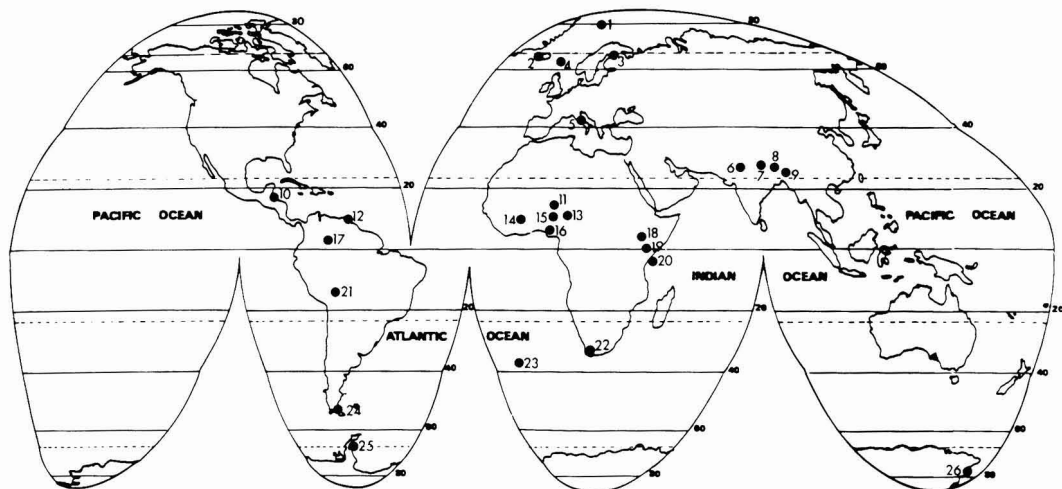


Figure 1. Geographical distribution of the 26 sample sites.

Table I. Information on the 26 Sample Sites

site	lat.	long.	altitude, m	no. of samples	plant species
1. Spitsbergen	78° N	15° E	0	20	lichens, mosses
2. Iceland	65° N	20° W	100–500	8	lichens, mosses
3. Scandinavia	70–60° N	18–33° E	500–700	18	lichens, mosses
4. Foroyar	62° N	7° W	100–500	9	lichens, mosses
5. Italy	46–41° N	9–16° W	100–300	2	lichens
6. New Delhi	29° N	77° E	250	8	mango
7. Nepal	29–27° N	84–87° E	800–2500	21	lichens, mosses
8. Nepal Mountains	29–27° N	84–87° E	2500–4700	32	lichens, mosses
9. Everest	28° N	87° E	5600	6	lichens, mosses
10. Guatemala	16–14° N	89–91° W	600–2500	4	mango, lichens
11. Mali-Guinea	12–9° N	8–10° W	200–500	12	mango
12. Delta Amacuro	11–8° N	60–63°	0	7	lichens, mosses
13. Benin Burkina Faso	12–6° N	2° E	0–300	7	mango
14. Ghana Suhum	8° N	1° E	100–200	20	mango
15. Ivory Coast	7° N	5° E	200–500	5	mango
16. Ghana Accra	6° N	1° E	0	32	mango
17. Amazonas	5–4° N	67–68° W	200–500	16	lichens, mosses
18. Mount Kenya	0°	37° E	3100–4900	23	lichens, mosses
19. Kenya Nairobi	1° S	37° E	1700	2	mango
20. Kenya Mombasa	4° S	39° E	0	5	mango
21. Bolivia	18° S	68° W	3800–5300	9	lichens, mosses
22. Capetown	33° S	18° E	0	1	mango
23. Tristan da Cunha	38° S	12° W	0	10	lichens, mosses
24. Tierra del Fuego	54° S	68° W	0	6	lichens, mosses
25. Antarctic Peninsula	65–68° S	65° W	0	12	lichens, mosses
26. Kay Island	74° S	165° E	0	11	lichens, mosses

extention of a previous investigation, analyzing more samples from different areas of the world with the aim of contributing to the understanding and quantification of the global cycling of these xenobiotics.

Materials and Methods

Selection of Foliage Samples. In cold and temperate areas and at high altitudes (above 2500 m), lichen and moss samples were collected. In tropical areas, fallen mango leaves (*Mangifera indica*) were chosen due to their wide distribution.

All the samples were wrapped in aluminum foil, kept cold (~5 °C) whenever possible, and then stored at –20 °C until pretreatment.

Sample Collection. A total of 300 samples (~10 g each) were collected in 26 areas of the world.

A detailed description of the type of sampling would be lengthy and unnecessary but as a general rule in each area

a variable number of samples were collected along transects of tens to hundreds of kilometers of length, which were considered as representative of the entire geographic area.

The sample collectors were, in a few cases, volunteers, but most of the work was done by the authors of this paper within 1985–1988. Two sampling programs in West Africa and in Antarctica were considered necessary for interpreting the results.

Only a few samples were obtained from Iceland, Capetown, Nairobi, Kenya, and Italy and these were pooled due to the low weight of the biomass but were included in the paper as representative of the areas. Figure 1 shows the sample sites on a world map while Table I gives geographic areas, numbers of samples, types of plants collected, approximate altitudes above sea level, latitude, and longitude.

Chemical Analysis. After partial oven-drying, minced samples were extracted in a Soxhlet apparatus with *n*-hexane as solvent. Residual water content was measured

Table II. Selected Physicochemical Properties of the Molecules Studied

	MW	VP P_{sat}^a Pa	water sol C_{sat}^a mol/m ³	log K_{ow}	H , Pa m ³ /mol
HCB	284.8	1.5×10^{-3}	1.7×10^{-5}	6.0	88
α -HCH	290.9	3.0×10^{-3}	6.9×10^{-3}	3.8	0.43
γ -HCH	290.9	4.0×10^{-3}	2.4×10^{-2}	3.8	0.17
<i>p,p'</i> -DDT	354.5	2.5×10^{-5}	8.5×10^{-6}	6.0	2.9
<i>o,p'</i> -DDT	354.5	4.5×10^{-4}	8.5×10^{-6}	6.0	53
<i>p,p'</i> -DDE	318.0	8.0×10^{-4}	1.3×10^{-4}	5.0	6.2

^a At 20 °C.

on homogeneous subsamples (105 °C, 24 h). Sulfuric acid cleanup was followed by Florisil column chromatography. Samples were analyzed with a Perkin-Elmer Sigma-3B chromatograph, using a 30 m \times 0.2 mm (i.d.) SPB-5 bonded-phase (0.25- μ m film thickness) fused-silica capillary column from Supelco. Carrier gas: argon-methane 95/5%, 100 kPa, split ratio 66/1; injector and EC detector temperatures were 220 and 280 °C, respectively; oven temperature 100 °C for 10 min to 280 °C at 3 °C/min and maintained for 40 min.

Statistical Treatment of the Data. A log-probit analysis was performed on the foliage concentration of samples from the same area according to a BASIC computer program suggested by Trevors (18) but slightly modified. This statistical approach was used by Bacci et al. (17) and recently has been suggested as appropriate by Travis and Land (19) and by Helsel (20).

A median C50 was calculated for each group of samples. The values corresponding to probit 4 and 6 (C16–C84), indicating the range around the median where ~68% of the results were expected, were also calculated; from these values the slope of the sample distribution line was obtained. A χ^2 test gave an indication of the homogeneity of the sample population and was significant in almost all cases.

Physicochemical Parameters. A review of the literature was performed in order to estimate the main parameters relevant to understanding environmental distribution processes. Table II shows data on vapor pressure, water solubility, and octanol–water partition coefficients (log K_{ow}) critically selected from a number of literature sources (5,21–27).

Vapor pressure data are in good agreement with a series of experimental values recently produced by B. Rordorf (personal communication).

Results

Mean concentrations, calculated as C50, of the six molecules, for the 26 sample sites, are reported in Table III. The χ^2 values and the slopes of the sample distribution lines are also shown in the table.

For hexachlorobenzene (HCB) and for the sum of hexachlorocyclohexanes (HCHs) and DDTs a log-probit analysis has also been performed on the mean values for the different sites in order to obtain a more easily comparable picture of the global range of values.

The distribution lines, reported in Figure 2, indicate that HCB shows relatively low concentrations, with a C50 of 0.12 ng/g. The C50 values for total HCHs and DDTs are more than 1 order of magnitude higher.

The concentrations in plant foliage here reported are consistent with the published data; see, for example, pine needles from several samples in Germany (28), Italy (15), and other European countries (11), lichens from Sweden,

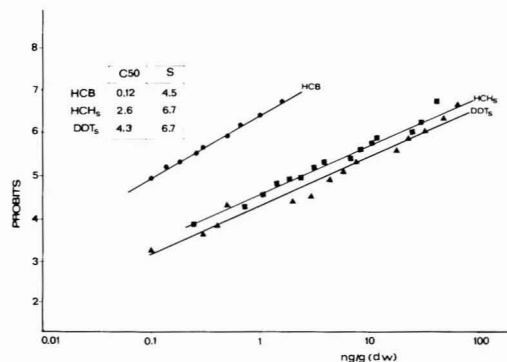


Figure 2. Log-probit distribution of the mean values of concentration in foliage in the 26 sample sites for HCB and the sum of HCHs and DDTs. The C50 values and the slopes (S) are also reported.

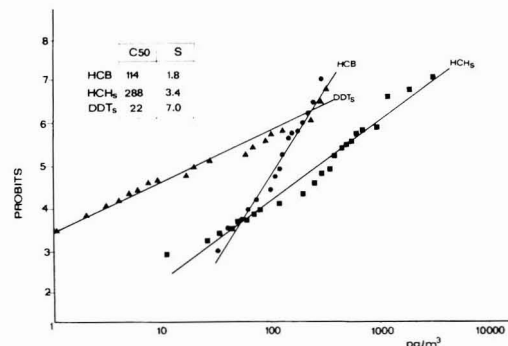


Figure 3. Log-probit distribution of air concentration values for HCB and the sum of HCHs and DDTs taken from the literature (2, 5, 7, 33–35). C50 values and the slopes (S) are also reported.

Norway, and France (29–31), and mango foliage from Colombia (32).

Discussion

Chlorinated hydrocarbons have been found in foliage in all parts of the world. The concentration means and ranges are variable according to the areas studied, but high enough to permit reliable analysis and thus the use of foliage as a biomonitor of presence of chlorinated hydrocarbons even in remote areas where problems may arise for air sampling. Conceptually, this kind of approach could be used to monitor other persistent chemicals with comparable circulation patterns.

As foliage contamination from organochlorinated hydrocarbons is believed to depend on the concentration in the atmosphere (11, 15), a survey of the literature has been made in order to compare global air concentrations with global plant concentrations measured in this work. Figure 3 shows the levels in the atmosphere taken from the literature (2, 5, 7, 33–35) treated with the same log-probit statistical analysis. Results indicate a different ranking among the compounds in comparison with foliage. In air the lowest mean values are for DDTs, in the middle in HCB, and the highest values are for HCHs.

From the global levels in foliage and in air, a bioconcentration factor (BCF) can be calculated as the ratio between the C50 in the two compartments. The values obtained are in good agreement with those experimentally measured in simulation chambers by Bacci et al. (12), as shown in Table IV. This seems to confirm that some

Table III. Mean Concentrations (C50 in ng/g Dry Weight) and Statistical Parameters (χ^2 , Degrees of Freedom (DF), and Slope (S) of the Log-Probit Line for the Organochlorines in the 26 Sample Sites*

site	HCB	α -HCH	γ -HCH	p,p' -DDT	o,p' -DDT	p,p' -DDE	site	HCB	α -HCH	γ -HCH	p,p' -DDT	o,p' -DDT	p,p' -DDE
1. Spitsbergen							14. Ghana Suhum						
C50	1.00	3.42	0.52	0.30	ND	0.20	C50	<0.1	0.30	2.80	2.40	0.80	0.40
χ^2	4.98	9.44	14.54	7.82		16.40	χ^2		12.60	8.60	2.50	3.50	11.10
DF	17	17	17	14		14	DF		17	17	17	17	17
S	2.7	2.2	1.8	1.6		1.7	S		1.7	2.7	2.1	2.0	1.9
2. Iceland							15. Ivory Coast						
x	1.47	4.90	0.78	0.39	ND	0.10	C50	<0.1	0.69	0.35	3.30	0.70	1.60
3. Scandinavia							χ^2		0.38	0.49	0.82	0.82	1.19
C50	0.68	8.59	3.69	1.60	0.90	0.40	DF		2	2	2	2	2
χ^2	4.36	3.82	2.05	3.60	8.61	7.18	S		1.6	1.9	1.8	1.4	4.9
DF	15	15	15	14	14	14	16. Ghana Accra						
S	2.6	2.8	2.7	3.0	3.0	3.3	C50	<0.1	0.30	1.00	15.00	1.50	1.90
4. Föroyar							χ^2		23.60	26.50	44.00	26.10	19.70
C50	0.27	0.81	0.66	2.90	ND	0.70	DF		29	29	29	29	29
χ^2	0.42	5.29	0.50	2.45		2.47	S		1.6	1.7	2.9	3.1	2.3
DF	6	6	6	6		6	17. Amazonas						
S	1.6	2.3	2.0	2.5		4.0	C50	<0.1	41.39	0.15	52.20	7.70	6.50
5. Italy							χ^2		2.11	6.27	3.20	2.98	5.81
x	1.41	26.93	9.95	12.40	ND	8.40	DF		13	13	13	13	13
6. New Delhi							S		5.3	6.1	10.3	7.8	10.6
C50	<0.1	106.9	13.55	77.80	10.80	21.00	18. Mount Kenya						
χ^2		0.19	0.60	1.10	0.90	1.70	C50		0.52	7.93	0.78	4.00	1.00
DF		5	5	5	5	5	χ^2		7.40	4.54	9.75	18.40	8.50
S		2.4	3.3	1.7	1.4	1.9	DF		20	20	20	20	20
7. Nepal							S		2.0	2.4	4.4	2.7	4.6
C50	0.10	21.52	3.46	13.70	2.40	1.90	19. Nairobi, Kenya						
χ^2	4.10	28.42	9.29	15.46	9.20	7.15	x	<0.1	1.45	0.88	13.50	2.10	6.70
DF	13	18	18	18	18	18	20. Mombasa, Kenya						
S	2.4	3.1	3.5	3.1	3.0	2.4	C50	<0.1	2.71	0.78	13.80	5.70	25.44
8. Nepal Mountains							χ^2		0.75	0.44	1.06	1.45	0.48
C50	0.25	35.74	4.47	10.50	4.00	1.60	DF		2	2	2	2	2
χ^2	6.09	19.42	9.68	3.61	5.15	11.87	S		2.4	1.3	2.0	1.6	1.7
DF	24	28	28	28	29	28	21. Bolivia						
S	2.6	2.7	2.3	2.4	2.0	2.2	C50		0.18	1.10	0.79	1.20	0.40
9. Everest							χ^2		1.16	1.23	1.31	0.97	1.28
C50	0.48	9.50	1.15	2.10	1.80	0.30	DF		6	6	6	6	6
χ^2	0.63	0.69	0.34	0.75	1.59	1.17	S		1.7	1.9	2.1	2.9	3.6
DF	3	3	3	3	3	3	22. Capetown						
S	1.8	1.7	1.8	2.4	2.0	2.5	x		0.12	0.58	0.77	4.40	<0.1
10. Guatemala							23. Tristan Da Cunha						
C50	0.14	0.45	0.32	2.90	0.40	1.10	C50	<0.1	0.19	<0.1	ND	ND	ND
χ^2	0.28	0.34	0.55	0.54	0.01	0.10	χ^2			1.39			
DF	4	4	4	4	4	4	DF		7				
S	1.4	1.6	2.2	2.4	3.5	2.8	S		1.5				
11. Mali-Guinea							24. Tierra del Fuego						
C50	<0.1	0.50	0.20	37.00	4.30	8.10	C50		0.15	0.21	<0.1	0.15	0.20
χ^2		6.89	5.12	2.25	2.44	1.42	χ^2		0.64	0.68		0.51	1.69
DF		9	9	9	9	9	DF		3	3		2	2
S		2.2	2.2	6.2	8.2	4.8	S		1.5	2.7		2.0	1.9
12. Delta Amacuro							25. Antarctic Peninsula						
C50	<0.1	7.58	0.30	27.50	2.10	2.60	C50		0.49	0.32	0.71	0.30	ND
χ^2		1.43	1.68	0.45	1.58	1.15	χ^2		2.23	3.55	1.61	1.50	2.50
DF		4	4	4	4	4	DF		9	9	9	9	9
S		3.7	4.9	8.5	5.0	8.8	S		1.6	1.7	1.5	2.5	2.0
13. Benin-Burkina Faso							26. Kay Island						
C50	<0.1	0.60	<0.1	5.10	1.00	1.00	C50		0.30	0.17	0.04	0.20	ND
χ^2		2.50		0.80	0.90	1.70	χ^2		3.21	3.42	2.74	3.27	4.76
DF		4		4	4	4	DF		8	8	8	8	8
S		2.3		4.7	5.3	11.0	S		2.7	1.6	2.0	2.0	2.0

*ND, not detected. A geometric mean (x) is reported if samples were too few for a complete statistical evaluation.

Table IV. Values of Foliage-Air BCF for HCB, HCHs, and DDTs Calculated as Mass Ratio between Global Mean Concentrations (C50) in Foliage and Air, Compared to Experimentally Measured Values in Simulation Chambers (12)

	HCB	HCHs	DDTs
BCF (C50 ratio)	1.3×10^3	1.1×10^4	2.4×10^5
BCF (exptl)	1.9×10^3	4.6×10^3 (α) 3.4×10^3 (γ)	1.9×10^5 (p,p' -DDT) 1.3×10^5 (p,p' -DDE)

aspects of the global behavior of these molecules can be predicted from small-scale experiments and/or theoretical evaluations.

It could thus be suggested that vegetation can be used as an indicator of air contamination, although some sources of variability exist and cannot be controlled.

Possibly the use of old vegetation takes into account the different rates of absorption/release kinetics, but other pitfalls or sources of error (e.g., chemical reactions, translocation, local meteorological conditions) cannot be evaluated.

In the following paragraphs, some comments on the single substances will be presented.

Hexachlorobenzene (HCB). According to Atlas and Giam (4), HCB is, along with HCHs, one of the predominant chlorinated hydrocarbons in the marine atmosphere, with a relatively homogeneous distribution in the two

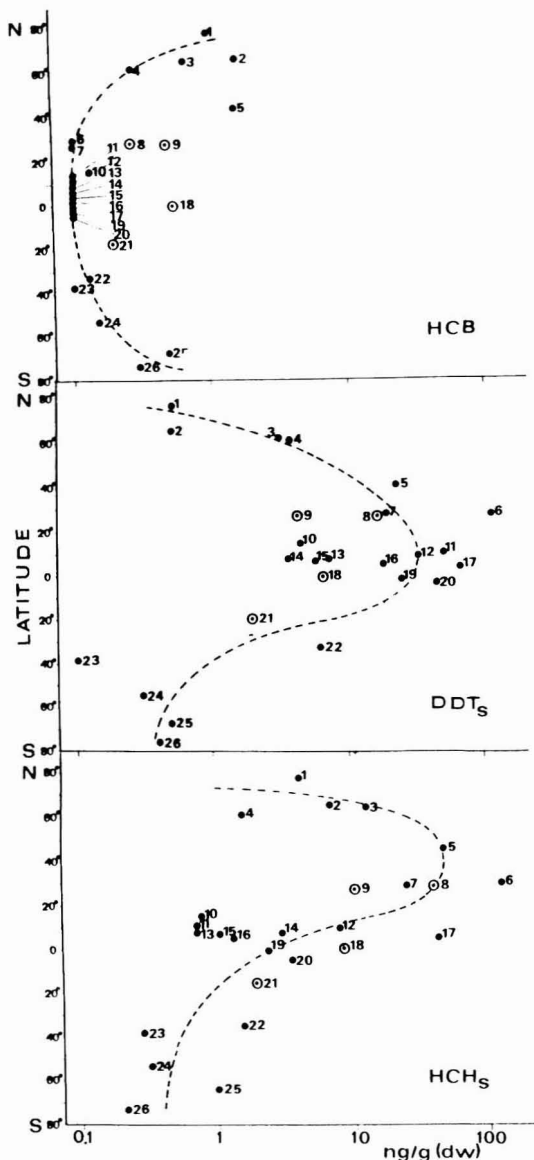


Figure 4. Distribution of HCB and sum of DDT and sum of HCH mean concentrations in the 26 sample sites as a function of the latitude. Circled points represent mountain sites.

hemispheres. In contrast, a high interhemispheric gradient has been suggested by Wittlinger and Ballschmitter (3) but this is based only on a limited quantity of data.

Differences in atmospheric distribution between compounds are related to differences in source strength and in atmospheric residence times. On the basis of its physicochemical properties, in particular its relatively high Henry's law constant, it is expected that HCB will have an atmospheric residence time longer than other chlorinated hydrocarbons. Consequently, Atlas and Giam (4) predicted and found a small interhemispheric gradient. This hypothesis has also been recently proposed in a wide literature survey carried out by GESAMP (5) and is confirmed by Figure 3, which indicates that atmospheric concentrations of HCB extend over a relatively small

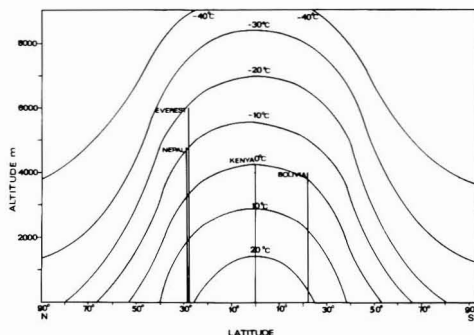


Figure 5. Global distribution of mean temperatures as a function of latitude and height. The four mountain sites considered in the present survey are indicated.

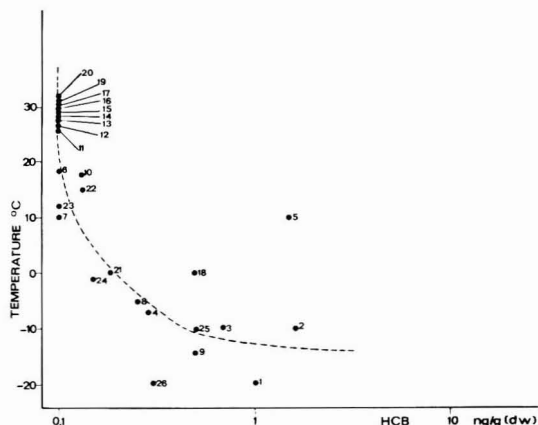


Figure 6. Relationship between HCB mean concentrations and mean temperature of the sampling sites.

range. Concentrations of HCB in plants verify this hypothesis, even if the differences among the slopes of the various molecules are less evident (Figure 2).

A better explanation of the variability of HCB concentrations in plants is given in Figure 4. From the figure it appears that, together with a slight difference between hemispheres, a difference between low and high latitudes is more evident. In tropical areas HCB concentrations in plants are always negligible and increase toward cold regions. Relatively high values in tropical or subtropical areas were found only in high-altitude samples (Nepal, Kenya, etc.).

On the basis of an approximate distribution of mean temperature in function of latitude and height (Figure 5) it is possible to find a good relationship between HCB concentrations and annual temperature averages, the only exception being Italian samples (Figure 6).

This trend can be explained by a "cold condenser" effect, particularly important with a volatile molecule such as HCB. These data indicate that the observed concentrations of HCB in the areas sampled in this survey are the result of a long-term distribution, regulated by global processes and physicochemical properties more than by direct contamination.

Italian data appear as outliers due to the fact that they derive from the only highly developed and industrialized temperate area included in the survey, where contamination due to use can be considered the prevailing process. HCB levels in Italian pines are comparable to those in plants from other developed countries (United States,

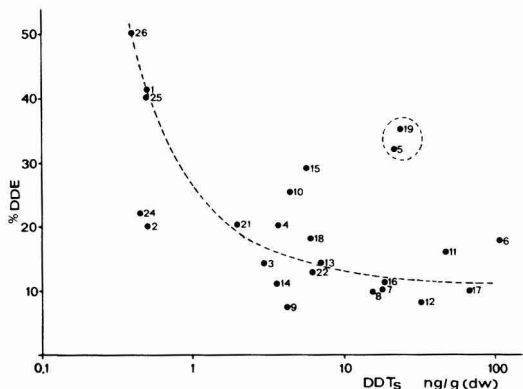


Figure 7. Relationship between DDT concentrations in foliage and the percentage of p,p' -DDE.

Yugoslavia) (15), but are not reported in this survey due to different sampling methodology.

DDTs. The most common DDT forms in the environment are p,p' -DDT, its isomer o,p' -DDT present in the technical product, and its degradation product p,p' -DDE, though in some cases other degradation products, such as DDDs, can be present at significant levels.

Total DDT introduced before the 1972 ban should exist primarily in the form of degradation products (mainly DDE) (36). However, DDT is still heavily used in several developing countries, accounting for the nonhomogeneous distribution of total DDT concentrations in the atmosphere (see slope in Figure 3). Current usage of DDT also affects concentrations measured in foliage. Higher concentrations were measured where an intensive use is still present or took place in the recent past.

In contrast to HCB, DDT plant concentrations are highest in tropical and subtropical areas (Figure 4).

In Figure 7 a relationship between the total amount of DDTs measured in foliage and the percent of DDE is evident. The highest values of DDT concentrations with low percentage of DDE are typical of areas where DDT is still in use in large amounts (e.g., India), whereas low levels of total DDTs correspond, in general, to high DDE percentages, and this can indicate long-range, indirect contamination. Only Italy and Kenya behave as outliers, being areas of high but not recent contamination.

Total DDT distribution is not related to temperature, unlike HCB. Nevertheless, for o,p' -DDT, a relationship with temperature was observed (Figure 8). This is in agreement with the physicochemical properties of the molecules (Table II) and in particular with the high Henry's law constant of o,p' -DDT, although very cold areas are not considered in the figure due to the low levels of DDTs that make unreliable the calculations of the percentage of the DDT forms.

Hexachlorocyclohexanes (HCHs). HCHs are used in the form of nearly pure γ isomer (lindane) or as technical product, a mixture of five isomers where the α form is the prevalent with an amount of ~55–80%. At present, the pure γ form is the most widely used but large amounts of the technical product are still produced and employed, mainly in the Far East (7).

HCHs show relatively high concentrations in the atmosphere and a gradient between the Northern and Southern Hemispheres has been observed (3–5).

Several authors indicated α -HCH as the major component of total HCH (1, 7, 8). Bidleman et al. (7) proposed two possible explanations: a long-range transport from

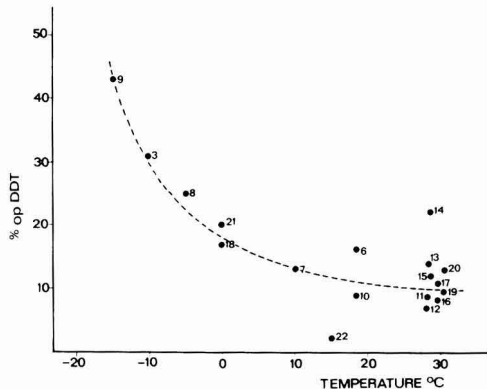


Figure 8. Relationship between the percentage of o,p' -DDT and the mean temperature of the sampling sites.

developing countries where the technical product is largely used, and an isomerization process from the γ to the α form.

On the other hand, Atlas and Giam (35) hypothesized that the ratio α -HCH/ γ -HCH is an indication of the age of an air parcel. A high α/γ ratio indicates older air. They observed that air masses with trajectories directly from Europe, where only the γ form is used, had an α/γ ratio of ~5/1, while background air had ratios near 50/1.

Foliage data measured in this survey show a relatively high C50 (Figure 2), comparable with the DDT value, and a flat slope, indicating a very wide range of concentrations.

The geographical distribution (Figure 4) confirms a gradient between Northern and Southern Hemispheres for total HCHs. The mean value (C50) of Northern samples is ~5 times higher than those of the Southern Hemisphere. The ratio between α and γ isomers confirms, with some exceptions, the prevailing role of α -HCH. Nevertheless it is very difficult to understand distribution patterns because the relative amounts of α and γ isomers are affected by at least two factors: the present use of the technical product or of the pure lindane, and the isomerization of γ - to α -HCH. The concurrence of those two factors can give very conflicting results. For example, the high α/γ ratios observed in some areas of Latin America (Amazonas, Delta Amacuro) can be assumed to be an indication of a strong use of technical product rather than of old contamination; in fact, the flat slopes observed in these extended areas seem to be an indication of recent and direct contamination. In contrast, the very low levels of α/γ ratio in some African areas indicate a recent use of the pure γ form. In conclusion, the levels of HCHs and the ratios between the two forms seem to be strongly affected by the present high use in different formulations rather than by long-range distribution processes and by the role of physicochemical properties, which are very similar for both isomers (Table II).

In the interpretation of the global distribution of persistent organic chemicals in vegetation based on physicochemical properties, it is important to use data from areas without relatively recent usage of the chemical. For HCB, only the Italian samples can be assumed not to have this characteristic. Thus, the main features of the observed distribution of HCB appear influenced more by long-range processes regulated by molecular properties and environmental phenomena (e.g., cold condenser effect) than by contamination due to use.

For HCHs and DDTs the problem is more complex due to the actual use of these molecules, in particular in de-

veloping countries from which most of the samples examined in this survey derive. Therefore only partial deductions can be made.

Conclusions

The present work and other literature on chemicals in vegetation indicate the following general conclusions: (a) there is a linear relationship between concentration of chemicals in foliage and in air (12), and the role of root translocation is, for the studied compounds, negligible (10); (b) chlorinated hydrocarbons can be detected in plant foliage from different species and the choice of the species is relatively irrelevant in relation to the aim of the investigation (15), especially when dealing with global distribution; (c) concentration in foliage is a suitable monitor of atmospheric contamination (11, 15, 31); (d) parent compound and metabolite ratios can provide information on the age of contamination (16, 36); (e) slopes of the frequencies of concentration (probits) within groups of samples (i.e., from the same geographical areas) can give indications of actual use and redistribution (17); (f) concentrations in lichens and mosses in Antarctica have been studied with the assumption that this area would have been the cleanest part of the world, being the farthest from the technological world (16); the findings however did not confirm this hypothesis (17), at least for certain substances (i.e., HCB); (g) chlorinated hydrocarbons distribute and cycle between air-water and air-soil by means of deposition-volatilization periods, with the so-called "grasshopper effect" (37); (h) according to literature data, substances with subcooled liquid vapor pressure (P_l) higher than 10^{-5} Pa tend to be distributed mainly in the vapor phase of the atmosphere, confirming the essential role of vapor movements in the global transport of these chemicals (38); (i) tropical areas have been identified, mainly due to climatic and meteorological reasons, more as contamination sources than as contamination receivers; this last role is more suited to the cold areas (cold condenser effect) (17).

Acknowledgments

We thank every person or organization contributing to the samples collection and B. Rordorf for providing unpublished data.

Literature Cited

- (1) Atlas, E. L.; Giam, C. S. *Science* 1981, 211, 163-165.
- (2) Tanabe, S.; Hidaka, H.; Tatsukawa, R. *Chemosphere* 1983, 12, 277-288.
- (3) Wittlinger, R.; Ballschmitter, K. *Fresenius J. Anal. Chem.* 1990, 336, 193-200.
- (4) Atlas, E. L.; Giam, C. S. In *The role of air-sea exchange in geochemical cycling*; Bouat-Menard, P., Ed.; NATO-ASI Series C 185; Reidel Publishing Co.: Dordrecht, The Netherlands, 1986; pp 295-329.
- (5) GESAMP, Joint Group of Experts on Scientific Aspects of Marine Pollution. *Rep. Stud.*-GESAMP 1989, No. 38, 1-111.
- (6) Tateya, S.; Tanabe, S.; Tatsukawa, R. In *Toxic contamination in large lakes*; Schmidtke, N. W., Ed.; Lewis Publishers: Chelsea, MI, 1988; Vol. III, pp 273-281.
- (7) Bidleman, T. E.; Wideqvist, U.; Jansson, B.; Soderlund, R. *Atmos. Environ.* 1987, 21, 641-654.

- (8) Patton, G. W.; Hinckley, D. A.; Walla, M. D.; Bidleman, T. F.; Hartgrave, B. T. *Tellus* 1989, 41B, 243-255.
- (9) Buckley, E. H. *Science* 1982, 216, 520-522.
- (10) Bacci, E.; Gaggi, C. *Bull. Environ. Contam. Toxicol.* 1985, 35, 673-681.
- (11) Ericksson, G.; Jensen, S.; Kylin, H.; Strachan, W. *Nature* 1989, 34, 42-44.
- (12) Bacci, E.; Calamari, D.; Gaggi, C.; Vighi, M. *Environ. Sci. Technol.* 1990, 24, 885-889.
- (13) Riederer, M. *Environ. Sci. Technol.* 1990, 24, 829-836.
- (14) Trapp, S.; Matthies, M.; Scheunert, I.; Topp, E. M. *Environ. Sci. Technol.* 1990, 24, 1246-1251.
- (15) Gaggi, C.; Bacci, E.; Calamari, D.; Fanelli, R. *Chemosphere* 1985, 14, 1673-1686.
- (16) Bacci, E.; Calamari, D.; Gaggi, C.; Fanelli, R.; Focardi, S.; Morosini, M. *Chemosphere* 1986, 15, 747-754.
- (17) Bacci, E.; Calamari, D.; Gaggi, C.; Biney, C.; Focardi, S.; Morosini, M. *Chemosphere* 1988, 17, 693-702.
- (18) Trevors, J. T. *Bull. Environ. Contam. Toxicol.* 1986, 37, 18-26.
- (19) Travis, C. C.; Land, M. L. *Environ. Sci. Technol.* 1990, 24, 961-962.
- (20) Helsel, D. R. *Environ. Sci. Technol.* 1990, 24, 1766-1774.
- (21) Hansch, C.; Leo, A. J. *Substituent constants for correlation analysis in chemistry and biology*; John Wiley: New York, 1979.
- (22) Lyman, W. J.; Reehl, W. F.; Rosenblatt, D. H. *Handbook of chemical property estimation methods*; McGraw-Hill Book Co.: New York, 1982.
- (23) Suinto, L. R.; Shiu, W. Y.; Mackay, D.; Seiber, J. N.; Glotfelty, D. *Rev. Environ. Contam. Toxicol.* 1987, 103, 1-59.
- (24) Worthing, C. R.; Walker, S. B. *The Pesticide Manual*, 8th ed.; The British Crop Protection Council: Lavenham, Suffolk, U.K., 1987.
- (25) Verschuere, K. *Handbook of environmental data on organic chemicals*, 2nd ed.; Van Nostrand Reinhold Co.: New York, 1983.
- (26) Morris, C. R.; Cabral, J. R. P. *Hexachlorobenzene: proceedings of an international symposium*; IARC Scientific Publication 77; International Agency for Research on Cancer: Lyon, France, 1986.
- (27) De Bruijn, J.; Busser, F.; Seinen, W.; Hermens, J. *Environ. Toxicol. Chem.* 1989, 8, 499-512.
- (28) Reishl, A.; Reissinger, M.; Hutzinger, O. *Chemosphere* 1987, 16, 2647-2663.
- (29) Villeneuve, J. P.; Holm, E. *Chemosphere* 1984, 13, 1133-1138.
- (30) Carlberg, G.; Baumann-Ofstad, E.; Drangholt, H.; Steinnes, E. *Chemosphere* 1983, 12, 341-356.
- (31) Villeneuve, J. P.; Fogelquist, E.; Cattini, C. *Chemosphere* 1988, 17, 399-403.
- (32) Schrimpf, E. *Water, Air, Soil Pollut.* 1984, 21, 279-315.
- (33) Guicherit, R.; Schulting, F. L. *Sci. Total Environ.* 1985, 43, 193-219.
- (34) Nakano, T.; Tasuji, M.; Okuno, T. *Chemosphere* 1987, 16, 1781-1786.
- (35) Atlas, E. L.; Giam, C. S. *Water, Air, Soil Pollut.* 1988, 38, 19-36.
- (36) Rapaport, R. A.; Urban, N. R.; Capel, P. D.; Baker, J. E.; Looney, B. B.; Eisenreich, S. J.; Gorham, E. *Chemosphere* 1985, 14, 1167-1173.
- (37) Mackay, D.; Paterson, S.; Schroeder, W. H. *Environ. Sci. Technol.* 1986, 20, 810-816.
- (38) Bidleman, T. F.; Billings, W. N.; Foreman, W. T. *Environ. Sci. Technol.* 1986, 20, 1038-1043.

Received for review January 23, 1991. Revised manuscript received April 18, 1991. Accepted April 22, 1991.

Mutagenicity of Indoor Air Containing Environmental Tobacco Smoke: Evaluation of a Portable PM-10 Impactor Sampler

Paris E. Georgioulou,* Philip Blagden, David A. Snow, and Linda Winsor

Department of Chemistry, Memorial University of Newfoundland, St. John's, Newfoundland, Canada A1B 3X7

David T. Williams

Health and Welfare Canada, Environmental Health Directorate, Monitoring and Criteria Division, Tunney's Pasture, Ottawa, Ontario, Canada K1A 0L2

■ An indoor air sampling impactor (IASI) was used to sample inhalable suspended particulate matter (PM-10) in indoor air. The unit, which is convenient to use, light weight and portable, was compared in a controlled indoor setting with a Sierra-Andersen dichotomous sampler (DICHOT) equipped with a PM-10 inlet. The two samplers were used for coreplicate sampling in the same test room both in the presence of and in the absence of environmental tobacco smoke (ETS). Gravimetric analyses and mutagenicity testing of solvent extracts of the particulate matter, using the microspuspension modification of the *Salmonella typhimurium* mutagenicity test, were used to compare the two samplers. In a limited field trial of the IASI sampler in various residential indoor environments containing low and high ETS levels, PM-10 concentrations ranged from 20 to 3000 $\mu\text{g}/\text{m}^3$. Mutagenic responses in the presence of the S9 metabolizing system ranged from 13 to 13 000 revertants/ m^3 .

Introduction

Nonindustrial indoor environments are significant contributors to human exposure to airborne pollutants (1). It has been estimated that individuals spend up to 90-95% of their time indoors (2), where commonly encountered indoor air pollutants (3) include inhalable particulate matter (IPM). A considerable effort has been devoted to the sampling and evaluation of IPM in ambient air (4-6). Dichotomous samplers have been developed to fractionate the particulate matter (PM) having mean median diameters of $<10\ \mu\text{m}$ (PM-10) into coarse inhalable (2.5-10 μm) and fine inhalable ($<2.5\ \mu\text{m}$) fractions (7). It has been shown that IPM and PM-10 concentrations in nonindustrial indoor environments can exceed outdoor ambient concentrations (8-10). Residential wood combustion (9), environmental tobacco smoke (ETS) (11), and the improper use of portable ultrasonic humidifiers with tap water (12) are significant contributors to IPM in many indoor environments.

Methods for assessing personal exposure to indoor air pollutants are not as well developed as those for ambient air monitoring (13, 14). Liou et al. (15) and Lewtas et al. (16) have reported the use of medium-volume samplers (0.70 and 0.21 m^3/min , respectively) and relatively large sampling times (8 and 24 h, respectively) to collect sufficient indoor air particulate matter to allow their mutagenicity to be determined. A study by Mumford et al. (17) employed high- (1.1 m^3/min) and medium-volume (0.11 m^3/min) samplers in relatively high particulate laden indoor environments for sampling periods of 6-40 min to collect sufficient particulate matter for mutagenicity testing. Lofroth et al. (18) employed personal samplers to sample ETS in indoor public areas. The samplers, whose cut size was not specified, employed glass fiber filters and low sampling rates of 0.002 m^3/min over sampling times ranging from <1 to 6 h. For the small sample

sizes obtained, Kado's microspuspension modification (19) of the Ames mutagenicity assay (20) was required.

As a result of the recent promulgation of the ambient air PM-10 standard by the U.S. Environmental Protection Agency (21), we were interested in developing methodologies for assessing the levels and mutagenicity of indoor air PM-10. This required a sampler capable of collecting PM-10 quietly and unobtrusively for relatively short sampling periods (1-2 h) and yet providing a sufficiently large sample for mutagenicity testing. An inexpensive and convenient to use portable indoor air sampling impactor (IASI) capable of collecting PM-10 at 10 L/min on membrane filters has been developed by Marple et al. (22). This sampler has been intercompared with a dichotomous sampler in an outdoor study (23) in which only glass fiber filters were employed. We report here our results from studies in which we used the IASI to sample several residential indoor air locations. In some cases, by coreplicate sampling, we have compared the IASI with a dichotomous sampler equipped with a PM-10 inlet. In all cases, Teflon membrane filters were employed to minimize the potential for artifact formation observed when glass fiber filters were used (24). The mutagenic activities of solvent extracts of the sampled particulate matter were determined by a modification of the microspuspension procedure of Kado et al. (19, 25) for the Ames *Salmonella typhimurium*/microsome mutagenicity assay (20).

Materials and Methods

Samplers. An indoor air sampling impactor (IASI) with a 10- μm cut size and a 10.0 L/min flow rate was used as specified by the manufacturer, Air Diagnostics and Engineering Inc., Naples, ME. The pumping unit of the IASI is housed in a 43 cm \times 24 cm \times 33 cm carrying case and the impactor unit is 26 cm high. The noise output measured at 1 m is less than 45 dB. Other characteristics of the impactor have been described previously (22, 23). A Sierra-Andersen Series 240 dichotomous sampler (DICHOT) with a PM-10 inlet was used in the intercomparison experiments. This sampler operates at a 16.7 L/min flow rate and divides the collected particulate matter into fine ($<2.5\ \mu\text{m}$) and coarse (2.5-10 μm) fractions. The flow rates of each sampler were checked with a 1.00-L bubble flowmeter at the beginning and end of each sampling period.

Teflon membrane filters (37-mm diameter, 2- μm pore size) purchased from Sierra-Andersen Inc. were used in both samplers. Antistatic ^{210}Po devices were used to remove static charge on the filters prior to weighing of the filters. The filters were preweighed on a Cahn 4100 microbalance, stored in glass Petri dishes between layers of aluminum foil until use, returned to the Petri dishes immediately after sampling to minimize potential contamination from the filter holders (26), and weighed within 24 h of sampling. All filters were weighed in triplicate (results to $\pm 10\ \mu\text{g}$). The relative humidity and temperature in the

Table I. Mass of PM-10 Sampled Coreplicately with a Sierra-Andersen Sampler DICHOT and an Indoor Air Sampler (IASI)^a

test no.	DICHOT		IASI	
	mass of combined coarse + fine fractns, μg	PM-10 concn, $\mu\text{g}/\text{m}^3$	mass of PM-10, μg	PM-10 concn, $\mu\text{g}/\text{m}^3$
1	1049	2430 \pm 92	750	2780 \pm 104
2	903	1390 \pm 51	555	1400 \pm 37
3	1108	1630 \pm 34	803	1890 \pm 42
4	1972	3910 \pm 69	1294	4200 \pm 76
5	832	236 \pm 2	510	254 \pm 4
6	1098	2110 \pm 30	714	2160 \pm 43
7	1886	1380 \pm 19	1252	1460 \pm 21
8	587	8.42 \pm 0.21	353	7.79 \pm 0.22
9	901	9.76 \pm 0.22	535	9.32 \pm 0.18
10	1149	9.59 \pm 0.15	875	11.50 \pm 0.22
11	105	5.68 \pm 0.76	64	5.29 \pm 0.83

^a Conditions for tests described in Materials and Methods.

weighing room were 60–65% RH and 20–21 °C. After being weighed, the loaded filters were stored at –20 °C in the glass Petri dishes sealed with Parafilm until the filters were extracted for bioassay.

Test Locations. Coreplicate sampling experiments (Table I) were conducted in an empty 40-m³ office with painted gypsum-board walls and a carpeted floor. All samples were collected with the door closed. When necessary, the room was ventilated by opening a window. Three different sampling experiments were carried out with the window open, and seven different experiments with it closed. During sampling with the window closed, the room temperature was maintained at 20 °C and the air was mixed by using a household circulating fan with a 38-cm-diameter propeller. The sampler inlets were set 1.0 m from each other and 166 cm above the floor. ETS for comparison of the two samplers in the test room was generated mechanically in six experiments (tests 1–6) and once by two volunteer smokers (test 7). In the former cases, cigarettes were attached by means of short lengths of Tygon tubing to Air Cadet Model 1730-40 pumps, through which air was drawn. Two cigarettes were burned at a time and the air flow was controlled by a flow-regulating valve that was adjusted to burn the two cigarettes in 4.5 min. This apparatus was positioned 2.0 m from the samplers. Sampling periods ranged from 20 min to 3.5 h and on several occasions had to be terminated because blockage of the DICHOT fine particulate filter caused pressure buildup and reduction of the flow. Since the objective of generating and sampling the cigarette smoke was only to compare the sampling characteristics of the two samplers and to rapidly produce samples large enough to be assayed for mutagenicity, ventilation rates were not determined during these experiments.

Three coreplicate sampling tests were carried out in the absence of ETS in the same test room, with the window open (tests 8–10). Coreplicate sampling was also conducted in an empty bedroom in a residence in which no smoking occurred (test 11).

Field Sampling. Field sampling experiments (Table IV) using only the IASI sampler were conducted in several different single-family dwellings in St. John's, NF. Two samples (1.5- and 3.5-day sampling times) were collected in the kitchen of a house where the residents did not smoke. The remaining samples were collected during parties at four different residences where heavy cigarette smoking occurred. The windows of the dwellings in which the parties occurred were kept closed during the sampling

periods. The sampling was conducted during the winter months of December 1987–January 1988. The handling, storage, and transportation of blank and sampled filters was conducted exactly in the same manner as those that were generated in the laboratory. Ventilation rates were not determined during these experiments.

Extraction of Particulate Matter. The methods used for extraction and concentration of particulate matter were similar to those described by Kado et al. (25). Dichloromethane-methanol-toluene (1:1:1) was used to extract the particulate samples. In a typical extraction, 5 mL of the extraction solvent was added to a 20 \times 125 mm screw-capped tube containing the filter, followed by sonication for 20 min in the dark, in a Bransonic water bath, at 40–45 °C. The solvent was removed with a syringe and the sonication was repeated with a fresh 5-mL aliquot of the solvent. The combined extract was filtered through a 0.5- μm Fluoropore filter, using a Millipore microsyringe filter holder, and the filtrate transferred into the 10-mL receiving vessel of a Kuderna-Danish apparatus. A clean boiling chip was added and the vessel was attached to a microcondenser and placed in a 40–45 °C water bath. A steady flow of nitrogen was blown onto the surface of a solution via a Pasteur pipet inserted in the condenser. The volume of solution was reduced to less than 0.5 mL and was transferred to a 2-dram amber vial. The receiving vessel was washed with two small portions of clean solvent, which were added to the vial. The vial was placed in a 35 °C water bath and the solvent remaining in the vial was then removed by nitrogen blowdown. The vial was sealed with a Teflon-lined cap and was stored at –20 °C until needed for mutagenicity assays. Evaporation to dryness was the method chosen since other investigators have reported that chemical transformations occurred for samples stored in dimethyl sulfoxide (DMSO) (27).

Each of the filters used during the coreplicate sampling in tests 1–4 (Table I) was cut into two approximately equal halves, which were then weighed. Halves from each of the fine and coarse fractions obtained with the DICHOT sampler were combined and were extracted together.

Mutagenicity Testing. Mutagenicity testing of each of the extracts was conducted with *S. typhimurium* strain TA98 using a modification (28) of the microsusension procedure of Kado et al. (19). Fifty microliters or more of dimethyl sulfoxide (DMSO) was added to the extracts and the mixtures were sonicated for 5 min at 35 °C to bring the material into solution. Duplicate plates were tested at three or more doses selected to fall in the linear portion of the dose-response curve. Plate counts were determined with a Biotran II automatic colony counter (New Brunswick Scientific Inc.). Maximum slopes from the initial linear dose-response regions of each set of data were determined by using the Ames Fit program (29). Duplicates of all zero-dose plates were run and the spontaneous revertants were determined by subtracting the numbers of preexisting revertants (28). S9 prepared from Arochlor-pretreated male Sprague-Dawley rats was purchased from Litton Bionette Inc. and had a stated protein content of 29 mg/mL. The S9 optimum concentration for samples collected in the presence of tobacco smoke was found to be 5 μL per plate (5% S9 mix). Unexposed filters were extracted and tested in the same manner as those used in particulate sampling. No mutagenic response was observed with these extracts either in the absence of S9 or in the presence of 1, 5, or 10% S9 per plate. To minimize interday variability, the corresponding extracts from each sampler were tested for mutagenicity in the same assay. Duplicates of single-dose plates each containing 0.5 μg of

Table II. Mutagenic Activities of PM-10 Sampled Coreplicately with a Sierra-Andersen Dichotomous Sampler (DICHOT) and an Indoor Air Sampler (IASI) Determined by the *Salmonella typhimurium* TA98 Microsuspension Assay with S9 Activation

assay no.	spontaneous revertants, rev/plate	mutag response of control, ^a rev/plate	DICHOT		IASI	
			mutag activ of combined fractns, rev/ μ g	mutag activ of combined fractns, rev/m ³	mutag activ of PM-10, rev/ μ g	mutag activ of PM-10, rev/m ³
1	23 \pm 3	167 \pm 6	5.1 \pm 0.8	12 400 \pm 2400	4.7 \pm 0.6	13 000 \pm 2000
2	42 \pm 8	347 \pm 23	10.5 \pm 0.7	14 500 \pm 1500	9.1 \pm 1.2	12 700 \pm 2000
3	26 \pm 4	171 \pm 10	8.5 \pm 0.6	13 800 \pm 1200	5.9 \pm 0.2	11 200 \pm 700
4	23 \pm 8	160 \pm 24	10.2 \pm 0.4	39 700 \pm 2100	8.4 \pm 0.5	35 500 \pm 2600
5	29 \pm 6	326 \pm 40	1.7 \pm 0.2	17 \pm 1	2.5 \pm 0.3	29 \pm 3

^a Control, 0.5 μ g of BaP.

benzo[a]pyrene (BaP) were used as controls in each assay. Results were within expected ranges (104–407 induced revertants in the presence of 5% S9).

Results and Discussion

Table I contains data obtained from 11 separate experiments in which the IASI and DICHOT were compared in the same test locations. The relative performances of the two samplers were evaluated by comparing the respective concentrations of PM-10 sampled. In the case of the DICHOT, the combined masses of the fine and coarse fractions were computed and used to calculate the corresponding values. Regression analysis of the concentrations obtained with each of the samplers showed that the Pearson product correlation coefficient (r^2) was 0.99, the slope was 1.08, and the regression line intercept was $-2.9 \mu\text{g}/\text{m}^3$. The data suggested that the IASI samples a slightly greater mass of PM-10 per unit volume than the DICHOT. These findings are consistent with the ambient air intercomparison study conducted by Liou et al. (23), but extend over a much wider range of PM-10 concentrations (5–4200 $\mu\text{g}/\text{m}^3$ in indoor air versus 20–80 $\mu\text{g}/\text{m}^3$ in ambient air).

The microsuspension modification to Maron and Ames' mutagenicity assay procedures developed by Kado et al. (19) has substantially increased the sensitivity of the assay, thereby reducing the amount of material required for mutagenicity testing. It has been used for the analysis of the fine fraction of PM-10 from outdoor ambient air (25), for the measurements of indoor air containing ETS (30), and in a study of the PM-10 in an indoor ice arena (31). It was therefore the method of choice for this study.

Table II contains results of the mutagenicity testing of the extracts of some of the PM-10 samples coreplicately collected by use of the two samplers. Five sets of samples from Table I (tests 1–4 and 10) were extracted for mutagenicity testing (assays 1–4 and 5, respectively). Mutagenic activities (revertants/ μg and revertants/ m^3) were estimated from the maximum slopes calculated from the initial linear dose-response regions (29) of each set of data.

In the presence of ETS (assays 1–4), both samplers collected PM-10 that was highly mutagenic with S9 activation (+S9). Without metabolic activation (–S9), only one of the samples (assay 4, data not shown) exhibited detectable mutagenicity (3140 and 4240 revertants/ m^3 , or 0.80 and 0.89 revertants/ μg of PM-10 for the DICHOT and IASI, respectively). In the absence of ETS, and with the window of the test room open (assay 5), it was necessary to sample for a much longer period of time to obtain sufficient PM-10 for analysis. Under these conditions, mutagenic activity could be detected at much lower concentrations per volume of air and direct acting mutagenicity of 12–20 revertants/ m^3 (1.3–1.8 revertants/ μg of PM-10) was detectable. With metabolic activation these

samples exhibited only a 25–33% increase in mutagenic activity.

A Student *t* test (32) was used to compare the slopes of the linear portion of the dose-response curves of the corresponding IASI and DICHOT samples within each assay. With the slopes calculated as revertants/ m^3 there was no significant difference ($p = 0.05$) between any of the paired samples collected in the presence of ETS. In the absence of ETS, and with the window open, the mutagenicity of the PM-10 sampled by the IASI was greater than that of the DICHOT sample.

The expression of mutagenicity in terms of revertants per microgram of PM-10 (specific mutagenic activity) is useful for comparing the sampling characteristics of the two samplers. In the presence of ETS the specific mutagenic activity of the combined DICHOT filters was greater than that of the corresponding IASI filter. This difference was statistically significant ($p < 0.05$) for two of the four assays (assays 3 and 4). On the basis of our experiments alone, it is difficult to explain unequivocally the reasons for the differences. Dissimilarities in the impactor design and the sampling rates could account for these observed differences. Since the IASI samples had lower specific mutagenic activities (revertants/ μg of PM-10), a possible explanation could be that relatively larger amounts of more volatile, less mutagenic compounds present in ETS, e.g., nicotine, are adsorbed as aggregates onto the PM sampled on the IASI filters. Furthermore, as the IASI samples at a lower overall rate than the DICHOT, the corresponding mass loss during sampling due to evaporation of the more volatile components on the filters could conceivably be less for the former. Alternatively, or in addition, the sampling characteristics of the IASI could favor its collecting relatively larger amounts of the coarser fraction within the PM-10 than the DICHOT does. These factors would tend to mask the specific mutagenic activity of the IASI samples tested since it has been reported that the mutagenic compounds are mostly located on particles smaller than 2.0–3.3 μm (33).

However, when the mutagenicity was calculated as revertants/ m^3 of air sampled, as recommended by van Houdt (33), the mutagenic activities between the IASI and DICHOT samples were found to be not significantly different ($p = 0.05$). Calculating mutagenic activity in this way takes into account the different sampling rates of the two samplers and also indicates that the two devices sample the same mutagenic components in the ETS-containing air.

When longer sampling times were employed in the test room with the window open and in the absence of ETS, (assay 5) the mutagenic activity (+S9) of the samples was considerably lower for both the DICHOT and IASI samples. There was a significant difference ($p = 0.05$) between the mutagenic activity of the two samples regardless of how it was calculated, with the IASI demonstrating the higher

Table III. Comparison of Mutagenic Activities of Both Halves^a of IASI PM-10 Filters Assayed on Different Days by Using the *Salmonella typhimurium* TA98 Microsuspension Assay with S9 Activation

test no.	filter half A			filter half B		
	spontaneous revertants, rev/plate	mutag response of control, ^b rev/plate	mutag activ of PM-10, rev/ μ g	spontaneous revertants, rev/plate	mutag response of control, ^b rev/plate	mutag activ of PM-10, rev/ μ g
1	23 \pm 3	167 \pm 6	4.7 \pm 0.6	29 \pm 4	315 \pm 10	7.67 \pm 0.9
2	42 \pm 8	347 \pm 23	9.1 \pm 1.2	22 \pm 9	196 \pm 9	11.2 \pm 1.5
3	26 \pm 4	171 \pm 10	5.9 \pm 0.2	22 \pm 9	196 \pm 9	11.1 \pm 1.5

^aThese filter halves were obtained from tests 1-3, Table I. ^bControl, 0.5 μ g of BaP.

Table IV. Gravimetric Analyses and Mutagenic Activities of PM-10 Sampled with an Indoor Air Sampling Impactor (IASI) in Various Field Trials Assayed by the *Salmonella typhimurium* TA98 Microsuspension Assay with and without S9 Activation^a

filter no.	sampling and gravimetric data				mutagenicity data			
	location	total mass, μg	flow rate, L/min	sampling time, min	S9, %	dose	mutag activ	
						range, μg	rev/ μg	rev/ m^3
ESa	kitchen during cooking	1352 \pm 4	10.3	6420	0	7–53	0.25 \pm 0.07	5.2 \pm 1.4
ESb					0	26–72	0.51 \pm 0.11	0.2 \pm 2.3
					5	26–72	0.64 \pm 0.06	13.0 \pm 1.3
EZ	kitchen + 1 cigarette smoked	1215 \pm 4	10.0	2202	0	26–121	0.23 \pm 0.06	12.4 \pm 3.3
					1	26–121	0.53 \pm 0.08	29.2 \pm 4.2
DC	party 1, sample 1	603 \pm 4	10.6	120	0	4–30	nr	nr
					7	4–30	4.8 \pm 0.54	2280 \pm 260
DD	party 1, sample 2	531 \pm 4	10.6	120	1	3–26	5.9 \pm 1.5	2460 \pm 630
					5	3–26	5.7 \pm 0.5	2380 \pm 210
DH	party 2, sample 1	393 \pm 7	10.5	65	0	3–20	nr	nr
					5	3–20	10.4 \pm 0.3	5970 \pm 750
DG	party 2, sample 2	1008 \pm 7	10.5	65	0	13–101	0.48 \pm 0.09	709 \pm 130
					5	13–101	8.8 \pm 0.87	12950 \pm 130
DK	party 3	446 \pm 4	10.6	60	0	9–45	0.41 \pm 0.17	288 \pm 120
					5	9–45	2.6 \pm 0.21	1840 \pm 150
ECa	party 4, sample 1	2024 \pm 4	10.3	60	0	20–93	nr	nr
					5	20–93	1.4 \pm 0.1	4700 \pm 330
EDa	party 4, sample 2 (split into two equal halves)	1040 \pm 4	10.4	60	0	11–55	nr	nr
EDb					5	11–55	3.2 \pm 0.6	5330 \pm 670
					0	11–48	nr	nr
					5	11–48	3.3 \pm 0.3	5480 \pm 570

^anr denotes that the Ames fit program (29) failed to detect a nonzero slope. Spontaneous revertants were in the range 27-66.

mutagenic activities. This suggests that there is a difference in the characteristics of the mutagenic components present in the PM-10 that did not contain ETS.

The range for specific mutagenic activities (revertants/ μ g) in assays 1-4 (Table II), which were determined on different days, can be attributed to interassay variability. Three of the IASI samples that had been split into equal halves were assayed on different days. Significant variability between the interday assay results were observed (Table III), which is consistent with findings reported by ourselves (31) and others (18, 34). The higher mutagenic activity in revertants/m³ observed for assay 4 (Table II) can be attributed to the much larger sample loading that was obtained during the corresponding sampling test (test 4, Table I).

Several field tests were conducted with the IASI alone. Table IV summarizes the data obtained. The sampler was used over test periods ranging from as low as 1 h at several parties at which there was extensive cigarette smoking to 107 h in one home where nonsmokers live. The numbers of cigarettes smoked in the parties were not counted, but it was estimated that the numbers were between approximately 15 and 30 cigarettes/h. The PM-10 levels measured ranged from a high value of 3280 μ g/m³, observed during one party in which the room air was sampled for

1 h, to a low value of 417 μ g/m³ at another party in which the room air was sampled for 2 h. These values are well within the range of PM-10 levels generated under controlled conditions in our test room and are among the highest values reported (11, 35) to date. The mutagenic responses (with 5% S9) from these samples varied from a high of 12950 \pm 130 to 2380 \pm 210 revertants/m³. By comparison, the mutagenic response from the samples obtained from the relatively smoke free environment, which was sampled for up to 107 h, was only 13 revertants/m³. The mutagenic responses with TA98 in the presence of S9 of the extracts of PM-10 from the environments containing ETS were 2-16 times greater than those observed for environments that did not contain ETS. Mutagenic responses with TA98 in the absence of S9 were observed in only two of the samples (DG and DK). All samples demonstrated mutagenic responses, with the largest responses being in the presence of high levels of ETS.

It is apparent from these field tests that the IASI can be used to collect indoor PM-10 samples in sufficient amounts for gravimetric analyses and mutagenicity testing with a modification of the Ames *S. typhimurium* assay. The IASI proved to be quiet and unobtrusive and was well-tolerated by the inhabitants of the test houses/loca-

tions that were sampled. The fact that it can sample PM-10 at 10.0 L/min enables it to be used in virtually any indoor setting for periods of as low as 1 h if samples are needed for mutagenicity assays. Based on our findings, a lower limit of detection of mutagenic activity (+S9) of 0.5–1.0 revertant/m³ is feasible. The mass losses for PM-10 sampled over long periods were not determined. For PM-10 samples that are required only for gravimetric analyses, lower sampling times can be used. The consistency observed in this study and by others (23) between the IASI and the well-studied DICHOT sampler should add further confidence in its use.

Acknowledgments

The Department of Chemistry and the Department of Biology, Memorial University of Newfoundland, are thanked for their assistance.

Literature Cited

- (1) *Exposure Guidelines for Residential Indoor Air Quality*; A Report of the Federal-Provincial Advisory Committee on Environmental and Occupational Health, prepared for the Environmental Health Directorate, Health Protection Branch, Health and Welfare Canada, Tunney's Pasture, Ottawa, Canada, April 1987.
- (2) Sexton, K.; Liu, K.-S.; Treitman, R. D.; Spengler, J. D.; Turner, W. A. *Environ. Int.* **1986**, *12*, 265.
- (3) Meyer, B. *Indoor Air Quality*; Addison-Wesley Publishing Co.: Reading, MA, 1983.
- (4) Wedding, J. B. *Environ. Sci. Technol.* **1982**, *16*, 154.
- (5) Ortiz, C. A.; McFarland, A. R. *J. Air Pollut. Control Assoc.* **1985**, *35*, 1057.
- (6) Wedding, J. B.; Wiegand, M.; John, W.; Wall, S. *Environ. Sci. Technol.* **1980**, *14*, 1367.
- (7) Loo, B. W.; Jaklevic, J. M.; Goulding, F. S. In *Fine Particles: Aerosol Generation, Measurement, Sampling and Analysis*; Liu, B. Y. H., Ed.; Academic Press: New York, 1976; p 311.
- (8) Dockery, D. W.; Spengler, J. D. *Atmos. Environ.* **1981**, *15*, 335.
- (9) Sexton, K.; Spengler, J. D.; Treitman, R. D. *Atmos. Environ.* **1984**, *18*, 1371.
- (10) Sexton, K.; Webber, L. M.; Hayward, S. B. *Environ. Int.* **1986**, *12*, 351.
- (11) Repace, J. L. In *Environmental Carcinogens. Passive Smoking*; O'Neill, I. K., Brunneemann, K. D., Dodet, B., Hoffmann, D., Eds.; IARC Scientific Publications No. 81; International Agency for Research on Cancer: Lyon, France, 1987; Vol. 9, pp 141–162.
- (12) Highsmith, V. R.; Rodes, C. E.; Hardy, R. J. *Environ. Sci. Technol.* **1988**, *22*, 1109.
- (13) Spengler, J. D.; Soczek, M. L. *Environ. Sci. Technol.* **1984**, *18*, 268A.
- (14) Fletcher, R. A. *J. Air Pollut. Control Assoc.* **1984**, *34*, 1014.
- (15) Liou, P. J.; Avdenko, M.; Harkov, R.; Atherholt, T.; Daisey, J. M. *J. Air Pollut. Control Assoc.* **1985**, *35*, 653.
- (16) Lewtas, J.; Goto, S.; Williams, K.; Chuang, J. C.; Petersen, B. A.; Wilson, N. K. *Atmos. Environ.* **1987**, *21*, 443.
- (17) Mumford, J. L.; Harris, D. B.; Williams, K.; Chuang, J. C.; Cooke, M. *Environ. Sci. Technol.* **1987**, *21*, 308.
- (18) Lofroth, G.; Ling, P. I.; Agurell, E. *Mutat. Res.* **1988**, *202*, 103.
- (19) Kado, N. Y.; Langley, D.; Eisenstadt, E. *Mutat. Res.* **1983**, *121*, 25.
- (20) Maron, D. A.; Ames, B. N. *Mutat. Res.* **1983**, *113*, 173.
- (21) *Fed. Regist.* **1987**, *52*, 24634–24750.
- (22) Marple, V. A.; Rubow, K. L.; Turner, W. A.; Spengler, J. D. *JAPCA* **1987**, *37*, 1303.
- (23) Liou, P. J.; Wainman, T.; Turner, W.; Marple, V. A. *JAPCA* **1988**, *38*, 668.
- (24) Van Cauwenbergh, K.; Van Vaeck, L. *Mutat. Res.* **1983**, *116*, 1.
- (25) Kado, N. Y.; Guirguis, G. N.; Flessel, C. P.; Chan, R. C.; Chang, K.-I.; Wesolowski, J. J. *Environ. Mutagen.* **1986**, *8*, 53.
- (26) Feeney, P.; Cahill, T.; Olivera, J.; Guidara, R. *J. Air Pollut. Control Assoc.* **1984**, *34*, 376.
- (27) Morin, R. S.; Tulis, J. J.; Claxton, L. D. *Toxicol. Lett.* **1987**, *38*, 279.
- (28) Georgiou, P. E.; Blagden, P. A.; Winsor, L.; Williams, D. T. *Mutat. Res.* **1989**, *225*, 33.
- (29) Moore, D.; Felton, J. S. *Mutat. Res.* **1983**, *119*, 95.
- (30) Ling, P. I.; Lofroth, G.; Lewtas, J. *Toxicol. Lett.* **1987**, *35*, 147.
- (31) Georgiou, P. E.; Blagden, P. A.; Snow, D. A.; Winsor, L.; Williams, D. T. *JAPCA* **1989**, *39*, 1583.
- (32) Zhar, J. H. *Biostatistical Analysis*; Prentice-Hall Inc.: Englewood Cliffs, NJ, 1974.
- (33) van Houdt, J. J. *Atmos. Environ.* **1990**, *24B*, 207.
- (34) Watts, R. R.; Drago, R. J.; Merrill, R. G.; Williams, R. W.; Perry, E.; Lewtas, J. *JAPCA* **1988**, *38*, 652.
- (35) *Indoor Air '90. Proceedings of the 5th International Conference on Indoor Air Quality and Climate*; Toronto, Canada, 1990.

Received for review September 25, 1990. Revised April 1, 1991. Accepted April 15, 1991. This work was supported through a contract awarded by Supply and Services Canada on behalf of Health and Welfare Canada.

Influence of Sorbate Structure on Nonequilibrium Sorption of Organic Compounds

Mark L. Brusseau*

Soil and Water Science Department, 429 Shantz Building, 38, University of Arizona, Tucson, Arizona 85721

P. Suresh C. Rao

Soil Science Department, University of Florida, Gainesville, Florida 32611

■ We investigate the relationship between sorbate structure and nonequilibrium sorption. The rate-limited sorption of compounds representing eight classes of organic chemicals, including chlorinated benzenes, unsubstituted and alkyl-substituted aromatics, chlorinated ethenes and ethanes, chlorinated phenols, nitrogen heterocycles, *s*-triazines, substituted amides, and substituted ureas, was examined by use of a single sorbent (sandy aquifer material) and the miscible displacement technique. The breakthrough curves were analyzed by using a bicontinuum model wherein sorption is assumed instantaneous for a fraction of the sorbent and rate limited for the remainder. Sorbate structure was shown to exert minimal impact on the nature of rate-limited sorption for nonionic, low-polarity compounds comprising relatively simple structures and for ionogenic compounds in neutral form. In contrast, sorbate structure appeared to have a significant impact for compounds comprising more complex structures (i.e., pesticides). First-order reverse rate constants determined for the pesticides were at least 1 order of magnitude smaller than those of the non-pesticides. This difference was attributed to differences in degree of constraint on diffusion within the polymeric structure of organic matter.

Introduction

Several investigations of the rate-limited sorption (both adsorption and desorption) of nonionic, low-polarity "hydrophobic" organic compounds (HOCs) by natural sorbents have recently been reported. Chlorinated aromatics have received the majority of attention (cf. refs 1-7), with polynuclear aromatics (7, 8) and chlorinated ethenes (6, 7, 9, 10) receiving lesser attention. Knowledge of the role of solute (or sorbate), solvent, and sorbent properties on mediating nonequilibrium sorption is required for a complete understanding of this process. Such knowledge is also required to successfully model and predict the effect of nonequilibrium sorption on the transport and fate of contaminants in soils, sediments, and aquifers. Unfortunately, few systematic investigations of this type have been reported.

The nature of the sorbent apparently has only a second-order effect on the nature of nonequilibrium sorption, as evident in the similarity of rate-limited sorption of numerous HOCs for a wide variety of soils, sediments, and aquifer materials (1, 7, 11, 12). This holds for only natural sorbents, however, as values for sorption rate constants measured for systems comprising natural sorbents were significantly different from those measured for synthetic sorbents (e.g., organic-modified silica) (7). Conversely, the nature of the solvent (e.g., polarity) has been shown to significantly affect the kinetics of sorption of HOCs (13-16). For example, a model that describes a log-linear increase in the reverse rate constant with increasing volume fraction of organic cosolvent was presented by Brusseau et al. (13, 14).

Qualitative observations of a relationship between degree of nonequilibrium or values of rate constants and sorbate

hydrophobicity, which is a reflection of the nature and size of the sorbate molecule, have been reported by several researchers (cf. refs 1, 4, and 17). The relationship between sorption kinetics and equilibrium sorption has recently been quantified by Brusseau and Rao (11), who analyzed literature data using the linear free energy relationship approach. They reported the first-order, reverse rate constant to be a log-log-linear inverse function of the equilibrium sorption constant for a number of HOCs and a wide variety of natural sorbents. This functionality has since been substantiated by experiment (6, 7, 12).

The size of the sorbate molecule appears to have a major influence on the degree of nonequilibrium sorption experienced by a given sorbate, based on the observations reported above. However, the structure of the sorbate molecule (e.g., nature, size, and reactivity of functional groups) may also significantly affect nonequilibrium sorption (7, 11). On the basis of their analysis of literature data, Brusseau and Rao (11) reported the degree of nonequilibrium sorption exhibited by relatively complex sorbates, such as pesticides, to be significantly greater than that exhibited by simpler sorbates such as alkyl- and chlorobenzenes. These observations are tentative, however, considering that the data were gathered from many literature sources, were obtained by several different experimental techniques, and represent many different sorbents. The number of carbons comprising the alkyl functional group was shown to affect the degree of nonequilibrium sorption for a series of substituted benzenes (7). These two appear to be the only published reports concerning a quantitative analysis of the influence of sorbate structure on nonequilibrium sorption of HOCs.

The purpose of this work is to specifically investigate the relationship between sorbate structure and nonequilibrium sorption. This was accomplished by examining the rate-limited sorption of compounds representing eight classes of organic chemicals, including chlorinated benzenes, unsubstituted and alkyl-substituted aromatics, chlorinated ethenes and ethanes, chlorinated phenols, nitrogen heterocycles, *s*-triazines, substituted amides, and substituted ureas, by a single sorbent. In addition, the nature of nonequilibrium sorption of ionogenic chemicals in their neutral form is investigated.

Experimental Section

Materials. The following analytical grade chemicals were used for the experiments: benzene, toluene, *p*-xylene, naphthalene, chlorobenzene, 1,3-dichlorobenzene, 1,2,4-trichlorobenzene, 1,2-*trans*-dichloroethane, 1,1,1-trichloroethane, 1,2-*trans*-dichloroethene, trichloroethene, tetrachloroethene, *p*-chlorophenol, 2,4-dichlorophenol, 2,4,6-trichlorophenol, 2,3,4,5-tetrachlorophenol, pentachlorophenol, quinoline, atrazine, cyanazine, simazine, trietazine, alachlor, propachlor, monuron, and monolinuron. The structures, and pK_a values where appropriate, of all chemicals discussed are provided in Figure 1.

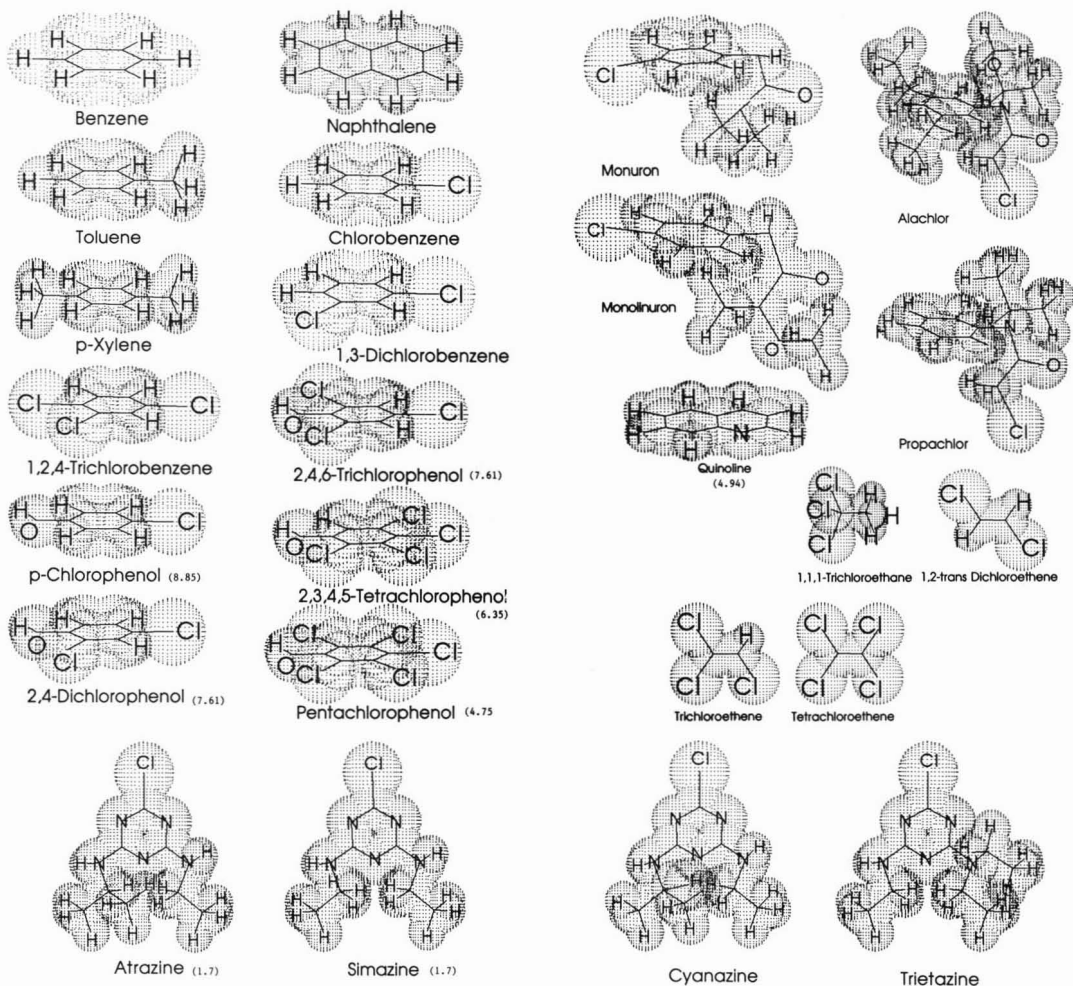


Figure 1. Structures for sorbates. pK_a values (in parentheses) from refs 36 and 37.

Pentafluorobenzoic acid was used as a nonsorbing tracer to characterize the hydrodynamic properties of the column.

The <2-mm size fraction of a sandy aquifer material with a moderately low organic carbon content (1.3 g kg^{-1}) was used as the sorbent. This material was collected from an increment 2–2.5 m below the surface, near a site located in Tampa, FL, that is contaminated with solvents (trichloroethene, tetrachloroethene). The sample collection point was outside the contaminated zone (18). Textural analysis revealed the material to be 971 g kg^{-1} sand, 23 g kg^{-1} silt, and 6 g kg^{-1} clay.

Experimental Apparatus and Methods. Miscible displacement techniques identical with those described by Brusseau et al. (6) were used for these experiments. A preparative chromatography column made of precision-bore borosilicate glass, with an internal diameter of 2.5 cm and a length of 10.6 cm, was packed in incremental steps with dry material to establish a uniform bulk density of 1.64 g cm^{-3} . After completion of packing, electrolyte solution (0.01 N CaCl_2) was pumped through the column until steady-state water saturation (volumetric water content of 0.42) was established. Two single-piston HPLC pumps (Gilson Medical Electronics, Model 302) were connected to the column, with a Rheodyne switching valve (Model 7060) placed in-line to facilitate switching between

solutions that did or did not contain the solute of interest. Single-solute solutions, with concentrations approximately 1–20% of saturation, were prepared by placing aliquots of a saturated stock solution in a matrix of 0.01 N CaCl_2 . The system was designed so that solute would contact only stainless steel, glass, or Teflon.

A flow-through, variable-wavelength UV detector (Gilson Holochrome) was used to continuously monitor solute concentration in the column effluent for all experiments except that involving 1,1,1-trichloroethane and 1,2-trans-dichloroethane. In the latter case, a ternary-solute solution of 1,1,1-trichloroethane, 1,2-trans-dichloroethane, and trichloroethene was used, and effluent fractions were collected for subsequent analysis by gas chromatography (GC). The GC analysis was performed using a Perkin-Elmer Sigma 3B equipped with a flame ionization detector, a 30-m, 0.53-mm-i.d. capillary column (J&W Scientific, JW624), and using a Hewlett-Packard integrator (HP3390) for signal monitoring. Direct liquid injections ($2 \mu\text{L}$) were made into an injection block maintained at 200°C , followed by isothermal analysis at 62°C . The performance of the flow-through UV detection and effluent fraction collection methods were compared and were found to provide identical results, as previously shown by Brusseau et al. (6).

The flow rate used for all experiments was 3 mL/min (average pore-water velocity of 90 cm/h). Experiments for most compounds were performed under ambient pH conditions (pH of 7–8). Note that quinoline will exist in the neutral form at this pH. For the experiments using the chlorophenols, the pH was adjusted to 2 by addition of acid (HCl) so that the phenols would be present only as the neutral species. To investigate the potential impact of the pH change on observed nonequilibrium sorption, the chlorobenzene and dichlorobenzene experiments were also performed at pH 2.

Data Analysis. The various models available for simulating nonequilibrium sorption are reviewed elsewhere (6, 17). The results of the miscible displacement experiments using the sorbing solutes were analyzed by use of a first-order bicontinuum model of the type presented by several authors (cf. refs 8, 19, and 20). This model has been successfully used to model nonequilibrium sorption and transport of organic chemicals (cf. refs 1, 3, 6–8, and 10–15). With the bicontinuum model, sorption is conceptualized to occur in two domains:



where

$$S_1 = FK_p C \quad (2)$$

$$dS_2/dt = k_1 S_1 - k_2 S_2 \quad (3)$$

and where C is the solution-phase solute concentration ($M L^{-3}$), S_1 is the sorbed-phase concentration ($M M^{-1}$) in the "instantaneous" domain, S_2 is the sorbed-phase concentration ($M M^{-1}$) in the rate-limited domain, K_p is the linear equilibrium sorption constant ($L^3 M^{-1}$), F is the fraction of sorbent for which sorption is instantaneous, t is time, and k_1 and k_2 are forward and reverse first-order rate constants (T^{-1}), respectively.

The following nondimensional equations describe the transport of sorbing solutes during one-dimensional, steady water flow in a homogeneous porous medium:

$$\beta R \partial C^*/\partial p + (1 - \beta) R \partial S^*/\partial p = (1/P) \partial^2 C^*/\partial X^2 - \partial C^*/\partial X \quad (4)$$

$$(1 - \beta) R \partial S^*/\partial p = \omega(C^* - S^*) \quad (5)$$

where

$$C^* = C/C_0 \quad (6a)$$

$$P = vl/D \quad (6b)$$

$$S^* = S_2/(1 - F)K_p C_0 \quad (6c)$$

$$R = 1 + (\rho/\theta)K_p \quad (6d)$$

$$p = vt/l \quad (6e)$$

$$\beta = (1 + F(\rho/\theta)K_p)/R \quad (6f)$$

$$X = x/l \quad (6g)$$

$$\omega = k_2(1 - \beta)Rl/v \quad (6h)$$

and where D is the dispersion coefficient (L^2/T), v is the average pore-water velocity (L/T), x is distance (L), l is column length (L), p is dimensionless time in pore volumes, ρ is soil bulk density ($M L^{-3}$), θ is volumetric soil-water content, C_0 is concentration of solute in the influent solution, P is the Peclet number, which represents the dispersive-flux contribution to transport, R is the retardation factor, which represents the effect of sorption on transport, β is the fraction of instantaneous retardation, and ω is the Damkohler number, which is a ratio of hydrodynamic

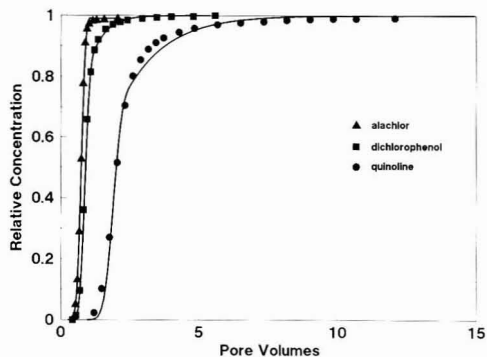


Figure 2. Representative measured breakthrough curves (data points) and simulations produced with the bicontinuum model (solid lines).

residence time to characteristic time for sorption. These last two terms specify the degree of nonequilibrium existent in the system, which decreases as either of the two increase in magnitude. Development of the dimensional equations may be found in several sources (cf. refs 17, 19, and 20).

To run the model, knowledge of the following parameters is required: P , R , β , ω , and T_0 , the size of the input solute pulse in pore volumes. The value for P was obtained from the breakthrough curve of a nonsorbing solute, pentafluorobenzoic acid, by use of a nonlinear, least-squares optimization program (21) to solve the advective-dispersive local equilibrium transport model. The value for R , and thus K_p (see eq 6d), was obtained by moment analysis (6) for all solutes except the pesticides. For these, the values for R determined by moment analysis are uncertain because of the high degree of nonequilibrium, reflected in the very small values of ω (22). Hence, K_p values for the pesticides were measured by using a standard batch isotherm technique, with equilibration periods of 24–48 h. The data were represented well by linear isotherms. The sorption of the non-pesticides was also linear, as determined by comparing the front and back segments of the breakthrough curves (17). The size of the solute pulse, T_0 , is known from measurement. The two unknown parameters are thus β and ω . A nonlinear, least-squares optimization program using the bicontinuum model (21) was used under flux-type boundary conditions to determine values for the two unknowns. Values for k_2 were obtained by using eq 6h. Much of the forthcoming analyses will employ the linear free energy relationship (LFER) technique, as used by Brusseau and Rao (11), where the logarithms of k_2 are regressed against the logarithms of K_p .

Results

The breakthrough curve for pentafluorobenzoic acid was symmetrical, whereas those for the sorbing solutes were asymmetrical and exhibited some degree of "tailing", or delayed approach to $C/C_0 = 1$ or 0. This behavior suggests that the nonequilibrium is caused by a sorption-related rather than a transport-related mechanism (6, 15, 17). Representative breakthrough curves and the simulations produced with the bicontinuum model are shown in Figure 2. Comparison of the simulations and the data reveals that the model provided good descriptions of the data. The parameter values for all experiments are reported in Table I; 95% confidence intervals obtained by first-order uncertainty analysis are included for all optimized parameters.

Table I. Parameter Values

chemical	pH	R	K_p	β^a	ω^a	k_2^a	SSQ ^b
TOL	8	1.18	0.05	0.92 (0.92–0.93)	0.17 (0.12–0.22)	15.1 (10.9–19.3)	0.006
XYL	8	1.53	0.14	0.79 (0.79–0.80)	0.35 (0.30–0.39)	8.4 (7.3–9.5)	0.004
NAP	8	1.87	0.22	0.79 (0.78–0.81)	0.45 (0.36–0.54)	9.5 (7.6–11.4)	0.01
CB	2	1.35	0.09	0.86 (0.85–0.86)	0.24 (0.21–0.27)	10.1 (8.8–11.4)	0.003
DCB	2	2.49	0.38	0.69 (0.68–0.70)	0.57 (0.49–0.66)	6.1 (5.2–7.0)	0.01
TCB	8	3.85	0.73	0.62 (0.62–0.63)	0.98 (0.90–1.06)	5.5 (5.1–5.9)	0.003
TCA	8	1.11	0.03	0.95 (0.94–0.95)	0.10 (0.07–0.14)	14.5 (8.3–20.7)	0.002
DCE	8	1.18	0.05	0.89 (0.88–0.90)	0.30 (0.25–0.35)	18.8 (15.7–21.9)	0.001
TCE	8	1.36	0.09	0.82 (0.81–0.82)	0.26 (0.22–0.29)	8.1 (7.0–9.2)	0.003
TCE2 ^c	8	1.32	0.08	0.82 (0.81–0.83)	0.21 (0.15–0.27)	7.2 (5.1–9.3)	0.01
PCE	8	2.36	0.35	0.54 (0.52–0.55)	0.58 (0.50–0.66)	4.3 (3.7–4.9)	0.02
CP	2	1.29	0.07	0.94 (0.92–0.95)	0.03 (0.01–0.09)	10.2 (3.9–16.5)	0.04
DCP	2	1.38	0.10	0.92 (0.91–0.92)	0.24 (0.21–0.28)	16.4 (13.4–18.8)	0.0008
TCP	2	1.93	0.24	0.79 (0.78–0.80)	0.42 (0.35–0.49)	8.4 (6.9–9.9)	0.01
TeCP	2	4.64	0.94	0.82 (0.81–0.82)	0.41 (0.37–0.44)	3.9 (3.5–4.3)	0.003
PCP	2	15.08	3.63	0.71 (0.70–0.72)	0.74 (0.67–0.81)	1.4 (1.3–1.5)	0.006
quinoline	8	2.75	0.45	0.82 (0.80–0.84)	0.42 (0.30–0.55)	7.0 (4.9–9.1)	0.01
AT	8	1.42	0.11	0.82 (0.81–0.82)	0.03 (0.03–0.04)	1.1 (0.8–1.4)	0.002
CYN	8	1.32	0.08	0.89 (0.89–0.89)	0.01 (0.04–0.02)	2.8 (2.2–3.4)	0.002
SIM	8	3.12	0.55	0.51 (0.49–0.52)	0.10 (0.05–0.15)	0.5 (0.2–0.8)	0.08
TRI	8	2.90	0.49	0.51 (0.50–0.51)	0.06 (0.03–0.09)	0.3 (0.1–0.5)	0.03
ALA	8	1.55	0.14	0.74 (0.74–0.75)	0.01 (0.01–0.02)	0.2 (0.1–0.6)	0.003

^a95% confidence intervals. ^bSSQ = sum of the squares. ^cExperiment performed with TCA and DCA.

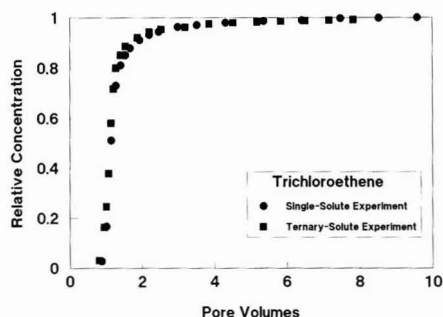


Figure 3. Comparison of trichloroethene breakthrough curves obtained by using single- and ternary-solute solutions. The single-solute experiment used flow-through UV detection, while the ternary-solute experiment used fraction collection followed by GC analysis.

The trichloroethene breakthrough curve obtained from the experiment performed with a single-solute solution is compared in Figure 3 to the breakthrough curve obtained from the experiment performed with the ternary-solute solution. The two breakthrough curves are essentially identical, which is reflected in the similarity of parameter values obtained from the two experiments (see Table I). This similarity exemplifies the reproducibility of the miscible displacement technique, as well as demonstrating that the flow-through and fraction collection methods produce identical results. In addition, the similarity suggests that neither the magnitude nor the rate of sorption of trichloroethene was affected by the presence of cosolutes. Trichloroethene and *p*-xylene breakthrough curves obtained by using single- and binary-solute solutions were reported by Lee et al. (10) to be similar.

A plot of the reverse rate constants (k_2) versus the equilibrium sorption constants (K_p) is provided in Figure 4. The results of the benzene, 1,2-*trans*-dichloroethane, monuron, monolinuron, and propachlor experiments are not included because unique solutions could not be obtained as a result of R values that were very close to 1 (insufficient sorption). Regressions performed for the individual chemical classes, excluding the pesticides, were statistically indiscriminate (i.e., overlapping confidence intervals). Thus, the k_2 - K_p relationships for the chloro-

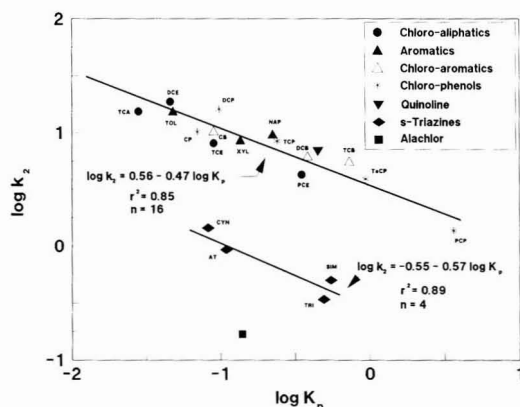


Figure 4. Relationship between the first-order reverse rate constant (k_2 , h^{-1}) and the equilibrium sorption constant (K_p , $mL\ g^{-1}$). Key: TOL, toluene; XYL, *p*-xylene; NAP, naphthalene; TCA, 1,1,1-trichloroethane; DCE, 1,2-*trans*-dichloroethene; TCE, trichloroethene; PCE, tetrachloroethene; CP, *p*-chlorophenol; DCP, 2,4-dichlorophenol; TCP, 2,4,6-trichlorophenol; TeCP, 2,3,4,5-tetrachlorophenol; PCP, pentachlorophenol; CB, chlorobenzene; DCB, 1,3-dichlorobenzene; TCB, 1,2,4-trichlorobenzene; CYN, cyanazine; AT, atrazine; SIM, simazine; TRI, trietazine.

benzenes, alkylbenzenes, and chloroethenes/chloroethanes, as well as the neutral species of chlorophenols and quinoline could be described with a single function. Several tentative conclusions may be drawn from this. First, sorbates containing single or multiple substitutions of methyl or chlorine appear to exhibit k_2 - K_p relationships similar to that of unsubstituted aromatic hydrocarbons (naphthalene). Second, chlorinated alkenes/alkanes appear to exhibit a k_2 - K_p relationship similar to that of the unsubstituted and substituted aromatics. Third, it appears that the neutral species of ionogenic compounds exhibit kinetic behavior similar to that of nonionic compounds. It is apparent that, for these compounds, sorbate structure has a minor impact on the nature of rate-limited sorption. The major factor controlling nonequilibrium sorption appears to be the sorptivity (K_p value) of the compound, which can be related to its hydrophobicity and molecular size.

Inspection of Figure 4 reveals that the chlorobenzene and dichlorobenzene data points, which were collected under low-pH conditions, are similar to the data points collected under high-pH conditions. This similarity suggests that pH has a negligible impact on the nature of nonequilibrium sorption exhibited by nonionic, low-polarity HOCs. It should be noted, however, that pH can have a significant effect on nonequilibrium sorption of ionogenic HOCs (7).

It is clear that the reverse rate constants of the pesticides are much smaller than those of the non-pesticide HOCs and that the differences are statistically significant (see Table I and Figure 4). While the slopes of the LFERs are similar, the intercept for the triazines is 1 order of magnitude smaller than that for the non-pesticide HOCs. The magnitude of the intercept is a measure of the characteristic time of the sorption "reaction". Thus, sorption of the pesticides is rate limited to a significantly greater degree than is that of the non-pesticide HOCs.

Discussion

The inverse nature of the k_2 - K_p relationship presented in Figure 4 suggests that a diffusion-limited mechanism is responsible for the observed nonequilibrium (7, 11, 17). While several researchers have proposed some form of a diffusion-limited mechanism as the cause of nonequilibrium sorption for HOCs, it has not been possible to discriminate between the two primary sorption-related, diffusion-limited mechanisms: intrasorbent diffusion and retarded intraparticle diffusion. Recent research (7), however, has shown that diffusion within the matrix of sorbent organic matter, or intraorganic matter diffusion, appears to be responsible for the rate-limited sorption of HOCs by nonaggregated sorbents. A model that interprets the nonequilibrium sorption in terms of diffusion of sorbate within a polymeric structure was presented by Brusseau et al. (7). The model relates the first-order reverse rate constant to polymer diffusivity as follows:

$$k_2 = \alpha / (1 - F) \text{ and } \alpha = c D_{py} / l^2 \quad (7)$$

where α is a mass-transfer constant (T^{-1}), c is a shape factor, D_{py} is the diffusion coefficient ($L^2 T^{-2}$) in the polymer, and l is the characteristic diffusion length (L).

Diffusion in polymers is dependent upon the physicochemical properties of the polymer, the diffusing molecule, and the solvating medium. For a given polymer and solvent, the diffusion coefficient decreases exponentially with increasing molecular weight (MW) or size of the sorbate, i.e., $D_{py} \propto (MW)^{-n}$ (23–25). The log-log-linear inverse relationship that exists between k_2 and K_p is a reflection of the strong dependency of D_{py} on molecular size of the sorbate (7). The shape of the diffusing molecule can also have an impact on diffusion in polymers (23, 26). Branched molecules (e.g., benzene with various functional groups), for example, have been shown to have smaller D_{py} values in comparison to unbranched molecules (26, 27). The addition of functional groups to a molecule such as benzene results in an increased potential for entanglement with the polymer mesh, which will constrain diffusion. Such behavior has been reported for sorption of alkylbenzenes by a sandy soil, where k_2 values for propylbenzene and butylbenzene were smaller than the LFER established for the unsubstituted series of benzene, naphthalene, and anthracene (7).

The fact that the k_2 values for all the non-pesticide HOCs can be described by a single LFER suggests that the relatively simple functional groups associated with these molecules do not significantly affect their diffusive behavior. This confirms the preliminary observations of

Brusseau and Rao (11). Inspection of the structures of the pesticides (see Figure 1) reveals that they comprise relatively complex functional groups. Such functional groups could certainly result in an increased hindrance to diffusion, which would be reflected in smaller k_2 values. The large difference in intercepts between the pesticides and the non-pesticide HOCs may thus arise from this factor.

It is possible, however, that another factor instead of, or in addition to, the diffusive constraint discussed above, may be involved. The sorption of neutral HOCs is generally considered to involve van der Waal type interactions between the sorbate and sorbent. In contrast, sorption of the classes of pesticides employed herein can, in some cases, involve specific sorbate-sorbent interactions such as charge transfer between the sorbate and functional groups of the organic matter components of the sorbent, as well as van der Waals interactions (28–34). The characteristic time of reaction associated with specific sorbate-sorbent interactions can be significantly greater than that of van der Waals interactions, which are rapid. Hence, the difference in sorption rate constants (i.e., intercepts of the LFERs) observed for the pesticides and the non-pesticide HOCs may result from some combination of diffusive constraint and specific sorbate-sorbent interactions.

An attempt to delineate which factor may predominate can be made by using the polymer diffusion analogue discussed by Brusseau et al. (7). As discussed above, D_{py} is an exponential function of molecular weight. Inspection of eq 7 reveals that this functionality results in k_2 being a function of molecular weight. The k_2 -MW functionality with n equal to 4 describes the data reported by Brusseau et al. (7). This functionality can be used to estimate the magnitude of the difference that would be expected between k_2 values of the pesticides and the non-pesticides if only diffusive constraints were involved. The predicted differences can then be compared to the observed differences, revealing the fraction of the observed difference that may be associated with diffusive constraint.

This was done with chlorobenzene (MW = 112.5), atrazine (MW = 216.1), and alachlor (MW = 269.5) as the representative sorbates. The predicted difference between the k_2 values of chlorobenzene and atrazine is 1.1 (log units), while the observed difference is 1.0. The predicted difference between the k_2 values of chlorobenzene and alachlor is 1.5, while the observed difference is 1.7. The similarity between the predicted and observed differences suggests that diffusive constraint may be the predominate factor for the large differences between the rate constants obtained for the pesticides and non-pesticides.

The large difference between the rate constants obtained for the pesticides and non-pesticides has implications regarding the mechanism responsible for the nonequilibrium sorption observed in these experiments. As previously mentioned, several authors have postulated that some type of diffusion-limited mechanism is responsible for nonequilibrium sorption. Some authors have considered diffusion within organic matter (cf. references cited in ref 17) while others have proposed retarded diffusion within microporous mineral components (4, 35). The large difference in rate constants between the pesticides and non-pesticides reported herein is inconsistent with the retarded intraparticle diffusion model, which would predict a difference of approximately 0.5 log unit between the values for alachlor and toluene. The predicted difference contrasts sharply with the observed difference of 2 log units. The observed difference is, however, consistent with the intraorganic matter diffusion model, as evidenced by

the results discussed in the previous paragraph. Hence, the data reported herein provide support for diffusion within organic matter as the rate-limiting mechanism for sorption of HOCs by nonaggregated sorbents and are in accordance with the results reported by Brusseau et al. (7).

Conclusions

The data presented in Figure 4 support the hypothesis of Brusseau and Rao (11) that a series of roughly parallel LFERs may be expected to describe the k_2 - K_p relationships for diverse groups of chemicals, with the magnitude of the intercept dependent upon the nature of the sorbate. The LFER for simple molecules such as benzene and chlorobenzene represents a "standard-state" behavior, with deviations from the standard being a function of the relative degree of additional or lesser constraint affecting sorbate-sorbent interactions. For example, sorbates with relatively complex structures, such as some pesticides, may have additional constraints relating to diffusion and specific interactions. These additional constraints result in larger characteristic times of sorption and smaller rate constants, as observed for the pesticides in this report. Conversely, sorbates whose sorption involves cation exchange, for example, may have characteristic times of sorption much smaller than HOCs, resulting in larger rate constants (7). The structure of the sorbate should be considered when the nonequilibrium sorption of organic chemicals is evaluated.

Literature Cited

- Karickhoff, S. W.; Morris, K. R. *Environ. Toxicol. Chem.* **1985**, *4*, 469-479.
- Oliver, B. G. *Chemosphere* **1985**, *14*, 1087-1106.
- Coates, J. T.; Elzerman, A. W. *J. Contam. Hydrol.* **1986**, *1*, 191-210.
- Wu, S.; Gschwend, P. M. *Environ. Sci. Technol.* **1986**, *20*, 717-725.
- Witkowski, P. J.; Jaffe, P. R.; Ferrara, R. A. *J. Contam. Hydrol.* **1988**, *2*, 249-269.
- Brusseau, M. L.; Jessup, R. E.; Rao, P. S. C. *Environ. Sci. Technol.* **1990**, *24*, 727-735.
- Brusseau, M. L.; Jessup, R. E.; Rao, P. S. C. *Environ. Sci. Technol.* **1991**, *25*, 134-142.
- Karickhoff, S. W. In *Contaminants and Sediments*; Baker, R. A., Ed.; Ann Arbor Press: Ann Arbor, MI, 1980; Vol. 2, Chapter 11.
- Curtis, G. P.; Roberts, P. V.; Reinhard, M. A. *Water Resour. Res.* **1986**, *22*, 2059-2068.
- Lee, L. S.; Rao, P. S. C.; Brusseau, M. L.; Ogwada, R. A. *Environ. Toxicol. Chem.* **1988**, *7*, 779-793.
- Brusseau, M. L.; Rao, P. S. C. *Chemosphere* **1989**, *18*, 1691-1706.
- Brusseau, M. L.; Reid, M. E. *Chemosphere* **1991**, *22*, 341-350.
- Brusseau, M. L.; Rao, P. S. C.; Wood, A. L. *Natl. Meet.—Am. Chem. Soc., Div. Environ. Chem.* **1989**, 29(2), 137-140.
- Brusseau, M. L.; Wood, A. L.; Rao, P. S. C. *Environ. Sci. Technol.* **1991**, *25*, 903-910.
- Nkedi-Kizza, P.; Brusseau, M. L.; Rao, P. S. C.; Hornsby, A. G. *Environ. Sci. Technol.* **1989**, *23*, 814-820.
- Shorten, C. V.; Elzerman, A. W. *Natl. Meet.—Am. Chem. Soc., Div. Environ. Chem.* **1989**, 29(2), 134-136.
- Brusseau, M. L.; Rao, P. S. C. *CRC Crit. Rev. Environ. Cont.* **1989**, *19*, 33-99.
- Hicks, R. W.; Stodhill, A. M. DER, Florida Department of Environmental Regulation, Groundwater Investigation Report No. 88-06, June 1988.
- Selim, H. M.; Davidson, J. M.; Mansell, R. S. Summer Computer Simulation Conference; Washington, DC, 1976.
- Cameron, D. R.; Klute, A. *Water Resour. Res.* **1977**, *13*, 183-188.
- Van Genuchten, M. Th. Research Report No. 119, USDA Salinity Laboratory, Riverside, CA, 1981.
- Brusseau, M. L.; Jessup, R. E.; Rao, P. S. C. *Water Resour. Res.* **1989**, *25*, 1971-1988.
- Park, G. S. *Trans Faraday Soc.* **1951**, *47*, 1007.
- Klein, J. *Nature* **1978**, *271*, 143.
- Rogers, C. E. In *Polymer Permeability*; Comyn, J., Ed.; Elsevier: London, 1985; Chapter 2, pp 11-73.
- Rogers, C. E.; Fels, M.; Li, N. N. In *Recent Developments in Separation Science*; Li, N. N., Ed.; CRC Press: Cleveland, OH, 1972; Vol. II, pp 77-105.
- Prager, S.; Long, F. A. *J. Am. Chem. Soc.* **1951**, *73*, 4072.
- Weber, J. B.; Weed, S. B.; Ward, T. M. *Weed Sci.* **1969**, *17*, 417-421.
- Hayes, M. H. B. *Residue Rev.* **1970**, *32*, 131-174.
- Dunigan, E. P.; McIntosh, T. H. *Weed Sci.* **1971**, *19*, 279-282.
- Senesi, N.; Testini, C. *Geoderma* **1982**, *28*, 129-146.
- Ward, T. M.; Upchurch, R. P. *J. Agric. Food Chem.* **1965**, *13*, 334-338.
- Briggs, G. C. *Nature* **1969**, *223*, 1288-1290.
- Gaillardon, P.; Calvet, R.; Gaudry, J. C. *Weed Res.* **1980**, *20*, 201-204.
- Ball, W. P.; Roberts, P. V. *Environ. Sci. Technol.*, in press.
- Callahan, M. A.; Slimak, M. H.; Gabel, N. W.; May, I. P.; Fowler, C.; Freed, J. R.; Jennings, P.; Durfee, R. L.; Whitmore, F. C.; Maestri, B.; Mabey, W. R.; Holt, B. R.; Gould, C. *Water-Related Environmental Fate of 129 Priority Pollutants*; EPA-440/4-79-029a and EPA-440/4-79-029b; U.S. Environmental Protection Agency: Washington, DC, 1979; Vol. I and II.
- Worthing, C. R. *The Pesticide Manual*, 8th ed.; British Crop Protection Council: Thornton Heath, UK, 1987.

Received for review August 20, 1990. Revised manuscript received April 16, 1991. Accepted April 18, 1991. We thank Linda Lee, Alison Browne, and Randy McCrady for their assistance in the GC analyses and Zeina Hinedi for Figure 1. This work was supported, in part, by Florida Department of Environmental Regulation Contract WM-254 and by U.S. Department of Agriculture CSRS Project ARZT-136402-H-21-060. Approved for publication as Arizona Agricultural Experiment Station Journal Series No. 7334 and Florida Agricultural Experiment Station Journal Series No. R-00979.

COMMUNICATIONS

Phenol Oxidation in Supercritical Water: Formation of Dibenzofuran, Dibenzo-*p*-dioxin, and Related Compounds

Thomas D. Thornton, Douglas E. LaDue, III, and Phillip E. Savage*

Department of Chemical Engineering, The University of Michigan, Ann Arbor, Michigan 48109-2136

Introduction

Supercritical water is a good medium for the complete oxidation of organic compounds, and this chemistry forms the basis for a novel technology currently being advanced for the ultimate destruction of hazardous wastes. Above its critical point ($T_c = 374^\circ\text{C}$, $P_c = 218\text{ atm}$), water has a high solubility for both organics (1) and oxygen (2), so a single phase containing a homogeneous mixture can exist at reaction conditions. This elimination of potential interphase transport limitations coupled with the moderately high operating temperatures and pressures leads to rapid oxidation rates.

Much of the previous research dealing with oxidation in supercritical water has been devoted to either demonstrating the technology (3-7) or measuring the disappearance kinetics for relatively simple compounds (8-12). Only very limited work (3, 12), however, has been devoted to identifying and quantifying the reaction products from the supercritical water oxidation of organic compounds. Such research is clearly important from an environmental viewpoint, especially when one considers that incineration, another thermal oxidation process, can produce undesired, high molecular weight condensation products such as dibenzofurans and dibenzo-*p*-dioxins from phenols (13-18). We have undertaken and completed this study to determine whether the oxidation of phenol, a representative organic pollutant, in near- and supercritical water can lead to the formation of similar high molecular weight products.

Experimental Section

Oxidation reactions were accomplished in both batch and flow reactors. For the flow reactor studies, phenol oxidation was carried out in an isothermal reactor that was constructed from a 1- or 4-m length of $1/8$ -in.-o.d. Hastelloy C-276 tubing. The reactor feed streams were prepared by dissolving high-pressure oxygen into deionized water in a stirred vessel and loading a mixture of phenol dissolved in deionized water into a second vessel. The two feed streams were pumped and preheated separately in 2-m lengths of $1/16$ -in.-o.d. Hastelloy C-276 tubing coiled inside a temperature-controlled fluidized sand bath. Employing this split feed arrangement ensured that the phenol and oxygen did not contact each other until the streams had been pressurized and preheated to the desired reaction conditions. We verified that the phenol did not react in the preheater line by pyrolyzing phenol in supercritical water in a batch reactor, under conditions identical with those used in the flow reactor studies, and observing no measurable conversion and detecting no reaction products. The feed streams were mixed at the reactor inlet, and after passing through the heated reactor, the reactor effluent was cooled rapidly in a heat exchanger, depressurized, and separated into liquid and vapor phases. Additional details

regarding the reactor design and operation have been reported elsewhere (19).

The batch reactor studies were completed in constant-volume reactors constructed from $3/8$ -in.-o.d. 316 stainless steel tubing fitted with 316 stainless steel Swagelok end caps. The reactors were loaded with a measured volume of an aqueous stock solution of phenol in order to achieve the desired reactor pressure for each reaction temperature. The loading and sealing of the reactors were completed in an oxygen-filled glovebag. Thus, phenol, water, and oxygen were the only compounds initially present within each reactor. After the reactors were loaded and sealed, they were next immersed in a preheated, isothermal fluidized sand bath. When the desired residence time was reached, the reactors were removed from the sand bath and quenched in an ambient temperature water bath. Each reactor was opened, and the liquid-phase product was retained for further analysis.

The concentration of unreacted phenol was determined by reverse-phase, high-performance liquid chromatography (HPLC), and more details are available elsewhere (19). Prior to further analysis, the liquid product samples were subjected to a benzene solvent extraction protocol in which the liquid product was contacted with benzene in a 5:1 volume ratio. The extraction step transferred the organic compounds in the aqueous phase into the benzene, thereby concentrating the samples. The benzene layer was transferred to a vial and retained for further analysis.

Identification of the reaction products was accomplished using a Hewlett-Packard (HP) Model 5890 gas chromatograph (GC) with a Model 5970 mass selective detector and a computer workstation. Quantification of the product concentrations was accomplished using an HP 5890 GC equipped with a flame ionization detector and an HP 7673 autosampler/injector. In both gas chromatograph systems, a 12 m \times 0.2 mm \times 0.33 μm film thickness HP-1 capillary column separated the sample constituents.

The concentrations of each of the products were determined by first preparing a set of aqueous standard solutions containing different concentrations of each product. We next subjected these standards to the solvent extraction protocol used for the reaction products, separated the benzene and aqueous phases, injected 1 μL of the benzene phase into the GC, and recorded the integrated area of the resulting peak on the chromatogram. Plotting these integrated areas as a function of the concentration of the compound in the standard solution resulted in a linear calibration. We used these calibrations to determine the concentrations of the different reaction products in the samples taken from the flow reactor. Multiple injections of samples withdrawn from the same vial revealed that the GC analyses were reproducible as the integrated peak area varied by $\pm 6\%$ at the 95% con-

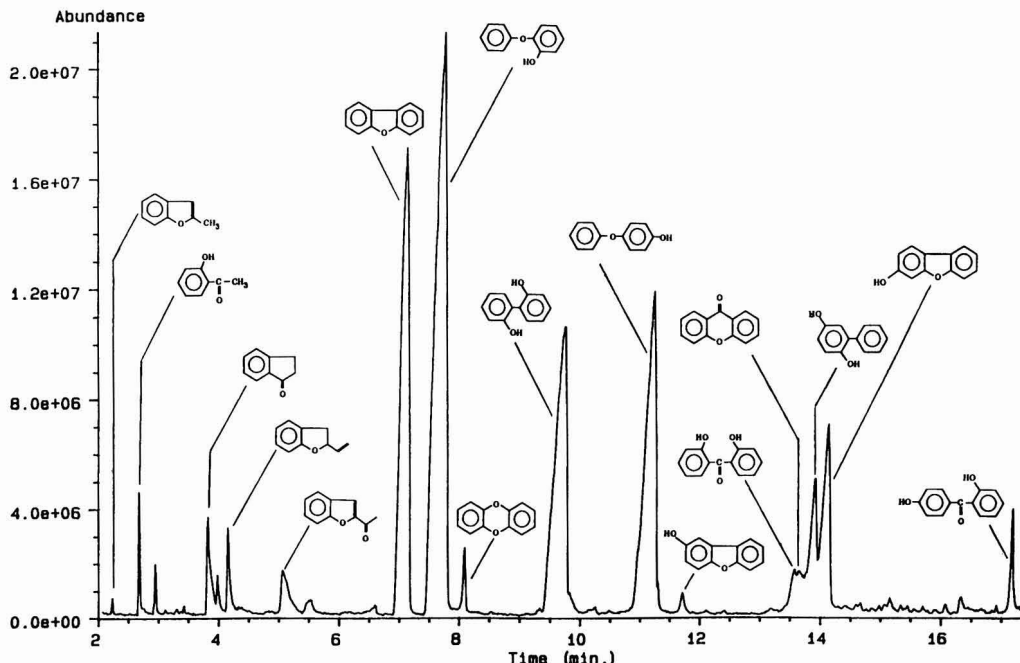


Figure 1. Total ion chromatogram of phenol oxidation products (380 °C, 233 atm, 875 ppm phenol, 40% excess oxygen, and 33-s residence time).

fidence level. Additionally, background analyses verified that the deionized water, phenol, and benzene used in the experiments were each free of high molecular weight impurities.

Results and Discussion

The nominal reaction conditions used in our experiments included temperatures of 300, 380, and 420 °C and pressures of 218, 233, and 278 atm. We intentionally operated at temperatures somewhat lower than the temperatures of 400–650 °C typically proposed for commercial applications of supercritical water oxidation technology (5, 7) so that the products from the incomplete oxidation of phenol could be detected. The operating pressure was comparable to that proposed for commercial operation. The initial phenol concentrations were from 100 to 1000 parts per million on a mass basis (ppm), and the initial oxygen concentrations ranged from the precise stoichiometric amount required for the complete conversion of phenol to carbon dioxide and water (0% excess oxygen) to 11 times the stoichiometric amount (1000% excess oxygen). Through the combination of both flow and batch reactor work, a wide range of residence times could be tested. The residence times investigated in the flow reactor ranged from 3 to 109 s, and much longer residence times from 300 to 29 000 s (5 min to about 8 h) were tested in the batch reactor. These residence times covered a broader range than those proposed for commercial operation.

Gas chromatography-mass spectrometry analysis of the benzene extracts revealed the presence of a very large number of individual reaction products. Figure 1 displays a representative total ion chromatogram, which corresponds to a sample produced by oxidizing 875 ppm phenol with 40% excess oxygen at 380 °C and 233 atm for 33 s in the flow reactor. We tentatively identified each of the compounds by searching the computer library of mass spectra and selecting the one that best matched its mass

spectrum. The structures that appear near the individual peaks in Figure 1 summarize the results of the computer matches of the mass spectra. Note that these identifications remain tentative for most of the compounds. Four of the compounds (4-phenoxyphenol, 2,2'-biphenol, dibenzofuran, and dibenzo-*p*-dioxin), however, were positively identified by comparing both their retention times and mass spectra with those of authentic compounds. Additionally, we are confident that the identification of 2-phenoxyphenol is also correct because of the very good match of its mass spectrum with the library spectrum.

Table I provides a summary of representative experimental results obtained under the different reaction conditions. Inspection of the data in Table I reveals that at shorter residence times 2-phenoxyphenol, 4-phenoxyphenol, and 2,2'-biphenol were typically present in higher concentrations than were dibenzofuran and dibenzo-*p*-dioxin. At longer residence times, however, dibenzofuran was typically the product present in the highest concentrations. In no experiment did the dibenzo-*p*-dioxin concentration ever exceed 0.3 ppm, and for several sets of operating conditions it was not detected as a product.

Figure 2 displays the temporal variations of the concentrations of the five products whose identities are certain. These data were obtained by operating the flow reactor at 380 °C and 278 atm and using a feed stream with an initial phenol concentration of 100 ppm and 800% excess oxygen. At short reaction times the concentrations of the two phenoxyphenol isomers were the highest. These concentrations increased rapidly with time until they reached maximum values near 13 s. As time increased, however, the concentrations of the phenoxyphenols decreased until they were present in very low concentrations at the long reaction times. The concentration of 2,2'-biphenol showed a similar trend with time, but its concentration was always much lower than that of the phenoxyphenols. The dibenzofuran concentration was always greater than 0.9 ppm, and it increased slowly with reaction

Table I. Product Concentrations for Selected Operating Conditions

temp, °C	pressure, atm	resid time, s	init phenol concn, ppm	excess oxygen, %	phenol convrsn, %	product concn, ppm				
						dibenzo-furan	2-phenoxy-phenol	dibenzo-dioxin	2,2'-biphenol	4-phenoxy-phenol
300	278	27	242	294	21	0.0	3.8	0.0	2.4	6.0
300	278	47	244	284	40	0.2	4.0	0.0	2.7	6.1
300	278	78	230	318	82	0.0	1.5	0.0	0.7	2.2
300	278	109	240	275	95	0.2	0.0	0.0	0.0	0.0
380	278	4	96	985	17	1.4	3.7	0.0	0.4	2.4
380	278	10	98	923	27	1.6	4.5	0.3	0.4	2.4
380	278	24	101	858	59	1.3	7.1	0.1	0.2	2.5
380	278	98	96	872	98	2.4	0.3	0.1	0.0	0.0
380	278	16	973	4	32	1.5	57.7	0.1	32.6	12.2
380	278	32	951	13	61	2.9	36.3	0.2	15.1	8.3
380	278	65	965	6	73	2.4	23.0	0.0	6.5	5.6
380	278	12	243	228	27	2.3	21.9	0.2	4.4	8.3
380	278	41	242	280	69	3.4	14.8	0.3	1.5	4.1
380	278	78	246	276	93	2.9	2.6	0.1	0.0	1.0
380	278	900	151	250	100	2.4	0.0	0.0	0.0	0.4
380	278	1800	151	250	100	2.5	0.0	0.0	0.0	0.3
380	278	29040	151	250	100	0.0	0.0	0.0	0.0	0.0
380	218	3	258	180	4	1.1	4.5	tr < 0.1	0.9	1.6
380	218	7	249	193	10	1.0	8.1	0.0	0.7	3.2
380	218	13	225	253	13	1.1	11.5	tr < 0.1	2.7	5.0
380	218	600	590	250	100	8.0	0.0	0.2	0.0	0.0
380	218	900	590	250	100	3.6	0.0	0.0	0.0	0.0
380	218	1800	590	250	100	5.6	0.0	0.2	0.0	0.0
380	218	3600	590	250	100	3.8	0.0	0.0	0.0	0.0
420	278	4	98	781	16	1.6	7.6	0.0	0.0	2.1
420	278	12	92	871	29	2.1	12.9	0.0	0.0	3.1
420	278	16	98	668	40	2.7	16.0	0.0	0.0	3.1
420	278	41	92	868	75	2.2	9.0	0.0	0.0	1.1
420	278	300	750	263	94	12.5	3.5	0.3	0.0	0.0
420	278	1800	750	263	100	9.7	0.0	0.0	0.0	0.0
420	278	3600	750	263	100	9.7	0.0	0.0	0.0	0.0
420	278	28800	750	263	100	0.0	0.0	0.0	0.0	0.0

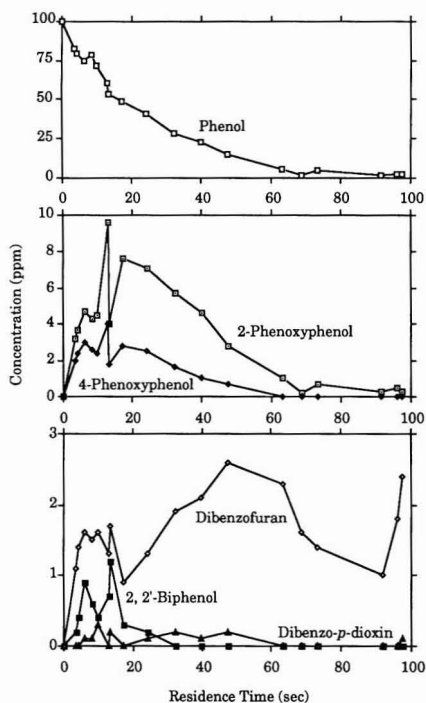


Figure 2. Temporal variation of concentrations of selected products (380 °C, 278 atm, 100 ppm phenol, and 800% excess oxygen).

time. The concentration of dibenzo-*p*-dioxin was always very low, and its maximum value was 0.3 ppm at 9.9 s.

The data in Figure 2 indicate that the 2,2'-biphenol and phenoxyphenols were oxidized on roughly the same time scale as was phenol, the original reactant. The batch reactor results in Table I, however, show that the dibenzofuran was more resistant to degradation. For example, oxidation of 750 ppm phenol at 420 °C and 278 atm for 3600 s (1 h) resulted in a dibenzofuran concentration of 9.7 ppm. After 28 800 s (8 h) of oxidation at these conditions, however, the dibenzofuran was completely degraded. These results show that of the five condensation products detected in the present work, dibenzofuran was the product most resistant to oxidative degradation in supercritical water, but even this persistent product can be destroyed at long residence times.

The data in Figure 2 also show that a large fraction of the original phenol goes into the formation of the high molecular weight products. For example, at a residence time of 13 s, the total concentration of the five identified condensation products was 15.6 ppm and the phenol concentration was 63 ppm. Thus, 37 ppm of phenol had reacted to form other products, so approximately 42% of that phenol went into the formation of these higher molecular weight products. The balance of the phenol that reacted apparently formed other products (e.g., catechol, hydroquinone, *p*-benzoquinone, carboxylic acids, carbon monoxide, and carbon dioxide) that we have identified in earlier investigations using HPLC analysis of the liquid product and GC analysis of the vapor phase (19).

To summarize, this work has been the first to identify 2-phenoxyphenol, 4-phenoxyphenol, 2,2'-biphenol, dibenzofuran, and dibenzo-*p*-dioxin as products from oxidation of phenol in supercritical water under a variety of different reaction conditions. Furthermore, it is evident that these products contain a significant proportion of the organic carbon originally present in the reactant. Finally,

these products formed from the supercritical water oxidation of phenol are also formed from phenol incineration (13-18). This observation suggests that there may be a relationship between the two thermal oxidation processes, even though supercritical water oxidation operates at much lower temperatures and much higher pressures than does incineration.

Literature Cited

- (1) Connolly, J. F. *J. Chem. Eng. Data* 1966, 11, 13.
- (2) Pray, H. A.; Schweickert, C. E.; Minnich, B. H. *Ind. Eng. Chem.* 1952, 44, 1146.
- (3) Modell, M. U.S. Patent 4 543 190, 1985.
- (4) Thomason, T. B.; Modell, M. *Hazard. Waste* 1984, 1, 453.
- (5) Modell, M. In *Standard Handbook of Hazardous Waste Treatment and Disposal*; Freeman, H. M., Ed.; McGraw-Hill: New York, 1989; pp 8.153-8.168.
- (6) Staszak, C. N.; Malinowski, K. C.; Killilea, W. R. *Environ. Prog.* 1987, 6, 39.
- (7) Bramlette, T. T.; et al. Destruction of DOE/DP Surrogate Wastes with Supercritical Water Oxidation Technology. Sandia National Laboratory Report, SAND90-8229; 1990.
- (8) Helling, R. K.; Tester, J. W. *Energy Fuels* 1987, 1, 417.
- (9) Helling, R. K.; Tester, J. W. *Environ. Sci. Technol.* 1988, 22, 1319.
- (10) Rofer, C. K.; Streit, G. E. Kinetics and Mechanism of Methane Oxidation in Supercritical Water. Los Alamos

National Laboratory Report, LA-11439-MS (DOE/HWP-64); 1988.

- (11) Wightman, T. J. M.S. Thesis, University of California, Berkeley, 1981.
- (12) Yang, H. H.; Eckert, C. A. *Ind. Eng. Chem. Res.* 1988, 27, 2009.
- (13) Choudhary, G. G.; Olie, K.; Hutzinger, O. In *Chlorinated Dioxins and Related Compounds: Impact on the Environment*; Hutzinger, O., Frei, R. W., Merian, E., Pocchiari, F., Eds.; Pergamon: Oxford, U.K., 1982; pp 275-301.
- (14) Eklund, G.; Pedersen, J. R.; Strömberg, B. *Nature* 1986, 320, 155.
- (15) Stehl, R. H.; Lamparski, L. L. *Science* 1977, 197, 1008.
- (16) Ballschmiter, K.; Swerev, M. *Fresenius Z. Anal. Chem.* 1987, 328, 125.
- (17) Born, J. G. P.; Louw, R.; Mulder, P. *Chemosphere* 1989, 19, 401.
- (18) Shaub, W. M.; Tsang, W. *Environ. Sci. Technol.* 1983, 17, 721.
- (19) Thornton, T. D.; Savage, P. E. *J. Supercrit. Fluids* 1990, 3, 240.

Received for review March 27, 1991. Revised manuscript received May 24, 1991. Accepted May 27, 1991. This work was supported in part by the National Science Foundation (CTS-8906859 and CTS-8906860), the Shell Faculty Career Initiation Fund, and the Amoco Foundation.

Sonochemical Destruction of Chlorinated Hydrocarbons in Dilute Aqueous Solution

H. Michael Cheung,* Ashish Bhatnagar, and Greg Jansen

The University of Akron, Department of Chemical Engineering, Akron, Ohio 44325-3906

Introduction

Power ultrasound in the range of 20-100 kHz has found application in cleaning (the common laboratory ultrasonic cleaner operates in this frequency range), plastic welding, emulsification, and chemical reactivity. Most sonochemical research to date has focused on synthetic aspects of ultrasound. Both homogeneous and heterogeneous ultrasound can produce sonochemistry, a recent review by Suslick (1) provides a concise overview of the current state of the art. A more extensive tutorial in sonochemistry can be found in the book by Mason (2).

Homogeneous sonochemistry results from the formation of cavitation bubbles in the solvent. The bubble collapse leads to surprisingly high local temperatures and pressures. Locally the temperature and pressure may reach 5000 °C and 500 atm, respectively (3). These rather extreme conditions are very short lived, but have been shown to produce several reactive species in aqueous systems including H_2O_2 , HO_2 , H^\cdot , and OH^\cdot (4). The reactions that take place in aqueous solution are similar to combustion (5) though strong reduction as well as oxidation reactions have been observed (6).

We are currently exploring the use of homogeneous ultrasound in destroying chlorinated hydrocarbons in dilute aqueous solution. We have thus far examined the sonochemical destruction of methylene chloride, carbon tetrachloride, 1,1,1-trichloroethane, and trichloroethylene in concentrations in the 100-1000 ppmv range. Ultrasound appears to be quite effective in the destruction of the compounds examined thus far. Quantitative results with GC/MS have been obtained for methylene chloride, qualitative results from pH measurements have been ob-

tained for the other compounds.

Experimental Section

The experimental setup consisted of a Heat Systems W-385 ultrasonicator and a 2-L glass reaction vessel equipped with a stainless steel cooling coil. The W-385 ultrasonicator is capable of delivering 475 W of ultrasonic energy. The temperature and pH of the reactor contents were continuously monitored. The sonicator was operated at its maximum output setting and typically delivered 40% (approximately 250 W) of its rated power to the reactor. The chlorinated hydrocarbons were all of at least 99% purity and were used as received. A Hewlett-Packard GC/MS (5890 GC, 5970 mass sensitive detector, and 9133 Chem Station) with a 12 m \times 0.2 mm \times 0.33 μm film thickness HP Ultra 1 capillary column coated with cross-linked methylsilicone gum was used for determination of methylene chloride concentrations. Regular tap water was used in the cooling coils to prevent temperature rise due to the sonication. The temperature was not controlled but ranged from 15 to 20 °C. We are planning to install a temperature-controlled circulation bath on the reactor.

Temperature and pH data were recorded at regular intervals with the sonicator on standby. The sonicator interfered with the stability of the pH reading. For methylene chloride, 10-mL samples were withdrawn for GC/MS analysis. The analytical protocol involved combining the 10-mL sample with 1 mL of hexane and shaking for 2-5 min by hand. After at least 10 min of equilibration, 1 μL of the hexane phase was injected into the GC/MS. A calibration curve utilizing aqueous samples of known

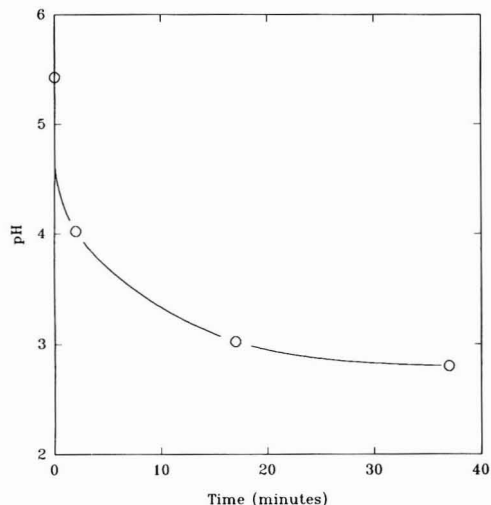


Figure 1. Solution pH versus sonication time for the homogeneous sonochemical destruction of 120 ppmv methylene chloride in water.

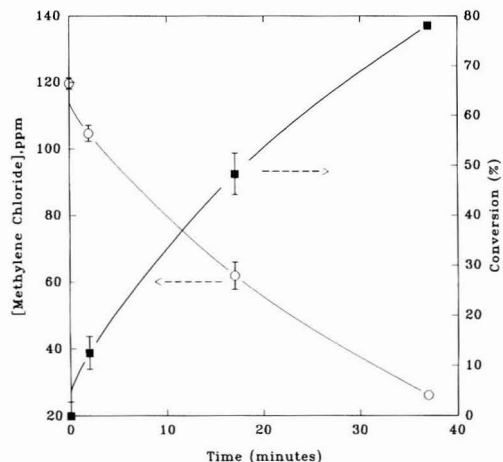


Figure 2. Methylene chloride concentration and conversion versus sonication time for the homogeneous sonochemical destruction of 120 ppmv methylene chloride in water.

methylene chloride concentration was developed by use of the same hexane extraction protocol. The calibration curve was linear over the 25–1000 ppmv range.

Results and Discussion

The pH of the reactor contents decreased rapidly in all cases, indicating the probable formation of HCl from the chlorinated reactants. The GC/MS results indicate a corresponding rapid decrease in the concentration of methylene chloride. Figure 1 shows the pH versus sonication time data for 120 ppmv methylene chloride. Figure 2 shows the GC/MS-determined concentrations and conversion for the same experiment. The shape of the curves is indicative of first-order kinetics, and a fit of the data yielded a first-order rate constant of $3.93 \times 10^{-2} \pm 2.7 \times 10^{-3} \text{ min}^{-1}$.

Similar pH results are obtained for carbon tetrachloride (Figure 3), trichloroethylene, and 1,1,1-trichloroethane. The pH results for the carbon tetrachloride are particularly interesting since it contains no hydrogen. We conclude that it is likely that the hydrogen for the HCl formation

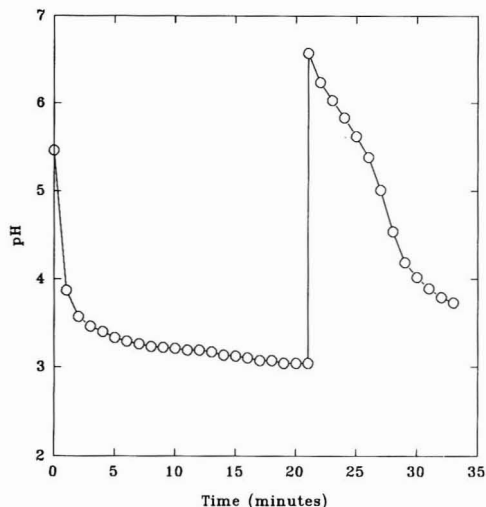


Figure 3. Solution pH versus sonication time for the homogeneous sonochemical destruction of 100 ppmv carbon tetrachloride in water. The vertical discontinuity at 21 min is due to the addition of sodium hydroxide solution to raise the system pH.

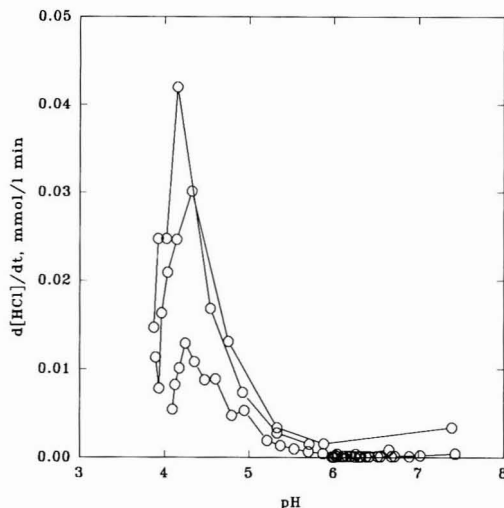


Figure 4. Rate of HCl formation versus solution pH for the sonochemical destruction of 100 ppmv methylene chloride in water.

is obtained from the water. Another feature of the pH measurements is that after they appear to become asymptotic, the rapid pH decline can be repeated following the addition of sodium hydroxide to increase the system pH. Figure 3 demonstrates this for the case of 100 ppmv carbon tetrachloride. Much of this effect is due to pH being minus the logarithm of the hydrogen ion concentration; however, it appears that the selectivity toward HCl formation (or at least hydrogen ion production) is pH dependent. Figure 4 plots the rate of HCl formation (inferred from the pH measurements) versus solution pH for the sonication of 100 ppmv methylene chloride. The rate of HCl formation seems to peak at approximately pH 4. It is speculative at this early stage, but it appears that pH may be useful in driving the reaction toward HCl as the final chlorinated product. We have not identified any other chlorinated species produced yet. The GC/MS results indicate no other chlorinated organics are present in

the sonication of methylene chloride (at least to the detection threshold of the instrument). We suspect that Cl_2 is being formed, but have not yet attempted to detect it.

We are presently developing the calibration curves needed for GC/MS analysis of carbon tetrachloride, 1,1,1-trichloroethane, and trichloroethylene. We plan to test the reactor vessel headspace for the presence of Cl_2 in the hopes of closing the chlorine atom balance on the reactor. Sonochemical destruction of chlorinated hydrocarbons appears to be a potentially powerful method of remediation, which may compete with or serve as an adjunct to other advanced oxidation processes.

Literature Cited

(1) Suslick, K. S. *Science* **1990**, 247, 1439.

- (2) Mason, T. J.; Lorimer, J. P. *Sonochemistry: Theory, Applications, and Uses of Ultrasound in Chemistry*; John Wiley & Sons: New York, 1988.
- (3) Suslick, K. S.; Hammerton, D. A.; Cline, R. E., Jr. *J. Am. Chem. Soc.* **1986**, 108, 5641.
- (4) Riesz, P.; Berdahl, D.; Christman, C. L. *Environ. Health Perspect.* **1985**, 64, 233.
- (5) Henglein, A. *Ultrasonics* **1985**, 25, 6.
- (6) Margulis, M. A. *Ultrasonics* **1985**, 23, 157.

Received for review April 5, 1991. Revised manuscript received May 6, 1991. Accepted May 8, 1991. We gratefully acknowledge the financial support of the Ohio Board of Regents through the Research Challenge Enhancement Awards program.

For the most vital news and important information . . .

Environmental Science & Technology

ES&T offers peer-reviewed research and a magazine section -- ensuring you that each monthly issue covers all areas of science and engineering in the environmental field.

You'll gain access to the very best minds . . . top environmental science

scholars. . . directors of leading laboratories . . . influential government regulatory experts . . . top industrial pollution experts. . . and other researchers on the cutting edge of environmental science today.

Timely. Detailed. Thorough.

ES&T standards are highest in the discipline, without exception.

Plus, ES&T presents hard facts on every aspect of the environment, included in these regular features:

- **RESEARCH** The most current, comprehensive peer-reviewed research makes ES&T "the place to publish" for top researchers in environmental science.
- **FEATURES** New materials and engineering approaches, special series of articles on the hottest topics in the field today.
- **REGULATIONS** Reports of changes in the state and federal regulatory picture and how those changes may affect your operation.
- **VIEWS** Short articles commenting on timely events and developments. These up-to-the-minute commentaries will keep you abreast on a range of environmental topics.
- **CURRENTS** News briefs on topics that are state-wide, federal, and international in scope. Awards are also noted in this popular section.
- **PLUS . . .** Book reviews, classified ads, and a consulting services directory round out ES&T, making it your full service publication!

Too much is happening in the field of environmental science! Don't go without your monthly issues of ES&T.

ACS Guarantee: If you are not satisfied with your ES&T subscription, you may cancel at any time, and receive a refund for all undelivered issues. No questions asked!

1991 SUBSCRIPTION RATES

Volume 25, ISSN: 0013-936X

		U.S.	Canada & Mexico	Europe*	All Other Countries*
Members	One Year	\$ 39	\$ 55	\$ 75	\$ 84
	Two Years	\$ 66	\$ 98	\$ 138	\$ 156
Nonmembers (personal)	One Year	\$ 73	\$ 89	\$ 109	\$ 118
	Two Years	\$ 124	\$ 156	\$ 196	\$ 214
Nonmembers (institutional)	One Year	\$ 329	\$ 345	\$ 365	\$ 374
	Two Years	\$ 559	\$ 591	\$ 631	\$ 649

*Includes air service.

Member subscription rates are for personal use only.

To subscribe to ES&T, contact:

American Chemical Society,
Marketing Communications Dept.,
Washington, D.C. 20036
TELEX: 440159 ACSPIU or 89 2582 ACS PUBS
FAX: (202)872-4615

Foreign payment must be made in U.S. dollars by international money order, UNESCO coupons, or U.S. bank draft. Orders accepted through your subscription agency. For nonmember rates in Japan, contact MARUZEN Co., Ltd. Please allow 45 days for delivery of your first issue.

Editor: William H. Glaze, University of North Carolina, Chapel Hill

Associate Editors: W. Giger, EAWAG, Switzerland • R.A. Hites, Univ. of Indiana • J.H. Seinfeld, California Institute of Technology
J.L. Schnoor, Univ. of Iowa • J. Suflita, Univ. of Oklahoma, Norman

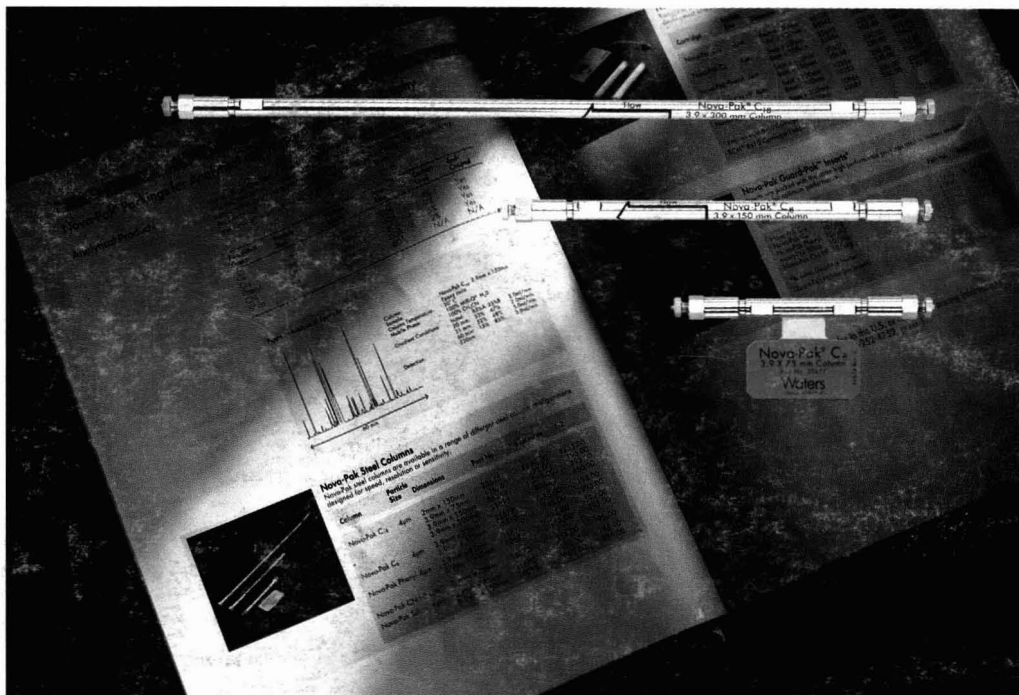
Advisory Board: R. Atkinson, Univ. of California, Riverside • J.M. Daisey, Lawrence Berkeley Lab.

F.H. Frimmel, Engler-Bunte-Institut der Univ. Karlsruhe, Germany

G.R. Helz, Univ. of Maryland • R. Mitchell, Harvard Univ. • J.M. Norbeck, Ford Motor Co.

W.J. Weber, Jr., Univ. of Michigan • A.J.B. Zehnder, Agricultural Univ. of Wageningen, The Netherlands • R.G. Zepp, U.S. EPA

In a hurry? Call TOLL FREE 800-227-5558 (U.S. and Canada). For Orders in the D.C. area or outside the U.S. and Canada call (202) 872-4363.



IF THIS MAKES YOU ANXIOUS, YOU SHOULD BE IN ANALYSIS.

Analytical chromatographers everywhere are anxious to get their hands on this informative new publication. It's the *Waters Chromatography Columns and Supplies Catalog*, and it's a convenient way to order the world's leading brand of HPLC columns.

Like our Nova-Pak® columns and cartridge columns. They're available in C₁₈, C₈, phenyl, cyano and silica, and they're the ideal choice for everything from microbore chromatography to lab scale purification. Especially now that we're offering our 3.9 mm i.d. x 150 mm columns at a new low price: **just \$295**. (Other sizes and quantity discounts also available.)

Only Nova-Pak packing is made from uniform, 4 µm and 6 µm spherical particles—particles we manufacture and pack ourselves in our cGMP material synthesis facility. And because of Waters exclusive, highly controlled bonding and endcapping process, you can count on Nova-Pak columns and cartridge columns for consistent results column-to-column, year after year.

GET THE BIG PICTURE.

Just call **1-800-252-4752**, in Puerto Rico call **809-747-8444**. We'll mail you a free copy of the *Waters Chromatography Columns and Supplies Catalog*.



Waters
Division of MILLIPORE

